Methods in Molecular Biology 1342

Springer Protocols

Amanda S. Coutts
Louise Weston *Editors*

Cell Cycle Oscillators

Methods and Protocols

EXTRAS ONLINE

Humana Press

METHODS IN MOLECULAR BIOLOGY

Series Editor
John M. Walker
School of Life and Medical Sciences
University of Hertfordshire
Hatfield, Hertfordshire, AL10 9AB, UK

For further volumes:
http://www.springer.com/series/7651

Cell Cycle Oscillators

Methods and Protocols

Edited by

Amanda S. Coutts

Department of Oncology, University of Oxford, Oxford, UK

Louise Weston

Scientific writer, London, UK

Humana Press

Editors
Amanda S. Coutts
Department of Oncology
University of Oxford
Oxford, UK

Louise Weston
Scientific writer
London, UK

ISSN 1064-3745 ISSN 1940-6029 (electronic)
Methods in Molecular Biology
ISBN 978-1-4939-2956-6 ISBN 978-1-4939-2957-3 (eBook)
DOI 10.1007/978-1-4939-2957-3

Library of Congress Control Number: 2015945586

Springer New York Heidelberg Dordrecht London

Printed on acid-free paper

Humana Press is a brand of Springer
Springer Science+Business Media LLC New York is part of Springer Science+Business Media (www.springer.com)

Preface

In order to multiply, all cells must go through a series of highly regulated and ordered events in order to complete a cell division cycle, or cell cycle. Understanding the dynamic interaction of small molecules, genes, and proteins that facilitate such a sophisticated biological process remains a challenging scientific problem. Oscillatory networks underlie the cycle of cell division, a process that in addition to driving both reproduction and the development of living systems also facilitates proliferative diseases and cancer. In *Cell Cycle Oscillators*, expert researchers discuss recent progress in the field from both holistic and reductionist perspectives. Moreover, they provide the latest developments in molecular biology techniques, biochemistry, and computational analysis used for studying oscillatory networks. Written in the highly successful Methods in Molecular Biology series format, chapters include introductions to their respective topics, lists of the necessary materials and reagents, step-by-step, readily reproducible laboratory protocols, and key tips on troubleshooting and avoiding known pitfalls. We hope you will agree that this book brings together a unique collection of protocols that cover standard, as well as novel and more specialized, techniques. Because of this range, the protocols will be useful for those new to the field as well as the more experienced scientist. Importantly, we hope these techniques will be used to gain further insight into the complex and incompletely understood processes that are involved in the cell cycle and its regulation by oscillatory networks. Lastly, we would also like to thank all the authors for their excellent contributions, John Walker for his expert advice and assistance, and Springer Press for all their efforts.

Oxford, UK — ***Amanda S. Coutts***
London, UK — ***Louise Weston***

Contents

Contributors

Diala Abd-Rabbo • *Département de Biochimie, Université de Montréal, Succursale Centre-Ville, Montréal, QC, Canada; Centre Robert-Cedergren, Bio-Informatique et Génomique, Université de Montréal, Succursale Centre-Ville, Montréal, QC, Canada*

Karen Akopyan • *Department of Cell and Molecular Biology, Karolinska Institutet, Stockholm, Sweden*

J. Julian Blow • *Centre for Gene Regulation & Expression, University of Dundee, Dundee, UK*

J. Bohlen • *German Cancer Research Center (Deutsches Krebsforschungszentrum; DKFZ), Heidelberg, Germany; Center for Molecular Biology of Heidelberg University (Zentrum für Molekulare Biologie der Universität Heidelberg; ZMBH), Heidelberg, Germany*

Michael J. Booth • *Département de Biochimie, Université de Montréal, Succursale Centre-Ville, Montréal, QC, Canada; Merton College, University of Oxford, Oxford, UK*

Michael Brandeis • *The Department of Genetics and The Bio-Imaging Unit, The Hebrew University of Jerusalem, Jerusalem, Israel*

Nicholas G. Brown • *Department of Structural Biology, St Jude Children's Research Hospital, Memphis, TN, USA*

M. Rowan Brown • *College of Engineering, Swansea University, Swansea, UK*

Alain de Bruin • *Department of Pathobiology, Faculty of Veterinary Medicine, Utrecht University, Utrecht, The Netherlands; Division of Molecular Genetics, Department of Pediatrics, University Medical Center Groningen, Groningen, The Netherlands*

Gaganmeet Singh Chadha • *Centre for Gene Regulation & Expression, University of Dundee, Dundee, UK*

Harry Charbonneau • *Department of Biochemistry and Center for Cancer Research, Purdue University, West Lafayette, IN, USA*

Courtney H. Coschi • *Department of Biochemistry, London Regional Cancer Program, Children's Health Research Institute, Western University, London, ON, Canada*

Kevin Creavin • *Centre for Gene Regulation & Expression, University of Dundee, Dundee, UK*

Attila Csikász-Nagy • *Randall Division of Cell and Molecular Biophysics, King's College London, Strand, London, UK; Institute for Mathematical and Molecular Biomedicine, King's College London, London, UK; Department of Computational Biology, Research and Innovation Centre, Fondazione Edmund Mach, San Michele all'Adige, Italy*

Christian Cuba • *Department of Mechanical Engineering, University of California, Riverside, Riverside, CA, USA*

Frederick A. Dick • *Department of Biochemistry, London Regional Cancer Program, Children's Health Research Institute, Western University, London, ON, Canada; Cancer Research Labs, London, ON, Canada*

Po Hien Ear • *Département de Biochimie, Université de Montréal, Succursale Centre-Ville, Montréal, QC, Canada; Department of Genetics, Harvard Medical School, Boston, MA, USA*

B.A. Edgar • *German Cancer Research Center (Deutsches Krebsforschungszentrum; DKFZ), Heidelberg, Germany; Center for Molecular Biology of Heidelberg University (Zentrum für Molekulare Biologie der Universität Heidelberg; ZMBH), Heidelberg, Germany*

Christie L. Eissler • *Department of Biochemistry and Center for Cancer Research, Purdue University, West Lafayette, IN, USA*

Monika Engelhardt • *Department of Hematology, Oncology and Stem Cell Transplantation, University Medical Center, Freiburg, Germany*

Rachel J. Errington • *Institute of Cancer and Genetics, School of Medicine, Cardiff University, Cardiff, UK*

Marie Follo • *Core Facility, Department of Hematology, Oncology and Stem Cell Transplantation, University Medical Center, Freiburg, Germany*

Elisa Franco • *Department of Mechanical Engineering, University of California, Riverside, Riverside, CA, USA*

Olivier Gavet • *Institut Gustave Roussy, UMR 8200 CNRS, Villejuif Cedex, France*

Lilia Gheghiani • *Sorbonne Universités, UPMC Paris VI, Paris, France*

Peter J. Gillespie • *Centre for Gene Regulation & Expression, University of Dundee, Dundee, UK*

Roy M. Golsteyn • *Cancer Cell Laboratory, Department of Biological Sciences, University of Lethbridge, Lethbridge, AB, Canada*

Christine Greil • *Department of Hematology, Oncology and Stem Cell Transplantation, University Medical Center, Freiburg, Germany*

Victoria Griesdoorn • *Institute of Cancer and Genetics, School of Medicine, Cardiff University, Cardiff, UK*

Mark C. Hall • *Department of Biochemistry and Center for Cancer Research, Purdue University, West Lafayette, IN, USA*

Conrad Hall • *Department of Biology, McGill University, Montreal, QC, Canada*

Christian E. Isaac • *Department of Biochemistry, London Regional Cancer Program, Children's Health Research Institute, Western University, London, ON, Canada*

Marc A. Jarvis • *Research Institute of Molecular Pathology (IMP), Vienna Biocenter (VBC), Vienna, Austria*

Jongmin Kim • *Wyss Institute for Biologically Inspired Engineering, Harvard University, Boston, MA, USA*

Jacqueline Kowarzyk • *Département de Biochimie, Université de Montréal, Succursale Centre-Ville, Montréal, QC, Canada*

Kazunori Kume • *Department of Molecular Biotechnology, Graduate School of Advanced Sciences of Matter, Hiroshima University, Higashi-Hiroshima, Japan*

Cody W. Lewis • *Cancer Cell Laboratory, Department of Biological Sciences, University of Lethbridge, Lethbridge, AB, Canada; Department of Oncology, Cross Cancer Institute, University of Alberta, Edmonton, AB, Canada*

Arne Lindqvist • *Department of Cell and Molecular Biology, Karolinska Institutet, Stockholm, Sweden*

Chunxiong Luo • *The State Key Laboratory for Artificial Microstructures and Mesoscopic Physics, School of Physics, Peking University, Beijing, China; Center for Quantitative Biology, Academy for Advanced Interdisciplinary Studies, Peking University, Beijing, China*

Naomi Melamed-Book • *The Department of Genetics and The Bio-Imaging Unit, The Hebrew University of Jerusalem, Jerusalem, Israel*
Michael Melesse • *Department of Biochemistry and Center for Cancer Research, Purdue University, West Lafayette, IN, USA*
Stephen W. Michnick • *Département de Biochimie, Université de Montréal, Succursale Centre-Ville, Montréal, QC, Canada; Centre Robert-Cedergren, Bio-Informatique et Génomique, Université de Montréal, Succursale Centre-Ville, Montréal, QC, Canada*
Erik Müllers • *Department of Cell and Molecular Biology, Karolinska Institutet, Stockholm, Sweden*
Ivan Mura • *Faculty of Engineering, EAN University, Bogotá, Colombia*
Julia Neusiedler • *Centre for Gene Regulation & Expression, University of Dundee, Dundee, UK*
Jan-Michael Peters • *Research Institute of Molecular Pathology (IMP), Vienna, Austria*
Randy Y.C. Poon • *Division of Life Science, Center for Cancer Research, Hong Kong University of Science and Technology, Clear Water Bay, Hong Kong; State Key Laboratory of Molecular Neuroscience, Hong Kong University of Science and Technology, Clear Water Bay, Hong Kong*
Brendan L. Powers • *Department of Biochemistry and Center for Cancer Research, Purdue University, West Lafayette, IN, USA*
Gemma S. Puts • *Department of Biochemistry & Molecular Biology, University of Maryland School of Medicine, Baltimore, MD, USA*
Brenda A. Schulman • *Department of Structural Biology and Howard Hughes Medical Institute, St Jude Children's Research Hospital, Memphis, TN, USA*
Matthaeus Schwarz-Schilling • *Systems Biophysics and Bionanotechnology, Physik Department and WSI/ZNN, Technische Universität München, Garching, Germany*
Hadas Segev • *The Department of Genetics and The Bio-Imaging Unit, The Hebrew University of Jerusalem, Jerusalem, Israel*
Kristian Shulist • *Department of Biology, McGill University, Montreal, QC, Canada*
Friedrich C. Simmel • *Systems Biophysics and Bionanotechnology, Physik Department and WSI/ZNN, Technische Universität München, Garching, Germany*
Kobi J. Simpson-Lavy • *The Department of Genetics and The Bio-Imaging Unit, The Hebrew University of Jerusalem, Jerusalem, Israel*
Paul J. Smith • *Institute of Cancer and Genetics, School of Medicine, Cardiff University, Cardiff, UK*
Natasha Spadafora • *School of Biosciences, Cardiff University, Cardiff, UK*
M. van Straaten • *German Cancer Research Center (Deutsches Krebsforschungszentrum; DKFZ), Heidelberg, Germany; Center for Molecular Biology of Heidelberg University (Zentrum für Molekulare Biologie der Universität Heidelberg; ZMBH), Heidelberg, Germany*
Zhaohua Tang • *W.M. Keck Science Center, The Claremont Colleges, Claremont, CA, USA*
Ryan G. Taylor • *Cancer Cell Laboratory, Department of Biological Sciences, University of Lethbridge, Lethbridge, AB, Canada*
Ingrid Thurlings • *Department of Pathobiology, Faculty of Veterinary Medicine, Utrecht University, Utrecht, The Netherlands*
Michael J. Thwaites • *Department of Biochemistry, London Regional Cancer Program, Children's Health Research Institute,Western University, London, ON, Canada*

Ryan VanderLinden • *Department of Structural Biology and Howard Hughes Medical Institute, St Jude Children's Research Hospital, Memphis, TN, USA*
Jackie Vogel • *Department of Biology, McGill University, Montreal, QC, Canada*
Shujing Wang • *The State Key Laboratory for Artificial Microstructures and Mesoscopic Physics, School of Physics, Peking University, Beijing, China; Center for Quantitative Biology, Academy for Advanced Interdisciplinary Studies, Peking University, Beijing, China*
Ralph Wäsch • *Department of Hematology, Oncology and Stem Cell Transplantation, University Medical Center, Freiburg, Germany*
Edmond R. Watson • *Department of Structural Biology, St Jude Children's Research Hospital, Memphis, TN, USA*
Maximilian Weitz • *Systems Biophysics and Bionanotechnology, Physik Department and WSI/ZNN, Technische Universität München, Garching, Germany*
Marie Wiltshire • *Institute of Cancer and Genetics, School of Medicine,, Cardiff University, Cardiff, UK*
Wei-Sheng Wu • *Department of Electrical Engineering, National Cheng Kung University, Tainan City, Taiwan*
Drora Zenvirth • *The Department of Genetics and The Bio-Imaging Unit, The Hebrew University of Jerusalem, Jerusalem, Israel*
Tongli Zhang • *Biochemistry Department, University of Oxford, Oxford, UK*
N. Zielke • *German Cancer Research Center (Deutsches Krebsforschungszentrum; DKFZ), Heidelberg, Germany; Center for Molecular Biology of Heidelberg University (Zentrum für Molekulare Biologie der Universität Heidelberg; ZMBH), Heidelberg, Germany*

Part I

Reviews

Chapter 1

Cell Cycle Control: A System of Interlinking Oscillators

Randy Y.C. Poon

Abstract

The cell cycle is the sequence of events through which a cell duplicates its genome, grows, and divides. Key cell cycle transitions are driven by oscillators comprising cyclin-dependent kinases and other kinases. Different cell cycle oscillators are inextricably linked to ensure orderly activation of oscillators. A recurring theme in their regulation is the abundance of auto-amplifying loops that ensure switch-like and unidirectional cell cycle transitions. The periodicity of many cell cycle oscillators is choreographed by inherent mechanisms that promote automatic inactivation, often involving dephosphorylation and ubiquitin-mediated protein degradation. These inhibitory signals are subsequently suppressed to enable the next cell cycle to occur. Although the activation and inactivation of cell cycle oscillators are in essence autonomous during the unperturbed cell cycle, a number of checkpoint mechanisms are able to halt the cell cycle until defects are addressed. Together, these mechanisms orchestrate orderly progression of the cell cycle to produce more cells and to safeguard genome integrity.

Key words APC/C, Cell division, Cell growth, Checkpoints, Cyclin-dependent kinases, Cyclin, DNA replication, Mitosis, Phosphorylation, pRb, Proteolysis, Ubiquitin-mediated degradation

1 Introduction

The cell cycle is the sequence of events through which a cell duplicates its genome, grows, and divides into two daughter cells. It encompasses one of the most fundamental properties of life.

The cell cycle is divided into four phases (Fig. 1). After cell division, daughter cells undergo a period of growth (G_1) when cellular macromolecules including proteins, RNA, and membranes are synthesized. G_1 is followed by a period of DNA synthesis (S). After another period of growth (G_2), cells undergo mitosis (M), during which the DNA is divided equally into two daughter cells, cumulating in cytokinesis. Most nondividing cells exit the cell cycle at G_1 into quiescence (G_0).

Progress in the past several decades has revealed that the eukaryotic cell cycle is driven by an evolutionarily conserved engine composed of a family of protein kinases called cyclin-dependent kinases (CDKs). Although the orderly progression of the cell cycle depends

Amanda S. Coutts and Louise Weston (eds.), *Cell Cycle Oscillators: Methods and Protocols*, Methods in Molecular Biology, vol. 1342, DOI 10.1007/978-1-4939-2957-3_1,

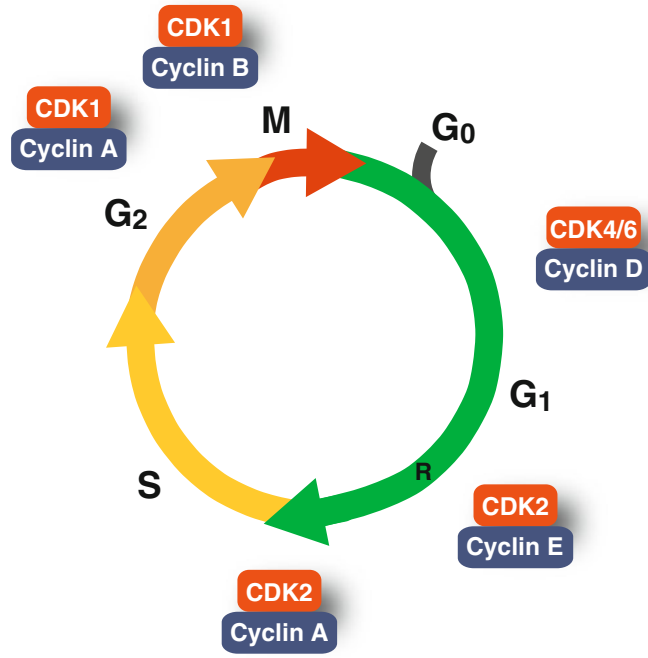

Fig. 1 The cell cycle and cyclin–CDK complexes. The cell cycle is divided into four phases: Gap 1 (G_1), DNA synthesis (S), Gap 2 (G_2), and mitosis (M). Most nondividing mammalian cells exit the cell cycle at G_1 into a quiescent state (G_0). After passing the restriction point (R), a cell is committed to another round of cell cycle and becomes independent of proliferation stimulants. The cyclin–CDK complexes involved in different periods of the cell cycle are shown

on a number of factors, the sequential switching on and off of different CDKs to promote different stages of the cell cycle remains a good approximation (Fig. 1). Accordingly, the activities of CDKs are stringently regulated by mechanisms including protein–protein interaction, phosphorylation, and ubiquitin-mediated proteolysis.

This review summarizes the fundamental concepts of cell cycle oscillators. Although the basic mechanisms of cell cycle control are conserved in all eukaryotic cells, details such as the complexity of protein families involved and checkpoint regulation do vary between organisms and between embryonic and somatic cells. Here the emphasis is placed on the somatic cell cycle of mammalian cells.

1.1 Anatomy of a Cell Cycle Oscillator

The cell cycle is steered by successive waves of cell cycle oscillators. Myriad mechanisms are developed to ensure that cell cycle regulators are turned on and off a timely fashion and in proper order. These oscillators are characterized by several features, including (a) an activating mechanism; (b) an auto-amplifying loop to ensure switch-like cell cycle transitions; an additional kick-starting mechanism may also be involved; (c) an auto-inactivating mechanism that automatically turns off the oscillator; (d) a mechanism to prevent the

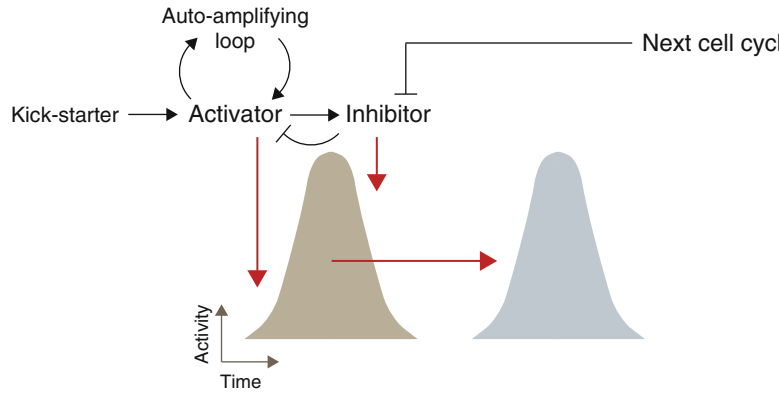

Fig. 2 Cell cycle oscillators. Due to the periodic nature of the cell cycle, activating mechanism of a cell cycle oscillator is followed by an inactivating one. The latter then has to be suppressed to enable a subsequent cell cycle. Several features are frequently found in cell cycle oscillators, including (**a**) an activating mechanism; (**b**) an auto-amplifying and a kick-starting mechanism; (**c**) an auto-inactivating mechanism; (**d**) a mechanism to prevent the reactivation of the oscillator during the same cell cycle; and a way to remove this inhibitory signal during the next cell cycle; as well as (**e**) a stimulator of the next oscillator in the cell cycle (*blue*)

reactivation of the oscillator during the same cell cycle; and a way to remove this inhibitory signal during the next cell cycle; and (e) a stimulator of the next oscillator in the cell cycle (Fig. 2). Not all of these features are present in every cell cycle oscillator. Emphasis is placed in the subsequent sections to identify these components in each cell cycle oscillator.

1.2 Checkpoints: Putting a Break on Cell Cycle Oscillators

Once passed the restriction point, the cell cycle can be viewed as a succession of autonomous oscillators (*see* Subheading 2). However, the free running of the cell cycle engine is restrained by surveillance mechanisms termed checkpoints. By temporarily halting the cell cycle, checkpoints ensure that each stage of the cell cycle is completed before the next stage is initiated.

In general, checkpoints include a sensor that monitors cell cycle defects, a transducer that transmits and amplifies the signal, and an effector that stop the cell cycle. Several major checkpoints, including those that monitor proper spindle assembly, completion of DNA replication, and DNA damage are discussed here.

2 Entering the Cell Cycle and G_1–S

Whether a cell stays in the cell cycle depends on the integration of extracellular signals from cell surface receptors responding to mitogenic growth factors and growth inhibitory factors. This decision

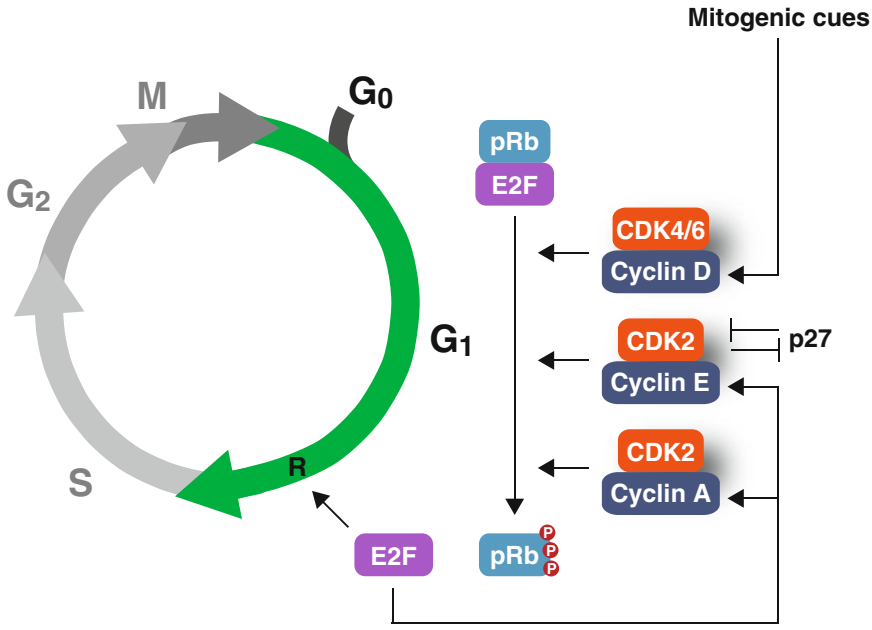

Fig. 3 Regulation of G_1–S. Both the transcription and stability of cyclin D increase when quiescent cells are stimulated to enter the cell cycle by extracellular growth signals. Hyperphosphorylation of pRb by cyclin D–CDK4/6 releases pRb from E2F, allowing E2F to activate transcription. Increased E2F-dependent transcription enables cells to pass through the restriction point (R). Among other genes, E2F increases the expression of cyclin E and cyclin A, which activates CDK2 and further boosts the phosphorylation of pRb in a positive feedback loop. Sequestering of $p21^{CIP1/WAF1}$ and $p27^{KIP1}$ by cyclin D–CDK4/6 further increases the activity of cyclin E–CDK2. Cyclin E–CDK2 also reduces $p27^{KIP1}$ by targeting it to SCF^{SKP2}-dependent degradation. Resetting pRb to a hypophosphorylated state is carried out by PP1 at the end of mitosis

is made at a transition toward the end of G_1 called the restriction point (R). Cells exit the cell cycle into G_0 if insufficient mitogenic signals are present to overcome the restriction point. After passing the restriction point, a cell is committed to another round of cell cycle and becomes independent of external stimuli. Mechanistically, the restriction point involves phosphorylation of the retinoblastoma gene product pRb by G_1 cyclin–CDK complexes (Fig. 3). After DNA damage, the G_1–S cell cycle engine is suppressed by the G_1 DNA damage checkpoint.

2.1 Cyclin D as a Mitogenic Sensor for the Cell Cycle

Transcription of D-type cyclins (D1, D2, and D3) increases when quiescent cells are stimulated with growth factors. The strong dependence of cyclin D expression on extracellular mitogenic cues, coupling to the relatively short half-live of the protein (~30 min), enables cyclin D to act as an effective mitogenic sensor that conveys extracellular signals to the cell cycle.

The promoters of D-type cyclins are under the control of multiple cell surface receptors and signaling pathways [1]. For example, activation of RAS–RAF–MEK–ERK signaling cascade, either

in response to soluble growth factors binding to cell surface tyrosine kinase receptors or extracellular matrix (ECM) binding to integrins, activates the transcription of cyclin D1. This is mediated by the downstream transcription factors AP-1 (including members of the FOS, JUN, and ATF families) of the RAS signaling pathway. In addition, RAS also activates AKT/PKB through phosphoinositide 3-kinase (PI3K). AKT/PKB then phosphorylates and inactivates GSK-3β, thereby preventing β-catenin from degradation; the accumulated β-catenin then recruits the TCF/LEF family of transcription factors to activate cyclin D1 transcription. In this connection, activation of β-catenin by the canonical Wnt signaling pathway also increases the transcription of cyclin D1. As degradation of cyclin D1 involves phosphorylation by GSK-3β (at residue threonine (Thr) 286, generating a phosphodegron that is recognized by the ubiquitin ligase SCF^{FBX4}), inhibition of GSK-3β by AKT/PKB also has an additional effect of stabilizing cyclin D1 protein [2].

2.2 Phosphorylation of pRb Underlies the Restriction Point

Once cyclin D is synthesized, it binds and activates two cyclin-dependent kinases, CDK4 and CDK6. The cyclin D–CDK4/6 complexes then phosphorylate the retinoblastoma gene product pRb (and the related p107 and p130) [3].

One of the key functions of pRb (and related proteins) before it is phosphorylated by cyclin D–CDK4/6 (hypophosphorylated) is to sequester E2F. Several members of the E2F family (E2F1-3) bind DP proteins (DP1 or DP2), forming transcription factors critical for transcribing genes important for entry into S phase [4]. Hypophosphorylated pRb inhibits E2F by both blocking the transactivating domain as well as recruiting other proteins to repress E2F-mediated transcription. One mechanism involves the association of pRb with chromatin remodeling enzymes including histone deacetylase (HDAC), thereby indirectly targeting HDAC to the promoters bound by E2F–DP [3]. This represses the transactivation of the promoter through chromatin remodeling. Phosphorylation of pRb by cyclin D–CDK4/6 releases pRb from E2F (removing HDAC at the same time), liberating E2F–DP complexes to activate transcription. Hyperphosphorylation of pRb is initiated by cyclin D–CDK4/6, but is then maintained by cyclin E–CDK2 and cyclin A–CDK2. Unlike that of cyclin D, the expression of cyclin E and cyclin A is independent of extracellular signals. A large number of genes, many yet to be characterized, are transcriptionally activated by E2F–DP complexes. Among these are cyclin E and cyclin A, which activate CDK2 and further increase the phosphorylation of pRb. The pRb–E2F pathway therefore functions as a switch to convert graded growth factor stimulations into an all-or-none E2F response.

Several members of the E2F family including E2F4 and E2F5 are transcriptional repressors. During G_0, E2F4 and E2F5 repress E2F-responsive genes that promote entry into G_1. Following mitogenic

stimulation, phosphorylation of pRb by cyclin–CDK complexes results in the release of E2F repressors and the accumulation of newly synthesized E2F activators (E2F1-3) [4].

Negative regulators of the G_1 cyclin–CDK complexes including CDK inhibitors can modulate the threshold of the restriction point. Binding of cell surface receptors by TGF-β stimulates a signaling pathway involving Smad proteins, eventually leading to the synthesis of $p15^{INK4B}$ [5]. As a cyclin D-specific inhibitor, $p15^{INK4B}$ inhibits cyclin D–CDK4/6 by blocking the formation of the complexes. It also has an additional effect of displacing the $p21^{CIP1/WAF1}$/$p27^{KIP1}$ that normally associates with cyclin D–CDK4/6 to redistribute to other cyclin–CDK complexes. The protein $p27^{KIP1}$ is further stabilized by TGF-β signaling through destruction of SKP2 [6].

The levels of some of the CDK inhibitors are modulated during the cell cycle. For example, $p27^{KIP1}$ is degraded by the ubiquitin ligase SCF^{SKP2} complex. SKP2 itself is destroyed by APC/C^{CDH1} during G_1 [7, 8]. The accumulation of $p27^{KIP1}$ conferred by APC/C^{CDH1} therefore contributes to the inhibition of CDK2 activity during G_1. When cyclin D accumulates during G_1, it drags $p21^{CIP1/WAF1}$ and $p27^{KIP1}$ away from cyclin E–CDK2 complexes, thereby liberating cyclin E–CDK2 from the CDK inhibitors. For cyclin D–CDK4/6 complexes, the kinase activity towards pRb is actually unaffected by $p21^{CIP1/WAF1}$ and $p27^{KIP1}$ (in fact, these proteins stimulate the formation of cyclin D–CDK4/6 complexes).

After cyclin E–CDK2 is turned on, it phosphorylates $p27^{KIP1}$ and stimulates SCF^{SKP2}-dependent degradation of $p27^{KIP1}$. This in turn allows more cyclin E–CDK2 to be activated to promote G_1–S. As described above, signaling by RAS activates AKT/PKB. AKT/PKB also phosphorylates $p21^{CIP1/WAF1}$ and $p27^{KIP1}$ and blocks their nuclear accumulation, thereby preventing these CDK inhibitors from acting on the G_1 cyclin–CDK complexes.

Phosphorylation of pRb is reset to the hypophosphorylated state by the phosphatase PP1 at the end of mitosis, at a time when the levels of cyclin D, cyclin E, and cyclin A are at their lowest during the cell cycle [9]. The overcoming of the restriction point becomes once again dependent on extracellular cues and the accumulation of cyclin D.

2.3 The G_1 DNA Damage Checkpoint

DNA damage occurring during G_1 phase activates a checkpoint that pauses the cell cycle to allow time for DNA repair. The molecular mechanism underlying this checkpoint is comprised of a p53-dependent mechanism that feeds into the pRb pathway [10]. In the absence of DNA damage, p53 is suppressed by one of its own transcriptional targets called MDM2 in a negative feedback loop. MDM2 binds to the amino (N)-terminal transactivation

domain of p53 and inhibits p53-mediated transcription, shuttles p53 out of the nucleus, and promotes ubiquitin-dependent degradation of p53. The last effect is due to the fact that MDM2 is itself an ubiquitin ligase.

DNA damage activates sensors that facilitate the activation of the PI3K-related protein kinases ATM and ATR. They in turn activate the checkpoint kinases CHK1 and CHK2. ATM/ATR, CHK1/CHK2, and other DNA damage-activated protein kinases phosphorylate the N-terminal region of p53. Phosphorylation of these sites abolishes the MDM2–p53 interaction, leading to a rise in p53 level and transcriptional activity.

One of the transcriptional targets of p53 is the CDK inhibitor $p21^{CIP1/WAF1}$. The accumulated $p21^{CIP1/WAF1}$ then binds and inhibits cyclin A/E–CDK2. This diminishes the phosphorylation of pRb, thereby stopping the cell cycle in G_1 phase (*see* Subheading 2.2).

Another important control of the p53 pathway comes from the *INK4A* gene, which encodes both the CDK inhibitor $p16^{INK4A}$ and a protein called $p14^{ARF}$. The inhibition of p53 by MDM2 is interrupted by $p14^{ARF}$ because it sequesters MDM2 to the nucleolus. The *INK4A* gene is generally activated in response to oncogenic stresses. The ensuing increase in $p16^{INK4A}$ and $p14^{ARF}$ reduces cyclin D–CDK4/6 activity and elevates p53 expression, respectively. Both of these events eventually suppress pRb phosphorylation and arrest the cell cycle in G_1.

3 Control of S Phase

The key issues concerning the regulation of S phase are (1) how DNA replication occurs only in S phase, and (2) how replication is initiated once and once only per cell cycle (Fig. 4). Centrosome duplication also occurs during S phase and is in part coupled with the mechanisms that govern DNA replication. The replication checkpoint is responsible for delaying S phase progression and preventing mitosis in the presence of stalled replication forks.

3.1 Initiation of S Phase

Although it is well established that initiation of DNA replication occurs at chromosomal locations known as origins of replication, *S. cerevisiae* is the only known eukaryote with a defined initiation sequence. Several proteins, including origin recognition complex (ORC, which is composed of ORC1-6), CDC6, and CDT1 are assembled at the origins of replication during G_1. This facilitates the loading of double hexamers of the MCM2-7 core helicase, forming the so-called pre-replication complex (pre-RC). The formation of pre-RC on origins is called origin licensing [11].

During G_1–S transition, the origins are activated by CDK2 and another kinase called CDC7. CDK2 is activated by cyclin A and

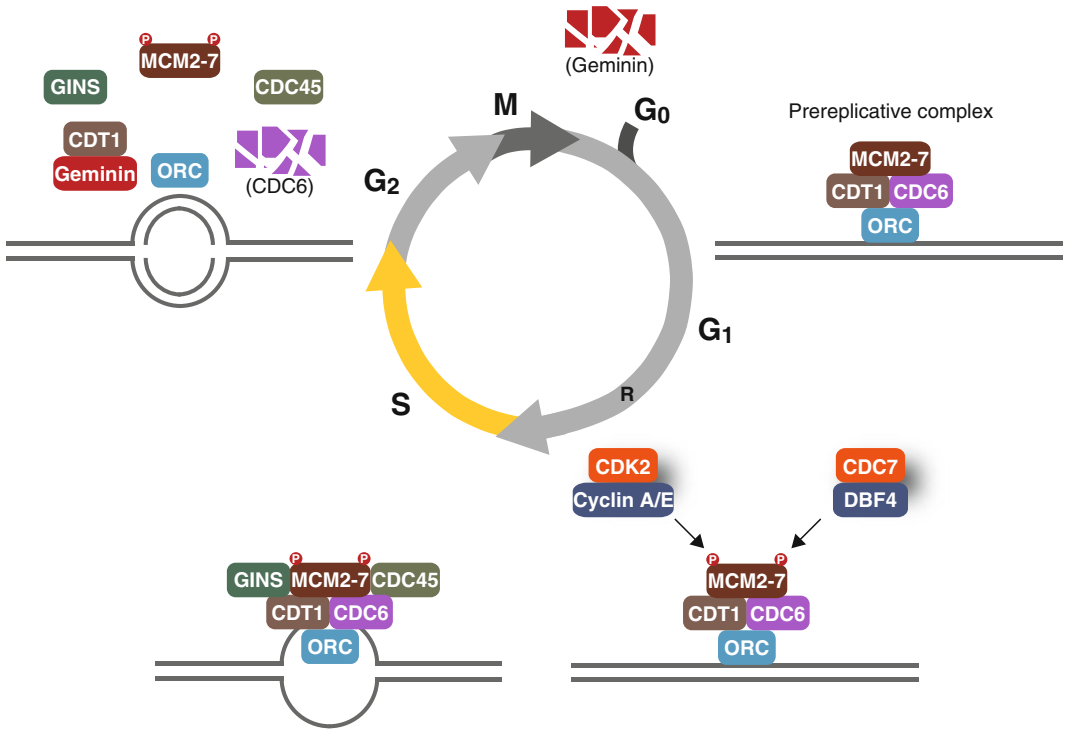

Fig. 4 Regulation of S phase. Initiation of DNA replication occurs at origins of replication. During G_1 phase, the origins are licensed by binding to the pre-replication complex. During G_1–S transition, cyclin A, cyclin E, and DBF4 are transcriptionally activated by E2F. Pre-replication complex components including MCM2-7 are phosphorylated by cyclin A/E–CDK2 and DBF4–CDC7, thereby stimulating the recruitment of CDC45 and GINS. This activates the MCM2-7 helicase to unwind the origin. Finally, the unwound DNA allows the recruitment of DNA polymerases and other components of the DNA synthesis machinery to initiate DNA synthesis. After DNA replication, several mechanisms including degradation of CDC6 and binding of CDT1 to newly synthesized geminin prevent re-replication. These mechanisms are reset later in G_1 (including the removal of geminin by APC/C shown in the figure)

cyclin E and CDC7 is activated by a protein called DBF4 (ASK in humans) [12]. Higher eukaryotes contain a second DBF4-like protein called DRF1 or ASKL1. Similar to cyclin–CDK pairs, while the level of CDC7 remains relatively constant during the cell cycle, the level of DBF4/ASK oscillates during the cell cycle, being absent during G_1 and accumulating during S and G_2. Similar to cyclin A and cyclin E, transcription of *DBF4/ASK1* is activated during late G_1 and S phase by E2F.

CDK2 and CDC7 phosphorylate components of the pre-RC including the MCM2-7 complex, thereby triggering the recruitment of two helicase co-activators, CDC45 and GINS. The MCM2-7 helicase is then activated and unwinds the origin. The single-stranded DNA is subsequently stabilized by binding to replication protein A (RPA). Finally, the unwound DNA facilitates the recruitment of DNA polymerases and other components of the DNA synthesis machinery to initiate DNA synthesis.

Cyclin A/E–CDK2 also coordinates the initiation of DNA replication with the centrosome cycle [13]. The centrosome is located near the nucleus and contains the microtubule organizing center, playing important roles in the establishment of the interphase cytoplasmic microtubule network and bipolar mitotic spindles. Since each daughter cell receives just one centrosome after cell division, the centrosome has to duplicate once before the next mitosis. Centrosome duplication occurs during S phase and is coupled to the cell cycle, at least in part, by the activity of cyclin A/E–CDK2.

3.2 Prevention of Re-replication

Once the genome has been replicated, formation of the pre-RC is inhibited by multiple mechanisms until the next cell cycle. Cyclin E is degraded by the ubiquitin ligase SCF^{FBW7} after S phase, thereby turning off the cyclin E-CDK2 kinase activity. The phosphodegron recognized by SCF^{FBW7} is created by CDK2-dependent autophosphorylation as well as by GSK-3β. On the other hand, DBF4/ASK1 is degraded by APC/C only after mitosis.

The accumulation of CDK activity during late G_1, S, and G_2 prevents the reassembly of the pre-RC through several mechanisms. Although cyclin E is degraded during S phase, the expression of cyclin A persists till mitosis. CDK-dependent phosphorylation excludes MCM2-7 from the nucleus, targets CDT1 and CDC6 for degradation, and dissociates ORC from the chromatin. Furthermore, accumulation of geminin during S and G_2 results in the formation of a tight geminin–CDT1 complex, thereby preventing CDT1 from loading onto the pre-RC.

Cyclin A–CDK2 also phosphorylates E2F1 and E2F3, decreasing their DNA binding capability and terminating the transcription of genes involve in S phase control [14, 15]. SCF^{SKP2}-dependent degradation of E2F1 during S and G_2 further limits the activity of E2F after S phase [16]. Several members of the E2F family including E2F7 and E2F8 are transcriptional repressors. After G_1–S, these transcriptional repressor E2Fs attenuate the transcription of genes activated earlier by E2F1-3. They also directly repress the expression of transcriptional activator E2Fs such as E2F1 [4]. Together, these mechanisms prevent the expression of E2F-activating genes after G_1–S.

Assembly of the pre-RC can occur again in early G_1 because destruction of cyclin A and cyclin B during mitosis provides an environment of low CDK activity. Proteolysis of geminin by APC/C during mitosis also unleashes CDT1 to form the pre-RC. Hence, APC/C resets the mechanisms that safeguard re-replication during the previous cell cycle.

3.3 Replication Checkpoint

Stalled replication forks activate a checkpoint involving ATR [17]. Replication fork progression is disrupted by either an insufficient supply of nucleotides or lesions and obstacles on the DNA. Several proteins including ATRIP, Claspin, and TopBP1 are involved in

recruiting ATR to single-stranded DNA present at the stalled replication forks. Specifically, ATR is activated by binding to the single-strand binding protein RPA-coated single-stranded DNA. The activated ATR then phosphorylates and activates CHK1. CHK1 subsequently activates WEE1 and inactivates CDC25 (*see* Subheading 4.2). Consequently, this alters the inhibitory phosphorylation status of CDKs, tipping the balance towards inhibition of the cyclin–CDK complexes involved in both replication (*see* Subheading 3.1) and mitotic entry (*see* Subheading 4). Hence, the replication checkpoint regulates origin firing, replication forks progression, as well as preventing untimely mitosis. These mechanisms provide the cell with time to restart or repair the stalled replication forks. Significantly, the checkpoint is essential during unperturbed S phase even in the absence of exogenous stresses.

4 G_2–Mitosis

Several dramatic events occur during mitosis, including chromosome condensation, nuclear envelope breakdown, formation of mitotic spindles, attachment of chromosomes to the mitotic spindles, and separation of sister chromatids. In essence, mitosis is driven by the activation of CDK1 (Fig. 5). Working in concert with a number of kinases and phosphatases, the activation of CDK1 is characterized by feedback mechanisms that ensure CDK1 is activated rapidly.

4.1 Cyclin B–CDK1 as the Engine of Mitosis

The key event for mitotic entry is the activation of CDK1. Although CDK1 is present at constant levels throughout the cell cycle, it is active only during mitosis due to regulation by several mechanisms including binding to cyclins and phosphorylation.

The mitotic cyclins (cyclin A and cyclin B) are synthesized and destroyed around the time of mitosis (cyclin A also functions in S phase) [18]. Mammalian cells contain two A-type cyclins (A1 and A2) and three B-type cyclins (B1, B2, and B3). While cyclin A2 is present in all proliferating somatic cells, cyclin A1 is critical only during spermatogenesis. Cyclin B1 is the major mitotic cyclin partner of CDK1. Cyclin B2 is co-expressed with cyclin B1 in the majority of dividing cells but is less abundant. The expression of cyclin B3 is restricted to developing germ cells and in the adult testis.

A salient characteristic of the mitotic cyclins is their periodicity. Cyclin A starts to accumulate during late G_1, continues through S phase and G_2, before being rapidly destroyed during mitosis. Cyclin B is synthesized and destroyed slightly later than cyclin A. The cell cycle expression of cyclin A and cyclin B is regulated at the levels of transcription and proteolysis [18]. For example, several transcription factors, including B-MYB, E2F, FOXM1, and NF-Y, regulate the mRNAs of cyclin B1 so that they accumulate during G_2 and diminish after mitosis. The sharp decrease of the mitotic cyclins at

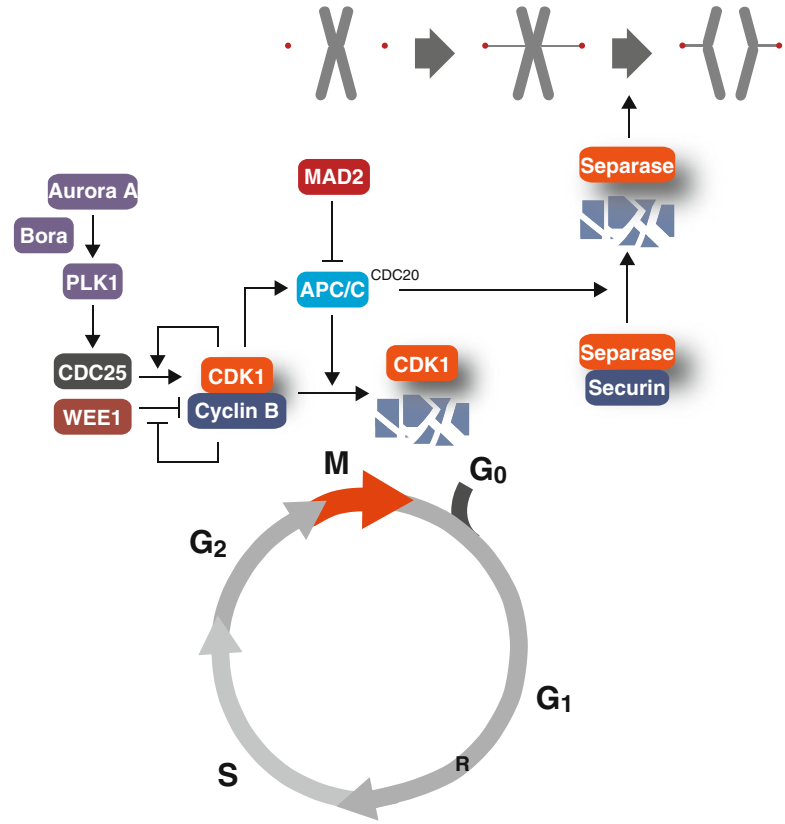

Fig. 5 Regulation of mitotic entry and exit. After cyclin B is synthesized and bound to CDK1, the complex is kept in an inactive state by WEE1/MYT1-dependent phosphorylation of CDK1. Dephosphorylation of CDK1 by members of the CDC25 phosphatase family during G_2–M transition activates cyclin B–CDK1. Cyclin B–CDK1 activation is autocatalytic because CDK1 activates CDC25 and inactivates WEE1/MYT1. Initial activation of CDC25 may be carried out by PLK1, which in turn is activated by Aurora A and Bora. During early mitosis, APC/C^{CDC20} is turned on by cyclin B–CDK1 and other mitotic kinases. However, its activity is suppressed by MAD2 from the spindle-assembly checkpoint. Once all kinetochores are properly attached, the spindle-assembly checkpoint is silenced to allow APC/C^{CDC20} activation. APC/C then targets several proteins including cyclin B, PLK1, Aurora A, and securin to ubiquitin-mediated degradation. Proteolysis of securin releases separase, which in turn cleaves cohesin to allow sister chromatid separation. Reactivation of CDK1 during G_1 is safeguarded by another APC/C complex involving CDH1. APC/C also resets conditions required for forming of the pre-replication complex for the next S phase (not shown)

the end of mitosis, however, is caused mainly by proteolysis involving APC/C-dependent mechanisms (*see* Subheading 5).

4.2 Feedback Control Ensures Biphasic Activation of CDK1

The defining characteristic of CDK1 activation is a system of feedback loops that converts the slow accumulation of cyclin B into an abrupt activation of CDK1. Monomeric CDK1 is inactive and unphosphorylated. On binding to cyclin B, the kinase activity of

CDK1 is initially suppressed by inhibitory phosphorylation of $CDK1^{Thr14/Tyr15}$ by MYT1 and WEE1 [19]. WEE1 is a dual-specificity kinase that phosphorylates tyrosine (Tyr) 15 (but not Thr14). MYT1, a kinase that is normally bound to the endoplasmic reticulum and Golgi complex, can phosphorylate both Thr14 and Tyr15, but has a stronger preference for Thr14.

At the end of G_2, the stockpile of inactive cyclin B–CDK1 complexes is rapidly activated by members of the CDC25 phosphatase family (A, B, and C) [20]. CDC25B is believed to be the initial activator of cyclin B–CDK1 at the centrosomes. This is followed by the complete activation of cyclin B–CDK1 by CDC25A and CDC25C in the nucleus. Significantly, active CDK1 activates more CDC25 and inactivates WEE1 by directly phosphorylating these proteins. Hence, a small amount of active cyclin B–CDK1 can lead to a rapid and complete activation of all the complexes by this autocatalytic loop. Phosphorylation of WEE1 by CDK1 (as well as by PLK1) also creates a phosphodegron for $SCF^{\beta TrCP}$-dependent degradation. Thus cyclin B–CDK1 is essentially a biphasic switch system that becomes autocatalytic once a critical portion is activated.

4.3 Kick-Starting the CDK1 Activating Loops

Given that the activation of cyclin B–CDK1 is autocatalytic, how the initial batch of cyclin B–CDK1 is activated becomes a salient issue. The available data indicate that the multifunctional protein kinase PLK1 may initiate the system by activating CDC25 and inactivating WEE1/MYT1 [21].

In addition, PLK1 also promotes the translocation of cyclin B into the nucleus during prophase [22]. During G_2, binding of the export mediator CRM1 to the nuclear export sequence (NES) of cyclin B1 promotes cytoplasmic localization of cyclin B1. Phosphorylation of residues in the NES by kinases including CDK1 and PLK1 is important for the nuclear translocation of cyclin B1, presumably by disrupting the CRM1–cyclin B1 interaction. This mechanism enables the localization of cyclin B1–CDK1 to the nucleus (involving binding of cyclin B1 to importin-β) when the complexes are active.

The activation of PLK1 involves phosphorylation by Aurora A, an event that is assisted by a protein called Bora [23]. Binding of Bora to PLK1 is stimulated by cyclin B–CDK1, thereby creating another positive feedback loop in the activation of cyclin B–CDK1. PLK1 then phosphorylates Bora and generates a phosphodegron motif that is recognized by the ubiquitin ligase $SCF^{\beta TrCP}$, targeting Bora for degradation [24]. Degradation of Bora allows the redistribution of Aurora A from a cytoplasmic Bora-containing complex to a TPX2-containing complex at the mitotic spindle. Activation of Aurora A during mitosis involves binding to cofactors such as TPX2 and autophosphorylation of a residue in the T-loop.

Both Aurora A and PLK1 are also important for various centrosome functions, including centrosome separation, maturation,

and mitotic spindle formation. Separation of duplicated and matured centrosomes in late G_2 is crucial for the formation of bipolar mitotic spindles. At the end of mitosis, both Aurora A and PLK1 are degraded by APC/C^{CDH1}-mediated ubiquitination.

4.4 Greatwall (MASTL) Helps Maintain the Mitotic State

Phosphorylation events during mitosis are reversible. To ensure that mitotic cells do not reverse to G_2, it is important both to maintain the activities of the mitotic kinases as well as to suppress the phosphatases that counteract the kinases' actions.

Greatwall (MASTL in humans) is a kinase that phosphorylates ARPP19 and α-endosulfine (ENSA), promoting their inhibition of the phosphatase PP2A–B55. As PP2A–B55 is a major phosphatase that dephosphorylates cyclin B–CDK1 substrates, Greatwall activity is important for maintaining the phosphorylation of CDK1 substrates during mitosis [25].

Greatwall also regulates the activation of CDK1 by maintaining the phosphorylation of CDC25, thereby keeping CDK1 in a Thr14/Tyr15-dephosphorylated state. Greatwall itself appears to be activated during mitosis by CDK1 in a feedback loop. At the end of mitosis, Greatwall is reset to an inactive state by PP2A–B55-dependent dephosphorylation of an essential CDK phosphorylation site (Thr194). Dephosphorylation of ENSA/ARPP19 is mediated by the phosphatase FCP1 [26].

4.5 The G_2 DNA Damage Checkpoint

The G_2 DNA damage checkpoint involves the activation of the protein kinases ATM/ATR followed by CHK1/CHK2 similarly to the G_1 DNA damage checkpoint. CHK1/CHK2 then activates WEE1 and inactivates all three isoforms of the CDC25 family (CDC25A, CDC25B, and CDC25C). Together, these mechanisms promote $CDK1^{Thr14/Tyr15}$ phosphorylation, leading to the inactivation of CDK1 and cell cycle arrest in G_2 [27].

CDC25C is inactivated by CHK1/CHK2-dependent phosphorylation both directly and indirectly through the creation of a 14-3-3 binding site. Binding of 14-3-3 to CDC25C masks a proximal nuclear localization sequence, thereby anchoring CDC25C in the cytoplasm and preventing efficient access to cyclin B–CDK1. The centrosomal CDC25B is also phosphorylated by CHK1, creating a docking site for 14-3-3 that disrupts access to CDK1. In contrast to other CDC25 isoforms, CDC25A is targeted for rapid degradation by CHK1/CHK2. CDC25A stability is usually controlled by APC/C^{CDH1} complexes during early G_1 and by $SCF^{\beta TrCP}$ complexes during interphase. Importantly, the $SCF^{\beta TrCP}$-mediated degradation of CDC25A is enhanced after DNA damage through phosphorylation by CHK1. In addition to acting on CDC25, CHK1/CHK2 also appears to phosphorylate and activate WEE1 by promoting 14-3-3 binding.

5 Mitosis–G_1

The key event in mitotic exit is the onset of anaphase, which is driven by APC/C-dependent ubiquitination. Degradation of APC/C substrates including cyclin B and securin promotes several events during mitotic exit, including sister chromatid separation, spindle disassembly, chromosome decondensation, cytokinesis, and reformation of the nuclear envelope. How to keep APC/C inactivate before all the chromosomes are attached to the spindle correctly is the major feedback that orchestrates mitotic exit (Fig. 5).

5.1 APC/C Drives Mitotic Exit

Bipolar spindle formation and proper attachment of chromosomes are highly regulated to ensure that chromosomes are segregated equally to the daughter cells. Several kinases that are targeted to unattached kinetochores, including CDK1, PLK1, and NEK2, phosphorylate key kinetochore proteins such as HEC1 and contribute to the stabilization of microtubule–kinetochore interactions [19].

The chromosomal passenger complex (CPC, composed of Aurora B, Borealin, INCENP, and Survivin) plays a major role in spindle assembly and cytokinesis. CPC localizes to the kinetochores and chromosomes during early mitosis and functions in microtubule–kinetochore interactions, sister chromatid cohesion, and the spindle-assembly checkpoint. CPC corrects misattachments of chromosomes until they are bioriented and under tension. CPC is relocated to the central spindle at anaphase and subsequently to the midbody to promote cytokinesis [28].

Once all kinetochores are properly attached, the ubiquitin ligase APC/C is activated to degrade the mitotic cyclins and other proteins [29]. Both A- and B-type cyclins contain a short sequence at the N-terminal region known as the destruction box (D-box). The D-box targets the mitotic cyclins to the multi-subunit ubiquitin ligase APC/C. Two targeting subunits called CDC20 and CDH1 are involved in facilitating the ubiquitination of cyclins by APC/C. While CDC20 is present only during mitosis, CDH1 remains constant during the cell cycle, but only associates with APC/C during G_1. The ubiquitinated cyclins are then rapidly degraded by a constitutively active proteasome complex.

Importantly, activated cyclin B–CDK1 stimulates the activity of APC/C^{CDC20} through phosphorylation of several subunits of APC/C and CDC20. APC/C is also phosphorylated and activated by PLK1. Hence, cyclin B primes its own destruction and ensures that APC/C^{CDC20} is activated only after mitotic entry. However, the activity of APC/C^{CDC20} is suppressed by the spindle-assembly checkpoint until all the all kinetochores are properly attached (*see* Subheading 5.2).

In addition to cyclin B, APC/C^{CDC20} also degrades several substrates including securin and geminin [30]. Degradation of

securin is important for sister chromatid separation during anaphase. After DNA is replicated, sister chromatids are tethered together by cohesin, a ring-shaped complex consisting of four SMC subunits. This involves a cohesin-interacting protein called sororin, which protects the removal of cohesin by PDS5 and WAPL. Cohesin is removed from chromosomes in a two-step manner during mitosis: while cohesin at the chromosome arms is removed during early mitosis, the centromeric cohesin is protected until anaphase.

During prophase, CDK1, PLK1, and Aurora B collaborate to phosphorylate cohesin and sororin, inducing WAPL-dependent removal of cohesin from chromosome arms. However, a pool of cohesin at centromeres is protected by Shugoshin (SGO1). The primary signal for localizing SGO1 to centromeres is BUB1 (a component of the spindle-assembly checkpoint)-dependent phosphorylation of histone $H2A^{Ser121}$. SGO1 interacts with the phosphatase PP2A, thereby keeping cohesin and sororin in a hypophosphorylated state and maintaining centromeric cohesion. During metaphase-anaphase transition, proper kinetochore–microtubule attachment creates tension across sister kinetochores and triggers the removal of SGO1. Kinetochore tension also silences the spindle-assembly checkpoint. This allows the APC/C^{CDC20} to degrade securin, leading to activation of the protease separase. Separase then cleaves centromeric cohesin to facilitate sister-chromatid separation.

Another substrate of APC/C^{CDC20} is geminin. Degradation of geminin by APC/C^{CDC20} releases CDT1, a subunit required for the initiation of DNA replication (*see* Subheading 3). Hence, by simultaneously destroying the mitotic cyclins, securin, and geminin, APC/C^{CDC20} coordinates several important processes during the mitosis–G_1 transition and prepares the cell for the next S phase.

In addition to CDC20, APC/C can also associate with a targeting subunit called CDH1 [30]. In contrast to APC/C^{CDC20}, APC/C^{CDH1} is turned off during mitosis because phosphorylation by cyclin B–CDK1 alters the conformation of CDH1 and prevents its interaction with APC/C. Destruction of cyclin B at anaphase therefore relieves the inhibition of APC/C^{CDH1}, enabling it to degrade CDC20 and take over the task of degrading any remaining or newly synthesized cyclin B during G_1. Finally, APC/C^{CDH1} is also responsible for destroying several important mitotic regulators including PLK1, CDC25A, Aurora A, and SGO1.

During late G_1, E2F is released from pRb and activates the transcription of cyclin A (*see* Subheading 2). Cyclin A–CDK complexes then phosphorylates CDH1 and inhibits its association with APC/C. APC/C^{CDH1} and APC/C^{CDC20} are also turned off by binding to EMI1, which begins to accumulate at late G_1 (also transcriptionally activated by E2F). EMI1 has to be removed subsequently to allow APC/C to function in mitotic exit. This is achieved by PLK1-dependent phosphorylation, targeting EMI to ubiquitin-mediated degradation by $SCF^{\beta TrCP}$.

5.2 The Spindle-Assembly Checkpoint

The spindle-assembly checkpoint is activated by either the presence of unattached kinetochores or the absence of tension between paired kinetochores [31]. Consequently the spindle-assembly checkpoint ensures that chromosomes have achieved correct bipolar attachment to the mitotic spindles before cyclin B and other proteins are degraded by APC/C (Fig. 5).

Unattached kinetochores attract several components of the checkpoint sensors (including BUB1, BUBR1, BUB3, CENP-E, MAD1, MAD2, and MPS1), catalyzing the formation of diffusible complex called mitotic checkpoint complexes (MCC, components include MAD2, BUBR1, and BUB3). These checkpoint components act as signal transducers, resulting in the inhibition APC/C^{CDC20} through the sequestration of CDC20 by MAD2. Binding to CDC20 requires a conformational change of MAD2 from a less stable open conformation (known as O-MAD2) to the more stable close conformation (C-MAD2). Although the mechanism remains incompletely understood, several lines of evidence suggest that C-MAD2 can convert more C-MAD2 from O-MAD2 in an autocatalytic manner [32].

Once all kinetochores are properly attached, the spindle-assembly checkpoint is silenced to allow APC/C^{CDC20} activation. Several mechanisms have been implicated in switching off the checkpoint, including those that involve PP1 [33] and a MAD2-binding protein called $p31^{comet}$ [31]. However, the precise mechanism of how $p31^{comet}$ inactivates MAD2 remains incompletely understood.

Acknowledgements

Related works in my laboratory are supported in part by the Research Grants Council of Hong Kong.

References

1. Wang C, Li Z, Fu M, Bouras T, Pestell RG (2004) Signal transduction mediated by cyclin D1: from mitogens to cell proliferation: a molecular target with therapeutic potential. Cancer Treat Res 119:217–237
2. Lin DI, Barbash O, Kumar KG, Weber JD, Harper JW, Klein-Szanto AJ, Rustgi A, Fuchs SY, Diehl JA (2006) Phosphorylation-dependent ubiquitination of cyclin D1 by the SCF(FBX4-alphaB crystallin) complex. Mol Cell 24:355–366
3. Henley SA, Dick FA (2012) The retinoblastoma family of proteins and their regulatory functions in the mammalian cell division cycle. Cell Div 7:10
4. Chen HZ, Tsai SY, Leone G (2009) Emerging roles of E2Fs in cancer: an exit from cell cycle control. Nat Rev Cancer 9:785–797
5. Massague J (2008) TGFbeta in Cancer. Cell 134:215–230
6. Liu W, Wu G, Li W, Lobur D, Wan Y (2007) Cdh1-anaphase-promoting complex targets Skp2 for destruction in transforming growth factor beta-induced growth inhibition. Mol Cell Biol 27:2967–2979
7. Bashir T, Dorrello NV, Amador V, Guardavaccaro D, Pagano M (2004) Control of the SCF(Skp2-Cks1) ubiquitin ligase by the APC/C(Cdh1) ubiquitin ligase. Nature 428:190–193

8. Wei W, Ayad NG, Wan Y, Zhang GJ, Kirschner MW, Kaelin WGJ (2004) Degradation of the SCF component Skp2 in cell-cycle phase G1 by the anaphase-promoting complex. Nature 428:194–198
9. Nelson DA, Krucher NA, Ludlow JW (1997) High molecular weight protein phosphatase type 1 dephosphorylates the retinoblastoma protein. J Biol Chem 272:4528–4535
10. Sherr CJ, McCormick F (2002) The RB and p53 pathways in cancer. Cancer Cell 2:103–112
11. Masai H, Matsumoto S, You Z, Yoshizawa-Sugata N, Oda M (2010) Eukaryotic chromosome DNA replication: where, when, and how? Annu Rev Biochem 79:89–130
12. Matthews LA, Guarne A (2013) Dbf4: the whole is greater than the sum of its parts. Cell Cycle 12:1180–1188
13. Hinchcliffe EH, Sluder G (2001) "It takes two to tango": understanding how centrosome duplication is regulated throughout the cell cycle. Genes Dev 15:1167–1181
14. Dynlacht BD, Moberg K, Lees JA, Harlow E, Zhu L (1997) Specific regulation of E2F family members by cyclin-dependent kinases. Mol Cell Biol 17:3867–3875
15. Krek W, Xu G, Livingston DM (1995) Cyclin A-kinase regulation of E2F-1 DNA binding function underlies suppression of an S phase checkpoint. Cell 83:1149–1158
16. Marti A, Wirbelauer C, Scheffner M, Krek W (1999) Interaction between ubiquitin-protein ligase SCFSKP2 and E2F-1 underlies the regulation of E2F-1 degradation. Nat Cell Biol 1:14–19
17. Friedel AM, Pike BL, Gasser SM (2009) ATR/Mec1: coordinating fork stability and repair. Curr Opin Cell Biol 21:237–244
18. Fung TK, Poon RY (2005) A roller coaster ride with the mitotic cyclins. Semin Cell Dev Biol 16:335–342
19. Ma HT, Poon RY (2011) How protein kinases co-ordinate mitosis in animal cells. Biochem J 435:17–31
20. Lindqvist A, Rodriguez-Bravo V, Medema RH (2009) The decision to enter mitosis: feedback and redundancy in the mitotic entry network. J Cell Biol 185:193–202
21. van Vugt MA, Medema RH (2005) Getting in and out of mitosis with Polo-like kinase-1. Oncogene 24:2844–2859
22. Porter LA, Donoghue DJ (2003) Cyclin B1 and CDK1: nuclear localization and upstream regulators. Prog Cell Cycle Res 5:335–347
23. Lens SM, Voest EE, Medema RH (2010) Shared and separate functions of polo-like kinases and aurora kinases in cancer. Nat Rev Cancer 10:825–841
24. Macurek L, Lindqvist A, Medema RH (2009) Aurora-A and hBora join the game of Polo. Cancer Res 69:4555–4558
25. Hunt T (2013) On the regulation of protein phosphatase 2A and its role in controlling entry into and exit from mitosis. Adv Biol Regul 53:173–178
26. Hegarat N, Vesely C, Vinod PK, Ocasio C, Peter N, Gannon J, Oliver AW, Novak B, Hochegger H (2014) PP2A/B55 and Fcp1 regulate Greatwall and Ensa dephosphorylation during mitotic exit. PLoS Genet 10:e1004004
27. Chen Y, Poon RY (2008) The multiple checkpoint functions of CHK1 and CHK2 in maintenance of genome stability. Front Biosci 13:5016–5029
28. Carmena M, Wheelock M, Funabiki H, Earnshaw WC (2012) The chromosomal passenger complex (CPC): from easy rider to the godfather of mitosis. Nat Rev Mol Cell Biol 13:789–803
29. Teixeira LK, Reed SI (2013) Ubiquitin ligases and cell cycle control. Annu Rev Biochem 82:387–414
30. Manchado E, Eguren M, Malumbres M (2010) The anaphase-promoting complex/cyclosome (APC/C): cell-cycle-dependent and -independent functions. Biochem Soc Trans 38:65–71
31. Musacchio A, Salmon ED (2007) The spindle-assembly checkpoint in space and time. Nat Rev Mol Cell Biol 8:379–393
32. Mapelli M, Massimiliano L, Santaguida S, Musacchio A (2007) The Mad2 conformational dimer: structure and implications for the spindle assembly checkpoint. Cell 131:730–743
33. Lesage B, Qian J, Bollen M (2011) Spindle checkpoint silencing: PP1 tips the balance. Curr Biol 21:R898–R903

Chapter 2

Model Organisms for Studying the Cell Cycle

Zhaohua Tang

Abstract

Regulation of the cell-division cycle is fundamental for the growth, development, and reproduction of all species of life. In the past several decades, a conserved theme of cell cycle regulation has emerged from research in diverse model organisms. A comparison of distinct features of several diverse model organisms commonly used in cell cycle studies highlights their suitability for various experimental approaches, and recaptures their contributions to our current understanding of the eukaryotic cell cycle. A historic perspective presents a recollection of the breakthrough upon unfolding the universal principles of cell cycle control by scientists working with diverse model organisms, thereby appreciating the discovery pathways in this field.

A comprehensive understanding is necessary to address current challenging questions about cell cycle control. Advances in genomics, proteomics, quantitative methodologies, and approaches of systems biology are redefining the traditional concept of what constitutes a model organism and have established a new era for development of novel, and refinement of the established model organisms. Researchers working in the field are no longer separated by their favorite model organisms; they have become more integrated into a larger community for gaining greater insights into how a cell divides and cycles. The new technologies provide a broad evolutionary spectrum of the cell-division cycle and allow informative comparisons among different species at a level that has never been possible, exerting unimaginable impact on our comprehensive understanding of cell cycle regulation.

Key words Cell-division cycle (*cdc*) phenotype, Checkpoints, Yeast genetics, Maturation-promoting factor (MPF), Cyclin-dependent kinases (Cdks), Protein kinases, Phosphorylation, Domino model, Clock model

1 Introduction: Why Is Cell Cycle Regulation Important?

The development of model organisms has been driven by the fundamental questions that stimulate biologists and the amenability of species for experimental investigation in laboratories. Historically, cell function has been mainly elucidated from studies using a few unicellular organisms—primarily *Escherichia coli* and yeasts; what we have learned about animal development has been largely based on the genetics of the fruit fly and worm, as well as exploration of the frog and mouse; our understanding of the molecular and developmental biology of plants came from examining *Arabidopsis*.

Amanda S. Coutts and Louise Weston (eds.), *Cell Cycle Oscillators: Methods and Protocols*, Methods in Molecular Biology, vol. 1342, DOI 10.1007/978-1-4939-2957-3_2,

The cast of conventional model organisms is considerably small compared with the biodiversity that exists on Earth, but they have been serving as the representatives of individual groups in research to address a variety of biological questions, constituting the core of biological knowledge [1].

This chapter provides a review of several diverse model organisms commonly used in cell cycle analyses, including yeasts, frogs, fruit flies, and mammalian cells. A traditional meaning of the term model organism is: a life-form that has been established as an experimental system with common tools and reagents accessible to the community members, who focus on the model to seek answers to questions about biology [2]. Model organisms are crucial for a comprehensive understanding of a biological process at any scale. However, since every organism may be limited by its suitability for only specific types of approaches, each system may harbor imperfections, and a single route to discovery may bear biases in research, such as in cell cycle studies. Comparing the mechanisms of cell cycle regulation among different organisms deciphers whether conclusions being reached independently can be generalized across species.

Research in eukaryotes as divergent as yeasts, frogs, fruit flies, and mammalian cells has revealed the conservation of the fundamental principles in cell cycle regulation. At the same time, the unique features of cell cycle control in various organisms studied have helped, and will continue to help, illuminate how fidelity of the cell cycle can be achieved in different ways (for review, *see* refs. 3–6). Historically, cell cycle research communities based in different model systems, often in isolation from one another, have gained insight into the general principles that underlie the cell cycle control in all eukaryotic cells. Changes in technologies with the availability of complete genome sequences from many species, are reframing our concept of what consists of a model organism [1, 2]. These advances have greatly facilitated informative comparisons between different species and have increased interactions among organism-based cell cycle research communities, thereby enabling fresh and exciting opportunities in this field.

1.1 The Cell as a Structural Unit of Life

A great variety of organisms have evolved on Earth with diverse shapes, sizes, and lifestyles that nonetheless all work under a common framework of cellular mechanics. In 1838, botanist Matthias Schleiden and zoologist Theodor Schwann proposed "all organisms are composed of essentially like parts, namely cells"—the cell theory [5]. The cell theory states that:

1. All life forms are made from one or more cells.
2. Cells are the smallest form of life.
3. Cells only arise from preexisting cells.

It took 20 years for Rudolf Virchow, a German pathologist to add the third tenet of the cell theory about cell reproduction. He

discovered that cancer is an uncontrolled growth of cells—hyperplasia in its extreme form, as he put it: *ominis cellula e cellula* [7]. That constitutes the above third tenet of the cell theory.

After the birth of the cell theory, the cell biology field was forever changed. While life on Earth consists of immensely diverse forms, the cell theory provides us with an operational definition of life: the cell as a common basic unit for all organisms, the appearance of which can be drastically diverse. Amazingly, the principles of cell cycle regulation in all eukaryotes are fundamentally the same.

Eukaryotic organisms can grow quite large and develop many different tissues types. For example, adult humans are composed of about 10^{13} (ten trillion) cells that all arise from a single fertilized egg via subsequent cell divisions. Furthermore, the cell-division cycle is still indispensible after reaching the adult stage, as cellular renewal is crucial for functional physiology of multicellular organisms. A human body loses 10^9 cells each day and reforms its entire skin every 7 days. Without this regeneration ability, we would lose the lining of our intestines in 2 days; our skin would fall apart in 3 weeks; and our blood cells including red blood cells would run out in 4 months. Afterwards, we would only have some organs left. This necessary regeneration is accomplished via the cell-division cycle of precursor cells of various types. During a human life-span, the cells in the body undergo about 10^{16} (ten thousand trillion) divisions [8].

1.2 The Cell as a Functional Unit of Life

"*Cells do it all*: *heredity*, *development*, *disease*, *and death*." [4]. There are more than 200 types of different cells in a human body and not every cell can divide forever. Two classes of stem cells, embryonic stem (ES) cells and adult stem cells, are responsible for replenishing old, dying cells [9]. The distinctions between them are their growth and developmental potentials. Embryonic stem cells are pluripotent cells that can divide indefinitely and generate all types of cells in the body. Adult stem cells are multipotent cells that possess limited ability to proliferate and are more restricted in what they can become. Both embryonic and adult stem cells are capable of responding to particular differential factors in the environment and developing into the corresponding precursor cells. Blood precursor cells will become mature blood cells and skin precursor cells will become mature skin cells, and so on. Therefore, the fate of these cells in a normal environment from then on is more or less determined, not to say it cannot be reversed based on recent studies on induced pluripotent stem (iPS) cells [10].

In addition to the essential cell-division cycle for organism development and renewal, programed cell death, known as apoptosis, is required for normal development. Interestingly, about a hundred thousand cells are produced every second in a human by mitosis, and a similar number of cells die by apoptosis through a physiological suicide process [11]. On the other hand, cells that do not kill themselves can go awry in many ways. Errors in cell

division routinely occur and mutations can accumulate to activate oncogenes, which promote cell growth and division, and/or inactivate tumor-suppressor genes, which restrain cell growth and division, leading to cancer in complex organisms such as mice and humans. In a sense, every time a cell divides, it is at risk of producing errors that may contribute to cancer development in humans. The risk for individuals increases with age due to the genetic mutations accumulated as one's life span extends.

1.3 Natural Selection Is Not Natural Perfection

Remarkably complex adaptations have evolved in living organisms; however, humans are still very vulnerable to a wide range of diseases. Cancer perhaps is among the most enigmatic and tragic of illnesses, because it is derived from the cells of our own body that have escaped the normal controls of the cell cycle. Furthermore, cancer is not rare. In the US, the cancer incidence is one in every three people and the mortality rate is one in every four people. Three people are diagnosed and one person dies of cancer every minute. Globally, cancer causes eight million deaths per annum. It is anticipated that a woman in the US has a 39 % chance, while a man has a 45 % chance of being diagnosed with some type of cancer in their lifetime [7]. The startling fact is that tumors afflicting us are not foreign parasites that have acquired sophisticated strategies for attacking our bodies; tumors are made of our own cells turned against us. Cancer cells arise as variants from normal cells in that they have lost their usual controls for growth and division [7]. Yet cancer is complex, since it comprises numerous ways to flee from cell cycle controls, gain growth advantages, and become cancerous. In this sense, cancer is not one disease but many types of diseases.

Natural selection has only a limited ability to prevent cancer. It has provided some defenses for the survival of species involved, but these measures tend to delay the diseases until late in life rather than eliminating it entirely. Since most cancer occurs in the post-reproductive period, it is unlikely to be selected against, as the criterion of a species' fitness is its reproducibility. Moreover, as some scientists argue, the selective pressure may even have resulted in tools that help tumors grow [12].

Evolutionary forces have apparently favored some genes that promote proliferation and migration during organism growth and development. These genes may get hijacked by cancer cells and be turned on when they would normally be silent after the developmental stages. The ability of some gene products to stimulate new blood vessel formation and aggressive growth serves a tumor just as it does a placenta. Therefore, natural selection is not natural perfection. It lacks the power to erase cancer from humans, partly due to its focus on reproduction rather than on longevity of species [12].

In principle, at a cellular level, aging starts with a reduced ability in cell growth and division, finally reaching the senescence state without reentry into the cell cycle, whereas cancer development

begins with unrestrained proliferation and genomic instability during growth and division. Without understanding the normal balances and checks that ensure the orderly cell-division cycle, we cannot design effective strategies for cancer prevention and treatment.

2 Basic Properties of the Cell-Division Cycle

What is the cell-division cycle? The cell cycle is the universal process by which cells reproduce, and it underlies the growth and development of all living species. There are four successive phases of a standard eukaryotic cell cycle: G_1 (growth phase 1), S (synthesis phase), G_2 (growth phase 2), and M phase (Fig. 1). During interphase (G_1, S, and G_2) a cell grows continuously and in M phase it divides. DNA replication is confined to a part of interphase known as S phase.

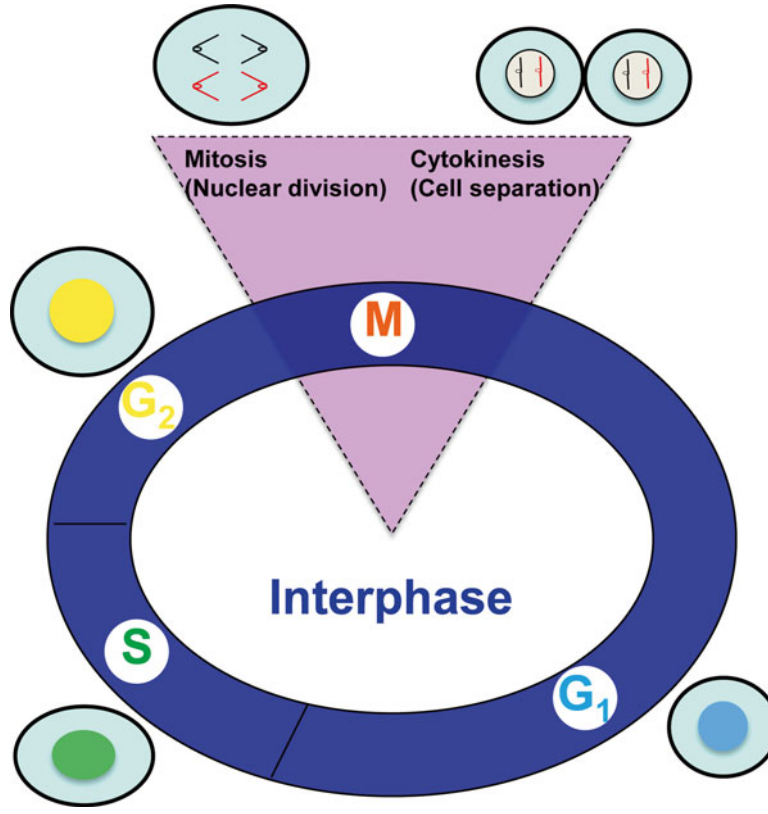

Fig. 1 Four successive phases of a standard mitotic cell cycle of eukaryotes. G_1 (growth phase 1 or gap 1), S (synthesis phase), G_2 (growth phase 2 or gap 2), and M phases. M phase consists of mitosis (nuclear division) and cytokinesis (cell separation). A cell grows continuously during interphase (G_1, S, and G_2) and divides in M phase. DNA replication is confined to a part of interphase known as S phase

The M phase consists of nuclear division/mitosis and cell separation/cytokinesis, the changes during which are visible under a microscope. Although a typical M phase only occupies a small fraction of the cell cycle, it is the stage that has dramatic morphological changes. The other much longer part of the cell cycle is known as interphase with relatively less discernible morphological changes (Fig. 1). At metaphase-anaphase transition, the chromosome pairs first line up to form the mitotic spindle plate and then quickly break apart from each other and race to the spindle poles (Fig. 2). The precision and concerted manner of the process is very striking. There is no doubt that a decisive switch is at work to ensure the event occurs rapidly, accurately, and completely.

The central issue of cancer prevention is the fidelity of the cell cycle, that is, all eukaryotic cells must replicate their DNA during S phase, only replicate once per cell cycle, and distribute the resulting identical copies of genetic information to daughter cells at mitosis (Fig. 3). It is important to understand not only how the cell-division cycle is accomplished, but also how its precision is achieved. The high fidelity of mitotic chromosome transmission is necessary in order to ensure the genome stability. Usually errors occur once in 10^5–10^6 divisions. There are three major restriction

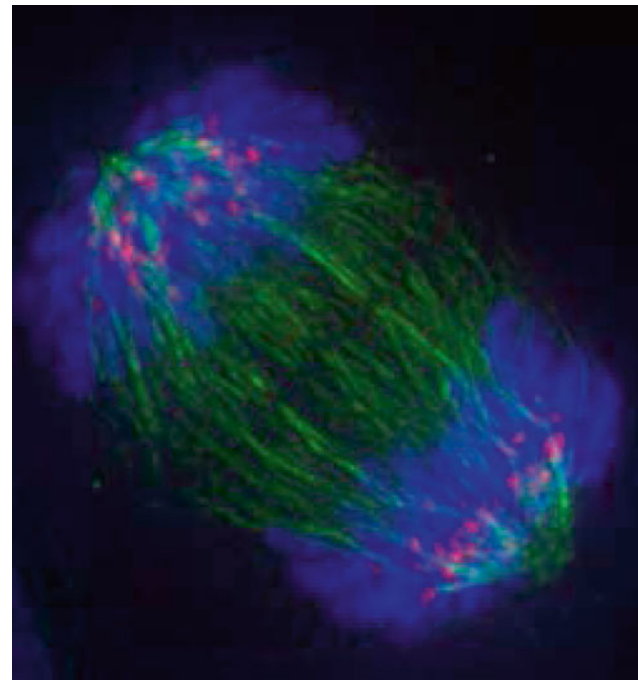

Fig. 2 A cell in anaphase. Lengthening microtubules push the two sets of chromosomes apart. *Blue*: chromosomes, *green*: mitotic spindle. (Image captured by Roy van Heesbeen posted on http://upload.wikimedia.org/wikipedia/commons/9/91/Anaphase_IF.jpg)

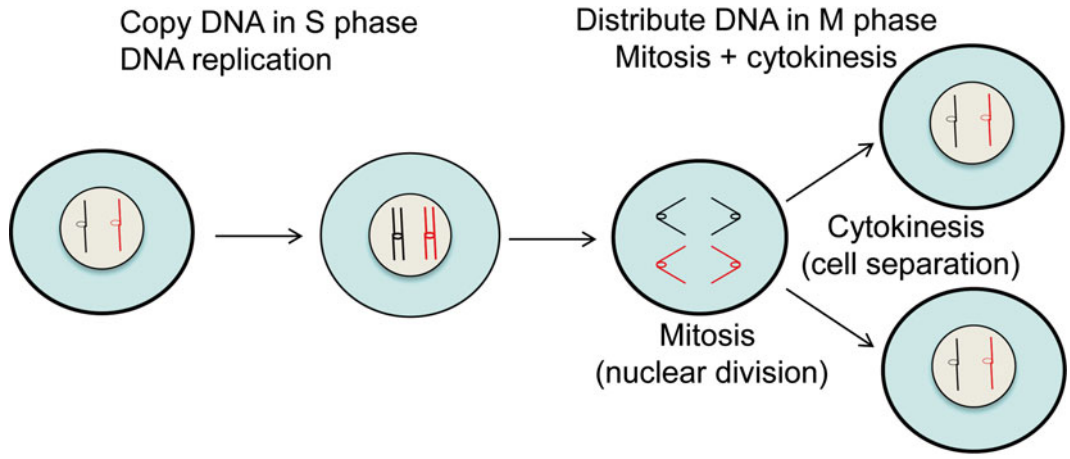

Fig. 3 Two critical steps of the cell-division cycle: DNA replication and nuclear division. To produce healthy cells, eukaryotes must accurately replicate their DNA during S phase and precisely distribute the resulting copies of genetic information to daughter cells at mitosis

points or important transitions in the cell cycle: the start or a restriction point before the G1–S transition to initiate DNA replication, the G2–M transition to enter mitosis, and the metaphase–anaphase transition to exit from the mitosis (Fig. 4). These phase transitions are discrete points of cell cycle control.

What is a phase transition of the cell-division cycle? It is a unidirectional change in the state of the cell cycle. The fidelity of the cell cycle requires that each phase transition occurs at the right time in the right order, which is stringently monitored. Two types of processes must be coordinated for a cell to divide. First, the initiation of a transition is dependent upon the completion of a previous transition. For example, the initiation of mitosis must be coupled to the completion of DNA replication, in order to exert the checkpoint control on the precise phase transitions. All eukaryotic cells synthesize their DNA during S phase, replicate DNA only once per cell cycle, and distribute the resulting identical copies of genetic information to daughter cells at mitosis. When mammalian cells such as baby hamster cells in S phase are treated with an inhibitor of DNA synthesis, for example, aphidocolin or hydroxyurea, the cells halt in S phase and will not progress into mitosis until the inhibitor is removed and DNA replication has been completed. However, in the presence of 2 mM caffeine, cells enter mitosis without finishing DNA replication, increasing the genomic instability of the cells [13]. These experiments indicate that incompletely replicated DNA blocks the onset of mitosis, while caffeine disconnects the coupling between DNA replication and mitosis.

Second, the cell size must be coordinated with the progression of the cell-division cycle. Eukaryotic cells can complete cell cycle

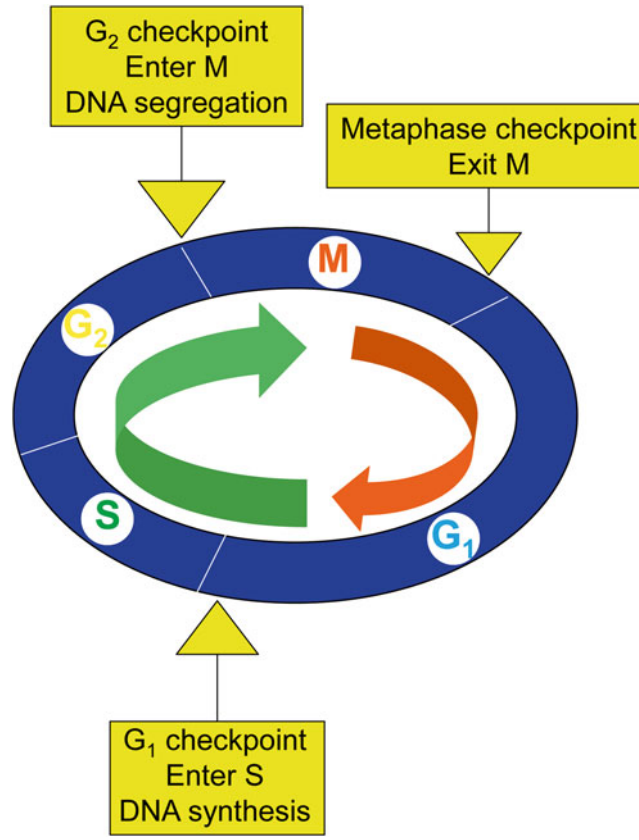

Fig. 4 Phase transitions and restriction points of cell cycle control. Phase transitions are unidirectional changes in the state of the cell cycle. The three major transitions in the cell cycle are the start or a restriction point before G1–S transition to initiate DNA replication, G2–M transition to enter mitosis, and the metaphase–anaphase transition to exit from the mitosis

events such as DNA replication during S phase and chromosome segregation at mitosis in less time than it takes to double in size. If cells keep dividing without attaining a standard size, they would become smaller with each generation. Figure 5 shows the relationship between cell growth, cell size, and cell division in a free-living organism such as a yeast cell. If cell division continued at an unchanged rate when cells are starved, the daughter cells produced at each division would become progressively smaller and eventually be too small to be viable—mitotic catastrophe. Yeast cells have evolved the ability to respond to poor nutritional conditions by slowing the rate of cell division in the population — a cell size control. A cell cannot proceed past a specific point in the division cycle until it has attained a standard size; thus the rate of cell division slows down and cell size remains more or less unchanged.

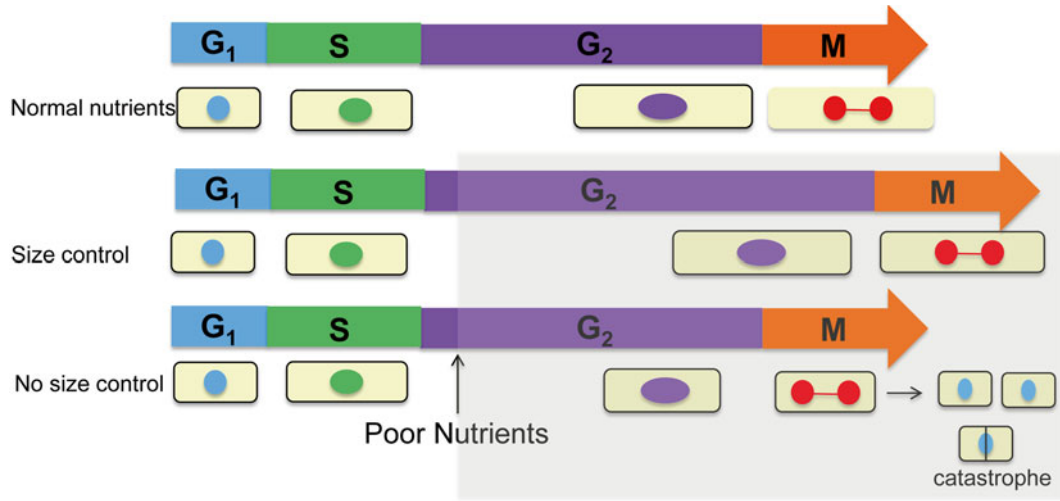

Fig. 5 The coordination of cell size and cell division in free-living yeast cells. Yeast cells have evolved the ability to respond to poor nutritional conditions by slowing the rate of cell division in the population—a cell size control. If cells keep dividing at an unchanged rate when cells are starved, the daughter cells generated at each division would become progressively smaller and eventually unviable, reaching catastrophe

3 Exploring Mechanisms of Cell Cycle Control in Different Model Organisms

Although the fundamental mechanisms of the cell cycle have been conserved for a billion years, from yeasts to humans through evolution, various organisms possess different features in cell cycle regulation. The studies on the cell-division cycle have been conducted in diverse eukaryotic systems, but the significance of an analysis relies on the suitability of the model organism chosen for addressing the questions of interest in cell cycle. Importantly, cell cycle studies in different experimental systems allow us to assess the conservation and variation in the mechanisms of cell cycle regulation, gaining a comprehensive understanding of the cellular process fundamental for all eukaryotes. The most commonly used model organisms are unicellular yeasts, the early embryos of frogs and fruit flies, and mammalian cells in cell culture. *What are the features of the cell cycle in these different organisms? What are advantages and disadvantages of each system used as a model organism to examine the regulation of the cell cycle?* A comprehensive review of these model organisms with respect to cell cycle analyses is valuable for us to appreciate how our knowledge of cell cycle control has expanded, how the completion of genome sequences has empowered the established model organisms, as well as how systems biology and quantitative approaches influence the research of the cell cycle. Exciting possibilities are emerging and renewed emphasis on cell cycle analyses are created by the new technologies developed in the post-genomic era and research advances using these model organisms in the past decades.

3.1 Yeasts

3.1.1 An Overview

Yeasts belong to unicellular Ascomycota fungi, a branch of eukaryotes. More than 80,000 living fungi species have been described [1]. These include the models of great importance for genetics, *Saccharomyces cerevisiae*, *Schizosaccharomyces pombe*, *Neurospora crassa*, and *Aspergillus nidulans*, as well as animal and plant pathogens. The budding yeast *Saccharomyces cerevisiae* and the fission yeast *Schizosaccharomyces pombe* are unicellular and considered to be among the best genetically tractable organisms for a comprehensive understanding of biology. Budding yeast was the eukaryote whose genome was sequenced first in 1996 [14], followed by the genome sequence of fission yeast, which was completed in 2002 [15]. 5885 and 4914 protein-coding genes have been predicted in *S. cerevisiae* and *S. pombe*, respectively [14, 16]. Research employing these yeasts has made tremendous impacts on the elucidation of the biological principles of complex organisms. Moreover, comparative genome analysis suggests that *S. cerevisiae* and *S. pombe* diverged about 1 billion years ago [1]. Their genomes share no obvious synteny and are quite distinct in their biology (Fig. 6).

S. cerevisiae was established as an experimental system earlier than *S. pombe*. It was the first eukaryotic organism to be transformed by plasmids, to have precise gene knockouts, and to have its genome sequenced. *S. cerevisiae* has also been the model eukaryote for pioneering research in chemical genomics [17–20].

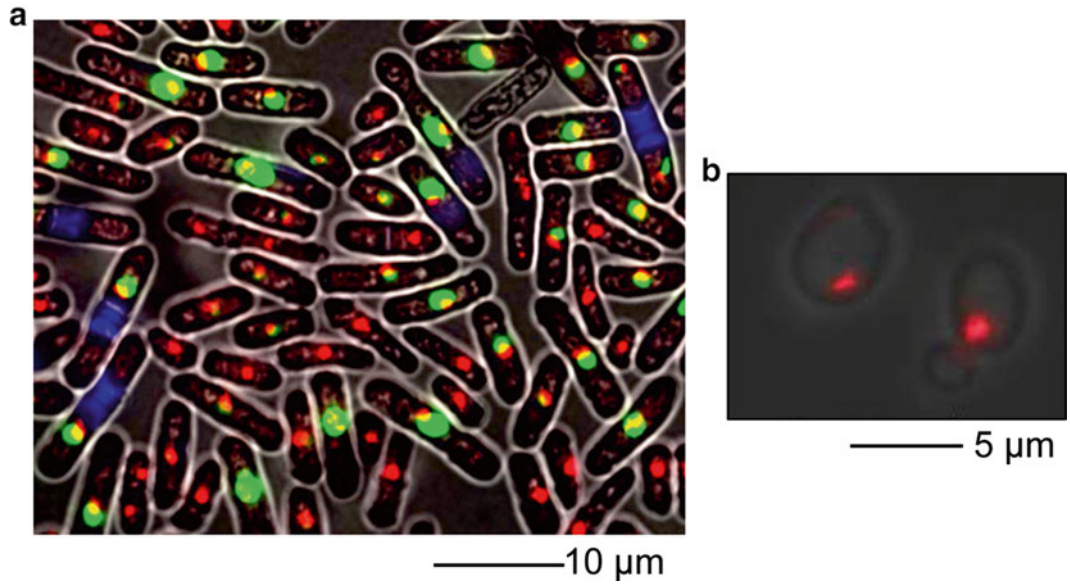

Fig. 6 Morphology of fission yeast *S. pombe* and budding yeast *S. cerevisiae* under fluorescence microscopy. The images were acquired at room temperature with cells grown in rich medium. *Red*, DAPI (4′,6′-diamidino-2-phenylindole) staining has been used to visualize DNA. (**a**) *Schizosaccharomyces pombe* cells. *Blue*, calcofluor has been used for detecting septa; *green*, a GFP (green fluorescent protein)-tagged RNA processing factor. (**b**) *Saccharomyces cerevisiae* cells. The image was captured by Dr. Gretchen Edwalds-Gilbert's laboratory

Although started later, research using *S. pombe* has been particularly influential in studies of cell cycle regulation, DNA damage/repair mechanisms, and chromosome dynamics, including RNA interference (RNAi) [21]. Furthermore, the fission yeast *S. pombe* harbors less genome duplication compared with other eukaryotes so far sequenced and holds the smallest sequenced eukaryotic genome, which led to its rising popularity as a eukaryotic model in the last decade. Based on current information, out of 4914 protein coding genes in *S. pombe*, 3385 fission yeast proteins have one or more orthologues in humans (http://listserver.ebi.ac.uk/pipermail/pombelist/2013/003783.html). Therefore, investigators studying mammalian cell biology are increasingly using *S. pombe* to test their gene of interest, as it may be present in only one copy, bestowing fission yeast the nickname "micro-mammal" [22]. The equivalent logic can be applied to budding yeast *S. cerevisiae*, building the concept of surrogate genetics: testing a gene from one organism such as a human gene in the context of another model system such as yeasts to provide an assessment of the potential function of the gene [2]. A milestone case for a proof of principle is the substitution of a fission yeast cell-division cycle (*cdc*) gene, *cdc2*, coding for a master protein kinase in cell cycle regulation, by a human orthologous gene, *CDC2* in a cross-species complementary assay [23]. (*See* later part of Subheading 3.1.) In fact, many methods now used for complex organisms were first developed and optimized in the yeast model organisms. Studying human protein homologs in yeasts allows researchers to extrapolate information about human proteins and gain insight into genetic networks that are more difficult to uncover in humans (reviewed in [24]).

3.1.2 The Haploid and Diploid State of Yeast Life Cycle

Both budding yeast *S. cerevisiae* and fission yeast *S. pombe* are able to exist in either a diploid or a haploid state. Although most strains of yeasts used in the laboratory are haploid strains, in the wilderness, budding yeast tends to live as a diploid, whereas fission yeast prefers to be in a haploid form. The proportion of the life cycle they spend in the diploid or haploid state varies, depending on the environment. When nutrients are plentiful, budding yeast proliferate as diploid cells [13]. If starved, they undergo meiosis to form haploid spores. The spores germinate to become haploid cells when conditions improve. These haploid cells can then either proliferate or conjugate in G_1 phase to reform diploid cells. In contrast, fission yeast typically proliferate as haploid cells. They fuse in response to starvation to form diploid cells, and the diploid cells promptly undergo meiosis and sporulation. The spores hatch to regenerate the haploid cells when nutrients become available again [25]. Thus, the diploid and haploid states are two alternative ways for yeast cells to divide.

3.1.3 Advantages of Using Yeast Systems as Experimental Models

S. cerevisiae and *S. pombe* are especially suitable for biological research for a number of reasons. The two yeasts are non-pathogenic and thus safe to handle. Their reproduction cycles are fast and easy to monitor, with doubling times from 90 min for wild-type cells in rich medium to a few hours for mutant cells. Both yeasts lend themselves to diverse experimental approaches, from genetics to systems biology, cytological and biochemical, making them useful for comprehensive investigations of biological processes. Moreover, the available online resources for the yeast models (yeastgenome.org and pombase.org) and supporting research communities facilitate data analysis by researchers and students.

Although the two yeasts differ from one another in a range of features, they share the fact that they have well-established and fast-evolving genetic tools. *S. cerevisiae* and *S. pombe* are genetically tractable and readily amenable to both classical and molecular genetic analyses. They have been used for decades in forward genetics, to identify genes important for a process of interest, including cell cycle regulation [26, 27]. They are also the only eukaryotes with collections of genome-wide gene deletions available [16], allowing systematic reverse genetic analyses for genotype–phenotype relationships. The functional analyses in budding and fission yeasts have been further facilitated by the availability of accurate and well-annotated genome sequences, since they entered the post-genomic era more than a decade ago [15, 28, 29].

A primary goal of any genetic screen or selection is to identify the players in a process of interest or a role of a gene product in such a process. The haploid phase of the yeast life cycle expedites the isolation of genes involved in a cellular process [30]. The haploid life cycle of the yeasts is particularly useful in determining the normal function of a gene, as it reveals a phenotype rendered by a recessive, loss-of-function mutation that is normally masked by the presence of the other allele in a diploid cell. Another advantage of yeast genetics is the availability of nutritional and drug markers. Inserting a marker, for example a marker that complements a specific nutritional requirement, in the gene locus of interest disrupts the gene and the subsequent expression of the marker can be conveniently selected for generating the null mutant. If successful, an auxotroph (supply-dependent) for a particular nutrient would be conferred a prototroph (self-sufficient) for that nutrient, confirming that the gene has been knocked out [31]. The isolation of *cdc* mutants in yeasts allowed scientists to identify important protein regulators in cell cycle.

Since *S. cerevisiae* and *S. pombe* diverged from the common ancestor more than a billion years ago, they are not closer relatives to each other than to humans with respect to the evolutionary distance between them as to each to humans. The divergence between the two yeasts actually serves as a useful criterion when we explore the conservation of a cellular process. For example, if a relevant

orthologue is identified in both yeasts, the corresponding gene or gene product is likely to be conserved in humans as well. *S. cerevisiae* and *S. pombe* differ from each other in a number of aspects, including cell cycle organization, heterochromatin, complexity of centrosomes and DNA replication origins, and the prevalence of introns [16]. The long evolutionary distance between the two yeasts makes their comparison beneficial for defining genes and processes common to all eukaryotes. On the other hand, the variation between the two yeasts in cellular processes, such as the regulation of the cell cycle, is valuable for us to inquire whether conserved or alternative mechanisms have been evolved to solve identical biological problems that all eukaryotes, including humans, face throughout evolution.

3.1.4 Distinct Features of the Cell Cycles in *S. cerevisiae* and *S. pombe*

Both *S. cerevisiae* and *S. pombe* undergo closed mitosis, during which the nuclear envelope does not break down. In contrast, most multicellular animal cells usually undergo open mitosis: the nuclear envelope breaks down (Fig. 7) [5]. Although both are yeasts, the cell cycles of *S. cerevisiae* and *S. pombe* have distinct features. Fission yeast cells go through a typical eukaryotic cell cycle with consecutive G_1, S, G_2, and M phases (Fig. 8). Conversely, the budding yeast cell cycle appears to consist of only clear G_1 and S phases; the G_2/M boundary is fuzzy, as spindle assembly starts to occur in S phase (Fig. 9) [13]. Therefore, the control at the G_2–M transition is more visible in fission yeast *S. pombe*, while the G_1–S transition—*Start*, is the major control of the cell-division cycle in budding yeast *S. cerevisiae*.

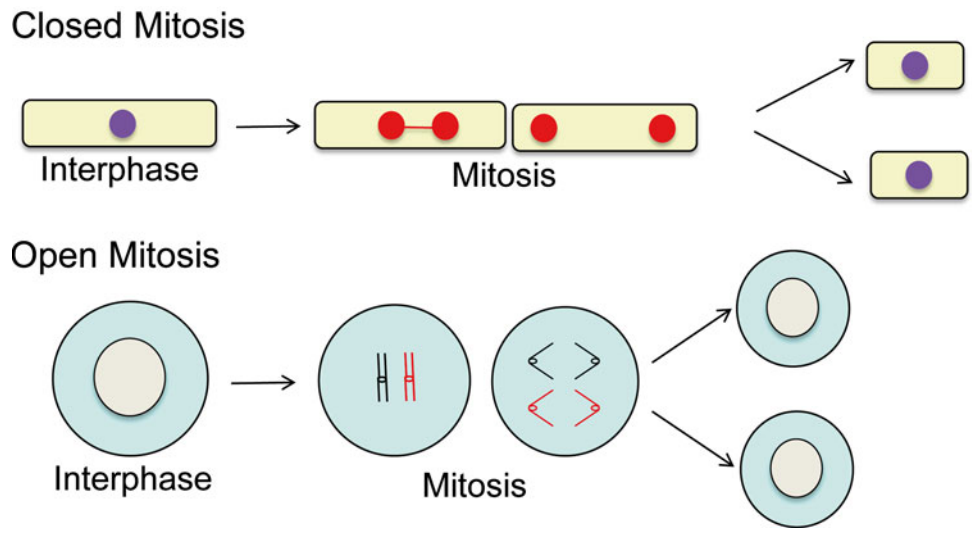

Fig. 7 Different morphologies of mitosis between yeasts and animal cells. Both *S. cerevisiae* and *S. pombe* undergo closed mitosis, at which the nuclear envelope does not break down; while most multicellular animal cells usually undergo open mitosis: the nuclear envelope breaks down

3.1.5 Fission Yeast (Schizosaccharomyces pombe) Cell Cycle

Two properties of fission yeast *S. pombe* make it especially suitable for analyzing the relationship between cell size and cell cycle. First, unlike budding yeast, fission yeast cells divide symmetrically by forming a septum in the middle of the cell, thus the cell size at a particular position of the cell cycle is well defined for a cell. Second, fission yeast cells grow only in length, not in diameter; measuring individual cell lengths provides a convenient and precise way of following cell growth during the cell cycle. Therefore, fission yeast as a study system permits detailed analysis of cell size as a parameter to follow cell cycle progression. Among the four phases of the cell cycle, G_2 is the longest while G_1 may be the shortest or least visible in fission yeast. Normally, after completing cytokinesis, two daughter cells are born passing G_1 (Fig. 8). Consequently, G_1/S control is not visible unless the cell entry into S phase is blocked. It is not surprising that most of cell-division cycle (*cdc*) mutants originally isolated from fission yeast arrest in G_2. The G_2–M transition in fission yeast therefore acts as a major control in the mitotic cell cycle. Because of its distinct cell cycle features, fission yeast has historically been used as a model organism for genetic studies of G_2–M transition. The research in fission yeast *S. pombe* has contributed greatly to our understanding of the mechanisms of mitotic cell cycle control, especially for identifying key regulators such as Cdc2 protein kinase, Cdc25 tyrosine phosphatase, and Wee1 tyrosine kinase [5, 26, 32, 33].

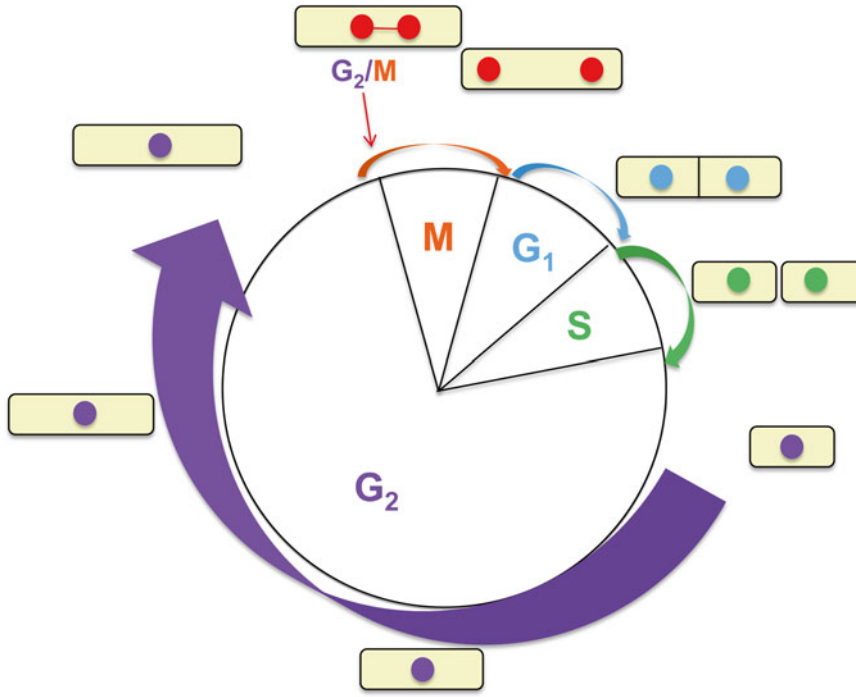

Fig. 8 Features of the *S. pombe* cell cycle. Fission yeast cells have a typical eukaryotic cell cycle with consecutive G_1, S, G_2, and M phases. The major restriction point is at the G_2–M transition

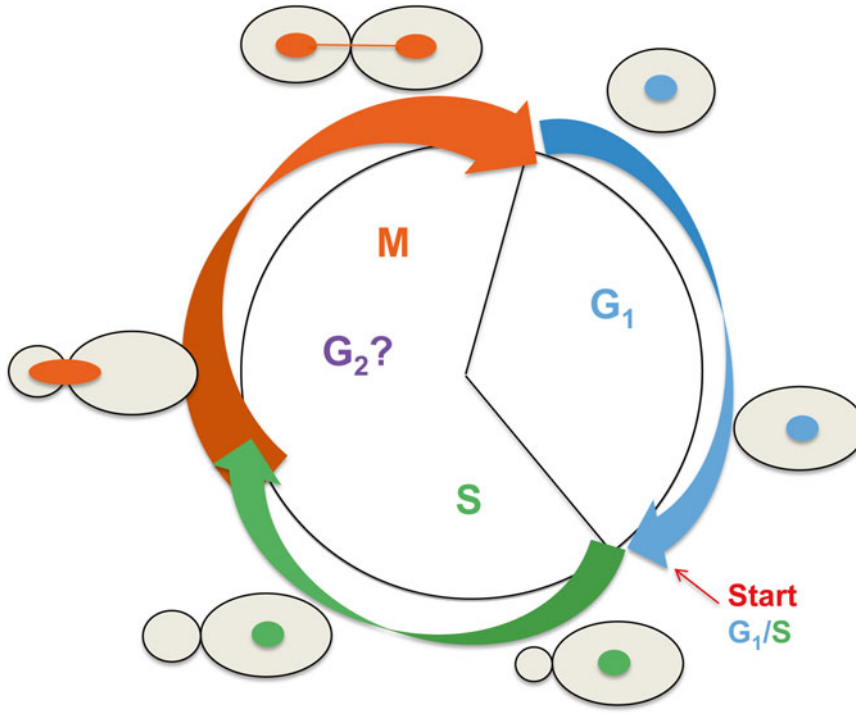

Fig. 9 Features of the *S. cerevisiae* cell cycle. The budding yeast cell cycle appears to consist of only clear G_1 and S phases; the G_2–M boundary is blurry. The G_1–S transition—*Start*, is the major control of the cell-division cycle

3.1.6 Budding Yeast (Saccharomyces cerevisiae) Cell Cycle

Since budding yeast *S. cerevisiae* divides asymmetrically by budding before entering S phase, it is convenient to follow the progress of the cell cycle in living cells by observing the size of the bud. A small bud forms early in the cell cycle of budding yeast. The bud enlarges continually and ultimately separates from the mother cell. Moreover, the ratio between the size of the mother and the bud gives a rough estimate of a cell's position in the cell cycle. Since the bud appears after the Start, it provides a morphological marker for the event of G_1–S transition. We can look at the cells under a microscope and examine the presence or absence of a bud and measure the bud size to assess the cell cycle progression, or a possible cell cycle arrest at the major control of cell cycle in budding yeast—G_1–S transition [34].

3.1.7 Identifying Key Players in Cell Cycle Control Using Yeast Conditional Mutants

Our present understanding of the cell cycle regulation comes partly from a systematic search for mutations in genes encoding components of cell cycle machinery in yeasts [35, 36]. Geneticists analyze mutants to identify the genetic information responsible for specific traits. These approaches can be broadly grouped into two categories: forward genetics and reverse genetics. Forward genetic analyses begin by obtaining mutants that display a specific phenotype, followed by identifying the particular gene alteration(s) responsible for the observed trait. Reverse genetic analyses involve targeted

gene mutation(s) and observation of the resultant phenotype to determine the function of a specific gene. The logic of reverse genetics relies on a "reverse destructive" strategy—targeting a gene of interest for a loss of function mutation or deletion and observing the resulting phenotype. The possible role of the gene in the corresponding process can then be proposed. In this paradigm, each gene is analogous to a worker in an automobile assembly line. Removing a worker will have a car produced with some missing part [37]. These genetic methods allow researchers to identify and assemble a cast of players in phase transitions of the cell cycle. Once the gene(s) responsible for a trait has been identified, genetic studies can branch off in various directions to investigate the mechanisms of the gene function, including biochemical analysis of encoded proteins and determination of spatial and/or temporal expression patterns. One of the strengths of the yeasts as model organisms to study the cell cycle is the wealth of defined wild-type strains against which other isolated mutants can be compared [2].

Leland Hartwell and Paul Nurse began to search for mutations that affect the cell cycle in budding yeast and fission yeast, respectively in 1970s [35, 36]. They examined collections of temperature-sensitive (*ts*) mutants that specifically arrest at a discrete stage of the cell-division cycle or that divide at a smaller size at the restrictive temperature. What are *ts* mutants? Why would it not work to simply create a loss-of-function mutation or deletion of a gene? Since cell division is essential for viability, a haploid mutant that is unable to complete a cell-division cycle cannot be propagated. As result, a mutant would be lethal if it harbors a loss-of-function mutation or a null deletion in a gene that is required for completing the cell cycle. To circumvent this problem, *conditional mutants* are developed for identifying the genes involved in the cell cycle. Conditional mutants are the cells in which a gene product is inactive under one condition but not another. The most common conditional mutants used in cell cycle studies are temperature-sensitive, cell-division cycle (*cdc*) mutants. In a *ts* mutant the gene product can function at a lower temperature, the permissive temperature, but not at a higher, restrictive (or non-permissive) temperature. For yeasts, the permissive temperature is usually at room temperature (20–25 °C), and the restrictive temperature is 35–37 °C. Temperature-sensitive *cdc* mutants can be selected, isolated, and maintained only as conditional mutations.

What are the distinct features of *cdc* mutants? Cells in a *cdc* mutant population growing at a permissive temperature are in various stages of the cell cycle and thus are asynchronous. After arresting at the same stage of the cell cycle at a restrictive temperature, they become synchronous (Fig. 10) and are ready to progress through the cell cycle synchronously upon being released from the block by shifting down from the restrictive to a permissive temperature. The affected genes in these mutants are called *cdc* genes, which may function in a particular phase transition of the cell cycle.

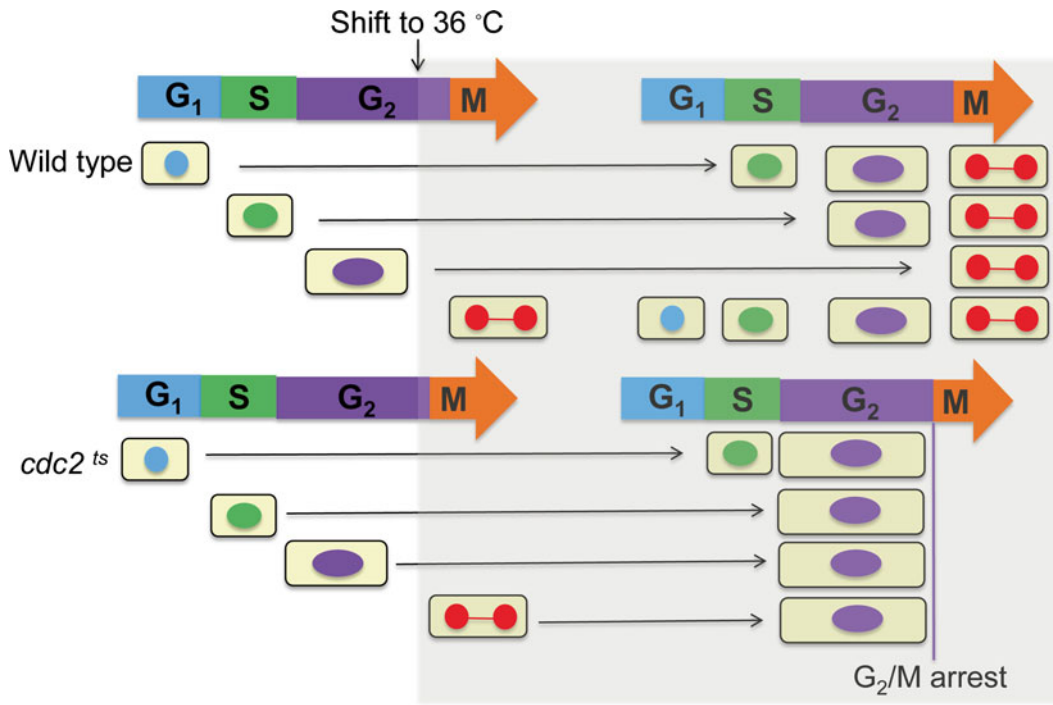

Fig. 10 *cdc* mutants arrest at a specific stage of the cell cycle. Cells in a *cdc* mutant population growing at a permissive temperature are asynchronous in the cell cycle. at a restrictive temperature, they are blocked at a specific stage of the cell cycle and become synchronous. *cdc2ts* mutant cells are all arrest at G_2–M transition at 36 °C, since *cdc2*$^+$ gene is required for the cell entry into mitosis but it is not functioning at the restrictive temperature

In contrast, non-*cdc* mutants may be deficient in continuous processes such as ATP production, necessary for biosynthesis and growth throughout all phases; thus, it may halt at any stage of the cell cycle as soon as the ATP reservoir runs out.

To identify genes that are directly involved in the control of the cell cycle, the search was focused on two mutant phenotypes. In the first type, all of the cells in the same mutant population arrest at the same point in the cell cycle—*cdc* phenotype at restrictive temperature. Cells blocked at the specific phase of the cell cycle in a particular *cdc* mutant population display similar phenotypes. For example, the mutations in *CDC28* gene in budding yeast or *cdc2* gene in fission yeast result in arrest at the restrictive temperature at G_1–S or G_2–M transition, respectively. The second type of mutations display the so-called *wee* (derived from a Scottish word for small) phenotype in fission yeast, as the mutants divides at a smaller size than normal cells [36]. The *wee* mutants are defective in gene products that normally inhibit passage through the G_2–M transition without attaining a standard cell size [38]. It has been known that Wee1 protein mediates the control of cell size in response to the availability of nutrients in the external environment and internal synthesis cues, such as DNA replication.

Several dozens of *cdc* genes were originally identified in fission yeast and budding yeast by using forward genetics [34–36]. We now know probably more than hundreds of genes are cell cycle regulated by genome-wide analyses [39, 40]. In human HeLa cells, more than 500 genes are implicated in mitosis [41]. However, not all of these genes identified by the forward genetics approach are directly involved in regulating the cell cycle. In fact, among the genes originally identified as *cdc* genes, substantial numbers of those encode proteins that contribute to the mechanics of a cell cycle event, such as those that comprise the DNA replication machinery for completing S phase. They may not have a role in the regulation of cell cycle progression, such as DNA polymerases or enzymes that synthesize the precursors for DNA replication, for example. On the other hand, forward genetics has not exhausted the search for cell cycle regulators yet. Negative regulators of the cell cycle, extrinsic to cell cycle progression, including those that regulate checkpoints, would be overlooked, as the loss-of-function of those genes does not exhibit *cdc* phenotypes.

Nonetheless, investigation of yeast cell cycle mutants revealed the *cdc2*$^+$/*CDC28*$^+$ gene product as a pivotal, decisive component for driving the cell into mitosis: when *cdc2* is defective, mitosis fails to occur in fission yeast, leading to cell elongation (Fig. 11, upper part); while when *CDC28* is not functional, cells arrest before the Start without a bud in budding yeast (Fig. 11, lower part). Conversely, if this master gene is released from the normal control, mitosis or S phase takes place prematurely in fission yeast or budding yeast, respectively. Most *cdc* mutants of fission yeast exhibit an altered cell length at a restrictive temperature. The majority of the *cdc* mutants are recessive, temperature sensitive and blocked at the G_2–M transition before entry into mitosis at the restrictive temperature. Using this forward genetics approach, scientists discovered a cast of important players in cell cycle control, including Cdc2/Cdc28 and Wee1 protein kinases, as well as Cdc25 tyrosine phosphatase [38, 42].

The early studies of these mutants, defective in cell cycle progression, also revealed the order of the cell cycle events. If a *cdc* mutant is blocked in S phase without completing DNA synthesis, it cannot initiate a later phase such as mitosis. This sequential order of the cell cycle events underlines the concept of checkpoint pathways, which are a series of cell signaling events to ensure the proper order of phase transition in the cell cycle. The results of these genetic studies provide the evidence for the interdependence of the cell cycle events—the central idea of checkpoint control in cell-division cycle [43].

3.1.8 The Cloning of the cdc Genes

Although the genetic studies of the *cdc* mutants, including tetrad analysis and genetic mapping, defined the discrete genes involved [35, 36], the molecular nature of the genes and the corresponding proteins encoded by these genes were not known. In-species complementation assays were used to clone several *cdc* genes crucial for

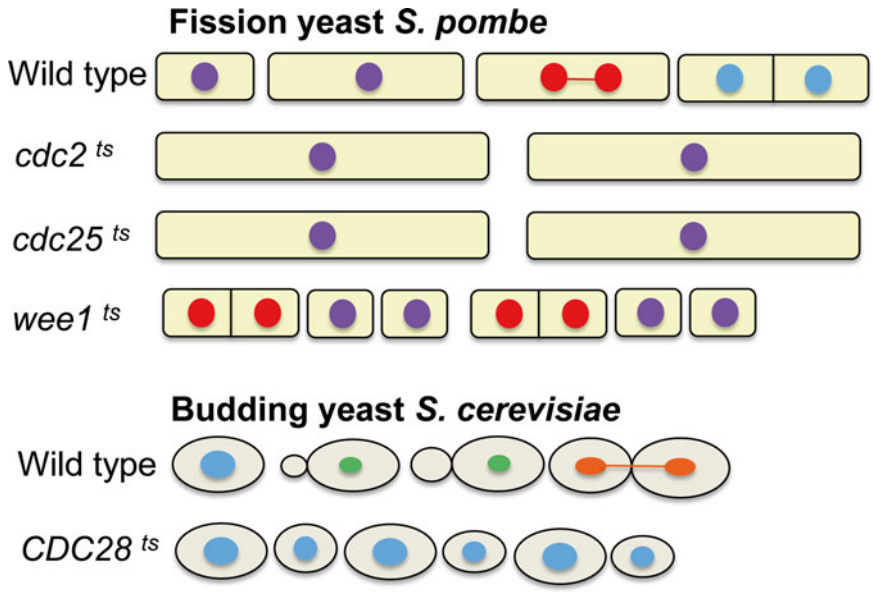

Fig. 11 Schematic presentations of yeast mutants with cell cycle phenotypes. The *upper part* shows wild-type cells of fission yeast *S. pombe* at different stages of the cell cycle; *cdc2ts* and *cdc25ts* mutants are blocked at the G_2–M transition at 36 °C, giving rise to cell elongation; *wee1ts* mutants dividing prematurely, resulting in small cell size [44]. The *lower part* illustrates asynchronous wild-type cells of *S. cerevisiae* budding yeast; *CDC28 ts* mutants arrest before the Start at the G_1–M transition at 36 °C without budding [31]

the cell cycle regulation in yeasts [44]. For example, cloning the *cdc2*$^+$ gene allowed the amino acid sequence of the Cdc2 protein to be deducted from the nucleotide sequence of the gene, providing valuable clues about its homology to protein kinases [45]. This clue was exciting to researchers in the field, because the pattern of protein phosphorylation had been known to change when cells enter mitosis, and it had long been suspected that maturation-promoting factor (MPF), identified in the frog embryos was a protein kinase.

Generally, all the *cdc* genes can be cloned by using the complementation assay. We can clone a gene by isolating a DNA fragment that would complement a *ts* mutation phenotype. This logic should work for all systems in which tools of genetic manipulation are available for complementing the phenotype caused by mutations. One advantage of the approach is that the selection depends on functional rescuing rather than structural similarity. To clone the fission yeast *cdc2*$^+$ gene, a library of plasmids containing fission yeast DNA fragments was introduced into *cdc2ts* cells, and the cells were then shifted from 25 °C to 35 °C [44]. Individual recipient cells could intake different plasmids from the library. The vast majority of cells received a plasmid that did not contain the *cdc2*$^+$ gene and failed to divide and grow into colonies at 35 °C. But a small fraction of cells that received a plasmid containing the *cdc2*$^+$ gene were capable of restoring the mitotic entry, thereby giving

rise to colonies. The plasmids were then recovered, amplified in bacteria, and used to determine the sequence of the gene. Other genes genetically interacting with *cdc2*$^+$ may also be isolated by this method, such as the suppressor of *cdc2*$^+$ gene, which may function in the same pathway as *cdc2*$^+$ [46].

3.1.9 Cloning of Orthologous Genes in Cell Cycle Regulation

The same logic of the in-species complementation assay can be applied to isolating orthologous genes in other organisms, the cross-species complementation assay. In this assay, the source of the DNA containing a potential orthologous gene, is from an organism of interest. The gene selection is based on the ability of the gene to complement the phenotype of interest in yeasts. The first proof-of-principle work was the milestone work by Lee and Nurse, in which they successfully cloned the human *cdc2*$^+$ gene, encoding the protein counterpart of Cdc2/Cdc28 protein [23]. The result demonstrates that human Cdc2 and fission yeast Cdc2 protein are true orthologues of each other, based not only on their sequence relationship, but also on their functional substitution. It provides convincing evidence for the conservation of the fundamental principles of cell cycle regulation for a billion years through evolution. Moreover, it also offers a new methodology to identify orthologues in diverse organisms. The strength of the method is the functional selection of orthologous genes, which surpasses the sequence-based selections.

3.2 Early Embryo of Frog (*Xenopus laevis*)

Many biological processes are best studied in cells that are specialized for particular tasks. For example, historically, studies on nerve cells have been a principal route to understanding the electrical properties of cells, and research in muscle have provided the foundation of our knowledge about how chemical energy is converted to movement. Eggs of the frog *Xenopus laevis* are a special type of cell very useful for cell cycle studies. The eggs of amphibians, marine invertebrates and insects are large cells and they divide very rapidly following fertilization in early embryo development. An oocyte of a frog *Xenopus* grows for many months in the ovary of the mother frog, without dividing, and finally matures into an egg. Upon fertilization, the egg cleaves very rapidly, initially at a rate of one cycle every 30 min, forming a multicellular tadpole within a day or two. The cells get progressively smaller as no growth can occur until the tadpole begins feeding.

What is the distinguishing feature of early embryonic cell cycle in frog? In the early embryonic cycle, no cell growth occurs and each daughter cell produced from a cell division is half the size of the parent cell. Therefore, compared with the standard cell division, the duration of the frog egg cycle is extraordinarily short, only consisting of alternating S phase and M phase without intervening G_1 or G_2 phase (Fig. 12) [5, 13]. The first cell-division cycle of a frog embryo lasts 75 min and is followed by 11 synchronous cell cycles each 30 min long. The rapid cleavage pattern of the early frog embryo determines their unique features of cell division cycle.

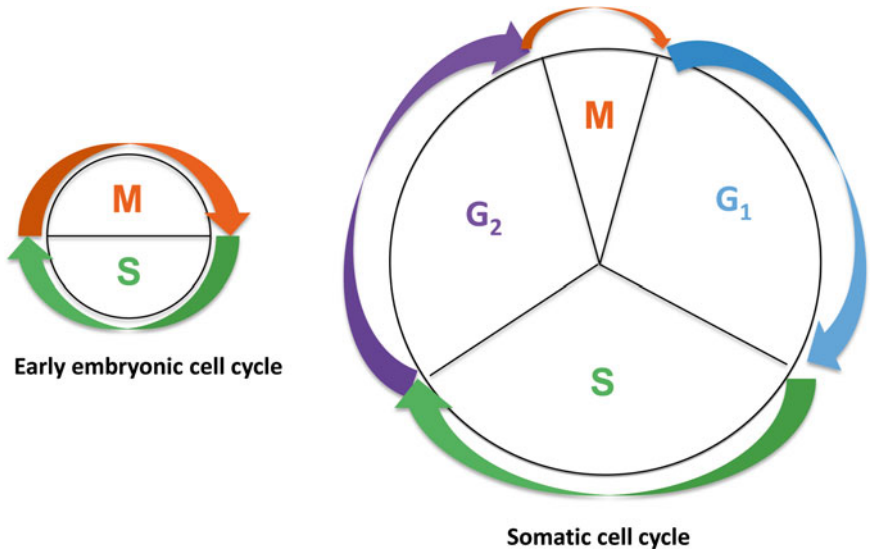

Fig. 12 Comparison of the early embryonic cell cycle with the somatic cell cycle. The somatic cell cycle consists of four phases while the early embryonic cell cycle alternates between S and M phases without intervening G_1 and G_2 phases

Because of the specialized rapid cell division of the frog embryo, they are very useful for studying the mechanisms of interphase–M phase transition. The early development of the frog *X. laevis* embryo provides a particularly powerful system to analyze the factors that drive cells into mitosis. A female frog is able to produce several thousands of eggs, which can be fertilized in vitro to produce a large population of embryos proceeding synchronously through several cell-division cycles. A frog egg is a large structure of about 1 mm in diameter. It has 100,000 times more cytoplasm than an average somatic cell and is a vast store of macromolecules, thus serving as a good resource for biochemically isolating protein factors of specific cell cycle stages. Since the 1970s a lot of what we know about the control mechanisms of the mitotic cell cycle has been learned from the studies on the interphase–M phase transition in the frog egg system [3].

3.2.1 Identifying and Purifying Maturation-Promoting Factor (MPF) in Frog Xenopus laevis Eggs

An inspiring way to illustrate the strength of the frog embryonic system is to revisit several experiments crucial for establishing the existence of a cytoplasm-based control activity and the molecular nature of the activity that operates in all dividing cells to initiate phase transitions in the cell cycle.

3.2.2 Xenopus Oocyte Injection Assay

A fully grown oocyte arrests in G_2, when triggered by hormone, the oocyte matures into an egg and arrests in metaphase of the meiosis II. Fertilization releases the metaphase arrest, so that the egg completes its second meiotic division and enters the interphase of the first embryonic cell cycle. Since an immature oocyte arrests in meiotic G_2, whereas a mature egg arrests in meiotic M phase, the

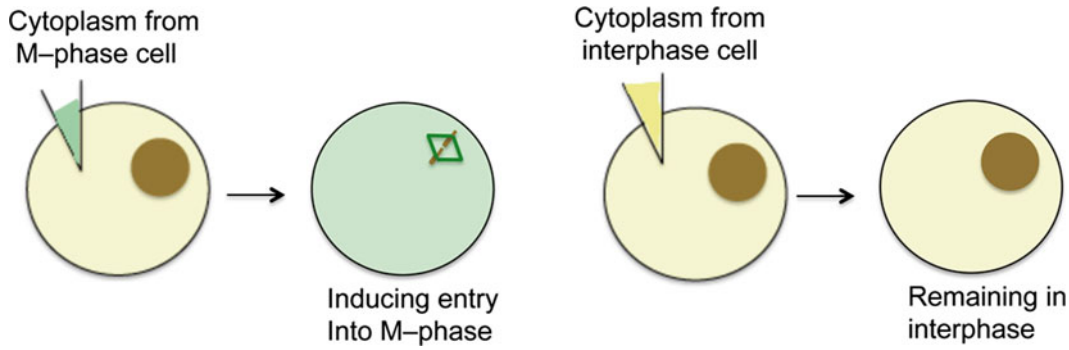

Fig. 13 Oocyte injection experiment. Injection of the cytoplasm from a mature egg in M phase into an immature oocyte in interphase induces the oocyte to become mature and enter M phase

abundant source of the cytoplasm can be extracted from these embryonic cells at defined stages of the cell cycle. Moreover, because of their big size, they are amenable for injecting materials such as a molecule of interest or protein lysates into them, or for extracting out of the cytoplasm. When M-phase cytoplasm from a mature egg is injected into a G_2-phase immature oocyte, the oocyte is driven into M phase and completes its maturation (Fig. 13) [47]. The cytoplasmic activity identified in the assay was initially called maturation-promoting factor (MPF) because it induces the maturation of an immature oocyte into a mature egg.

3.2.3 Cell Fusion Experiment

Mammalian cells are generally not as large as frog oocytes; therefore, it is not as easy to use them for cytoplasmic injections. However, we can perform a logically equivalent test by fusing a mitotic cell with an interphase cell, so that the nucleus of the interphase cell is exposed to any active components present in the cytoplasm of the mitotic cell. In such experiments the interphase cell is directly driven into mitosis, no matter whether it is in G_1, S, or G_2, and whether it has replicated its DNA or not [48]. This cytoplasmic activity is also named MPF—M-phase-promoting factor. It became clear several years later that MPF plays a general role in mitotic induction in somatic cells of all eukaryotic cells from yeasts to humans [49–53].

3.2.4 Egg Splitting and Bouncing Egg Experiments

An activated frog egg can be constricted by a loop of fine human baby hair before it has completed the first division, so that it is split into two separate parts: one containing the nucleus, the other not. As expected, the nucleated part continues the normal program of rapid cleavages. Remarkably, the non-nucleated part also undergoes a series of oscillations, seen as repeated cycles of contractions with almost perfect synchrony with the cleavages of the nucleated part. Similar patterns were observed in the famous "bouncing frog egg" experiment presented at a cell cycle symposium in 1980 by

Kirschner [3]. Frog eggs need fertilization to start rapid cleavages in nature. Alternatively, we can artificially "activate" frog eggs in various ways to initiate the mitotic cell cycle. In Kirschner's experiments, he removed the nuclei from *Xenopus* oocytes and observed striking contractions of the enucleated egg, expanding as mitosis began and then contracting during interphase. The cycles of contractions seen in both egg-splitting and bouncing egg experiments are due to the activity of the MPF in the cytoplasm. The peak of the MPF activity overlaps with the onset of mitosis. These results provide evidence for MPF as a cytoplasmic oscillator in the cleaving *Xenopus* embryo. This oscillator operates even in the absence of a nucleus [3].

3.2.5 Discovering Cyclins

Although the division cycles in the cleaving embryo can occur in the absence of DNA, they cannot occur in the absence of protein synthesis: blocking protein synthesis in early interphase prevents both the activation of MPF and the next mitosis. Protein synthesis was examined in sea urchin eggs by Tim Hunt. The fertilized eggs were incubated with water containing the radioactive amino acid, ^{35}S-methionine. Samples were removed at allocated time points and analyzed by SDS-PAGE (polyacrylamide gel electrophoresis). The experiment revealed a novel class of proteins, appearing in a periodic fashion, although most proteins in sea urchin eggs accumulate continuously after fertilization. The family of oscillating proteins increases steadily during interphase until the metaphase–anaphase transition, at which they are suddenly abolished. The proteins are thus given the name of cyclin because of their characteristic cycling pattern during the cell cycle [54]. The result suggests the possible model that one or more cyclins need to build up to a threshold concentration to activate MPF, and the destruction of cyclin is coupled to the inactivation of MPF and the cell exit from mitosis.

3.2.6 Reconstituting Cell Cycle Events in Cell-Free Extracts of Frog Xenopus laevis Eggs

The reconstitution of a biological process in a cell-free system is an ultimate goal of biochemical research to study the mechanism of a biological process at a molecular level. The frog egg has several unequaled advantages for such an approach. It is essentially pure cytoplasm, containing stockpiles of cellular components. It arrests as a single state of the cell cycle, either in G_2 phase as an immature oocyte or in M-phase as a mature egg, and it can be made to go from one state to the other state of the cell cycle by adding purified molecules. Cell-free extracts were developed in 1980s to reproduce cell cycle events in vitro. Activated frog eggs are broken open by centrifugation. The undiluted cytoplasm is then collected. Sperm nuclei are added together with ATP to monitor the alternating M phase and interphase in the "cycling" extracts [55].

How is the alternating M phase and interphase monitored in the *Xenopus* egg extracts? The sperm nuclei undergo decondensation in interphase and condensation at the onset of the

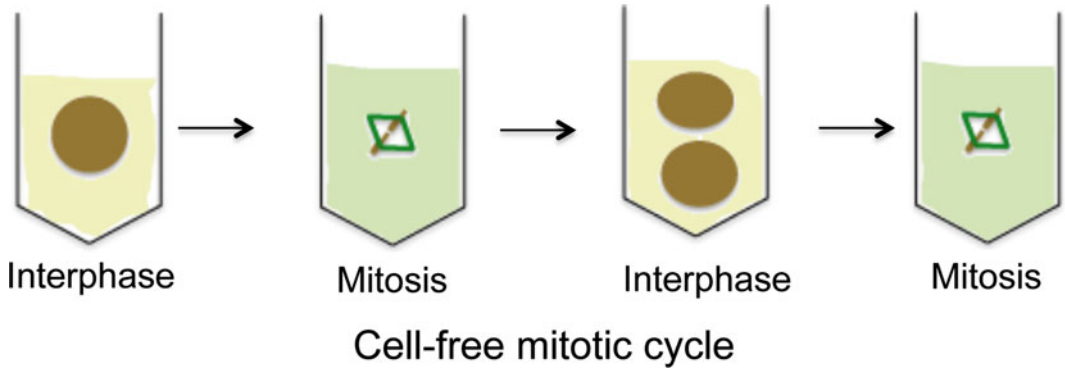

Fig. 14 Reproducing mitotic cell cycle in a cell-free system of frog egg extracts. The sperm nuclei undergo de-condensation in interphase and condensation at the onset of the mitosis, in parallel with nuclear envelope disassembly and reassembly, respectively, serving as an indicator to distinguish interphase and M phase. These morphological changes can be observed under a fluorescence microscope to follow the cell cycle events occurring in the cell-free system

mitosis, in parallel with nuclear envelope disassembly and reassembly, respectively, serving as an indicator to distinguish interphase and M phase. The extracts reproduce the events of conversion between the two phases. We can observe these morphological changes under a fluorescence microscope to follow the cell cycle events occurring in the cell-free system (Fig. 14). This system makes it possible to characterize functionally the role of a protein in the interphase–M phase transition. An inhibitor slows down the transition, while an activator speeds up the transition. The long arduous work to purify MPF from the M-phase extracts was accomplished utilizing this "biochemically tractable" system, as the MPF-enriched fractions of the extracts induce the conversion from interphase to mitosis in the extracts [56]. One culminating work was using the frog egg extracts, depleted of endogenous transcripts and adding cyclin mRNA back to the extracts, to elegantly demonstrate that cyclin alone fulfilled the entire protein synthesis requirement of the interphase–M phase transition. Therefore, cyclin is the only protein needed, rather than total protein synthesis, for the onset of the mitosis [57]. Furthermore, the linkage of MPF to Cdc2 and ultimately to cyclin was also established in this biochemical assay system [58]. The studies using the system provide insights into the molecular nature of the MPF and the control mechanisms of the mitotic transition.

3.3 The Fruit Fly Drosophila melanogaster

Fruit Fly *Drosophila melanogaster* is a valuable model organism for cell cycle studies. The components of the cell cycle control system in *Drosophila* are structurally and functionally similar to humans. Particularly, both fruit flies and humans share common developmental and physiological constrains that are unique for multicellular organisms [59]. The generation time of *Drosophila* is 2 weeks and it is relatively easy to grow and maintain them in a laboratory.

Drosophila has a genome size of about 14,000 genes, which is 2–3 times of yeasts and about half the number in humans. Efficient genetic tools are established and available in *Drosophila* to identify and analyze the genes involved in regulation and progression of the cell-division cycle [60], although the diploid chromosome content makes the subsequent characterization of these genes more complex than the haploid yeasts.

An early *Drosophila* embryo undergoes rapid and synchronous nuclear divisions after the fusion of egg and sperm nuclei to give rise to a zygote nucleus. These divisions each last less than 10 min and proceed without gap phases, resulting in a syncytium, in which many nuclei share the same cytoplasm. The nuclei subsequently move to the surface of the embryo after nine divisions and start cytokinesis to form about 6000 cells at the end of the 13th division. The synchronous progression of the nuclear division in early *Drosophila* embryos provides a good resource to isolate important regulators of the cell cycle. However, the analysis of a mutant phenotype in such system is complicated by the presence of maternal gene products, required for completing the first 13 divisions. Consequently, mutations in a zygotic gene may not generate a visible phenotype until the stock of the maternal gene products is depleted.

3.4 Mammalian Cells

Although the fundamental principles of cell cycle control are studied efficiently in simpler systems including yeasts and *Drosophila*, it cannot supersede the research in the mammalian cell cycle. Only in mammalian cells can we ultimately decipher the complex circuits regulating the cell cycle. However, in complex multicellular organisms such as humans, various cells divide at very different rates. The cells that line our intestine live only 3 days and must be constantly replaced by the division of precursor cells. On the other hand, the life span of liver cells is more than a year, thus cell division in this organ is rare. The cell cycle in mammalian cells varies greatly. The variability in the length of the cell cycle of different cells occurs mainly in G_1 and G_2. It reflects the ability of cells to exit from the cell cycle during either G_1 or G_2 phase (Fig. 15). Many cells can withdraw from the cell cycle, entering G_0 or a stable G_2 arrest. Cells in G_0 have left the cycle after division but before the restriction point at the G_1–S transition. These cells account for most of the non-growing, non-proliferating cells in the human body. Some cells such as epidermal cells leave the cycle during G_2 and arrest without growth or proliferation [5].

It is difficult to study cell proliferation in intact multicellular animals; therefore, most studies of cell cycle control are performed on cells proliferating in culture. The tissue culture studies on the cell cycle contribute to our understanding of cancer development at a cellular level. Insights into the regulation of cell growth and proliferation in mammals have been provided by studies of cell lines and transformed cancer cells in cell culture. No matter how different

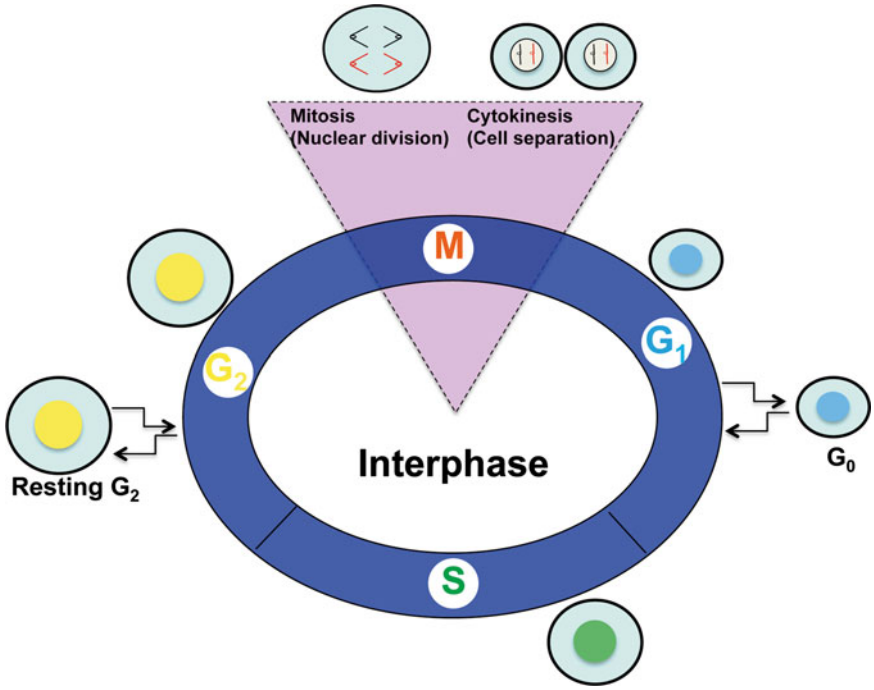

Fig. 15 Features of the cell cycle of human cells. The human cell cycle varies in length. The variability reflects the ability of cells to exit from the cell cycle during either phase of G_1 or G_2

individual paths of cancer development are from each other and how diverse the origins that cancer derives from, all cancer cells abandon normal growth regulation and continuously cycle. Cancer cells proliferate excessively and give rise to malignant tumors. In essence, cancer is a cellular disease in multicellular organisms and uncontrolled cell proliferation is the hallmark of cancer. Usually, multiple genetic changes are necessary to affect properties of cell growth and proliferation that eventually lead to cancer. Several properties are used as parameters to judge the normality of cells in culture:

- Limited generation time and death at crisis—a point at which most of the cells die.
- Anchorage dependence—cells need a firm surface to attach to.
- Serum dependence or growth factor dependence—serum that contains growth factors is essential for cell proliferation.
- Density-dependent inhibition—cell growth is inhibited via cell–cell contact.
- Cell shape—cells are usually flat and extended on the growth surface due to the cytoskeletal organization.

Growth of normal cells result in a monolayer in culture because of these properties. Primary cells, immortal cell lines and transformed cell lines have been used to study cell cycle control in tissue culture environment.

3.4.1 Primary Cells Reach Replicative Senescence in Culture

Ideally, cells freshly removed from animals—primary cells are used. Primary cells are the immediate descendants of cells taken directly from an animal organism. We can culture them in plastic dishes with medium containing nutrients and growth factors. Although primary cells faithfully mimic the in vivo properties, they can only survive for a relatively short period in culture. Human primary cells usually divide 25–50 times in culture before reaching replicative senescence or a crisis. The proliferative life span of mouse cells is even shorter—about 15 generations of cell divisions [61]. The replicative senescence probably caused by telomere degeneration and the culture condition that drastically differs from the normal environment of the animal body [62]. The limitation of the life span of most primary cells makes it necessary to also explore options of employing non-transformed cells—immortal but not transformed cell lines, even if it is not perfect.

3.4.2 Cultured Cell Lines

To examine the pathways and aberrant events that enable cells to bypass normal cell cycle controls and develop tumors, we need to recognize the differences in proliferation properties among primary cells, immortal and transformed cell lines in culture. During cell adaptation to culture environment, cells may first convert to immortal cell lines, continue to evolve and finally become transformed, in which the aforementioned characteristics of primary cells are completely lost. Cells in an established cell line can divide indefinitely. Cell lines are evolved through a step of immortalization. When the growth of primary cells from a vertebrate animal ceases in culture, reaching replicative senescence—a crisis, the majority of the cells die. However, among them a few cells survive the crisis, keep proliferating, and eventually form a line of endless dividing cells. Although changed to become immortalized, the cells in such a cell line still remain non-tumorigenic and display the other features similar to those of primary cells.

As these cell lines can perpetuate endlessly, they may continue to change while adapting to the culture environment. They may lose anchorage dependence for growth on solid surfaces, gain the ability to grow without serum supply, and become insensitive to contact inhibition and form multiple layers of cells—tumor foci in culture. The last stage of transformation is metastasis, at which point, cells become mobile and are capable of migrating to new sites, establishing new colonies in culture [5]. Fully transformed cells capture the malignancy of cancer—the ability to invade normal tissue.

The combined changes of cell immortalization and transformation in culture provide a paradigm for cancer development at the cellular level. An assay that is commonly used to identify transformation agents is called the transfection assay. The assay is based on the ability of a molecule to convert a “normal” cell line into a transformed cell line. Many oncogenes/proto-oncogenes harbored in retrovirus and tumor DNA have been identified and isolated by using the transfection assay [63]. In contrast, it is difficult to

identify tumor-suppressor genes using the transfection assay, due to the recessive nature of the mutations, unless both alleles in the cell are altered. Certain steps converting normal cells into transformed cells may provide models for the process of cancer development.

Although studies using normal and transformed cell lines in culture contribute to our understanding of cell cycle controls and cancer development at a cellular level, we must keep in mind that these cell lines have changed to form distinct identities from primary cells. Even normal cell lines can only serve as an approximate mimic of in vivo controls. All cell lines, normal or transformed, are consequences of genetic changes that affect cell cycle control.

3.4.3 New Gene-Manipulation Tools in Mammalian Cells

The large size of mammalian cells makes them excellent for cytological and biochemical analyses of the cell cycle. Traditionally, the main drawback of the mammalian cell system is the lack of efficient means for genetic manipulations. Development of two methodologies has opened immense potential for genetic analyses in mammalian cells: systematic gene deletions using small-interfering RNAs (siRNAs) and gene editing, regulating and targeting employing the clustered, regularly interspaced, short palindromic repeat (CRISPR) technology [64, 65]. There has been success in using the siRNAs approach in cell cycle studies, including an exceptionally large-scale project by Neumann et al. [41]. In this work, Neumann et al. reduced protein expression with siRNA from 21,000 genes, used time-lapse microscopy to measure defects in mitosis, and identified more than 500 genes implicated in mitosis. Although the siRNA method is versatile, it may suffer from partial knockdown and off-target effects [66]. These problems render this method less straightforward for assigning gene functions compared with complete gene ablation in yeasts.

CRISPR-Cas systems are RNA-guided nucleases, such as Cas9, derived from adaptable immune mechanisms used by many bacteria to protect themselves from foreign nucleic acids including viruses and plasmid DNAs. The guide RNA assembles into complexes with Cas9 and target the nuclease to a specific DNA sequence by base pairing. The programmable feature of the DNA-targeting system enables researchers to efficiently modify endogenous genes in many cell types and organisms including mammalian cells, which are traditionally challenging for genetic manipulations [65].

4 Diverse Biological Systems, Conserved Mechanisms: A Historic Perspective

Before the genomics era of the 1990s, cell division was mainly studied using genetic manipulations in yeasts and biochemical analyses of early embryonic cell divisions in frog eggs. Isolating yeast mutants with perturbed cell cycle control helped identify genes involved in the sequential execution of cell cycle phase

transitions. In early development, the rapid cleavage of frog eggs and the cell-free extracts proved useful in biochemically characterizing a key cell cycle regulator: MPF, whose activity oscillated in synchrony with the mitotic cycle. These different approaches led to two seemingly distinct models: the domino model in yeasts and the clock model in frog eggs. The domino model emphasizes the interdependence of the cell cycle events or phase transitions, whereas the clock model envisions a cytoplasmic timer controlling the onset of mitosis, which is independent to other events in the cell cycle. The divergent models were originally proposed based on research in yeasts and early embryonic frog cells, respectively. The identification of the proteins with crucial functions in both models allowed scientists to reconcile the divergent models, and highlights fundamental principles of cell cycle regulation that are exquisitely conserved through evolution in all eukaryotic organisms.

4.1 Lessons from Yeasts: The Domino Model

In the 1970s, Paul Nurse and Leland Hartwell pioneered the search for mutations that affect the cell cycle in fission yeast and budding yeast, respectively [35, 36]. They identified mutants based on either the aforementioned phase-specific arrest, so-called *cdc* phenotype, or on the abnormally small cell size phenotype, known as the *wee* mutants. The mutants identified in both yeasts are temperature-sensitive (*ts*). Using this genetic approach, researchers identified a cast of vital players in cell cycle control, including the genes encoding Cdc2, Wee1 protein kinases, as well as Cdc25 tyrosine phosphatase. The discoveries also provide the basis for the concept of checkpoint control of cell division [34, 43]. If mutant cells lose a functional gene necessary for completing an early phase, they cannot proceed to the later phases. The interdependence of cell cycle events ensures that each phase transition of the cell cycle occurs at a specific time and in a defined order. Thus, the initiation of a later cell cycle phase is dependent on the proper completion of a prior phase, known as the *domino model* of cell cycle regulation. This sequential order of the cell cycle events is achieved through a series of cell signaling events; checkpoint pathways for the faithful phase transitions of the cell cycle.

4.2 Lessons from Frog Eggs: The Clock Model

The rapid cleavage of early *Xenopus laevis* eggs and the frog egg extracts provide a valuable system to functionally analyze and purify the factors that drive a cell into mitosis. It is this model organism that enables researchers to biochemically purify MPF and functionally identify the key regulators of the cell cycle including, Cdc2, later named as cyclin-dependent kinase1 (Cdk1), Cdc25 tyrosine phosphatase, and Wee1 tyrosine kinase.

The tight timing of the onset of mitosis in early frog embryos indicates a fast biochemical switch responsible for speedy and accurate phase transition. Remarkably, in the egg-splitting and bouncing-egg experiments, the eggs underwent a series of oscillations, seen as

repeated cycles of contractions with almost perfect synchrony as to the onset of mitosis. Since the driving force for cell entry into mitosis had then been identified as MPF and MPF peak activity overlaps with the onset of mitosis, scientists soon established that the surge or fluctuation of the MPF activity, occurring every 30 min in the cleaving frog *Xenopus* embryo, acts as a cytoplasmic oscillator or a cytoplasmic timer/clock. In fact, this clock continues ticking even in the absence of a nucleus [3]. The results from biochemical studies in early frog embryos apparently suggest a very different mechanism of cell cycle regulation—what is known as the clock model. In this model, the timing for the onset of mitosis is controlled by the MPF activity that resides in the cytoplasm and is turned on every 30 min, independent of other cell cycle events.

4.3 Reconciliation of the Two Divergent Views

Are the governing principles of the cell cycle conserved in different organisms through evolution? Is there any generality in cell cycle regulation? The genetic isolation and analysis of *cdc* mutants in yeasts revealed a fundamental nature of cell cycle control—the execution of late events depends on the prior completion of early events. This concept has become the theme for the domino model. In contrast, the rapid contractions of an enucleated *Xenopus* egg illustrated a cytoplasmic clock that sets the timing of mitotic entry, representing the idea known as the clock model. The domino model suggests that the cell cycle events are interdependent, whereas the clock model implies that the timing for cell entry into mitosis is not influenced by other events. Back in the 1980s, researchers conducting cell cycle analyses in yeast and frog eggs using different experimental systems, mainly genetic and biochemical, were mutually impressed by each other's accomplishments, depth of thinking and cleverness of approaches at conferences, yet walked away disappointingly seeing little commonality in the cell cycle among different organisms [3, 34].

The clues about the functional links of the genetic and biochemical approaches came from the molecular identifications of the key players in cell cycle regulation. Genetic studies in yeasts identified a central gene in the network of cell cycle control: *cdc2*$^+$ in fission yeast and *CDC28*$^+$ in budding yeast. Budding yeast *CDC28*$^+$ gene transformed into fission yeast *cdc2 ts* mutant could rescue its elongation phenotype and restore the normal cell cycle, establishing that Cdc2 and Cdc28 proteins are functionally equivalent in the yeasts. Cdc2/Cd28d is thus crowned as the master regulator of the cell cycle in yeasts, just like the royal status of MPF in frog eggs.

A giant leap came in 1987. Using the same cross-species complementation assay, Melanie Lee and Paul Nurse discovered the human counterpart of fission yeast *cdc2*$^+$, based on the ability of human *CDC2*$^+$ to entirely replace the function of *cdc2*$^+$ in fission yeast. All three homologous genes, *cdc2*$^+$ in fission yeast, *CDC28*$^+$ in budding yeast and *CDC2*$^+$ in humans, appeared to be

closely related protein kinases. "One small step for yeast…one giant leap for mankind," reflects the significance of the result and the promising potential of utilizing yeasts as model organisms for rapid understanding of cell cycle control in humans (www.nature.com/celldivision/milestones/full/milestone11.html). Since Cdc2 is evolutionarily conserved from yeast to humans, the next logical question is: how are Cdc2/Cdc28 proteins in yeasts related to MPF in animal cells?

Scientists in the field suspected that MPF in frog eggs and mammalian cells might also be a master protein kinase in charge of protein phosphorylation cascades. As long predicted, MPF isolated from the frog extracts was finally confirmed as a specific protein kinase. In fact, it was further defined as a two-subunit protein complex, the catalytic subunit being a protein kinase with a size of 34 kDa. Using clever heterologous strategy, scientists introduced the fission yeast Cdc2 protein into frog egg extracts, and found that the 34 kDa component of frog MPF was actually the same kinase as the Cdc2 protein in fission yeast [58]! The frog eggs and yeast cells, which originally appeared dramatically different, are fundamentally the same in the master regulator of the cell cycle. It has been one of the most unifying discoveries in cell biology—the fission yeast Cdc2 protein, budding yeast Cdc28 protein, and MPF in *Xenopus* are all related serine-threonine protein kinases.

The master kinase that triggers downstream events for mitotic transition consists of two proteins: cyclin-dependent kinase1 (Cdk1/Cdc2) and a regulatory subunit, cyclin. To form an activated MPF at the G_2–M transition, Cdc2 (the 34 kDa protein subunit of MPF) is associated with cyclin B (the 48 kDa protein subunit of MPF). The two views of cell cycle regulation were finally unified at the identification of the molecular identity of MPF: the same protein kinase is required for cell entry into mitosis in both yeasts and animals. Furthermore, different Cdks control the onset of S phase and M phase, acting as a "cell cycle engine" [5]. This conclusion is both satisfying and surprising for two reasons. Firstly, there is a wide evolutionary distance between yeasts and vertebrates. Secondly, the morphological events of mitosis are significantly distinct between yeast and animal cells. In yeasts, "closed" mitosis takes place without disassembly of the nuclear envelope, while in animal cells, "open" mitosis occurs with breakdown of nuclear membrane in despite of the drastic differences from single-cellular to multicellular eukaryotes including humans, the function of the master kinase is conserved. Therefore, in many diverse biological systems, the main components of the cell cycle machinery for phase transitions are fundamentally the same [3, 26]. The domino model and clock model reflect the mechanisms in specialized cell types, proliferating cells and early embryos, respectively. The specific mechanisms governing the functions of these regulators, as well as the complexity of the signaling pathways may vary with

phase transitions, developmental stages, organisms, and environment. These distinct aspects of cell cycle regulation constitute fascinating areas for further research.

5 Gaining a Comprehensive Understanding of Cell-Division Cycle

The fundamental theme controlling the cell-division cycle underlies the growth, development, and reproduction of all eukaryotes. A comprehensive understanding of the molecular regulatory mechanisms is one of the most important goals of modern cell biology. In the past decades, we have seen remarkable advances in our understanding of cell cycle control. These advances are built mainly on the knowledge gained from studying the cell cycle in different model organisms using various experimental approaches. Given the conservation of the cell-division cycle through evolution, the findings in these simpler model organisms are relevant to the control mechanisms in humans. Researchers also explored the cell cycle regulation in the context of development, tumorigenesis, and human diseases, proving the value of model organism research for meeting the critical translational challenges of the current age.

One singe model organism alone with one specialized experimental approach, genetic, cytological, or biochemical would not have led us to what we know now about cell cycle regulation. One particular model would be imperfect for addressing all questions about cell cycle control. Informative comparisons of cell cycle regulators in different organisms allow the identification of gene products that are implicated more universally in a cell cycle event or phenomenon [67]. These comparisons also provide a logical route to reduce system biases inherent in individual organisms. Successful examples include, the converging of the diverging domino and clock models, as well as the level changes of certain RNAs at the transitions of cell cycle stages in a conserved manner in multiple organisms [40].

The cell-division cycle as a vital process of life is complex and dynamic. Many interacting components involved are prone to unexpected outcomes, reflecting emergent properties characteristic of life. Lots of challenging questions about the cell cycle still await us to answer them. Even certain control circuits of the cell cycle have emerged from the research in the past decades, to reveal that the linkages in the network are not always hard-wired. How and when they may break, reform, or connect to new components, remain elusive. In addition, often, cell cycle regulators such as protein kinases, have pleiotropic roles. Also, little is known about the unique benefit provided by the redundancy of gene functions in cell cycle networks. Uncovering these genetic interactions would have a special impact on cancer treatments, which could result in synthetic lethal interactions [2]. A comprehensive understanding of the cell-division cycle is necessary to further our knowledge about the important processes of biology.

Yeasts with small genomes of 5000–6000 genes are relatively straightforward organisms for use in systems genomic analyses. The availability of genome-wide gene deletion collections, as well as other methods for forward genetics, allows the identification of as many genes involved in cell cycle control as possible [2, 16]. Discoveries in zinc-finger nucleases (ZFNs), transcription activator-like effector nucleases (TALENs), and more lately clustered regulatory interspaced short palindromic repeats (CRISPRs), make it possible for targeted genome editing in all organisms including human cells. The application of bioinformatics procedures would enable us to link the genes identified with specific biochemical and molecular functions. Employing stable-isotope labeling of amino acids in culture (SILAC) for global analysis of Cdk1 substrate phosphorylation sites sets an elegant example of chemical genomics for signaling pathways in cell cycle regulation [68, 69]. Quantitative methodologies have been developed to manage large database sets, in addition to the development of mathematical modeling as a tool for analyzing cell cycle control networks [70, 71]. The new technologies have empowered cell cycle studies in the model organisms to investigate the regulatory mechanisms at a higher level with respect to cellular phenomena and morphologies, changes in the gene expression program, protein modification and protein degradation at large scales and in a cell cycle-dependent manner.

Because of the progress in genome annotation and the conservation of the cell cycle throughout evolution, orthologous genes or proteins from a variety of organisms in a range of situations can be compared extensively at a level that was never possible decades ago. It is no longer a fantasy to test a human gene in yeasts to determine its potential function in the cell cycle—surrogate genetics. Although researchers have enriched their common toolboxes and reagents by working with individual model organisms to fulfill their goals in scientific discovery, they are becoming more integrated into larger communities than before. Changes in technologies and the applicability of new methodologies have renewed interests and opened exciting opportunities in cell cycle studies using different model organisms, allowing the gain of a comprehensive understanding of the fundamental processes of all eukaryotes.

Biological research is used to relying on a small number of traditional model organisms. The species chosen are usually based on their amenability for experimental approaches to investigate biological problems ranging from genetics, cell biology, biochemistry, development, and evolution. Advances in genome sequencing and editing, proteomics, quantitative analyses, as well as systems biology approaches are reshaping our concept of a model organism. The introduction of next-generation sequencing technology has changed the landscape of genetics [72]. The capability of processing millions of sequence reads in parallel, in much shorter time periods, with lower costs than conventional sequencing methods, also

influences the cast of potential model organisms. The living species used in biological research have been vastly expanded from relatively small numbers, to a large variety of organisms. New species have been introduced to laboratories as emerging model organisms, including Butterfly (*Bicyclus anynana*), Cricket (*Gryllus bimaculatus*), Fruit Bat (*Carollia perspicillata*), Social Ameba (*Dictyostelium discoideum*), and Tomato (*Solanum lycopersicum*) [73]; just name a few. For example, tiger pufferfish is characterized as a vertebrate model with a compact genome [74]. We have entered a new era of model organism development, in which expansion of model organisms, comparison among and refinement of the established model organisms will be driven by both exciting biological questions and fascinating advancements of technologies. The new technologies provide a broad evolutionary perspective of cell-division regulation and allow informative comparisons among different species at a level that has never been possible, exerting unimaginable impact on our comprehensive understanding of cell cycle regulation.

Acknowledgement

I thank my colleagues at Keck Science Department, Claremont Colleges, CA, Dr. Gretchen Edwalds-Gilbert for providing an image of budding yeast *S. cerevisiae*; Dr. Bryan Thines and Dr. Babak Sanii for reading and the feedback on the manuscript. I also thank Dr. Louise Weston for editing and the feedback on the manuscript.

References

1. Hedges SB (2002) The origin and evolution of model organisms. Nat Rev Genet 3:838–849
2. Rine J (2014) A future of the model organism model. Mol Biol Cell 25:549–553
3. Kirschner M (1992) The cell cycle then and now. Trends Biochem Sci 17:281–285
4. Nurse P (2000) A long twentieth century of the cell cycle and beyond. Cell 100:71–78
5. Murray A, Hunt T (1993) The cell cycle: an introduction. Oxford University Press, New York, NY
6. Morgan DO (2007) The cell cycle: principles of control. New Science Press Ltd, London
7. Mukherjee S (2011) The emperor of all maladies: a biography of cancer. Scribner, New York, NY
8. Bianconi E, Piovesan A, Facchin F, Beraudi A, Casadei R, Frabetti F, Vitale L, Pelleri MC, Tassani S, Piva F, Perez-Amodio S, Strippoli P, Canaider S (2013) An estimation of the number of cells in the human body. Ann Hum Biol 40: 463–471
9. Fischbach GD, Fischbach RL (2004) Stem cells: science, policy, and ethics. J Clin Invest 114:1364–1370
10. Yamanaka S (2007) Strategies and new developments in the generation of patient-specific pluripotent stem cells. Cell Stem Cell 1:39–49
11. Vaux DL, Korsmeyer SJ (1999) Cell death in development. Cell 96:245–254
12. Zimmer C (2007) Evolved for cancer? Sci Am 296:68–74, 75A
13. Alberts B, Johnson A, Lewis J, Raff M, Roberts K, Walter P (2007) Molecular biology of the cell. Garland Science, New York, NY
14. Goffeau A, Barrell BG, Bussey H, Davis RW, Dujon B, Feldmann H, Galibert F, Hoheisel JD, Jacq C, Johnston M, Louis EJ, Mewes

HW, Murakami Y, Philippsen P, Tettelin H, Oliver SG (1996) Life with 6000 genes. Science 274(546):563–567

15. Wood V, Gwilliam R, Rajandream MA, Lyne M, Lyne R, Stewart A, Sgouros J, Peat N, Hayles J, Baker S, Basham D, Bowman S, Brooks K, Brown D, Brown S, Chillingworth T, Churcher C, Collins M, Connor R, Cronin A, Davis P, Feltwell T, Fraser A, Gentles S, Goble A, Hamlin N, Harris D, Hidalgo J, Hodgson G, Holroyd S, Hornsby T, Howarth S, Huckle EJ, Hunt S, Jagels K, James K, Jones L, Jones M, Leather S, McDonald S, McLean J, Mooney P, Moule S, Mungall K, Murphy L, Niblett D, Odell C, Oliver K, O'Neil S, Pearson D, Quail MA, Rabbinowitsch E, Rutherford K, Rutter S, Saunders D, Seeger K, Sharp S, Skelton J, Simmonds M, Squares R, Squares S, Stevens K, Taylor K, Taylor RG, Tivey A, Walsh S, Warren T, Whitehead S, Woodward J, Volckaert G, Aert R, Robben J, Grymonprez B, Weltjens I, Vanstreels E, Rieger M, Schafer M, Muller-Auer S, Gabel C, Fuchs M, Fritzc C, Holzer E, Moestl D, Hilbert H, Borzym K, Langer I, Beck A, Lehrach H, Reinhardt R, Pohl TM, Eger P, Zimmermann W, Wedler H, Wambutt R, Purnelle B, Goffeau A, Cadieu E, Dreano S, Gloux S, Lelaure V et al (2002) The genome sequence of Schizosaccharomyces pombe. Nature 415:871–880
16. Kim DU, Hayles J, Kim D, Wood V, Park HO, Won M, Yoo HS, Duhig T, Nam M, Palmer G, Han S, Jeffery L, Baek ST, Lee H, Shim YS, Lee M, Kim L, Heo KS, Noh EJ, Lee AR, Jang YJ, Chung KS, Choi SJ, Park JY, Park Y, Kim HM, Park SK, Park HJ, Kang EJ, Kim HB, Kang HS, Park HM, Kim K, Song K, Song KB, Nurse P, Hoe KL (2010) Analysis of a genome-wide set of gene deletions in the fission yeast Schizosaccharomyces pombe. Nat Biotechnol 28:617–623
17. Parsons AB, Lopez A, Givoni IE, Williams DE, Gray CA, Porter J, Chua G, Sopko R, Brost RL, Ho CH, Wang J, Ketela T, Brenner C, Brill JA, Fernandez GE, Lorenz TC, Payne GS, Ishihara S, Ohya Y, Andrews B, Hughes TR, Frey BJ, Graham TR, Andersen RJ, Boone C (2006) Exploring the mode-of-action of bioactive compounds by chemical-genetic profiling in yeast. Cell 126:611–625
18. Hillenmeyer ME, Fung E, Wildenhain J, Pierce SE, Hoon S, Lee W, Proctor M, St Onge RP, Tyers M, Koller D, Altman RB, Davis RW, Nislow C, Giaever G (2008) The chemical genomic portrait of yeast: uncovering a phenotype for all genes. Science 320:362–365
19. Hoon S, St Onge RP, Giaever G, Nislow C (2008) Yeast chemical genomics and drug discovery: an update. Trends Pharmacol Sci 29:499–504
20. Costanzo M, Baryshnikova A, Bellay J, Kim Y, Spear ED, Sevier CS, Ding H, Koh JL, Toufighi K, Mostafavi S, Prinz J, St Onge RP, VanderSluis B, Makhnevych T, Vizeacoumar FJ, Alizadeh S, Bahr S, Brost RL, Chen Y, Cokol M, Deshpande R, Li Z, Lin ZY, Liang W, Marback M, Paw J, San Luis BJ, Shuteriqi E, Tong AH, van Dyk N, Wallace IM, Whitney JA, Weirauch MT, Zhong G, Zhu H, Houry WA, Brudno M, Ragibizadeh S, Papp B, Pal C, Roth FP, Giaever G, Nislow C, Troyanskaya OG, Bussey H, Bader GD, Gingras AC, Morris QD, Kim PM, Kaiser CA, Myers CL, Andrews BJ, Boone C (2010) The genetic landscape of a cell. Science 327:425–431
21. White SA, Allshire RC (2008) RNAi-mediated chromatin silencing in fission yeast. Curr Top Microbiol Immunol 320:157–183
22. Forsburg SL, Rhind N (2006) Basic methods for fission yeast. Yeast 23:173–183
23. Lee MG, Nurse P (1987) Complementation used to clone a human homologue of the fission yeast cell cycle control gene cdc2. Nature 327:31–35
24. Botstein D, Fink GR (2011) Yeast: an experimental organism for 21st century biology. Genetics 189:695–704
25. MacNeill SA, Nurse P (1997) The molecular and cellular biology of the yeast saccharomyces. Cold Spring Harbor Laboratory Press, New York, NY
26. Nurse P (1990) Universal control mechanism regulating onset of M-phase. Nature 344:503–508
27. Botstein D, Chervitz SA, Cherry JM (1997) Yeast as a model organism. Science 277:1259–1260
28. Melese T, Hieter P (2002) From genetics and genomics to drug discovery: yeast rises to the challenge. Trends Pharmacol Sci 23:544–547
29. Roguev A, Wiren M, Weissman JS, Krogan NJ, Roguev A, Krogan NJ (2007) High-throughput genetic interaction mapping in the fission yeast Schizosaccharomyces pombe SIN-fully silent: HDAC complexes in fission yeast. Nat Methods 4:861–866, Epub 2007 Sep 23
30. Alfa C, Fantes P, Hyams J, McLeod M, Warbrick E (1993) Experiments with fission yeast, a laboratory course manual. Cold Spring Harbor Laboratory Press, New York, NY
31. Forsburg SL (2001) The art and design of genetic screens: yeast. Nat Rev Genet 2:659–668
32. Lee MG, Nurse P (1987) Cell cycle genes of the fission yeast. Sci Prog 71:1–14

33. Morgan DO (1995) Principles of CDK regulation. Nature 374:131–134
34. Hartwell LH, Culotti J, Pringle JR, Reid BJ (1974) Genetic control of the cell division cycle in yeast. Science 183:46–51
35. Hartwell LH, Mortimer RK, Culotti J, Culotti M (1973) Genetic control of the cell division cycle in yeast: v. genetic analysis of cdc mutants. Genetics 74:267–286
36. Nurse P, Thuriaux P, Nasmyth K (1976) Genetic control of the cell division cycle in the fission yeast Schizosaccharomyces pombe. Mol Gen Genet 146:167–178
37. Sullivan W (1993) The salvation of doug. Generations (Genet Soc Am) 1:3
38. Russell P, Nurse P (1987) Negative regulation of mitosis by wee1+, a gene encoding a protein kinase homolog. Cell 49:559–567
39. Spellman PT, Sherlock G, Zhang MQ, Iyer VR, Anders K, Eisen MB, Brown PO, Botstein D, Futcher B (1998) Comprehensive identification of cell cycle-regulated genes of the yeast Saccharomyces cerevisiae by microarray hybridization. Mol Biol Cell 9:3273–3297
40. Rustici G, Mata J, Kivinen K, Lio P, Penkett CJ, Burns G, Hayles J, Brazma A, Nurse P, Bahler J (2004) Periodic gene expression program of the fission yeast cell cycle. Nat Genet 36:809–817
41. Neumann B, Walter T, Heriche JK, Bulkescher J, Erfle H, Conrad C, Rogers P, Poser I, Held M, Liebel U, Cetin C, Sieckmann F, Pau G, Kabbe R, Wunsche A, Satagopam V, Schmitz MH, Chapuis C, Gerlich DW, Schneider R, Eils R, Huber W, Peters JM, Hyman AA, Durbin R, Pepperkok R, Ellenberg J (2010) Phenotypic profiling of the human genome by time-lapse microscopy reveals cell division genes. Nature 464:721–727
42. Russell P, Nurse P (1986) cdc25+ functions as an inducer in the mitotic control of fission yeast. Cell 45:145–153
43. Hartwell LH, Weinert TA (1989) Checkpoints: controls that ensure the order of cell cycle events. Science 246:629–634
44. Beach D, Durkacz B, Nurse P (1982) Functionally homologous cell cycle control genes in budding and fission yeast. Nature 300:706–709
45. Simanis V, Nurse P (1986) The cell cycle control gene cdc2+ of fission yeast encodes a protein kinase potentially regulated by phosphorylation. Cell 45:261–268
46. Draetta G, Brizuela L, Potashkin J, Beach D (1987) Identification of p34 and p13, human homologs of the cell cycle regulators of fission yeast encoded by cdc2+ and suc1+. Cell 50:319–325
47. Masui Y, Markert CL (1971) Cytoplasmic control of nuclear behavior during meiotic maturation of frog oocytes. J Exp Zool 177:129–145
48. Johnson RT, Rao PN, Hughes HD (1970) Mammalian cell fusion. 3. A HeLa cell inducer of premature chromosome condensation active in cells from a variety of animal species. J Cell Physiol 76:151–157
49. Gerhart J, Wu M, Kirschner M (1984) Cell cycle dynamics of an M-phase-specific cytoplasmic factor in Xenopus laevis oocytes and eggs. J Cell Biol 98:1247–1255
50. Newport JW, Kirschner MW (1984) Regulation of the cell cycle during early Xenopus development. Cell 37:731–742
51. Sunkara PS, Wright DA, Rao PN (1979) Mitotic factors from mammalian cells: a preliminary characterization. J Supramol Struct 11:189–195
52. Kishimoto T, Kuriyama R, Kondo H, Kanatani H (1982) Generality of the action of various maturation-promoting factors. Exp Cell Res 137:121–126
53. Tachibana K, Yanagishima N, Kishimoto T (1987) Preliminary characterization of maturation-promoting factor from yeast Saccharomyces cerevisiae. J Cell Sci 88(Pt 3):273–281
54. Evans T, Rosenthal ET, Youngblom J, Distel D, Hunt T (1983) Cyclin: a protein specified by maternal mRNA in sea urchin eggs that is destroyed at each cleavage division. Cell 33:389–396
55. Lohka MJ, Masui Y (1983) Formation in vitro of sperm pronuclei and mitotic chromosomes induced by amphibian ooplasmic components. Science 220:719–721
56. Lohka MJ, Hayes MK, Maller JL (1988) Purification of maturation-promoting factor, an intracellular regulator of early mitotic events. Proc Natl Acad Sci U S A 85:3009–3013
57. Murray AW, Kirschner MW (1989) Cyclin synthesis drives the early embryonic cell cycle. Nature 339:275–280
58. Dunphy WG, Brizuela L, Beach D, Newport J (1988) The Xenopus cdc2 protein is a component of MPF, a cytoplasmic regulator of mitosis. Cell 54:423–431
59. Edgar BA, Lehner CF (1996) Developmental control of cell cycle regulators: a fly's perspective. Science 274:1646–1652
60. Lee LA, O-W TL (2003) Regulation of cell cycles in Drosophila development: intrinsic and extrinsic cues. Annu Rev Genet 37:545–578

61. Todaro GJ, Green H (1963) Quantitative studies of the growth of mouse embryo cells in culture and their development into established lines. J Cell Biol 17:299–313
62. Ramirez RD, Morales CP, Herbert BS, Rohde JM, Passons C, Shay JW, Wright WE (2001) Putative telomere-independent mechanisms of replicative aging reflect inadequate growth conditions. Genes Dev 15:398–403
63. Land H, Parada LF, Weinberg RA (1983) Cellular oncogenes and multistep carcinogenesis. Science 222:771–778
64. Novina CD, Sharp PA (2004) The RNAi revolution. Nature 430:161–164
65. Sander JD, Joung JK (2014) CRISPR-Cas systems for editing, regulating and targeting genomes. Nat Biotechnol 32:347–355
66. Sioud M (2011) Promises and challenges in developing RNAi as a research tool and therapy. Methods Mol Biol 703:173–187
67. Nurse P, Hayles J (2011) The cell in an era of systems biology. Cell 144:850–854
68. Holt LJ, Tuch BB, Villen J, Johnson AD, Gygi SP, Morgan DO (2009) Global analysis of Cdk1 substrate phosphorylation sites provides insights into evolution. Science 325:1682–1686
69. Koivomagi M, Valk E, Venta R, Iofik A, Lepiku M, Morgan DO, Loog M (2011) Dynamics of Cdk1 substrate specificity during the cell cycle. Mol Cell 42:610–623
70. Allen NA, Chen KC, Shaffer CA, Tyson JJ, Watson LT (2006) Computer evaluation of network dynamics models with application to cell cycle control in budding yeast. Syst Biol 153:13–21
71. Brazhnik P, Tyson JJ (2006) Cell cycle control in bacteria and yeast: a case of convergent evolution? Cell Cycle 5:522–529
72. Mardis ER (2008) The impact of next-generation sequencing technology on genetics. Trends Genet 24:133–141
73. Hudson A et al (2009) Emerging model organisms: a laboratory manual. Cold Spring Harbor Laboratory Press, New York, NY
74. Brenner S, Elgar G, Sandford R, Macrae A, Venkatesh B, Aparicio S (1993) Characterization of the pufferfish (Fugu) genome as a compact model vertebrate genome. Nature 366:265–268

Chapter 3

Role of Computational Modeling in Understanding Cell Cycle Oscillators

Attila Csikász-Nagy and Ivan Mura

Abstract

The periodic oscillations in the activity of the cell cycle regulatory program, drives the timely activation of key cell cycle events. Interesting dynamical systems, such as oscillators, have been investigated by various theoretical and computational modeling methods. Thanks to the insights achieved by these modeling efforts we have gained considerable insights about the underlying molecular regulatory networks that can drive cell cycle oscillations. Here we review the basic features and characteristics of biological oscillators, discussing from a computational modeling point of view their specific architectures and the current knowledge about the dynamics that the life evolution selected to drive cell cycle oscillations.

Key words Cell cycle oscillators, Mathematical models, Nonlinearity, Predictive simulation, Regulation, Cross-talk

1 Introduction to Biological Oscillators

The ordered and regulated execution of the cell reproduction process relies on a complex set of interactions that are able to sense and integrate multiple signals from the cell environment into a fundamental network, with a molecular oscillator as the core engine driving the events of the cell cycle.

Oscillatory behaviors are interesting and complex. Their dynamical equilibria are able to maintain information about time progression and the state of variables, enabling native patterns of behavior to be coupled with external stimuli that modulate the final resulting responses. Similarly, the cell cycle oscillator is controlled by several environmental inputs, which set the frequency of the oscillation and stop it if the environment does not support cell division.

So effective are oscillators in flexibly governing the many regulated phenomena inside living systems, that we find more and more evidence of their existence in many key cellular processes, for instance the p53 response to DNA damage [1, 2], or the dynamics of key transcription factors such as NF-kB [3, 4].

Amanda S. Coutts and Louise Weston (eds.), *Cell Cycle Oscillators: Methods and Protocols*, Methods in Molecular Biology, vol. 1342, DOI 10.1007/978-1-4939-2957-3_3,

Cell reproduction cycles, circadian rhythms and seasonal clocks in plants are all examples of combined time and signal dependent modulation of cellular function regulation, which result in the concerted activation or repression of genes responsible for periodical phenotypical expression.

Oscillatory behaviors are complex to understand. One of the very first and simplest oscillators, the Lotka self-catalytic module, which was originally discovered and analyzed in 1920 [5], couples two chemical reactions involving just two species, yet it gives rise to a type of dynamical behavior that could hardly be predicted by other means than via simulation of a model. By their very time-dependent essence, oscillators escape classical equilibrium analysis, as they never rest in a steady state, and reveal sensitivities that can account for distinct types of system responses. Both frequency and amplitude of oscillating effectors may be crucial in exerting regulation upon a biological phenomenon as information can be coded in either or both frequency and amplitude of a biological oscillation.

The reasons for such rich behaviors of oscillators are rooted in the existence of nonlinear relationships among variables. Nonlinearity is a general concept in systems theory, which essentially provides for generating response outputs that are not proportional to the input variables. In the absence of nonlinear relations among variables, a system can only provide outputs that satisfy the superposition principle; changes in the input would be mapped into proportional variations of the output, which implies that oscillations could only be relayed but not be generated. When the relations among variables involve nonlinearities, the analysis of the possible system behaviors soon becomes complex. Mathematical models of nonlinear systems are comparatively much easier to build than to solve. They are hardly tractable from an analytical viewpoint, and call for the deployment of approximated numerical and/or simulation techniques.

The rest of this review paper is organized as follows. In Subheading 2 we focus on cell cycle computational model based research, with a short historical perspective that accounts for the evolution of the field, and then discuss the main modeling approaches that have been deployed.

In Subheading 3 we review the most influential models of the cell cycle, which in a sense are distilling the knowledge gained by decades of computational modeling in the field. As it always happens in biology, every subsystem connects to the whole systems in a number of ways, the machinery regulating cell cycle oscillations does not escape the rule. In this same section we review some of the many interactions that cell cycle oscillator components have with other periodically regulated cellular functions. Conclusions and perspectives for future research are provided in Subheading 4.

2 Cell Cycle Modeling

Cell cycle oscillating phenomena are not an exception to the above-mentioned complexity, and their study has largely benefited from computational approaches based on the definition and simulation of mathematical models. In the decades from the 1960s to the 1980s, yet before the molecular interactions that sustain the cyclic behavior were explored, models were developed [6–14] that attempted to explain, at a phenomenological level, the experimentally observed correlation between cell cycle and cell size.

Later on, extensive experimental work on model organisms began to unveil the details of the intracellular network generating the oscillating behavior of cyclins and cyclin-dependent kinases. This information fostered new modeling efforts aimed at understanding a growing set of intertwined molecular interactions that, through positive and negative feedback, generate bistability, hysteretic switches, and cyclic behaviors. A number of computational models were developed, in particular for the cell cycle of budding yeast *Saccharomyces cerevisiae* [15–18], fission yeast *Schizosaccharomyces pombe* [19–26], and Xenopus frog embryos [27–29]. Models for the cell cycle of embryonic cells of the fruit fly *Drosophila melanogaster* [30] and of the sea urchin [31] were also built. The modeling of the mammalian cell cycle is a complex task, due to the many regulatory mechanisms that control cell reproduction in complex organisms. Nevertheless, many different aspects of the cell cycle in mammals have been the subject of computational modeling studies; *see* for instance [32–45].

Various approaches to the mathematical modeling of the interactions among the molecular components of the cell cycle network have been used, each one using a different abstraction level. We succinctly explain in Fig. 1 the main concepts of the three main modeling methods, namely Boolean, Continuous-Deterministic, and Discrete-Stochastic, and the outputs provided by their computationally implemented versions. A common requirement for all the modeling methods is that they must be able to provide a prediction of the dynamics of the system over time.

A quick look at the mathematical approaches applied for the computational modeling of the cell cycle reveals that continuous-deterministic techniques have been the first choice tools. Quite obviously, when dealing with nonlinearity, limit cycles and switches, the mathematics of differential equations comes in straightforwardly, with its rich set of simulation and analysis techniques. In the continuous-deterministic setting, the variables of interest are the concentrations of species (*see* Fig. 1b), and their time evolution is modeled through the effect that the interactions among species have on the derivatives of the concentrations [49, 50].

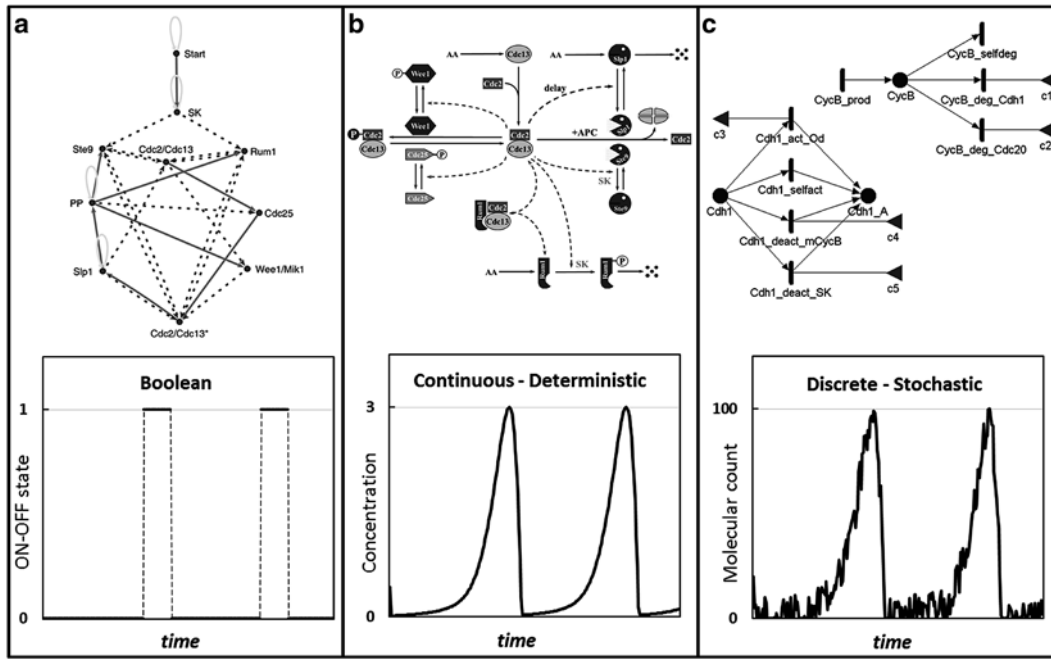

Fig. 1 Computational and mathematical methods used for cell cycle oscillator modeling. (**a**) Boolean models consider how various proteins activate (*solid*) or inhibit (*dashed)* each other (adapted from ref. [46]). Each molecule can be in either active (1) or inactive (0) forms and transitions between these driven by regulators. Simulations (*bottom*) show how each molecule switches between the two states. (**b**), Ordinary Differential Equation models (adapted from ref. [47]) consider the continuous transitions between states (*solid arrows*) driven by regulator molecules (*dashed*) in a deterministic form, capturing the average cell behavior by simulating changes in the concentration of each form. (**c**) Various stochastic methods can be used to follow the changes in molecule numbers and the noise observed in individual cells. The notation of the wiring corresponds to the Petri-Net formalism (adapted from ref. [48])

When constructing a model of a system's dynamics, a continuous-deterministic model is just one of the possible interpretations, mostly used to capture the average behavior of cells. In those cases when the molecular noise plays a role in determining the emerging behavior of the oscillatory system, discrete-stochastic modeling methods can provide additional information, which is not necessarily captured by continuous-deterministic abstractions built upon the same knowledge base. In a discrete-stochastic interpretation, variables are integer molecular counts (*see* Fig. 1c), and interactions among species are rendered as reactions with integer stoichiometry, which occur at random times. Thanks to the many available implementations of the stochastic simulation algorithm of Gillespie [51], many models-based studies of the cell-cycle regulatory networks have been conducted [48, 52–57]. Stochasticity has been considered as well in the continuous setting to model molecular noise by Langevin equations, whereby random terms are directly added to the differential equations [53, 58].

On the other hand, when the focus of the research is on understanding the properties of the dynamics that are determined by the structure (topology) of the interaction network rather than by the kinetics of the reactions, other interpretations based on Boolean modeling techniques become of interest [46, 59, 60]. In a Boolean model, time progression is abstracted as stepwise increments, and the state of a molecule is abstractly represented by a binary variable, whose two possible values can be used to model two distinct behaviors, for instance when the molecule is phosphorylated and active, or unphosphorylated and inactive (*see* Fig. 1a). The transition between states is determined by the values taken by Boolean functions, which depend on the states of interacting molecules and are evaluated at the discrete time steps.

No matter which angle was taken at the time of implementing the model, the process of identifying the involved entities and their interactions always resulted in a refinement and systematization of the biological knowledge. Because they must be executable on a computing system, by their very nature computational models are not ambiguous, and require a complete specification of the biochemical transformations in mathematical or logical terms. This means that each phenomenon, such as a repression or activation, which has a clear semantic for biologists, needs to be detailed in terms of molecular interactions. Consequently, model definition is an inter-disciplinary activity that sets the ground for gaining new insights into the design of biological systems and requires the interaction of mathematicians, computer scientists, and physicists with the experimental biologists [61].

The objective of building a computational model is twofold: from one side the model provides a precise encoding of the available knowledge about a phenomenon, and on the other one, at least for the class of dynamical models we are considering in this context, it allows generating predictions about system evolution over time. When these predictions can reproduce experimentally observed behaviors, the model is valid, and its predictions can be extended to scenarios that have not been explored before. Hence, a valid model allows rapidly conducting in-silico experiments, analyzing what-if scenarios, simulating conditions that could hardly be run or that would be very costly in the wet-lab. Moreover, the obtained insights about system behavior can drive additional experimental work, to verify specific aspects or to dig into areas that require refining biological knowledge. Furthermore, models that cannot be validated, i.e., cannot reproduce parts of the experimentally observed behaviors, are also conductive to additional experimental work, in that they are usually pointing out limitations of the available knowledge. These all reflect to the famous quote by George EP Box “all models are wrong, but some are useful”, which underlines that models just represent the summary of our current knowledge and when they fail then the problem is with our current knowledge, not with the model itself.

Computational modeling studies of the cell cycle have been instrumental in providing many insights about the intricacies of oscillatory behavior and the regulatory effects exerted by external environmental and cellular processes. Especially, significant advances have been obtained in those circumstances when computational modeling progressed hand-in-hand with experimental research in the lab. For instance, the group of Béla Novák and John J. Tyson, which has been working for the last 30 years on cell cycle modeling with the support of the team of experimentalists led by Fred Cross, was able to propose many hypotheses about the design principles of the cell cycle oscillator, which were lately proved by experiments. For instance, the bistability features of the Cdk control system [16, 29], the existence of a dedicated switch point controlling the entry into the DNA synthesis phase of the cycle in *Saccharomyces cerevisiae* [15], and interactions with yet unobserved species [18], were all predicted through the definition and analysis of computational models of the cell cycle. The group of James Ferrell also contributed to our knowledge on cell cycle regulation by combining theory and modeling [28, 62, 63]. Recent results from other interactions between theorists and experimentalists have led to further new results that help us to understand the dynamical features of cell cycle oscillations.

3 Models of Cell Cycle Oscillators

Oscillations can be generated in various ways. The simplest, and in engineering the most used version, is the ring oscillator, whereby processes activate or inhibit each other in a cyclical manner (Fig. 2). Indeed the transcriptional waves of the cell cycle were associated with such a system [64].

Activation of genes that regulate a specific cell cycle stage or transition is induced by specific transcription factors. The yeast cell cycle regulatory transcription factors are connected in a way that one transcription factor induces the next one in the cycle, which induces the following one, until they close the loop of the cell cycle [65]. These oscillations are autonomous; they can run even in a cell cycle block, when the core Cdk control system is halted, whereas in normal circumstances the period of the transcriptional oscillations is controlled by the Cdk regulatory module [66]. These transcriptional waves were also subjects of modeling approaches [67, 68].

Similarly, a loop of transcriptional repressors can induce oscillations as it has been showed by synthetic construction of a three transcription factor loop called *repressilator* [69] (Fig. 2). Combination of positive and negative effects in a loop can also induce oscillation, the necessary criteria is that the loop should have an odd number of negative signs and cause enough delay to allow the active forms to reach a critical level (Fig. 2). Indeed one of the

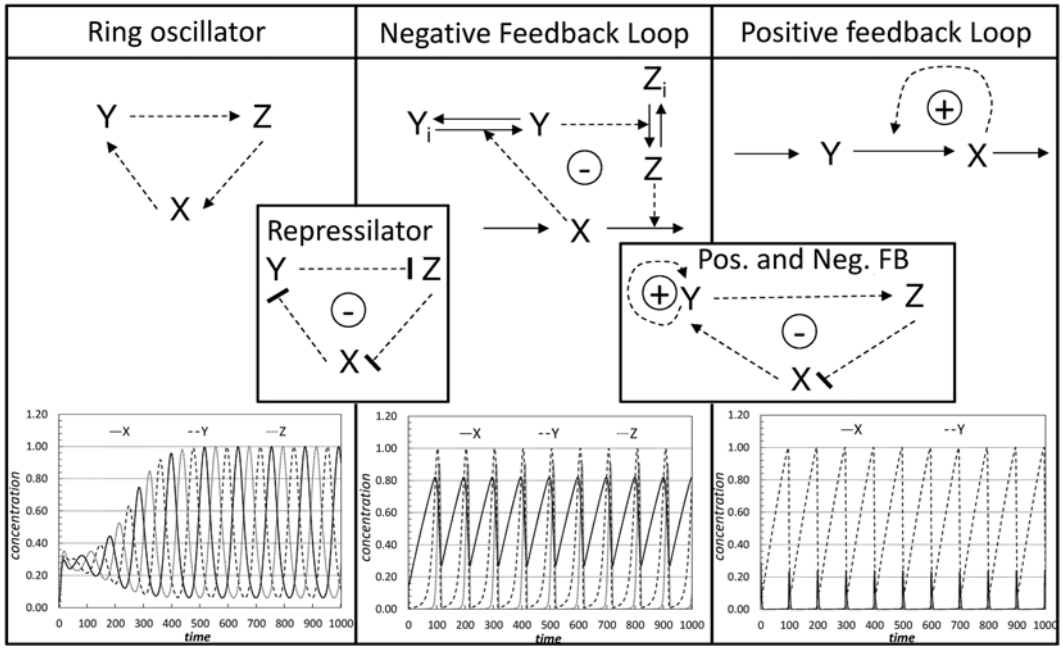

Fig. 2 Regulatory networks that can create oscillations. In ring oscillators each component activates the next component closing on a loop where activatory waves follow each other. Negative feedback loops also contain a ring, but the signs of the interactions could be both negative and positive, the crucial point is that an odd number of negative interactions and a long enough loop are needed for oscillations. The repressilator is a special type of negative feedback loop that inherited concepts of a ring oscillator from engineering. Oscillations are also possible with positive feedback and substrate depletion, where a substrate (Y) is totally used up by an autocatalytic reaction and the active (X) form is unstable. Positive and negative feedbacks can be combined, leading to the most robust oscillators

earliest models of cell cycle regulation is based on a three component negative feedback loop where Cdk is activated by a cyclin, which is destroyed by a protease that was activated by Cdk [70].

Positive feedback can also lead to oscillations, in the case where the autocatalytic reactions lead to the depletion of the substrate of the autocatalytic reaction (Fig. 2). An alternative model of the Cdk-cyclin oscillations was proposed by Tyson [71], where the fast, autocatalytic transition from inactive to active Cdk leads to the depletion of the inactive form and at the same time induces the degradation of the active form. Thus, in the 1990s, the core Cdk oscillations were explained by both positive and negative feedback oscillations. By now we have learned that the combination of positive and negative feedback loops can lead to the most robust cell cycle oscillations [62] and indeed these might stand in the core of most cell cycle oscillators [50, 72]. It is still a controversial question whether normal cell cycles run as a limit cycle or the system moves between steady states as it passes through cell cycle transitions. In the case of embryonic cell cycles the system might be indeed

free-running, without checkpoints being activated, although the importance of positive feedbacks and hysteresis have been first predicted [27], and later experimentally shown in *Xenopus* embryonic cycles [28]. Similarly, the importance of positive feedback in the stabilization of cell cycle stages and the irreversibility in the transitions between them, have been proposed following theoretical considerations [73] and later proved experimentally [74].

Probably the most influential cell cycle model (known in the community as 'Chen model') is the result of the computational modeling work on the Start (G1 to S) and Finish (M to G1) transitions of the budding yeast cell cycle. The very first model, focusing on the Start transition, was published in 2000 [15]. Predictions from this work were experimentally tested and the model adjusted to fit new data in 2002 [16]. Finally, this Start model was extended with the molecular regulatory network controlling mitotic exit in 2004 [17]. The final version of Chen's model is able to account for several physiological observations on wild type and on 132 mutant strains at various growth conditions [17]. The relevance of this result is backed up by the rigorous process used in model definition: the values assigned to a basic parameter set were solely determined to fit wild type behavior; simulating the behavior of mutants only requires changing the parameters of the reactions that get perturbed in the corresponding mutation. Based on this model and on models of fission yeast [23] and mammalian [34] cell cycles, a generic model of eukaryotic cell cycle regulation was created [50]. This model could capture the similarities and differences between the cell cycle control of the key eukaryotic test organisms. This model was later used as a starting point for investigations of cell cycle coupling to other processes [1, 58].

We have already discussed that the transcriptional oscillations and the core Cdk oscillations can be uncoupled and both can run autonomously [66]. There are other periodic processes connected to the cell cycle that could oscillate even when uncoupled from the core cell cycle machinery [75]. The transcriptional and centrosome duplication cycles can be uncoupled from the Cdk activity cycles, similarly to the recently discovered oscillations in the localization of a major cell cycle regulator phosphatase Cdc14 [76, 77]. In normal conditions all of these oscillators are tightly coupled to the oscillations in Cdk activity, but can also feed back and slow down or halt the Cdk cycles in case there is a failure in these loops. Similar coupling connects the cell cycle oscillator to other periodic processes such as the circadian clock and metabolic oscillations [78, 79]. Various modeling approaches were established to investigate the importance and selective advantage of such coupling between the core and auxiliary cell cycle and related oscillators [75, 80], but there is still a long way ahead until we will understand and will be able to control the complex oscillatory network that controls the cell division cycle.

4 Conclusions and Future Perspectives

We know more and more about the molecular regulatory networks that control the cell division cycle. A detailed map of the cell cycle regulatory network of yeast is available [72] and cell cycle controlling pathways in mammals are also characterized in fine detail [81, 82].

However, this increasing knowledge is also setting new challenges for the computational biology community. First of all, there is the necessity to develop tools that can deal with such large amount of data. The promise of computational and systems biology is the ability to integrate data coming from the different omics into coherent representations of biological processes. Moreover, we know that the cell cycle behavior emerges from the interaction of many biological processes and is influenced by the availability of nutrients and by the presence of physical factors, such as light radiation. Therefore, we also need to be able to combine various existing models of the core systems to reach a global model that can capture and successfully predict all the dynamical details of cell cycle oscillators. Such an integration calls for the development of hybrid modeling techniques, whereby continuous representations of parts of the system can be effectively included into more detailed models of molecular interactions built at a discrete-stochastic level.

Another key area of research has to do with the availability of reliable data that can be used to quantitatively characterize cellular phenomena. Molecular counts, volumes, and reaction kinetics are all input data to predictive models. Their quality determines the predictive ability of models. Historically, experimental biology has been more a qualitative than a qualitative science. This is somehow changing, thanks to the appearance of single cell measurement techniques, which allow measuring concentrations and even molecular counts avoiding the averaging effects of traditional techniques.

There is a long way to go in developing a complete predictive model of the cell cycle, which could account for the many factors that influence cell reproduction. The availability of such a predictive model would have profound impact on health research. In the mammalian system, it would aid cancer research as, at the single cell level, defects of the cell cycle control system lie at the core of cancerous proliferation [83].

References

1. Toettcher JE, Loewer A, Ostheimer GJ, Yaffe MB, Tidor B, Lahav G (2009) Distinct mechanisms act in concert to mediate cell cycle arrest. Proc Natl Acad Sci U S A 106(3):785–790. doi:10.1073/pnas.0806196106
2. Liu B, Bhatt D, Oltvai ZN, Greenberger JS, Bahar I (2014) Significance of p53 dynamics in regulating apoptosis in response to ionizing radiation, and polypharmacological strategies, Sci Rep 4, Article number: 6245 doi:10.1038/srep06245
3. Ihekwaba AE, Broomhead DS, Grimley R, Benson N, White MR, Kell DB (2005) Synergistic control of oscillations in the NF-kappaB signalling pathway. Syst Biol (Stevenage) 152(3):153–160

4. Mengel B, Hunziker A, Pedersen L, Trusina A, Jensen MH, Krishna S (2010) Modeling oscillatory control in NF-κB, p53 and Wnt signaling. Curr Opin Genet Dev 20(6):656–664. doi:10.1016/j.gde.2010.08.008
5. Lotka AJ (1920) Undamped oscillations derived from the law of mass action. J Am Chem Soc 42:1595–1599
6. Prescott DM (1956) Relation between growth rate and cell division. III. Changes in nuclear volume and growth rate and prevention of cell division in Amoeba proteus resulting from cytoplasmic amputations. Exp Cell Res 11:94–98
7. Brooks RF, Bennett DC, Smith JA (1980) Mammalian cell cycles need two random transitions. Cell 19:493–504
8. Castor LN (1980) A G1 rate model accounts for cell-cycle kinetics attributed to 'transition probability'. Nature 287:857–859
9. Koch AL, Schaechter M (1962) A model for statistics of the cell division process. J Gen Microbiol 29:435–454
10. Koch AL (1980) Does the variability of the cell cycle result from one or many chance events? Nature 286:80–82
11. Shields R (1977) Transition probability and the origin of variation in the cell cycle. Nature 267:704–707
12. Smith JA, Martin L (1973) Do cells cycle? Proc Natl Acad Sci U S A 70:1263–1267
13. Tyson JJ (1983) Unstable activator models for size control of the cell cycle. J Theor Biol 104:617–631
14. Tyson JJ, Hannsgen KB (1986) Cell growth and division: a deterministic/probabilistic model of the cell cycle. J Math Biol 23:231–246
15. Chen KC, Csikasz-Nagy A, Gyorffy B et al (2000) Kinetic analysis of a molecular model of the budding yeast cell cycle. Mol Biol Cell 11:369–391
16. Cross FR, Archambault V, Miller M et al (2002) Testing a mathematical model for the yeast cell cycle. Mol Biol Cell 13:52–70
17. Chen KC, Calzone L, Csikasz-Nagy A et al (2004) Integrative analysis of cell cycle control in budding yeast. Mol Biol Cell 15:3841–3862
18. Queralt E, Lehane C, Novak B et al (2006) Downregulation of PP2A(Cdc55) phosphatase by separase initiates mitotic exit in budding yeast. Cell 125:719–732
19. Csikasz-Nagy A, Kapuy O, Gyorffy B et al (2007) Modeling the septation initiation network (SIN) in fission yeast cells. Curr Genet 51:245–255
20. Lygeros J, Koutroumpas K, Dimopoulos S et al (2008) Stochastic hybrid modeling of DNA replication across a complete genome. Proc Natl Acad Sci U S A 105:12295–12300
21. Novak B, Tyson JJ (1995) Quantitative analysis of a molecular model of mitotic control in fission yeast. J Theor Biol 173:283–305
22. Novak B, Tyson JJ (1997) Modeling the control of DNA replication in fission yeast. Proc Natl Acad Sci U S A 94:9147–9152
23. Novak B, Csikasz-Nagy A, Gyorffy B et al (1998) Mathematical model of the fission yeast cell cycle with checkpoint controls at the G1/S, G2/M and metaphase/anaphase transitions. Biophys Chem 72:185–200
24. Novak B, Pataki Z, Ciliberto A et al (2001) Mathematical model of the cell division cycle of fission yeast. Chaos 11:277–286
25. Sveiczer A, Csikasz-Nagy A, Gyorffy B et al (2000) Modeling the fission yeast cell cycle: quantized cycle times in wee1-cdc25Delta mutant cells. Proc Natl Acad Sci U S A 97:7865–7870
26. Vasireddy R, Biswas S (2004) Modeling gene regulatory network in fission yeast cell cycle using hybrid petri nets. In: Neural information processing. Springer, Berlin, pp 1310–1315
27. Novak B, Tyson JJ (1993) Numerical analysis of a comprehensive model of M-phase control in Xenopus oocyte extracts and intact embryos. J Cell Sci 106(Pt 4):1153–1168
28. Pomerening JR, Sontag ED, Ferrell JE (2003) Building a cell cycle oscillator: hysteresis and bistability in the activation of Cdc2. Nat Cell Biol 5:346–351. doi:10.1038/ncb954
29. Sha W, Moore J, Chen K et al (2003) Hysteresis drives cell-cycle transitions in Xenopus laevis egg extracts. Proc Natl Acad Sci U S A 100:975–980
30. Calzone L, Thieffry D, Tyson JJ et al (2007) Dynamical modeling of syncytial mitotic cycles in Drosophila embryos. Mol Syst Biol 3:131
31. Ciliberto A, Tyson JJ (2000) Mathematical model for early development of the sea urchin embryo. Bull Math Biol 62:37–59
32. Hatzimanikatis V, Lee KH, Bailey JE (1999) A mathematical description of regulation of the G1-S transition of the mammalian cell cycle. Biotechnol Bioeng 65:631–637
33. Kohn KW (1998) Functional capabilities of molecular network components controlling the mammalian G1/S cell cycle phase transition. Oncogene 16:1065–1075
34. Novak B, Tyson JJ (2004) A model for restriction point control of the mammalian cell cycle. J Theor Biol 230:563–579
35. Pfeuty B, David-Pfeuty T, Kaneko K (2008) Underlying principles of cell fate determination during G1 phase of the mammalian cell cycle. Cell Cycle 7:3246–3257

36. Qu Z, Weiss JN, MacLellan WR (2003) Regulation of the mammalian cell cycle: a model of the G1-to-S transition. Am J Physiol Cell Physiol 284:C349–C364
37. Swat M, Kel A, Herzel H (2004) Bifurcation analysis of the regulatory modules of the mammalian G1/S transition. Bioinformatics 20:1506–1511
38. Singhania R, Sramkoski RM, Jacobberger JW, Tyson JJ (2011) A hybrid model of mammalian cell cycle regulation. PLoS Comput Biol 7(2):e1001077
39. Alfieri R, Barberis M, Chiaradonna F, Gaglio D, Milanesi L, Vanoni M, Klipp E, Alberghina L (2009) Towards a systems biology approach to mammalian cell cycle: modeling the entrance into S phase of quiescent fibroblasts after serum stimulation. BMC Bioinform 10(Suppl 12):S16. doi:10.1186/1471-2105-10-S12-S16
40. Conradie R, Bruggeman FJ, Ciliberto A, Csikász-Nagy A, Novák B, Westerhoff HV, Snoep JL (2010) Restriction point control of the mammalian cell cycle via the cyclin E/Cdk2:p27 complex. FEBS J 277(2):357–367. doi:10.1111/j.1742-4658.2009.07473.x
41. Kapuy O, He E, Uhlmann F, Novák B (2009) Mitotic exit in mammalian cells. Mol Syst Biol 5:324. doi:10.1038/msb.2009.86
42. Haberichter T, Mädge B, Christopher RA, Yoshioka N, Dhiman A, Miller R, Gendelman R, Aksenov SV, Khalil IG, Dowdy SF (2007) A systems biology dynamical model of mammalian G1 cell cycle progression. Mol Syst Biol 3:84. doi:10.1038/msb4100126
43. Gérard C, Goldbeter A (2009) Temporal self-organization of the cyclin/Cdk network driving the mammalian cell cycle. Proc Natl Acad Sci U S A 106(51):21643–21648. doi:10.1073/pnas.0903827106
44. Pfeuty B (2012) Strategic cell-cycle regulatory features that provide mammalian cells with tunable G1 length and reversible G1 arrest. PLoS One 7(4):e35291. doi:10.1371/journal.pone.0035291
45. Iwamoto K, Hamada H, Eguchi Y, Okamoto M (2011) Mathematical modeling of cell cycle regulation in response to DNA damage: exploring mechanisms of cell-fate determination. Biosystems 103(3):384–391. doi:10.1016/j.biosystems.2010.11.011
46. Davidich MI, Bornholdt S (2008) Boolean network model predicts cell cycle sequence of fission yeast. PLoS One 3(2):e1672. doi:10.1371/journal.pone.0001672
47. Tyson JJ, Chen KC, Novák B (2001) Network dynamics and cell physiology. Nat Rev Mol Cell Biol 2:908–916. doi:10.1038/35103078
48. Kar S, Baumann WT, Paul MR, Tyson JJ (2009) Exploring the roles of noise in the eukaryotic cell cycle. Proc Natl Acad Sci U S A 106:6471
49. Tyson JJ, Chen KC, Novak B (2003) Sniffers, buzzers, toggles and blinkers: dynamics of regulatory and signaling pathways in the cell. Curr Opin Cell Biol 15(2):221–231. doi:10.1016/S0955-0674(03)00017-6
50. Csikász-Nagy A, Battogtokh D, Chen KC, Novák B, Tyson JJ (2006) Analysis of a generic model of eukaryotic cell-cycle regulation. Biophys J 90(12):4361–4379. doi:10.1529/biophysj.106.081240
51. Gillespie DT (1977) Exact stochastic simulation of coupled chemical reactions. J Phys Chem 81(25):2340–2361. doi:10.1021/j100540a008
52. Sveiczer A, Tyson JJ, Novak B (2001) A stochastic, molecular model of the fission yeast cell cycle: role of the nucleocytoplasmic ratio in cycle time regulation. Biophys Chem 92:1–15. doi:10.1016/S0301-4622(01)00183-1
53. Steuer R (2004) Effects of stochasticity in models of the cell cycle: from quantized cycle times to noise-induced oscillations. J Theor Biol 228:293–301. doi:10.1016/j.jtbi.2004.01.012
54. Mura I, Csikász-Nagy A (2008) Stochastic Petri Net extension of a yeast cell cycle model. J Theor Biol 254:859–860. doi:10.1016/j.jtbi.2008.07.019
55. Palmisano A, Mura I, Priami C (2009) From ODEs to language-based, executable models of biological systems. In: Proceedings of the Pacific Symposium on Biocomputing 14, Kohala Coast, Hawaii, USA, pp 239–250.
56. Ballarini P, Mazza T, Palmisano A, Csikász-Nagy A (2009) Studying irreversible transitions in a model of cell cycle regulation. Electron Notes Theor Comput Sci 232:39–53. doi:10.1016/j.entcs.2009.02.049
57. Csikász-Nagy A, Mura I (2010) Role of mRNA gestation and senescence in noise reduction during the cell cycle. In Silico Biol 10(1):81–88. doi:10.3233/ISB-2010-0416
58. Zámborszky J, Hong CI, Csikász-Nagy A (2007) Computational analysis of mammalian cell division gated by a circadian clock: quantized cell cycles and cell size control. J Biol Rhythms 22:542–553
59. Fauré A, Naldi A, Chaouiya C, Thieffry D (2006) Dynamical analysis of a generic Boolean model for the control of the mammalian cell cycle. Bioinformatics 22(14):e124–e131. doi:10.1093/bioinformatics/btl210
60. Li F, Long T, Lu Y, Ouyang Q, Tang C (2004) The yeast cell-cycle network is robustly designed. Proc Natl Acad Sci U S A 101(14):4781–4786. doi:10.1073/pnas.0305937101

61. Kitano H (2002) Computational systems biology. Nature 420(6912):206–210. doi:10.1038/nature01254
62. Tsai TYC, Choi YS, Ma W, Pomerening JR, Tang C, Ferrell JR (2008) Robust, tunable biological oscillations from interlinked positive and negative feedback loops. Science 321(5885):126–129. doi:10.1126/science.1156951
63. Santos SDM, Ferrell JE (2008) Systems biology: on the cell cycle and its switches. Nature 454:288–289. doi:10.1038/454288
64. Simmons Kovacs LA, Orlando DA, Haase SB (2008) Transcription network and cyclin/CDKs: the yin and yang of cell cycle oscillators. Cell Cycle 7(17):2626–2629. doi:10.4161/cc.7.17.6515
65. Orlando DA, Lin YC, Bernard A, Wang JY, Socolar JES, Iversen ES, Hartemink AJ, Haase SB (2008) Global control of cell-cycle transcription by coupled CDK and network oscillators. Nature 453:944–947. doi:10.1038/nature06955
66. Simmons LA, Kovacs LA, Mayhew MB, Orlando DA, Jin Y, Li Q, Huang C, Reed SI, Mukherjee S, Haase SB (2012) Cyclin-dependent kinases are regulators and effectors of oscillations driven by a transcription factor network. Mol Cell 45(5):669–679. doi:10.1016/j.molcel.2011.12.033
67. Sevim V, Gong X, Socolar JES (2010) Reliability of transcriptional cycles and the yeast cell-cycle oscillator. PLoS Comput Biol 6(7):e1000842. doi:10.1371/journal.pcbi.1000842
68. Sriram K, Bernot G, Képès F (2007) A minimal mathematical model combining several regulatory cycles from the budding yeast cell cycle. IET Syst Biol 1(6):326–341. doi:10.1049/iet-syb:20070018
69. Elowitz MB, Leibler S (2000) A synthetic oscillatory network of transcriptional regulators. Nature 403:335–338. doi:10.1038/35002125
70. Goldbeter A (1991) A minimal cascade model for the mitotic oscillator involving cyclin and cdc2 kinase. Proc Natl Acad Sci U S A 88(20):9107–9111. doi:10.1073/pnas.88.20.9107
71. Tyson JJ (1991) Modeling the cell division cycle: cdc2 and cyclin interactions. Proc Natl Acad Sci U S A 88(16):7328–7332. doi:10.1073/pnas.88.16.7328
72. Kazunari K, Samik G, Yukiko M, Hisao M, Yuki S-Y, Hiroaki K (2010) A comprehensive molecular interaction map of the budding yeast cell cycle. Mol Syst Biol 6:1. doi:10.1038/msb.2010.73
73. Novak B, Tyson JJ, Gyorffy B, Csikasz-Nagy A (2007) Irreversible cell-cycle transitions are due to systems-level feedback. Nat Cell Biol 9:724–728. doi:10.1038/ncb0707-724
74. López-Avilés S, Kapuy O, Novák B, Uhlmann F (2009) Irreversibility of mitotic exit is the consequence of systems-level feedback. Nature 459:592–595. doi:10.1038/nature07984
75. Oikonomou C, Cross FR (2010) Frequency control of cell cycle oscillators. Curr Opin Genet Dev 20(6):605–612. doi:10.1016/j.gde.2010.08.006
76. Lu Y, Cross FR (2010) Periodic cyclin-Cdk activity entrains an autonomous Cdc14 release oscillator. Cell 141(2):268–279. doi:10.1016/j.cell.2010.03.021
77. Manzoni R, Montani F, Visintin C, Caudron F, Ciliberto A, Visintin R (2010) Oscillations in Cdc14 release and sequestration reveal a circuit underlying mitotic exit. J Cell Biol 190(2):209–222. doi:10.1083/jcb.201002026
78. Matsuo T, Yamaguchi S, Mitsui S, Emi A, Shimoda F, Okamura H (2003) Control mechanism of the circadian clock for timing of cell division in vivo. Science 302(5643):255–259. doi:10.1126/science.1086271
79. Klevecz RR, Bolen J, Forrest G, Murray DB (2003) A genomewide oscillation in transcription gates DNA replication and cell cycle. Proc Natl Acad Sci U S A 101(5):1200–1205. doi:10.1073/pnas.0306490101
80. Mirollo RE, Strogatz SH (1990) Synchronization of pulse-coupled biological oscillators. SIAM J Appl Math 50(6):1645–1662. doi:10.1137/0150098
81. Kanae O, Yukiko M, Akira F, Hiroaki K (2005) A comprehensive pathway map of epidermal growth factor receptor signaling. Mol Syst Biol 1:1. doi:10.1038/msb4100014
82. Laurence C, Amélie G, Andrei Z, François R, Emmanuel B (2008) A comprehensive modular map of molecular interactions in RB/E2F pathway. Mol Syst Biol 4:1. doi:10.1038/msb.2008.7
83. Malumbres M, Barbacid M (2009) Cell cycle, CDKs and cancer: a changing paradigm. Nat Rev Cancer 9:153–166. doi:10.1038/nrc2602

Chapter 4

E2F Transcription Factors Control the Roller Coaster Ride of Cell Cycle Gene Expression

Ingrid Thurlings and Alain de Bruin

Abstract

Initially, the E2F transcription factor was discovered as a factor able to bind the adenovirus E2 promoter and activate viral genes. Afterwards it was shown that E2F also binds to promoters of nonviral genes such as *C-MYC* and *DHFR*, which were already known at that time to be important for cell growth and DNA metabolism, respectively. These findings provided the first clues that the E2F transcription factor might be an important regulator of the cell cycle. Since this initial discovery in 1987, several additional E2F family members have been identified, and more than 100 targets genes have been shown to be directly regulated by E2Fs, the majority of these are important for controlling the cell cycle.

The progression of a cell through the cell cycle is accompanied with the increased expression of a specific set of genes during one phase of the cell cycle and the decrease of the same set of genes during a later phase of the cell cycle. This roller coaster ride, or oscillation, of gene expression is essential for the proper progression through the cell cycle to allow accurate DNA replication and cell division. The E2F transcription factors have been shown to be critical for the temporal expression of the oscillating cell cycle genes.

This review will focus on how the oscillation of E2Fs and their targets is regulated by transcriptional, post-transcriptional and post-translational mechanism in mammals, yeast, flies, and worms. Furthermore, we will discuss the functional impact of E2Fs on the cell cycle progression and outline the consequences when E2F expression is disturbed.

Key words E2F transcription factors, Cell cycle, Oscillation, Gene expression, RB/E2F pathway

1 Introduction

Quiescent cells are able to enter the cell cycle in G1-phase upon proper mitogenic stimulation (Fig. 1). Growth factors activate the RB/E2F-pathway, an important pathway for cell cycle progression, by stimulating G1-Cyclins and Cyclin-dependent kinases (CDKs) to form complexes. Activated Cyclin-CDK complexes will phosphorylate Rb-family members (RB, p107, p130), which are bound to E2Fs. Hyperphosphorylation of Rb-family members is the point of no return in the cell cycle, committing the cell to a full cycle of DNA replication and cell division. It leads to a conformational change of RB, releasing E2Fs from the complex.

Amanda S. Coutts and Louise Weston (eds.), *Cell Cycle Oscillators: Methods and Protocols*, Methods in Molecular Biology, vol. 1342, DOI 10.1007/978-1-4939-2957-3_4,

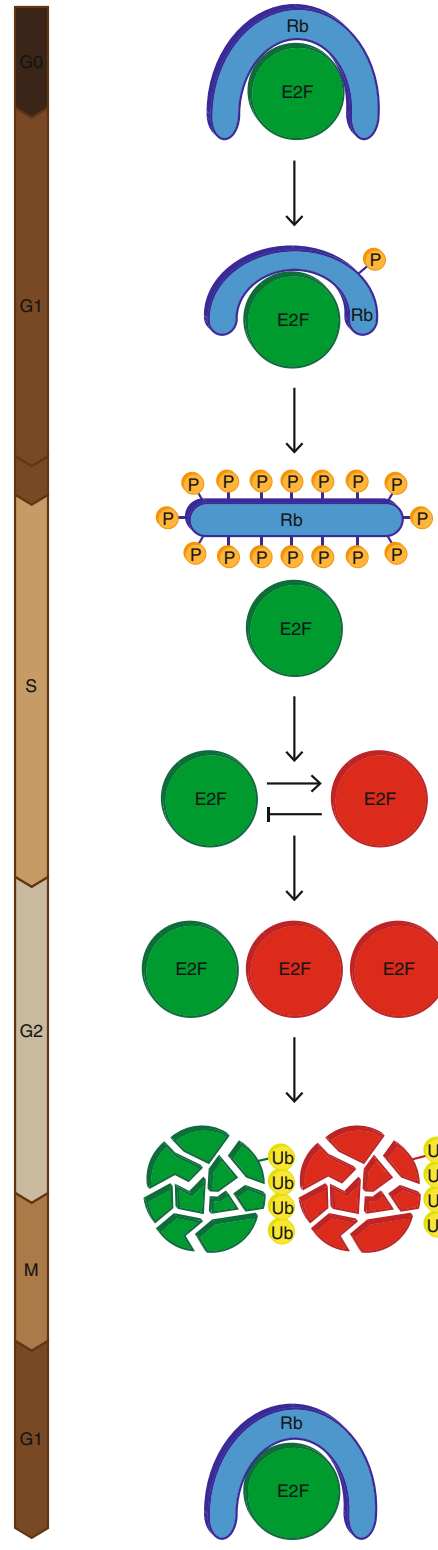

Fig. 1 The pRb/E2F pathway is activated by growth signals when a cell enters a new round of the cell cycle. Cyclin D-CDK4/6-complexes phosphorylate Rb-family members, leading to release of activator E2Fs and progression into S-phase. Activated repressor E2Fs bring down the levels of activator E2Fs, guiding the cells to G2-phase and mitosis, when the transcription factors are degraded

The accumulation of free activating E2Fs leads to increased expression of their target genes. Activating E2Fs mainly bind to promoters of genes that are important for S-phase progression leading to the initiation of DNA replication [1–4]. This critical upswing of S-phase gene expression is followed by a downswing and is induced by the action of atypical E2Fs, the newest members of the mammalian family of E2F transcription factors, which are induced by activator E2Fs [5–11]. This mechanism of transcriptional repression to shut down S-phase gene expression during late S- and G2-phase is most likely required for the timely progression through G2–M; however, experimental evidence is still lacking.

In addition to downregulating S-phase gene expression, atypical E2Fs repress classical E2F activators during G2, creating a direct negative feedback-loop to control the oscillating expression pattern of E2F target genes. Interestingly, atypical E2Fs also repress their own transcriptional activity [10, 11], providing a second negative feedback-loop, most likely to guarantee the repressive activity has been shut down before a cell starts the next cell cycle. A posttranslational mechanism has been identified on top of the transcriptional mechanism to induce degradation of S-phase proteins during G2–M, for example through the SCF-SKP2 complex in G2-phase, or anaphase-promoting complex or cyclosome (APC/C) mediated degradation from anaphase onwards [12–14]. Together these findings demonstrate that a complex mechanism exists to control the roller coast ride of E2F target gene expression during the cell cycle.

2 Regulation of Oscillating E2F Target Gene Expression in Mammals

Proper oscillating E2F target gene expression is vital for cell cycle progression. Their altered expression can have detrimental consequences for the cell, such as speeding up or slowing down the cell cycle. In some occasions, it can even result in a cell cycle arrest or apoptosis, for example when the expression of specific members of the E2F family is altered.

The mammalian E2F family consists of eight members, which are divided into activators (E2F1–3) and repressors (E2F4–8). E2F1–6 are classical E2Fs, with one DNA-binding domain, and are required to heterodimerize with DP1/DP2 proteins before they can bind target gene promoters and activate or repress their expression. E2F7 and E2F8 are considered as atypical E2Fs. They have two DNA-binding domains, and they can repress target genes independent of DP heterodimerization. Instead, they can form homodimers and heterodimers with each other [10, 15, 16].

The protein expression of the activator E2F1–3 increases in G1, peaks during S, and decreases in G2-phase [17]. RB blocks the

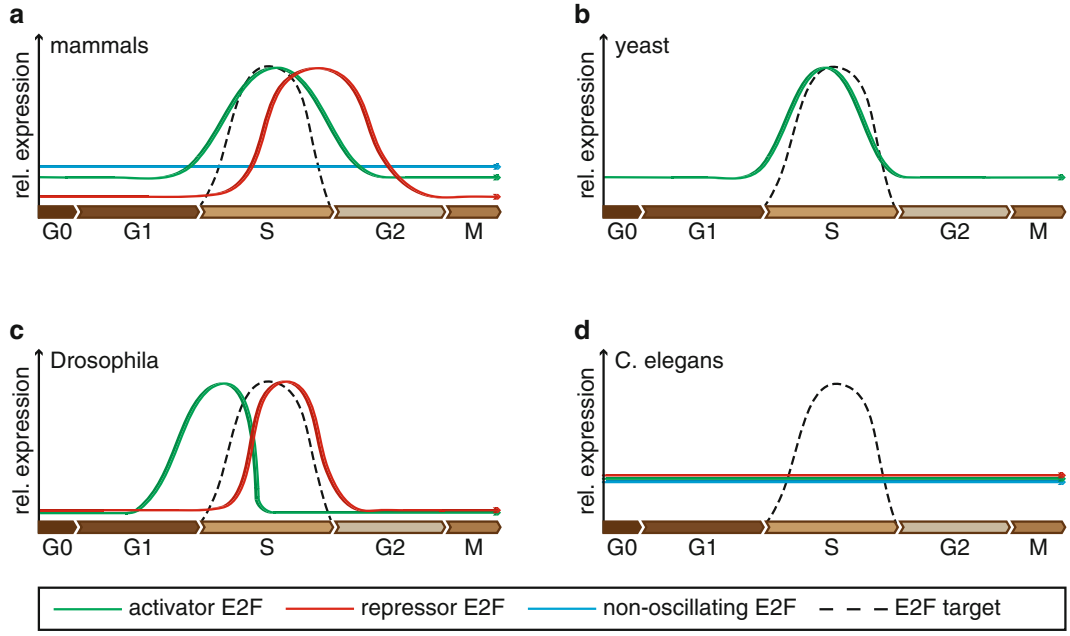

Fig. 2 E2F expression patterns. (**a**) The mammalian E2F family consists of activator, repressor, and non-oscillating E2Fs. (**b**) Yeast contains one oscillating, activator E2F. (**c**) The *Drosophila* E2F family consists of an activator and a repressor E2F, both E2Fs are oscillating. (**d**) The *C. elegans* E2F family consists of three members, all of which are non-oscillating

transcriptional activity of the activator E2Fs in G1 through the occupation of their transactivation domain. The RB-E2F complex dissociates upon RB hyperphosphorylation, and activation of E2F target gene expression starts, followed by entry into S-phase (Fig. 2a) [2, 18, 19].

The individual loss of E2F1, E2F2, or E2F3 has minor effects on the target gene expression and the cell cycle progression. Cells have a lengthened S-phase, but keep proliferating (*see* Table 1) [20–26]. However, the combined loss of E2F1–3 abolishes the possibility for mouse embryonic fibroblasts to enter S-phase and proliferate (*see* Table 1). This loss triggers a p53-p21^{Cip1} response and leads to a G1-phase arrest. However, as long as there is still one functional allele of one of the three activators, cells are able to continue through the cell cycle. These findings demonstrate a clear redundancy between the activating E2Fs [27, 28]. Remarkably, the requirement of E2F1–3 for cell cycle progression appears to be cell type specific, as deletion of the activator E2Fs has no effect on cell cycle progression in epithelial stem cells and lens progenitor cells. Nevertheless, the lens progenitor cells deficient for E2F1–3 display increased expression of cell cycle regulated genes, high levels of DNA damage and an activated p53-pathway, leading to massive apoptosis later in development, suggesting that E2F1–3 function as transcriptional repressors in stem cells most likely via

Table 1
Impact of altering E2F expression: deletion

	Oscillation	Level	Cell cycle progression	Cell fate	Reference
E2F1	No effect	No effect	Lengthened S-phase	No effect	[20–22]
E2F2	Earlier upswing	Increased	Enhanced S-phase	Hyper-proliferation	[23–25]
E2F3	Delayed upswing	Decreased	Lengthened S-phase	Apoptosis	[21, 26]
E2F1–3	No upswing	Decreased	G1-phase arrest	Apoptosis, hyperploidy	[27, 28, 66]
E2F6	No effect	No effect	No effect	No effect	[37]
E2F7	No effect	No effect	No effect	No effect	[10]
E2F8	No effect	No effect	No effect	No effect	[10]
E2F7–8	No downswing	Increased	No effect	Apoptosis	[10]
SBF	Unknown	Decreased	G1-phase arrest	Apoptosis	[39, 41, 43–45]
MBF	Unknown	Decreased	G1-phase arrest	No effect	[39, 41, 45]
dE2F1	No upswing	Decreased	G1-phase arrest	Unknown	[19, 53]
dE2F2	Unknown	Increased	No effect	No effect	[19, 56]
EFL-1	Unknown	Increased	Enhanced S phase	Reduced apoptosis, endoduplication	[58, 59, 61]

their interaction with Rb [18]. The ectopic expression of activator E2Fs is sufficient to bypass upstream signals and drive cells into S-phase (*see* Table 2). When the activator E2F levels remain high after S-phase entry, cells will undergo apoptosis [2, 7, 29]. High levels of activator E2Fs lead to the induction of apoptotic target genes, such as APAF1 and p73, especially in response to DNA damage [2, 30].

E2F4 and E2F5 play important roles in keeping cells in quiescence, the resting phase of the cell cycle (G0). During this time, E2F4 and E2F5 form repressing complexes with the Rb-family members p107 and p130. Their binding to promoters of E2F target genes leads to inhibition of their expression and results in blockage of cell cycle progression. E2F4 and E2F5 are constitutively expressed throughout the cell cycle (Fig. 2a), but their subcellular localization changes during cell cycle progression to regulate their repressing transcriptional activity [31, 32]. In G0 and early G1, E2F4/5 are present in the nucleus to inhibit E2F target gene expression, but upon p107/p130 hyperphosphorylation through enhanced CDK activity during G1, E2F4/5 can be relocated to

Table 2
Impact of altering E2F expression: overexpression

	Oscillation	Level	Cell cycle progression	Cell fate	Reference
E2F1	Unknown	Increased	Enhanced G1-phase	Apoptosis	[2, 7, 29]
E2F2	Unknown	Increased	Induced S-phase entry	No effect	[2, 95]
E2F3	Earlier upswing	Increased	Induced S-phase entry	Hyper-proliferation	[2, 96]
E2F6	Earlier downswing	Decreased	S-phase arrest	Unknown	[37, 97]
E2F7	Earlier downswing	Decreased	During G1: S-phase arrest	Apoptosis	[5, 6, 11]
E2F8	Unknown	Decreased	S-phase arrest	Unknown	[8, 9, 98]
SBF	Unknown	Increased	Enhanced G1/S	Toxic	[46]
MBF	Unknown	No effect	No effect	Toxic	[46]
dE2F1	Unknown	Increased	During G1: induction S phase During S: G1-arrest	Apoptosis	[54]
dE2F2	Unknown	Decreased	No effect	No effect	[19]
EFL-1	Unknown	Unknown	Unknown	Sterility	[61, 99]

the cytoplasm [33]. Experiments in synchronized cell populations have shown that E2F4 is able to repress and activate target genes during the cell cycle, suggesting a more versatile role for this transcription factor than its known function during quiescence [34].

E2F6–8 are transcriptional repressors, and are important for inhibiting the expression of target genes in S/G2-phase, most likely to ensure proper cell cycle progression. Like E2F1–3, the expression of E2F6–8 oscillates during the cell cycle. Since E2F1–3 induce the expression of E2F6–8, the upswing of E2F6–8 expression occurs a couple of hours later compared to the upswing of E2F1–3 expression. E2F6–8 expression peaks at S-G2 and declines during G2–M (Fig. 2a). They appear to function independent of Rb-family members, because they lack the classical pocket protein binding domain [6, 8, 11, 33, 35–37].

The exact role of E2F6 in cell cycle regulation and the effects of the loss or gain of this transcription factor are still unclear (Tables 1 and 2). It has been shown that E2F6 binds to promoters of target genes that are important for G1/S-phase progression during G2/M phase, repressing their expression so the cells can continue the cell cycle [37]. A loss of E2F6 can be compensated by E2F4, since this transcription factor is also able to bind to the same target gene promoters, and co-deletion of both E2F4 and E2F6 leads to a derepression of their target genes during S-phase [35, 37].

Cells lacking both E2F7 and E2F8 continue cycling as well, even though the RNA levels of the E2F target genes are strongly derepressed during S/G2-phase (Table 1). One possible explanation for the continuation of the cell cycle is that other E2F repressors, such as E2F4 or E2F6, can compensate for the loss of E2F7/8 to partially repress E2F target genes [10]. In addition, enhanced production of E2F target protein in response to loss of E2F7/8 will be most likely compensated through enhanced degradation mechanisms during G2/M.

Remarkably, the effects on cell cycle progression of ectopic expression of E2F7 depend on the phase of the cell cycle (Table 2). The induction of E2F7 during G1-phase leads to a strong repression of its target genes involved in DNA replication, metabolism and repair, and to an early S-phase arrest. However, when E2F7 is induced later, during S-G2, cell cycle progression is not disturbed. Prolonged ectopic expression of E2F7 results in DNA damage and apoptosis [11]. Overexpression of E2F8 has been shown to reduce the proliferation rate [9]. However, overexpression studies where E2F8 is induced at different phases of the cell cycle are still missing.

2.1 Regulation of Oscillating E2F Target Gene Expression in Yeast, Flies, and Worms

E2Fs are highly conserved through evolution. This strong conservation of the E2Fs throughout different species allows us to use less complex systems to learn more about the general mechanisms that regulate the oscillating E2F target gene expression pattern.

2.1.1 E2Fs in Yeast

There is a robust functional similarity between the mammalian and yeast E2F proteins, but there is no detectable sequence homology throughout the protein [38]. The budding yeast E2F family consists of two activating proteins, SBF and MBF, which overlap in function. As in mammals, SBF and MBF are present in G1-phase, but they are bound to Whi5, the yeast protein functionally comparable to RB. SBF and MBF are released from its binding partner Whi5 by CDK-dependent hyperphosphorylation of Whi5, and become active in late G1-phase to promote target gene expression and subsequent cell cycle progression into S-phase (Fig. 2b) [38, 39]. SBF and MBF are inactivated in S-G2/M by B-type cyclins. SBF and MBF promote expression of B-type cyclins in late G1, which in turn inhibit the expression of SBF and MBF by phosphorylation [38, 40]. This phosphorylation leads to nuclear export of SBF and MBF [41]. A second level of regulation of MBF target genes is via Nrm1, a G1-target of MBF. This factor can bind MBF and together they form an inhibitory complex, repressing MBF target gene expression [42].

Deletion of SBF or MBF leads to a G1-phase arrest accompanied with a decreased expression of the target genes (Table 1), which can lead to apoptosis [39, 41, 43–45]. Overexpression of SBF or MBF leads to an enhanced G1–S-phase transition and is toxic to the cells (Table 2) [46].

2.1.2 E2Fs in Flies

Compared to mammals, *Drosophila melanogaster* has E2F family members that are both functionally and sequentially more conserved than in yeast. *Drosophila* has two E2F proteins, an activator E2F (dE2F1), with over 65 % sequence homology to human E2F1 in the DNA binding domain and 50 % homology in the RB-interacting domain [47], and a repressor E2F (dE2F2), with a similar level of homology as dE2F1 [48]. The Rb homologue RBF1 is a strong regulator of dE2F1, and is important to limit dE2F1-regulated activation of target genes in G1-phase, similar to its function in mammals [49–51]. dE2F1 accumulates in G1-phase, when RBF1 is phosphorylated and dissociates from the transcription factor. Once the cells progress into S-phase, dE2F1 is rapidly degraded by the $Cul4^{Cdt2}$ E3 ubiquitin ligase, via a PCNA-interacting-protein motif (Fig. 2c) [52].

The loss of dE2F1 leads to a G1-phase arrest, as there is no upswing of the activator target genes to push the cells forward into S-phase (Table 1) [19, 53]. Ectopic expression of dE2F1 in S-phase has effects on the cell in the following cell cycle (Table 2). Cells are unable to enter the next S-phase with continued expression of dE2F1. However, if the ectopic expression is limited to G1, there will be a strong induction of S-phase due to high levels of target genes. A subset of these genes regulates apoptosis, leading cells with high dE2F1 levels to their fate [54].

An important function of dE2F2 is to antagonize the function of dE2F1 through repression of their common E2F target genes. This competition between the activator and repressor E2F is important for cell cycle progression, as the cell cycle progression phenotypes caused by deletion of dE2F1 can be rescued by deletion of dE2F2 [19, 54, 55].

The deletion or overexpression of dE2F2 has no clear effects on the cell cycle (Tables 1 and 2). There is an increase in its target genes when dE2F2 is absent, but without any resulting phenotypes. Ectopic expression of dE2F2 leads to a decrease in target gene expression, but surprisingly also without any effect on cell cycle progression or cell fate [19, 56].

2.1.3 E2Fs in Worms

C. elegans has three E2F transcription factors, namely EFL-1, EFL-2, and the recently identified EFL-3. None of their expression levels appear to be cell cycle regulated (Fig. 2d). E2F proteins in *C. elegans* are important during development, regulating tightly controlled cell divisions redundantly with several regulatory pathways, including the RAS/MAP kinase cascade [57]. EFL-1 shares its structure with mammalian E2F4 and E2F5, its DNA binding domain is highly conserved and the dimerization domains have 38 % homology [58]. This transcription factor acts as a transcriptional repressor and thereby inhibits S-phase entry [59]. It forms a repressor complex with LIN-35 (most homologous to p107 and p130, overall 19 % and 20 % amino acid homology, respectively) in

G1, repressing G1/S genes [57, 58]. In G1-phase, the Cyclin D1 (CYD1)/CDK-4 complex phosphorylates the LIN-35/EFL-1 complex, relieving the inhibitory effect on target genes like Cyclin E (CYE1), pushing the cells into S-phase [57, 60].

The loss of EFL-1 in *C. elegans* leads to enhanced S-phase entry and hyperplasia, as the negative regulation is gone and target genes are derepressed, similar to the loss of LIN-35 (Table 1). There is not much known about the effects of ectopic expression of EFL-1 on the cell cycle, only that *C. elegans* overexpression mutants are sterile (Table 2) [61].

EFL-2 is most similar to mammalian E2F3 and E2F6 (the dimerization domain homology is 37 %) and is proposed to act as an E2F activator during the cell cycle. However, current data only supports a transcriptional activator role during apoptosis [58, 61]. EFL-3 is a novel homologue of the mammalian E2F7 and E2F8, and it does not appear to be essential for regulating cell cycle progression. However, it has been shown that EFL-3 acts as a repressor in cooperation with Hox to regulate apoptosis [62, 63].

The function of the activator E2Fs to stimulate target gene expression and moving the cell into S-phase is highly conserved from yeast to mammals. Furthermore, the inhibitory effect of RB interaction with E2F activators is strongly conserved as well. In contrast, the evolution of E2F repressors in different species is quite diverse. In line with this observation, different mechanisms have evolved in mammals, yeast, flies, and worms to regulate the downswing of E2F target gene expression. The relevance of down-regulation of E2F target genes for cell cycle progression remains obscure, since inactivation of E2F repressors has no major impact on cell cycle progression and cells continue to proliferate even in the absence of E2F repressors. Recent studies provide evidence that loss of E2F repressors such as E2F7/8 can lead to hyperproliferation or inhibition of abortive cell cycles [64, 65]. Future studies are necessary to determine what the long-term effects are of deleting E2F repressors to understand functional impact on tissue homeostasis, aging, and tumorigenesis.

3 Mechanisms That Regulate the Oscillation of the E2F Transcription Factors

There are several mechanisms that tightly regulate the oscillating E2F expression during the cell cycle to prevent aberrant cell cycle progression. These mechanisms are on transcriptional, post-transcriptional, and post-translational levels. Transcriptionally, the most common regulation of E2Fs in proliferating cells is via a feedback-loop by E2Fs themselves [1, 66]. Activator E2Fs promote the expression of repressor E2Fs by binding to their promoter sites. Repressor E2Fs can bind to the promoters of activator E2Fs and inhibit their transcription, creating a negative feedback within the system [1].

E2Fs are also strongly regulated by c-Myc [67, 68]. c-Myc binds to the promoter of activator E2Fs after cells are triggered to start proliferating, leading to increasing levels of E2F mRNA and consequently E2F protein, and activation of E2F target genes [69]. It has also been shown that c-Myc is essential for the loading of E2F1 on activator E2F promoters. Immunoprecipitation experiments for c-Myc and E2F1 on endogenous E2F2 promoters after serum stimulation show that c-Myc binds from 4 h after stimulation onwards, while E2F1 does not bind until 16 h after serum stimulation. Importantly, mutations in E box elements in the promoter abolishes both c-Myc and E2F1 binding to the promoter [69].

In recent years, it has been shown that E2Fs are also under post-transcriptional regulation by microRNAs (miRNAs); short noncoding RNAs that are involved in many biological processes such as cell proliferation, differentiation, and oncogenesis. For instance, c-Myc activates a cluster of six miRNAs. Two of these miRNAs can inhibit the expression of E2F1, namely miR-17-5p and miR-20a. The inhibition of E2F1 by these miRNAs seems to be a mechanism to control E2F activation by c-Myc via a negative feedback loop in G1-phase, preventing uncontrolled activation of E2F1 [70]. Another example of miRNA regulation is the repression of E2F7 via miR-26a in acute myeloid leukemia (AML) cells. The E2F7 3′-UTR contains two putative binding sites for miR-26a, and E2F7 levels are increased after knockdown of this miRNA [71].

E2Fs are also regulated through post-translational regulation. Chk1 is an important kinase for the regulation of cell cycle progression after replication stress and DNA damage. During replication stress, E2F6 replaces the activator E2Fs on the target gene promoters, repressing their expression. Once the DNA damage caused by replication stress is repaired and the DNA replication checkpoint is satisfied, Chk1 phosphorylates E2F6. This leads to the dissociation of E2F6 from the promoters, and freeing them for activator E2Fs to bind again and promote cell cycle progression [35].

Transcriptional repression of transcription factors is an important step in limiting target gene expression, but this no longer has any effect on the already synthesized pool of proteins. Cyclin-CDK complexes are vital in E2F regulation. These complexes phosphorylate and inactivate Rb and E2Fs during different phases of the cell cycle [3, 72].

The regulation of protein turnover is another way to control the activity of E2Fs. The decrease of E2F1–3 in late S-G2 phase is caused via the SKP2-CUL1 complex, which targets the proteins for degradation [12]. A second degradation mechanism acts primarily in mitosis, namely via APC/C^{Cdh1}. The levels of E2F3 are slowly decreased upon cell cycle exit through APC/C^{CDh1}. E2F3 interacts with both Cdh1 and Cdc20 in vitro, but it seems to be a predominant target of Cdh1 in vivo [73]. Another substrate for APC/C is E2F1. E2F1 interacts with Cdh1 and Cdc20 in vitro,

similar to E2F3, but is mainly degraded by Cdc20 in vivo [13]. There are currently no reports on APC/C-mediated degradation of repressor E2Fs, but their oscillating expression pattern during the cell cycle suggests that these transcription factors are degraded as well [6, 8].

4 Mechanism of Controlling Target Gene Transcription by E2Fs

Activator and repressor E2Fs work together to control the oscillating expression pattern of E2F target genes. It is known that activator and repressor E2Fs can bind to a common set of promoters to balance target gene expression in vivo, for instance in the liver and placenta [64–66]. Loss of activator E2F1–3 in the mouse liver results in downregulation of target genes, while loss of repressor E2F7/8 leads to upregulation of the same target genes [65, 66]. However, it is still unknown how different E2Fs regulate the expression of target genes at the promoter levels.

All E2Fs can bind to the E2F consensus sequence TTTSSCGC, but the different E2F factors can also bind to non-consensus motifs [11, 34, 74]. One possible mechanism is that activating and repressing E2Fs compete for the same E2F binding sites, and the E2F factor with the highest DNA-binding affinity or the highest expression levels has a stronger effect on the transcriptional outcome (Fig. 3) [11, 75]. Another possibility is that binding to certain promoters or low-affinity sites is stabilized in cooperation with other transcription factors, for instance the binding of E2F7/8 to hypoxia-induced factor (HIF) during hypoxia, as HIF is essential for inhibiting cell cycle proliferation under this condition [76–78].

Since many promoters contain multiple consensus and non-consensus E2F binding sites, an alternative mechanism would be that different E2Fs bind to different sites on the same promoter

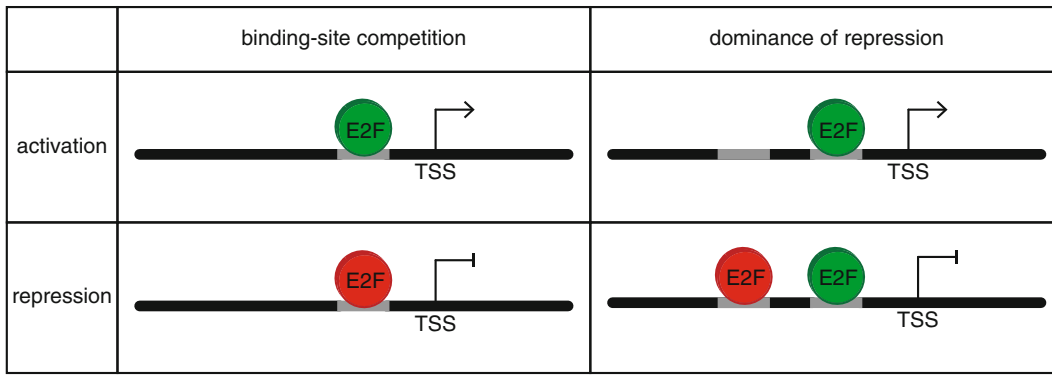

Fig. 3 There are two main models of E2F target gene regulation. The first shows competition between activator and repressor E2Fs for the same binding site, the second shows simultaneous binding and a dominant effect of repressor binding

and the combinatorial activating and repressing transcriptional activity of each individual E2F factor determines the transcriptional outcome. Previous studies provide evidence for the presence of positive- and negative-acting E2F promoter elements, for example in the *CDK1* and *CCNB1* promoter, whereby E2F1–3 bind to the positive acting site and E2F4 to negative acting sites [74, 79]. The expression patterns of E2F1–3 and E2F6–8 show a strong overlap especially during S-phase, so it is likely that they have overlapping binding sites as well. Currently it is unclear whether the competitor model or the activator/repressor specific-site model is critical to determine the transcriptional outcome of E2F target genes during S-phase.

Recently, it has been shown that E2F1 and E2F7 can bind to the same binding sites in the E2F1 promoter utilizing the gel shift assay [80]. Interestingly, it was also demonstrated that E2F1 and E2F7 can form a complex, and that the binding of E2F1-E2F7 heterodimer towards the promoter required the presence of two adjacent E2F binding sites [80]. Together, these findings show that activator and repressor E2Fs can bind to the same binding site, but also to different E2F sites in the same promoter, providing support for both models outlined above. However, it still unclear how the different binding options for activator and repressor E2Fs regulate the transcriptional activity of the target gene. For example, does induced expression of repressor E2F lead to disappearance of activator E2Fs from the promoter and vice versa? Does the number of consensus and non-consensus E2F sites in a promoter influence the transcriptional activity of a promoter? Do activator and repressor E2Fs bind to the same promoter in vivo during S-phase? Does the distance between E2F binding sites and the transcriptional start site influence the transcription rate? Future studies will be necessary to unravel the mechanism of how activator and repressor E2Fs regulate the expression of target genes at the promoter level.

4.1 Altered Regulation of E2F Target Gene Expression

The majority of human cancers show enhanced expression of E2Fs and E2F target genes (reviewed in [81]), providing evidence that proper control of E2F target expression is critical to avoid uncontrolled proliferation. Altered expression of E2F target genes is often caused by specific mutations in upstream regulators of the RB/E2F pathway, such as Cyclin D amplification [82], or by mutations of the RB/E2F pathway itself (reviewed in [81]). Transgenic mouse models for E2F activators demonstrated that enhanced expression of E2F1–3 leads to enhanced E2F target gene expression and spontaneous tumor formation (reviewed in [81]). Moreover, deletion of activator E2Fs in mouse models of cancer can reduce tumorigenesis, such as inactivation of E2F3 in a mouse model of mammary cancer [83]. Importantly, E2F activators have oncogenic potential, but can also function as tumor suppressors in specific tissues. E2F1 plays an important role in repressing skin

carcinogenesis by inducing DNA repair and apoptosis in response to DNA damage [84, 85].

The role of repressor E2Fs (E2F6–8) in controlling tumorigenesis is still undetermined, and it is unclear whether the timely downswing of oscillating E2F target gene expression is critical to suppress tumorigenesis. Preliminary data from our group show that inactivation of atypical E2Fs leads to spontaneous tumor formation in mice (unpublished data), providing strong evidence that enhanced expression of E2F target genes can lead to uncontrolled proliferation and cancer. Further support that repressor E2Fs can function as tumor suppressors is provided by studies showing that E2F7 is involved in cellular senescence and DNA damage. During oncogene-induced senescence or DNA damage, E2F7 is a direct transcriptional target of p53 and represses target genes that are involved in cell cycle progression to promote a strong cell cycle arrest [86–89].

Tight control of E2F target expression is not only important to prevent tumorigenesis but also for development. Inactivation of E2Fs in mice and zebrafish and the subsequent deregulation of E2F target gene expression results in many developmental defects of the placenta [64, 66] and the embryo [10, 78, 81]. Studies performed in the mammalian placenta and liver, as well as in flies and plants, revealed that E2Fs are not only important for regulating the normal cell cycle, but are also critical for the control of abortive cell cycles (reviewed in [90]). Abortion of the cell cycle can occur before entering mitosis (endocycle), during mitosis (endomitosis) or during cytokinesis (incomplete cytokinesis) and leads to the formation of polyploid cells, cells with increased numbers of chromosome sets. Remarkably, inactivation of the repressors E2F7/8 prevents the formation of polyploid cells in hepatocytes and giant trophoblast cells, while inactivation of activator E2F1 enhances polyploidization [65, 66]. These findings demonstrate that low levels of E2F target gene expression promote an abortive cell cycle leading to the formation of polyploid cells in the placenta and liver. In contrast, when the levels of E2F target gene expression were increased through inactivation of the repressors E2F7/8, cells completed a normal cell cycle and polyploidization was blocked. This suggests that the levels of E2F target gene expression determine whether a hepatocyte or trophoblast cell enters a normal or an abortive cell cycle.

5 Outstanding Questions

There have been great advancements in understanding how E2Fs function since their discovery in the late 1980s [91]. However, there are still many open questions concerning the regulation of the oscillating E2F target expression. Since many cancers are characterized by the deregulation of E2F target expression, it will

be critical to understand the mechanism that influences E2F target gene expression in more detail. For example, what are the dynamics of expression of E2Fs and its targets in single cells in response to growth signals or DNA damage? What is the expression profile of all E2Fs in different tissue and cell types during cell cycle progression? What is the direct impact of the acute deletion or overexpression of E2Fs on the length of each cell cycle phase? A bottleneck in answering these questions has been the redundancy in the mammalian E2F family members, and the limitations of the techniques by looking at cell populations. Recent developments in single cell analysis techniques have made it possible to take the next step. It is now feasible to analyze the gene expression pattern of a single cell by single cell transcriptomics, which can provide more detailed knowledge about the regulation of E2Fs and their target genes [92, 93]. This will allow one to study whether each cell within a particular tissue has the same expression pattern, or whether there are subsets of cells within a tissue that have distinct expression profiles.

Another strong tool to help elucidate questions about E2F functions during the cell cycle is live time lapse microscopy of cells expressing fluorescent cell cycle indicators, such as the ubiquitination-based cell cycle indicator (FUCCI) system [68, 94]. Thus, cell cycle progression of single cells over time can be visualized, and the effects of manipulating the activity of specific E2Fs can be monitored. Combining these two single cell techniques makes it possible to analyze in detail the entire network of E2F target genes during specific phases of the cell cycle.

Utilizing these novel single cell analysis technologies will help to provide answers to the burning fundamental questions about the dynamics and mechanism of expression of E2Fs and its targets. Moreover, it will help to design novel strategies to avoid or inhibit altered E2F target gene expression patterns in diseases such as cancer.

Acknowledgements

We thank B. Westendorp and W.J. Bakker for critically reviewing the manuscript.

References

1. Wong JV, Dong P, Nevins JR et al (2011) Network calisthenics: control of E2F dynamics in cell cycle entry. Cell Cycle 10:3086–3094
2. DeGregori J, Leone G, Miron A et al (1997) Distinct roles for E2F proteins in cell growth control and apoptosis. Proc Natl Acad Sci U S A 94:7245–7250
3. Weinberg R (2013) The biology of cancer, 2nd edn. Garland Science, New York, NY
4. Sun A, Bagella L, Tutton S et al (2007) From G0 to S phase: a view of the roles played by the retinoblastoma (Rb) family members in the Rb-E2F pathway. J Cell Biochem 102:1400–1404. doi:10.1002/jcb.21609

5. Di Stefano L, Jensen MR, Helin K (2003) E2F7, a novel E2F featuring DP-independent repression of a subset of E2F-regulated genes. EMBO J 22:6289–6298. doi:10.1093/emboj/cdg613
6. de Bruin A, Maiti B, Jakoi L et al (2003) Identification and characterization of E2F7, a novel mammalian E2F family member capable of blocking cellular proliferation. J Biol Chem 278:42041–42049. doi:10.1074/jbc.M308105200
7. Logan N, Delavaine L, Graham A et al (2004) E2F-7: a distinctive E2F family member with an unusual organization of DNA-binding domains. Oncogene 23:5138–5150. doi:10.1038/sj.onc.1207649
8. Christensen J, Cloos P, Toftegaard U et al (2005) Characterization of E2F8, a novel E2F-like cell-cycle regulated repressor of E2F-activated transcription. Nucleic Acids Res 33:5458–5470. doi:10.1093/nar/gki855
9. Maiti B, Li J, de Bruin A et al (2005) Cloning and characterization of mouse E2F8, a novel mammalian E2F family member capable of blocking cellular proliferation. J Biol Chem 280:18211–18220. doi:10.1074/jbc.M501410200
10. Li J, Ran C, Li E et al (2008) Synergistic function of E2F7 and E2F8 is essential for cell survival and embryonic development. Dev Cell 14:62–75. doi:10.1016/j.devcel.2007.10.017
11. Westendorp B, Mokry M, Groot Koerkamp MJA et al (2012) E2F7 represses a network of oscillating cell cycle genes to control S-phase progression. Nucleic Acids Res 40:3511–3523. doi:10.1093/nar/gkr1203
12. Nakayama KI, Nakayama K (2006) Ubiquitin ligases: cell-cycle control and cancer. Nat Rev Cancer 6:369–381. doi:10.1038/nrc1881
13. Peart MJ, Poyurovsky MV, Kass EM et al (2010) APC/C(Cdc20) targets E2F1 for degradation in prometaphase. Cell Cycle 9:3956–3964
14. GeleyS,KramerE,GieffersCetal(2001)Anaphase-promoting complex/cyclosome-dependent proteolysis of human cyclin A starts at the beginning of mitosis and is not subject to the spindle assembly checkpoint. J Cell Biol 153:137–148
15. Trimarchi JM, Lees JA (2002) Sibling rivalry in the E2F family. Nat Rev Mol Cell Biol 3:11–20. doi:10.1038/nrm714
16. Lammens T, Li J, Leone G, De Veylder L (2009) Atypical E2Fs: new players in the E2F transcription factor family. Trends Cell Biol 19:111–118. doi:10.1016/j.tcb.2009.01.002
17. Leone G, DeGregori J, Yan Z et al (1998) E2F3 activity is regulated during the cell cycle and is required for the induction of S phase. Genes Dev 12:2120–2130
18. Wenzel PL, Chong J-L, Sáenz-Robles MT et al (2011) Cell proliferation in the absence of E2F1-3. Dev Biol 351:35–45. doi:10.1016/j.ydbio.2010.12.025
19. Frolov MV, Huen DS, Stevaux O et al (2001) Functional antagonism between E2F family members. Genes Dev 15:2146–2160. doi:10.1101/gad.903901
20. Logan TJ, Evans DL, Mercer WE et al (1995) Expression of a deletion mutant of the E2F1 transcription factor in fibroblasts lengthens S phase and increases sensitivity to S phase-specific toxins. Cancer Res 55:2883–2891
21. Humbert PO, Verona R, Trimarchi JM et al (2000) E2f3 is critical for normal cellular proliferation. Genes Dev 14:690–703
22. Dos Reis Vasques L, Pujiz RS, Strauss BE, Krieger JE (2010) Knockdown of E2f1 by RNA interference impairs proliferation of rat cells in vitro. Genet Mol Biol 33:17–22. doi:10.1590/S1415-47572009005000104
23. Degregori J, Johnson DG (2006) Distinct and overlapping roles for E2F family members in transcription, proliferation and apoptosis. Curr Mol Med 6:739–748
24. Zhu JW, Field SJ, Gore L et al (2001) E2F1 and E2F2 determine thresholds for antigen-induced T-cell proliferation and suppress tumorigenesis. Mol Cell Biol 21:8547–8564. doi:10.1128/MCB.21.24.8547-8564.2001
25. Laresgoiti U, Apraiz A, Olea M et al (2013) E2F2 and CREB cooperatively regulate transcriptional activity of cell cycle genes. Nucleic Acids Res 41:10185–10198. doi:10.1093/nar/gkt821
26. Chong J-L, Tsai S-Y, Sharma N et al (2009) E2f3a and E2f3b contribute to the control of cell proliferation and mouse development. Mol Cell Biol 29:414–424. doi:10.1128/MCB.01161-08
27. Wu L, Timmers C, Maiti B et al (2001) The E2F1-3 transcription factors are essential for cellular proliferation. Nature 414:457–462. doi:10.1038/35106593
28. Tsai S-Y, Opavsky R, Sharma N et al (2008) Mouse development with a single E2F activator. Nature 454:1137–1141. doi:10.1038/nature07066
29. Stevens C, Smith L, La Thangue NB (2003) Chk2 activates E2F-1 in response to DNA damage. Nat Cell Biol 5:401–409. doi:10.1038/ncb974
30. Carnevale J, Palander O, Seifried LA, Dick FA (2012) DNA damage signals through differentially modified E2F1 molecules to induce apoptosis. Mol Cell Biol 32:900–912. doi:10.1128/MCB.06286-11

31. Müller H, Moroni MC, Vigo E et al (1997) Induction of S-phase entry by E2F transcription factors depends on their nuclear localization. Mol Cell Biol 17:5508–5520
32. Verona R, Moberg K, Estes S et al (1997) E2F activity is regulated by cell cycle-dependent changes in subcellular localization. Mol Cell Biol 17:7268–7282
33. Attwooll C, Lazzerini Denchi E, Helin K (2004) The E2F family: specific functions and overlapping interests. EMBO J 23:4709–4716. doi:10.1038/sj.emboj.7600481
34. Lee B-K, Bhinge AA, Iyer VR (2011) Wide-ranging functions of E2F4 in transcriptional activation and repression revealed by genome-wide analysis. Nucleic Acids Res 39:3558–3573. doi:10.1093/nar/gkq1313
35. Bertoli C, Klier S, McGowan C et al (2013) Chk1 inhibits E2F6 repressor function in response to replication stress to maintain cell-cycle transcription. Curr Biol 23:1629–1637. doi:10.1016/j.cub.2013.06.063
36. Lyons TE, Salih M, Tuana BS (2006) Activating E2Fs mediate transcriptional regulation of human E2F6 repressor. Am J Physiol Cell Physiol 290:C189–C199. doi:10.1152/ajpcell.00630.2004
37. Giangrande PH, Zhu W, Schlisio S et al (2004) A role for E2F6 in distinguishing G1/S- and G2/M-specific transcription. Genes Dev 18:2941–2951. doi:10.1101/gad.1239304
38. Cross FR, Buchler NE, Skotheim JM (2011) Evolution of networks and sequences in eukaryotic cell cycle control. Philos Trans R Soc Lond B Biol Sci 366:3532–3544. doi:10.1098/rstb.2011.0078
39. Charvin G, Oikonomou C, Siggia ED, Cross FR (2010) Origin of irreversibility of cell cycle start in budding yeast. PLoS Biol 8, e1000284. doi:10.1371/journal.pbio.1000284
40. Amon A, Tyers M, Futcher B, Nasmyth K (1993) Mechanisms that help the yeast cell cycle clock tick: G2 cyclins transcriptionally activate G2 cyclins and repress G1 cyclins. Cell 74:993–1007
41. Bähler J (2005) Cell-cycle control of gene expression in budding and fission yeast. Annu Rev Genet 39:69–94. doi:10.1146/annurev.genet.39.110304.095808
42. de Bruin RAM, Kalashnikova TI, Chahwan C et al (2006) Constraining G1-specific transcription to late G1 phase: the MBF-associated corepressor Nrm1 acts via negative feedback. Mol Cell 23:483–496. doi:10.1016/j.molcel.2006.06.025
43. Igual JC, Johnson AL, Johnston LH (1996) Coordinated regulation of gene expression by the cell cycle transcription factor Swi4 and the protein kinase C MAP kinase pathway for yeast cell integrity. EMBO J 15:5001–5013
44. Verma R, Smiley J, Andrews B, Campbell JL (1992) Regulation of the yeast DNA replication genes through the Mlu I cell cycle box is dependent on SWI6. Proc Natl Acad Sci U S A 89:9479–9483
45. Koch C, Moll T, Neuberg M et al (1993) A role for the transcription factors Mbp1 and Swi4 in progression from G1 to S phase. Science 261:1551–1557
46. Sopko R, Huang D, Preston N et al (2006) Mapping pathways and phenotypes by systematic gene overexpression. Mol Cell 21:319–330. doi:10.1016/j.molcel.2005.12.011
47. Ohtani K, Nevins JR (1994) Functional properties of a Drosophila homolog of the E2F1 gene. Mol Cell Biol 14:1603–1612
48. Sawado T, Yamaguchi M, Nishimoto Y et al (1998) dE2F2, a novel E2F-family transcription factor in Drosophila melanogaster. Biochem Biophys Res Commun 251:409–415. doi:10.1006/bbrc.1998.9407
49. Dimova DK, Stevaux O, Frolov MV, Dyson NJ (2003) Cell cycle-dependent and cell cycle-independent control of transcription by the Drosophila E2F/RB pathway. Genes Dev 17:2308–2320. doi:10.1101/gad.1116703
50. Lee H, Ragusano L, Martinez A et al (2012) A dual role for the dREAM/MMB complex in the regulation of differentiation-specific E2F/RB target genes. Mol Cell Biol 32:2110–2120. doi:10.1128/MCB.06314-11
51. Ji J-Y, Miles WO, Korenjak M et al (2012) In vivo regulation of E2F1 by Polycomb group genes in Drosophila. G3 (Bethesda) 2:1651–1660. doi:10.1534/g3.112.004333
52. Shibutani ST, la Cruz de AFA, Tran V et al (2008) Intrinsic negative cell cycle regulation provided by PIP box- and Cul4Cdt2-mediated destruction of E2f1 during S phase. Dev Cell 15:890–900. doi:10.1016/j.devcel.2008.10.003
53. Duronio RJ, O'Farrell PH (1994) Developmental control of a G1-S transcriptional program in Drosophila. Development 120:1503–1515
54. Asano M, Nevins JR, Wharton RP (1996) Ectopic E2F expression induces S phase and apoptosis in Drosophila imaginal discs. Genes Dev 10:1422–1432
55. Frolov MV, Moon N-S, Dyson NJ (2005) dDP is needed for normal cell proliferation. Mol Cell Biol 25:3027–3039. doi:10.1128/MCB.25.8.3027-3039.2005
56. Ambrus AM, Nicolay BN, Rasheva VI et al (2007) dE2F2-independent rescue of proliferation in

cells lacking an activator dE2F1. Mol Cell Biol 27:8561–8570. doi:10.1128/MCB.01068-07
57. Koreth J, van den Heuvel S (2005) Cell-cycle control in Caenorhabditis elegans: how the worm moves from G1 to S. Oncogene 24:2756–2764. doi:10.1038/sj.onc.1208607
58. Ceol CJ, Horvitz HR (2001) dpl-1 DP and efl-1 E2F act with lin-35 Rb to antagonize Ras signaling in C. elegans vulval development. Mol Cell 7:461–473
59. Boxem M, van den Heuvel S (2002) C. elegans class B synthetic multivulva genes act in G(1) regulation. Curr Biol 12:906–911
60. Roy SH, Tobin DV, Memar N et al (2014) A complex regulatory network coordinating cell cycles during C. elegans development is revealed by a genome-wide RNAi screen. G3 (Bethesda) 4:795–804. doi:10.1534/g3.114.010546
61. Schertel C, Conradt B (2007) C. elegans orthologs of components of the RB tumor suppressor complex have distinct pro-apoptotic functions. Development 134:3691–3701. doi:10.1242/dev.004606
62. van den Heuvel S, Dyson NJ (2008) Conserved functions of the pRB and E2F families. Nat Rev Mol Cell Biol 9:713–724. doi:10.1038/nrm2469
63. Winn J, Carter M, Avery L, Cameron S (2011) Hox and a newly identified E2F co-repress cell death in Caenorhabditis elegans. Genetics 188:897–905. doi:10.1534/genetics.111.128421
64. Ouseph MM, Li J, Chen H-Z et al (2012) Atypical E2F repressors and activators coordinate placental development. Dev Cell 22:849–862. doi:10.1016/j.devcel.2012.01.013
65. Pandit SK, Westendorp B, Nantasanti S et al (2012) E2F8 is essential for polyploidization in mammalian cells. Nat Cell Biol 14:1181–1191. doi:10.1038/ncb2585
66. Chen H-Z, Ouseph MM, Li J et al (2012) Canonical and atypical E2Fs regulate the mammalian endocycle. Nat Cell Biol 14:1192–1202. doi:10.1038/ncb2595
67. Hölzel M, Kohlhuber F, Schlosser I et al (2001) Myc/Max/Mad regulate the frequency but not the duration of productive cell cycles. EMBO Rep 2:1125–1132. doi:10.1093/embo-reports/kve251
68. Dong P, Maddali MV, Srimani JK et al (2014) Division of labour between Myc and G1 cyclins in cell cycle commitment and pace control. Nat Commun 5:4750. doi:10.1038/ncomms5750
69. Leung JY, Ehmann GL, Giangrande PH, Nevins JR (2008) A role for Myc in facilitating transcription activation by E2F1. Oncogene 27:4172–4179. doi:10.1038/onc.2008.55
70. O'Donnell KA, Wentzel EA, Zeller KI et al (2005) c-Myc-regulated microRNAs modulate E2F1 expression. Nature 435:839–843. doi:10.1038/nature03677
71. Salvatori B, Iosue I, Mangiavacchi A et al (2012) The microRNA-26a target E2F7 sustains cell proliferation and inhibits monocytic differentiation of acute myeloid leukemia cells. Cell Death Dis 3, e413. doi:10.1038/cddis.2012.151
72. Fung TK, Poon RYC (2005) A roller coaster ride with the mitotic cyclins. Semin Cell Dev Biol 16:335–342. doi:10.1016/j.semcdb.2005.02.014
73. Ping Z, Lim R, Bashir T et al (2012) APC/C (Cdh1) controls the proteasome-mediated degradation of E2F3 during cell cycle exit. Cell Cycle 11:1999–2005. doi:10.4161/cc.20402
74. Xu X, Bieda M, Jin VX et al (2007) A comprehensive ChIP-chip analysis of E2F1, E2F4, and E2F6 in normal and tumor cells reveals interchangeable roles of E2F family members. Genome Res 17:1550–1561. doi:10.1101/gr.6783507
75. Grant GD, Brooks L, Zhang X et al (2013) Identification of cell cycle-regulated genes periodically expressed in U2OS cells and their regulation by FOXM1 and E2F transcription factors. Mol Biol Cell 24:3634–3650. doi:10.1091/mbc.E13-05-0264
76. Goda N, Ryan HE, Khadivi B et al (2003) Hypoxia-inducible factor 1alpha is essential for cell cycle arrest during hypoxia. Mol Cell Biol 23:359–369
77. Ortmann B, Druker J, Rocha S (2014) Cell cycle progression in response to oxygen levels. Cell Mol Life Sci 71:3569–3582. doi:10.1007/s00018-014-1645-9
78. Weijts BGMW, Bakker WJ, Cornelissen PWA et al (2012) E2F7 and E2F8 promote angiogenesis through transcriptional activation of VEGFA in cooperation with HIF1. EMBO J 31:3871–3884. doi:10.1038/emboj.2012.231
79. Zhu W, Giangrande PH, Nevins JR (2004) E2Fs link the control of G1/S and G2/M transcription. EMBO J 23:4615–4626. doi:10.1038/sj.emboj.7600459
80. Liu B, Shats I, Angus SP et al (2013) Interaction of E2F7 transcription factor with E2F1 and C-terminal-binding protein (CtBP) provides a mechanism for E2F7-dependent transcription repression. J Biol Chem 288:24581–24589. doi:10.1074/jbc.M113.467506
81. Chen H-Z, Tsai S-Y, Leone G (2009) Emerging roles of E2Fs in cancer: an exit from cell cycle control. Nat Rev Cancer 9:785–797. doi:10.1038/nrc2696

82. Okami K, Reed AL, Cairns P et al (1999) Cyclin D1 amplification is independent of p16 inactivation in head and neck squamous cell carcinoma. Oncogene 18:3541–3545. doi:10.1038/sj.onc.1202837
83. Wu L, de Bruin A, Wang H et al (2015) Selective roles of E2Fs for ErbB2- and Myc-mediated mammary tumorigenesis. Oncogene 34:119–128. doi:10.1038/onc.2013.511
84. Russell JL, Weaks RL, Berton TR, Johnson DG (2006) E2F1 suppresses skin carcinogenesis via the ARF-p53 pathway. Oncogene 25:867–876. doi:10.1038/sj.onc.1209120
85. Biswas AK, Mitchell DL, Johnson DG (2014) E2F1 responds to ultraviolet radiation by directly stimulating DNA repair and suppressing carcinogenesis. Cancer Res 74: 3369–3377. doi:10.1158/0008-5472.CAN-13-3216
86. Aksoy O, Chicas A, Zeng T et al (2012) The atypical E2F family member E2F7 couples the p53 and RB pathways during cellular senescence. Genes Dev 26:1546–1557. doi:10.1101/gad.196238.112
87. Carvajal LA, Hamard P-J, Tonnessen C, Manfredi JJ (2012) E2F7, a novel target, is up-regulated by p53 and mediates DNA damage-dependent transcriptional repression. Genes Dev 26:1533–1545. doi:10.1101/gad.184911.111
88. Zalmas LP, Zhao X, Graham AL et al (2008) DNA-damage response control of E2F7 and E2F8. EMBO Rep 9:252–259. doi:10.1038/sj.embor.7401158
89. Zalmas L-P, Coutts AS, Helleday T, La Thangue NB (2013) E2F-7 couples DNA damage-dependent transcription with the DNA repair process. Cell Cycle 12:3037–3051. doi:10.4161/cc.26078
90. Pandit SK, Westendorp B, de Bruin A (2013) Physiological significance of polyploidization in mammalian cells. Trends Cell Biol 23:556–566. doi:10.1016/j.tcb.2013.06.002
91. Reichel R, Kovesdi I, Nevins JR (1987) Developmental control of a promoter-specific factor that is also regulated by the E1A gene product. Cell 48:501–506
92. Avital G, Hashimshony T, Yanai I (2014) Seeing is believing: new methods for in situ single-cell transcriptomics. Genome Biol 15:110. doi:10.1186/gb4169
93. Grindberg RV, Yee-Greenbaum JL, McConnell MJ et al (2013) RNA-sequencing from single nuclei. Proc Natl Acad Sci U S A 110:19802–19807. doi:10.1073/pnas.1319700110
94. Sakaue-Sawano A, Kurokawa H, Morimura T et al (2008) Visualizing spatiotemporal dynamics of multicellular cell-cycle progression. Cell 132:487–498. doi:10.1016/j.cell.2007.12.033
95. Joyce NC, Harris DL, Mc Alister JC et al (2004) Effect of overexpressing the transcription factor E2F2 on cell cycle progression in rabbit corneal endothelial cells. Invest Ophthalmol Vis Sci 45:1340–1348
96. Rady B, Chen Y, Vaca P et al (2013) Overexpression of E2F3 promotes proliferation of functional human β cells without induction of apoptosis. Cell Cycle 12:2691–2702. doi:10.4161/cc.25834
97. Cartwright P, Müller H, Wagener C et al (1998) E2F-6: a novel member of the E2F family is an inhibitor of E2F-dependent transcription. Oncogene 17:611–623. doi:10.1038/sj.onc.1201975
98. Logan N, Graham A, Zhao X et al (2005) E2F-8: an E2F family member with a similar organization of DNA-binding domains to E2F-7. Oncogene 24:5000–5004. doi:10.1038/sj.onc.1208703
99. Reddien PW, Andersen EC, Huang MC, Horvitz HR (2007) DPL-1 DP, LIN-35 Rb and EFL-1 E2F act with the MCD-1 zinc-finger protein to promote programmed cell death in Caenorhabditis elegans. Genetics 175:1719–1733. doi:10.1534/genetics.106.068148

Part II

Methods

Chapter 5

Cell Synchronization of Mouse Embryonic Fibroblasts

Michael J. Thwaites, Courtney H. Coschi, Christian E. Isaac, and Frederick A. Dick

Abstract

A fundamental need in the analysis of the cell cycle is the ability to isolate relatively homogeneous populations of cells in different phases. This is complicated by the variable proliferative properties and responses to synchronizing methods of different cancer-derived cell lines. Paradoxically, cell lines with genetic defects in cell cycle control are sometimes chosen because they are amenable to chemical synchronization. Embryonic fibroblasts from mice present the opportunity to study the effects of defined genetic modifications on a normal cell cycle. However, synchronization of these cells has often been challenging. In this chapter we outline three basic protocols for isolating mouse fibroblasts at the G1-to-S-phase transition, in S phase, and during mitosis.

Key words Flow cytometry, DNA replication, Aphidicolin, Serum starvation, Nocodazole

1 Introduction

The mammalian cell division cycle is marked by a number of phases through which cells progress prior to division. G1, S, G2, and mitosis are distinct phases of the cell cycle that undertake specific molecular tasks related to division. Fidelity of the biochemical events that define these phases is ensured by checkpoints and other mechanisms that regulate the unidirectional transition between phases. These mechanisms are essential to propagate all living organisms [1]; however mistakes in the cell division cycle can lead to unwanted effects on development and fuel the progression of diseases such as cancer [2].

A long-standing challenge in understanding cell cycle control at a molecular level is the distinction between cause and consequence. A pathway that controls advancement of the cell cycle from one phase to the next could be mistaken for one that participates directly in distinct events during the next phase. Normal mouse embryonic fibroblast cells (MEFs) deficient for cell cycle

Amanda S. Coutts and Louise Weston (eds.), *Cell Cycle Oscillators: Methods and Protocols*, Methods in Molecular Biology, vol. 1342, DOI 10.1007/978-1-4939-2957-3_5,

regulators have been invaluable in determining requirements for cell cycle control as well as making distinctions between cause and consequence [3–6]. Serum starvation (G0) and contact inhibition (G1) methods readily allow for isolation of cells from these phases. However, the ability to synchronize MEFs later in the cell cycle for biochemical experiments is more challenging when compared with established cancer cell lines.

In this chapter we outline protocols to isolate relatively uniform populations of MEFs for the analysis of events at the G1-to-S-phase transition, in early S phase, and mitosis. The first is a serum deprivation and restimulation protocol to obtain cell populations in late G1 or early S phase to investigate the regulation and timing of the transition between these phases. The second is a protocol to isolate uniform populations of early S-phase cells and it can also be used to create enriched populations of mitotic cells. Lastly, we describe a nocodazole shake-off method for isolation of mitotic cells. In this way we have established simple methods for isolating MEFs in commonly studied phases of the cell cycle and we have used these routinely in our studies [7–9].

Investigators that are new to cell synchronization should be cautious in the implementation of these methods. It is critical that methods for assessing the degree of synchronization by flow cytometry be established in parallel. Methods for assessing cell cycle phases using BrdU and propidium iodide staining have been described previously [10], and flow cytometric techniques for detecting histone H3-S10 phosphorylation in mitosis are also available [11]. While we focus on the use of MEFs, we expect that these methods will be amenable for adaptation to other primary cell culture systems that best represent normal cell cycle regulation.

2 Materials

2.1 Generation and Culture of Mouse Embryonic Fibroblasts

1. Pregnant female mice, day 13.5 of gestation.
2. Stereomicroscope for dissection, equipped for top lighting.
3. Sterile phosphate-buffered saline (PBS).
4. Tissue culture-grade disposable plastics including 6 cm tissue culture dishes, T75 tissue culture flasks, 10 and 15 cm tissue culture dishes, and 50 ml conical tubes.
5. Sterile razor blades, watch maker's forceps, and scissors.
6. Growth media: Dulbecco's modified Eagle's medium containing 100 U/ml penicillin, 10 μg/ml streptomycin, 200 mM L-glutamine, and 10 % fetal bovine serum.
7. Trypsin-EDTA: 0.05 % Trypsin, 0.7 mM EDTA in Hanks' balanced salt solution.

8. Basic supplies for mammalian cell culture including incubators, laminar flow hood, tabletop centrifuge, and cell culture pipets.
9. 2 ml cryogenic vials (e.g., Thermo Scientific 5000-0020).
10. Slow cooling cryogenic container (e.g., Mr Frosty Freezing container, Thermo Scientific 5100-0001).

2.2 Cell Synchronization

1. Low-serum media: Dulbecco's modified Eagle's medium containing 100 U/ml penicillin, 10 μg/ml streptomycin, 200 mM L-glutamine, and 0.1 % fetal bovine serum.
2. 3 mM aphidicolin: 1 mg/ml in ethanol (250× stock). Store in the dark at −20 °C and remake weekly.
3. 150 μM nocodazole: 0.045 mg/ml in DMSO (1000× stock). Store in the dark at −20 °C.

3 Methods

3.1 Preparation of Mouse Embryonic Fibroblast

The generation of primary mouse embryonic fibroblast cultures (MEFs) is relatively ubiquitous. The basic protocol that we follow is devised to generate cultures from individual embryos. This creates the advantage that crosses designed to produce control and mutant embryos in the same litter will be processed in parallel and can be genotyped in isolation. In addition, cultures derived from individual embryos of the same genotype represent separate biological replicates. The biggest challenge in culturing MEFs is that oxidative DNA damage limits their proliferative capacity [12], and requires judicious protocol planning to ensure that they are used at as early a passage as possible. In addition, culture at low cell density is also detrimental to long-term proliferative capacity. The following protocol describes the generation of MEFs and illustrates how to organize cell cycle analysis experiments at the earliest passage possible.

1. Euthanize pregnant mother at day 13.5 of gestation. Dissect out uterus and submerge in PBS in a 10 cm dish.
2. Isolate individual embryos and transfer to separate 6 cm dishes containing PBS.
3. Under dissecting microscope use forceps to hook, poke, and scratch out organs and remove brain. Save these tissues or the yolk sac for DNA extraction and genotyping if desired.
4. Place carcass in a fresh, dry 6 cm dish and continue dissecting other embryos.
5. Once all embryos in a litter have been dissected, aspirate residual PBS and cover each embryo with 1 ml trypsin-EDTA. Mince tissue finely with a sterile razor blade.
6. Tip dish on edge to allow tissue and trypsin solution to pool, and place in 37 °C humidified incubator for 30 min on edge.

7. Pipet up and down ten times through a Pasteur pipet. Then add 4 ml of growth media, and pipet to mix.
8. Transfer cell suspension to a T75 flask and add 15 ml of growth media and incubate for 2 days (this is the first passage; *see* **Note 1**).
9. Rinse cells in PBS and dissociate with 3 ml trypsin-EDTA. Add 7 ml of growth media and pipet to break up small aggregates of cells. Allow larger aggregates to settle out to remove them from future cultures. Subculture cell suspension into three, 15 cm dishes in 30 ml of media per dish.
10. Culture for approximately two additional days and freeze in log growth phase. Trypsinize cells as above in **step 9**, resuspend in growth media containing 10 % DMSO at a density of three million cells per ml, and aliquot into cryogenic vials in 1 ml aliquots. These cells are in mid-passage 2 and each embryo should yield approximately 20 vials. Slowly freeze cells in a cryogenic container at −80 °C for 24 h. Following this slow freeze, cryovials are transferred to a −150 °C freezer (or liquid nitrogen vapor) for long-term storage.
11. Thaw a single cryovial per 10 cm dish or equivalent, and culture until it reaches confluence (end of passage 2). Subculture onto five, 10 cm dishes for passage 3. This will yield greater than 20×10^7 cells. Subculture again at the desired density for the start of passage 4 and use in the synchronization methods described below (*see* **Note 2**).

3.2 Cell Synchronization in G1 and at the G1-to-S-Phase Transition

In this section we describe how to synchronize cells at the G1-S-phase boundary. Using this technique we are able to enrich for cells in the early stages of S phase using a relatively gentle induction of quiescence through serum deprivation. Cells are then stimulated to progress into the cell cycle with growth media containing 10 % serum. We find that this approach leads to adequate synchrony at the G1/S boundary without the use of drugs, which could affect the proliferative capacity of the cells or the integrity of the data. Figure 1 contains data depicting a time course following serum stimulation with growth media. Once a time course has been performed, particular time points can be selected for experiments in G1 phase (10–12 h in our example) and the G1/S boundary (approximately 18 h). In general, cells that do not reach S phase in the first 20 h enter the cell cycle more slowly. For this reason, unsynchronized cells in these cultures are earlier in the cell cycle and generally do not affect analysis of the G1/S boundary in these experiments.

1. Plate passage 4 MEFs at a density of 7×10^5 cells per 10 cm plate or equivalent for each time point in growth media (*see* **Note 3**).

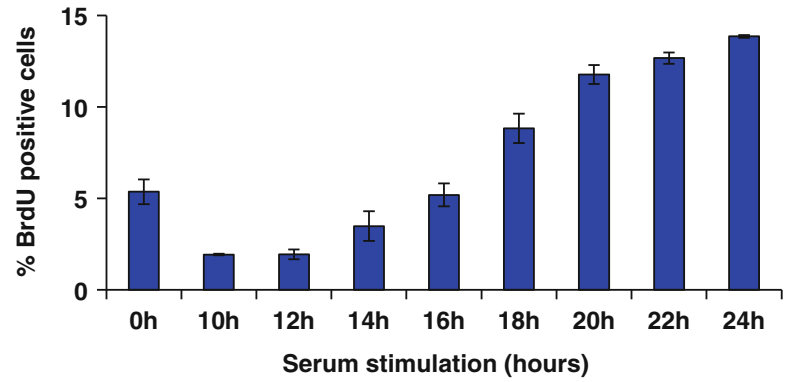

Fig. 1 Time course of serum stimulation: Wild-type MEFs were stimulated with 10 % serum to reenter the cell cycle. Cells were pulse labeled with BrdU beginning 1 h before the indicated time points. The percentage of BrdU-positive cells at each time point was determined by flow cytometry

2. The following day wash the cells three times with PBS and re-feed with low-serum media.
3. Following 72 h of serum deprivation, standard growth media containing 10 % serum is added to each culture (*see* **Note 4**).
4. Harvest cells for cellular analyses, fractionation, RNA, or protein at the desired time point(s).

3.3 Generating Synchronous S-Phase and Mitotic Populations of Cells

The following section outlines our methods for isolating a highly synchronous S-phase population of cells. This method makes use of the DNA polymerase inhibitor aphidicolin to initially block cell cycle advancement in early S phase. In our experience, hydroxyurea and thymidine block techniques are too toxic for MEFs, and the cells cease to proliferate in response to these treatments. Since all of these chemicals unavoidably rely on a replication block that activates a DNA damage response, we do not recommend analyzing cells at the point of arrest. Our protocol removes aphidicolin and allows the cells to resume DNA synthesis before harvesting, thus obtaining a bona fide S-phase population. Cells synchronized in this manner can also be followed into M phase to enrich for mitotic figures.

1. At the end of passage 3, allow the cells to become fully confluent by leaving them for three additional days, for a total of 6 days following subculture.
2. Resume proliferation of cells by subculturing them at your desired cell density, but not less than 7×10^5 cells for a 10 cm dish, to ensure maintenance of robust proliferation (*see* **Note 3**).
3. Ten hours following subculture, supplement media with 12 μM aphidicolin and culture for an additional 10 h.
4. Aspirate media, wash cells three times with PBS, and re-feed with fresh growth media.

5. Culture for an additional 2 h to allow the cells to resume DNA replication (*see* **Note 5**).
6. Cells can be cultured further and at 8 h post-aphidicolin removal, the peak of mitotic enrichment occurs (*see* **Note 6**).

3.4 Generating Large Quantities of Mitotic Cells

Mitotic shake-off approaches rely on the fact that mitotic cells round up compared to their interphase neighbors. This leads to poor attachment and consequently they are readily isolated by shearing forces associated with tapping the side of the dish or washing with media. Many human cancer cell lines can be arrested in mitosis with microtubule inhibitors for prolonged periods of time, leading to extensive mitotic enrichment. Murine cells are less amenable to accumulation at this cell cycle stage because they adapt to the arrest and decondense their chromosomes [13]. Consequently, shorter drug treatments are necessary and lower yields need to be expected. We have used the following brief protocol and it has allowed us to isolate large quantities of mitotic cells and even to undertake biochemical fractionation experiments (*see* Fig. 2).

1. Plate passage 4 MEFs at a density of at least 7×10^5 cells per 10 cm plate or equivalent.
2. Two days later supplement the media with 150 nM nocodazole and return the cells to the incubator for 4 h (*see* **Note 7**).
3. Harvest weakly adherent cells first by removing 6 ml of culture media from each 10 cm dish and place in a centrifuge tube. This media is removed to prevent splashing.
4. Vigorously tap the cell culture dish on its side to detach cells. Remove this media and add to the first aliquot.
5. Wash cells vigorously with PBS using a strong stream of liquid from a tissue culture pipet to further remove cells. Add this PBS wash to the media already collected.
6. Concentrate cells by centrifugation at $400 \times g$ for 10 min, resuspend in a small volume of PBS, and proceed with use in downstream applications (*see* **Note 8**).

4 Notes

1. If genotyping to select particular embryos, complete this step before the next passage. In this way undesired genotypes of cells can be discarded before passaging to conserve cell culture supplies.
2. When cells are thawed into a 10 cm dish virtually all cells should be viable and the plate should become confluent in 1–2 days. Batches of cells that exhibit poor viability upon thawing or that fail to proliferate appropriately in the initial 2 days

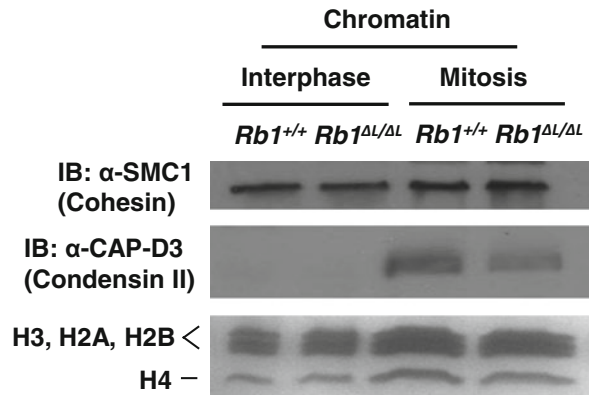

Fig. 2 Shake-off isolation of mitotic cells and analysis of chromatin: Mitotic MEF cells of the indicated genotypes were isolated by nocodazole treatment and shake-off. Isolated cells, and remaining adherent interphase cells, were processed to isolate chromatin fractions [14]. Interphase and mitotic chromatin preparations were normalized to histone protein content. Levels of SMC1 (a component of cohesin) and CAP-D3 (a component of condensin II) were determined by western blotting. Coomassie staining of histone proteins serves as a loading control

should be discarded as they will not generate reproducible data. We generally design experiments where control and mutant genotypes are thawed simultaneously and carried through the entire experiment in parallel to ensure that they are as comparable as possible.

3. It is advisable to plate multiple dishes of cells for each desired time point. This will allow a parallel culture to be pulse labeled with BrdU 1 h prior to the desired time point. These cells are then harvested in parallel to experimental cultures and used to monitor cell cycle position by flow cytometry. This is the approach used to generate the data in Fig. 1.
4. Growth media containing 20 % FBS can be used to stimulate more cells to enter the cell cycle at the beginning of this experiment.
5. We typically find that BrdU pulse labeling followed by analysis by flow cytometry at this time point results in 60 % positive cells. In addition, it is advisable to assay for replication stress following aphidicolin washout by western blotting for a marker such as phospho-serine 345 on Chk1.
6. At 8 h post-aphidicolin washout, pulse labeling with BrdU and flow cytometry reveals that cells are typically less than 20 % BrdU positive. Approximately 5–10 % will be in mitosis. This is ideal for analysis of mitotic events by microscopic methods as asynchronous MEF cultures will contain less than 1 % mitotic figures.

7. The exact cell density is less critical in this method. Cells can be plated at a higher initial density and drug treated sooner. It is important that cells are highly proliferative. Since your yields can be relatively low, using sparse cultures is unproductive.
8. A small quantity of cells should be fixed and used for H3-S10p staining and flow cytometry analysis, or processed for generating mitotic spreads to count mitotic figures. We typically obtain a 15 % yield of mitotic cells from cultures using this experimental approach.

Acknowledgements

The authors wish to thank the CIHR strategic training program in cancer research and technology transfer for fellowship support. F.D. is the Wolfe Senior Research Fellow in Tumor Suppressor Genes at Western University. Research in the Dick lab is supported by the Canadian Institutes of Health Research, the Canadian Cancer Society Research Institute, and the Cancer Research Society.

References

1. Harashima H, Dissmeyer N, Schnittger A (2013) Cell cycle control across the eukaryotic kingdom. Trends Cell Biol 23(7):345–356
2. Massague J (2004) G1 cell-cycle control and cancer. Nature 432:298–306
3. Kozar K, Ciemerych MA, Rebel VI, Shigematsu H, Zagozdzon A, Sicinska E, Geng Y, Yu Q, Bhattacharya S, Bronson RT, Akashi K, Sicinski P (2004) Mouse development and cell proliferation in the absence of D-cyclins. Cell 118:477–491
4. Geng Y, Yu Q, Sicinska E, Das M, Schneider JE, Bhattacharya S, Rideout WM, Bronson RT, Gardner H, Sicinski P (2003) Cyclin E ablation in the mouse. Cell 114(4):431–443
5. Brugarolas J, Moberg K, Boyd S, Taya Y, Jacks T, Lees J (1999) Inhibition of cyclin-dependent kinase 2 by p21 is necessary for retinoblastoma protein-mediated G1 arrest after gamma-irradiation. Proc Natl Acad Sci U S A 96:1002–1007
6. Santamaria D, Barriere C, Cerqueira A, Hunt S, Tardy C, Newton K, Caceres JF, Dubus P, Malumbres M, Barbacid M (2007) Cdk1 is sufficient to drive the mammalian cell cycle. Nature 448(7155):811–815
7. Isaac CE, Francis SM, Martens AL, Julian LM, Seifried LA, Erdmann N, Binne UK, Harrington L, Sicinski P, Berube NG, Dyson NJ, Dick FA (2006) The retinoblastoma protein regulates pericentric heterochromatin. Mol Cell Biol 26(9):3659–3671
8. Coschi CH, Martens AL, Ritchie K, Francis SM, Chakrabarti S, Berube NG, Dick FA (2010) Mitotic chromosome condensation mediated by the retinoblastoma protein is tumor-suppressive. Genes Dev 24(13):1351–1363
9. Cecchini MJ, Thwaites M, Talluri S, Macdonald JI, Passos DT, Chong JL, Cantalupo P, Stafford P, Saenz-Robles MT, Francis SM, Pipas JM, Leone G, Welch I, Dick FA (2014) A retinoblastoma allele that is mutated at its common E2F interaction site inhibits cell proliferation in gene targeted mice. Mol Cell Biol 34:2029–2045
10. Cecchini MJ, Amiri M, Dick FA (2012) Analysis of cell cycle position in mammalian cells. J Vis Exp 59:e3491. doi:10.3791/3491
11. Taylor WR (2004) FACS-based detection of phosphorylated histone H3 for the quantitation of mitotic cells. Methods Mol Biol 281:293–299
12. Parrinello S, Samper E, Krtolica A, Goldstein J, Melov S, Campisi J (2003) Oxygen sensitivity

severely limits the replicative lifespan of murine fibroblasts. Nat Cell Biol 5(8):741–747

13. Rieder CL, Maiato H (2004) Stuck in division or passing through: what happens when cells cannot satisfy the spindle assembly checkpoint. Dev Cell 7:637–651

14. Mendez J, Stillman B (2000) Chromatin association of human origin recognition complex, cdc6, and minichromosome maintenance proteins during the cell cycle: assembly of prereplication complexes in late mitosis. Mol Cell Biol 20(22):8602–8612

Chapter 6

Cell Cycle Synchronization in *Xenopus* Egg Extracts

Peter J. Gillespie, Julia Neusiedler, Kevin Creavin, Gaganmeet Singh Chadha, and J. Julian Blow

Abstract

Many important discoveries in cell cycle research have been made using cell-free extracts prepared from the eggs of the South African clawed frog *Xenopus laevis*. These extracts efficiently support the key nuclear functions of the eukaryotic cell cycle in vitro under apparently the same controls that exist in vivo. The *Xenopus* cell-free system is therefore uniquely suited to the study of the mechanisms, dynamics and integration of cell cycle regulated processes at a biochemical level. Here, we describe methods currently in use in our laboratory for the preparation of *Xenopus* egg extracts and demembranated sperm nuclei. We detail how these extracts can be used to study the key transitions of the eukaryotic cell cycle and describe conditions under which these transitions can be manipulated by addition of drugs that either retard or advance passage. In addition, we describe in detail essential techniques that provide a practical starting point for investigating the function of proteins involved in the operation of the eukaryotic cell cycle.

Key words Xenopus, Egg extract, In vitro, Cell-free system, DNA replication, Cell cycle, Synchronization

1 Introduction

For more than 30 years we have used cell-free extracts prepared from the eggs of the South African clawed frog, *Xenopus laevis*, to study the control of cell cycle progression and DNA replication. Originally conceived to study chromatin remodeling [1], this embryonic model system is used to conduct research in fields as diverse as DNA replication, apoptosis, nucleocytoplasmic transport, kinetochore formation and spindle microtubule dynamics and sister chromatid cohesion and condensation.

That these soluble egg extracts recapitulate the key nuclear transitions of the eukaryotic cell cycle in vitro under apparently the same controls that exist in vivo is dependent upon some key properties of early *Xenopus* embryos [2–4]. The eggs, as in other vertebrates, are arrested in metaphase II of meiosis. Progression into the first mitotic interphase occurs upon fertilization. In only 7 h after

Amanda S. Coutts and Louise Weston (eds.), *Cell Cycle Oscillators: Methods and Protocols*, Methods in Molecular Biology, vol. 1342, DOI 10.1007/978-1-4939-2957-3_6,

fertilization the eggs undergo 11 rounds of synchronous cell division. It is only after this stage—at the mid-blastula transition—that zygotic transcription occurs [5, 6]. The eggs therefore contain an abundant stockpile of material to support genome duplication and segregation up to DNA concentrations found at the onset of zygotic transcription: ~13 ng DNA per 0.5 μl egg, pre-S phase, in cell cycle 12, with approximately ~4000 cells per embryo at the transition. The continuing translation of a single protein, cyclin B, can support passage through the whole cell cycle [7].

DNA added to extract prepared from unfertilized, metaphase arrested, eggs is first assembled into chromatin and then condensed into rod-like fibers [3]. Upon activation and release of the extract into interphase the DNA is first decondensed and then assembled into structures corresponding to interphase nuclei [3, 4]. Upon nuclear assembly the added DNA is efficiently replicated, producing interphase nuclei with a 4C DNA content [8, 9]. Advancement of the extracts into mitosis supports first the condensation and resolution of paired sister chromatids and ultimately their separation on the spindle, all in vitro [10]. That these extracts support this wide range of activities in vitro makes this model system uniquely suited to the study of the mechanisms, dynamics and integration of cell cycle regulated processes at a biochemical level.

The regulation of cell cycle progression and DNA replication in egg extract occurs under the same controls as occur in vivo. Cytostatic factor (CSF) maintains the block to cell cycle progression in extracts prepared from unfertilized eggs [11]. Activation of these extracts by the addition of calcium, mimicking the Ca^{2+} wave at fertilization, promotes cyclin B destruction facilitating meiotic exit and entry into the first mitotic cycle [12]. The complete duplication of DNA present in the now interphase extract requires the activation of many thousands of origins of replication. To ensure genetic stability these origins must fire once and only once in each cell cycle. To this end two distinct signals are required to permit origin activation: origin "licensing" and "activation." The activation of the Anaphase Promoting Complex (APC/C) upon exit from anaphase of meiosis II permits activation of the "replication licensing system" [13, 14]. This allows Mcm2–7 double hexamers to be loaded onto DNA, "licensing" these sites to act as replication origins in the upcoming S phase [15–17].

During S phase replication forks are initiated, only at licensed origins, by the combined action of two protein kinases: S phase cyclin-dependent kinases (CDKs) and Dbf4-dependent kinases (DDKs) [18–22]. It is likely that nuclear assembly and protein import permits the concentration of these two kinases within the nucleus to a critical concentration that promotes the initiation of replication forks. Nuclear protein import also prevents re-replication of DNA by reactivating the licensing inhibitor geminin [14, 23]. The combination of CDK and DDK activity promotes the recruitment of replisome proteins to origins, which activates the helicase

activity of Mcm2–7 to unwind template DNA at the replication fork [24]. Activated origins revert to an unlicensed state upon initiation as Mcm2–7 moves away with the replication forks. Terminated Mcm2–7 hexamers are removed from the DNA under the control of ubiquitination [25, 26]. The sequential activation of the license and initiation signals ensures the faithful duplication of the genome [15, 27].

Upon completion of genome duplication the translation of cyclin B promotes passage into the first mitotic metaphase in vitro [7, 28]. At the chromatin level, high mitotic CDK activity drives sister chromatid resolution and condensation [7, 29, 30]. These condensed chromosomes form into a cognate metaphase plate with bi-orientated amphitelic sister chromatids. The sisters can then be induced to separate as the extract undergoes the metaphase-to-anaphase transition and reenters into interphase.

Importantly, by using well-characterized inhibitors of individual proteins that function in these phase transitions we are able to perturb cell cycle progression in vitro. In this article we describe the methods currently in use in our laboratory for the study of cell cycle progression and DNA replication using the *Xenopus* cell-free system. In addition to a description of the methods used for extract preparation, we detail their application for studying protein function in this system. These recently developed and revised techniques provide a practical starting point for investigation of cell cycle progression and DNA replication using this system.

2 Materials

Buffer storage temperatures are indicated in parenthesis and are abbreviated as follows:

temperature, as indicated, °C; RT—room temperature; RS—refrigerated stock; FS—frozen stock. All solutions are made up with Milli-Q H_2O.

2.1 Preparation of Demembranated *Xenopus laevis* Sperm Nuclei

1. EB (4 °C, freshly made): 50 mM KCl, 5 mM $MgCl_2$, 2 mM dithiothreitol (DTT) or β-mercaptoethanol, 50 mM HEPES–KOH, pH 7.6.
2. SuNaSp (4 °C, freshly made): 0.25 M sucrose, 75 mM NaCl, 0.5 mM spermidine, 0.15 mM spermine, 15 mM HEPES–KOH, pH 7.6.
3. Lysolecithin (−20 °C FS to 4 °C): 5 mg/ml, in H_2O.
4. Hoechst 33258 (−20 °C FS to 4 °C): 10 mg/ml in H_2O; prepare 20 μg/ml dilution on the day.
5. MS222 (RT, freshly made, immediately before use): 0.2 % w:v Tricaine mesylate MS222, ~0.5 % w:v $NaHCO_3$, to pH 7.5.

2.2 Preparation of Metaphase Arrested Xenopus laevis Egg Extract

1. 10× MMR (RT): 1 M NaCl, 20 mM KCl, 10 mM $MgCl_2$, 20 mM $CaCl_2$, 1 mM EDTA, 50 mM HEPES–NaOH, pH 7.8.
2. 20× XB Salts (4 °C RS): 2 M KCl, 40 mM $MgCl_2$, 2 mM $CaCl_2$.
3. XBE2 (4 °C to RT): 1× XB salts, 1.71 % w:v sucrose, 5 mM K-EGTA, 10 mM HEPES–KOH, pH 7.7.
4. LFB 1/50 (−20 °C FS or freshly made, 4 °C): 10 % w:v sucrose, 50 mM KCl, 2 mM $MgCl_2$, 1 mM EGTA, 2 mM DTT, 20 mM K_2HPO_4/KH_2PO_4 pH 8.0, 40 mM HEPES–KOH, pH 8.0.
5. Energy Regenerator (−20 °C FS to 4 °C): 1 M phosphocreatine disodium salt, 600 μg/ml creatine phosphokinase in 10 mM HEPES–KOH pH 7.6.
6. Cytochalasin D (−20 °C FS to RT): 10 mg/ml, in DMSO.
7. Protease inhibitors (−20 °C FS to RT): aprotinin, 10 mg/ml in H_2O; leupeptin, 10 mg/ml in H_2O; pepstatin, 10 mg/ml in dimethylformamide.
8. Dejellying solution (RT, freshly made, immediately before use): 2 % cysteine w:v in H_2O, to pH 7.8 with NaOH.

2.3 Preparation of Interphase Xenopus laevis Egg Extract

1. 10× MMR (RT): 1 M NaCl, 20 mM KCl, 10 mM $MgCl_2$, 20 mM $CaCl_2$, 1 mM EDTA, 50 mM HEPES–NaOH, pH 7.8.
2. Barth solution (RT): 88 mM NaCl, 2 mM KCl, 1 mM $MgCl_2$, 15 mM Tris–HCl pH 7.4, 0.5 mM $CaCl_2$.
3. Calcium ionophore A23187 (−20 °C FS to RT): 10 mg/ml in dimethyl sulfoxide (DMSO).
4. Extraction buffer (EB) (4 °C, freshly made): 50 mM KCl, 50 mM HEPES–KOH (pH 7.6), 5 mM $MgCl_2$, 2 mM DTT or β-mercaptoethanol.
5. Extract dilution buffer with sucrose (EDB-S) (−20 °C FS to 4 °C): 50 mM KCl, 50 mM HEPES–KOH (pH 7.6), 10 % (w/v) sucrose, 2 mM DTT, 0.4 mM $MgCl_2$, 0.4 mM EGTA, and pepstatin, leupeptin, and aprotinin (1 μg/ml each).

2.4 Use of Xenopus Egg Extract: General Use and Determination of Extract Integrity and Cell Cycle Status

1. Xenopus egg extract (−80 °C/liquid nitrogen to RT immediately before RT water bath thaw) and demembranated Xenopus sperm nuclei ~400 ng DNA/μl (−80 °C/−20 °C FS to 4 °C).
2. Energy Regenerator (−20 °C FS to 4 °C): 1 M phosphocreatine disodium salt, 600 μg/ml creatine phosphokinase in 10 mM HEPES–KOH pH 7.6.
3. Cycloheximide (−20 °C FS to 4 °C): 10 mg/ml, in H_2O.
4. $CaCl_2$ (−20 °C FS to 4 °C): 50 mM, in H_2O.
5. Hoechst 33258 (−20 °C FS to 4 °C): 10 mg/ml in H_2O; prepare 20 μg/ml dilution on the day.

2.5 Use of Metaphase Arrested Egg Extract: In Vitro Release into First Mitotic Interphase and Manipulation by Drug Addition

As Subheading 2.4, and the following:

1. Roscovitine (−20 °C FS to RT): 400 mM, in DMSO.
2. 6-DMAP (−20 °C FS to 4 °C): 50 mM, in H_2O.
3. Microcystin LR (−20 °C FS to RT): 100 μM, in DMSO.
4. D-box peptide (−20 °C FS to 4 °C): 26 mM, in LFB1/50.
5. MG132 (−20 °C FS to RT): 40 mM, in DMSO.
6. Bortezomib (−20 °C FS to RT): 200 mM, in DMSO.

2.6 Use of Interphase Egg Extract: Manipulation by Drug Addition

As Subheading 2.4, and the following:

1. Wheat germ agglutinin (−20 °C FS to 4 °C): 20 mg/ml, in H_2O.
2. GeminiDEL (−80 °C/liquid nitrogen FS to 4 °C): used at ~100 nM (~2.6 ng/μl), in LFB 1/50.
3. $p27^{Kipl}$ (−80 °C/liquid nitrogen FS to 4 °C): used at ~100 nM (~5.2 μg/ml), in LFB 1/50.
4. $p21^{Cipl}$ (−80 °C/liquid nitrogen FS to 4 °C): used at ~0.5 μM (~21.1 μg/ml), in LFB 1/50.
5. Roscovitine (−20 °C FS to RT): 400 mM, in DMSO.
6. PHA-767491 (−20 °C FS to RT): 100 mM, in DMSO and diluted in 40 mM HEPES–KOH pH 7.0 immediately prior to use, mixing well to avoid precipitates.
7. Aphidicolin (−20 °C FS to RT): 18 mM. in DMSO.

2.7 Interphase-to-Mitosis Extract Conversion

As Subheading 2.4, and the following:

Non-destructible mutant mitotic cyclins, e.g., cyclin A1 NΔ56 [31, 32] or cyclin BΔ90 [33] (−80 °C/liquid nitrogen FS to 4 °C), or metaphase-arrested egg extract (−80 °C/liquid nitrogen to RT immediately before RT water bath thaw).

2.8 Quantifying DNA Replication

As Subheading 2.4, and the following:

1. Stop-C (RT): 0.5 % w:v SDS, 5 mM EGTA, 20 mM Tris HCl, pH 7.5.
2. Proteinase K (−20 °C): 20 mg/ml proteinase K, 50 % v:v glycerol, 10 mM Tris HCl, pH 7.5.
3. 5 % TCA (4 °C RS): 5 % w:v TCA, 0.5 % w:v $Na_4P_2O_7 \cdot 10H_2O$.
4. 10 % TCA (4 °C RS): 5 % w:v TCA, 2 % w:v $Na_4P_2O_7 \cdot 10H_2O$.
5. α^{32}P-dATP (high activity: typically 10 mCi/ml) (4 °C RS).
6. 25 mm Paper filter disks.
7. 25 mm Glass microfiber filter disks.
8. Vacuum manifold (Millipore).
9. Gel preparation buffer (RT): 50 mM NaCl, 1 mM EDTA.

10. Gel running buffer (RT): 50 mM NaOH, 1 mM EDTA.
11. StopN (RT): 20 mM Tris HCl pH 8.0, 200 mM NaCl, 5 mM EDTA, 0.5 % SDS.
12. 7 % (w:v) TCA (4 °C RS).
13. Phenol–chloroform–isoamyl alcohol (25:24:1) (e.g., Sigma P-3803) (4 °C RS).
14. 10 mM EDTA (RT).
15. 100 % ethanol (−20 °C).
16. 70 % ethanol (RT).
17. 2× alkaline loading buffer (RT): 100 mM NaOH, 2 mM EDTA, 2.5 % Ficoll, 0.025 % bromocresol green, H_2O.
18. Eppendorf Phase Lock gel tube.
19. 6× 3MM paper, 20 cm × 20 cm.
20. 12× paper towel.
21. 2× glass plates, 20 cm × 20 cm.
22. 8× large bulldog clips.
23. Large polythene box 25 cm × 25 cm.
24. End-radiolabeled molecular weight markers—1 kb lambda DNA HindIII digested, see below.
25. 10× End-labeling buffer: 5 mM dCTP, 5 mM dGTP, 5 mM dTTP, 500 mM Tris HCl, pH 8.0, 100 mM $MgCl_2$.
26. Reaction mix (10 µl): 1 µl 10× end-labeling buffer, 1 µl DNA (500 µg/ml) 1 kb lambda-HindIII, 0.5 µl Klenow exo− (10 units/µl), 0.3 µl 32P-dATP (10 mCi/ml), 7.2 µl H_2O.

2.9 Immuno-depletion and Immunoprecipitation

As Subheading 2.4, and the following:

1. A source of antibody, either crude serum or a purified fraction.
2. Either, agarose beads (rProtein A- or rProtein G-FF; GE Healthcare) or magnetic beads (Dynabeads Protein A or G; Dynal-Life Technologies) (4 °C RS).
3. LFB 1/50 (−20 °C FS or freshly made, 4 °C): 10 % w:v sucrose, 50 mM KCl, 2 mM $MgCl_2$, 1 mM EGTA, 2 mM DTT, 20 mM K_2HPO_4/KH_2PO_4 pH 8.0, 40 mM HEPES–KOH, pH 8.0.
4. 100 mM HEPES–KOH, pH 8.0 (−20 °C FS or freshly made, 4 °C).
5. Xenopus egg extract (−80 °C/liquid nitrogen to RT immediately before RT water bath thaw) and demembranated Xenopus sperm nuclei ~400 ng DNA/µl (−80 °C/−20 °C FS to 4 °C).
6. Energy Regenerator (−20 °C FS to 4 °C): 1 M phosphocreatine disodium salt, 600 µg/ml creatine phosphokinase in 10 mM HEPES–KOH pH 7.6.

7. Cycloheximide (−20 °C FS to 4 °C): 10 mg/ml, H_2O.
8. $CaCl_2$ (−20 °C FS to 4 °C): 50 mM in H_2O.
9. Magnetic tube stand.
10. PMSF (−20 °C FS to RT): 100 mM, in 100 % ethanol.
11. Gel loading fine pipette tips.
12. 50 ml Falcon tube.
13. 25 μm Nybolt filter.
14. Sepharose wash buffer (4 °C, freshly made): 40 mM HEPES, 20 mM K_2HPO_4/KH_2PO_4, pH 8.0, 2 mM $MgCl_2$, 1 mM DTT, 2 mM EGTA, 10 % (w:v) sucrose, 10 μg/ml each of leupeptin, pepstatin, and aprotinin, 100 mM KCl.
15. Dynabead wash buffer (4 °C, freshly made): 20 mM Na_2HPO_4/NaH_2PO_4 pH 8.0, 150 mM NaCl, 0.1 % Tween 20.

2.10 Immunofluorescent Staining of Chromosomes and Nuclei Assembled In Vitro

1. 24-well plates.
2. 13 mm coverslips—optionally coated with poly-lysine.
3. XBE2 plus 30 % sucrose (4 °C, freshly made): 1× XB salts, 5 mM K-EGTA, 10 mM HEPES–KOH pH 7.7, 30 % (w:v) sucrose.
4. 20× XB Salts (4 °C RS): 2 M KCl, 40 mM $MgCl_2$, 2 mM $CaCl_2$.
5. Formaldehyde stock (typically 37 %, freshly prepared immediately before use or high-grade commercial stock, typically 16 %, at 4 °C).
6. PBS plus 0.1 M glycine pH 7.0 (RT)—alternatively 750 mM Tris–HCl pH 7.0.
7. PBS plus 0.1 % (v:v) Tween and 3 % (w:v) BSA (RT).
8. VECTASHIELD (Vector Laboratories) (4 °C RS).
9. PBS plus 0.1 % (v:v) Tween (RT).
10. PBS plus 0.1 % (v:v) Triton (RT).
11. Secondary Antibodies (Alexa Fluor recommended).
12. DAPI: 1 mg/ml, in PBS (−20 °C FS); use at 1/1000, freshly made, immediately before use.

3 Methods

3.1 Preparation of Demembranated Xenopus laevis Sperm Nuclei

Although able to support the replication of a range of DNA templates - single and double stranded plasmids and extracted mammalian nuclei - the physiological substrate for replication in Xenopus laevis egg extracts are Xenopus laevis sperm nuclei. The sperm nuclei, recovered from the testes postmortem, remain stable for extended periods after demembranation.

Frogs are euthanized by means of a lethal dose of anesthetic and the testes are recovered postmortem. The preparation procedure is composed of two parts: after removing unwanted tissue from around the isolated testes the sperm are released; the released nuclei are then demembranated and prepared for storage. Sperm yield may be increased by hormone injection (*see* **Note 1**).

1. Place the frogs in MS222 solution in individual opaque chambers. When their heads drop below water and they stop moving when touched (after approximately 5–10 min), check for life by placing a forefinger deep into the frog's mouth—if the frog performs a reflex sucking response then it is alive. Keep the frog in MS222, checking every minute or so until the reflex is lost.
2. Remove the frog from the MS222 and place it on its back on a protected work surface. Ensure death by quickly opening up the abdomen using sharp scissors or a scalpel and cutting the main arteries around the heart. Remove the testes as soon as possible, cutting carefully so as not to cut or damage them, and place them in EB solution on ice (*see* **Note 2**).
3. Wash the testes in ~20 ml of EB in a 9 cm petri dish and clean them, being careful to avoid bursting them, using two pairs of dissection forceps, to remove any blood vessels and extraneous tissue.
4. Transfer the cleaned testes to a fresh petri dish containing 10 ml EB. Chop the testes with a razor blade as finely as possible; pool all chopped material and store on ice.
5. Filter the homogenate through a 25 μm mesh nylon filter (e.g., Nitex or Nybolt), e.g., mounted over the end of a 50 ml tube (*see* **Note 3**). The filtered material will look quite cloudy.
6. Spin the filtered material in a 15 ml tube at 2000 × *g* in a swinging bucket rotor for 5 min at 4 °C; repeat the spin if the supernatant appears cloudy. If the sperm preparation contains a significant contamination of erythrocytes these will appear as a red fraction at the bottom of the pellet. Separate these cells by careful resuspension and transfer of the sperm to a second tube—the recovered sperm should be respun and the still pelleted bloods cells in the original tube discarded.
7. Resuspend the pellet in a total volume of 0.5 ml SuNaSp per testis at room temperature. Supplement with 25 μl lysolecithin per testis and incubate for 5–10 min at room temperature. Check for demembranation of the sperm after incubation by mixing 1 μl of sample with 1 μl of Hoechst 33258 (20 μg/ml) and view by UV microscopy. Demembranated sperm appear as small fat "squiggles" which stain bright blue with Hoechst; non-demembranated sperm will not stain with Hoechst. If <95 % are demembranated, then respin and resuspend the sperm in fresh SuNaSp and repeat the lysolecithin treatment.

8. Centrifuge the demembranated sperm at 2000 × *g* in a swinging bucket rotor for 5 min at 4 °C. Discard the supernatant and quench the lysolecithin by resuspending the total pelleted material in 0.5 ml SuNaSp containing 3 % (w:v) BSA per testis.
9. Centrifuge again and resuspend the pellet in 0.5 ml EB per testis and then repeat. Resuspend the twice washed pellet in 100 μl EB plus 30 % glycerol per testis.
10. To count the sperm make a small aliquot of the resuspended pellet and dilute 1:100 in EB. Use a haemocytometer to count the number of sperm and large somatic-type nuclei (*see* **Note 4**). The DNA concentration of the preparation can be determined, given that the Xenopus haploid genome is ~3 pg DNA. We typically recover 100–200 μg DNA (33,000,000–66,000,000 haploid nuclei) per testis.
11. Dilute the stock in EB plus 30 % glycerol to give a final concentration of ~400 ng DNA/μl (133,000 haploid nuclei/μl). Freeze in 80 μl aliquots and store in Eppendorf tubes at −80 °C.

3.2 Preparation of Metaphase Arrested *Xenopus laevis* Egg Extract

In the more than 30 years since the original method of Lohka and Masui was described [2], small but significant optimizations have been developed for preparing *Xenopus* egg extracts suited for studying different aspects of the cell cycle. In particular, methods for preparing extracts that support efficient DNA replication differ from methods for preparing extracts that support efficient passage through mitosis. Since the focus of research in our lab historically has been DNA replication we developed a method appropriate for this purpose. However, with the broadening of research interests over the last decade we have incorporated key aspects of metaphase arrested extract preparation protocols into our scheme, giving rise to an extract that is suitable for both interphase and metaphase studies.

Extracts can be frozen and stored under liquid nitrogen, or at −80 °C, and remain stable without loss of quality for at least 10 years. Whereas frozen extracts support efficient and rapid DNA replication, they are unable to cycle into mitosis without further manipulation. A method for preparing extracts that cycle in and out of mitosis in vitro has been described [7]. It should also be noted that there is a specialized method for preparing "nucleoplasmic" extracts which can support the replication of DNA in the absence of nuclear assembly [34, 35].

3.2.1 General Considerations for Egg Production and Extract Preparation

1. The single most important consideration when preparing extracts is the quality of the starting material, the eggs. Eggs of the very best quality are essential for preparation of a high quality extract. In this regard it is vitally important that the *Xenopus* colony is maintained in prime health.

2. *Xenopus* eggs are arrested at metaphase of meiosis II. Metaphase arrested eggs can be identified by the clear circumferential distinction between the larger sized dark colored animal pole and the smaller sized lightly colored vegetal pole—essentially, eggs appear half black and half white. The animal pole contracts upon activation, so that from the top eggs appear almost totally white but for a small black dot.
3. When eggs spontaneously enter interphase in the absence of fertilization they will apoptose in due course. Apoptotic eggs, which may float on the top surface of the egg mass, appear as large white or gray spheres, often visibly greater in volume than an intact egg.
4. Activated or apoptotic eggs in a batch should be removed. On preparation the contents of the eggs mix together. Since activation and apoptosis are enzyme mediated processes, a small contamination with active or apoptotic eggs may render your extract useless. It is therefore advisable to remain vigilant and make considerable effort to remove activated and apoptotic eggs from your preparation during the early stages. The longer the time that the eggs lie before extract preparation the greater the likelihood there is of the eggs spontaneously activating and/or apoptosing.
5. Collection of the eggs into a high salt buffer helps maintain the metaphase arrest. We find the egg collection buffer we currently use, MMR, is optimal in this regard. Furthermore, to guarantee egg freshness we make a number of egg collections throughout the day.
6. We collect the eggs from individual frogs in separate glass beakers. The collected eggs are assessed for quality and pooled accordingly into at least three groups—highest quality: the vast majority of eggs remain visibly in metaphase during the early steps of extract preparation and there are few, if any, apoptotic eggs; acceptable quality: contains a small percentage of either activated or apoptosed eggs and only a limited fraction are seen to activate or apoptose during the early steps of extract preparation; poorest quality: contains a large fraction of activated and/or apoptosed eggs, or strings of apparently connected immature eggs, which are of an indeterminate cell cycle status. These poorest quality eggs, together with any batches in which the laying buffer has turned opaque white-gray with the contents of ruptured apoptotic eggs, should be discarded. Extract can be made from both the highest and acceptable quality eggs, although these should be prepared separately. During laying the frogs may shed excessive amounts of skin or regurgitate food, discoloring the laying buffer. Extracts can be prepared from these “dirty” eggs after removal of the detritus, but

we would not consider these eggs as high quality irrespective of their standard.

7. We rest the frogs for a minimum of 4 months after each ovulation; after 8–12 ovulations egg quality and quantity becomes unacceptable.
8. Female frogs are primed with 50 units of Folligon (Pregnant Mare Serum Gonadotrophin) 3 days before the eggs are required to increase the number of stage 6 mature oocytes. We typically inject ~15 frogs per preparation. At approximately 4 pm on the day before eggs are required, frogs are injected with 500 units of Chorulon (Chorionic Gonadotrophin) and placed in individual laying tanks at 18–21 °C in 2 l of 1× MMR egg laying buffer. The first egg collection of the day is made by 9.30 am; to avoid unnecessary delay all materials required during the process are readied prior to beginning.

3.2.2 Protocol for the Preparation of Metaphase Arrested Xenopus laevis Egg Extract

1. Egg volume and quality are recorded.
2. Rinse eggs several times in 1× MMR to remove debris.
3. Remove activated and apoptosed eggs with a Pasteur pipette and any that subsequently appear.
4. Pour off excess MMR and add dejellying solution; swirl gently, at intervals. After 3–4 min remove and replace the dejellying solution; continue until the eggs are dejellied and pack tightly together.
5. Wash the dejellied eggs twice with room temperature XBE2 and then once with the XBE2 plus protease inhibitors (final concentration 10 μg/ml for each component).
6. Transfer the eggs to 14 ml centrifuge tubes containing 1 ml XBE2 plus protease inhibitors and cytochalasin D (final concentration 100 μg/ml), using as few as possible. Remove excess buffer from the settling eggs.
7. Pack the eggs by centrifugation at 3000 rpm (~1400×*g*) in a Beckman JS13.1 (or similar) swinging bucket rotor for 1 min at 16 °C. Remove excess buffer and any remaining activated or apoptosed eggs that resolve to the top surface during packing using a Pasteur pipette.
8. Spin-crush the eggs by centrifugation at 10,000 rpm (~16,000×*g*) in a Beckman JS13.1 (or similar) swinging bucket rotor for 10 min at 16 °C. Collect the dirty brown cytoplasmic layer—approximately 1/3 of the sample, between the bright yellow lipid at the top and the gray yolk platelets at the bottom—using a 20 G needle and a 1 ml syringe via side puncture. From this point onwards the extract is kept on ice.
9. Supplement the extract with a 1:1000 dilution of cytochalasin D (final concentration 10 μg/ml), 1:1000 dilution of protease

inhibitors (final concentration of 10 μg/ml for each component), 1:80 dilution of energy regenerator and LFB1/50 to 15 % v:v. Mix the extract thoroughly using a 3 ml plastic Pasteur pipette.

10. Load precooled SW55 ultracentrifuge tubes (or equivalent) with 3–5 ml of extract, on ice, using as few tubes as possible. Centrifuge the extract at 30,000 rpm (approximately 84,000 × *g*) in a precooled SW55 rotor for 20 min at 4 °C. This spin results in a small black insoluble pellet, a larger loose brown membranous pellet above it, a clear golden cytoplasmic fraction with a variable amount of white membranous material floating in it, and a small yellow lipid plug.
11. Remove the lipid plug from the top of the tube with an ethanol-cleaned and dried spatula. Collect the golden cytoplasmic layer, including the wispy membranes floating immediately below the lipid plug. Do not disturb the "dirty yellow" membrane layer below the cytoplasm; this layer contains the mitochondria which promote apoptosis on freeze-thawing. If this layer is disturbed do not collect any more extract. The interface between layers can be more easily distinguished when the tube is well illuminated with a backlight. Optionally, at this stage, extract may be filtered through a 25 μm mesh nylon filter (e.g., Nitex or Nybolt).
12. Supplement the recovered cytoplasm to 2 % (v:v) glycerol and mix thoroughly, but very gently, using a 3 ml plastic Pasteur pipette. Record final extract volume.
13. Freeze the extract by dropping 20 μl aliquots into plastic Petri dishes containing liquid nitrogen using a micropipette tip with the end cut off. The beads should then be stored under liquid nitrogen. Alternatively, place single use aliquots into appropriately sized Eppendorf tubes with needle-punctured caps, and freeze in liquid nitrogen; after freezing, the tubes, but not the beads, may be stored at −80 °C.

3.3 Preparation of Interphase Xenopus laevis Egg Extract

Xenopus eggs are arrested at metaphase of meiosis II. Release from metaphase arrest activates unfertilized eggs and the replication licensing system; extracts can be prepared from eggs that have been briefly activated in vivo by treatment with a calcium ionophore—the exogenous Ca^{2+} mimics the calcium wave generated at fertilization. We typically find that extracts prepared from activated eggs show a larger variability in quality than those prepared from unactivated eggs. However, ionophore activation is a useful technique when it is important to ensure exit from meiosis prior to extract preparation, for example if extracts that have efficiently activated the licensing system in vivo are required. Although the general strategy for preparation of in vivo activated extracts is the same as for the preparation of metaphase arrested, there are a number of significant changes, most notably with the buffer system used;

whereas the buffer system used for metaphase extract preparation is optimized to limit calcium availability, for in vivo activated extract preparation calcium is provided.

1. Egg volume and quality are recorded.
2. Rinse eggs several times in 1× MMR to remove debris.
3. Remove activated and apoptosed eggs with a Pasteur pipette.
4. Pour off excess MMR and add dejellying solution; swirl gently, at intervals. After 3–4 min remove and replace the dejellying solution; continue until the eggs are dejellied and pack tightly together.
5. Wash the dejellied eggs thrice with room temperature Barth solution, leaving the eggs in approximately 100 ml solution.
6. Activate the eggs by adding 10 μl A23187—final concentration 2 μg/ml; upon activation the eggs roll animal side up and the dark pigment contracts. Incubate until the vast majority of the eggs activate, typically 5–10 min.
7. Wash the dejellied eggs thrice with room temperature Barth solution.
8. Wash the eggs thrice with EB at 4 °C; all further steps are taken at 4 °C.
9. Transfer the eggs to precooled 14 ml centrifuge tubes, using as few as possible. Remove excess buffer from the settling eggs.
10. Pack the eggs by centrifugation at 3000 rpm (~1400×*g*) in a Beckman JS13.1 (or similar) swinging bucket rotor for 1 min at 4 °C. Remove excess buffer and any apoptosed eggs that resolve to the top surface during packing using a Pasteur pipette.
11. Spin-crush the eggs by centrifugation at 10,000 rpm (~16,000×*g*) in a Beckman JS13.1 (or similar) swinging bucket rotor for 10 min at 4 °C. Collect the dirty brown cytoplasmic layer—approximately 1/3 of the sample, between the bright yellow lipid at the top and the gray yolk platelets at the bottom—using a 20 G needle and a 1 ml syringe via side puncture.
12. Supplement the extract with a 1:1000 dilution of cytochalasin D (final concentration 10 μg/ml) and EDBS to 15 % v:v. Mix the extract thoroughly using a 3 ml plastic Pasteur pipette.
13. Load precooled SW55 ultracentrifuge tubes (or equivalent) with 3–5 ml of extract, on ice, using as few tubes as possible. Centrifuge the extract at 20,000 rpm (approximately 37,000×*g*) in a precooled SW55 rotor for 20 min at 4 °C. This spin results in a small black insoluble pellet, a larger loose brown membranous pellet above it, a clear golden cytoplasmic fraction with a variable amount of white membranous material floating in it, and a small yellow lipid plug.

14. Remove the lipid plug from the top of the tube with an ethanol-cleaned and dried spatula. Collect the golden cytoplasmic layer, including the wispy membranes floating immediately below the lipid plug. Do not disturb the "dirty yellow" membrane layer below the cytoplasm; this layer contains the mitochondria which promote apoptosis on freeze-thawing. If this layer is disturbed do not collect any more extract. The interface between layers can be more easily distinguished when the tube is well illuminated with a backlight.
15. Filter the extract through a 25 μm mesh nylon filter (e.g., Nitex or Nybolt).
16. Supplement the recovered cytoplasm to 2 % (v:v) glycerol and mix thoroughly, but very gently, using a 3 ml plastic Pasteur pipette. Record final extract volume.
17. Freeze the extract by dropping 20 μl aliquots into plastic Petri dishes containing liquid nitrogen using a micropipette tip with the end cut off. The beads should then be stored under liquid nitrogen.

3.4 Use of Xenopus Egg Extract: General use and Determination of Extract Integrity and Cell Cycle Status

Prior to experimental use we determine the cell cycle status and integrity of the prepared extract by following nuclear morphology upon the addition of sperm nuclei, plus and minus calcium, over 8 h by microscopy; extracts are supplemented with the translation inhibitor cycloheximide, preventing resynthesis of cyclin B and thereby preventing interphase extracts from progressing into mitosis. During this period the nuclei should remain stable; in apoptotic extracts chromatin condensation, nuclear and chromosomal DNA fragmentation will be apparent: these extracts should not be used for any purpose.

Sperm nuclei added to a metaphase arrested extract, in the absence of Ca^{2+} will not form nuclei. After primary nucleoplasmin-mediated decondensation chromatin is seen to recondense and form into a network of rod like chromosomes that separate and resolve in time. Extracts may escape from metaphase arrest during preparation and form nuclei in the absence of exogenous calcium ions that remain otherwise stable. Addition of Ca^{2+} to a metaphase arrested extract will facilitate metaphase exit and passage into interphase; added sperm—and sperm added directly to an interphase extract—will form into nuclei and undergo DNA replication.

1. The required number of frozen beads (or volume) of extract are transferred to an Eppendorf tube and thawed in a room-temperature water bath (*see* **Note 5**).
2. Supplement egg extract with ER (1/40 stock) and cycloheximide (1/40 stock) (*see* **Note 6**), ± $CaCl_2$ (1/167 stock), as required (*see* **Note 7**). In vitro reactions are performed at 23 °C.
3. Add sperm nuclei at the desired concentration, typically 3–10 ng/μl (*see* **Note 8**). Most importantly, if multiple samples

are to be prepared from one extract treatment aliquots should be made as early as is appropriate.

4. Follow chromatin and nuclear morphology throughout the course of your reaction (*see* **Note 9**): mix 1 μl of sample with 1 μl of Hoechst 33258 (20 μg/ml) and view by microscopy. It is advisable to check morphology at a number of time points, typically 15 min apart, as appropriate, throughout the incubation (*see* **Note 10**).

3.5 Use of Metaphase Arrested Egg Extract: In Vitro Release into First Mitotic Interphase and Manipulation by Drug Addition

Extracts prepared from eggs arrested in metaphase II of meiosis provide a means to investigate metaphase entry and exit, including nuclear envelope breakdown (NEBD), chromosome condensation/decondensation, kinetochore formation, spindle microtubule dynamics, APC/C function, and the dynamic kinase–phosphatase balance, in addition to the events that occur early in interphase of the eukaryotic cell cycle prior to DNA replication, including replication licensing, nuclear formation and cohesin chromatin association.

Metaphase arrested extracts contain high levels of the mitotic kinases cyclin B-Cdk1 (Cdc2) [maturation promoting factor or MPF], Plk1 [Polo-like kinase 1], and Aurora B. A key feature of *Xenopus* egg extracts, however, is their ability to maintain metaphase arrest and prevent progression even with high cyclin B-CDK/MPF activity. This is due to the presence of a cytostatic factor (CSF), which depends on the activity of the Mos/MAPK and cyclin E-Cdk2 pathways, and the APC/C inhibitor Emi2 [36–38]. The APC/C is a multiprotein ubiquitin E3 ligase that catalyzes the ubiquitination and subsequent degradation of cell cycle regulators, such as cyclin B, in a defined sequence, establishing the temporal order of mitotic events in somatic cell cycles. APC/C complexes require an adaptor protein, either Cdc20 or Cdh1, for activity. At metaphase II of meiosis in Xenopus eggs APC/C activity is kept in an inactive state and cell cycle progression is inhibited by Emi2 competing with Cdc20 for APC/C binding. Emi2 is stabilized and activated by the MAPK-mos-rsk pathway, which recruits PP2A, bound to its regulatory subunit B56β/ε, to Emi2 to counteract the inactivating phosphorylations of the mitotic kinases [39]. PP2A, with the B55δ regulatory subunit, is largely responsible for counteracting CDK dependent phosporylations during mitotic exit. As such, it is necessary to inhibit this activity to maintain metaphase arrest. CDK dependent activation of Greatwall kinase leads to global suppression of PP2A. Therefore, through the combined action of Emi2 and cyclin B-Cdk1, metaphase arrested extracts are characterized by both high CSF and MPF activity. The presence of both MPF and CSF ensures these extracts are primed for rapid entry into the cell cycle.

Unactivated metaphase-arrested extracts can induce NEBD in previously formed interphase nuclei (see below). Sperm nuclei added directly to these extracts become loaded with condensins I and II,

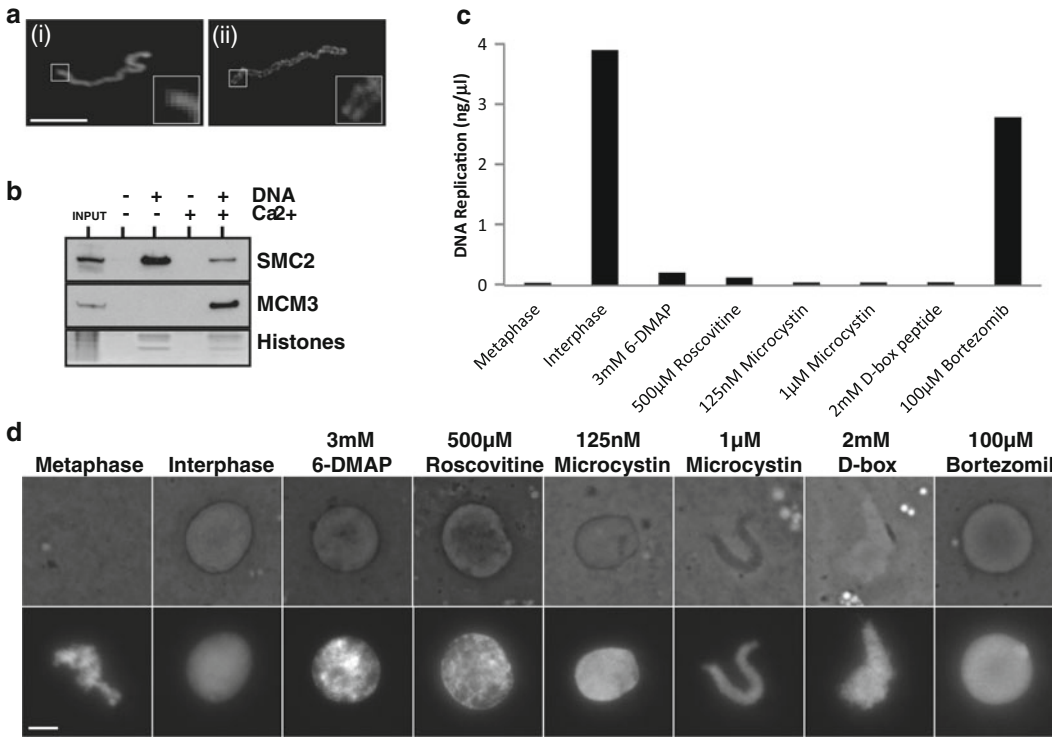

Fig. 1 Manipulation of the metaphase-to-anaphase transition. (**a**) (*i*) A single condensed chromatid: sperm nuclei were added directly to metaphase-arrested egg extract and incubated for 2 h. (*ii*) Condensed sister chromatids: sperm nuclei were added to interphase egg extract to allow DNA replication to occur; after 2 h 2 volumes of metaphase-arrested egg extract were added to the interphase reaction and incubated for 2 h to promote mitotic entry. For both *i* and *ii*, chromatids were fixed, isolated, and stained with anti-condensin (SMC2) antibody and visualized under UV microscopy. *Insets* show close-ups of selected regions. Scale bar, 5 μm. (**b**) Sperm nuclei were incubated in metaphase-arrested or interphase egg extract for 15 min. Chromatin was isolated and immunoblotted for condensin (SMC2) and replication licensing (Mcm3). The lower portion of the gel was stained with Coomassie to visualize histones as a loading control. (**c**, **d**) Sperm nuclei were added at 5 ng/μl to extract which was metaphase arrested, released into interphase, or pretreated for 10 min with various drugs prior to release with Ca^{2+}: 3 mM 6-DMAP, 500 μM roscovitine, 250 nM microcystin, 1 μM microcystin, 2 mM D-box peptide or 100 μM bortezomib. (**c**) shows total DNA replication assayed 90 min after the addition of sperm. (**d**) shows phase contrast (*top panel*) and UV (*bottom panel*) microscopy 40 min after the addition of sperm. Scale bar, 10 μm

and together with the combined action of CDK1, Plk1 and Aurora B, generate long thin chromosome fibers—in the absence of DNA replication no paired sister chromatids are formed and only condensed single fibers are seen (Fig. 1a). The addition of calcium to metaphase arrested extracts, which mimics fertilization, activates CamKII. This triggers the Plk1 and SCF-βtrCP dependent destruction of Emi2, leading to the activation of the APC/C. APC/C activity then facilitates the metaphase to anaphase transition and release of the extract into the first interphase of the mitotic embryonic cleavage cycles [40]. APC/C E3 ubiquitin ligase activity results in

the destruction of cyclin B and securin, thereby allowing destruction of cohesin and also inactivates geminin, to activate the replication licensing system. Together this promotes chromatin decondensation, replication licensing and nuclear assembly (Fig. 1b–d).

3.5.1 Manipulation of the Metaphase to Anaphase Transition

Metaphase arrested egg extracts can be manipulated to generate distinct cell cycle states, with limited activities, by drug addition, thus facilitating the study of specific cell cycle regulated processes and proteins, uncoupled from cell cycle progression. The major activities known to date that control metaphase release involve regulating the kinase–phosphatase balance and the ubiquitin-degradation system, and as such these activities are the main targets for manipulation in a metaphase arrested extract. For this type of experiment extract quality is of prime importance and it must be unequivocally arrested. The addition of inhibitors to extract is made prior to release with $CaCl_2$. This allows manipulation of the earliest stages of metaphase release and avoids potent feedback circuits, which drive mitotic progression. These types of studies can be carried out to characterize a single process or protein in the treated extract alone or in the context of the whole cell cycle by combining additional extract types or by nuclear/extract transfer procedures.

Addition of CDK inhibitors, such as roscovitine [41, 42] or broad-spectrum kinase inhibitors such as 6-DMAP or staurosporine [43, 44], to metaphase arrested extract promotes passage into an "interphase-like" state without the calcium-dependent activation of the APC/C. These interphase-like extracts support chromatin decondensation and nuclear assembly but cannot undertake replication licensing (Fig. 1c, d). Previously licensed templates will replicate efficiently in treated extract however. This combination of activities is explained by the disruption of the kinase–phosphatase balance and subsequent uncoupling of APC/C activity from progression into the first interphase of the mitotic cell cycle. Cyclin B-Cdk1 activity is largely responsible for the mitotic state and inhibition of this kinase leads to PP2A-dependent dephosphorylation of CDK targets [45, 46]. B-type cyclins are a major target of the APC/C and their destruction is an important event for promoting entry into the next cell cycle. CDK inhibition generates extracts with activities that resemble interphase extracts without APC/C activation; the destruction of cyclin B and other key APC/C targets such as geminin and cell cycle progression are therefore inhibited (*see* **Note 11**). These extracts facilitate the study of APC/C target proteins in early cell cycle processes, the role of mitotic phosphorylation on proteins of interest, as well as nuclear assembly processes uncoupled from DNA replication.

The addition of the PP1 and PP2A phosphatase inhibitor microcystin to metaphase arrested extracts disrupts the kinase–phosphatase balance in favor of kinase activity. Upon calcium addition

to microcystin treated extracts, the APC/C targets cyclin B, securin, and geminin are destroyed; however, CDK target proteins which are usually dephosphorylated upon mitotic exit by PP2A remain modified even in the absence of CDK activity. Mitotic CDK targets include histones and condensin—which facilitates chromosome condensation—lamin—which control nuclear envelope formation—and subunits of the origin recognition complex (ORC) complex and Cdc6 to prevent replication licensing. Treatment of metaphase arrested extracts with 250 nM microcystin, which has been shown to reduce PP1/PP2A activity to 82–58 % [47], promotes nuclear membrane formation and chromatin decondensation. However, these extracts are not permissive for DNA replication; the addition of greater than 500 nM drug, which has been shown to reduce PP1/PP2A activity to <12 %, generates extracts that are unable to initiate chromatin decondensation, nuclear formation or DNA replication. This is due to the untimely CDK-dependent activation of condensin-mediated chromosome condensation and inhibition of lamin assembly which prevents nuclear formation and in turn DNA replication [47] (Fig. 1c, d). These treated extracts can be used to study the role of mitotic phosphorylation in the activation/inhibition of a protein/process of interest.

The D-box protein domain, which facilitates protein-protein interactions with the APC/C, is a defining feature of APC/C substrates and results in the ubiquitin dependent destruction of the substrate protein. A peptide containing the D-box of the prototypical APC/C target cyclin B can be generated for use as a competitive inhibitor of the APC/C. This inhibitor enables functional studies of the APC/C E3 ubiquitin ligase activity, identification of APC/C substrates and the role of target proteins in early cell cycle events. Addition of high concentrations (~3 mM) of D-box peptide to extract prior to $CaCl_2$ generates a metaphase arrested extract that enables the study of mitotic events occurring downstream of $CaCl_2$ addition and upstream of APC/C activity. So treated, extract maintains metaphase properties such as chromatin condensation, inhibition of nuclear envelope assembly and the inhibition of DNA replication (Fig. 1c, d); these extracts allow for a study of the signal transduction pathways activated upon calcium addition uncoupled from mitotic exit. Addition of this inhibitor at intervals after calcium enables functional studies of the APC/C E3 ubiquitin ligase activity, identification of APC/C substrates and the role of target proteins in early cell cycle events.

In *Xenopus* egg extract the 26S proteasome is not essential for release from metaphase arrest: addition of either 800 μM MG132 [41] or 100 μM Bortezomib [26] (Fig. 1c, d), inhibitors of the 26S proteasome, prior to release with $CaCl_2$, results in the stabilization of ubiquitylated proteins; this, however, does not affect an extract's ability to support DNA replication. This is because the

activities of both cyclin B-Cdk1 and geminin can be inhibited by ubiquitylation without requiring protein degradation [14, 41, 48], triggering mitotic exit and activation of the replication licensing system. The addition of proteasome inhibitors to extracts enables the study of ubiquitin chain formation, chain topology on target proteins and the role of deubiquitinating enzymes.

1. Transfer the required number of frozen beads (or volume) of metaphase-arrested extract to an Eppendorf tube and thaw in a room-temperature water bath.
2. Supplement egg extract with ER (1/40 stock) and cycloheximide (1/40 stock).
3. Add drugs at the required concentration and mix well: add roscovitine to a final concentration of 0.2–1 mM—alternatively, for example 6-DMAP at a final concentration of 3 mM can be used; add microcystin to a final concentration of 0.25–1 μM, as required; add D-box peptide, as required; add MG-132 or Bortezomib to a final concentration of 800 μM or 100 μM, respectively.
4. Add $CaCl_2$ at 0.3 mM (1/167 stock) and mix well.
5. Add sperm nuclei at the desired concentration, typically 3–10 ng/μl, mix well and incubate at 23 °C.
6. Follow nuclear morphology throughout the course of your reaction: mix 1 μl of sample with 1 μl of Hoechst 33258 (20 μg/ml) and view by UV microscopy. It is advisable to check morphology at a number of time points, typically 15 min apart, as appropriate, throughout the incubation.

3.6 Use of Interphase Egg Extract: Manipulation by Drug Addition

In order to further study DNA replication and repair, the establishment of sister chromatid cohesion and nuclear envelope formation during interphase a number of drugs can be added to egg extract to manipulate the cell cycle, either to advance or retard progression. These agents, used in combination with biochemical assays—chromatin isolation, blotting, immunoprecipitation (IP) and depletion, and immunofluorescence—are a powerful tool for elucidating cell cycle regulated molecular function.

3.6.1 Nuclear Assembly and Wheat Germ Agglutinin

The replication of DNA added to *Xenopus* egg extract is dependent on nuclear formation [49–51]. However, not all steps in the pathway leading to actual DNA synthesis are nuclear: replication licensing occurs and can only occur (under normal circumstance) in the absence of a nuclear envelope [15]; although DDK activity can be recruited to licensed chromatin prior to nuclear assembly, this occurs more efficiently after nuclear assembly has taken place [21, 22, 52]. In contrast, operative levels of CDK activity require nuclear formation. To study a cell cycle regulated process it may therefore be of interest to disrupt nuclear function. This can be

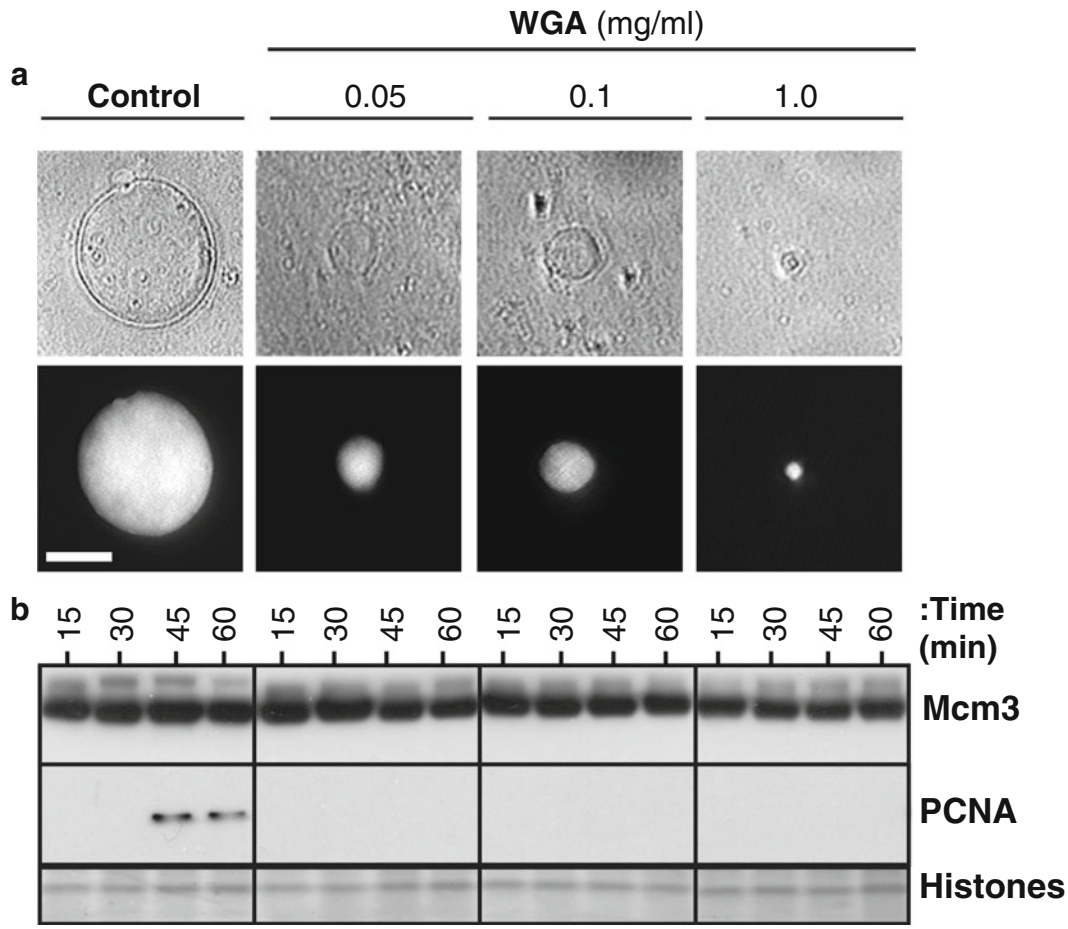

Fig. 2 Wheat germ agglutinin inhibits nuclear assembly. Sperm nuclei were incubated in interphase egg extract supplemented with different concentrations of wheat germ agglutinin (WGA). (**a**) After 40 min nuclei were visualized by phase contrast (*top panel*) and UV microscopy (*bottom panel*). Scale bar, 10 μm. (**b**) At the indicated times chromatin was isolated and immunoblotted for Mcm3 and PCNA. The lower portion of the gel was stained with Coomassie to visualize histones as a loading control

achieved using wheat germ agglutinin (WGA), which binds to *N*-acetyl-D-glucosamine, which is conjugated to a number of nuclear pore glycoproteins. Increasing concentrations of the drug, in the range 0.05–1 or 2 mg/ml, progressively limit and then abolish nuclear assembly and hence DNA synthesis (Fig. 2a) [52]. Under these circumstances the array of chromatin associated proteins and activities is altered, e.g., WGA restricts the efficient phosphorylation of MCM4 by DDK by reducing Cdc7 chromatin association [52]; likewise, the chromatin association of PCNA, which is dependent on both nuclear DDK and CDK activity, is abolished upon WGA treatment (Fig. 2b).

1. Transfer the required number of frozen beads (or volume) of extract to an Eppendorf tube and thaw in a room-temperature water bath.
2. Supplement egg extract with ER (1/40 stock) and cycloheximide (1/40 stock), ± $CaCl_2$ (1/167 stock)—extract can be activated for 15 min prior to **step 3** to ensure metaphase exit.
3. Add WGA, as required, mix well and incubate at 23 °C for 5 min.
4. Add sperm nuclei at the desired concentration, typically 3–10 ng/μl. If multiple samples are to be prepared from one extract treatment aliquots should be made as early as is appropriate.
5. Follow nuclear morphology throughout the course of your reaction: mix 1 μl of sample with 1 μl of Hoechst 33258 (20 μg/ml) and view by UV microscopy. It is advisable to check morphology at a number of time points, typically 15 min apart as appropriate, throughout the incubation.

3.6.2 Replication Licensing

The binding of Mcm2–7 proteins to chromatin licenses the DNA for one round of replication in the upcoming S phase. Mcm2–7 chromatin association is mediated by the combined action of the licensing factors ORC, Cdc6, and Cdt1, together with hydrolyzable ATP. The major inhibitor of licensing in *Xenopus* egg extracts is geminin, a specific inhibitor of Cdt1 [13, 42, 53]. Since geminin is inactivated at the metaphase to anaphase transition by the APC/C we use a bacterially expressed and purified, constitutively active, geminin mutant that is not recognized by the APC/C—geminin^{DEL}—to manipulate licensing [54]. This enables the study of activities dependent on Mcm2–7 chromatin association.

Geminin not only inhibits licensing but also prevents Scc2 and cohesin chromatin association [55, 56]. Nuclei forming in a geminin-treated egg extract grow more slowly and nuclear pore complex assembly is impaired [57, 58]. Consistent with this, the chromatin association of the nuclear pore seeding protein, ELYS, and downstream nucleoporins, such as Nup133, and the mAb414 antigens, are delayed in geminin treated extracts; the absence of Mcm2–7 complex on chromatin lowers the affinity of ELYS for chromatin, which in turn slows the nuclear assembly and growth [57]. Importantly, inhibition of replication by geminin addition has a great effect on the chromatin proteome: only 15–20 % of the ≥600 proteins identified remain unaffected upon treatment. Proteins analyzed in cell cycle related clusters show different patterns [58]. Although all clusters show changes upon replication inhibition, the S phase peak is the most perturbed.

Geminin^{DEL} can be added to extract either before or after release into interphase and at varying times either before or after sperm addition, depending on the desired effect. When geminin is

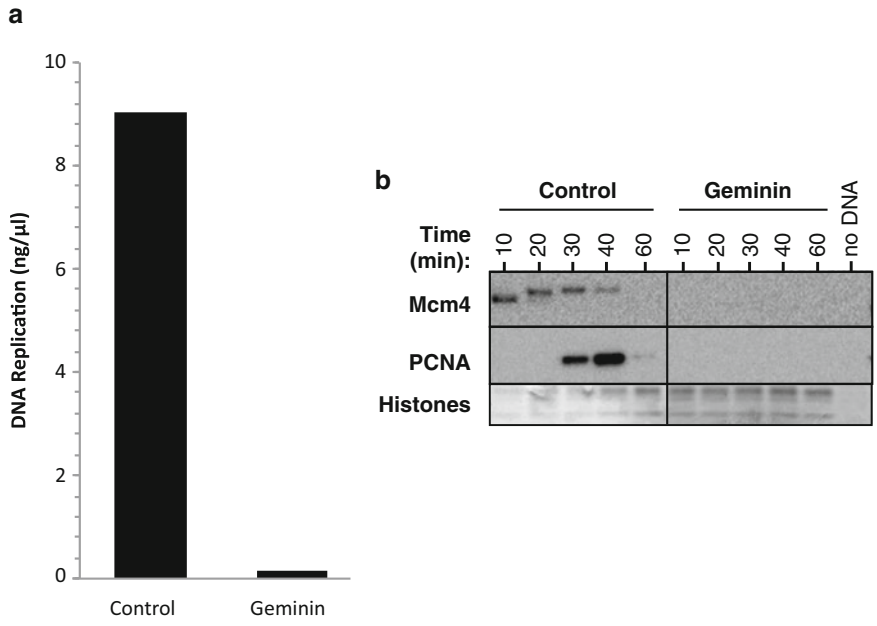

Fig. 3 Geminin inhibits DNA replication and Mcm2–7 chromatin association. Sperm nuclei were incubated at 10 ng/µl in interphase egg extract or in interphase egg extract pretreated for 5 min with 100 nM geminin. (**a**) Total DNA replication was assayed 90 min after sperm addition. (**b**) At the indicated times chromatin was isolated and immunoblotted for Mcm4 and PCNA. The lower portion of the gel was stained with Coomassie to visualize histones as a loading control

added prior to DNA addition, Cdc6 is stabilized on the chromatin [59] but Mcm2–7 chromatin association, replication licensing and DNA synthesis are completely inhibited (Fig. 3a, b). The late addition of geminin to an interphase extract—20 min after sperm addition—by which time replication licensing is complete but nuclear envelope has not yet formed—affects neither bulk DNA replication nor cohesin chromatin association [60].

During the licensing period an excess of Mcm2–7 complexes are loaded onto chromatin over the number of origins that are normally used during S phase [61]; this DNA is said to be "maximally licensed." Unactivated Mcm2–7 molecules on maximally licensed DNA provide excess potential, i.e., otherwise "dormant," replication origins that can be used under conditions of replication stress and DNA damage. These origins do not fire in an unperturbed S phase because they are rapidly replicated and inactivated by forks emanating from neighboring origins [60, 62, 63].

When geminin is added to interphase extract ~3 min after sperm nuclei addition, the number of DNA bound Mcm2–7 complexes is limited to ~10 % of maximum; this "minimally licensed" chromatin will support complete DNA replication in an unperturbed S phase with the same kinetics as otherwise fully licensed chromatin [59, 60]. Although maximally and minimally licensed

DNA show similar replication kinetics and the same average origin spacing, minimally licensed DNA is sensitive to a range of replication inhibitors, such as mitomycin C (a cross-linking agent), etoposide (a topoisomerase II inhibitor), aphidicolin (a polymerase inhibitor), or actinomycin D (a DNA intercalator) [60]. The use of minimally licensed chromatin can therefore be used to study the response to replication stress and DNA damage.

In order to completely inhibit DNA replication:

1. Transfer the required number of frozen beads (or volume) of extract to an Eppendorf tube and thaw in a room-temperature water bath.
2. Supplement egg extract with ER (1/40 stock) and cycloheximide (1/40 stock), ± $CaCl_2$ (1/167 stock)—extract can be activated for 15 min prior to **step 3** to ensure metaphase exit.
3. Add gemimin at 100 nM (2.6 ng/μl) to block DNA replication; mix well and incubate at 23 °C for 5 min.
4. Add sperm nuclei at the desired concentration, typically 3–10 ng/μl. If multiple samples are to be prepared from one extract treatment aliquots should be made as early as is appropriate.
5. Follow nuclear morphology throughout the course of your reaction: mix 1 μl of sample with 1 μl of Hoechst 33258 (20 μg/ml) and view by UV microscopy. It is advisable to check morphology at a number of time points, typically 15 min apart as appropriate, throughout the incubation.

Alternatively, to prepare a minimally licensed template:

1. Add sperm nuclei at the desired concentration, typically 3–10 ng/μl and incubate at 23 °C.
2. 3 min after sperm addition, add gemimin at 100 nM (1.5–2.6 ng/μl) to inhibit further licensing and mix well. If multiple samples are to be prepared from one extract treatment aliquots should be made as early as is appropriate.

3.6.3 Replication Initiation

The activation of licensed origins during S phase is triggered by two S phase promoting kinases, CDK and DDK, which promote assembly of the Cdc45-MCM-GINS (CMG) replicative helicase. DNA polymerases are recruited to the CMG, facilitating replication initiation. CDK activity is required to support the initiation of replication throughout S phase, and does not affect DDK activity [21, 22, 64].

Cdc7 is an essential serine/threonine kinase, conserved from yeast to humans, that promotes the initiation of DNA replication by phosphorylating several components of the replicative machinery, including multiple subunits of the Mcm2–7 complex [65].

The kinase is activated by associating with a regulatory partner Dbf4 or Dbf4-related-factor 1 (Drf1) whose levels can vary during the cell cycle to regulate kinase activity. In *S. cerevisiae*, Cdc7 targets the structurally disordered N-terminal serine/threonine-rich domain (NSD) of Mcm4, apparently relieving an inhibitory activity that blocks S phase progression [66]. In early *Xenopus* embryos the Drf1 has been identified as the major activator of Cdc7 kinase activity [67]. Cdc7 also functions in cohesin chromosome association [55, 68].

Unlike CDKs, DDK activity is essential only early in S phase and is not limiting for progression through the replication timing program in Xenopus egg extracts [52]. The effects of Cdc7-mediated MCM hyperphosphorylation can be reversed by protein phosphatase 1 (PP1). Upon DNA damage or replication inhibition the checkpoint kinases induce the association of PP1 with chromatin which results in an increased rate of MCM dephosphorylation, thereby counteracting Cdc7 function and inhibiting further replication initiation [52].

Three CDKs are known to be present in the early *Xenopus* embryo: cyclin B-Cdk1, cyclin A-Cdk1 and cyclin E-Cdk2 [69]. Cyclin B is degraded at the end of mitosis whereas cyclin E remains constant at a relatively high concentration throughout the early embryonic cell cycle. Cyclin A, which is present at a relatively low concentration, is degraded around the time of nuclear envelope breakdown in cycling egg extracts [31]. Cyclin A-Cdk1 and cyclin E-Cdk2 support DNA replication [18, 19, 32, 70]. Formation of an active helicase requires the recruitment of Cdc45 and the GINS complex to licensed origins [71, 72]. In budding yeast, formation of the CMG complex requires CDK phosphorylation of Sld2 and Sld3, which then bind to their partner Dbp11, facilitating GINS and Cdc45 recruitment [73, 74]. In *Xenopus* and human cells the loading of Cdc45 is achieved when Treslin, the Sld3 homologue, associates with Dpb11/TopBP1 (also known as Cut5 or Mus101) [75, 76].

We have characterized a range of CDK and DDK inhibitors in the *Xenopus* cell-free system: $p27^{Kip1}$, $p21^{Cip1}$, and roscovitine inhibit CDK activity and PHA-767491 inhibits DDK activity. Addition of these drugs to egg extract inhibits DNA replication (Fig. 4a) but does not perturb nuclear formation. We typically add these inhibitors to the extract together with, or shortly before, DNA addition, but well-timed addition after nuclear formation will have a partial affect. Use of these inhibitors permits investigation of the role of DDK and CDK phosphorylation on a protein of interest, e.g., when studying protein chromatin association and modification, the apparent increase in molecular weight associated with DDK phosphorylation of Mcm4 on chromatin is abolished by PHA-767491 but not $p27^{Kipl}$ (Fig. 4b).

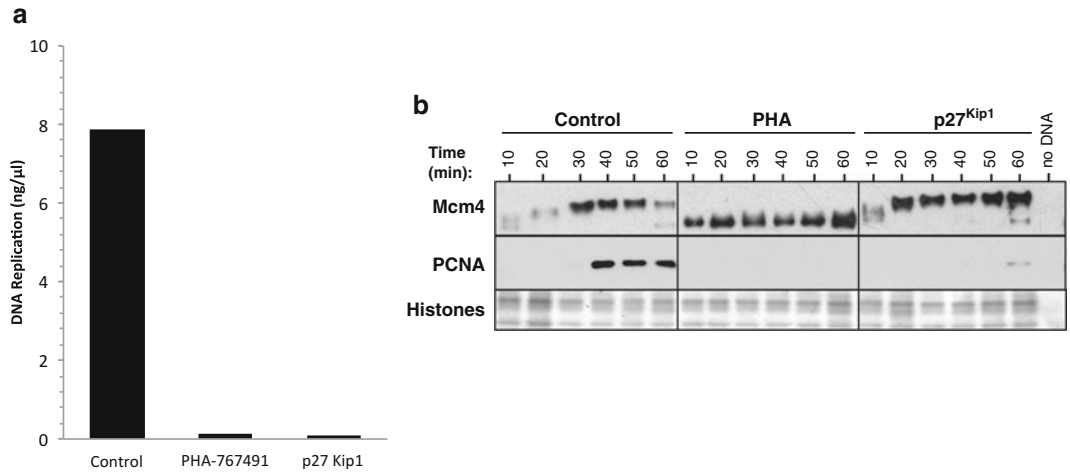

Fig. 4 Both DDK and CDK activity are required for DNA Replication. Sperm nuclei were incubated at 10 ng/µl in interphase egg extract or in interphase egg extract pretreated for 5 min with 50 µM PHA-767491 or 100 nM $p27^{Kipl}$. (**a**) Total DNA replication was assayed 90 min after sperm addition. (**b**) At the indicated times chromatin was isolated and immunoblotted for Mcm4 and PCNA. The lower portion of the gel was stained with Coomassie to visualize histones as a loading control

In order to completely inhibit DNA replication:

1. Transfer the required number of frozen beads (or volume) of extract to an Eppendorf tube and thaw in a room-temperature water bath.
2. Supplement egg extract with ER (1/40 stock) and cycloheximide (1/40 stock), ± $CaCl_2$ (1/167 stock)—extract can be activated for 15 min prior to **step 3** to ensure metaphase exit.
3. Add inhibitors to the extract at the required concentration to inhibit DNA replication, mix well and incubate at 23 °C for 5 min: $p27^{Kipl}$ is added to extract at 100 nM (~5 µg/ml) (*see* **Note 12**); $p21^{Cipl}$ is added to egg extract at 0.5 µM (~20 µg/ml) (*see* **Note 13**); Roscovitine is used at a final concentration in egg extract of 0.5–1 mM (*see* **Note 14**); Addition of 50 µM PHA-767491 to egg extract is sufficient to inhibit Mcm4 phosphorylation and DNA replication (*see* **Note 15**).
4. Add sperm nuclei at the desired concentration, typically 3–10 ng/µl. If multiple samples are to be prepared from one extract treatment aliquots should be made as early as is appropriate.
5. Follow nuclear morphology throughout the course of your reaction: mix 1 µl of sample with 1 µl of Hoechst 33258 (20 µg/ml) and view by UV microscopy. It is advisable to check morphology at a number of time points, typically 15 min apart as appropriate, throughout the incubation.

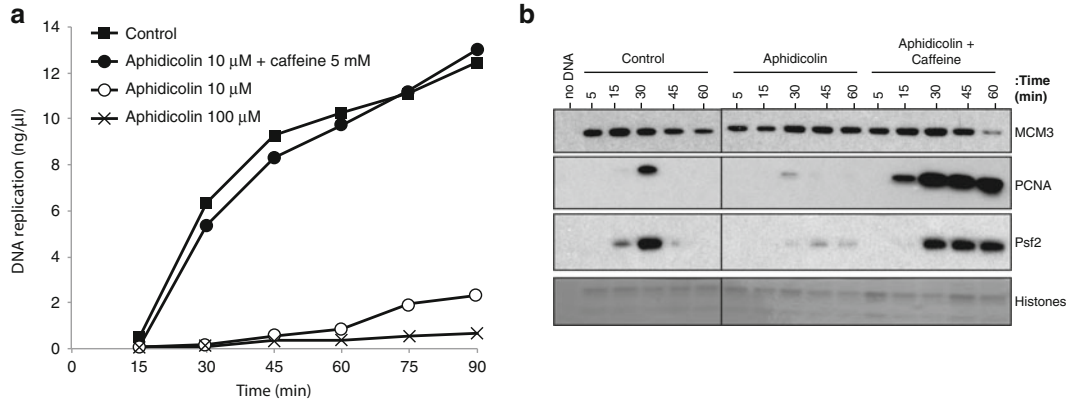

Fig. 5 Inhibition of DNA replication and activation of a replication checkpoint using aphidicolin. (**a**) Sperm nuclei were incubated at 10 ng/μl in interphase egg extract or in interphase egg extract pretreated for 5 min with either a low (10 μM) or high (100 μM) concentration of aphidicolin plus or minus 5 mM caffeine. The extent of DNA replication was assayed at the indicated times. (**b**) Sperm nuclei were incubated in interphase egg extract or in interphase egg extract pretreated for 5 min with 10 μM aphidicolin plus or minus 5 mM caffeine. At the indicated times chromatin was isolated and immunoblotted for Mcm3, PCNA, and Psf2 (GINS complex). The lower portion of the gel was stained with Coomassie to visualize histones as a loading control

3.6.4 Replication Elongation

In order to perturb the progression of replicating nascent DNA strands and to study checkpoint activation, induction and effectors, as well as checkpoint regulated processes, we commonly use two drugs, aphidicolin and caffeine (Fig. 5). Other drugs, such as mitomycin C (a cross-linking agent), etoposide (a topoisomerase II inhibitor) or actinomycin D (a DNA intercalator), cause replicative stress and induce caffeine sensitive checkpoint activation in egg extract.

1. Transfer the required number of frozen beads (or volume) of extract to an Eppendorf tube and thaw in a room-temperature water bath.
2. Supplement egg extract with ER (1/40 stock) and cycloheximide (1/40 stock), +$CaCl_2$ (1/167 stock)—extract can be activated for 15 min prior to **step 3** to ensure metaphase exit.
3. Add aphidicolin to extract in the range 10–100 μM, as required and mix well (*see* **Note 16**). If required add 5 mM caffeine to the treated extract, mix well and incubate at 23 °C for 5 min (*see* **Notes 16** and **17**).
4. Add sperm nuclei at the desired concentration, typically 3–10 ng/μl. If multiple samples are to be prepared from one extract treatment aliquots should be made as early as is appropriate.
5. Follow nuclear morphology throughout the course of your reaction: mix 1 μl of sample with 1 μl of Hoechst 33258

(20 μg/ml) and view by UV microscopy. It is advisable to check morphology at a number of time points, typically 15 min apart as appropriate, throughout the incubation.

3.7 Interphase-to-Mitosis Extract Conversion

The *Xenopus* cell-free system is capable of reproducing cell cycle-specific chromosomal events in vitro: upon conversion from interphase to mitosis, nuclear envelope breakdown occurs and duplicated chromatin is converted into condensed metaphase chromosomes with paired sister chromatids [3, 10]. Mitotic chromosome condensation is mediated by the "condensin" complex. In *Xenopus laevis*, XCAP-C (SMC4) and XCAP-E (SMC2) function as the core subunits of condensin [77–79]. The SMC—structural maintenance of chromosomes—proteins are a family of chromosomal ATPases that function during the cell cycle: SMC 1 and 3 form the core of the "cohesin" complex that mediates sister chromatid cohesion and SMC 5 and 6 form a complex that functions in DNA repair and the checkpoint response.

In order to study the interphase to mitosis transition—sister chromatid cohesion and chromosome condensation, kinetochore formation and spindle microtubule dynamics, as well as the dynamic interaction of proteins with chromatin across the cell cycle—interphase egg extract incubations can be advanced into mitosis; due to the nature of the freezable extracts we prepare, this progression is dependent upon addition of mitotic CDKs or the activating cyclin partner. Metaphase arrested whole egg extract can be used to convert interphase extract into a mitotic state—the volume of addition required varies from extract to extract, and should be determined in advance (for both the interphase and metaphase extracts used), but typically the addition of one half to two volumes is sufficient (Fig. 6). Alternatively, the addition of a mitotic cyclin, either cyclin A or cyclin B, to extract will promote mitotic entry—typically non-destructible mutant proteins are used, recombinant cyclin A1 NΔ56 [31, 32] or cyclin BΔ90 [33]. These cyclins must be titrated on an extract to extract basis.

In order to perturb the interphase to metaphase transition the activity of the key mitotic kinases—CDKs, Polo-like kinase and Aurora B—can be depleted from the extract or chemically inhibited. These manipulations permit investigation of the role of these key kinases on proteins and processes of interest during the transition to metaphase. Consistent with CDK inhibition when studying the metaphase to anaphase transition, and S phase, metaphase CDK activity can be reduced by addition of broad-spectrum kinase inhibitors such as 6-DMAP or more specific inhibitors such as roscovitine.

Aurora B is a serine/threonine kinase required for the mitotic phosphorylation of histone H3 on serine10. Aurora B kinase activity facilitates bulk cohesin chromatin dissociation in prophase and inhibition of activity impairs the alignment of chromosomes

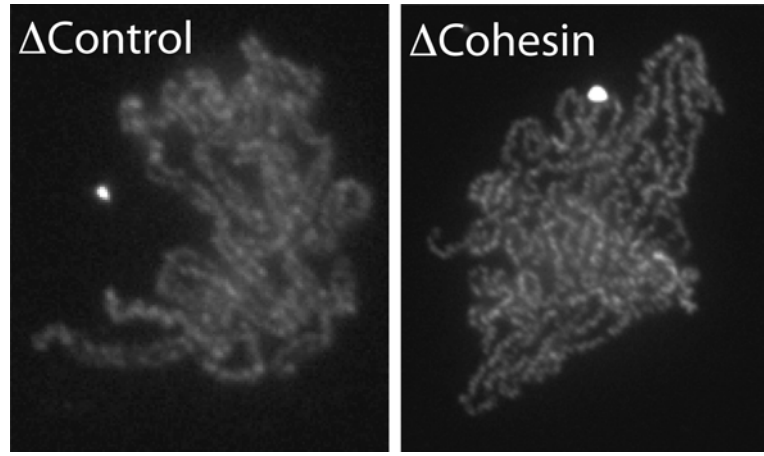

Fig. 6 Interphase-to-mitosis extract conversion. Sperm nuclei were incubated in control- (Δ control) or cohesin-depleted (Δ cohesin) interphase egg extract. After 2 h, 2 volumes of metaphase-arrested egg extract were added to promote passage into mitosis. After 2 h, chromosomes were fixed, isolated, and stained with anti-condensin (SMC2) antibody and visualized under UV microscopy. Scale bar, 10 μm

at the equator of the mitotic spindle. Aurora B kinase activity can be inhibited by a range of drugs, including ZM447439, Hesperadin, VX-680/MK-0457, AT9283, and Barasertib. In metaphase-arrested extracts preassembled kinetochores disassemble after inhibiting Aurora B activity by either drug addition or antibody neutralization; kinetochore disassembly, induced by Aurora B inhibition, is rescued by restraining protein phosphatase 1 (PP1) activity [80].

The polo-like kinase 1 (Plk1), acts in concert with Aurora B and cyclin B-Cdk1, to promote entry into mitosis. In the absence of Plk1 metazoan cells fail to establish a bipolar spindle and to properly attach microtubules to the kinetochores. As a consequence cells are arrested in mitosis by the activation of the spindle assembly checkpoint, which monitors the correct attachment of chromosomes to the mitotic spindle. In *Xenopus* egg extract, depletion of the Plk1 orthologue Plx1 prevents activation of Cdk1 and thus mitotic entry [81].

Within the same experiment, various assays can be performed in both the interphase and the converted mitotic extract. Nuclear envelope formation and breakdown can be followed directly by phase contrast light microscopy and by the membrane dye $DiIC_{18}$ (10 μg/ml) or by immunofluorescence on fixed nuclei using antibodies against specific proteins such as lamin or nuclear pore proteins, e.g., mAb414 [82]. DNA decondensation/condensation can be followed by microscopy under UV light when the DNA is stained by a fluorescent dye, e.g., Hoechst 33258, in either fresh

or fixed samples. Condensin-mediated mitotic chromosome condensation can be assayed by staining fixed samples for the SMC or non-SMC subunits of condensin—this procedure is the basis of the sister chromatid cohesion assay, in which the paired axes of sisters chromatids are visualized by condensin staining [83]. Replication progression can be followed by radiolabeled nucleotide incorporation and TCA precipitation (see below). Additionally, replication can also be assayed in fixed microscopy samples when biotinylated nucleotides, e.g., 10 μM biotin–16-dUTP, added to the replication reaction, are visualized by incubation with fluorescent streptavidin after fixation [9]. Chromatin fractions can be prepared for immunoblotting as previously described [84]. A good choice of control proteins to follow during conversion experiments is one of the cohesin and one of the condensin subunits: cohesin associates with chromatin during interphase but the vast majority (≥95 %) of the complex dissociates upon mitotic conversion. In contrast, condensin subunits, e.g., SMC2 or SMC4, associate with chromatin only in mitosis.

If performing mitotic conversion with metaphase-arrested egg extract:

1. Perform an interphase incubation, as described (Subheading 3.4). This reaction should be incubated such that sufficient time is given to allow DNA replication to be completed—whether control, depleted or drug treated, the interphase extract used for mitotic conversion should have been previously characterized so that the kinetics of DNA replication are known.
2. 15 min prior to the completion of the interphase incubation transfer the required number of frozen beads (or volume) of extract to an Eppendorf tube and thaw in a room-temperature water bath.
3. Supplement egg extract with ER (1/40 stock) and cycloheximide (1/40 stock), and incubate at 23 °C until completion of the interphase incubation.
4. Upon completion of the interphase incubation add the previously determined volume of metaphase-arrested extract to each reaction and incubate at 23 °C for up to 2 h.
5. Follow nuclear morphology: mix 1 μl of sample with 1 μl of Hoechst 33258 (20 μg/ml) and view by UV microscopy. It is advisable to check morphology at a number of time points, typically 15 min apart as appropriate, throughout the incubation.

If performing mitotic conversion with mutant non-destructible cyclin:

1. Perform an interphase incubation, as described (Subheading 3.4). This reaction should be incubated such that sufficient time is given to allow DNA replication to be completed—whether

control, depleted, or drug treated, the interphase extract used for mitotic conversion should have been previously characterized so that the kinetics of DNA replication are known.

2. Upon completion of the interphase incubation add the previously determined concentration of cyclin to each reaction and incubate at 23 °C for up to 2 h.
3. Follow nuclear morphology: mix 1 μl of sample with 1 μl of Hoechst 33258 (20 μg/ml) and view by UV microscopy. It is advisable to check morphology at a number of time points, typically 15 min apart as appropriate, throughout the incubation.

3.8 Quantifying DNA Replication

To determine the kinetics of DNA replication, assays based on the incorporation of exogenous radiolabeled nucleotide (α^{32}P-dATP) into replicating DNA are used. Although DNA synthesis can be roughly assessed using non-denaturing agarose gel electrophoresis, accurate quantitation can be achieved using an assay based on TCA precipitation [8]. To analyze elongating DNA and properly resolve replication intermediates we use denaturing alkaline agarose gels, although urea–polyacrylamide gels may also be used.

3.8.1 TCA Replication Assay

Reactions, terminated by addition of a solution containing SDS and protease, are added to cold 10 % TCA to facilitate DNA precipitation. The precipitated DNA is separated from the unincorporated radiolabel by filtration and the level of radioactivity in each sample is measured by scintillation counting; the extent of DNA replication is determined by calculating the percentage of incorporated radiolabel.

1. Transfer the required number of frozen beads (or volume) of extract to an Eppendorf tube and thaw in a room-temperature water bath.
2. Supplement egg extract: ER (1/40 stock), cycloheximide (1/40 stock), $CaCl_2$ (1/167 stock), and sperm nuclei at the required concentration, with 50 nCi/μl α^{32}P-dATP and incubate at 23 °C—extract can be activated for 15 min at 23 °C prior to sperm nuclei and α^{32}P-dATP addition to ensure metaphase exit (*see* **Note 18**).
3. Terminate the reaction by addition of 160 μl Stop-C plus 0.2 mg/ml proteinase K—freshly added—mix well and incubate at 37 °C for 30 min.
4. Precipitate the digested sample by addition of 4 ml of 4 °C 10 % (w:v) TCA; incubate for a minimum of 30 min at 4 °C.
5. Invert the tube at least four times to mix the sample well. Spot 40 μl of the TCA/precipitate mix onto a paper filter disk for measurement of total 32P.

6. Filter the remaining sample, under vacuum, on a manifold, through a glass fiber filter pre-wetted with 10 % (w:v) TCA. Rinse the empty tube with 4 ml 10 % (w:v) TCA and apply to the same filter.
7. Wash the glass fiber filter twice with 8 ml of 4 °C 5 % (w:v) TCA and then with 8 ml of room temperature 100 % ethanol. After the ethanol wash allow the filters to dry.
8. Quantify the 32P on the filters in a scintillation counter: place each filter—both paper and glass fiber, separately—into a scintillation counter tube and add enough scintillant (e.g., Ultima Gold F; Perkin Elmer) to entirely wet the filter; a wide open or "Cerenkov" channel is appropriate because the filter reduces the recorded energy of emission.
9. The extract contains an endogenous dATP pool of ~50 μM [8]. The percentage of total 32P incorporated into the DNA is calculated by dividing the 32P incorporated into DNA captured on the glass fiber filter by the total 32P on the paper filter—this represents 1 % of total α^{32}P-dATP, e.g., 40 μl of 4 ml.
10. The total amount of DNA synthesized, expressed in ng DNA/μl extract, can then be calculated by multiplying percent total 32P incorporated by a factor of 0.654—this calculation assumes an average molecular weight of dNMPs of 327 Da and equal quantities of all four dNTPs incorporated into DNA (weight of dNMP incorporated in ng/μl = (percent total 32P incorporated/100) × 50 × 10^{-6} × 4 × 327 × 10^{3}).

3.8.2 Alkaline Agarose DNA Gels

Alkaline agarose gels can be prepared in advance on the day of the experiment.

1. Add the required agarose to a volume of gel buffer—we typically prepare a 250 ml 1 % (w:v) agarose gel using a 20 × 15 cm mold and 20 wells.
2. Boil the mixture taking care to ensure all of the agarose is dissolved, pour the gel and allow to set at room temperature.
3. Place the gel into the running tank and allow it to equilibrate for 1 h at room temperature with alkaline gel running buffer—remove excess buffer after equilibration so that the comb holes stand out.
4. Supplement egg extract: ER (1/40 stock), cycloheximide (1/40 stock), $CaCl_2$ (1/167 stock) and sperm nuclei at the required concentration, with 50 nCi/μl α^{32}P-dATP and incubate at 23 °C—extract can be activated for 15 min at 23 °C prior to sperm nuclei and α^{32}P-dATP addition to ensure metaphase exit. For this procedure we typically use 40–50 μl extract per individual sample, with DNA concentrations ranging from 10 to 20 ng/μl. Note that increased DNA concentrations may slow down replication kinetics [59].

5. Stop the reaction by resuspending in 300 µl StopN containing 2 µg/ml freshly added RNase and incubate for 10 min at 37 °C.
6. Add proteinase K at 200 µg/ml and incubate for a further 30 min at 37 °C.
7. Add 300 µl of phenol–chloroform–isoamyl alcohol (25:24:1) and vortex briefly. Transfer to an Eppendorf Phase Lock gel tube—this enhances separation between DNA and phenol—and centrifuge for 6000×*g* for 5–10 min at room temperature.
8. Precipitate the DNA by adding 3 volumes of 100 % ice-cold ethanol and place in dry ice for 10 min. Centrifuge the sample at 20,000×*g* at room temperature for 10–15 min. Wash the pellet with 70 % room temperature ethanol—let the ethanol evaporate completely at room temperature, it is important that no trace of ethanol remains—and resuspend in 10 µl 1 mM EDTA pH 7.5.
9. Add an equal volume of 2× alkaline loading buffer—do not use classical dyes, such as bromophenol blue or xylene cyanol, as they are not stable in an alkaline environment.
10. Load the samples and run on the gel at 2 V/cm for 10–18 h (e.g., 30–50 V for 15 cm gels) together with end-radiolabeled molecular weight markers (*see* **Note 19**).
11. Remove gel from running apparatus using a spatula as a lever and wearing double gloves—make sure that the well end is lifted first, as all the free 32P is in the buffer tank at the opposite pole.
12. Optional: in order to prevent loss of small fragments (<150 nt), the gel may be fixed by incubating in 7 % (w:v) TCA for 20 min in a polythene box on a shaker.
13. Dry the gel: take a glass plate the approximate size of the 3MM sheets and place six paper towels onto it; onto this place three sheets of 3MM paper, labeling the top sheet, as required.
14. Carefully place the gel onto the labeled top sheet and cover this with the three remaining sheets of 3MM paper.
15. Onto this place the other six paper towels and then finally the second glass plate. Clamp the two glass plates together with eight large bulldog clips, two on each side.
16. Leave the sandwich for 30 min or until the gel is flattened.
17. Remove the paper towels and carefully peel off the 3MM paper from on top of the gel, which should remain stuck to the labeled under sheet.
18. Cover the gel and paper with plastic wrap, and autoradiograph for 4–24 h using a Fuji Screen or up to 8 days if using film; for a typical example *see* Fig. 3 [60].

3.9 Immunodepletion and Immunoprecipitation

In order to first determine, and then characterize, the potential role of any protein (or protein complex) in a biochemical process it can be of particular interest to perform a specific assay in the absence of the protein(s) of interest. Since *Xenopus laevis* eggs are not transcriptionally active until passage through the mid-blastula transition, depletion cannot be mediated genetically but only at the protein level; this is achieved using specific antibodies raised against the protein of interest. Using agarose or magnetic beads as a support for antibody incubations in extract allows the bead–antibody conjugate and bound protein of interest to be separated by physical means from the extract as a whole. The depleted extract can be used in a specific assay, together with a control (non-immune) depletion, to study the protein of interest. It is essential that the specificity of the depletion is determined, to ensure that the observed phenotype is a consequence of the loss of the target protein. Rescue experiments, where a depleted extract is supplemented with either purified native or recombinant—wild-type or mutant—protein, can be undertaken to demonstrate depletion specificity. Furthermore, this can be combined with immunoprecipitation experiments to study protein-protein interactions and together with mass spectrometry, identify interacting partners of your target protein. The mass spectrometry of immunoprecipitated samples is also used to characterize antibody specificity.

3.9.1 General Considerations for Antibody Production

We first generate an antibody against the protein of interest. This requires the expression and purification of an antigen. In order to expedite antibody production we have developed a strategy for antigen generation.

1. The amino acid sequence of a target protein is first verified by EST matching. The verified sequence is next assessed for hydrophobicity; sequences with a low hydrophobic residue content are preferred immunogens. If suitable, we typically select a 100 amino acid sequence from either or both termini as antigen, as our experience suggests that these have a higher likelihood of giving antibodies capable of efficiently immunodepleting native protein complexes.
2. Bacterial expression plasmids are then generated by subcloning an in vitro synthesized oligonucleotide and the cloned sequence is expressed in *E. coli* and the protein purified using standard methods.
3. We typically raise antibodies in rabbit but also use sheep regularly; although they are usually better for immunoblotting, we find that antibodies raised in sheep are often not as efficient for depletion.
4. To generate the antibody the purified protein is systematically injected into the host animal over a period of months, with blood being recovered at intervals. The recovered blood is

processed to remove erythrocytes and clotting factors; this final serum is a complex mix of albumin and globulins, and contains significant protease activity. Only a relatively low amount of specific IgGs is present.

5. Once generated, the serum is assayed by immunoblotting and immunoprecipitation against whole egg extract; precipitated proteins are identified by mass spectrometry in order to confirm the presence of the intended target and ascertain antibody specificity. In recent trials this strategy has yielded a success rate of 80 % for the production of useful antibodies.
6. Depending upon serum specificity, antibodies can be purified from this solution by either one of two methods: IgG or affinity purification.
7. Taking advantage of the high affinity of *Staphylococcus aureus* protein A and *Streptococcus* protein G for rabbit or sheep heavy chains respectively, undesirable proteases and the bulk of serum proteins can be separated out, generating a solution of purified IgGs. As this solution will contain all IgGs present in the serum there will be a significant proportion of nonspecific antibodies in this preparation. For particularly "dirty" sera, containing high levels of cross-reacting antibodies, an alternative purification method is used to isolate only IgGs that are specific for the cognate antigen. Specific IgGs are affinity purified from serum using a 1 ml HiTrap NHS-activated column, to which 0.5–5 mg of the specific protein antigen has been conjugated. Antibodies are recovered from the column at low pH and quickly neutralized in high concentration Tris (base). This process eliminates serum proteins and nonspecific IgGs, generating a pure fraction of antibodies that react specifically with the chosen antigen. One caveat to this technique is that antibodies with the highest affinity for the antigen may resist pH elution and will be lost on the column.
8. Purified antibodies can then be used for immunoblotting, immunoprecipitation experiments and extract immunodepletion as well as immunofluorescence.

3.9.2 Preparing Antibody–Bead Conjugates for Immunodepletion

We use porous agarose beads (rProtein A- or rProtein G-FF Sepharose) for serum and protein A/G purified IgG-based depletions, and for affinity purified antibody depletions solid support magnetic beads (Dynabeads Protein A or Protein G). Preparing antibody–bead conjugates using either agarose or magnetic beads is the same but for the use of either a centrifuge or magnet, respectively, to recover the beads during washes and preparation. For rabbit antibodies we use protein A support and for sheep protein G.

1. It is important to first determine the quantity of beads required: for both types of beads used we typically deplete extract at a ratio of 60–80 % (v:v) beads to extract, i.e., to deplete 100 µl

of extract we use 60–80 μl of antibody bound beads; whereas two rounds of depletion are required for agarose-based methods, magnetic bead depletion typically requires three rounds; agarose beads are prepared using 2 volumes of sera (or 2 volume equivalents of protein A/G purified) per 1 volume of beads and magnetic beads are incubated with 0.3 μg/μl of affinity purified IgG, 20 % above the binding capacity of these beads (0.25 μg/μl IgG)—this ensures saturation of the beads with antibody and the supernatant from the coupling reaction can be reused after requantification. A small number of agarose beads may be lost on early processing so we typically prepare 20 % more beads than absolutely required.

2. Wash the required quantity of agarose beads in 100 mM Hepes pH 8.0 to reduce the concentration of starting buffer is reduced to <0.1 % (v:v) (*see* **Note 20**). Agarose beads are recovered by centrifugation at 500–1000 × *g* in a swinging bucket rotor for 2 min at 4 °C. After washing the beads should be transferred to an appropriately sized Eppendorf tube. Magnetic beads should be washed as per manufacturer's instruction.
3. Adjust serum or purified IgG to 100 mM Hepes pH 8.0 from a 1 M stock. Add serum/antibody to agarose beads and incubate on a horizontal/flat-bed roller at 4 °C overnight or at room temperature for 1 h. Bind affinity purified antibodies to magnetic beads as per manufacturer's instruction.
4. Wash the agarose beads as in **step 2** in 100 mM Hepes pH 8.0. After washing, remove excess buffer and add an equal volume of 100 mM Hepes freshly supplemented with 1 mM PMSF and incubate on a horizontal/flat-bed roller at room temperature for 15 min. Magnetic beads should be washed as per manufacturer's instruction.
5. Wash the agarose beads as in **step 2** in 100 mM Hepes pH 8.0.
6. Wash the agarose beads as in **step 2** into LFB1/50.
7. For agarose beads: recover the beads and measure the final bed volume. Remove excess buffer and add an equal volume of LFB1/50 to give a 50 % slurry. For magnetic beads: resuspend the beads back to starting volume in LFB1/50.

3.9.3 Immunodepletion: Serum and Agarose Beads

1. Make a 50 % (v:v) slurry of antibody bound agarose beads in LFB1/50. Resuspend the slurry using a wide-mouth cut pipette tip. Transfer the required volume of beads to two 0.5 ml Eppendorfs—two tubes per depletion (*see* **Note 21**).
2. Check each tube contains the required volume of wet beads either by briefly spinning down (500–1000 × *g* at 4 °C) in a swinging bucket rotor or placing on ice and allowing to settle under gravity. Continue to add/subtract beads until you have

the required volume. Remove all but a thin cover of buffer from the beads and keep on ice.

3. Prepare your volume of extract as required; supplement with ER (1/40 stock), cycloheximide (1/40 stock) and, if you require interphase extract, $CaCl_2$ (1/167 stock), and incubate for 15 min at 23 °C.
4. Using a "gel loading" fine pipette tip placed at the bottom of the tube, remove all liquid from the beads immediately before use, i.e., one round of depletion at a time. The beads should have a "cracked" appearance when the last of the buffer is removed—this may take several removals/tips as the gel loader tip can easily get blocked. It is important to remove as much buffer as possible from the beads at this stage as the extract can tolerate very little dilution.
5. Add the extract to the beads: to mix beads and extract DO NOT vigorously pipette up and down but mix the liquid into the beads gently or by stirring with a tip.
6. Place the tube securely, using a wad of tissue paper, in a 50 ml Falcon tube and incubate on a horizontal/flat-bed roller at 4 °C for 40 min.
7. Prepare a filter: cut two 1 ml pipette tips so that they stack one on top of another and place a small square of 25 μm Nybolt filter between them; place into an appropriately sized tube. Pipette the extract plus beads on top of the filter and spin in a swinging bucket rotor at 700 × *g* for 2 min at 4 °C. Recover the filtered extract.
8. Dry the second aliquot of beads with a "gel loading" tip and repeat **steps 6** and 7.
9. Use depleted extract immediately or freeze in 10 μl drops directly in liquid nitrogen. The extent of depletion of the protein of interest should be quantified by immunoblotting the depleted extract versus a serial dilution of non-depleted extract, e.g., 0.5 μl of depleted extract and an equal volume of 1:5, 10, 20, 50, and 100 diluted non-depleted extract; for a typical example see Figure S1B in ref. 57. In the first instance a top-to-toe blot of depleted extract should be carried out to ensure that any nonspecific bands recognized by the antibody are not also depleted with your target protein.

3.9.4 Immunodepletion: Affinity-Purified Antibody and Magnetic Beads

Using a magnet in place of the centrifuge and filter system, immunodepletion of egg extract using magnetic beads is essentially the same as that described above (Subheading 3.9.3) for depletion using agarose beads. The required volume of beads is transferred to an Eppendorf tube. Using the magnet, buffer is removed from the beads immediately before use. Extract and beads are mixed and incubated at 4 °C on a horizontal/flat-bed roller, as above.

Typically three rounds of depletion of 30 min each are required. The extract is separated from the beads using the magnet and the final thrice-depleted extract is either used immediately or frozen in 10 µl drops directly in liquid nitrogen after recovery. The extent of extract depletion should be determined, as above (Subheading 3.9.3).

3.9.5 Immunoprecipitation

Immunoprecipitation experiments are used to study protein-protein interactions as well as to determine antibody specificity. Each antibody used requires optimization: type of beads used, the ratios of antibody to beads and of beads to extract, the length of antibody–bead incubation and the salt and detergent concentrations in the final wash buffers. In our lab one of two bead types is used for immunoprecipitation experiments: rProtein A- or rProtein G-FF Sepharose has a large capacity to bind IgG allowing for large amounts of antibody to be used for each IP. As such, Sepharose is typically used in combination with unprocessed serum or protein A/G purified antibodies. The physical properties of Sepharose, being large porous beads, results in significant pulldown of non-specific proteins, which require extensive washing to be removed. Wash times using this type of beads are relatively time consuming, as centrifugation is required to isolate the beads from the wash buffer. The second option is to use solid support magnetic Protein A or Protein G Dynabeads. These have a significantly (≥10-fold) lower capacity for antibodies than Sepharose and as such are typically used only in combination with affinity purified antibodies. To increase protein recovery the ratio of beads to extract can be optimized to pull-down sufficient levels of target protein. Wash steps are carried out simply and quickly by pelleting beads using a magnetic stand. For optimal results, antibodies are crosslinked to either Sepharose or Dynabeads according to manufacturer's protocols. This ensures that bound antibody is absent from the final IP eluate after boiling in SDS-PAGE sample buffer—this is essential for proteins that run at similar sizes to IgG heavy chain (~55 kDa) and light chain (~25 kDa) proteins.

1. Dilute 50 µl of metaphase arrested or interphase extract 1:5 with ice-cold LFB1/50—dilution reduces extract viscosity for the incubation and centrifugation steps of the protocol (*see* **Note 22**). Extracts can be centrifuged immediately after dilution to remove any precipitates or aggregates—use of this clarified extract may result in cleaner IPs. We would typically pre-clear extract by centrifugation at 20,000 × *g* for 20 min at 4 °C in a fixed angle rotor.
2. To the extract add 1–5 % (v:v) serum or 1–20 µg purified antibody and mix well (*see* **Note 23**).
3. Incubate the extract/antibody mixture for 1 h on ice or at 4 °C (*see* **Note 23**).

4. Add 10 μl of pre-washed Protein A/G Sepharose or 20 μl Protein A/G Dynabeads to the extract/antibody mixture, mix well and rotate at 4 °C for 1 h (*see* **Note 23**).
5. Wash the beads. Wash Protein A/G agarose beads three times with 400 μl of Sepharose wash buffer: add the buffer and mix gently by pipetting or inverting the tube six times (*see* **Note 23**). Protein A/G Sepharose is recovered, and unbound proteins in the wash supernatant separated out, by centrifugation at 2000 × *g* for 2 min at 4 °C in a swinging bucket rotor. Protein A/G Dynabeads are recovered in a magnetic stand on ice. Beads are washed three times with 200 μl of Dynabead wash buffer (*see* **Note 23**).
6. Proteins are recovered from the beads by boiling in SDS-PAGE loading buffer for 5 min at 95 °C. Samples can be then assayed by immunoblotting or further processed for mass spectrometric analysis.

3.10 Immunofluorescent Staining of Chromosomes and Nuclei Assembled In Vitro

Specific antibodies can be used to localize and track the dynamic interaction of a target protein with and within, chromosomes and nuclei. Chromosomes/nuclei isolated onto coverslips are incubated sequentially with a primary and then a fluorescently tagged secondary antibody. Staining is then visualized by UV microscopy.

1. At the required time add 100 μl of 1–4 % (v:v) formaldehyde prepared in XBE2 to 10 μl of reaction mixture—we typically use 4 % (v:v) formaldehyde. Incubate at room temperature for 10 min—do not exceed 20 min as excessive incubation with formaldehyde can damage the nuclei.
2. Optional: coverslip preparation. Coverslips can be coated with poly-L-lysine (Sigma) at a 1/10 dilution in H_2O, as per manufacturer's instructions. Incubate coverslips in the poly-L-lysine solution for 20–30 min and then dry them well by placing at 37 °C for 30 min or overnight at room temperature. The coated coverslips can be stored for up to 3 months at 4 °C.
3. Place a 13 mm diameter round coverslip into the desired number of wells of a 24-well plate. Add 2.4 ml of XBE2 plus 30 % sucrose cushion.
4. Load the fixed sample onto the sucrose cushion very gently; pellet the chromosomes/nuclei by centrifugation at 2400 × *g* in a swinging bucket rotor for 10 min at 4 °C. Carefully remove the liquid using either a pipette or an aspirating pump mounted with a p200 yellow tip.
5. Quench unreacted aldehyde by adding 500 μl PBS plus 0.1 M glycine pH 7.0 and incubate at room temperature for 20–30 min. Alternatively, 750 mM Tris–HCl pH 7.0 may be used.

6. Permeabilize the recovered sample by incubating with 500 μl 1× PBS plus 0.1 % (v:v) Triton for 3–5 min—this time should not be extended—and then wash the coverslip three times with 1 ml PBS alone.
7. Block the coverslips with 1 ml PBS plus 0.1 % (v:v) Tween and 3 % (w:v) BSA and incubate for 1 h at room temperature or overnight at 4 °C.
8. Prepare your primary antibody in PBS plus 0.1 % (v:v) Tween and 3 % (w:v) BSA. We use only affinity-purified antibodies for immunofluorescence: these are used typically in the range 1–5 μg/ml and we prepare 250 μl per well. Incubate the coverslips with antibody at room temperature for 1 h or 4 °C overnight.
9. Wash the reaction three times for 10 min with 1 ml PBS plus 0.1 %(v:v) Tween.
10. Prepare secondary antibody—250 μl per well—at the manufacturer's suggested dilution in PBS plus 0.1 % (v:v) Tween and 3 % (w:v) BSA. We preferably use Alexa Fluor secondary antibodies, as they are less sensitive to bleaching.
11. Incubate 45 min in the dark.
12. Wash as in **step 6**.
13. Incubate the coverslips with 250 μl DAPI (1/1000 in PBS) for 8 min at room temperature and then wash 2–3 times with PBS alone. Optional: one wash with high purity water can be added after the PBS washes in order to reduce salt contamination. DAPI containing mounting media, e.g., VECTASHIELD (Vector Laboratories) can be used, but usually the DNA staining is of better quality with traditional direct staining.
14. We mount coverslips using VECTASHIELD mounting media. Add a small drop (around 10 μl) of media to a slide—a number of coverslips may fit well onto one slide. Remove a coverslip carefully using forceps, dripping excess liquid onto a tissue and place it face down onto the media on the glass slide.
15. To prevent sample dehydration, use a transparent nail polish to seal the edges of the coverslip.
16. Leave for a minimum of 1 h at room temperature, in the dark.
17. Store at 4 °C in the dark.

4 Notes

1. To increase sperm yield male frogs can be primed with 150 units Chorulon (Chorionic Gonadotrophin) 7 ± 2 days before the testes are removed. We typically prepare nuclei from 15 frogs. Isolation of the testes and recovery of the sperm immediately

thereafter are time consuming and we typically divide the labor between two groups, preparing no more than three frogs simultaneously. Ethanol-rinse and dry already cleaned implements immediately prior to use.

2. The testes are located in the lower abdominal region. Often hidden in the body cavity they are readily distinguishable from the similarly colored digestive system—the testes are approximately bean/egg shaped and ivory in color and are typically 0.75–1.5 cm in length. Each frog typically has two testes.
3. Cut a large square from the top of the screw cap lid and use the cut lid to secure a square of nylon mesh over the end of the tube containing the sperm; the contents of the tube can then be filtered into another container through the lid top filter.
4. The sperm may look different depending on the angle from which they are viewed, ranging from a squiggle (side view) to a circle (top view). Preparations typically contain 1–5 % somatic nuclei. The count is repeated four times to ensure statistical accuracy. The mean number is then calculated, with somatic nuclei given a double weighting because they are diploid.
5. The extract should be used immediately and during sample processing should be kept at 4 °C until the replication reaction is started by the addition of DNA.
6. We make two essential additions extract: energy regenerator (ER) and cycloheximide. ER—25 mM phosphocreatine and 15 μg/ml creatine phosphokinase at final concentration—serves to keep ATP levels high throughout the duration of the reaction by providing a source of high-energy phosphate. Frozen extracts do not efficiently support protein synthesis, as the ribosomes are lost upon the hard clarifying spin during preparation and so do not usually progress into first mitosis. Addition of cycloheximide—250 μg/ml at final concentration—which acts to inhibit protein synthesis, ensures this block to progression.
7. Metaphase arrested extracts can be activated to progress into anaphase and the first mitotic interphase by addition of 0.3 mM $CaCl_2$ (1/167 of stock: 50 mM in H_2O). If performing an interphase reaction, we typically activate the extract for 15 min prior to template DNA addition.
8. The replication of sperm nuclei in egg extract is dependent upon nuclear assembly. In typical reactions, with DNA concentrations of 3–10 ng/μl, nuclei assemble between 20 and 40 min after sperm addition. Each nucleus forms a discrete unit of replication and the kinetics of DNA replication are absolutely dependent on the efficiency of nuclear assembly: at increased DNA concentrations, or in diluted extracts, assembly is less efficient resulting in slower replication [9]. Since the

initiation of DNA replication is dependent on nuclear assembly it is crucial that this is monitored in every experiment to rule out the nonspecific inhibition of DNA replication. The capacity of the extract to assemble demembranated sperm into nuclei is ~30 ng DNA/μl (~9500 haploid nuclei per μl), close to the concentration of chromosomal DNA in embryos at the mid-blastula transition; we typically use final DNA concentrations of 3–10 ng DNA/μl extract, however. The extract has a somewhat larger capacity to replicate preformed interphase nuclei [85], probably reflecting that nuclear envelope material becomes limiting when sperm nuclei are used as template. Dilution of the extract severely compromises nuclear assembly, so, ideally, the total volume of additions should be kept to <20 % extract volume. Drugs added to extract can be prepared in a number of solvents: H_2O, extract friendly buffer (e.g., LFB1/50) or DMSO, as appropriate. At high concentrations DMSO is toxic to the extract—we limit addition to 1 % v/v.

9. Nuclear assembly can be followed by UV and phase contrast light microscopy.
10. Over time the nuclei undergo a series of characteristic morphological changes: when added directly into interphase extract the sperm chromatin undergoes nucleoplasmin-mediated decondensation and increases in size within 5 min. The sperm nuclei acquire membrane components over the next 15–25 min and these are seen as black spots on the surface of the sperm under phase contrast. Upon full nuclear assembly, ~20–40 min after activation, phase contrast microscopy reveals the nuclear envelope as a solid black line around each nucleus. A time course showing micrographs of the different stages of nuclear assembly is given in ref. 84. The shape of nuclei formed in individual extracts varies. In our experience we find that nuclei formed in metaphase-arrested extracts activated in vitro appear larger and typically more circular than those formed in extracts prepared from activated eggs or in those extracts that escaped metaphase arrest during preparation.
11. Chromatin isolated from a 6-DMAP treated extract—and subsequently incubated with protein fractions purified from interphase extract—enabled the characterization of replication licensing, and the identification of the licensing factors Mcm2–7 and Cdt1 [13, 16, 43, 86].
12. By binding tightly to cyclin E-Cdk2 and cyclin D-Cdk4, $p27^{Kipl}$ (alternatively, $p27^{Xic1}$) becomes a potent inhibitor of their CDK activity in vitro in a stoichiometric manner [87, 88]. Recombinant GST-tagged $p27^{Kipl}$ is bacterially expressed and purified.
13. $p21^{Cip1}$ is a CDK inhibitor that is transcriptionally activated by p53 in response to DNA damage. $p21^{Cip1}$ effectively inhibits

Cdk2, Cdk3, Cdk4, and Cdk6 kinases but is much less effective toward cyclin B-Cdk1 and p35-Cdk5 and does not associate with cyclin H-Cdk7 [89–91]. Recombinant GST-tagged $p21^{Cipl}$ is bacterially expressed and purified.

14. Roscovitine is a potent, synthetic, purine-derived, inhibitor of cyclin-dependent kinases Cdks1/2/5/7/9 [92]. It acts as a competitive inhibitor of ATP binding. Roscovitine (Calbiochem) is dissolved in DMSO at 400 mM and used at a final concentration in egg extract of 0.5–1 mM which is sufficient to block S phase CDK activity [64]. Whereas the protein CDK inhibitors $p27^{Kipl}$ and $p21^{Cip1}$ are highly specific, roscovitine is less selective and may have off-target effects—at high concentration (≥1–2 mM) roscovitine affects nuclear envelope assembly, a process not known to be CDK sensitive. As such we prefer to use either $p27^{Kipl}$ and $p21^{Cip1}$ to inhibit CDK activity.
15. PHA-767491 is a potent and selective ATP-competitive dual Cdc7/Cdk9 inhibitor [93]. The activity of PHA-767491 in *Xenopus egg* extract has been fully characterized: Mcm4 phosphorylation is lost and DNA replication is inhibited at a concentration of 50 μM PHA-767491 [52]. In *Xenopus* egg extracts, DDK activity can be determined by the presence of hyperphosphorylated chromatin bound Mcm4, which is detected as an apparent upshift in molecular weight of the protein upon immunoblotting [52]. In order to prepare a working stock from the concentrated DMSO stock (100 mM) use 40 mM HEPES–KOH pH 7.0—the drug has to be made up freshly and mixed thoroughly before adding to the extract in order to avoid precipitates.
16. Aphidicolin, a competitive inhibitor of DNA polymerases α, δ and ε, limits DNA replication in two ways: firstly, by inhibiting the progression of active replication forks it decreases the size of nascent strands and secondly, by activating the ATM–ATR checkpoint response that inhibits further origin firing [64, 94, 95]. When added to *Xenopus* egg extracts at 10 μM, aphidicolin slows replication forks by approximately threefold; the major effect on replication at this concentration is to induce an ATR-dependent checkpoint that suppresses further initiation events [64]. The activity of the ATR kinase in extract can be inhibited by addition of 5 mM caffeine. When added to extract caffeine rescues the aphidicolin-induced inhibition of DNA replication at low concentrations of aphidicolin (≤20 μM) [60, 64]. However, at higher concentrations (80–100 μM) the checkpoints induced by aphidicolin are irreversibly activated and DNA replication cannot be rescued by caffeine addition. An aphidicolin stock, which can be stored frozen, is prepared in DMSO.

17. A 100 mM caffeine stock is prepared in H_2O and is added to extract at a final concentration of 5 mM; it is of the upmost importance that caffeine is prepared freshly, immediately prior to use.
18. Individual samples need be no more than 5–20 μl in volume. If multiple samples are to be prepared from one extract treatment, for example when performing a time course to determine replication kinetics, aliquots should be made as early as is appropriate.
19. Radiolabeling of molecular weight markers: incubate the reaction mix at room temperature for 20 min. Optionally, the enzyme can be heat deactivated (as per manufacturer's instruction). Typically we load 0.5–1 μl of marker on an agarose gel. Once labeled, the markers will be stable according to the half-life of the incorporated radio-nucleotide, e.g., 14 days for α^{32}P-dNTP, but we recommend making them up freshly for each experiment.
20. Agarose beads are supplied in an alcohol-based preservative. Since these beads are porous consider their volume as 100 % alcohol. Wash the beads, in an appropriately sized tube in order to reduce the alcohol to <0.1 %, e.g., 4× 10 volume washes reduces alcohol concentration to 0.01 %.
21. Premark the required volume on the outside of the tubes with permanent marker either by filling with autoclaved high purity water, which is then removed or by comparing with another tube filled to the desired volume.
22. Whole (undiluted) egg extract can be used for immunoprecipitation experiments; in this crude extract the nonspecific precipitation of proteins may confuse results, however.
23. A number of optimizations can be made to the immunoprecipitation protocol: the volume/concentration of serum/antibody added to extract; antibody incubation time—10 min to overnight; the choice of beads used, the ratio of beads to extract and the bead incubation time—10 min to 1 h. The bead washing steps can also be optimized: the number of washes and wash buffer components—in particular salt and detergent concentrations. Increasing both of these will clean the precipitate but may also disrupt native complex formation.

References

1. Laskey RA, Mills AD, Morris NR (1977) Assembly of SV40 chromatin in a cell-free system from Xenopus eggs. Cell 10:237–243
2. Lohka MJ, Masui Y (1983) Formation in vitro of sperm pronuclei and mitotic chromosomes induced by amphibian ooplasmic components. Science 220:719–721
3. Lohka MJ, Masui Y (1984) Effects of Ca2+ ions on the formation of metaphase chromosomes and sperm pronuclei in cell-free preparations from unactivated Rana pipiens eggs. Dev Biol 103:434–442
4. Lohka MJ, Masui Y (1984) Roles of cytosol and cytoplasmic particles in nuclear envelope

assembly and sperm pronuclear formation in cell-free preparations from amphibian eggs. J Cell Biol 98:1222–1230

5. Newport J, Kirschner M (1982) A major developmental transition in early Xenopus embryos: I. characterization and timing of cellular changes at the midblastula stage. Cell 30:675–686
6. Newport J, Kirschner M (1982) A major developmental transition in early Xenopus embryos: II. Control of the onset of transcription. Cell 30:687–696
7. Murray AW, Kirschner MW (1989) Cyclin synthesis drives the early embryonic cell cycle. Nature 339:275–280
8. Blow JJ, Laskey RA (1986) Initiation of DNA replication in nuclei and purified DNA by a cell-free extract of Xenopus eggs. Cell 47: 577–587
9. Blow JJ, Watson JV (1987) Nuclei act as independent and integrated units of replication in a Xenopus cell-free DNA replication system. EMBO J 6:1997–2002
10. Shamu CE, Murray AW (1992) Sister chromatid separation in frog egg extracts requires DNA topoisomerase II activity during anaphase. J Cell Biol 117:921–934
11. Lohka MJ, Hayes MK, Maller JL (1988) Purification of maturation-promoting factor, an intracellular regulator of early mitotic events. Proc Natl Acad Sci U S A 85:3009–3013
12. Murray AW, Solomon MJ, Kirschner MW (1989) The role of cyclin synthesis and degradation in the control of maturation promoting factor activity. Nature 339:280–286
13. Tada S, Li A, Maiorano D, Mechali M, Blow JJ (2001) Repression of origin assembly in metaphase depends on inhibition of RLF-B/Cdt1 by geminin. Nat Cell Biol 3:107–113
14. Hodgson B, Li A, Tada S, Blow JJ (2002) Geminin becomes activated as an inhibitor of Cdt1/RLF-B following nuclear import. Curr Biol 12:678–683
15. Blow JJ, Laskey RA (1988) A role for the nuclear envelope in controlling DNA replication within the cell cycle. Nature 332:546–548
16. Gillespie PJ, Li A, Blow JJ (2001) Reconstitution of licensed replication origins on Xenopus sperm nuclei using purified proteins. BMC Biochem 2:15
17. Gambus A, Khoudoli GA, Jones RC, Blow JJ (2011) Mcm2-7 form double hexamers at licensed origins in Xenopus egg extract. J Biol Chem 286:11855–11864
18. Blow JJ, Nurse P (1990) A cdc2-like protein is involved in the initiation of DNA replication in Xenopus egg extracts. Cell 62:855–862
19. Fang F, Newport JW (1991) Evidence that the G1-S and G2-M transitions are controlled by different cdc2 proteins in higher eukaryotes. Cell 66:731–742
20. Roberts BT, Ying CY, Gautier J, Maller JL (1999) DNA replication in vertebrates requires a homolog of the Cdc7 protein kinase. Proc Natl Acad Sci U S A 96:2800–2804
21. Jares P, Blow JJ (2000) Xenopus cdc7 function is dependent on licensing but not on XORC, XCdc6, or CDK activity and is required for XCdc45 loading. Genes Dev 14:1528–1540
22. Walter JC (2000) Evidence for sequential action of cdc7 and Cdk 2 protein kinases during initiation of DNA replication in Xenopus egg extracts. J Biol Chem 275:39773–39778
23. Yoshida K, Takisawa H, Kubota Y (2005) Intrinsic nuclear import activity of geminin is essential to prevent re-initiation of DNA replication in Xenopus eggs. Genes Cells 10:63–73
24. Pacek M, Walter JC (2004) A requirement for MCM7 and Cdc45 in chromosome unwinding during eukaryotic DNA replication. EMBO J 23:3667–3676
25. Maric M, Maculins T, De Piccoli G, Labib K (2014) Cdc48 and a ubiquitin ligase drive disassembly of the CMG helicase at the end of DNA replication. Science 346:1253596
26. Moreno SP, Bailey R, Campion N, Herron S, Gambus A (2014) Polyubiquitylation drives replisome disassembly at the termination of DNA replication. Science 346:477–481
27. Blow JJ, Dutta A (2005) Preventing re-replication of chromosomal DNA. Nat Rev Mol Cell Biol 6:476–486
28. Minshull J, Blow JJ, Hunt T (1989) Translation of cyclin mRNA is necessary for extracts of activated Xenopus eggs to enter mitosis. Cell 56:947–956
29. Lohka MJ, Maller JL (1985) Induction of nuclear envelope breakdown, chromosome condensation, and spindle formation in cell-free extracts. J Cell Biol 101:518–523
30. Sawin KE, Mitchison TJ (1991) Mitotic spindle assembly by two different pathways in vitro. J Cell Biol 112:925–940
31. Minshull J, Golsteyn R, Hill CS, Hunt T (1990) The A- and B-type cyclin associated cdc2 kinases in Xenopus turn on and off at different times in the cell cycle. EMBO J 9: 2865–2875
32. Strausfeld UP, Howell M, Descombes P, Chevalier S, Rempel RE, Adamczewski J, Maller JL, Hunt T, Blow JJ (1996) Both cyclin A and cyclin E have S-phase promoting (SPF) activity in Xenopus egg extracts. J Cell Sci 109(Pt 6):1555–1563

33. Solomon MJ, Glotzer M, Lee TH, Philippe M, Kirschner MW (1990) Cyclin activation of p34cdc2. Cell 63:1013–1024
34. Walter J, Sun L, Newport J (1998) Regulated chromosomal DNA replication in the absence of a nucleus. Mol Cell 1:519–529
35. Lebofsky R, Takahashi T, Walter JC (2009) DNA replication in nucleus-free Xenopus egg extracts. Methods Mol Biol 521:229–252
36. Masui Y (1974) A cytostatic factor in amphibian oocytes: its extraction and partial characterization. J Exp Zool 187:141–147
37. Masui Y (2001) From oocyte maturation to the in vitro cell cycle: the history of discoveries of Maturation-Promoting Factor (MPF) and Cytostatic Factor (CSF). Differentiation 69: 1–17
38. Liu J, Grimison B, Maller JL (2007) New insight into metaphase arrest by cytostatic factor: from establishment to release. Oncogene 26:1286–1289
39. Isoda M, Sako K, Suzuki K, Nishino K, Nakajo N, Ohe M, Ezaki T, Kanemori Y, Inoue D, Ueno H, Sagata N (2011) Dynamic regulation of Emi2 by Emi2-bound Cdk1/Plk1/CK1 and PP2A-B56 in meiotic arrest of Xenopus eggs. Dev Cell 21:506–519
40. Rauh NR, Schmidt A, Bormann J, Nigg EA, Mayer TU (2005) Calcium triggers exit from meiosis II by targeting the APC/C inhibitor XErp1 for degradation. Nature 437:1048–1052
41. Li A, Blow JJ (2004) Non-proteolytic inactivation of geminin requires CDK-dependent ubiquitination. Nat Cell Biol 6:260–267
42. Li A, Blow JJ (2005) Cdt1 downregulation by proteolysis and geminin inhibition prevents DNA re-replication in Xenopus. EMBO J 24: 395–404
43. Blow JJ (1993) Preventing re-replication of DNA in a single cell cycle: evidence for a replication licensing factor. J Cell Biol 122:993–1002
44. Kubota Y, Takisawa H (1993) Determination of initiation of DNA replication before and after nuclear formation in Xenopus egg cell free extracts. J Cell Biol 123:1321–1331
45. Mochida S, Hunt T (2007) Calcineurin is required to release Xenopus egg extracts from meiotic M phase. Nature 449:336–340
46. Mochida S, Ikeo S, Gannon J, Hunt T (2009) Regulated activity of PP2A-B55 delta is crucial for controlling entry into and exit from mitosis in Xenopus egg extracts. EMBO J 28: 2777–2785
47. Murphy J, Crompton CM, Hainey S, Codd GA, Hutchison CJ (1995) The role of protein phosphorylation in the assembly of a replication competent nucleus: investigations in Xenopus egg extracts using the cyanobacterial toxin microcystin-LR. J Cell Sci 108:235–244
48. Nishiyama A, Tachibana K, Igarashi Y, Yasuda H, Tanahashi N, Tanaka K, Ohsumi K, Kishimoto T (2000) A nonproteolytic function of the proteasome is required for the dissociation of Cdc2 and cyclin B at the end of M phase. Genes Dev 14:2344–2357
49. Newport J (1987) Nuclear reconstitution in vitro: stages of assembly around protein-free DNA. Cell 48:205–217
50. Sheehan MA, Mills AD, Sleeman AM, Laskey RA, Blow JJ (1988) Steps in the assembly of replication-competent nuclei in a cell-free system from Xenopus eggs. J Cell Biol 106:1–12
51. Blow JJ, Sleeman AM (1990) Replication of purified DNA in Xenopus egg extract is dependent on nuclear assembly. J Cell Sci 95:383–391
52. Poh WT, Chadha GS, Gillespie PJ, Kaldis P, Blow JJ (2014) Xenopus Cdc7 executes its essential function early in S phase and is counteracted by checkpoint-regulated protein phosphatase 1. Open Biol 4:130138
53. Kisielewska J, Blow JJ (2012) Dynamic interactions of high Cdt1 and geminin levels regulate S phase in early Xenopus embryos. Development 139:63–74
54. McGarry TJ, Kirschner MW (1998) Geminin, an inhibitor of DNA replication, is degraded during mitosis. Cell 93:1043–1053
55. Takahashi TS, Yiu P, Chou MF, Gygi S, Walter JC (2004) Recruitment of Xenopus Scc2 and cohesin to chromatin requires the pre-replication complex. Nat Cell Biol 6:991–996
56. Gillespie PJ, Hirano T (2004) Scc2 couples replication licensing to sister chromatid cohesion in Xenopus egg extracts. Curr Biol 14: 1598–1603
57. Gillespie PJ, Khoudoli GA, Stewart G, Swedlow JR, Blow JJ (2007) ELYS/MEL-28 chromatin association coordinates nuclear pore complex assembly and replication licensing. Curr Biol 17:1657–1662
58. Khoudoli GA, Gillespie PJ, Stewart G, Andersen JS, Swedlow JR, Blow JJ (2008) Temporal profiling of the chromatin proteome reveals system-wide responses to replication inhibition. Curr Biol 18:838–843
59. Oehlmann M, Score AJ, Blow JJ (2004) The role of Cdc6 in ensuring complete genome licensing and S phase checkpoint activation. J Cell Biol 165:181–190
60. Woodward AM, Gohler T, Luciani MG, Oehlmann M, Ge X, Gartner A, Jackson DA, Blow JJ (2006) Excess Mcm2-7 license dormant origins of replication that can be used under

conditions of replicative stress. J Cell Biol 173:673–683

61. Mahbubani HM, Chong JP, Chevalier S, Thommes P, Blow JJ (1997) Cell cycle regulation of the replication licensing system: involvement of a Cdk-dependent inhibitor. J Cell Biol 136:125–135
62. Blow JJ, Ge XQ (2009) A model for DNA replication showing how dormant origins safeguard against replication fork failure. EMBO Rep 10:406–412
63. Blow JJ, Ge XQ, Jackson DA (2011) How dormant origins promote complete genome replication. Trends Biochem Sci 36:405–414
64. Luciani MG, Oehlmann M, Blow JJ (2004) Characterization of a novel ATR-dependent, Chk1-independent, intra-S-phase checkpoint that suppresses initiation of replication in Xenopus. J Cell Sci 117:6019–6030
65. Masai H, Arai K (2002) Cdc7 kinase complex: a key regulator in the initiation of DNA replication. J Cell Physiol 190:287–296
66. Sheu YJ, Stillman B (2010) The Dbf4-Cdc7 kinase promotes S phase by alleviating an inhibitory activity in Mcm4. Nature 463:113–117
67. Takahashi TS, Walter JC (2005) Cdc7-Drf1 is a developmentally regulated protein kinase required for the initiation of vertebrate DNA replication. Genes Dev 19:2295–2300
68. Takahashi TS, Basu A, Bermudez V, Hurwitz J, Walter JC (2008) Cdc7-Drf1 kinase links chromosome cohesion to the initiation of DNA replication in Xenopus egg extracts. Genes Dev 22:1894–1905
69. Kobayashi H, Golsteyn R, Poon R, Stewart E, Gannon J, Minshull J, Smith R, Hunt T (1991) Cyclins and their partners during Xenopus oocyte maturation. Cold Spring Harb Symp Quant Biol 56:437–447
70. Krasinska L, Besnard E, Cot E, Dohet C, Mechali M, Lemaitre JM, Fisher D (2008) Cdk1 and Cdk2 activity levels determine the efficiency of replication origin firing in Xenopus. EMBO J 27:758–769
71. Moyer SE, Lewis PW, Botchan MR (2006) Isolation of the Cdc45/Mcm2-7/GINS (CMG) complex, a candidate for the eukaryotic DNA replication fork helicase. Proc Natl Acad Sci U S A 103:10236–10241
72. Ilves I, Petojevic T, Pesavento JJ, Botchan MR (2010) Activation of the MCM2-7 helicase by association with Cdc45 and GINS proteins. Mol Cell 37:247–258
73. Tanaka S, Umemori T, Hirai K, Muramatsu S, Kamimura Y, Araki H (2007) CDK-dependent phosphorylation of Sld2 and Sld3 initiates DNA replication in budding yeast. Nature 445:328–332
74. Zegerman P, Diffley JF (2007) Phosphorylation of Sld2 and Sld3 by cyclin-dependent kinases promotes DNA replication in budding yeast. Nature 445:281–285
75. Kumagai A, Shevchenko A, Shevchenko A, Dunphy WG (2011) Direct regulation of Treslin by cyclin-dependent kinase is essential for the onset of DNA replication. J Cell Biol 193:995–1007
76. Kumagai A, Shevchenko A, Shevchenko A, Dunphy WG (2010) Treslin collaborates with TopBP1 in triggering the initiation of DNA replication. Cell 140:349–359
77. Hirano T, Mitchison TJ (1994) A heterodimeric coiled-coil protein required for mitotic chromosome condensation in vitro. Cell 79: 449–458
78. Kimura K, Hirano T (1997) ATP-dependent positive supercoiling of DNA by 13S condensin: a biochemical implication for chromosome condensation. Cell 90:625–634
79. Hirano T, Kobayashi R, Hirano M (1997) Condensins, chromosome condensation protein complexes containing XCAP-C, XCAP-E and a Xenopus homolog of the Drosophila Barren protein. Cell 89:511–521
80. Emanuele MJ, Lan W, Jwa M, Miller SA, Chan CS, Stukenberg PT (2008) Aurora B kinase and protein phosphatase 1 have opposing roles in modulating kinetochore assembly. J Cell Biol 181:241–254
81. Qian YW, Erikson E, Taieb FE, Maller JL (2001) The polo-like kinase Plx1 is required for activation of the phosphatase Cdc25C and cyclin B-Cdc2 in Xenopus oocytes. Mol Biol Cell 12:1791–1799
82. Bernis C, Forbes DJ (2014) Analysis of nuclear reconstitution, nuclear envelope assembly, and nuclear pore assembly using Xenopus in vitro assays. Methods Cell Biol 122:165–191
83. Losada A, Hirano M, Hirano T (1998) Identification of Xenopus SMC protein complexes required for sister chromatid cohesion. Genes Dev 12:1986–1997
84. Gillespie PJ, Gambus A, Blow JJ (2012) Preparation and use of Xenopus egg extracts to study DNA replication and chromatin associated proteins. Methods 57:203–213
85. Dimitrova DS, Gilbert DM (1998) Regulation of mammalian replication origin usage in Xenopus egg extract. J Cell Sci 111(Pt 19): 2989–2998
86. Chong JP, Mahbubani HM, Khoo CY, Blow JJ (1995) Purification of an MCM-containing complex as a component of the DNA replication licensing system. Nature 375:418–421
87. Polyak K, Kato JY, Solomon MJ, Sherr CJ, Massague J, Roberts JM, Koff A (1994) p27Kip1,

a cyclin-Cdk inhibitor, links transforming growth factor-beta and contact inhibition to cell cycle arrest. Genes Dev 8:9–22

88. Toyoshima H, Hunter T (1994) p27, a novel inhibitor of G1 cyclin-Cdk protein kinase activity, is related to p21. Cell 78:67–74
89. Gu Y, Turck CW, Morgan DO (1993) Inhibition of Cdk2 activity in vivo by an associated 20K regulatory subunit. Nature 366: 707–710
90. Harper JW, Adami GR, Wei N, Keyomarsi K, Elledge SJ (1993) The p21 Cdk-interacting protein Cip1 is a potent inhibitor of G1 cyclin-dependent kinases. Cell 75:805–816
91. Xiong Y, Hannon GJ, Zhang H, Casso D, Kobayashi R, Beach D (1993) p21 is a universal inhibitor of cyclin kinases. Nature 366:701–704
92. Meijer L, Borgne A, Mulner O, Chong JP, Blow JJ, Inagaki N, Inagaki M, Delcros JG, Moulinoux JP (1997) Biochemical and cellular effects of roscovitine, a potent and selective inhibitor of the cyclin-dependent kinases cdc2, cdk2 and cdk5. Eur J Biochem 243:527–536
93. Montagnoli A, Valsasina B, Croci V, Menichincheri M, Rainoldi S, Marchesi V, Tibolla M, Tenca P, Brotherton D, Albanese C, Patton V, Alzani R, Ciavolella A, Sola F, Molinari A, Volpi D, Avanzi N, Fiorentini F, Cattoni M, Healy S, Ballinari D, Pesenti E, Isacchi A, Moll J, Bensimon A, Vanotti E, Santocanale C (2008) A Cdc7 kinase inhibitor restricts initiation of DNA replication and has antitumor activity. Nat Chem Biol 4:357–365
94. Santocanale C, Diffley JF (1998) A Mec1- and Rad53-dependent checkpoint controls late-firing origins of DNA replication. Nature 395:615–618
95. Shirahige K, Hori Y, Shiraishi K, Yamashita M, Takahashi K, Obuse C, Tsurimoto T, Yoshikawa H (1998) Regulation of DNA-replication origins during cell-cycle progression. Nature 395: 618–621

Chapter 7

Elutriation for Cell Cycle Synchronization in Fission Yeast

Kazunori Kume

Abstract

Cell synchronization is a powerful technique for studying the eukaryotic cell cycle events precisely. The fission yeast is a rod-shaped cell whose growth is coordinated with the cell cycle. Monitoring the cellular growth of fission yeast is a relatively simple way to measure the cell cycle stage of a cell. Here, we describe a detailed method of unperturbed cell synchronization, named centrifugal elutriation, for fission yeast.

Key words Synchronization, Elutriation, Cell cycle, Fission yeast, Cell morphology

1 Introduction

Synchronization of cells is a very effective method for the study of molecular mechanisms involved in cell cycle regulation. Synchronized cells are used to study the expression level of macromolecules (DNA, RNA, and protein) during the different stages of the cycle. The budding yeast *Saccharomyces cerevisiae* and the fission yeast *Schizosaccharomyces pombe* play significant roles as model eukaryotic cells in understanding the fundamental principles of cell cycle regulation [1, 2].

Fission yeast is a rod-shaped cell that grows by tip elongation in a cell-cycle-regulated manner [3]. After cell division, fission yeast cells initially grow in a monopolar manner, from the tip that existed before cell division (the old end) (Fig. 2a). In early G2 phase, after cells have attained completion of DNA replication and a critical cell size, the cells activate new end growth and switch to bipolar growth ("New End Take Off": NETO) [3, 4]. This growth polarity is maintained during the following interphase. At the onset of mitosis, the cell growth ceases and chromosome segregation occurs followed by cytokinesis which is accomplished by the construction of a septum through the middle of the cell (Fig. 2a). Thus, fission yeast cells coordinate cell growth and the cell cycle, indicating that monitoring cell growth (cell size and cell polarity) is a measure of the cell cycle stage of a cell [3–5].

Amanda S. Coutts and Louise Weston (eds.), *Cell Cycle Oscillators: Methods and Protocols*, Methods in Molecular Biology, vol. 1342, DOI 10.1007/978-1-4939-2957-3_7,

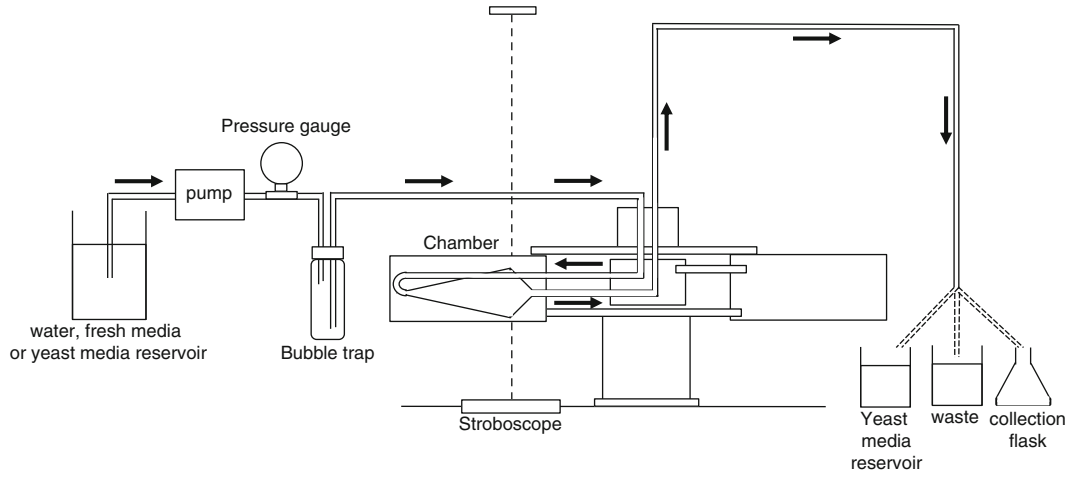

Fig. 1 Schematic diagram of centrifugal elutriation system

There are several techniques for cell synchronization, which can be categorized into two distinct approaches [6, 7]. One approach is the "block-and-release" method which includes use of cell cycle mutants, drug-induced arrest, nutrient starvation and pheromone-induced arrest, all of which can block the cell cycle at a particular point, resulting in a synchronous culture after release of the block [6, 7]. The other approach is the physical method including centrifugal elutriation and lactose gradient [6, 7]. The cell elutriation is the most physiological way to synchronize the culture. This method selects cells of uniform size, which are at the same stage of the cell cycle, from an asynchronous culture in a short time. This method has an important advantage over the block-and-release method, which is that selected cells are unperturbed, synchronized, and healthy. This chapter describes a protocol for synchronization of fission yeast cells by centrifugal elutriation (Fig. 1).

2 Materials

2.1 Elutriation System

1. Beckman-J-6M microprocessor-controlled elutriation centrifuge.
2. Beckman-JE-5.0 elutriator rotor.
3. MasterFlex Microprocessor Pump Drive and Pump Head (Cole-Parmer Instrument Inc.).
4. MasterFlex Tygon tube.
5. Masterflex silicone pump tube.

2.2 Yeast Strain, Growth Media, and Cell Measurement

1. *Schizosaccharomyces pombe* (e.g., wild-type strain 972, and temperature-sensitive NETO mutant strain *pol1-1546* [8]).
2. YES growth media (yeast extract + supplements [7]): 5 g/l yeast extract, 30 g/l glucose, 225 mg/l adenine, 225 mg/l L-histidine, 225mg/l L-leucine, 225 mg/l uracil, and 225 mg/l L-lysine.
3. Hematology Analyzer (Sysmex, F-820).
4. CellPack for dilution of cells (Sysmex, 884-0871-1).
5. 16 % Formaldehyde (methanol-free).
6. Calcofluor: dilute Calcofluor (Sigma F-6259) to 50 μg/ml.
7. DAPI: dilute 4′,6-diamidino-2-phenylindole (DAPI, Sigma D-9542) to 0.5 μg/ml. DAPI stock is 50 μg/ml in distilled water, stored in small aliquots at 4 °C.
8. Fluorescence microscopy with DAPI filter.

2.3 Cleaning Reagents for Elutriation System

1. 200 ml Bleach (5 % sodium hypochlorite): dilute sodium hypochlorite with sterile water.
2. 500 ml 70 % ethanol.
3. Two, 3 l flasks containing 2 l sterile water.

3 Methods

3.1 Sterilization of Elutriation System

1. Put an inlet and an outlet tube in 200 ml Bleach.
2. Pump the Bleach through the system at 30 ml/min (*see* **Note 1**).
3. Start the centrifugation to remove bubbles (2000 rpm, 895 × *g*) and set the centrifuge temperature to 25 °C (*see* **Notes 2** and **3**). Circulate it for at least 20 min.
4. Wash out the Bleach using 500 ml 70 % ethanol at 30 ml/min and circulate the 70 % ethanol for 20 min (*see* **Note 4**).

3.2 Setup Elutriation System

1. Place the inlet tube in the water reservoir (2 l in 3 l flask) and the outlet tube in the waste beaker (3 l or 5 l).
2. Set the flow rate at 100 ml/min and wash out the 70 % ethanol using 1 l of sterile water (*see* **Note 5**).
3. Replace the water with fresh YES media. Discard at least 500 ml of the YES media and then set the flow rate at 130 ml/min to circulate the rest of the YES media.
4. Start the centrifugation at 3500 rpm (2740 × *g*) to remove small bubbles and adjust the stroboscope to see the elutriation chamber through the hole of the door on the centrifuge.
5. Stop the centrifugation.

3.3 Synchronization of Cells

1. Put the inlet tube and the outlet tube in YES culture containing exponentially growing yeast cells ($1–1.2 \times 10^7$ cells/ml) to load them to the elutriation chamber (*see* **Note 6**).
2. Start centrifugation at 3500 rpm ($2740 \times g$) and flow rate 130 ml/min until the bottom line of the cell boundary fills 3/4 of the chamber (*see* **Note 7**).
3. Decrease the flow rate from 130 to 105 ml/min and reduce the centrifuge speed to 2800 rpm ($1750 \times g$).
4. Once the flow rate and the centrifuge speed are stabilized, transfer the outlet tube to an empty sterile flask (200 ml) and take 200 μl cells to measure the cell number (*see* **Note 8**).
5. Decrease the flow rate to between 100 and 95 ml/min to proceed with fine-tuning for obtaining synchronized small cells (*see* **Note 9**).
6. When the cell number is between 0.7×10^6 and 0.9×10^6 cells/ml, check the cell size by phase-contrast microscopy and start collecting cells in a new sterile flask (200 ml) (*see* **Note 10**).
7. Filter the collected cells and put them in pre-warm fresh YES media (*see* **Note 11**). Mix well and measure the cell number.
8. Put the flask containing synchronized cells on a shaker and start the time-course at 28 °C, 200 rpm.
9. To finish elutriation, stop the centrifuge and increase the flow rate to 130 ml/min. Remove residual yeast media from the elutriation chamber (*see* **Note 12**).
10. Rinse the elutriation system with five- to tenfold diluted natural detergent and wash the system completely with sterilized water (*see* **Note 13**).
11. To sterilize the system, rinse it with 70 % ethanol (*see* **Note 14**).

3.4 Counting Cell Number, Nuclear Number, and Cell Morphology Populations

1. For each time point, take 200 μl cells for counting cell number using the Sysmex, and mix 450 μl cells with 50 μl formaldehyde in a precooled 1.5 ml micro-centrifuge tube for cell fixation. Leave the cell-formaldehyde mix on ice for 10 min and wash it with precooled sterile water twice.
2. Count the cell number and fix cells with formaldehyde every 20 min for 3–6 h.
3. Count nuclear number and cell morphology (*see* **Note 15**).

4 Notes

1. Invert the bubble trap until it fills up. Make sure the Bleach reaches the whole of the inside of the bubble trap.
2. Once the speed of the centrifuge reaches 2000 rpm ($895 \times g$), stop the centrifugation and confirm whether the bubbles are

gone. If bubbles are still in the elutriation chamber, repeat the centrifugation with higher speed (e.g., 2500 rpm, $1400 \times g$ or 3000 rpm, $2012 \times g$).

3. It is recommended to use the same temperature at which the cells you plan to use are inoculated. Temperature affects yeast cell growth, especially when temperature-sensitive mutant strains are used.
4. These sterilized treatments can be done 1 day before using the elutriation system. In this case, the elutriation system including all tubes should be filled with the 70 % ethanol before using it, to keep the elutriation system clean.
5. Exponentially growing yeast cells are highly sensitive to both ethanol and bleach. Wash the tubes out using a sufficient amount of sterile water.
6. Cultivate an 800 ml culture in YES at 25 or 28 °C to $1–1.2 \times 10^7$ cells/ml (OD600 is about 1). For measurement of the cell number, we normally use a Hematology Analyzer (Sysmex, F-820). Sonication is needed before the measurement.
7. Do not stop the pump while the centrifuge is running. Loss of pressure from the pump results in cells accumulating in the narrow end of the elutriation chamber. In this case, stop the centrifuge, and restart the pump (130 ml/min) to remove the accumulated cells.
8. Take 200 μl cells from the flask in a 10 ml CellPack and measure the cell number using the Sysmex. The first fraction may be more than 1.2×10^6 cells/ml and population of the cells are not evenly distributed. This fraction should not be collected.
9. After reduction of the flow rate, wait until the pump pressure is stabilized and transfer the outlet tube to an empty sterile flask. If the cell number is still more than 1×10^6 cells/ml, decrease the flow rate in increments of 2 ml/min until the cell number is between 0.7×10^6 and 0.9×10^6 cells/ml. On the contrary, if the cell number is less than 0.7×10^6 cells/ml, increase the flow rate in increments of 2 ml/min until the cell number reaches between 0.7×10^6 and 0.9×10^6 cells/ml.
10. When 200 ml small cells are collected, transfer the outlet tube to a new sterile flask, and confirm whether the cells collecting from the outlet tube are still synchronized by counting the cell number using the Sysmex.
11. 50 ml or 100 ml YES media containing synchronized cells ($1.5–2 \times 10^6$ cells/ml) is enough for monitoring cellular morphology and nuclear division with specific dyes (calcofluor and DAPI). For this purpose, collect 200 ml of synchronized cells.
12. If it is difficult to remove remaining cells from the elutriation chamber, the chamber can be disassembled and washed by hand.
13. Do not use acetone for the wash. It will cause the tube to degrade.

14. Keeping the elutriation system filled with 70 % ethanol is a much easier way to maintain the system, when you repeatedly conduct the experiment over a short term.
15. Count 200 cells. For counting nuclear number using DAPI, which stains DNA, cells are classified into two groups: one nucleus in one cell and two nuclei in one cell with or without septum. For the observation of cellular morphology, we often use calcofluor which stains septa and newly synthesized cell wall in the growing cell end, which can be easily distinguished from the non-growing dark cell end. Cells are classified into three groups: monopolar cell, bipolar cell, and septated cell (Fig. 2a).

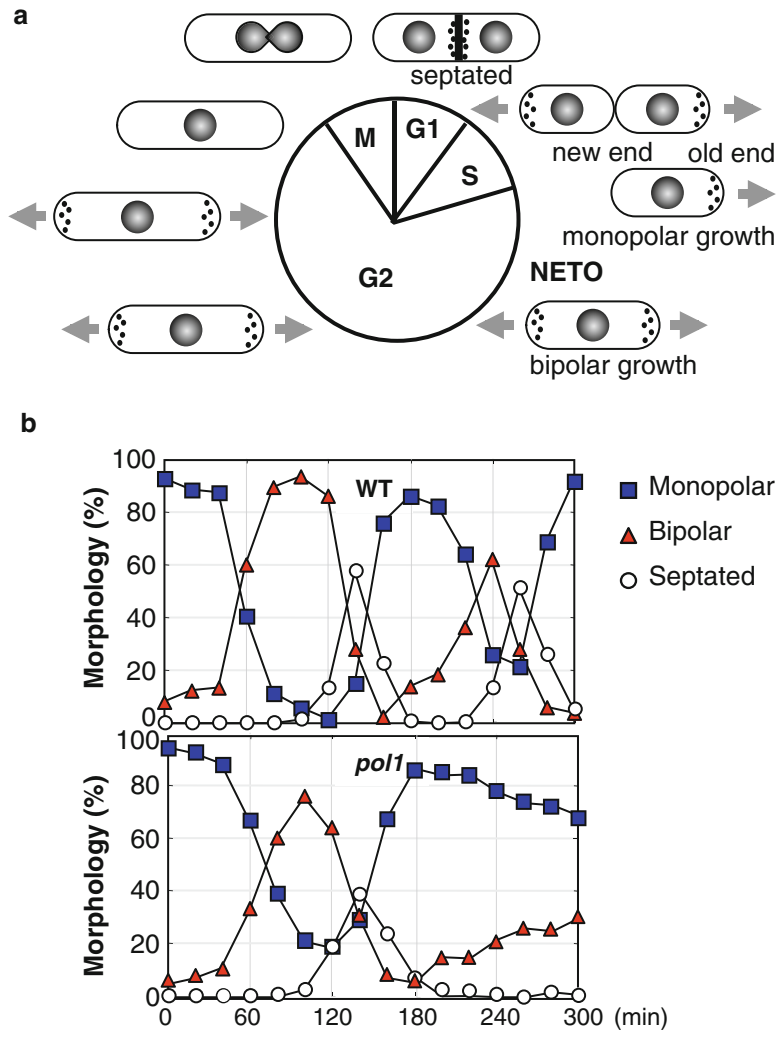

Fig. 2 Cell morphology is coordinated with cell cycle in fission yeast. (**a**) Cell morphology of wild-type cell during cell cycle. (**b**) Frequencies of monopolar, bipolar, and septated cells in synchronous culture from early G2 phase ($n > 200$). Wild-type cells and pol1 temperature-sensitive mutant cells are grown at 36 °C

At the beginning of the time course, most cells grow in a monopolar manner and 100 % of the cells have one nucleus, indicating a good synchronization. In these synchronized cells, population of septated cells will reach between 35 and 60 % at its peak (Fig. 2b).

References

1. Mitchison JM (2003) Growth during the cell cycle. Int Rev Cytol 226:165–258
2. Humphery T, Brooks G (2005) Cell cycle control. In: Humphery T, Brooks G (eds) Methods in molecular biology, vol 296. Humana Press, Totowa, NJ, pp 1–29
3. Hayles J, Nurse P (2001) A journey into space. Nat Rev Mol Cell Biol 2:647–656
4. Martin SG, Chang F (2005) New end take off: regulating cell polarity during the fission yeast cell cycle. Cell Cycle 4:4046–4049
5. Navarro FJ, Weston L, Nurse P (2012) Global control of cell growth in fission yeast and its coordination with the cell cycle. Curr Opin Cell Biol 24:1–5
6. Walker GM (1999) Synchronization of yeast cell populations. Methods Cell Sci 21:87–93
7. Forsburg SL, Rhind N (2006) Basic methods for fission yeast. Yeast 23:173–183
8. Kume K, Koyano T, Kanai M, Toda T, Hirata D (2011) Calcineurin ensures a link between the DNA replication checkpoint and microtubule-dependent polarized growth. Nat Cell Biol 13:234–242

Chapter 8

Spatiotemporal Investigation of Phosphorylation Events During Cell Cycle Progression

Lilia Gheghiani and Olivier Gavet

Abstract

Polo-like kinase 1 (Plk1) is an essential kinase for mitotic commitment and progression through mitosis. In contrast to its well characterized roles during mitosis, the precise molecular events controlled by Plk1 during G2/M progression and their spatiotemporal regulation are still poorly elucidated. We recently investigated Plk1-dependent regulation of Cdc25C phosphatase, an activator of the master mitotic driver Cyclin B1-Cdk1. To this end, we generated a genetically encoded FRET (Förster Resonance Energy Transfer)-based Cdc25C phosphorylation biosensor to observe Cdc25 spatiotemporal phosphorylation during cell cycle progression in live single cell assays. Because this approach proved to be powerful, we provide here guidelines for the development of biosensors for any phosphorylation site of interest.

Key words Phosphorylation, Kinase, Biosensor, FRET, Time-lapse imaging, Fluorescence microscopy

1 Introduction

1.1 Protein Phosphorylation

Protein phosphorylation is the most common post-translational modification used to finely tune any cellular process and is therefore a master regulatory mechanism for the maintenance of cell homeostasis. Reversible phosphorylation/dephosphorylation events are often associated with a switch in the active state of target proteins and reflect modifications over time by opposite protein kinase and phosphatase activities. Transcriptome and proteome analyses have revealed that most human diseases are associated with the deregulation of kinase and/or phosphatase expression levels. However, we frequently ignore the extent to which this will modify the spatiotemporal regulation of their enzymatic activities and as a consequence the phosphorylation states of their target proteins. A panel of elegant and powerful experimental approaches has recently emerged to identify target phosphorylation sites on a given protein and upstream kinase(s) and phosphatase(s) activities, including large-scale phosphoproteomic analyses, live-cell RNAi

Amanda S. Coutts and Louise Weston (eds.), *Cell Cycle Oscillators: Methods and Protocols*, Methods in Molecular Biology, vol. 1342, DOI 10.1007/978-1-4939-2957-3_8,

screens of protein kinase and phosphatase libraries and ATP analog labeling of protein kinase substrates [1–3]. Nevertheless, deciphering spatiotemporal regulation of any phosphorylation event, i.e. when and where this post-translational modification is initiated and/or turned off, is still a major challenge in cell biology. This is best illustrated by our weak understanding of how different signaling pathways are coordinated together into a coherent whole in space and time to control main cell cycle transitions as well as their spatiotemporal deregulations in tumoral conditions.

One popular approach, following the identification of a specific phosphorylation site, is the development of a corresponding phospho-specific antibody for qualitative and/or semi-quantitative immunofluorescence (IF) microscopy. In fact, IF is particularly powerful to detect any local phosphorylation of even a small fraction of a given protein. This will provide spatiotemporal information if the corresponding protein is concentrated at a particular subcellular location and if morphological landmarks are available. As an example, activating phosphorylation (T210P) of the mitotic Polo-like kinase 1 (Plk1) at the centrosome can be recorded during well identified mitotic stages (from prophase to anaphase) [4]. Conversely, phosphorylation states of diffusible proteins and/or absence of morphological landmarks are strongly limiting conditions. Accordingly, the activating phosphorylation kinetics of the diffusible cytoplasmic Plk1 pool during G2 phase progression has been under debate [4–6]. Also, IF detection of local phosphorylation events on fixed cells can be poorly informative of the underlying regulatory mechanisms taking place. In fact, local detection of active (T210P) Plk1 at the centrosome, as mentioned above, could reflect several scenarios: (1) its activation process could be restricted to this particular subcellular location, (2) following cytoplasmic activation, active Plk1 kinase could be recruited to the centrosome through unmasking of its anchoring domain (Polo-Box Domain), (3) initial activation of centromeric and cytoplasmic pools could be concurrent but the detection of cytoplasmic active Plk1 is limited by its diffusible distribution. FRET-based phosphorylation biosensors offer a powerful alternative to access the spatiotemporal regulation of phosphorylation events in live single cell assays.

1.2 Polo-Like Kinase 1 and Mitotic Commitment

Plk1 is an essential mitotic kinase for several processes including mitotic entry, centrosome maturation, sister chromatid resolution, stable attachment of chromosomes to the spindle apparatus and cleavage furrow formation [7–9]. Consistent with its involvement in the control of mitotic commitment, direct regulators (including activating phosphatases Cdc25B & C and inhibitory kinases Wee1 & Myt1) of the master mitotic driver Cyclin B1-Cdk1 have been found to be phosphorylated, at least in vitro, by Plk1. While the biological significance of Plk1-dependent Myt1 and Cdc25B phosphorylation is waiting further investigation, Plk1 has been shown

to promote Wee1 degradation through beta-TrCP-dependent mechanisms during G2/M progression, although it is not yet known whether this event precedes or follows mitotic entry [10]. Also, several reports show that Plk1 (or Plx1, *Xenopus laevis* homolog) stimulates Cdc25C (XCdc25C) phosphatase activity in vitro, by which it could promote Cyclin B1-Cdk1 initial activation and mitotic (meiotic) entry [11, 12]. Accordingly, hyperphosphorylation of Cdc25C during G2/M progression is sensitive to Plk1 inhibition. However, the different Plk1-dependent phosphorylation sites on Cdc25C and their spatiotemporal regulation during G2/M transition have been poorly characterized, strongly limiting our understanding of the relative importance of this regulatory mechanism for the control of mitotic commitment.

1.3 Plk1-Dependent Cdc25C Phosphorylation

We recently performed phosphoproteomic analysis to cover the whole Cdc25C protein sequence and identified eight Plk1-dependent phosphorylation sites, among them S38, 61 and 75 are fully conserved in vertebrates [6]. We generated a phospho-specific antibody against the S75 phosphosite which is surrounded by a canonical Plk1 consensus sequence and confirmed its Plk1-dependent phosphorylation during mitosis. Nevertheless, due to the diffusible cytoplasmic distribution of Cdc25C, we could not unambiguously determine when this phosphorylation event was initiated around the G2/M transition by IF, as discussed above. Instead, as described in the details of this chapter, we developed and optimized a FRET-based Cdc25C-S75 phosphorylation biosensor, which gave us access to its spatiotemporal regulation during cell cycle progression. We believe that this methodology could be broadly applied to investigate real-time regulation of any phosphorylation event following its previous identification by other experimental approaches.

1.4 Genetically Encoded Phosphorylation Biosensor

Genetically encoded FRET-based phosphorylation biosensors typically include a "sensor unit" which consists of a short phosphorylation sequence of interest (~10–20 amino acids) and a phosphorylation binding domain able to recognize this site in its phosphorylated state, both sandwiched between a pair of fluorescent proteins (usually CFP and YFP or their close derivatives). Conformational changes associated with the reversible phosphorylation of such biosensors affect the efficiency of non-radiative energy transfer between the donor (CFP) and the acceptor (YFP) fluorophores upon CFP excitation, which can be recorded in real time in live single cell assays. Efficient fluorescence resonance energy transfer between compatible fluorescent protein pairs is a function of the inverse sixth power of their absolute distance but is also strongly dependent on the relative orientation of their dipole moments. Optimization of these two parameters to improve the FRET dynamic range (sensitivity) of any biosensor can be a tedious process.

In order to override this main limitation, several FRET-dedicated vector libraries have recently emerged based on the use of differently connected circularly permutated forms of donor (CFP variant mTFP1) and/or acceptor (YFP variant Venus) fluorescent proteins to modulate their relative spatial orientation [13, 14]. Such libraries can also comprise short amino-acid sequences ("linkers") of different length between each fluorescent protein and the "sensor unit" to further modulate the orientation and/or absolute distance between them. From data currently available, it appears that using different circularly permutated forms is a more easy way to rapidly improve, as a first step, the dynamic range of any biosensor [13]. On the other hand, using linker random mutagenesis and large-scale (up to 1,00,000) bacterial colonies screening, Oliver Griesbeck's group recently selected calcium reporters exhibiting ratio changes of up to 1000 % in bacteria, demonstrating the potential to optimize linker sequences to generate highly sensitive biosensors [15].

Although commonly called "kinase biosensors," one should keep in mind that these sensors will, in most cases, report changes in the equilibrium between opposite kinase and phosphatase activities rather than modification of the kinase activity alone, i.e. when the phosphorylation of the target site becomes effective. As an example, this strategy proved to be powerful to decipher phosphorylation changes of Plk1-dependent kinetochore substrates during prometaphase to metaphase transition, which are finely tuned by the local recruitment of Plk1 and/or counteracting PP1 phosphatase [16]. A comprehensive list of phosphorylation site biosensors already available for several kinases (PKA, PKC, PKB/Akt, ERK, Aurora-B, CyclinB1-Cdk1, etc.) can be found at the following address: http://biosensor.dpb.carnegiescience.edu.

2 Materials

2.1 FRET-Dedicated Plasmid Library

We used a FRET-dedicated vector library previously developed by Carsten Schultz's group (EMBL, Germany; [13]). This library contains CFP variant mTurquoise as the fluorescent donor and YFP variant Venus or cp49Venus, cp157Venus, cp173Venus, cp229Venus as the fluorescent acceptors together with short linkers of different sizes (two, four, or eight amino acids). YPet fluorescent protein was also inserted as an alternative YFP variant acceptor [17] (Fig. 1a).

1. Cloning primers:

   FHA2 forward Primer 5′→3′ (**AgeI**) GCG **ACC GGT** AAG GGT AAT GGT AGG TTT TTA ACT

   FHA2 reverse Primer 5′→3′ (**MluI EcorI**) GCG **ACG CGT GAA TTC** TAA CTT TTT CAC CAA ATC TTT TTC T

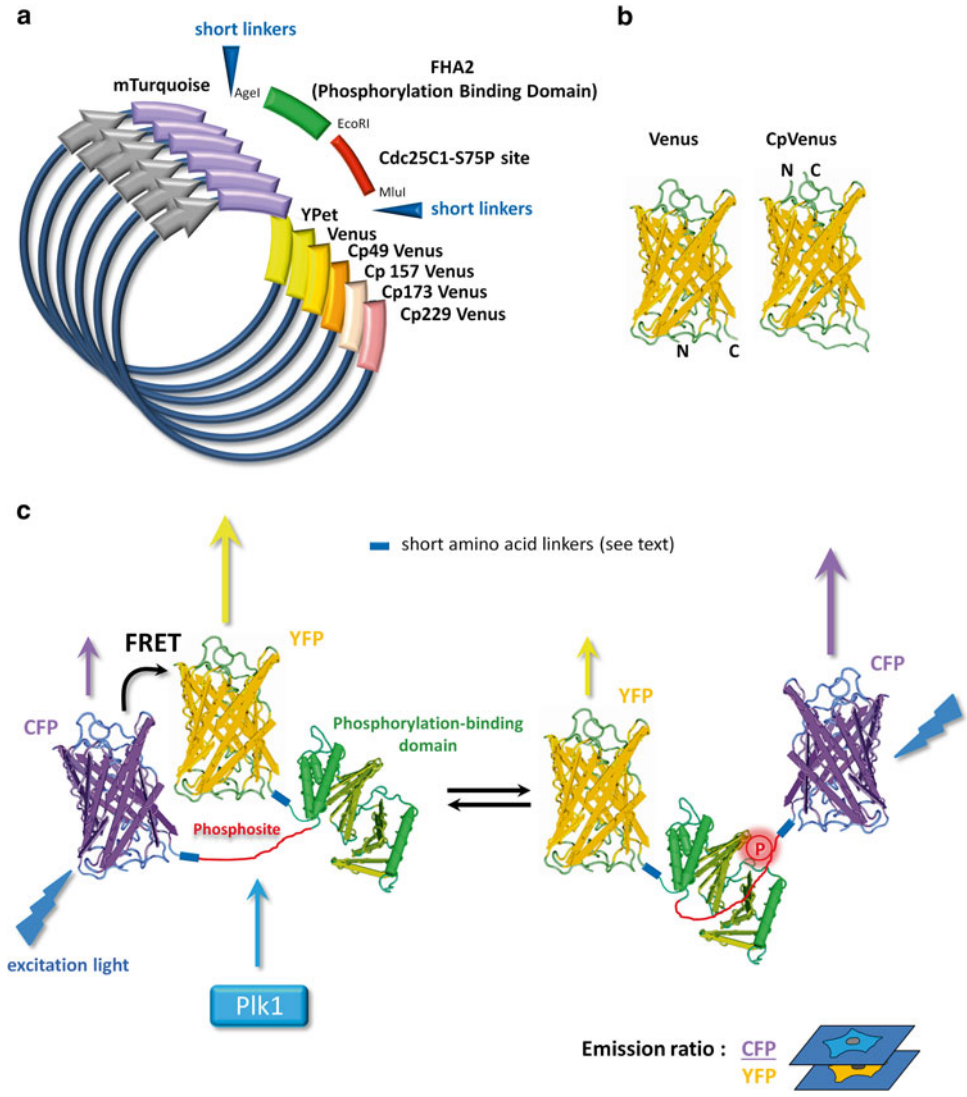

Fig. 1 (**a**) FRET-dedicated vector library containing fluorescent CFP donor (Turquoise), YFP acceptors (Ypet, Venus, and cpVenus) and short linker sequences (2, 4, or 8 amino acids) [13]. Restriction sites used for cloning are also indicated. (**b**) Schematic representation of differentially connected Venus and cpVenus. (**c**) General scheme of the FRET-based phosphorylation biosensor. Phosphorylation of a specific target residue induces its recognition by the phosphorylation binding domain and a conformational change occurs, affecting the efficiency of energy transfer between fluorescent donor and acceptor proteins

2. Restriction enzymes : AgeI (**ACC GGT**), MluI (**ACG CGT**), EcoRI (**GAA TTC**)
3. Vent DNA polymerase
4. T4 DNA ligase
5. Alkaline phosphatase, Calf Intestinal (CIP)

6. Competent bacteria: subcloning efficiency DH5a
7. LB-Kanamycin agar plates
8. Low melting point agarose

2.2 Cell Culture and Transfection

1. Homo sapiens cervix epithelial HeLa cell line.
2. Dulbecco's Modified Eagle's Medium supplemented with 10 % fetal bovine serum (FBS), 2 mM Glutamine, 100 U/ml penicillin, and 100 μg/ml streptomycin.
3. Fibronectin from human plasma.
4. JetPrime transfection reagent.
5. Nocodazole.
6. 24 glass-bottom well plate or 35-mm glass-bottom imaging dishes.
7. Phenol red free Dulbecco's Modified Eagle or Liebowitz-15 (L15) medium supplemented with 1 % fetal bovine serum (FBS) and 2 mM Glutamine.

2.3 Wide-Field Imaging

1. The imaging setup uses an inverted motorized microscope (Leica DMI6000) equipped with temperature and CO_2-humidified controller systems, adaptive focus control, fast emission filter wheel lambda 10-3 (Sutter Instruments, Novato, CA, USA), electron multiplier charge-coupled device camera (Evolve 512; Photometrics), HCX PL APO 40×/1.30 Oil objective and multi LED illumination system (spectra X-light engine, Lumencor). High NA oil immersion objectives are preferred due to their high light collecting efficiency.
2. Emission filters ET480/40, ET535/30m and CFP/YFP dichroic mirror 51017bs (Chroma Technology Corp., Brattleboro, VT, USA).

2.4 Image Acquisition

1. Wide-field imaging setup is controlled by Metamorph software (Molecular Devices, Sunnyvale, CA).

2.5 Image Analysis

1. Image analysis is performed using ImageJ software (NIH).

3 Methods

3.1 Design Intramolecular Cdc25C-S75 Phosphorylation Biosensors

We used AgeI and MluI sites inserted between donor and acceptor fluorescent protein sequences for subsequent cloning as described in Piljic et al. [13] (Fig. 1a).

1. Digest the CFP and YFP containing vectors with AgeI and MluI restriction enzymes, and dephosphorylate them with alkaline phosphatase enzyme.

2. Perform PCR amplification of the FHA2 phosphorylation binding domain sequence from yeast ScRad53p with 5′ and 3′ primers containing AgeI and MluI&EcoRI restriction sequences (*see* **Note 1**).
3. Digest the PCR product with AgeI and MluI restriction enzymes.
4. Run digested PCR products on a 0.5 % low melting point agarose gel.
5. Purify the digested product from the gel using standard protocols.
6. Insert the FHA2 fragment in the vector backbones using vector:insert molar ratios between 1:3 and 1:10 and T4 DNA ligase.
7. Transform the reaction mix into competent bacteria using standard protocols.
8. Plate the transformed bacteria on LB-Kanamycin agar plates.
9. Pick up individual colonies and inoculate LB medium containing Kanamycin antibiotic.
10. Prepare plasmid DNA using a plasmid miniprep kit.
11. Check plasmid constructs by DNA sequencing.
12. Design primers for the phosphorylation site of interest. We used complementary nucleotide sequences coding for the following peptide NH_2-G-G-A-P-K-R-C-L-L-**T**-N-L-I-COOH. This sequence is from HsCdc25C, residues 66–78, with Ser75 replaced with Thr and an Ile amino-acid inserted at +3 position in order to optimize FHA2 binding (*see* **Note 1**).
13. Anneal complementary oligonucleotides exhibiting overlapping 5′ ends for EcoRI & MluI restriction sites according to standard protocols.
14. Linearize the vector backbones containing the FHA2 domain with both EcoRI and MluI restriction enzymes. Do not dephosphorylate the vectors.
15. Subclone the annealed oligonucleotides into the different vector backbones.
16. Transform the different constructs into competent bacteria.
17. Plate the transformed bacteria on LB-Kanamycin agar plates.
18. Pick up individual colonies and inoculate LB medium containing Kanamycin antibiotic.
19. Prepare plasmid DNA using a plasmid miniprep kit (Plasmid DNA for transfection into mammalian cells should be preferentially prepared using commercial endotoxin-free MiniPrep and/or MaxiPrep kits to limit cell toxicity).
20. Check plasmid constructs by DNA sequencing.
21. If required, a protein-targeting domain can be inserted into the biosensor constructs (*see* **Note 2**).

3.2 Cell Culture

1. Culture human cervix carcinoma HeLa cells in Dulbecco's Modified Eagle Medium supplemented with 10 % fetal bovine serum (FBS), 2 mM Glutamine, 100 U/ml penicillin, 100 µg/ml streptomycin at 37 °C with 5 % CO_2.
2. Seed cells on a 24-well glass bottom plate or on a 35 mm glass bottom dish pre-coated with fibronectin (1 µg/cm^2) for 1–2 h at a density of 50,000 cells per well or 200,000 cells per dish, respectively.

3.3 Cell Transfection and Synchronization

The day after seeding, transfection of the different biosensor constructs can be carried out with a transfection reagent such as JetPrime, according to the manufacturer's recommendations. In brief:

1. Add 4 µl of JetPrime reagent and 1 µg of the plasmid construct to 200 µl of JetPrime buffer.
2. Mix gently by tapping and further incubate for 15 min at room temperature.
3. Add the mixture to the cells cultured in medium without antibiotics and incubate for 4 h.
4. Replace the culture medium and add thymidine 2.5 mM for ~15–20 h to synchronize the cells in S phase.
5. Add the microtubule depolymerizing drug Nocodazole (100 nM) 6 h post-thymidine release (G2 phase) for ~3–5 h to enrich for mitotic cells.

3.4 Screening

In order to determine the FRET dynamic range of each biosensor between phosphorylated and dephosphorylated states, we analyzed the average CFP/YFP emission ratio values in interphase (S phase) and mitotic synchronized cells. In fact, Plk1 protein is expressed from G2 phase onset and reaches a maximum activity level during mitosis [18].

1. Image acquisition is performed in CO_2-independent L15 culture medium (*see* **Note 3**).
2. Using the eyepieces, quickly select in each well several stage positions with healthy cells exhibiting appropriate fluorescent levels (*see* **Note 4**).
3. Avoid unnecessary exposure of the cells to excitation light.
4. Acquire CFPex/CFPem and CFPex/YFPem snapshot images of the different positions using the same exposure time (usually between 30 and 200 ms, depending on the biosensor expression level, illumination power and camera sensitivity (*see* **Note 5**)).

3.5 Data Analyses

All image analysis is performed using ImageJ software.

1. Draw a region of interest (ROI) around each fluorescent cell of interest.

2. Check that the cell remains inside the ROI during time-lapse experiments.
3. Save ROI-1 using ROI manager tool.
4. Choose a close region devoid of cells for fluorescence background correction.
5. Save ROI-2 using ROI manager tool.
6. Measure area, average and sum intensities of each ROI.
7. Export values to Excel or Prism software.
8. FRET ratio measurement is performed using the following formulae:
   (a) Whole cell signal = sum of the intensity of the pixels for ROI-1.
   (b) Background signal = average value per pixel for the region selected just beside the cell of interest (ROI-2).
   (c) Whole-cell signal corrected = whole cell signal – ((area selected=number of pixels for ROI-1) × background signal).
   (d) CFP/YFP emission ratio = whole cell CFP signal corrected/whole cell YFP signal corrected.
9. Determine the average CFP/YFP emission ratio from several cells expressing any biosensor construct in both control (S phase) and stimulation conditions (M-phase arrested cells).
10. Compare the average FRET (CFP/YFP emission ratio) dynamic range between both conditions for each biosensor construct (*see* **Note 6**).

3.6 Controls

Following the identification of the Cdc25C-S75 biosensor construct exhibiting the highest dynamic range between interphase and mitotic cells, we performed several control experiments.

1. An inactive biosensor mutated on its internal phosphorylation site (for example, to a non-phosphorylatable Ala residue) is used to confirm that FRET changes are dependent on its phosphorylation level and are not a consequence of morphological changes during the cell division process or due to differential photobleaching of the donor and/or acceptor fluorescent proteins during recording.
2. To confirm biosensor sensitivity to a specific kinase activity of interest, one could inhibit its expression by an RNA interference approach. Alternatively, we analyzed FRET changes in mitotic arrested cells following dose-dependent inhibition of Plk1 kinase using different selective compounds (BI 2536, BI6727).
3. Because Plk1 and checkpoint kinase Mps1 share closely related target sites, we also checked that the Cdc25C-S75 phosphorylation biosensor is insensitive to Mps1 inhibition

(Reversine + MG132). Note that Proteasome inhibitor (MG132) is required to prevent premature mitotic exit following Mps1 inhibition.

4. Finally, using a broad PP1 & PP2A inhibitor (okadaic acid, 500 nM) added on mitotic cells, we found that the raise of Cdc25C-S75 biosensor phosphorylation during mitosis is not due to the inactivation of counteracting phosphatase(s).

3.7 Generation of Biosensor Stably Expressing Cells

To facilitate subsequent microscopy analyses, we generated HeLa cell populations stably expressing the biosensor of interest:

1. Subclone the biosensor sequence into a vector containing an antibiotic resistance gene (*see* **Note 7**).
2. Transfect cells using the same protocol as for transient expression.
3. 2 days after transfection, select cells by the addition of the appropriate antibiotic into the culture medium.
4. Optional: transfected fluorescent cells can be sorted out at this time by flow cytometry.
5. Change the culture medium containing the antibiotic every 2–3 days to maintain selection pressure.
6. Clones of resistant cells can be observed after ~2 weeks of selection.
7. After 3–4 weeks, all clones are collected by trypsination and stably expressing cells are sorted by flow cytometry to generate a homogeneous cell population exhibiting equivalent fluorescent (YFP and/or CFP) expression levels (*see* **Note 8**).

3.8 Time-Lapse Experiments

1. For time-lapse experiments on a multi-well plate, a 40× air objective should be preferentially used to avoid air bubble formation during recording. Conversely, multi-position recording (up to ~40, depending on their absolute distance, exposure times and time-lapse intervals) of biosensor-expressing cells can be performed in a 35 mm dish using an oil objective at around 1 image/min for ~3–4 h duration or at 1 image/3 min for 10–24 h without cell phototoxicity (*see* **Note 9**).
2. Perform time-lapse image analysis as previously described in Subheading 3.5.
3. Plot CFP/YFP emission ratio values over time. To facilitate the comparison of different cells, the emission ratio can be expressed as a percentage of the initial value (Fig. 2a).
4. Pseudo-color Intensity-Modulated Display (IMD) representation of emission ratio values over time is performed using Metamorph Software. We selected the 8-color hues option with 32 intensities displayed for each color ranking from dark to bright (Fig. 2b). The max and min ratio values are generally

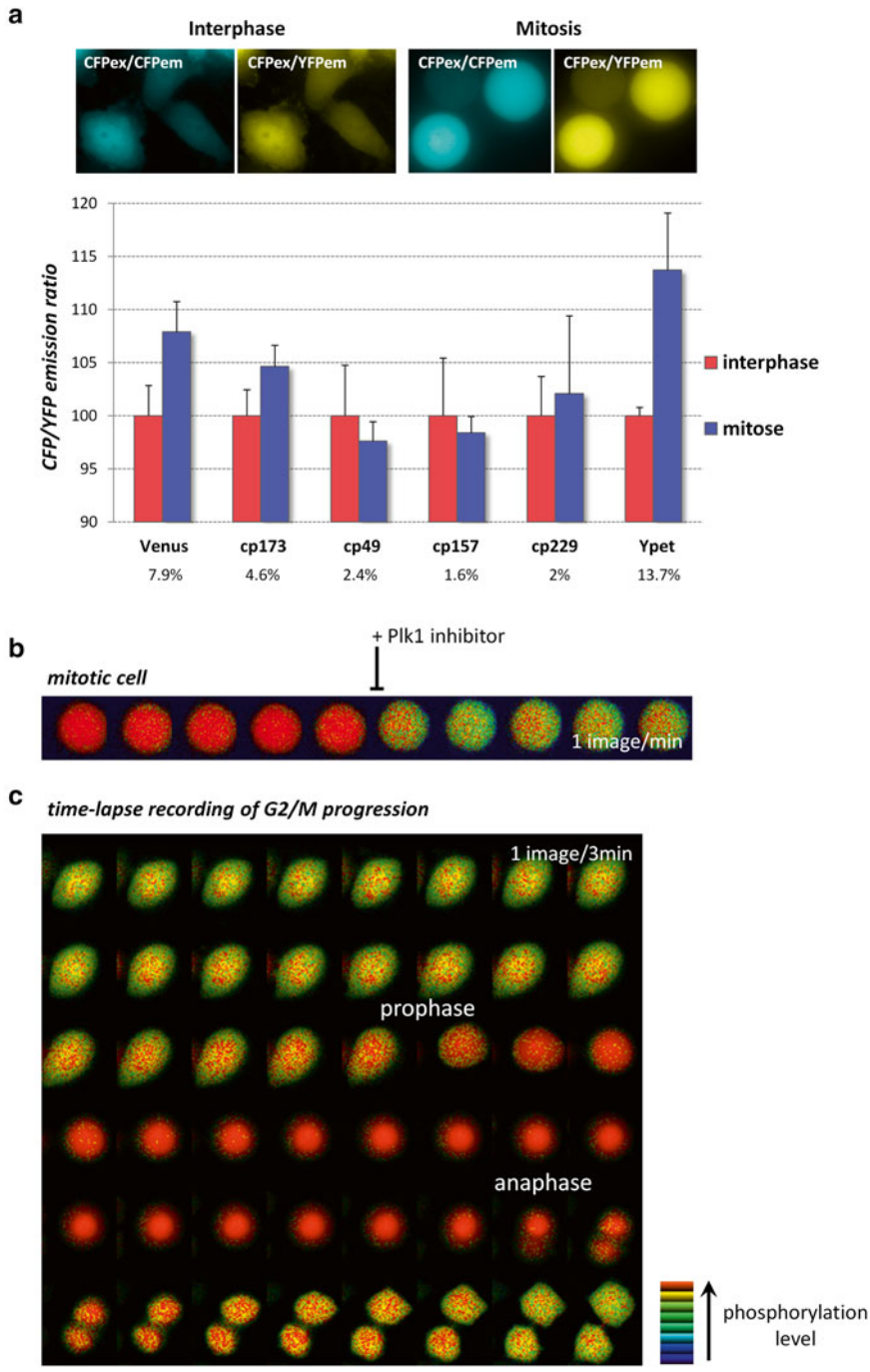

Fig. 2 (**a**) HeLa cells were transfected with the Cdc25C-S75 biosensor constructs containing different YFP acceptor fluorescent proteins as indicated. Transfected cells were either synchronized in interphase (S) or mitosis before CFPex/CFPem and CFPex/YFPem imaging. The average CFP/YFP emission ratio for each biosensor construct in both experimental conditions is displayed. The YPet-based Cdc25C-S75 biosensor exhibited the highest dynamic range and was used for subsequent experiments. Note that a secondary screen can be performed using amino-acid linkers of different sizes. (**b**) Cdc25C-S75 biosensor-expressing cells in mitosis were treated with a Plk1 inhibitor (BI2536 200 nM) (1 image/min). (**c**) Cdc25C-S75 biosensor-expressing cells were recorded during cell cycle progression (1 image/3 min)

fixed manually in a trial-and-error approach. The color intensities displayed for each hue are then determined automatically by the software [19].

4 Notes

1. Previous phosphoproteomics analyses revealed that recognition of Plk1 target sites is mostly based on adjacent N-terminal positions of phosphorylated serine/threonine residues [3]. In order to preserve the Plk1 specificity to the inserted Cdc25C-S75 phosphorylation peptide, we used the FHA2 domain of scRad53p as a phosphorylation-binding domain in our biosensor constructs. In fact, the FHA domains (denoted FHA1 and FHA2) exhibit amino-acid preferences at the three positions immediately C-terminal to the pT/pS, particularly at the +3 position (Asp residue for FHA1 and Ile for FHA2) [20]. Accordingly, the +3 position in the Cdc25C-S75 phosphorylation peptide was replaced by an Ile residue. Note also that the choice of the phosphorylation-binding domain will affect to a certain extent the dephosphorylation of biosensors and the FRET dynamics recorded. As an example, the dissociation constants of FHA1 and FHA2 domains for their respective optimal peptides are 530 nM and 10 μM [20, 21].
2. If the phosphorylation of a given substrate is taking place at a particular subcellular location or if one wants to investigate temporal phosphorylation/dephosphorylation kinetics at this place, insertion of a protein-targeting domain into the biosensor constructs will facilitate subsequent recording and image analyses. Several examples have been previously described including plasma membrane [22], nuclear or cytoplasmic [23], centrosome [24], chromatin [25] and inner centromere or kinetochore [26] targeting domains.
3. We used CO_2-dependent or -independent growth medium without phenol-red such as Dulbecco's Modified Eagle or Liebowitz-15 (L15) medium, respectively, for microscopy imaging. L-15 exhibited a lower auto-fluorescence level and was preferable due to the higher signal-to-noise ratio during short-term experiments. Conversely, we used Dulbecco's Modified Eagle medium and a CO_2-humidified controller system to prevent any evaporation during long-term (>20 h) experiments.
4. It is important to empirically select healthy and well adherent cells exhibiting appropriate expression levels of fluorescent biosensors. In indeed, a weak expression level will lead to a low signal-to-noise ratio. Conversely, high expression levels could affect cell properties and/or viability. Also, weakly adherent

cells have a tendency to round up and re-adhere over the time course of the experiment, which could affect the emission ratio baseline.

5. Different illumination sources can be used for FRET measurements. Whereas Xenon lamps are, in our hands, inappropriate for efficient CFP excitation, Mercury or metal-halide arc bulbs work quite well. Neutral density filters should be used to attenuate illumination power and to avoid photobleaching of the donor and/or acceptor fluorescent proteins, which will affect the emission ratio measurements. Also, we strongly recommend to insert UV filters (>400 nm long pass) in both epi- and trans-illumination light paths to limit phototoxicity. Finally, we recently used LED-based CFP excitation, which is superior in terms of light power stability for time-lapse experiments and further limits UV exposure. Several companies provide single- or multi-wavelength LED systems (for example, CoolLED, Lumencor).
6. Several screening approaches have been previously described to select phosphorylation biosensors with higher FRET dynamics between the control and stimulation conditions, including emission spectrum analysis of biosensor transfected cell extracts by a spectrofluorometer [22], fluorescence monitoring of biosensor library transfected cells in 96-well plates using a plate reader fluorometer [14] and large-scale screening of bacteria colonies co-expressing phosphorylation biosensors and the recombinant kinase of interest [27]. Nevertheless, because fluorescence properties and/or the dynamic range recorded by fluorescent microscopy could significantly differ, a secondary screen performed through live single cell assays is still required.
7. We used commercial mammalian pIRES expression vectors which allow co-expression of the biosensor of interest and the antibiotic resistance gene from the same bicistronic mRNA transcript. This significantly reduced the selection of false-positive colonies that only exhibit antibiotic resistance.
8. Using the same protocol, one could generate cell populations stably co-expressing the biosensor of interest and a RFP-fused cell cycle progression marker (PCNA, DNA ligase I, Cyclin B1, etc.). Red fluorescent proteins (such as mCherry and mRuby) will not interfere with the recording of CFP & YFP emission signals.
9. Focus drift is a frequent problem in video-microscopy, even when using automatic focus control systems that are generally based on infrared light reflection from the dish or plate bottom. In practice, we found that glass bottom dishes are more suitable for autofocus systems than fluorescent compatible plastic bottom dishes. Also, the choice of the stage dish holder, which depends on the dish used, is essential to prevent any movement

that may occur during time-lapse multi-positioning recording. Examples can be found at http://www.biosciencetools.com/catalog/. Finally, the stage dish holder was permanently maintained at 37 °C, and following dish positioning, we routinely waited for at least 1 h before starting recording. We found that this set-up significantly limited initial focus drift.

References

1. Schmitz MH, Held M, Janssens V et al (2010) Live-cell imaging RNAi screen identifies PP2A-B55alpha and importin-beta1 as key mitotic exit regulators in human cells. Nat Cell Biol 12:886–893, doi: ncb2092 [pii] 10.1038/ncb2092
2. Blethrow JD, Glavy JS, Morgan DO, Shokat KM (2008) Covalent capture of kinase-specific phosphopeptides reveals Cdk1-cyclin B substrates. Proc Natl Acad Sci U S A 105:1442–1447. doi:10.1073/pnas.0708966105
3. Kettenbach AN, Schweppe DK, Faherty BK et al (2011) Quantitative phosphoproteomics identifies substrates and functional modules of Aurora and Polo-like kinase activities in mitotic cells. Sci Signal 4:rs5. doi:10.1126/scisignal.2001497
4. Macurek L, Lindqvist A, Lim D et al (2008) Polo-like kinase-1 is activated by aurora A to promote checkpoint recovery. Nature 455:119–123, doi: nature07185 [pii] 10.1038/nature07185
5. Seki A, Coppinger JA, Jang C-YY et al (2008) Bora and the kinase Aurora a cooperatively activate the kinase Plk1 and control mitotic entry. Science 320:1655–1658. doi:10.1126/science.1157425
6. Gheghiani L, Loew D, Lombard B et al (2015) Plk1 pool activation in late G2 sets up commitment to mitosis
7. Lénárt P, Petronczki M, Steegmaier M et al (2007) The small-molecule inhibitor BI 2536 reveals novel insights into mitotic roles of polo-like kinase 1. Curr Biol 17:304–315. doi:10.1016/j.cub.2006.12.046
8. Lane HA, Nigg EA (1996) Antibody microinjection reveals an essential role for human polo-like kinase 1 (Plk1) in the functional maturation of mitotic centrosomes. J Cell Biol 135:1701–1713
9. Petronczki M, Glotzer M, Kraut N, Peters J-M (2007) Polo-like kinase 1 triggers the initiation of cytokinesis in human cells by promoting recruitment of the RhoGEF Ect2 to the central spindle. Dev Cell 12:713–725. doi:10.1016/j.devcel.2007.03.013
10. Watanabe N, Arai H, Iwasaki J et al (2005) Cyclin-dependent kinase (CDK) phosphorylation destabilizes somatic Wee1 via multiple pathways. Proc Natl Acad Sci U S A 102:11663–11668
11. Roshak AK, Capper EA, Imburgia C et al (2000) The human polo-like kinase, PLK, regulates cdc2/cyclin B through phosphorylation and activation of the cdc25C phosphatase. Cell Signal 12:405–411, doi: S0898-6568(00)00080-2 [pii]
12. Kumagai A, Dunphy WG (1998) Purification and molecular cloning of Plx1, a Cdc25-regulatory kinase from Xenopus egg extracts. Science 273:1377–1380
13. Pilji A, Wilmanns M, Schultz C et al (2011) Rapid development of genetically encoded FRET reporters. ACS Chem Biol 6:685–691. doi:10.1021/cb100402n
14. Fritz RD, Letzelter M, Reimann A et al (2013) A versatile toolkit to produce sensitive FRET biosensors to visualize signaling in time and space. Sci Signal 6:rs12. doi:10.1126/scisignal.2004135
15. Thestrup T, Litzlbauer J, Bartholomäus I et al (2014) Optimized ratiometric calcium sensors for functional in vivo imaging of neurons and T lymphocytes. Nat Methods 11:175–182. doi:10.1038/nmeth.2773
16. Liu D, Davydenko O, Lampson MA (2012) Polo-like kinase-1 regulates kinetochore-microtubule dynamics and spindle checkpoint silencing. J Cell Biol 198:491–499. doi:10.1083/jcb.201205090
17. Nguyen AW, Daugherty PS (2005) Evolutionary optimization of fluorescent proteins for intracellular FRET. Nat Biotechnol 23:355–360. doi:10.1038/nbt1066
18. Golsteyn RM, Mundt KE, Fry AM, Nigg EA (1995) Cell cycle regulation of the activity and subcellular localization of Plk1, a human protein kinase implicated in mitotic spindle function. J Cell Biol 129:1617–1628
19. Tsien R, Harootunian A (1990) Practical design criteria for a dynamic ratio imaging sys-

tem. Cell Calcium 11:93–109. doi:10.1016/0143-4160(90)90063-Z

20. Durocher D, Taylor IA, Sarbassova D et al (2000) The molecular basis of FHA domain:phosphopeptide binding specificity and implications for phospho-dependent signaling mechanisms. Mol Cell 6:1169–1182
21. Violin JD, Zhang J, Tsien RY, Newton AC (2003) A genetically encoded fluorescent reporter reveals oscillatory phosphorylation by protein kinase C. J Cell Biol 161:899–909, doi: 10.1083/jcb.200302125 jcb.200302125 [pii]
22. Yoshizaki H, Ohba Y, Kurokawa K et al (2003) Activity of Rho-family GTPases during cell division as visualized with FRET-based probes. J Cell Biol 162:223–232, doi: 10.1083/jcb.200212049 jcb.200212049 [pii]
23. Gavet O, Pines J (2010) Activation of cyclin B1-Cdk1 synchronizes events in the nucleus and the cytoplasm at mitosis. J Cell Biol 189:247–259. doi:10.1083/jcb.200909144
24. Agircan FG, Schiebel E (2014) Sensors at centrosomes reveal determinants of local separase activity. PLoS Genet 10(10), e1004672. doi:10.1371/journal.pgen.1004672
25. Fuller BG, Lampson MA, Foley EA et al (2008) Midzone activation of aurora B in anaphase produces an intracellular phosphorylation gradient. Nature 453:1132–1136, doi: nature06923 [pii] 10.1038/nature06923
26. Liu D, Vader G, Vromans MJ et al (2009) Sensing chromosome bi-orientation by spatial separation of aurora B kinase from kinetochore substrates. Science 323:1350–1353. doi:10.1126/science.1167000
27. Belal ASF, Sell BR, Hoi H et al (2014) Optimization of a genetically encoded biosensor for cyclin B1-cyclin dependent kinase 1. Mol Biosyst 10:191–195. doi:10.1039/c3mb70402e

Chapter 9

Cell Cycle Dynamics of Proteins and Post-translational Modifications Using Quantitative Immunofluorescence

Karen Akopyan, Arne Lindqvist, and Erik Müllers

Abstract

Immunofluorescence can be a powerful tool to detect protein levels, intracellular localization, and post-translational modifications. However, standard immunofluorescence provides only a still picture and thus lacks temporal information. Here, we describe a method to extract temporal information from immunofluorescence images of fixed cells. In addition, we provide an optional protocol that uses micropatterns, which increases the accuracy of the method. These methods allow assessing how protein levels, intracellular localization, and post-translational modifications change through the cell cycle.

Key words Quantitative immunofluorescence, Micropattern, Fluorescence microscopy, Image analysis, Cell cycle analysis

1 Introduction

With the rise of fluorescence microscopy, immunocytochemistry has become a fundamental technique of molecular biology. Samples are fixed and then stained using a huge variety of dyes or antibodies. For example, Antibodypedia (http://www.antibodypedia.org/) lists 1,426,650 antibodies as of October 15, 2014, corresponding to 19,285 genes, covering approximately 94 % of all human protein-coding genes [1]. Additionally, immunofluorescence can be used to detect glycans, lipids or small molecules, and even protein modifications or conformational changes. While immunofluorescence is a truly powerful tool to assess target molecule levels and localization, sample fixation generally leads to a loss of temporal information.

However, recent FACS-based approaches showed that it is feasible to deduce cell-cycle kinetics from the analysis of large numbers of immunostained cells [2, 3]. Now, we were able to reconstruct temporal information from fluorescence microscopy images of fixed cells [4]. To assign timings, we monitor markers that monotonically change throughout the cell cycle. For example,

Amanda S. Coutts and Louise Weston (eds.), *Cell Cycle Oscillators: Methods and Protocols*, Methods in Molecular Biology, vol. 1342, DOI 10.1007/978-1-4939-2957-3_9,

cellular DNA content steadily increases during replication from 2n to 4n. Similarly, the expression of cell-cycle regulators such as Cyclin A2 and Cyclin B1 gradually increases during S and G_2 phases [5]. Therefore, a cell containing high levels of DNA and Cyclins should be at a later stage in the cell cycle compared to a cell containing low levels. Using this information, cells can be assigned to their cell cycle position by ordering them according to increasing DNA, Cyclin A2 and/or Cyclin B1 levels (Fig. 1a). Our method relies only on standard immunofluorescence techniques, and a variety of markers can be used to arrange cells at the correct cell cycle position. In fact, others have obtained similar results by the use of an exogenously expressed marker [6].

The accuracy of the assigned timing largely depends on two factors: how many cells are analyzed (*see* **Note 1**) and how accurate the marker levels can be quantified [4]. Optimal quantification requires careful assessment of background signal, of autofluorescence from the cell, and unspecific antibody binding. The use of

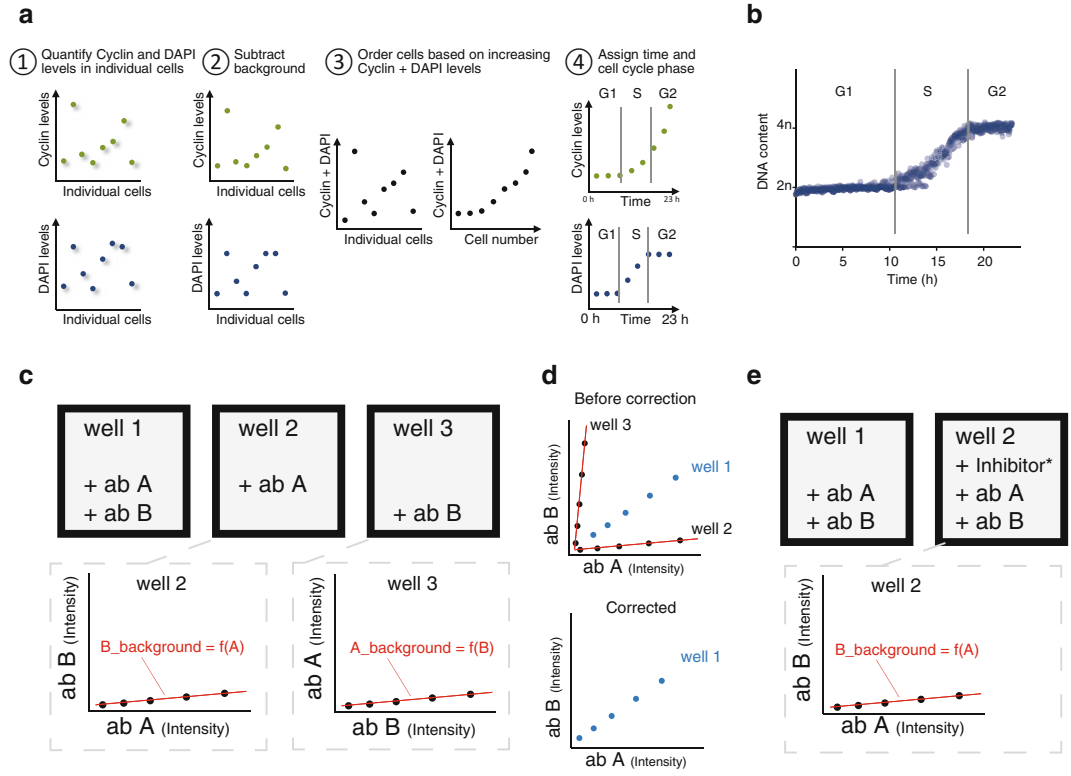

Fig. 1 (**a**) Schematic representation of how to assess kinetics from fixed cell microscopy images. (**b**) Representative DAPI profile. RPE cells ($n = 505$) were sorted for DAPI and Cyclin B1. (**c**) Schematic representation of general background estimation for antibody pair A and B. (**d**) Schematic representation of background subtraction. (**e**) Schematic representation of the background estimation when assessing post-translational modifications, here detected by antibody B. *, Specific inhibitor of the enzyme that catalyzes the post-translational modification detected by antibody B

Table 1
A comparison between standard quantitative immunofluorescence and quantitative immunofluorescence using micropatterns

Standard quantitative IF	Quantitative IF using micropatterns
• Simple, flexible setup yielding large cell numbers • Unperturbed cell growth • Coverage of the whole cell cycle • Easy processing of several different conditions • Segmentation of the cytoplasm is difficult • Possible artifacts from vignetting and uneven illumination	• Highly accurate quantifications • Precise segmentation of several organelles, e.g., cytoplasm, nucleus, centrosome • Robust against artifacts from vignetting and uneven illumination • Cell growth may be altered • Excludes analysis of the first 4–5 h of the cell cycle • Generally less cells to analyze

micropatterns to control cell shape and objective angle during image acquisition further improves the quality of quantifications of immunofluorescence [4]. In addition, the use of micropatterns may reduce variability due to cell-extrinsic factors, as cell–cell contacts are absent and cell–matrix contacts are similar for all cells. However, standard quantitative immunofluorescence generally allows for more experimental flexibility and yields higher cell numbers for analysis [6, 7] (Table 1). Here, we describe a protocol for assessing cell cycle dynamics based on immunofluorescence and an optional protocol to improve quantification of immunofluorescence using micropatterns.

2 Materials

2.1 Cell Culture

1. Phosphate-buffered saline (PBS; 10×): 0.1 M Na_2HPO_4, 0.018 M KH_2PO_4, 1.37 M NaCl, 0.027 M KCl, pH 7.4.
2. PBS containing 0.2 % EDTA (PBS-EDTA).
3. Micropatterns: CYTOOchips™ Custom (CYTOO, Grenoble, France).
4. Chamber for micropatterns: CYTOOchambers 1-well, 2-well, or 4-well (CYTOO, Grenoble, France).
5. 96-well imaging plates (BD Bioscience, Franklin Lakes, NJ, USA).

2.2 Immunofluorescence

1. 3.7 % formaldehyde.
2. Tris-buffered saline (TBS; 10×): 1.5 M NaCl, 0.1 M Tris–HCl, pH 7.4.
3. TBS containing 0.1 % Tween-20 (TBST).
4. Methanol.

5. Blocking solution: 2 % bovine serum albumin in TBST.
6. Cyclin A2 H-432; sc-751; diluted 1:400 in blocking solution (Santa Cruz Biotechnology, Santa Cruz, CA, USA).
7. Cyclin B1 V152; #4135; diluted 1:400 in blocking solution (Cell Signaling Technology, Danvers, MA, USA).
8. 4′,6-Diamidino-2-phenylindol (DAPI) (Sigma-Aldrich, St. Louis, MO, USA).

2.3 Microscopy

1. ImageXpress microscopy system (Molecular Devices/LLC, Sunnyvale, CA, USA): Nikon 10× Plan Fluor NA 0.3 objective; Nikon 40× S Plan Fluor ELWD 0.6 objective; MetaXpress 3.1.0.73 software.
2. Leica DMI6000 imaging system (Leica, Solms, Germany): HC PL FL 10× NA 0.30; HCX PL APO 40× NA 0.85 CORR; LAS Matrix: software.

2.4 Programs and Scripts

1. CellProfiler version 2.1.1 [8].
2. ImageJ version 1.45s [9].
3. MatLab (MathWorks, Natick, MA, USA).
4. Custom written scripts, pipelines and templates (http://www.lindqvistgroup.org, Table 2).

3 Methods

In Subheadings 3.1–3.3, we describe a simple and robust procedure to assess cell cycle kinetics from fixed cells. In addition, the Subheadings 3.4–3.7 cover the use of micropatterns as well as additional background considerations which facilitate highly accurate quantification and cell segmentation (Table 1).

Standard cell culture, immunofluorescence, and image acquisition procedures can be used if micropatterns are not used (*see* **Notes 2** and **3**). The immunofluorescence protocol should be optimized according to the antibodies used. The immunofluorescence protocol below is tested for the Cyclin A2 and Cyclin B1 antibodies described. Carry out all steps at room temperature unless otherwise noted.

3.1 Immunofluorescence and Image Acquisition

1. Remove the cell culture medium from the cells and fix them immediately with 3.7 % formaldehyde for 5 min.
2. Wash 2× with TBST. Fix and permeabilize the cells by 2 min incubation with −20 °C-cold methanol. Wash 2× with TBST.
3. Block with blocking solution for 1 h at room temperature or overnight at 4 °C.

Table 2
A list of recommended software and scripts for performing quantitative immunofluorescence

Name	Software	Description
Position list of single cells	MatLab	A MatLab script for making position list of single cells. The script will scan all images from chosen folder and make a position list of single cells. The script was adapted for two different microscope/software system: 1. ImageXpress/MetaXpress (Metamorph) 2. Leica/LAS Matrix Any other microscope/software can be easily added. The position list will be saved in MatLab folder (root folder)
Analyzing intensities of nucleus and cytoplasm	MatLab	A MatLab script for analyzing intensities of nucleus and cytoplasm. The script will scan all images from chosen folder and create data file (.xls) with mean and integrated intensities of nucleus and cytoplasm for every channel (channel 1—DAPI, channel 2—protein 1, channel 3—protein 2). The data file (.xls) will be saved in the destination folder you have chosen
Analyzing intensities of nucleus, kinetochores, and centrosomes	MatLab	A MatLab script for analyzing intensities of nucleus, kinetochores, and centrosomes. The script will scan all images from chosen folder and create data file (.xls) with mean and integrated intensities of nucleus, kinetochores, and centrosomes. The data file (.xls) will be saved in the MatLab folder (root folder)
Cell cycle kinetics pipeline	CellProfiler	A pipeline for analyzing intensities of nucleus and cytoplasm. The pipeline will analyze all images from chosen folder and create data file (.xls) with mean and integrated intensities of nucleus and cytoplasm for every channel (channel 1—DAPI, channel 2—marker antibody, channel 3—protein of interest)
Excel template	Excel	A template file for cell cycle sorting and assigning of times from raw measurements of "Nucleus Area" and fluorescence of "DAPI," "marker antibody," and "antibody of interest"
Excel macro	Excel	A macro-enabled workbook for automated cell cycle sorting and assigning of times from measurements of integrated intensities of three different channels

4. Dilute your antibody of interest, together with the marker antibody (Cyclin A2 H-432 or Cyclin B1 V152) in blocking solution and incubate for 1 h at room temperature or overnight at 4 °C.
5. Wash 3× with TBST. Incubate the cells with secondary antibodies at the recommended concentration and DAPI at 0.5 μg/ml in blocking solution for 1 h at room temperature. Wash 3× with TBST.
6. Acquire fluorescent images of DAPI, the marker antibody, and your antibody of interest using a microscopy setup with a high-resolution air objective (*see* **Notes 4** and **5**).

3.2 Image Analysis, Quantification, and Segmentation

The image analysis can be performed using any image analysis program that allows for segmentation of cell compartments according to a marker staining (*see* **Note 6**). We usually use CellProfiler [8] or ImageJ [9]. We provide a standard cell profiler pipeline at http://www.lindqvistgroup.org/?page_id=196. In addition, tutorials can be found at http://www.cellprofiler.org/tutorials.shtml and http://imagej.nih.gov/ij/docs/examples/.

1. Use the DAPI image to identify the primary objects, here the "Nuclei" (*see* **Note 7**).
2. Use the identified "Nuclei" as input objects to identify the "Cells" as secondary objects (*see* **Note 8**).
3. Measure the area of the "Nuclei" and "Cells" and obtain their mean signal intensity for all channels (DAPI, the marker antibody, and your antibody of interest).
4. Also obtain a quantification of an empty region to measure the general background signal for all channels.

3.3 Assessing Cell Cycle Kinetics

To assess cell cycle kinetics of a protein of interest, the cells have to be assigned to their cell cycle position by ordering them according to a monotonically changing marker. While a single marker is sufficient, the combination of multiple markers leads to a more accurate sorting [4, 6, 7]. In case more than one staining is used for ordering cells, it is essential to normalize the signal intensities from different channels (Fig. 1a). We generally use Microsoft Excel for the calculations (*see* **Note 9**). We provide template files and additional files for automated sorting of your data at http://www.lindqvistgroup.org/?page_id=196.

1. Calculate the integrated intensity for each measurement using the following formula: IntegratedIntensity = ObjectArea × (MeanObjectIntensity – MeanBackgroundIntensity).
2. Normalize the integrated intensity values for each channel by dividing with the median value of all measurements of this channel.
3. For each cell add the normalized values of DAPI and the marker antibody to obtain the sorting value.
4. Sort all columns with the normalized intensity values in ascending order according to the sorting value.
5. Assign time to each ordered cell according to the formula (*see* **Notes 10** and **11**): Time = CellCycleLength/(TotalCellNumber – 1) × (IndividualCellPosition – 1).
6. Plot the normalized values for each channel against the assigned cell cycle timing.
7. Finally, assign the G_1/S and S/G_2 borders according to the DAPI profile (Fig. 1b).

In the following Subheadings 3.4–3.7, we explain how micropatterns can be used for more advanced applications and automated processes of image acquisition, background subtraction, and image analysis (Table 1) (*see* **Note 12**).

3.4 Seeding Cells on Micropatterns

1. Carefully wash cells 3× with pre-warmed PBS. Add 500 µl of warm PBS-EDTA (for a 10 cm dish) and leave the cells in the incubator for about 5 min. To ensure that cells do not dry out, swirl the dish regularly to distribute the liquid over all of the cells. In the meantime, mount the chamber with the micropattern (*see* **Notes 13** and **14**).
2. Once the cells start rounding up and detaching, add 10 ml of fresh medium to compensate for the chelation of calcium by the EDTA.
3. Count the cells and resuspend them in medium to a final concentration of 60,000 cells/ml. Seed 400 µl/well (1-well chamber), 200 µl/well (2-well chamber), or 100 µl/well (4-well chamber) on the micropatterns (*see* **Note 15**). Switch off the cell culture hood to avoid vibrations. Put the cells back in the incubator very carefully.
4. Check after 15 min if cells are attached. If attached, wash the cells very gently with fresh medium to remove floating cells. Make sure that the cells do not dry out. Keep the cells warm by placing the chamber on a Styrofoam box or on top of a warm heating-block (37 °C). Fill the chamber with fresh medium—2 ml/well (1-well chamber), 800 µl/well (2-well chamber), or 300 µl/well (4-well chamber). Move the cells carefully back to the incubator and incubate for 5 h after seeding.
5. Fix and stain the cells for immunofluorescence as described above (*see* Subheading 3.1 and **Note 12**).

3.5 Image Acquisition

The image acquisition on micropatterns may be considered as a three-step process—screening with a low-resolution objective, identification of single cells, and image acquisition with a high-resolution objective. We provide a MatLab script to create the position list of single cells at http://www.lindqvistgroup.org/?page_id=196.

1. Acquire images for DAPI staining from entire coverslip by screening with a 10× objective.
2. Identify the coordinates of patterns with single cells and assemble these into a position list for the microscope (*see* **Note 16**).
3. Load the position list and revisit every position with a high-resolution objective (*see* **Note 4**).

3.6 Image Analysis, Quantification, and Segmentation

One of the advantages of using micropatterns is that the object of interest is located in the center of image, which makes the segmentation process much easier. The image analysis can be done with any image analysis program. We usually use MatLab. We provide MatLab scripts for automated image segmentation and quantification at http://www.lindqvistgroup.org/?page_id=196 (Table 2).

1. Crop the image based on the size of micropattern (leave 5–10 pixels from every side for initial background estimation).
2. Use the marker image to identify the ROI (region of interest; e.g., DAPI for the nucleus).
3. Use the size of the micropattern to identify the ROI for the whole cell.
4. For a ROI of cytoplasm simply subtract the ROI of nucleus from the ROI of cell.
5. Measure the area of all ROIs and obtain their mean fluorescence intensity for all channels.
6. Use the empty region next to the micropattern (*see* Subheading 3.7.1) to measure an initial background signal for all channels.

3.7 Background Subtraction

3.7.1 General Background Subtraction

1. An initial background based on a region close to the ROI should be subtracted for every cell and channel.
2. Remove cells where the background deviates more than 10 % from the median background, indicating aberrant staining or illumination.
3. For each antibody, estimate a background function by linear regression of the quantifications from cells where the primary antibody was left out (Fig. 1c).

   For example, for antibody pair A and B:

   The background function for antibody B (B_background = f(A)) should be estimated from a well with antibody A only (well 2, Fig. 1c).

   The background functions should be estimated separately for each segmented subcellular location (*see* **Note 17**).
4. Use the calculated background functions to subtract the background for each cell accordingly (Fig. 1d).

   For antibody B the corrected value will be: B_corrected = B(A) – B_background (A); For antibody A the corrected value will be: A_corrected = A(B) – A_background (B).

3.7.2 Background Subtraction When Assessing Post-translational Modifications

When quantifying post-translational modifications, an accurate estimation of the background signal can be obtained by the use of a specific inhibitor of the respective modifying enzyme. Images should be obtained in the same microscopy conditions both in the

presence and absence of the inhibitor. As the kinetics of the signal in the presence of the inhibitor already provide an accurate background estimation, a general background subtraction (*see* above) is not essential in this setup (*see* **Note 18**).

1. Estimate a background function (B_background = f(A)) by linear regression of the quantifications from cells where the inhibitor was added (Fig. 1e).
2. Use the calculated background functions to subtract the background for each cell accordingly: B_corrected = B(A) – B_background (A).

4 Notes

1. The theoretical accuracy of assigned time on single cells increases with the amount of cells quantified. A minimum of 300 cells should be quantified to reach an average accuracy of 20 min. Accuracy close to 10 min can be reached when analyzing 1200 or more cells [4].
2. It is very important to keep cells in non-stressful conditions at all times.
3. Make sure that cell growth is not perturbed for your specific cell line if using micropatterns.
4. The objective to be used should be based on the respective application. We have used 40× NA 0.6 or 40× NA 0.85 objectives.
5. Make sure to acquire a sufficient number of images to be able to analyze at least 500 (ideally 1000) cells for each condition.
6. In all setups the DAPI staining serves as a nuclear marker. If you do not include a pan-cellular stain to identify cells, most image analysis programs allow for a calculated estimation of the cytoplasmic region upon identification of the nucleus. When using micropatterns the size of an individual pattern provides a more accurate estimation of the whole cell size.
7. An accurate identification of single nuclei depends on correct filtering for appropriate size and shape. For even more accurate results the DAPI images can be screened manually.
8. The exact settings for object identification (e.g., object size, threshold parameters, or method of propagation) depend on multiple experimental parameters and should be optimized accordingly.
9. When processing the data it is essential that the different measurements for each cell (nuclear and cytoplasmic quantification of each channel) stay linked.

10. To assign correct cell cycle times the length of an average cell cycle has to be determined first. We find that the average cell cycle time of U2OS cells is 23 h [4]. Furthermore, it is essential that no cells in the population are undergoing cell cycle arrest.
11. In a standard immunofluorescence experiment the cell containing the lowest sorting value should be assigned the time 0 h. If using micropatterns the earliest time is determined by the time span from seeding to fixation. Generally, it should be around 4–5 h (*see* Subheading 3.4).
12. Make sure to have additional wells with cells, leaving out one primary antibody or all primary antibodies for later background estimation.
13. The numbers of single cells that can be obtained in a typical experiment are about 800–2500 (1-well chamber), 400–1000 (2-well chamber), or 200–400 (4-well chamber).
14. Once mounted, make sure that the micropattern chamber does not leak, by adding some PBS.
15. The exact number of cells seeded should be optimized according to the cell line used.
16. In case your microscope lacks the option to save a log file for every image, make sure to acquire low-resolution DAPI images without gaps between the single images. Thereby, position information for each cell can be reconstructed later.
17. A linear regression for the background estimation should only be used if the antibody signal shows a linear dependency to the cell cycle. We find that this often is the case as cells increase in size when progressing through the cell cycle.
18. In general accurate background kinetics can be obtained for any antibody by knockdown of its target. However, it is essential to achieve a complete knockdown and that the knockdown does not affect the cell cycle distribution.

Acknowledgements

This work was supported by the Swedish Research Council, the Swedish Foundation for Strategic Research, and the Swedish Cancer Society. We thank all members of the Lindqvist Lab for discussions.

References

1. Bjorling E, Uhlen M (2008) Antibodypedia, a portal for sharing antibody and antigen validation data. Mol Cell Proteomics 7(10):2028–2037. doi:10.1074/mcp.M800264-MCP200
2. Avva J, Weis MC, Sramkoski RM, Sreenath SN, Jacobberger JW (2012) Dynamic expression profiles from static cytometry data: component fitting and conversion to relative, "same scale" values. PLoS One 7(7), e38275. doi:10.1371/journal.pone.0038275
3. Jacobberger JW, Avva J, Sreenath SN, Weis MC, Stefan T (2012) Dynamic epitope expression from static cytometry data: principles and reproducibility. PLoS One 7(2), e30870. doi:10.1371/journal.pone.0030870
4. Akopyan K, Silva Cascales H, Hukasova E, Saurin AT, Mullers E, Jaiswal H, Hollman DA, Kops GJ, Medema RH, Lindqvist A (2014) Assessing kinetics from fixed cells reveals activation of the mitotic entry network at the S/G2 transition. Mol Cell. doi:10.1016/j.molcel.2014.01.031
5. Pines J, Hunter T (1990) p34cdc2: the S and M kinase? New Biol 2(5):389–401
6. Kafri R, Levy J, Ginzberg MB, Oh S, Lahav G, Kirschner MW (2013) Dynamics extracted from fixed cells reveal feedback linking cell growth to cell cycle. Nature 494(7438):480–483. doi:10.1038/nature11897
7. Müllers E, Silva Cascales H, Jaiswal H, Saurin AT, Lindqvist A (2014) Nuclear translocation of cyclin B1 marks the restriction point for terminal cell cycle exit G2 phase. Cell Cycle 13(17):2733–2743. doi:10.4161/15384101.2015.945831
8. Carpenter AE, Jones TR, Lamprecht MR, Clarke C, Kang IH, Friman O, Guertin DA, Chang JH, Lindquist RA, Moffat J, Golland P, Sabatini DM (2006) CellProfiler: image analysis software for identifying and quantifying cell phenotypes. Genome Biol 7(10):R100. doi:10.1186/gb-2006-7-10-r100
9. Schneider CA, Rasband WS, Eliceiri KW (2012) NIH Image to ImageJ: 25 years of image analysis. Nat Methods 9(7):671–675

Chapter 10

Building a Synthetic Transcriptional Oscillator

Matthaeus Schwarz-Schilling, Jongmin Kim, Christian Cuba, Maximilian Weitz, Elisa Franco, and Friedrich C. Simmel

Abstract

Reaction circuits mimicking genetic oscillators can be realized with synthetic, switchable DNA genes (so-called genelets), and two enzymes only, an RNA polymerase and a ribonuclease. The oscillatory behavior of the genelets is driven by the periodic production and degradation of RNA effector molecules. Here, we describe the preparation, assembly, and testing of a synthetic, transcriptional two-node negative-feedback oscillator, whose dynamics can be followed in real-time by fluorescence read-out.

Key words Gene oscillator, Transcription circuit, In vitro, Nonlinear dynamics, Negative-feedback oscillator, Genelet circuits

1 Introduction

Feedback is ubiquitous in the regulatory pathways of living organisms. Under certain conditions, negative-feedback circuits can exhibit oscillatory behavior (the famous Thomas' conjecture [1]), manifested through periodically varying concentrations of involved components [2]. Oscillations in naturally occurring systems perform essential functions such as timing circadian rhythms and cell division in a robust manner [3].

While the study of design principles of oscillating systems in vivo is extremely challenging, in vitro transcription circuits can be used to build simple network structures. Recently, a minimal toolbox comprised of short, linear, switchable genes (genelets) and two enzymes was used to build several feedback circuits, including a two-node negative-feedback oscillator [4, 5]. The reactions constituting this transcriptional oscillator are shown in Fig. 1; two genes mutually regulate their activity through their RNA outputs, which displace or reassemble part of the promoter regions. Nonlinearities required to establish oscillations are achieved through titration of inhibitors and activators [6]. This circuit was used as a timer for downstream molecular devices [7], and to study

Amanda S. Coutts and Louise Weston (eds.), *Cell Cycle Oscillators: Methods and Protocols*, Methods in Molecular Biology, vol. 1342, DOI 10.1007/978-1-4939-2957-3_10,

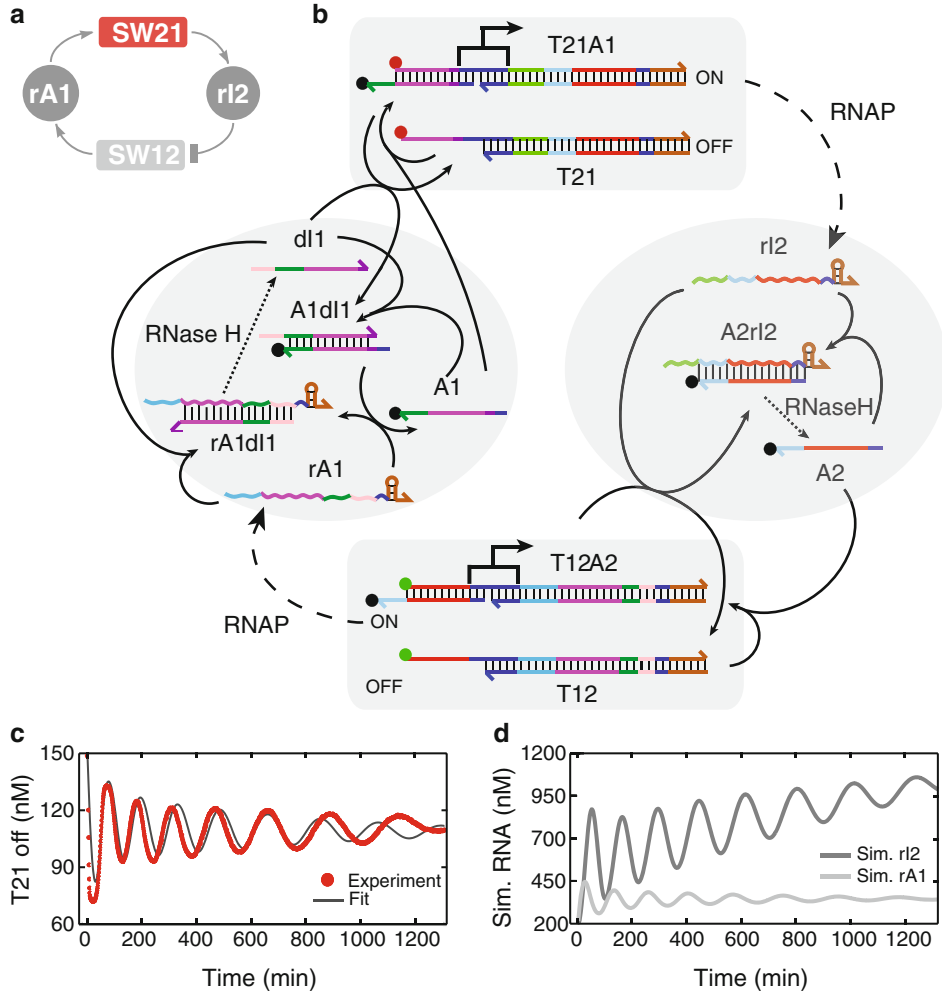

Fig. 1 A transcriptional oscillator circuit. (**a**) Simple scheme of a two-switch negative-feedback oscillator circuit. RNA signals produced from switches *Sw12* and *Sw21* mutually regulate the transcription activity of each other and lead to an overall negative feedback. The figure is reproduced from [5]. (**b**) Detailed molecular scheme of the reactions. DNA species are drawn as colored lines. RNA species are shown as wave-like lines. *Equal colors* indicate sequence complementarity. Hybridization and strand displacement reactions are shown as *arrow-headed solid lines*. Reactions involving enzymes are represented by *arrow-headed dashed lines. Grey-shaded shapes* indicate functional units shown in (**a**). Transcriptional switches (genelets) are comprised of a template and the corresponding activator. A typical oscillation reaction starts in the state *Sw12* ON, *Sw21* OFF. Starting there, *rA1* transcribed from *T12A2* displaces DNA activator *A1* from *A1dI1*. Released *A1* binds to *T21* and activates transcription of RNA inhibitor *rI2*. Produced *rI2* displaces *A2* by toehold-mediated strand displacement and consequently turns transcription from *Sw12* OFF. The reaction can be monitored by fluorescence read-out of the dye labels attached to *T21 and T12*; intensity is a measure of concentration of *Sw12 or Sw21 OFF*. The figure is reproduced from [5]. (**c**) Fluorescent time trace reporting the concentration of *Sw21 OFF* (*red dots*) from the oscillator circuit and the corresponding fit (*black line*). (**d**) A simulation of the concentrations of the RNA species *rA1* and *rI2*, which is based on the fit of *Sw21 OFF* in (**c**)

modularity in biochemical systems (*see* **Note 1**); this circuit was also encapsulated into femto- to picoliter-sized microemulsion droplets to identify the influence of partitioning noise on the dynamics of complex nonlinear systems [8].

An alternative toolbox for programming reactions in vitro, relying on DNA polymerase, a nickase and a nuclease has been successfully used to build feedback circuits [9, 10]. These circuits are remarkably tunable and robust, however, their reliance on nickases and nucleases and their high operation temperature may pose compatibility issues with most existing in vitro devices and circuits made with nucleic acids. In contrast, transcriptional oscillators may be easily interconnected with a variety of other DNA devices [7].

Here, we provide detailed protocols to prepare and experimentally test the two-node transcriptional oscillator described in [5].

2 Materials

Prepare all solutions using nuclease-free water. In principle, buffers and nucleic acids can be purchased from any vendor. However, we recommend that enzymes be purchased from the vendors listed below, due to the guaranteed purity, concentration, and high activity. Unless stated otherwise buffer and reagents can be stored at room temperature.

2.1 Oscillator

1. Nuclease-free water.
2. 10× reaction buffer: 400 mM Tris–HCl, 60 mM $MgCl_2$, 100 mM Dithiothreitol (DTT), 20 mM Spermidine, pH 7.9 at 25 °C. (New England Biolabs). Supplement with $MgCl_2$ to obtain final 30 mM $MgCl_2$ at 1×. Store at −20 °C (*see* **Note 2**).
3. Nucleoside Triphosphate (NTP) stock solution: 25 mM each NTP. Store at −20 °C (*see* **Note 3**).
4. Synthetic DNA strands (*see* Table 1 for sequences): T12 (genelet), T21 (genelet), dI1 (inhibitor of T21), A1 (activator of T21), A2 (activator of T12). Store at −20 °C (*see* **Note 4**).
5. 100× Inorganic Pyrophosphatase (Ppase) (Sigma-Aldrich, or New England Biolabs). Store at −20 °C (*see* **Note 5**).
6. T7 RNA Polymerase (RNAP). Store at −20 °C (*see* **Note 6**).
7. Ribonuclease H (RNase H) from *E. coli*. Store at −20 °C (*see* **Note 7**).

2.2 Polyacrylamide Gel Components

1. 10× TBE buffer: 0.89 M Tris–Borate, 22 mM Ethylenediaminetetraacetic acid (EDTA), pH 8.3 at 25 °C.
2. 50× TAE/Mg^{2+} buffer: 2 M Tris–Acetate, 50 mM EDTA, 0.625 M Magnesium Acetate, pH 8.3 at 25 °C.
3. Acrylamide/Bis-Acrylamide 19:1. Store at 4 °C.

Table 1

DNA sequences

T12-t	5′-TTT CTG ACT TTG TCA GTA TTA GTG TGT AGT AGT AGT TCA TTA GTG TCG TTC GTT CTT TGT TTC TCC CTA TAG TGA GTC G
T12-nt	5′-AAG CAA GGG TAA GAT GGA ATG ATA ATA CGA CTC ACT ATA GGG AGA AAC AAA GAA CGA ACG ACA CTA ATG AAC TAC TAC TAC ACA CTA ATA CTG ACA AAG TCA GAA A
T21-t	5′-TTT CTG ACT TTG TCA GTA TTA TCA TTC CAT CTT ACC CTT GCT TCA ATC CGT TTT ACT CTC CCT ATA GTG AGT CG
T21-nt	5′-*TexasRed*-CAT TAG TGT CGT TCG TTC ACA GTA ATA CGA CTC ACT ATA GGG AGA GTA AAA CGG ATT GAA GCA AGG GTA AGA TGG AAT GAT AAT ACT GAC AAA GTC AGA AA
dI1	5′-GTG TGT AGT AGT AGT TCA TTA GTG TCG TTC GTT CAC AG
A1	5′-TAT TAC TGT GAA CGA ACG ACA CTA ATG AAC TAC TAC-*Iowa Black RQ*
A2	5′-TAT TAT CAT TCC ATC TTA CCC TTG CTT CAA TCC GT-*Iowa Black RQ*

4. Urea (powder for scientific use).
5. $MgCl_2$ solution in nuclease-free water (typically 1 M).
6. Ammonium Persulfate (APS): 10 % (w/v) solution in nuclease-free water. At 4 °C the solution should be stable up to 12 h.
7. *N*,*N*,*N*′,*N*′-Tetramethyl-Ethylenediamine (TEMED).
8. 6× gel loading buffer for native gels: 10 mM Tris–HCl (pH 7.6), 0.03 % (w/v) Bromophenol Blue, 0.03 % (w/v) Xylene Cyanol, 60 % (v/v) Glycerol. Store at –20 °C.
9. 2× gel loading buffer for denaturing gels: 95 % (w/v) Formamide, 18 mM EDTA, 0.025 % (w/v) SDS, 0.025 % (w/v) Xylene Cyanol, 0.025 % (w/v) Bromophenol Blue. Store at –20 °C.
10. Crush-and-soak buffer: 0.3 M Sodium Acetate in ultrapure water of Type 1 (e.g. Milli-Q® water), pH 5.2 at 25 °C.
11. Ethanol (≥99.5 %).
12. 10-basepair dsDNA ladder. Store at –20 °C.
13. Staining solution, e.g. SYBR® Gold (Molecular Probes). Store at –20 °C.

2.3 Miscellaneous

1. Hexadecane (≥99 %).
2. RNase removal agent (e.g. RNase Zap, Ambion) is recommended to prevent RNase contamination.

3. 0.5 ml and 1.5 ml reaction tubes (*see* **Note 8**).
4. 15 ml tubes, e.g. Falcon® tubes.
5. Disposable gel cassettes.
6. Quartz micro-cuvettes (for use with a fluorometer), a well-plate (for use with a plate reader) or PCR tubes (for a real-time PCR machine with an optical reaction module) (*see* **Note 9**).

3 Methods

3.1 DNA Quantitation

1. Determine the concentration of single-stranded DNA components by measuring the absorption at 260 nm according to Beer Lambert's law using sequence-specific extinction coefficients.

3.2 Annealing of Switches

To minimize unintended secondary structures, anneal template (t) and non-template (nt) strands comprising switches T12 and T21, respectively.

1. Mix the single strands of either T12 or T21 in 1× reaction buffer, yielding a target concentration of 5 μM (*see* **Note 10**).
2. Apply a heat ramp on a thermocycler or PCR machine. A typical annealing protocol is heating the sample up to 95 °C, holding the maximum temperature for 5 min, and cooling to 20 °C at a rate of 1 °C/min.

3.3 Optional: Control of Annealing Performance

The annealing performance and stoichiometry of complementary strands can be controlled through polyacrylamide gel electrophoresis (PAGE) in a native 10 % TBE-polyacrylamide gel.

1. For an 8 cm × 8 cm gel, mix 7.4 ml H_2O, 1.3 ml TBE (10×), 4.3 ml acrylamide (30 %, 19:1), 130 μl APS, and 13 μl TEMED in a 15 ml falcon tube.
2. Mix the solution gently without creating bubbles and pour it into the gel cassette.
3. Insert a comb with at least seven wells and wait until the gel has polymerized (*see* **Note 10**).
4. Prepare the sample solutions for the volume of one well (typically 10–20 μl). Each solution should contain 100–200 ng of the relevant DNA and 1× native gel loading buffer.
5. Remove the comb from the gel and carefully pipette the samples into the wells. Avoid spillage of the sample to neighboring wells. Load the dsDNA ladder, the template (t) and non-template (nt) strands in the wells next to corresponding annealed switch.
6. Run the gel for 60 min at room temperature at 100 V. Use 1× TBE buffer as running buffer.

7. Dismount the gel from the cassette and place it in staining solution with 1× SYBR gold and 1× TBE buffer (running buffer can be used) for 10–40 min (*see* **Note 11**).
8. Position the gel on a UV-light plate in a dark chamber and image the fluorescence of the SYBR gold bound to the DNA with a CCD camera and an appropriate emission filter (typically transmission for light above $\lambda > 520$ nm).
9. In case of a successful annealing reaction and stoichiometry of the complementary strands, there should be one clear band in the lane of the annealed switches.
10. An unsuccessful annealing reaction can result in smearing of the band or two bands which correspond to two single strands (*see* **Note 12**). In case of strong deviations from stoichiometry of the two complementary strands, the strand in excess will show in a second band (*see* **Note 13**).

3.4 Assembling the Synthetic Oscillator

The following protocol assumes that enzymes have concentration and activity comparable to those available by the recommended vendors.

1. In a reaction tube, mix:
   (a) 1× reaction buffer
   (b) 7.5 mM each NTP
   (c) Synthetic DNA:
      - 80 nM T12 (genelet)
      - 150 nM T21 (genelet)
      - 500 nM dI1 (inhibitor of T21)
      - 150 nM A1 (activator of T21)
      - 250 nM A2 (activator of T12)
   (d) 1 unit/μl Ppase
2. Mix the sample using a benchtop vortex.

3.5 Fluorometry

Oscillations are measured by fluorometry experiments, where the concentration of the OFF switch T21 and/or T12 is tracked over time (*see* Fig. 1c). The choice of fluorescent labels should be made according to **Note 14**. We recommend using a xenon arc lamp fluorometer with monochromators (e.g. Horiba Fluorolog 3). To avoid lamp intensity fluctuations, the fluorometer lamp should be turned on at least 30 min prior to the beginning of the experiment.

1. Transfer the synthetic oscillator mix to a reaction container of your choice (e.g. a quartz micro-cuvette, plate well or PCR tube) and place it in the corresponding device (fluorometer, plate reader or real-time PCR) (*see* **Note 15**).
2. Make sure that the sample is protected from evaporation (*see* **Note 16**).

3. Allow the mix to equilibrate at the operation temperature of 37 °C (*see* **Note 17**).
4. Record the fluorescence signal from the dye attached to T21 (originally TexasRed) every 1 or 2 min for about 10 min, before adding the enzymes (*see* **Note 18**).
5. After about 10 min equilibration time, carefully add $6–10 \times 10^{-2}$ units/μl RNaseH and 10–12 units/μl RNAP through the hexadecane layer, which starts the reaction.
6. Mix the solution thoroughly and carefully (*see* **Note 19**).
7. Record the fluorescence over 30 h. Fluorescence will generally be measured through proprietary software provided by the fluorometer vendor. We recommend recording fluorescence every 1 or 2 min for about 30 h, with a 1 s measurement integration time and monochromator slit widths of 5 nm.

3.6 Gel Electrophoresis for Separating RNA Transcripts and Switch Components

Denaturing PAGE can visualize the oscillations in RNA concentration by separating the individual RNA transcripts, rA1 and rI2, from the rest of the reaction mixture for different time points (*see* Fig. 2).

1. Before gel preparation, assemble the synthetic oscillator according to Subheading 3.4 and add the enzymes in order to start the reaction.
2. Remove 5 μl every 0.5 or 1 h and add the same volume of 2× denaturing gel loading buffer. Heat the sample to 75 °C for 2 min and store the sample at –20 °C until all samples for the gel have been collected.
3. Prepare a denaturing polyacrylamide gel according to **steps 1–3** in Subheading 3.3 but with 8 % (w/v) 19:1 acrylamide:bis and 7 M urea.
4. After polymerization fill the buffer chamber with 1× TBE buffer and remove the comb. Rinse the wells with running buffer by using a pipette. Pre-run the gel for a minimum of 30 min at 45–55 °C with 5 V/cm.
5. Thaw the samples and heat them up to 75 °C for 1 min.
6. Load the samples and the 10-basepair dsDNA ladder as a size marker. For concentration determination add 150 ng of purified rA1 and rI2 in the last lane. The RNA purification protocol is described in Subheading 3.7.
7. Run the gel for 50–60 min with 10 V/cm at 65 °C.
8. Stain the gel with staining solution and collect the gel data as described in **steps 6** and 7 in Subheading 3.3.
9. Quantify the gel using band intensity of the control lane and software, e.g. Quantity One software package (BioRad) or ImageJ (*see* **Note 20**). The band intensity of the RNA species should oscillate with time.

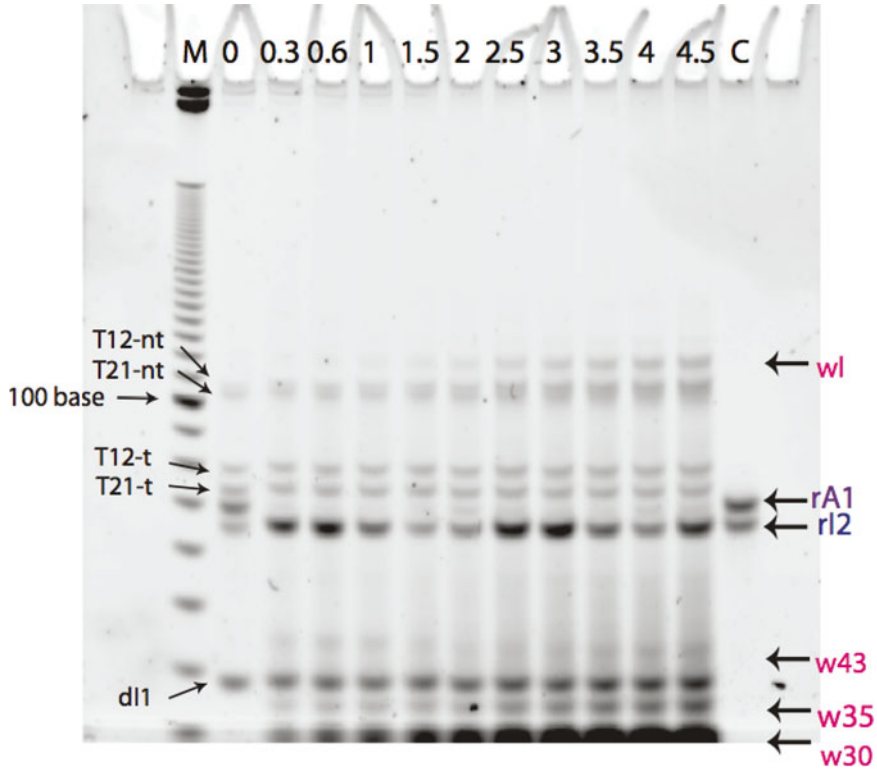

Fig. 2 Denaturing gel as described in Subheading 3.6. After assembly of the oscillator reaction, aliquots are taken at different times, as indicated above the gels in hours, and loaded onto the gel. The first lane shows a 10 bp dsDNA ladder. The last lane is loaded with 1 μM of purified rI2 (62 nucleotides) and rA1 (67 nucleotides) to serve as a control lane, as described in Subheading 3.7. The gel is stained with SYBR Gold. The change in the fluorescence intensity of the rI2 band over time reflects the oscillatory nature of the reaction. The intensity of rA1 is not significantly above background. The other bands in the gel can be accounted for as the DNA strands (T12 t and nt, T21 t and nt, dI1), potential self-coded elongation product of RNA transcript (wI), and presumed incomplete degradation products (w43, w35, and w30). The fluorescence intensity due to A1 and A2 is strongly absorbed by the quenchers. The figure is reproduced from [5]

3.7 RNA Purification Protocol

Purified RNA can be chemically synthesized and ordered directly from a vendor. Alternatively, one can purify the RNA from a transcription mix.

1. Assemble a transcription mix (typically 60 μl) as described in Subheading 3.4, for each switch and its activator (T12 and A2, T21 and A1) separately and without the RNase H and dI1. The RNAP can be increased to 20 % (v/v).
2. Incubate the reaction mix at 37 °C for 6 h.
3. Add 2.5 μl DNase I for 30 min to remove the DNA.
4. Add equal volume of 2× denaturing loading buffer to the reaction and heat the sample to 75 °C for 2 min.

5. The reaction solution should then be loaded on a 8 % denaturing gel, according to **steps 3**, **4**, **6** and **7** in Subheading 3.6.
6. Cut out one lane of the gel with an RNase-free scalpel. Stain and image the gel piece according to **steps 7–9** in Subheading 3.3.
7. Excise the RNA bands from the rest of the gel at the height indicated by the stained gel lane, and chop them in small gel pieces. Collect the pieces in a 1.5 ml tube.
8. Add 350 µl crush-and-soak buffer and incubate the tube at 42 °C overnight. Make sure that the tube is tightly sealed to avoid evaporation.
9. Transfer the supernatant to a fresh tube and add 100 µl of the crush-and-soak buffer to the gel pieces. Mix (e.g. vortex) the content and transfer the 100 µl of buffer to the other 350 µl in the fresh tube.
10. Add 1 ml of freezer cold Ethanol (−20 °C) to the supernatant and vortex.
11. Incubate the sample at −20 °C for at least 7 h, or at −80 °C for at least 30 min.
12. Spin the tube at >10,000 rcf at 4 °C for 15 min in a centrifuge.
13. Decant the supernatant with a pipette and air-dry the pellet for about 5 min at room temperature (a desiccator can also be used).
14. Re-suspend the pellet in nuclease-free water (typically 30 µl) and determine the concentration according to Subheading 3.1.

3.8 Gel Electrophoresis for Switch State Information

Non-denaturing PAGE provides information on the states of switches, e.g. it is possible to observe the switch states by scanning for labeled fluorophores: the ON-state switch has the quencher attached that reduces the fluorescence of the intercalating staining dyes. The concentration of the OFF-state switch, however, can be obtained by observing the fluorescence intensity of its band in the gel.

1. Before gel preparation, assemble a synthetic oscillator according to Subheading 3.4 at 37 °C and add all the enzymes in order to start the reaction. Remove 5 µl from the reaction mix every 0.5 or 1 h and add 5 µl of 2× denaturing gel loading buffer to it (*see* **Note 21**).
2. Prepare a non-denaturing gel according to **steps 1–4** in Subheading 3.3 but use 10 % 19:1 acrylamide/bis and 1× TAE/Mg^{2+} buffer (instead of 1× TBE buffer).
3. Load the samples and a 10-basepair dsDNA ladder as a size marker. Load 150 ng of T12 and T21 in the last lane as a control (*see* **Note 19**).
4. Run the gel for 100 min with 13 V/cm at 35 °C.

5. Stain and image the gel according to **steps 7** and **8** in Subheading 3.3, and quantify the concentration of the switches in the OFF state as described in **Note 19**. The band intensity of the Switches should oscillate.
6. Switches in the ON-state have lower fluorescence due to the quenchers attached to A1 and A2. Hence their bands cannot be clearly analyzed.

3.9 Tuning the Amplitude and Frequency

The genelet, activator, and inhibitor concentrations, together with the enzyme volumes given at Subheading 3.4 are expected to yield "nominal" oscillations in T21 concentration with a period of about 1.5–2 h, and amplitude in the range of 40–60 nM, which damp out after 16–20 h. However, enzyme activity can vary considerably from lot to lot (cf. Fig. 3d); in addition, oligonucleotide quantitation and pipetting may be inaccurate and introduce errors. These two sources of variability can significantly affect the operating point of the circuit, resulting in changes in period and amplitude of the oscillations.

1. To achieve the nominal oscillatory behavior, we recommend two tuning fluorimetry assays: (1) Vary the volume of RNase H (leaving all else unchanged). (2) Separately vary the concentration of inhibitor dI1 and activator A2 (leaving all else unchanged).
2. These experiments will help to identify what alterations to the base protocol (Subheading 3.4) are required to achieve the desired operating point.
3. Figure 3 shows examples of these tuning assays.

3.10 Support by Numerical Analysis and Data Fitting

Since all the components for the in vitro oscillator described here are known, mathematical modeling of the reaction network using mass action kinetics is straightforward (*see* Fig. 4).

1. Prior to initial experiments, mathematical analysis can point toward parameter regimes compatible with sustained oscillation for the concentrations of DNA strands and enzymes.
2. Normalized fluorescence trajectories or gel results can be used to determine a set of rate constants for the reaction equations. This can be implemented through a cost function using least-squared errors between the experimental data and the solution of the reaction equations. Furthermore some characteristics of the oscillations, such as oscillation amplitude, frequency, phase and damping coefficient can be considered in the cost function.
3. The resulting set of parameters can aid the further experimental exploration of the phase space of the oscillator.
4. The kinetic simulations and parameter fittings can be implemented in MATLAB and SBML.

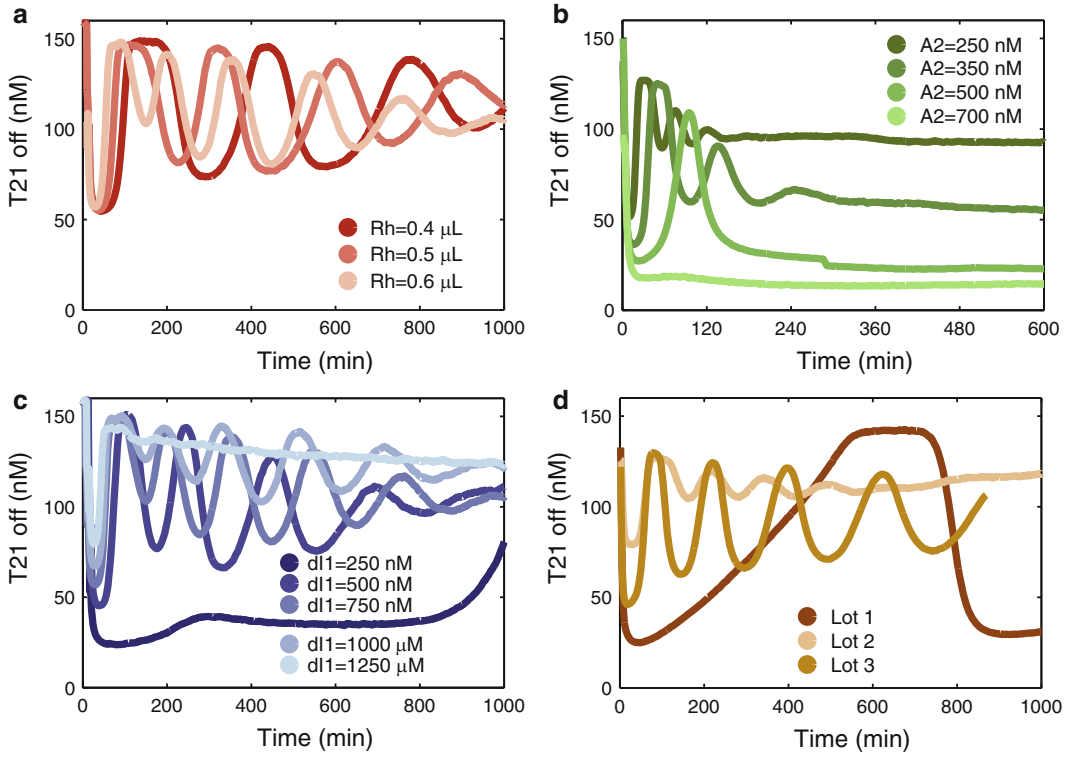

Fig. 3 By varying the enzyme volume (**a**), the concentration of DNA activator A2 (**b**) or the inhibitor dI1 (**c**), we obtain oscillations with different period and amplitude. These assays can be used to tune the oscillator to the desired amplitude/period. (**d**) The variations in the enzymatic activity between different lots of RNase H can have significant effects on the amplitude and period of the oscillator

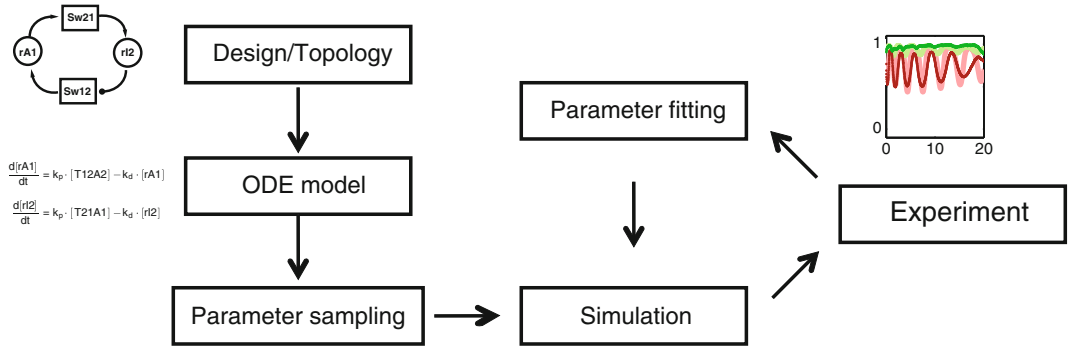

Fig. 4 A flowchart illustrating the implementation of the DNA/RNA oscillator. The circuit topology can be translated into differential equations, which can be used to find a parameter range for which the desired dynamical behavior may be observed. Once the first simulation and experiment have been made, one can feedback information from model to experiment and vice versa. New parameters are obtained from model fits, which are then used to improve the experiments, etc. This iteration can be helpful for orientation in parameter space and guidance toward sustained oscillations

4 Notes

1. This oscillator can be coupled with other nucleic acid devices [7]. Because DNA activators A1, A2 and the inhibitor dI1 all oscillate, each of these species can be used as an oscillatory input to downstream elements. We recommend the use of an additional genelet, which could be activated by A1 or A2, as a "buffering" or "insulating" element. A small amount of this additional genelet (10–200 nM), whose promoter activity will "oscillate" as with the concentration of A1 or A2, is able to produce a large amount of RNA output, which can be used by the downstream load.
2. To ensure constant grade, prepare aliquots and store at −20 °C. Mg^{2+} ions are supplemented to match the high concentration of NTP used in the experiment.
3. If separate NTPs are ordered, pre-mix the NTPs to yield a stock solution of 25 mM each.
4. We recommend to order the DNA strands purified by HPLC or PAGE. If the DNA strands are delivered as lyophilized powder dissolve them in a volume of nuclease-free water to yield stock concentrations of 100 μM according to the data sheet provided by the supplier. Quantify DNA concentrations according to the method described in Subheading 3.1. DNA switches are double-stranded molecules and have to be annealed. For this purpose, follow method in Subheading 3.2. After quantitation of DNA stocks, prepare working solutions of DNA strands A1, A2, and dI1 at a concentration of 10 μM. We recommend that each time before using a DNA stock, to vortex the solution for approximately 30 s and then to briefly spin it down in a microcentrifuge.
5. If inorganic Pyrophosphatase is purchased as lyophilized powder, dissolve in 20 mM Tris–HCl (pH 7.2 at 25 °C), 1 mM $MgCl_2$ and 50 % glycerol (v/v) yielding a 100 μg/mL stock solution, which corresponds to 100 units/μl according to the generally used definition.
6. We recommend T7 RNA polymerase from Epicentre with stock concentration of 200 units/μl.
7. We recommend RNase H from Ambion® with stock concentration of 10 units/μl. For oscillations a minimum value of RNase H activity is required [5]. Given that the enzymatic activity between different batches can fluctuate and that it might be affected by storage and handling, sometimes a new batch can restore or improve the oscillations. In some cases it might help to try other vendors, such as Thermo Scientific or Epicentre.

8. We recommend DNA-LoBind tubes (Eppendorf) for DNA stocks and Protein-LoBind tubes (Eppendorf) for the reaction assembly. Do not autoclave LoBind tubes.
9. The instruments and sample holders have different advantages. Typically, the well-plates and real-time PCR machines can hold more samples at once. The real-time PCR has often the best mechanism to avoid evaporation and condensation. In addition the sample volume can be reduced up to 20 μl, reducing resource costs but increasing the risk of pipetting inaccuracies. On the other hand, the fluorometers often have the best signal intensity.
10. Typical duration for polymerization is 2 h. Incomplete polymerization indicates degradation of APS. The comb should have at least seven wells, one for the dsDNA ladder, two for the switches and four for the single strands of the switches.
11. The staining solution should cover the whole gel (typically 50–100 ml) and should be protected from light. We recommend placing the container on a shaking plate, so that the gel is uniformly stained.
12. If mistakes in the execution of the PAGE can be ruled out, the following steps should improve the result: re-check the DNA sequences, the purity of the DNA stocks and the buffer conditions of the annealing reaction. Reapply the heat ramp.
13. From the height of the extra band one can identify the excess species and from the intensity of the extra band one can deduce the surplus in concentration (*see* **Note 19**). By adding the corresponding amount of the lesser species to the reaction solution and reapply the heat ramp one can correct for the deviations from stoichiometry of the reactants.
14. We recommend the use of Texas Red, TYE dyes, and TAMRA as fluorophores to monitor the active or inactive state of the switches. In principle, these fluorophores may be replaced with suitable alternatives. We recommend that alternative fluorophores be chosen with well separated emission/excitation spectra, to avoid "crosstalk" in the collected fluorescence data for the individual switches. Because fluorometry experiments have a duration of 16–30 h, fluorophores should present low photobleaching. Finally, the fluorophore's chemical and structural characteristics should be such that there is minimal interference with the hybridization and strand displacement kinetics of the oscillator. The recommended fluorophores satisfy all the above requirements.
15. Components must be transferred carefully, minimizing the contact surface of the solution with pipet tips and test tubes. Oligonucleotides and enzymes stick to plastic and glass

surfaces and excessive losses result in undesired alterations of the nominal operating point of the oscillator.

16. To prevent evaporation in the fluorometer, cover the mixture with sufficient volume of hexadecane (approximately 35 μl) (Attention: some well plate materials are not resistant to hexadecane!). For the plate reader, the plate should be sealed with a sticky transparent PCR foil. Most real-time PCR machines have a lid heating to prevent evaporation and condensation.
17. Prior to beginning a fluorometry experiment, sample holder (cuvettes, plates, and PCR tubes) should be placed in the sample chamber and pre-warmed to 37 °C. After the sample has been added to the pre-warmed sample holder, we recommend equilibrating its temperature inside the sample chamber for at least 10 min prior to starting the experiment. Fluorophores (like Texas Red, TYE dyes, and TAMRA) are sensitive to temperature, and temperature drifts result in fluorescence drifts.
18. The fluorescence intensity at this stage should report the maximum amount of T21 in the OFF state in the sample, since A1 is not paired with T21. Later on, this intensity value can be used to calculate the fraction of T21 in the OFF state during the different reaction steps. The same can be said for the fluorescence intensity of the dye attached to T12 (originally TAMRA), except that here the signal corresponds to the "background" fluorescence of the activated switch, since all of A2 should be bound to T12.
19. Care must be used when mixing enzymes, to avoid losses and to ensure their uniform distribution in the sample. When adding enzymes to the fluorometer samples, mix carefully by swirling the pipette tip sideways, avoiding the formation of air bubbles.
20. Quantification of the RNA concentration can be performed via image processing software. Typically, it is possible to quantify the total fluorescence of a user-specified area around the bands of interest. Background fluorescence can be subtracted by selecting an area of the same size in a blank region of the gel. A comparison to the intensity of the control band gives an estimate of the RNA concentration. In most cases the rA1 bands are not significantly above the background, whereas the rI2 bands should be clearly recognizable.
21. We recommend that 5 μl of the reaction mix are removed before adding the enzymes for the first data point in the gel. One has to adjust volume in advance to compensate for this step.

Acknowledgement

This work was supported by the Deutsche Forschungsgemeinschaft through the Cluster of Excellence Nanosystems Initiative Munich (NIM) and by NSF grants CMMI-1266402 and CCF-131729.

References

1. Thomas R (1981) On the relation between the logical structure of systems and their ability to generate multiple steady states or sustained oscillations. In: Della Dora J, Demongeot J, Lacolle B (eds) Numerical methods in the study of critical phenomena, Springer series in synergetics. Springer, Berlin, pp 180–193
2. Novak B, Tyson JJ (2008) Design principles of biochemical oscillators. Nat Rev Mol Cell Biol 9(12):981–991
3. Goldbeter A et al (2012) Systems biology of cellular rhythms. FEBS Lett 586(18):2955–2965
4. Kim J, White KS, Winfree E (2006) Construction of an in vitro bistable circuit from synthetic transcriptional switches. Mol Syst Biol 2:68
5. Kim J, Winfree E (2011) Synthetic in vitro transcriptional oscillators. Mol Syst Biol 7:465
6. Buchler NE, Louis M (2008) Molecular titration and ultrasensitivity in regulatory networks. J Mol Biol 384(5):1106–1119
7. Franco E et al (2011) Timing molecular motion and production with a synthetic transcriptional clock. Proc Natl Acad Sci U S A 108(40):E784–E793
8. Weitz M et al (2014) Diversity in the dynamical behaviour of a compartmentalized programmable biochemical oscillator. Nat Chem 6(4):295–302
9. Montagne K et al (2011) Programming an in vitro DNA oscillator using a molecular networking strategy. Mol Syst Biol 7:466
10. Padirac A, Fujii T, Rondelez Y (2012) Bottom-up construction of in vitro switchable memories. Proc Natl Acad Sci U S A 109(47):E3212–E3220

Chapter 11

The Use of SNAP Labeling to Study Cell Cycle Oscillatory Proteins

Christine Greil, Marie Follo, Monika Engelhardt, and Ralph Wäsch

Abstract

Tightly controlled degradation of specific regulatory proteins is crucial for transitioning to the next cell cycle phase, ensuring precise DNA replication and an equal distribution of chromosomes to provide genomic stability and avoid tumorigenesis. To study mitotic control at the metaphase-to-anaphase transition, a histone H2-GFP-based reporter system was established, allowing simultaneous monitoring of the alignment of mitotic chromosomes and cyclin B proteolysis. To depict the proteolytic profile, a chimeric cyclin B-SNAP reporter molecule that can be labeled with a fluorochrome-carrying SNAP substrate was generated for measurement of the decline in fluorescence intensity via live-cell imaging. This reporter system can be adapted for other cell cycle oscillatory proteins.

Key words Cell cycle, Spindle assembly checkpoint (SAC), Anaphase-promoting complex (APC/C), Cyclin B proteolysis, Ubiquitin-proteasome system

1 Introduction

The cell division cycle is regulated in an ordered manner, largely due to transcriptional and proteolytic control of regulatory proteins such as the cyclins or the mitotic kinases Polo and Aurora. To ensure the oscillation of cell cycle regulators by the ubiquitin-proteasome system, two ubiquitin ligases are employed: the SCF (Skp1-cullin-F box protein) complex at the G1-S and G2-M transitions, and the anaphase-promoting complex or cyclosome (APC/C) in mitosis and G1 (1).

The spindle assembly checkpoint (SAC) is a control mechanism inhibiting cell cycle progression at the metaphase-to-anaphase transition, until stable bipolar chromosomal attachment to the mitotic spindle is established. By inhibition of the activating APC/C subunit Cdc20, the SAC blocks proteolysis of securin and cyclin B, and thereby chromosome separation and mitotic exit. Improper attachment of chromosomes prevents silencing of SAC signaling and causes continuous inhibition of APC/C^{Cdc20}, until

Amanda S. Coutts and Louise Weston (eds.), *Cell Cycle Oscillators: Methods and Protocols*, Methods in Molecular Biology, vol. 1342, DOI 10.1007/978-1-4939-2957-3_11,

the problem is solved in order to avoid chromosome missegregation, aneuploidy, and tumorigenesis (2).

The influence of incorrect chromosomal spindle attachment on APC/C-dependent proteolysis can be studied by using depolymerizing or microtubule-stabilizing drugs that disturb chromosomal attachment to the mitotic spindle. These procedures bear a risk of inducing artificial effects, since interference with microtubule kinetics can affect transport and localization of critical regulators (3).

To study SAC interference with APC/C-dependent cyclin B proteolysis in unperturbed cell populations, a chimeric cyclin B reporter molecule was generated with a carboxy (C)-terminal SNAP moiety, which is able to bind covalently to an SNAP substrate carrying a fluorochrome (4, 5). SNAP reporter cells stably expressing this chimeric cyclin B-SNAP molecule are labeled through the addition of the membrane-permeable SNAP substrate to the growth medium (6, 7). The cyclin B-SNAP fluorescence intensity drops in a pulse-chase reaction-like manner, and the fluorescence intensity reflects levels of cyclin B degradation via APC/C-dependent proteolysis. In this way, the fluorescence intensity is a measure of APC/C activity and indirectly reflects the status of the SAC. The additional expression of histone H2-GFP allows simultaneous monitoring of metaphase alignment of mitotic chromosomes via live-cell imaging (*see* Fig. 1). The acquisition of proteolytic profiles of large numbers of cell divisions using image cytometry (Scan^R technology) allows for selection of single mitoses showing chromosome alignment errors, and to

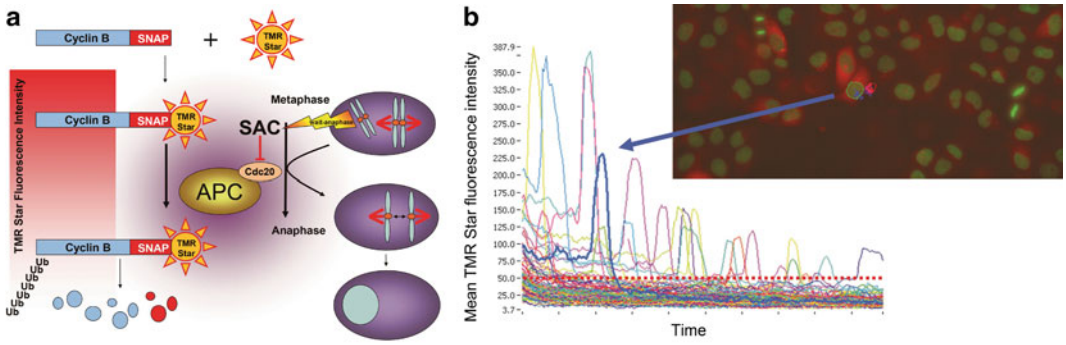

Fig. 1 Analysis of cyclin B proteolysis at the single-cell level. (**a**) To study pulsed-chased cyclin B proteolysis as a readout of APC/C-Cdc20 activity and spindle assembly checkpoint (SAC) surveillance, the decline of SNAP-tagged cyclin B fluorescence during degradation was analyzed. (**b**) Microscopic analysis: the corresponding images on the right allow the simultaneous visualization of histone H2-GFP (*green*) and cyclin B-SNAP (*red*). The decline of mean TMR-Star fluorescence intensities over time can be measured with the Scan^R analysis software (reproduced from ref. 4 with permission from Taylor & Francis)

define differences between the proteolytic profiles of aberrant and regular divisions (4, 5).

Because synthesis of cyclin B during mitosis has recently been suggested as an important mechanism in fostering a mitotic block in mice and humans by keeping cyclin B expression levels stable, the described system may be useful to analyze cyclin B proteolysis as one element of a balanced equilibrium (8–10). Moreover, screens using shRNA libraries with the reporter system may lead to the identification of novel mitotic regulators. It should also be useful in screening small molecules with regard to their potency in interfering with APC/C-dependent proteolysis in order to identify novel drugs for antimitotic therapy.

2 Materials

2.1 Cell Culture

1. SNAP reporter cells (i.e., U2OS (*see* **Note 1**) stably expressing the retroviral cyclin B-SNAP (*see* **Note 2**) construct and histone H2-GFP).
2. Growth medium: Phenol red-free medium supplemented with 10 % fetal bovine serum, penicillin/streptomycin, and sodium pyruvate. Optional: Sterile mineral oil suitable for mouse embryo culture (*see* **Note 3**).
3. Labeling medium: SNAP substrate (i.e., TMR-Star; *see* **Note 4**). The stock solution is dissolved in DMSO at a concentration of 400 μM and can be stored in aliquots at −20 °C. Prior to staining, dilute 0.5 μl of stock solution in 200 μl growth medium to obtain a final labeling concentration of 1 μM.
4. Incubator set for cell culture conditions: 37 °C, 100 % air humidity, 5 % CO_2.
5. Microscope chambers with glass or optical bottoms, 8- or 96-well: We have had good experience using chambers with optical bottoms which have been tissue culture treated, for example μ-Slide 8 well, Ibidi (Cat. 80826), or 96 Well Special Optics Clear Bottom Black Plate, Corning (Cat. 3720).
6. Portable heat block warmed to 37 °C.

2.2 Automated Microscope (Olympus Scan^R) (See Note 5)

1. GFP (H2-GFP, emission 510–550 nm) and TRITC (Cyclin B-SNAP-TMR-Star, emission 575–615 nm) filter sets.
2. 20× UPLSAPO (N.A. 0.75) objective.
3. Microscope climate chamber to allow incubation of the samples at 37 °C and at least 60 % humidity.
4. Scan^R acquisition software.
5. Scan^R analysis software.

3 Methods

3.1 Seeding of Cyclin B-SNAP Reporter Cells on Microscope Chamber Slides

1. Trypsinize subconfluent SNAP reporter cells which have been allowed to grow asynchronously in log phase for at least 48 h.
2. To achieve an even distribution across the entire surface of the microscope chamber, centrifuge 10,000 (5,000) cells at 300 × *g* for 5 min, resuspend in 350 (300) μl growth medium, and transfer cell suspension to an 8- (96-) well microscope chamber. For seeding of cells at a higher density in the center of the microscope chamber, load the chamber with 300 μl (15) growth medium and add 5,000 (1,500) cells carefully to the center of the microscope chamber. Depending on the total number of wells required for the experiment, adjust the cell number and the total volume of the suspension medium accordingly. A regular distribution of the cells across the surface of the entire well is recommended if only a single or a few positions are to be manually defined for analysis. Using a higher confluency of cells in the center region is recommended if you are performing automated acquisition across different wells, so that the center region can be used to position the images.
3. Allow the seeded cells to grow at least 18 h in the chamber/well.

3.2 Staining of Reporter Cells with SNAP Substrate

1. Aliquots of growth medium should be warmed up to 37 °C for 30 min prior to the staining procedure. Prepare enough aliquots for at least six changes of medium.
2. Remove the growth medium from the asynchronously growing cells and incubate in labeling medium for 25 min under standard culture conditions.
3. Remove the labeling medium and then wash the cells four times with pre-warmed growth medium. Incubate cells in 300 μl growth medium for 30 min. Prior to transporting to the microscope replace the medium again to remove any residual unbound SNAP substrate. For longer term incubations the cells can be layered with sterile, pre-saturated mineral oil, if desired (*see* **Note 3**).
4. Transport the plate to the microscope in a styrofoam box on a pre-warmed (37 °C) heat block to minimize temperature variation.

3.3 Measurement of Fluorescence Intensity Using Scan^R

1. At least 2 h prior to the planned experiment adjust the air temperature of the climate chamber to 37 °C while still in dry mode. Preheating before setting the humidity is important to avoid condensation and subsequent damage to the microscope. After the microscope has reached 37 °C, adjust the air humidity to 60 % and CO_2 level to 5 %.

Table 1
Standard settings for Scan^R Acquisition software

Autofocus settings	Histone H2-GFP (main object acquisition settings)	Cyclin B-SNAP labeled with TMR-Star (acquisition settings)	Acquisition cycle time
			Repetitions
Coarse autofocus ±39 μm 24 layers	*GFP filter set*:	*TRITC filter set*:	2–5 min (*see* **Note 6**)
Fine autofocus ±5.4 μm 14 layers *GFP filter set*: Exposure time: 12 ms Light intensity: 12.5 %	Exposure time: 100 ms Light intensity: 25 %	Exposure time: 50 ms Light intensity: 33.3 %	Up to 48 h of continued analysis (*see* **Note 3**)

2. Start the Scan^R acquisition software and define settings optimized for use with the 20× UPLSAPO (N.A. 0.75) objective (Table 1): In addition, define which wells are to be analyzed, the number of images per well and their spacing within the well, the acquisition cycle time, and the absolute number of acquisition cycles (*see* **Note 6**).
3. If hardware autofocus is available and analysis of multiple wells is desired select hardware autofocus; otherwise software autofocus can be used by itself (*see* **Notes 7** and **8**).
4. Start the image acquisition and supervise the first two cycles to ensure that the automatic focus is functioning well. The microscope should be set to focus on the histone H2-GFP signal using a GFP filter set, with subsequent acquisition of an image in that channel, before the filter is changed and the corresponding TMR-Star image is acquired with a TRITC filter set (4, 5, 8). This is repeated for all positions within a well and for each of the wells to be examined, before the next cycle starts.

3.4 Analysis of Proteolytic Profiles Using Scan^R (See Fig. 1)

1. Start the Scan^R analysis software and analyze the images. In setting up the assay, image processing should include background correction carried out on all channels using a size filter of 200 pixels. The cell nuclei, as visualized by histone H2-GFP, are used to define the main objects for analysis, using a threshold based on signal intensity and a watershed algorithm to assist in separating neighboring cells. A sub-object for the whole cell consisting of a nucleus with cytoplasm should be created for SNAP-substrate analysis. Important properties of the main object to include in the analysis are X and Y positions,

time, and maximum and mean GFP intensities, while the total intensity divided by the area should be included for the TMR-Star sub-object to give the mean TMR-Star intensity. This analysis process may take several hours to complete, due to the large amounts of data involved.

2. Change to "Trace View" to visualize changes in the sub-object mean TMR-Star fluorescence intensity over time (total TMR-Star intensity divided by area), assigned to the analyzed main objects. Within the "Kinetic Mode" configure the tracer to enable tracking with a main object range of 20 pixels when using the 20× objective. Within "Define Kinetic Parameters" add the lifetime parameter and the maximum of the "Mean Intensity" (GFP). The number of cells to be examined can be narrowed down by gating on those cells with a lifetime (total number of measurements) of 140 cycles or greater through the use of the lifetime parameter, and on those events with a high maximum intensity of H2-GFP to identify cells undergoing mitosis. Looking at larger numbers of cells within the "Trace View" allows a representative and objective first viewing of the cell population.
3. Within "Trace View" select a cell trace of interest to visualize histone H2-GFP and TMR-Star fluorescence simultaneously at the single-cell level.
4. Generate an exportable picture gallery to illustrate histone H2-GFP and cyclin B-SNAP TMR-Star for every single time point for a cell of interest.
5. Change back to the population mode of the Scan^R analysis software and draw a region around the cell, with the cell of interest located as represented on an X vs. Y dot plot.
6. Use the region as a gate in a new dot plot window in order to visualize mean TMR-Star fluorescence intensity over time.
7. Export data from the dot plot (time and fluorescence intensity) for further calculation (*see* **Note 9**).

4 Notes

1. Using the retroviral cyclin B-SNAP expression construct, a reporter cell line can be established by stable retroviral integration into any desired cell line (8).
2. The system can be adapted to other oscillatory cell cycle proteins of interest.
3. When imaging over time periods longer than 48 h, a small layer of sterile mineral oil can be added to limit the amount of

evaporation which takes place. The mineral oil should previously have been shaken and mixed with normal culture media and left overnight in order to saturate the oil with media components before using with the cells.

4. SNAP substrate molecules are readily available carrying different fluorochromes with different colors.
5. The reporter system was established based on the Scan^R software, but can be reproduced on any comparable microscope station.
6. A good starting point to use for the cycle time is from 2 to 5 min. The shortest cycle time which is achievable will be limited by the total number of positions to be acquired, as well as by the exposure times needed for the images. For longer cell survival, exposure times should be minimized as much as possible.
7. The use of histone H2-GFP, besides its requirement for monitoring chromosome alignment, helps to ensure fast and easy autofocusing. Autofocus and intensity settings also depend on the type of cell and have to be determined separately for each cell line.
8. The use of hardware autofocus, when larger numbers of wells are to be scanned, is more robust against losing the focus due to temperature drift of the sample over time than when using software autofocus alone, as well as against slight focal differences from well to well in the plate bottom.
9. Cyclin B-SNAP fluorescence intensities can be quantified using freeware image analysis programs such as ImageJ or Fiji (http://imagej.net/Welcome). Fluorescence intensity curves can be calculated based on the mean pixel intensity over time within a gate defining the X and Y coordinates of the mitotic cell (11). Within an isovolumetric window the shape and the volume of the cell remain nearly constant (4). This provides a rationale for using the same gate between nuclear envelope breakdown until early anaphase for measuring mean pixel intensities to manually estimate cyclin B proteolysis during prometaphase, metaphase, and early anaphase.

Acknowledgement

This work was supported by grants from the Deutsche Forschungsgemeinschaft (WA 1363/3-1) and Jose-Carreras Leukemia Foundation (DJCLS R 10/14).

References

1. Morgan DO (2007) The cell cycle: principles of control. New Science, London, UK
2. Musacchio A, Salmon ED (2007) The spindle-assembly checkpoint in space and time. Nat Rev Mol Cell Biol 8:379–393
3. Fletcher DA, Mullins RD (2010) Cell mechanics and the cytoskeleton. Nature 463:485–492
4. Schnerch D, Follo M, Krohs J, Felthaus J, Engelhardt M, Wäsch R (2012) Monitoring APC/C activity in the presence of chromosomal misalignment in unperturbed cell populations. Cell Cycle 11:310–321
5. Schnerch D, Follo M, Felthaus J, Engelhardt M, Wäsch R (2012) Studying proteolysis of cyclin B at the single cell level in whole cell populations. J Vis Exp 68:e4239
6. Keppler A, Gendreizig S, Gronemeyer T, Pick H, Vogel H, Johnsson K (2003) A general method for the covalent labeling of fusion proteins with small molecules in vivo. Nat Biotechnol 21:86–89
7. Jansen LE, Black BE, Foltz DR, Cleveland DW (2007) Propagation of centromeric chromatin requires exit from mitosis. J Cell Biol 176:795–805
8. Schnerch D, Follo M, Felthaus J, Engelhardt M, Wäsch R (2013) The 3' untranslated region of the cyclin B mRNA is not sufficient to enhance the synthesis of cyclin B during a mitotic block in human cells. PLoS One 8:e74379
9. Malureanu L, Jeganathan KB, Jin F, Baker DJ, van Ree JH, Gullon O, Chen Z, Henley JR, van Deursen JM (2010) Cdc20 hypomorphic mice fail to counteract de novo synthesis of cyclin B1 in mitosis. J Cell Biol 191: 313–329
10. Mena AL, Lam EW, Chatterjee S (2010) Sustained spindle-assembly checkpoint response requires de novo transcription and translation of cyclin B1. PLoS One 5
11. Wolthuis R, Clay-Farrace L, van Zon W, Yekezare M, Koop L, Ogink J, Medema R, Pines J (2008) Cdc20 and Cks direct the spindle checkpoint-independent destruction of cyclin A. Mol Cell 30:290–302

Chapter 12

A Computational Method for Identifying Yeast Cell Cycle Transcription Factors

Wei-Sheng Wu

Abstract

The eukaryotic cell cycle is a complex process and is precisely regulated at many levels. Many genes specific to the cell cycle are regulated transcriptionally and are expressed just before they are needed. To understand the cell cycle process, it is important to identify the cell cycle transcription factors (TFs) that regulate the expression of cell cycle-regulated genes. Here, we describe a computational method to identify cell cycle TFs in yeast by integrating current ChIP-chip, mutant, transcription factor-binding site (TFBS), and cell cycle gene expression data. For each identified cell cycle TF, our method also assigned specific cell cycle phases in which the TF functions and identified the time lag for the TF to exert regulatory effects on its target genes. Moreover, our method can identify novel cell cycle-regulated genes as a by-product.

Key words Yeast, Cell cycle, Transcription factor, Algorithm, Computational method, Dynamic model

1 Introduction

The eukaryotic cell cycle is a complex process and is precisely regulated at many levels. One important aspect of this regulation is at the transcriptional level. That is, many genes specific to the cell cycle are transcribed just before they are needed [1]. To have a good understanding of the cell cycle, it is essential to identify the cell cycle-regulated genes and their transcriptional regulators. DNA microarray analysis has revealed that the expression levels of ~800 genes vary in a periodic fashion during the yeast cell cycle, but little is known about the transcriptional regulation of most of these genes [2, 3]. To fill this gap, we aim to identify the cell cycle transcription factors (TFs) that regulate the cell cycle-regulated genes inferred by DNA microarray analysis [2].

Here, we describe a computational method (Fig. 1) to systematically identify cell cycle TFs by combining four data sources: transcription factor-binding site (TFBS), mutant, ChIP-chip, and cell cycle gene expression data. In order to reduce the high false-negative rate of the ChIP-chip data, we use current TFBS

Amanda S. Coutts and Louise Weston (eds.), *Cell Cycle Oscillators: Methods and Protocols*, Methods in Molecular Biology, vol. 1342, DOI 10.1007/978-1-4939-2957-3_12,

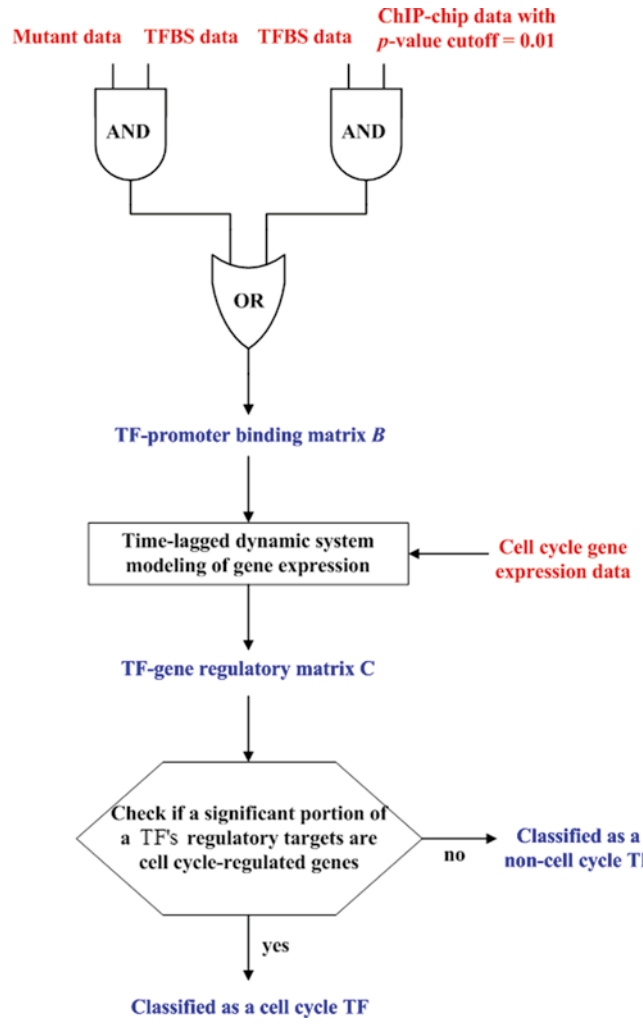

Fig. 1 Flow chart of the procedure of our method. This figure describes a computational method to systematically identify cell cycle TFs by combining four data sources: transcription factor-binding site (TFBS), mutant, ChIP-chip, and cell cycle gene expression data

data [4, 5] to avoid using a stringent p-value threshold (≤ 0.001) to determine TF-promoter binding. We assume that a TF binds to a specific promoter if (a) the p-value for the TF to bind the promoter is ≤ 0.01 in ChIP-chip data and (b) the promoter contains one or more binding sites of the TF. That is, we allow the p-value cutoff to be relaxed to 0.01 but the TF-promoter binding event must be supported by the TFBS data.

It is known that the ChIP-chip technique can only detect those TF-promoter binding events that happen under the same physiological condition in which the ChIP-chip experiment is conducted, so it can potentially miss many TF-promoter binding events. We use the mutant data [5] and the TFBS data [4, 5] to rescue some

of these false-negative TF-promoter binding events. We assume that a TF binds to a specific promoter if (a) the disruption of the TF results in a significant change of expression of the gene that has the specific promoter and (b) the promoter contains one or more binding sites of the TF. That is, the TF-promoter binding event can be assumed without using ChIP-chip data if it is supported by both the mutant and the TFBS data. This step can rescue some plausible TF-promoter binding events that are missing in the current ChIP-chip data.

From the above procedure, we can derive a high-confidence TF-promoter binding matrix (*see* Subheading 3). However, binding of a TF to the promoter of a gene does not necessarily imply regulation. A TF may bind to the promoter of a gene but has no regulatory effect on that gene's expression. Hence, additional information is required to solve this ambiguity inherent in the TF-promoter binding matrix. In this study, we use the additional information provided by the yeast cell cycle gene expression data [2] to solve this problem. We use a time-lagged dynamic system model of gene regulation to describe how the target gene's expression during cell cycle is controlled by the TFs that bind to its promoter (inferred from the TF-promoter binding matrix). Among these bound TFs, those that have significant regulatory effects on the target gene's expression can be extracted (*see* Subheading 3). From this procedure, we can refine the TF-promoter binding matrix into a high-confidence TF-gene regulatory matrix. Each TF-gene regulatory relationship in this matrix is supported by at least three data sources: gene expression, TFBS, and ChIP-chip or/and mutant data. From the high-confidence TF-gene regulatory matrix, the regulatory targets of each of the 203 TFs in yeast can be inferred. Finally, a TF is said to be a cell cycle TF if a statistically significant portion of its regulatory targets are cell cycle-regulated genes.

2 Materials

We use four data sources in this study. First, the ChIP-chip data are from Harbison et al. [6]. They used genome-wide location analysis to determine the genomic occupancy of 203 TFs in rich media conditions. Second, the TFBS data are from MacIsaac et al. [4] and the YEASTRACT database [5]. MacIsaac et al. used evolutionarily conservative criteria to computationally identify the binding sites of many TFs in yeast. The YEASTRACT database includes a set of computational tools that can be used to identify complex motifs overrepresented in the promoters of co-regulated genes. Third, the mutant data are from the YEASTRACT database [5]. The mutant data can tell us which gene's expression was changed significantly owing to the deletion (or mutation) of the gene that encodes a TF. The evidence may come from detailed gene-by-gene

analysis or genome-wide expression analysis. Finally, the yeast cell cycle gene expression data are from Spellman et al. [2]. The alpha factor data set is used because it was shown to have a better data quality than the other data sets [7]. Samples for all genes in the yeast genome are collected at 18 time points (0, 7, 14, 21, …, 119 min), which cover two cell cycles. That is, each gene has an 18-time point gene expression profile. The cubic spline method [8] is then used to reconstruct the missing values and interpolate extra data points into the original time profile. Note that genes that have more than one missing value in their gene expression profiles are excluded in this study.

3 Methods

3.1 Construction of a High-Confidence TF-Gene Regulatory Matrix

Using three data sources (ChIP-chip, mutant, and TFBS data), we can construct a high-confidence TF-promoter binding matrix $B = \left[b_{i,j} \right]$, where $b_{i,j} = 1$ if (a) the p-value for TFj to bind the promoter of gene i is ≤ 0.01 in the ChIP-chip data and the promoter of gene i contains one or more binding sites of TFj or (b) the disruption of TFj results in a significant change of the expression of gene i and the promoter of gene i contains one or more binding sites of TFj (*see* **Notes 1** and **2**). Otherwise, $b_{i,j} = 0$.

However, binding of a TF to the promoter of a gene does not necessarily imply regulation (*see* **Note 2**). Hence, additional information is required to solve this ambiguity inherent in the TF-promoter binding matrix. Using a time-lagged dynamic model of gene regulation, we can refine the TF-promoter binding matrix into a high-confidence TF-gene regulatory matrix. We consider the transcriptional regulatory mechanism of a target gene as a system with the regulatory profiles of several TFs as the inputs and the gene expression profile of the target gene as the output. The transcriptional regulation of a target gene is described by the following time-lagged dynamic system model [9–11]:

$$y[t] = \left(k + \sum_{i=1}^{N} d_i \cdot x_i[t - \tau_i] \right) - \lambda \cdot y[t-1] + \varepsilon[t] \qquad (1)$$

where $y[t]$ represents the target gene's expression profile at time point t, k represents the target gene's basal expression level induced by RNA polymerase II, N denotes the number of TFs that bind to the promoter of the target gene (inferred from the TF-promoter binding matrix B), d_i indicates the regulatory ability of TFi, $x_i[t]$ represents the regulatory profile of TFi at time point t, τ_i indicates the time lag for TFi to exert a regulatory effect on the target gene's expression, λ indicates the degrading effect of the target gene's expression value $y[t-1]$ at time point $t-1$ on the target gene's expression value $y[t]$ at time point t, and $\varepsilon[t]$ denotes the stochastic

noise due to the modeling error and the measuring error of the target gene's expression profile. $\varepsilon[t]$ is assumed to be a Gaussian noise with mean zero and unknown standard deviation σ. The biological meaning of Eq. 1 is that $y[t]$ (the target gene's expression value at time point t) is determined by $k+\sum_{i=1}^{N} d_i \cdot x_i\left[t-\tau_i\right]$ (the production effect of RNA polymerase II and TFi at time point $t-\tau_i$, where $i=1,\cdots,N$) and $-\lambda \cdot y[t-1]$ (the degradation effect of the target gene at time point $t-1$).

It has been shown that TF binding usually affects gene expression in a nonlinear fashion: below some level it has no effect, while above a certain level the effect may become saturated. This type of binding behavior can be modeled using a sigmoid function. Therefore, $x_i[t]$ (the regulatory profile of TFi at time point t) is defined as a sigmoid function of $z_i[t]$ (the gene expression profile of TFi at time point t) [12, 13]:

$$x_i[t]=f\left(z_i[t]\right)=\frac{1}{1+\exp\left[-g\left(z_i[t]-A_i\right)\right]}$$

where g denotes the transition rate of the sigmoid function and A_i denotes the mean of the gene expression profile of TFi. It is also known that the regulatory effect of a TF on its target genes may not be simultaneous but has a time lag [13–18]. Therefore, we incorporate a time lag term into our dynamic system model. The time lag τ_i between TFi and the target gene y is determined by $\tau_i=\arg_q \max r(q)$, where $r(q)$ is the correlation between $\vec{y}=\left(y[1],\cdots,y[M]\right)$ (the expression profile of the target gene y) and $\vec{x}_i=\left(x_i[1],\cdots,x_i[M]\right)$ (the regulatory profile of TF$_i$) with a lag of q time points [13, 14]:

$$r(q)=\left(\sum_{j=1}^{M-q}\left(y[j+q]-\bar{y}\right)\left(x_i[j]-\bar{x}_i\right)\right)/\left(\sqrt{\sum_{j=1}^{M-q}\left(y[j+q]-\bar{y}\right)^2}\cdot\sqrt{\sum_{j=1}^{M-q}\left(x_i[j]-\bar{x}_i\right)^2}\right),$$
$$q=0,1,\ldots,Q$$

where $\bar{y}=\left(\sum_{j=1}^{M-q} y[j+q]\right)/(M-q)$, $\bar{x}_i=\left(\sum_{j=1}^{M-q} x_i[j]\right)/(M-q)$, M is the number of time points of the target gene's expression profile, and Q is the maximal time lag of the TF's regulatory profile considered. The time lag may be interpreted as the time for a TF to exert a regulatory effect on its target gene's expression. The value of Q is chosen to make the maximal time lag approximately equal to two consecutive cell cycle phases because Simon et al. [3] found cases where a cell cycle TF that expresses in one phase of the cell cycle can regulate genes that function in the next phase.

After writing down the time-lagged dynamic system model of gene regulation, the next step is to estimate the unknown parameters in the model. We rewrite Eq. 1 into the following regression form:

$$y[t]=\left[x_1[t-\tau_1]\cdots x_N[t-\tau_N]\ 1-y[t-1]\right]\cdot\begin{bmatrix}d_1\\ \vdots\\ d_N\\ k\\ \lambda\end{bmatrix}+\varepsilon[t] \qquad (2)$$

Using the yeast cell cycle gene expression data from Spellman et al. [2], we can get the values of $\{x_i[v], y[v]\}$ for $i\in\{1,2,\cdots,N\}, v\in\{1,2,\cdots,M\}$. Equation 2 at different time points can thus be put together as follows:

$$\begin{bmatrix}y[w]\\ y[w+1]\\ \vdots\\ y[M]\end{bmatrix}=\begin{bmatrix}x_1[w-\tau_1] & \cdots & x_N[w-\tau_N] & 1 & y[w-1]\\ x_1[w+1-\tau_1] & \cdots & x_N[w+1-\tau_N] & 1 & -y[w]\\ \vdots & \vdots & \vdots & \vdots & \vdots\\ x_1[M-\tau_1] & \cdots & x_N[M-\tau_N] & 1 & -y[M-1]\end{bmatrix}\cdot\begin{bmatrix}d_1\\ \vdots\\ d_N\\ k\\ \lambda\end{bmatrix}+\begin{bmatrix}\varepsilon[w]\\ \varepsilon[w+1]\\ \vdots\\ \varepsilon[M]\end{bmatrix} \qquad (3)$$

where $w=1+\max_{i=1,\ldots,N}\tau_i$. For simplicity, we define the notations y, Φ, θ, and e to represent Eq. 3 as follows:

$$Y=\Phi\cdot\theta+e$$

where $Y=\left[y[w]\cdots y[M]\right]^T$, Φ is the system matrix, $\theta=\left[d_1\cdots d_N\,k\,\lambda\right]^T$ is the unknown parameter vector, and e is the error vector. The parameter vector θ can be estimated by the maximum likelihood (ML) method as follows:

$$\breve{\theta}=\left(\Phi^T\Phi\right)^{-1}\Phi^T Y=\left[\breve{d}_1\cdots\breve{d}_N\ \ \breve{k}\ \ \breve{\lambda}\right]^T$$

Since d_i stands for the regulatory ability of TFi, a large absolute value of d_i means that TFi has a large effect on the target gene's expression. We consider TFi to be a true regulator of the target gene if its regulatory ability d_i is statistically significantly different from zero. The test statistic $t=\dfrac{\breve{d}_i}{s\sqrt{u_{ii}}}$, a t-distribution with the degree of freedom equal to $(M-w+1)-(N+2)$, is used to assign a p-value for rejecting the null hypothesis H_0: $d_i=0$, where u_{ii} is the ith diagonal element of the matrix $\left(\Phi^T\Phi\right)^{-1}$ and $s=\sqrt{\dfrac{\left(Y-\Phi\cdot\breve{\theta}\right)^T\left(Y-\Phi\cdot\breve{\theta}\right)}{(M-w+1)-(N+2)}}$ is an unbiased estimator of σ (the

standard deviation of the stochastic noise $\varepsilon[t]$) [19]. The p-value computed by the t-distribution is then adjusted by the Bonferroni correction to represent the true alpha level in the multiple hypotheses testing [19]. Finally, TFi is said to be a true regulator of the target gene if the adjusted p-value $p_{\text{adjusted}} \le 0.05$.

From the above analysis, we can refine the TF-promoter binding matrix $B = \left[b_{i,j} \right]$ into a TF-gene regulatory matrix $C = \left[c_{i,j} \right]$. In this matrix, $c_{i,j} = 1$ if $b_{i,j} = 1$ and if TFj is shown by the time-lagged dynamic system model to exert a significant regulatory effect on the expression of gene i. Otherwise, $c_{i,j} = 0$.

3.2 Identification of Cell Cycle TFs

From the high-confidence TF-gene regulatory matrix, the regulatory targets of each of the 203 TFs in yeast can be inferred. Then a TF is said to be a cell cycle TF if a statistically significant portion of its regulatory targets are in the set of 800 cell cycle-regulated genes identified by Spellman et al. [2]. The hypergeometric distribution is used to test the statistical significance [20–23]. The procedure for checking whether TFj is a cell cycle TF as follows. Let S be the set of cell cycle-regulated genes identified by Spellman et al. [2], G be the set of genes that are regulated by TF_j (inferred from the TF-gene regulatory matrix), $T = S \cap G$ be the set of cell cycle-regulated genes that are also regulated by TF_j, and F be the set of all genes in the yeast genome. Then the p-value for rejecting the null hypothesis (H_0: TFj is not a cell cycle TF) is calculated as

$$p = P\left(x \ge |T|\right) = \sum_{x \ge |T|} \frac{\binom{|S|}{x}\binom{|F|-|S|}{|G|-x}}{\binom{|F|}{|G|}}, \tag{4}$$

where $|G|$ refers to the number of genes in set G. This p-value is then adjusted by the Bonferroni correction to represent the true alpha level in the multiple hypotheses testing [19]. TF_j is said to be a cell cycle TF if the adjusted p-value $p_{\text{adjusted}} \le 0.05$. This procedure is applied to each of the 203 TFs under study.

3.3 Identification of the Cell Cycle Phases in Which a Cell Cycle TF Functions

For each of the identified cell cycle TFs, we want to determine in which cell cycle phases it functions. We regard that a cell cycle TF functions in the X phase ($X = \text{MG}_1, \text{G}_1, \text{S}, \text{SG}_2, \text{G}_2\text{M}$) if a statistically significant portion of its regulatory targets belong to the X-phase cell cycle-regulated genes identified by Spellman et al. [2]. Equation 4 is again used to test the statistical significance. While G and F are defined as before, S now denotes the set of X-phase cell cycle-regulated genes identified by Spellman et al. [2] and $T = S \cap G$ now denotes the set of X-phase cell cycle-regulated genes that are also regulated by the cell cycle TF under study.

The p-value computed by Eq. 4 is then adjusted by the Bonferroni correction to represent the true alpha level in the multiple hypotheses testing. We say that a cell cycle TF functions in the X phase ($X = MG_1, G_1, S, SG_2, G_2M$) if the adjusted p-value $p_{adjusted} \leq 0.05$.

3.4 Identification of Novel Cell Cycle-Regulated Genes

For each of the identified cell cycle TFs, we look at their regulatory targets to find novel cell cycle-regulated genes. We regard a gene as a cell cycle-regulated gene if it is regulated by at least two of the identified cell cycle TFs. The requirement for defining a cell cycle-regulated gene to be regulated by at least two rather than one cell cycle TF is to reduce the number of false positives.

4 Notes

1. The choices of both the relaxed p-value and time-lag parameter have biological meanings. Two previous papers [6, 24] used a statistical error model to assign a p-value of the binding relationship of a TF-promoter pair. They found that if $p \leq 0.001$, the binding relationship of a TF-promoter pair is of high confidence and can usually be confirmed by promoter-specific PCR. If $p > 0.01$, the binding relationship of a TF-promoter pair is of low confidence and cannot be confirmed by promoter-specific PCR most of the time. However, if $0.001 < p \leq 0.01$, the binding relationship of a TF-promoter pair is ambiguous and can be confirmed by promoter-specific PCR in some cases but not in the other cases. Our aim is to solve this ambiguity, so we choose 0.01 to be the relaxed p-value. We say that an ambiguous binding relationship of a TF-promoter pair is plausible if $0.001 < p < 0.01$ and if the promoter contains one or more binding sites of the TF. As to the time-lag parameter, its value is chosen to make the maximal time lag approximately equal to two consecutive cell cycle phases because Simon et al. [3] found cases where a cell cycle TF that expresses in one phase of the cell cycle can regulate genes that function in the next phase.
2. Our method has four features that make it more powerful than existing approaches. First, it can reduce false negatives in determining TF-promoter binding events from current ChIP-chip data. Most previous methods [6, 24–28], except GRAM [26], used a stringent p-value threshold (≤ 0.001) to determine TF-promoter binding events in order to reduce the number of false positives, but it was at the expense of false negatives (~24 %) [6]. In comparison, our method allows the p-value cutoff to be relaxed to 0.01 but requires that the promoter must have one or more binding sites of the TF. Therefore, using additional information provided by the TFBS data, our method can rescue some false negatives without substantially increasing the number of false positives.

Second, it is known that ChIP-chip data can only indicate those TF-promoter binding events that happen under the same physiological condition in which the ChIP-chip experiments are conducted. Therefore, many plausible TF-promoter binding events may be missing in the current ChIP-chip data. In order to solve this problem, our method considers that a TF binds to a specific promoter if the disruption of the TF results in a significant change of the expression of the gene that has the specific promoter and if the promoter contains one or more binding sites of the TF. That is, using the information provided by the mutant and the TFBS data, our method can rescue many TF-promoter binding events that are missing in the current ChIP-chip data.

Third, our method can extract plausible TF-gene regulatory relationships from TF-promoter binding relationships. Most pervious methods [6, 24–27] regard the TF-promoter binding relationships provided by ChIP-chip data as the TF-gene regulatory relationships. This may not be true because the binding of a TF to the promoter of a gene does not necessarily imply regulation. A TF may bind to the promoter of a gene but has no regulatory effect on that gene's expression. To solve this problem, our method uses a time-lagged dynamic system model of gene regulation to extract the TFs that have significant regulatory effects on the target gene's expression from all TFs that bind to the promoter of the target gene. Through this process, our method can extract plausible TF-gene regulatory relationships from TF-promoter binding relationships. Thus, in our method each TF-gene regulatory relationship is supported by at least three data sources: gene expression, TFBS, and ChIP-chip or/and mutant data.

Fourth, our method can identify the time lag for a cell cycle TF to exert regulatory effects on its target genes. It is known that the regulatory effects of a TF on its target genes may have a time lag [14–18]. By using a time-lagged dynamical system model, our method takes the time lag into consideration, making it more realistic than those previous studies that did not allow a time lag [28–31].

Acknowledgements

I would like to thank Prof. Wen-Hsiung Li for helpful discussions. This work was supported by National Cheng Kung University and Ministry of Science and Technology of Taiwan (MOST-103-2221-E-006-174-MY2).

References

1. Rowicka M, Kudlicki A, Tu BP et al (2007) High-resolution timing of cell cycle-regulated gene expression. Proc Natl Acad Sci U S A 104(43):16892–16897
2. Spellman PT, Sherlock G, Zhang MQ et al (1998) Comprehensive identification of cell cycle-regulated genes of the yeast *Saccharomyces cerevisiae* by microarray hybridization. Mol Biol Cell 9:3273–3297
3. Simon I, Barnett J, Hannett N et al (2001) Serial regulation of transcriptional regulators in the yeast cell cycle. Cell 106:697–708
4. MacIsaac KD, Wang T, Gordon DB et al (2006) An improved map of conserved regulatory sites for Saccharomyces cerevisiae. BMC Bioinformatics 7:113
5. Teixeira MC, Monteiro P, Jain P et al (2006) The YEASTRACT database: a tool for the analysis of transcription regulatory associations in *Saccharomyces cerevisiae*. Nucleic Acids Res 34:D446–D451
6. Harbison CT, Gordon DB, Lee TI et al (2004) Transcriptional regulatory code of a eukaryotic genome. Nature 431:99–104
7. de Lichtenberg U, Jensen LJ, Fausbøll A et al (2005) Comparison of computational methods for the identification of cell cycle-regulated genes. Bioinformatics 21(7):1164–1171
8. Faires JD, Burden R (1998) Numerical methods, 2nd edn. Brooks/Cole Publishing Company, Pacific Grove
9. Wu WS, Li WH (2008) Systematic identification of yeast cell cycle transcription factors using multiple data sources. BMC Bioinformatics 9:522
10. Wu WS, Li WH, Chen BS (2008) Reconstructing a network of stress-response regulators via dynamic system modeling of gene regulation. Gene Regul Syst Bio 2:53–62
11. Wu WS, Li WH (2008) Identifying gene regulatory modules of heat shock response in yeast. BMC Genomics 9:439
12. Wu WS, Li WH, Chen BS (2006) Computational reconstruction of transcriptional regulatory modules of the yeast cell cycle. BMC Bioinformatics 7:421
13. Wu WS, Li WH, Chen BS (2007) Identifying regulatory targets of cell cycle transcription factors using gene expression and ChIP-chip data. BMC Bioinformatics 8:188
14. Kato M, Tsunoda T, Takagi T (2001) Lag analysis of genetic networks in the cell cycle of budding yeast. Genome Inform 12:266–267
15. Reis BY, Butte AJ, Kohane IS et al (2000) Approaching causality: discovering time-lag correlations in genetic expression data with static and dynamic relevance networks. RECOMB 2000:5
16. Schmitt WA Jr, Raab RM, Stephanopoulos G (2004) Elucidation of gene interaction networks through time-lagged correlation analysis of transcriptional data. Genome Res 14:1654–1663
17. Liping J, Tan KL (2005) Identifying time-lagged gene clusters using gene expression data. Bioinformatics 21:509–516
18. Qian J, Dolled-Filhart M, Lin J et al (2001) Beyond synexpression relationships: local clustering of time-shifted and inverted gene expression profiles identifies new, biologically relevant interactions. J Mol Biol 314:1053–1066
19. Mendenhall W, Sincich T (1995) Statistics for engineering and the sciences, 4th edn. Prentice-Hall, Englewood Cliffs
20. Wu WS, Chen BS (2007) Identifying stress transcription factors using gene expression and TF-gene association data. Bioinform Biol Insights 1:9–17
21. Wang H, Wang YH, Wu WS (2011) Yeast cell cycle transcription factors identification by variable selection criteria. Gene 485:172–176
22. Yang TH, Wu WS (2012) Identifying biologically interpretable transcription factor knockout targets by jointly analyzing the transcription factor knockout microarray and the ChIP-chip data. BMC Syst Biol 6:102
23. Lai FJ, Jhu MH, Chiu CC et al (2014) Identifying cooperative transcription factors in yeast using multiple data sources. BMC Syst Biol BMC Syst Biol. 2014;8 Suppl 5:S2
24. Lee TI, Rinaldi NJ, Robert F et al (2002) Transcriptional regulatory networks in Saccharomyces cerevisiae. Science 298:799–804
25. Banerjee N, Zhang MQ (2003) Identifying cooperativity among transcription factors controlling the cell cycle in yeast. Nucleic Acids Res 31:7024–7031
26. Bar-Joseph Z, Gerber GK, Lee TI et al (2003) Computational discovery of gene modules and regulatory networks. Nat Biotechnol 21: 1337–1342
27. Kato M, Hata N, Banerjee N et al (2004) Identifying combinatorial regulation of transcription factors and binding motifs. Genome Biol 5:R56
28. Gao F, Foat BC, Bussemaker HJ (2004) Defining transcriptional networks through

integrative modeling of mRNA expression and transcription factor binding data. BMC Bioinformatics 5(1):31

29. Liao JC, Boscolo R, Yang YL et al (2003) Network component analysis: reconstruction of regulatory signals in biological system. Proc Natl Acad Sci U S A 100: 15522–15527
30. Yu T, Li KC (2005) Inference of transcriptional regulatory network by two-stage constrained space factor analysis. Bioinformatics 21:4033–4038
31. Zhou XJ, Kao MC, Huang H et al (2005) Functional annotation and network reconstruction through cross-platform integration of microarray data. Nat Biotechnol 23:238–243

Chapter 13

Measuring Activity and Specificity of Protein Phosphatases

Brendan L. Powers, Michael Melesse, Christie L. Eissler, Harry Charbonneau, and Mark C. Hall

Abstract

Reversible protein phosphorylation plays essential roles in coordinating cell division and many other biological processes. Cell cycle regulation by opposing kinase and protein phosphatase activities is often complex and major challenges exist in identifying the direct substrates of these enzymes and the specific sites at which they act. While cell cycle kinases are known to exhibit strict substrate specificities important for coordinating the complex events of cell division, phosphatases have only recently been recognized to exert similarly precise regulatory control over cell cycle events through timely dephosphorylation of specific substrates. The molecular determinants for substrate recognition by many phosphatases that function in cell division are still poorly delineated. To understand phosphatase specificity, it is critical to employ methods that monitor the dephosphorylation of individual phosphorylation sites on physiologically relevant substrates. Here, using the cell cycle phosphatase Cdc14 as an example, we describe two methods for studying phosphatase specificity, one using synthetic phosphopeptide substrates and the other using intact phosphoprotein substrates. These methods are useful for targeted characterization of small substrate sets and are also adaptable to large-scale applications for global specificity studies.

Key words Protein phosphatase, Protein kinase, Cell cycle, Protein dephosphorylation, Multisite phosphorylation, Mass spectrometry, Protein phosphatase assay, Cdc14 phosphatase assay, Phosphopeptide substrates, High-throughput phosphatase assay

1 Introduction

Mitotic kinases coordinate orderly progression through the cell division cycle by phosphorylating specific substrates at precisely the right time and location. The regulation and substrate specificity of protein kinases are fundamental components of the cell cycle control system. Protein phosphatases, which catalyze removal of phosphate groups deposited by kinases, have historically been thought of as mostly unregulated enzymes whose purpose is to restore a basal phosphorylation state upon kinase inactivation [1]. It is now clear that mitotic phosphatases are precisely regulated enzymes that act at specific times toward specific substrates to help coordinate cell cycle progression and checkpoint responses [2–5].

Amanda S. Coutts and Louise Weston (eds.), *Cell Cycle Oscillators: Methods and Protocols*, Methods in Molecular Biology, vol. 1342, DOI 10.1007/978-1-4939-2957-3_13,

Understanding how phosphatases function in cell cycle control requires knowledge of the determinants for substrate selection and the identities of their direct substrates. Most cell cycle control proteins are regulated by multiple phosphorylation sites, sometimes controlled by multiple kinases and phosphatases [6, 7]. This regulatory complexity requires analytical methods capable of detecting and quantifying individual phosphorylation sites on physiologically relevant substrate proteins.

Many methods for monitoring protein phosphatase activity toward protein substrates report on the global phosphorylation status without providing site-specific information. This includes detecting release or loss of radioactive [^{32}P]-containing phosphate from protein substrates, a change in phosphorylation-induced gel mobility shift, and colorimetric detection of released free phosphate using malachite green dye [8–11]. Other methods use nonphysiological substrates like *p*-nitrophenyl phosphate or 6,8-difluoro-4-methylumbelliferyl phosphate in colorimetric or fluorometric assays or employ [^{32}P]-labeled artificial protein substrates, such as myelin basic protein. The use of nonphysiological substrates may have been influenced by the previously held view that protein phosphatases exhibit little substrate specificity.

Cdc14 phosphatases are members of the dual-specificity phosphatase subfamily of the protein tyrosine phosphatases [12, 13]. Despite their evolutionary and mechanistic relationship to tyrosine phosphatases, Cdc14 enzymes are highly selective for phosphoserine substrates [14]. They play roles in counteracting cyclin-dependent kinase (Cdk) phosphorylation during the cell division cycle [15–17] and exhibit a strong preference in vitro for the consensus sequence pSer-Pro-x-Lys/Arg [18], representing a subset of the Ser/Thr-Pro sites targeted by Cdks. The strong intrinsic selectivity of Cdc14 for a subset of Cdk sites deposited during the cell cycle was revealed using the methods described herein, highlighting the power of analytical methods that monitor individual phosphorylation sites.

We describe two protocols for measuring Cdc14 phosphatase activity on individual phosphorylation sites that have proven to be important in establishing the authenticity of candidate substrates [14, 18, 19] and are generally useful for studying phosphatase substrate specificity. The first uses synthetic phosphopeptides, measures the release of phosphate spectrophotometrically, and is easily adapted to high-throughput format for screening libraries of phosphatase peptide substrates, inhibitors, or activators. The second uses mass spectrometry (MS) to measure dephosphorylation at multiple individual sites on intact protein substrates. With yeast Cdc14, we found that the specificity observed with phosphopeptide substrates in vitro existed with intact proteins in cells [14, 18], indicating that these phosphopeptides mimic natural targets. However, many protein phosphatases recognize substrate features distal

from the sites of phosphorylation; thus phosphopeptides are not always useful analogs of physiological targets. The phosphopeptide assay is convenient, relatively inexpensive, and easy to implement with standard lab equipment. The MS assay requires more advanced instrumentation and is more technically challenging, but offers the advantage of studying single, or complex, mixtures of physiological protein substrates.

2 Materials

Prepare all solutions using ultrapure water. Store all reagents at room temperature unless otherwise noted. Solvents and liquid reagents should be of HPLC grade. Low-protein-binding microtubes should be used to minimize peptide/protein loss by adsorption.

2.1 Phosphopeptide Dephosphorylation Assay

1. Phosphopeptide stocks: Lyophilized synthetic phosphopeptides (*see* **Note 1**).
2. Phosphate standard solution: 10 mM K_2HPO_4 (or Na_2HPO_4) in water. Serially dilute to generate a set of concentrations between 0 and 40 μM (e.g., 4, 8, 16, 24, 32, and 40 μM) for creating standard curves. Use either water (for determining phosphopeptide concentration) or phosphatase reaction buffer (for enzyme assays) for the dilutions.
3. Phosphate detection reagent: BIOMOL GREEN™ (Enzo Life Sciences), store at 4 °C. Remove the appropriate volume required for an assay and allow it to reach room temperature (*see* **Note 2**).
4. 1 g Sep-Pak® C18 columns (Waters Corporation).
5. C18 mobile-phase solvents: Prepare 15 ml each of 5, 10, 20, 50, and 95 % acetonitrile (ACN) solutions, each containing 0.1 % trifluoroacetic acid (TFA).
6. Methanol.
7. α-Cyano-4-hydroxycinnamic acid: 5 mg/ml in 75 % ACN, 0.1 % TFA.
8. 50 mm borosilicate glass tubes.
9. Ashing reagent: 10 % $MgNO_3 \cdot 6H_2O$ in 95 % ethanol.
10. Phosphatase reaction buffer: 25 mM HEPES pH 7.5, 150 mM NaCl, 1 mM EDTA, 0.1 % β-mercaptoethanol (BME).
11. Purified recombinant Cdc14: Procedures for purification of recombinant Cdc14 fused to N-terminal 6×-histidine, glutathione S-transferase, or other affinity tags have been published (*see* ref. 14). We store purified Cdc14 in 25 mM Tris–HCl pH 7.5, 300 mM NaCl, 40 % glycerol, 2 mM EDTA, and 0.1 % BME in small aliquots at −80 °C. Working aliquots

are kept at –20 °C for up to 2 weeks. Dilute to 10× final concentration in phosphatase reaction buffer each day prior to use and keep on ice.

12. Clear plastic 96-well microplates suitable for measuring absorbance at visible wavelengths and/or semi-micro volume disposable cuvettes.
13. 15 ml conical tubes.

2.2 Intact Protein Dephosphorylation Assay

1. Kinase buffer: 10 mM HEPES pH 7.5, 10 mM $MgCl_2$, 50 mM NaCl, 10 % glycerol (*see* **Note 3**).
2. Phosphatase reaction buffer: 25 mM HEPES pH 7.5, 150 mM NaCl, 1 mM EDTA, 0.1 % BME.
3. Adenosine trisphosphate (ATP): 100 mM in 25 mM HEPES pH 7.5. Store at –20 °C.
4. 4× SDS sample buffer: 40 % glycerol, 240 mM Tris–HCl pH 6.8, 8 % SDS, 0.04 % bromophenol blue, 4 % BME.
5. Coomassie brilliant blue R-250: 0.05 % (w/v) in 25 % methanol, 10 % acetic acid.
6. Destain: 10 % acetic acid.
7. 100 mM ammonium bicarbonate (ABC) in water (must be made fresh).
8. Trypsin solution: 20 ng/μl proteomics-grade porcine trypsin in 100 mM ABC (*see* **Note 4**).
9. ACN.
10. Wash buffer: 50 mM ABC, 50 % ACN. Prepare by mixing 100 mM ABC and ACN at 1:1.
11. HPLC solvent A: 0.1 % formic acid.
12. HPLC solvent B: 95 % ACN, 0.1 % formic acid.
13. Purified proteins (*see* **Note 5**):
    (a) Cyclin-dependent kinase 1 (Cdk1) or other kinase.
    (b) Cdc14 or other phosphatase.
    (c) Protein substrate(s): Affinity-purified and retained on affinity beads.

3 Methods

3.1 Phoshopeptide Dephosphorylation Assay

Steps 1–9 are needed only for crude synthetic peptide stocks (*see* **Note 6**).

3.1.1 Substrate Preparation

1. Resuspend crude phosphopeptide in 2 ml of 0.1 % TFA (*see* **Note 7**). Remove and save ~3 μl pre-purification sample for MS analysis.

2. Condition a dry 1 g Sep-Pak® column with 3 ml methanol and then 3 ml 100 % ACN/0.1 % TFA (*see* **Note 8**). Drain the column by gravity flow for each step. Equilibrate column 2× with 3 ml 0.1 % TFA.
3. Apply peptide solution to the column and collect the flow through as one fraction in a 15 ml conical tube.
4. Wash column 2× with 3 ml 0.1 % TFA. Save the flow-through for MS analysis.
5. Step elution: Apply 3 ml 5 % ACN/0.1 % TFA to column and collect 1 ml fractions. Repeat with 3 ml 10, 20, and 50 % ACN/0.1 % TFA. There should be 12 total elution fractions.
6. Strip column 2× with 3 ml 100 % ACN/0.1 % TFA, collecting 1.5 ml fractions for analysis (*see* **Note 9**).
7. Analyze the elution fractions, starting peptide solution, and wash fractions by MALDI-TOF MS to find the desired phosphopeptide. A sample (typically 0.5 μl) of each fraction is spotted on the MALDI plate, and overlaid with 0.5 μl α-cyano-4-hydroxycinnamic acid solution (*see* **Note 10**).
8. Pool fractions containing the target peptide peak (based on MS intensity) and dry in a lyophilizer or centrifugal vacuum concentrator. Typically, the bulk of the peptide will be found in two to three fractions.
9. Resuspend phosphopeptide in water to the desired approximate concentration based on weight (make sure that it is fully soluble (*see* **Note 7**)—we usually start with 20 mM).
10. Add 50 μl of each phosphate standard solution (from above) or 50 μl of water to a 50 mm borosilicate glass tube (providing 0, 0.2, 0.4, 0.8, 1.2, 1.6, and 2 nmol phosphate). In triplicate, add two different volumes of purified phosphopeptide solution to separate tubes to achieve nmol amounts within this same range.
11. Add 25 μl ashing reagent to each tube. Mix and evaporate to dryness (an oven at ~50 °C works well).
12. Using a Bunsen burner, carefully heat the bottom of each tube until the brown fumes disappear and a white residue appears. Avoid prolonged heating, as black particles will form.
13. Allow tubes to cool in a rack and then dissolve the white residue in phosphate detection reagent (*see* **Note 11**).
14. Incubate for 20 min at room temperature and measure the absorbance at 640 nm in clean, phosphate-free cuvettes or microplate. The sample containing only water is used as a blank (*see* **Note 12**).

15. Create a standard curve of absorbance versus phosphate concentration and use it to calculate the concentration of the phosphopeptide solution.
16. Store phosphopeptide stocks in small aliquots at –80 °C to minimize freeze-thaw cycles. Prepare working stocks by diluting in phosphatase reaction buffer immediately prior to use. Prepare only the volume required for use each day.

3.1.2 Assay

1. Dispense 40 µl phosphatase reaction buffer per well in a 96-well plate and add 5 µl of phosphopeptide per well to achieve the desired final concentration. For Cdc14 endpoint assays we typically use substrates at 100 µM (*see* **Note 13**).
2. Add 5 µl of 10× Cdc14 working stock to each reaction well, mix thoroughly but carefully with a pipette to avoid creating bubbles, and incubate plate at 30 °C for 30 min (*see* **Note 14**).
3. Dispense 50 µl of each phosphate standard prepared above in reaction buffer into wells of the 96-well plate. Include one well with just 50 µl reaction buffer.
4. Add 100 µl of phosphate detection reagent to all wells to stop reaction and initiate color development. Incubate for 20 min at room temperature, and measure the absorbance at 640 nm in a plate reader.
5. Create a standard curve (as in Subheading 3.1.1, **step 15**) to calculate reaction rates from the absorbance values.

3.2 Intact Protein Dephosphorylation Assay

Keep proteins ice cold except where other incubation temperatures are noted.

3.2.1 Substrate Preparation (See **Note 15**)

1. Starting with affinity-purified substrate protein immobilized on the affinity matrix, equilibrate approximately 100 µg substrate by rinsing twice with several volumes kinase buffer, pelleting the resin at 1000 × *g* for 2 min, and discarding the supernatant (*see* **Note 16**).
2. Add 1 bead volume kinase buffer and ATP to 1 mM. Mix gently to resuspend the substrate-bound resin. Mix gently.
3. Add purified Cdk1 to the protein substrate resin, mix gently, and incubate suspension at 30 °C for 30 min (*see* **Note 17**).
4. Pellet the resin by centrifugation at 1000 × *g* for 2 min and discard the supernatant.
5. Wash the resin three times with at least 3 resin volumes of phosphatase reaction buffer to remove the kinase. Gently mix the solution each time and centrifuge at 1000 × *g* for 2 min. Carefully remove the supernatant and discard.
6. Optional: It is recommended to evaluate phosphorylation either by MS, using the procedure described below for the phosphatase assay, or by an alternative method such as Phos-Tag™ SDS-PAGE mobility shift.

3.2.2 Assay

The phosphatase assay can be conducted with the substrate still bound to the affinity resin, or after the substrate has been eluted. Here, we describe our procedure for assaying recombinant glutathione S-transferase-tagged substrates bound to glutathione-agarose resin (*see* **Note 18**).

1. Resuspend the resin with bound phosphorylated substrate in 4 volumes phosphatase reaction buffer.
2. Divide the resin into four equal aliquots (or additional aliquots if more time points are desired).
3. Add 4× SDS sample buffer to one aliquot and heat at 95 °C for 5 min. This will serve as the reference time = 0 sample.
4. Add Cdc14 to the remaining fractions at a final concentration of 100 nM and mix thoroughly by gentle agitation (*see* **Note 19**).
5. Incubate the reactions at 30 °C. Add 4× SDS sample buffer to one aliquot every 10 min (or other suitable time intervals) and heat immediately at 95 °C for 5 min (*see* **Note 20**).
6. Pellet the resin at 1000 × *g* for 2 min and transfer each supernatant to a low-bind microfuge tube.
7. Subject each sample to SDS-PAGE and stain with Coomassie blue. Destain thoroughly and store in ultrapure water prior to processing for MS analysis.

3.2.3 Peptide Preparation for MS Analysis

1. Excise bands of interest from gels using a clean razor blade. Chop each into roughly a half dozen smaller pieces and transfer to a low-bind microfuge tube (*see* **Note 21**).
2. Add 100 µl of wash buffer and incubate for 30 min, vortexing occasionally. Remove wash buffer and repeat until gel pieces are destained.
3. Add 500 µl ACN and incubate until gel pieces are dehydrated and appear small and white.
4. Remove and discard ACN. Air-dry gel pieces for 10 min.
5. Add enough trypsin solution to cover the gel pieces (typically 30–40 µl) and wait for 30 min to allow rehydration. Add additional trypsin solution to completely submerge gel pieces if necessary. Incubate overnight at 37 °C.
6. Add ACN (2× trypsin solution volume used) and incubate for 15 min at room temperature, vortexing occasionally. Transfer liquid to a new low-bind microfuge tube.
7. Repeat peptide extraction by rehydrating gel slices with 40 µl water for 10 min, adding 80 µl of ACN, incubating for 15 min, and pooling liquid with the first extraction.
8. Dry extracted peptides in a centrifugal vacuum concentrator or freeze and dry by lyophilization.

3.2.4 Liquid Chromatography-Mass Spectrometry (LC-MS) Acquisition and Analysis

The following protocol should be generally applicable for a wide variety of nanospray LC-MS systems.

1. Resuspend the dried peptides in a small volume of HPLC solvent A to a concentration suitable for MS analysis (typically ~0.2 μg/μl). Excess material may be stored at −80 °C (*see* **Note 22**).
2. Inject 1 μg (typically 5 μl) onto a C18 trap column and wash with HPLC solvent A.
3. Resolve the sample with a linear gradient from 5 to 40 % HPLC solvent B through a microcapillary C18 column and a nanoelectrospray emitter tip at a flow rate of ~300 nl/min (*see* **Note 23**).
4. Acquire MS survey and data-dependent MS/MS fragmentation scans during the entire linear gradient (*see* **Note 24**).
5. After data acquisition, peptides must be identified and quantified. Here we describe a procedure for identification of peptides using the Mascot database search engine and manual quantification of changes in abundance across time points. However, other options will work equally well (*see* **Note 25**).
6. Mascot is accessed from www.matrixscience.com. Parameter settings may vary depending on the instrument and other factors. The standard parameter settings that we use for peptide identification with the Mascot MS/MS Ions Search algorithm are presented in Table 1 (*see* **Note 26** for more detailed information on search settings).
7. Once peptides have been identified, the extracted ion current (XIC) for all phosphopeptides and for several non-phosphorylated "standard" peptides (minimum 4) must be obtained. An XIC simply represents the HPLC trace for a specific mass/charge value during the LC-MS experiment (*see* Fig. 1). The software from most instrument vendors includes functions for manually generating XICs for ions of interest. Alternatively, some freely available software packages, including MaxQuant (www.maxquant.org), will generate XICs automatically for all identified peptides (*see* **Note 27**). The procedure we describe is suitable for analysis of singly phosphorylated peptides. Analysis of peptides with multiple phosphorylation sites is more complicated.
8. The raw phosphopeptide XIC signals for each time point must be corrected using the non-phosphorylated standard peptides to account for sample-to-sample signal variation. We have used different approaches for this, but the simplest to implement is the following (*see* Fig. 2): (1) Normalize the XIC signals for all non-phosphorylated standard peptides and phosphopeptides, such that time = 0 is set to 1 and all other time points represent a fraction of the time = 0 signal. (2) Average these normalized values from the standard peptides to obtain a set of correction

Table 1
Mascot MS/MS ions search settings

Parameter	Setting
Database(s)	SwissProt
Enzyme	Trypsin
Allow up to # missed cleavages	2
Taxonomy	Select appropriate species
Fixed modifications	None, unless optional alkylation has been performed
Variable modifications	Oxidation (M), Phospho (ST), and/or Phospho (Y)
Peptide tolerance (ppm)	±10
MS/MS tolerance (Da)	±0.25
Peptide charge	+2, +3, and +4
Mass value	Monoisotopic
Data file	Locate and upload raw data file
Data format	Mascot accepts MGF, DTA, ASC, PKL, PKS, Sciex API III, XML, and mzML file formats
Instrument	Select type of instrument used

All parameters not listed can be left at their default settings

factors, one for each time point (the value for time = 0 will be 1). (3) Divide the normalized phosphopeptide values by the appropriate correction factor to obtain adjusted fractional phosphopeptide signals. With a robust instrument and carefully prepared samples, the corrections should be minimal (*see* **Note 28**).

9. Finally, generate dephosphorylation plots of the adjusted phosphopeptide signals. Time = 0 will be 1 and the other time points will represent the fraction of phosphopeptide remaining (*see* Fig. 2). The plots can generally be fit with an exponential decay equation to quantitatively compare rates of dephosphorylation.

4 Notes

1. Custom phosphopeptides are readily obtained commercially. Phosphopeptide length as well as the position of the phosphorylation site can vary according to need or preference. For Cdc14, we typically select a sequence of ~16 amino acids centered on the phosphorylated residue, or a sequence of ten amino acids with the phosphorylated residue at position 3. Both versions seem to yield similar results. Examples of phosphopeptide substrates used extensively for characterization

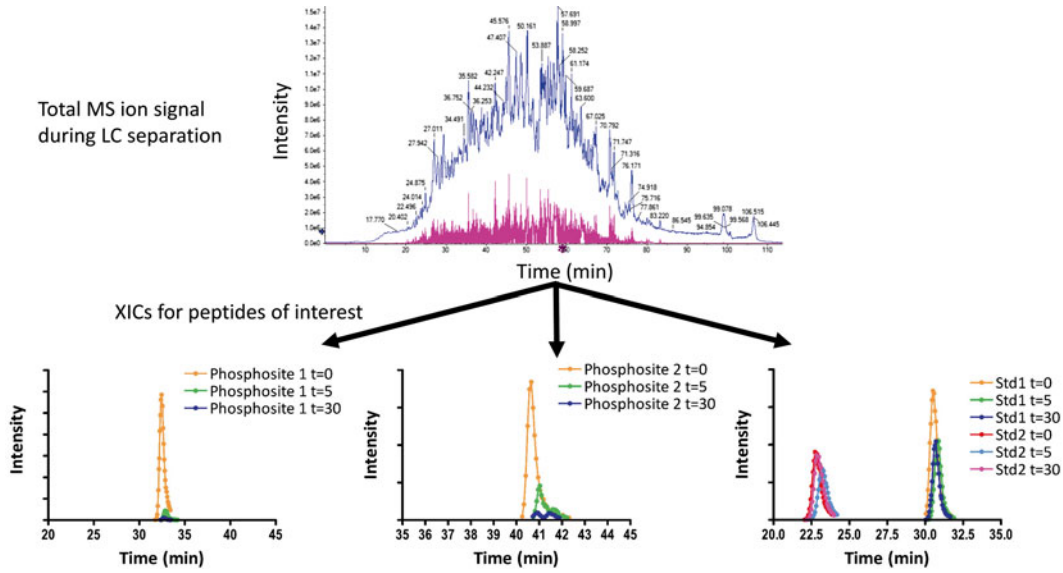

Fig. 1 Extraction of MS ion signals from LC-MS data. Raw LC-MS files are a composite of a broad range of measured mass/charge signals over the time course of an HPLC separation (*top plot, blue trace*). From this raw data, the mass/charge signal for specific peptides of interest, in this case two phosphopeptides (phosphosites 1 and 2) and two unphosphorylated standard peptides (Std1 and Std2), must be extracted (*bottom three plots*). Such plots are termed extracted ion currents, or XICs, and are obtained using software tools typically supplied with MS instruments. They require only the measured mass/charge value of the peptides of interest, obtained from the database search used to identify the peptides present

of budding yeast Cdc14 are VKGNELR**S**PSKRRSQI and MI**S**PSKKRTIL derived from the Acm1 protein [14]. Peptides are synthesized with an amide group at the C-terminus.

2. Other formulations of the malachite green/ammonium molybdate dye are commercially available as well. Vendor-specific instructions for use of other reagents should be followed. In addition, ammonium molybdate and malachite green reagents can be made and used as described [20].
3. The kinase buffer is optimized for budding yeast cyclin-dependent kinase 1 (Cdc28-Clb2 complex). The kinase buffer may need to be altered if other purified kinases are being used to create phosphoprotein substrates.
4. In our experience, unused trypsin solution can be stored in aliquots at −80 °C with minimal loss of activity. Alternatively, for long-term storage, resuspend trypsin at 100 ng/μl in 1 mM HCl and store in aliquots at −20 °C. Adjust pH and concentration with fresh 100 mM ABC prior to use.
5. Budding yeast Cdk1 can be purified as described [21]. Alternative protocols for Cdk1 purification from budding yeast or other species should be suitable but have not been evaluated. Cdc14 can be purified as described in Subheading 2.1, **item 11**, for the peptide assay. Substrates, either recombinant

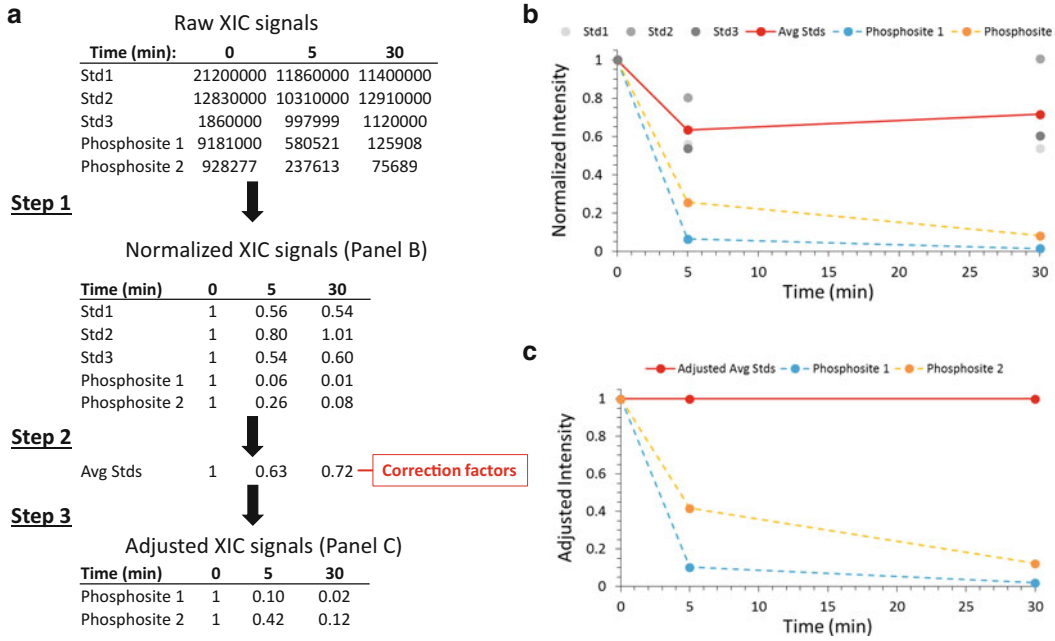

Fig. 2 Generation of dephosphorylation plots and normalization of XIC signals. Integration of XIC peaks shown in Fig. 1 provides quantitative values for plotting as a function of time during the phosphatase assay (*top table in panel* a) but these values must be adjusted first to correct for variation in sample processing, instrument performance, and other factors. In step 1 the raw XIC values for each peptide have been normalized by dividing each by the value at time = 0. This makes the first time point equal to 1 and the other time points a fraction relative to the first time point. A plot of these normalized values is shown in *panel* b. Notice that the signal for the standards varies between time points. In step 2 the normalized XIC values for just the standard peptides are averaged (*red line in panel* b) to create a set of correction factors, one for each time point. In step 3 the normalized phosphopeptide XIC signals are divided by the correction factor from the corresponding time point to generate the final adjusted XIC values that are plotted in *panel* c. Notice that the effect of this procedure is to correct the average standard peptide signals to 1, satisfying the assumption that the average abundance of these unphosphorylated standard peptides should be constant over time (*red line in panel* c). With additional data points, the adjusted phosphopeptide plots can be fit with an exponential decay equation to calculate rates of dephosphorylation

or from the native source, should be affinity purified and retained/stored on the affinity matrix until use. We commonly use a glutathione S-transferase fusion for affinity purification of substrate proteins expressed in *E. coli*. For recombinant substrates, affinity resin should be washed and resuspended in kinase buffer. For native substrates that are already phosphorylated, proteins can be left on the matrix or eluted into phosphatase reaction buffer or other suitable storage buffer.

6. If phosphopeptides are synthesized commercially, many companies also provide purification for an additional cost, eliminating the need for **steps 1–9**, Subheading 3.2.1. To achieve higher purity, conventional reverse-phase HPLC with a C18 column and ACN gradient elution can be employed as an alternative to the procedure described here.

7. Peptide solubility varies greatly. If solubility is a problem, lower concentrations or different solution conditions may be needed for the resuspension step.
8. We use 1 g Sep-Pak® 6 cc Vac cartridges (Waters catalog #186004621) for crude phosphopeptides up to 50 mg (a typical prep is 10 mg of crude phosphopeptide). A variety of Sep-Pak® C18 sizes are available to accommodate different peptide amounts.
9. Sep-Pak® columns can be regenerated and stored for repeated use by washing 3× with 3 ml methanol and then air-drying the column.
10. If MALDI-TOF or other MS analysis is not readily available, peptides should be purchased pre-purified. This routine MS analysis can often be provided by a core facility.
11. For measurements in semi-micro plastic cuvettes use 500–1000 µl. For 96-well plates use 100–200 µl.
12. Malachite green dye has a broad absorbance peak; thus any wavelength from 600 to 680 nm can be used.
13. The assay volume can be scaled down for use in high-throughput analyses in 384-well plates or scaled up for use with individual plastic cuvettes and a conventional spectrophotometer. Endpoint assays at a single substrate concentration below the K_M are an effective way to compare catalytic efficiency of many different substrates. Alternatively, k_{cat} and K_M values can be determined by measuring the reaction rate across a range of substrate concentrations.
14. We use a final concentration of 50–100 nM Cdc14 when optimal substrates are being assayed. Higher concentrations are needed for less efficient substrates. For other phosphatases, optimal enzyme concentrations as well as reaction times and temperatures may differ from those employed here. The amount of substrate consumed in reactions must be less than 10 % of the initial value.
15. This procedure is optimized for cyclin-dependent kinase 1 (Cdk1) and Cdc14 and may require modification to accommodate other protein kinases and phosphatases.
16. It is useful to obtain an estimate of the amount of substrate protein isolated on the affinity matrix. The most practical approach is to elute the substrate from a small, defined fraction of the matrix and perform a Bradford or BCA protein assay using commercially available reagents.
17. The goal is to achieve stoichiometric modification of substrate phosphorylation sites, and therefore the kinase concentration should be high and the incubation time may need to be adjusted. The stoichiometry of phosphorylation can usually be

estimated from the LC-MS data simply by comparing the signal intensity of phosphorylated and unphosphorylated peptide species.

18. For antibody-based affinity captures, it may be advantageous to elute substrates from the resin (e.g., by competition with antigenic peptide) prior to the phosphatase reaction, particularly if the substrate protein might co-migrate on SDS-PAGE with one of the antibody chains. The reducing agent required in the phosphatase reaction buffer may cause dissociation of antibody disulfide bonds leading to high levels of free antibody chains on SDS-PAGE in the subsequent steps.
19. We use 100 nM Cdc14 for substrates containing phosphosites efficiently targeted by Cdc14. The concentration of Cdc14 may need to be increased or decreased in accordance with the protein's efficacy as a substrate.
20. The appropriate incubation time will vary depending on the substrate, the substrate concentration, and the enzyme concentration and must be optimized.
21. Use gloves and a clean, dust-free environment when handling and processing gels to minimize keratin contamination. Use dedicated gel plates and staining trays cleaned only with isopropanol, and avoid handling them without gloves. Additional information on in-gel digest procedures, including optional cysteine reduction and alkylation steps, can be found here [22].
22. Peptide concentration can be difficult to measure accurately. To avoid consuming part of the sample we estimate the amount of protein from the Coomassie blue-stained gel band and assume 100 % protein digestion and 100 % peptide recovery from the in-gel digest.
23. We typically use a 60-min gradient, but shorter times may be sufficient for analysis of peptides derived from single proteins. In cases where a larger number of protein substrates are evaluated simultaneously, gradient length can be increased to enhance the number of peptides detected.
24. Specific method parameters will vary depending on the instrument. This includes flow rate, number and duration of MS/MS acquisitions per cycle, fragmentation settings, electrospray voltages, and dynamic exclusion window.
25. Use of Mascot with large LC-MS data files requires a license. Any database search program capable of identifying peptides and modified peptides should be suitable and several commonly used and freely accessible options exist. More detailed descriptions of the procedure for manual quantitation of phosphopeptide signals have been published elsewhere [14, 18, 21].

26. Notes on Mascot search parameter settings: Database—any database that contains the sequence of the protein(s) being analyzed will work. Enzyme—we have described the procedure for preparing samples by digestion with trypsin, but other site-specific endoproteinases can be used as well, particularly if specific phosphorylation sites of interest are not detected using trypsin. It is necessary to select the enzyme that was used to prepare the peptide samples. Fixed modifications—if the optional alkylation of cysteines has been performed with iodoacetamide during the in-gel digestion then "carbamidomethyl (C)" must be selected as a fixed modification. Variable modifications—oxidation (M) is not essential to select. However, in our experience, peptides containing methionine are almost always detected in both reduced and oxidized states. Peptide and MS/MS tolerance—these settings depend on both the type of mass analyzer and the quality of the calibration. The indicated values are our standard settings for a quadrupole-TOF instrument. Other analyzers may require very different tolerance settings. For example, Orbitraps may accommodate a more stringent peptide tolerance whereas conventional ion traps will require much less stringent peptide and MS/MS tolerances. The mass accuracy of an instrument can easily be determined using a collection of peptide standards. Peptide charge—this setting is overridden when the charge state of precursor peptides is provided in the LC-MS data file, as it almost always will be. Therefore this setting can usually be ignored. Mass value—this should always be set to monoisotopic unless a low-resolution analyzer is used that is not able to distinguish individual peptide isotope peaks. Data format—for instruments that generate raw data files in a proprietary format not supported by Mascot, conversion to one of these supported formats is required. Software is generally provided by instrument vendors for file conversion to nonproprietary formats and freely available tools exist as well.
27. Generation of an XIC for a peptide requires only its measured mass/charge value. Because multiple ions could have similar mass/charge values (this will become more frequent with increasing sample complexity), it is important that the XIC peaks used for quantitative analysis be matched to an MS/MS spectrum that identifies the peptide. An MS/MS spectrum identifying the peptide from at least one of the samples defines the peptide's LC retention time. The integrated XIC peak should match this retention time. MaxQuant will perform both the peptide identification step using the Andromeda search algorithm and the generation of integrated XIC values for all identified peptides. Information on use of MaxQuant has been published [23, 24] and is available from the MaxQuant website, www.maxquant.org.

28. The more non-phosphorylated peptides used to determine correction factors for each time point the better. We use a minimum of four. Try to select peptides that give a strong MS signal, do not have missed protease cleavage sites, and lack methionine and cysteine. Discard any peptide whose profile deviates dramatically from the average peptide profile.

References

1. Brautigan DL (2013) Protein Ser/Thr phosphatases—the ugly ducklings of cell signalling. FEBS J 280:324–345
2. Bollen M, Gerlich D, Lesage B (2009) Mitotic phosphatases: from entry guards to exit guides. Trends Cell Biol 19:531–541
3. Trinkle-Mulcahy L, Lamond A (2006) Mitotic phosphatases: no longer silent partners. Curr Opin Cell Biol 18:623–631
4. Virshup DM, Shenolikar S (2009) From promiscuity to precision: protein phosphatases get a makeover. Mol Cell 33:537–545
5. Wurzenberger C, Gerlich DW (2011) Phosphatases: providing safe passage through mitotic exit. Nat Rev Mol Cell Biol 12: 469–482
6. Fisher D, Krasinska L, Coudreuse D et al (2012) Phosphorylation network dynamics in the control of cell cycle transitions. J Cell Sci 125:4703–4711
7. Olsen JV, Vermeulen M, Santamaria A et al (2010) Quantitative phosphoproteomics reveals widespread full phosphorylation site occupancy during mitosis. Sci Signal 3:ra3
8. Hardie DG (1999) Protein phosphorylation: a practical approach. Oxford University Press, London
9. Moorhead G (2007) Protein phosphatase protocols. Humana Press, Totowa, NJ
10. Zhou B, Zhang Z-Y (2003) Measuring protein phosphatase activity with physiological substrates. Methods Enzymol 366:34–43
11. Geladopoulos TP, Sotiroudis TG, Evangelopoulos AE (1991) A malachite green colorimetric assay for protein phosphatase activity. Anal Biochem 192:112–116
12. Sheng Z, Charbonneau H (1993) The baculovirus Autographa californica encodes a protein tyrosine phosphatase. J Biol Chem 268: 4728–4733
13. Taylor GS, Liu Y, Baskerville C et al (1997) The activity of Cdc14p, an oligomeric dual specificity protein phosphatase from Saccharomyces cerevisiae, is required for cell cycle progression. J Biol Chem 272:24054–24063
14. Bremmer SC, Hall H, Martinez JS et al (2012) Cdc14 phosphatases preferentially dephosphorylate a subset of cyclin-dependent kinase (Cdk) sites containing phosphoserine. J Biol Chem 287:1662–1669
15. Clifford DM, Chen CT, Roberts RH et al (2008) The role of Cdc14 phosphatases in the control of cell division. Biochem Soc Trans 36:436–438
16. Mocciaro A, Schiebel E (2010) Cdc14: a highly conserved family of phosphatases with non-conserved functions? J Cell Sci 123: 2867–2876
17. Stegmeier F, Amon A (2004) Closing mitosis: the functions of the Cdc14 phosphatase and its regulation. Annu Rev Genet 38:203–232
18. Eissler CL, Mazon G, Powers BL et al (2014) The Cdk/Cdc14 module controls activation of the Yen1 holliday junction resolvase to promote genome stability. Mol Cell 54:80–93
19. Chin CF, Bennett AM, Ma WK et al (2012) Dependence of Chs2 ER export on dephosphorylation by cytoplasmic Cdc14 ensures that septum formation follows mitosis. Mol Biol Cell 23:45–58
20. Buss JE, Stull JT (1983) Measurement of chemical phosphate in proteins. Methods Enzymol 99:7–14
21. Eissler CL, Bremmer SC, Martinez JS et al (2011) A general strategy for studying multisite protein phosphorylation using label-free selected reaction monitoring mass spectrometry. Anal Biochem 418:267–275
22. Shevchenko A, Tomas H, Havlis J et al (2006) In-gel digestion for mass spectrometric characterization of proteins and proteomes. Nat Protoc 1:2856–2860
23. Cox J, Mann M (2008) MaxQuant enables high peptide identification rates, individualized p.p.b.-range mass accuracies and proteome-wide protein quantification. Nat Biotechnol 26:1367–1372
24. Cox J, Neuhauser N, Michalski A et al (2011) Andromeda: a peptide search engine integrated into the MaxQuant environment. J Proteome Res 10:1794–1805

Chapter 14

Combining the Optimized Yeast Cytosine Deaminase Protein Fragment Complementation Assay and an In Vitro Cdk1 Targeting Assay to Study the Regulation of the γ-Tubulin Complex

Po Hien Ear, Jacqueline Kowarzyk, Michael J. Booth, Diala Abd-Rabbo, Kristian Shulist, Conrad Hall, Jackie Vogel, and Stephen W. Michnick

Abstract

Cdk1 is the essential cyclin-dependent kinase in the budding yeast *Saccharomyces cerevisiae*. Cdk1 orchestrates cell cycle control by phosphorylating target proteins with extraordinary temporal and spatial specificity by complexing with one of the nine cyclin regulatory subunits. The identification of the cyclin required for targeting Cdk1 to a substrate can help to place the regulation of that protein at a specific time point during the cell cycle and reveal information needed to elucidate the biological significance of the regulation. Here, we describe a combination of strategies to identify interaction partners of Cdk1, and associate these complexes to the appropriate cyclins using a cell-based protein-fragment complementation assay. Validation of the specific reliance of the OyCD interaction between Cdk1 and budding yeast γ-tubulin on the Clb3 cyclin, relative to the mitotic Clb2 cyclin, was performed by an in vitro kinase assay using the γ-tubulin complex as a substrate.

Key words Yeast cyclin-dependent kinase (Cdc28 or Cdk1), Cyclin, Optimized yeast cytosine deaminase protein-fragment complementation assay (OyCD PCA), Budding yeast γ-tubulin (Tub4)

1 Introduction

Cyclin-dependent protein kinases (Cdk) are regulatory enzymes whose temporal and spatial selectivity for specific substrate proteins rely on their association with cyclin partner proteins [1]. In the budding yeast *Saccharomyces cerevisiae*, the essential and only Cdk, Cdk1 (Cdc28) binds to one of the nine available cyclin partner proteins (Cln1, Cln2, Cln3, Clb1, Clb2, Clb3, Clb4, Clb5, or Clb6) to recognize and phosphorylate their substrates [2]. The different

The original version of this chapter was revised. The erratum to this chapter is available at: DOI 10.1007/978-1-4939-2957-3_22

Amanda S. Coutts and Louise Weston (eds.), *Cell Cycle Oscillators: Methods and Protocols*, Methods in Molecular Biology, vol. 1342, DOI 10.1007/978-1-4939-2957-3_14, © Springer Science+Business Media New York 2016

Cdk1-cyclin complexes bind to and phosphorylate target proteins involved in orchestrating all of the processes necessary for cell division. Unlike Cdk1, cyclin concentrations vary throughout the cell cycle with the G1 cyclins, Cln1-3, peaking prior to START in G1, Clb3-6 peaking in S phase, and Clb1 and Clb2 peaking at the metaphase-anaphase transition [1, 3]. Identifying novel Cdk1 substrates and the cyclin(s) that mediate specific Cdk1-substrate interactions remains challenging due to the transient nature of the complexes and the low abundance of certain proteins forming these complexes [4, 5]. Additionally, some Cdk1 substrates are targeted for degradation upon phosphorylation (e.g., the yeast securin, Pds1 [6, 7]). Finally, a substrate of Cdk1 may be context/location dependent and thus be only a small fraction of the total pool of protein at a particular phase of the cell cycle. For example, phosphorylation of budding yeast γ-tubulin (Tub4) by Cdk1 occurs at the spindle pole, and cannot be detected in cytoplasmic pools or in asymmetric cells [8]. In this chapter we use Tub4 as an example, illustrating an in vivo strategy to identify a Tub4-specific cyclin necessary for its phosphorylation by Cdk1 and detailed methods for demonstrating Cdk1-cyclin-specific phosphorylation of Tub4 in vitro.

Tub4 is phosphorylated by Cdk1 at serine (S) 360, which lies in an evolutionarily conserved Cdk1 recognition motif found in both budding yeast and humans [8]. Keck et al. detected phosphorylated S360 in the subpopulation of Tub4 bound to purified spindle pole bodies, which represents ~10 % (~600 molecules) of the estimated total 7200 molecules of Tub4 in the cell [3, 9]. Phosphorylated S360 are specific to cells arrested in metaphase by inactivation of the anaphase-promoting complex, a condition in which cells have high levels of both early (Clb3,4) and late (Clb1,2) mitotic cyclins. Identification of the specific cyclin that mediates the interaction between Cdk1 and Tub4 is both a major challenge and key to understanding the biological significance of S360 phosphorylation, and requires a sensitive cell-based method of detection.

We previously reported a simple survival-selection screening method to detect protein-protein interactions in vivo based on the optimized yeast cytosine deaminase protein-fragment complementation assay (OyCD PCA) [10]. The OyCD PCA involves expressing two proteins of interest (bait and prey) fused to the amino (N)- or carboxyl (C)-termini of the OyCD fragments, OyCD-F[1] and OyCD-F[2] (i.e., proteinX-OyCD-F[1] and proteinY-OyCD-F[2]) and testing for their interaction in a yeast strain in which the gene expressing cytosine deaminase has been deleted. When the bait and prey proteins interact, the OyCD fragments rapidly fold and reconstitute the active yCD enzyme. The activity can be detected by either using an OyCD PCA death selection assay, where the reconstituted enzyme makes cells sensitive to the 5-fluorocytosine (5-FC) prodrug, or using an OyCD PCA survival selection assay, where *ura3Δ* cells with the reconstituted OyCD enzyme are able to convert cytosine to uracil and survive on minimal medium [10].

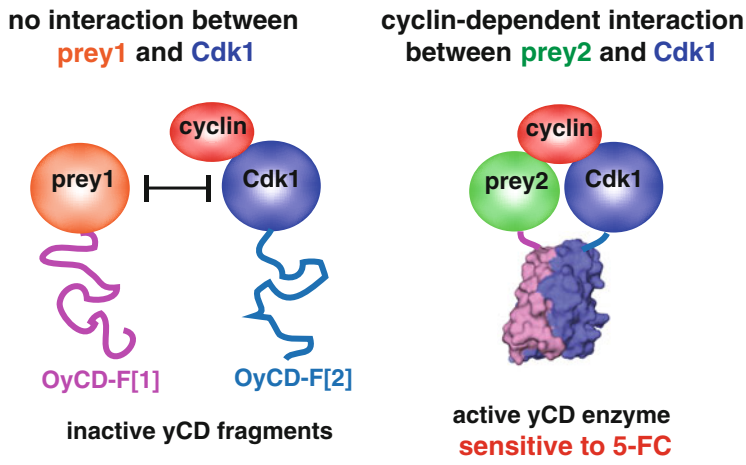

Fig. 1 Detecting protein-protein interactions between Cdk1 and candidate substrates (preys) using the death assay. Determine the activity of the OyCD PCA for Cdk1 and its preys in a yeast strain harboring all nine cyclin genes. Express each prey with Cdk1 fused to OyCD reporter fragments in yeast. Prey1 does not interact with Cdk1; cells are resistant to 5-FC. Prey2 interacts with Cdk1; cells are sensitive to 5-FC

The death selection assay of the OyCD PCA is particularly suitable for systematically identifying proteins ("prey") that interact with Cdk1 based on sensitivity to 5-FC (*see* Fig. 1).

To determine which cyclin(s) are required for recognition of a substrate by Cdk1, Cdk1:test-protein interactions are tested in a set of yeast strains with each strain bearing a null mutation in one of the nine cyclin genes (*see* Fig. 2a). For example, a Cdk1 substrate (prey2) interaction is shown to depend on Clb5 because when the OyCD PCA death assay is performed in a knockout strain for the *CLB5* gene (*clb5Δ*), death following treatment with 5-FC is prevented (*see* Fig. 2b). In the case of Tub4, we discovered that Clb3 is the mediator of the Cdk1-Tub4 interaction [11]. These cases are exceptional in that the Cdk1-substrate interaction could be attributed to a single cyclin. The majority of Cdk1-substrate interactions are mediated by more than one cyclin [11].

The early mitotic cyclin Clb3 is expressed concomitantly with the formation of microtubules at the newly duplicated mitotic spindle pole [1] and is known to regulate early steps in the process of mitotic spindle assembly [12, 13]. The identification of Clb3 as the cyclin that mediates interaction of Cdk1 with Tub4 is further tested by an in vitro kinase assay. We tested for phosphorylation of Tub4 by Cdk1-Clb3 relative to Cdk1-Clb2 using a purified, reconstituted γ-tubulin complex—the γ-tubulin small complex or γ-TUSC [14], which preserves the in vivo context of γ-tubulin (*see* Fig. 2a). The γ-tubulin complexes can be either γ-TUSCs or larger assemblies such as rings or filaments, contain Tub4, Spc97, Spc98, and an N-terminal fragment of the receptor protein Spc110,

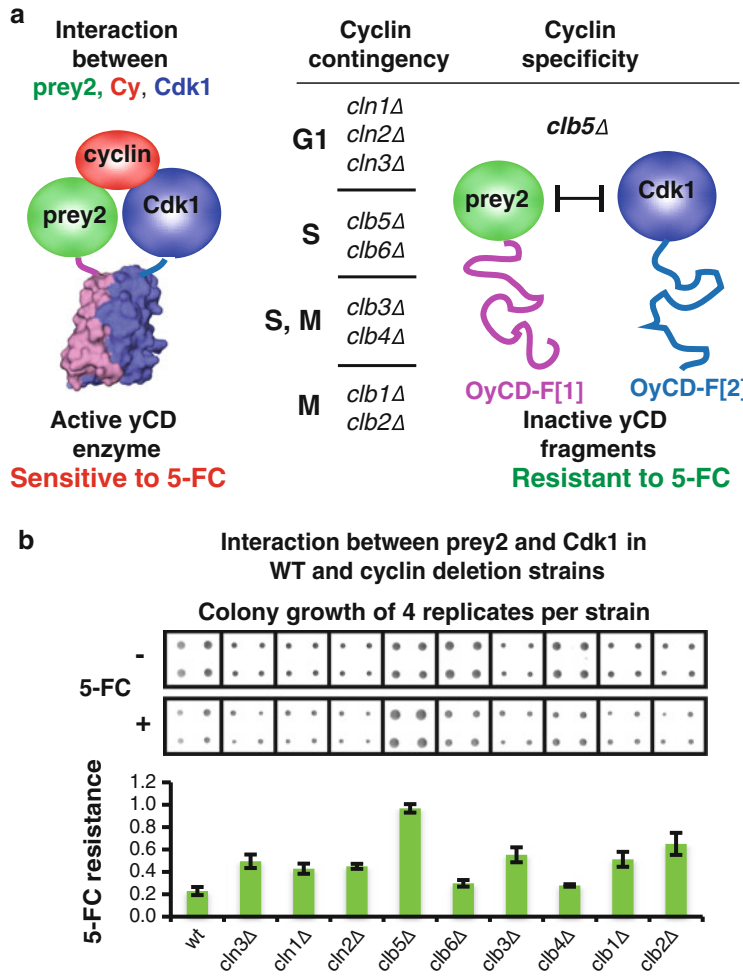

Fig. 2 Cyclin contingency tests using the death assay. (**a**) The presence of cyclin mediates the interaction between Cdk1 and a candidate substrate, resulting in sensitivity to 5-FC. If a cyclin is required for maintaining the interaction between Cdk1 and the prey protein, removal of the cyclin will block the interaction between Cdk1 and the substrate (Prey2), and cells will be resistant to 5-FC. (**b**) Example of cyclin contingency, showing resistance to 5-FC in a *CLB5* knockout strain (*clb5*Δ). Colony growth of 4 replicates per cyclin deletion strain, in the presence and absence of 5-FC, is shown. 5-FC resistance is determined by calculating the integrated intensity of each colony grown in the presence of 5-FC over the integrated intensity of colonies grown in the absence of 5-FC

is purified from Sf9 insect cells (*see* Fig. 3b) and treated with KCl to form γ-TUSCs. The structure of the complex is first verified by electron microscopy (*see* inset a, Fig. 3b). The specificity of Cdk1-Clb3 to Tub4 relative to Cdk1-Clb2 is shown in parallel in vitro kinase assays using purified Cdk1-Clb2 and Cdk1-Clb3 complexes (*see* Fig. 3b).

In a parallel study, we found that a phosphomimetic mutant of S360 decreases the number of the interpolar microtubules

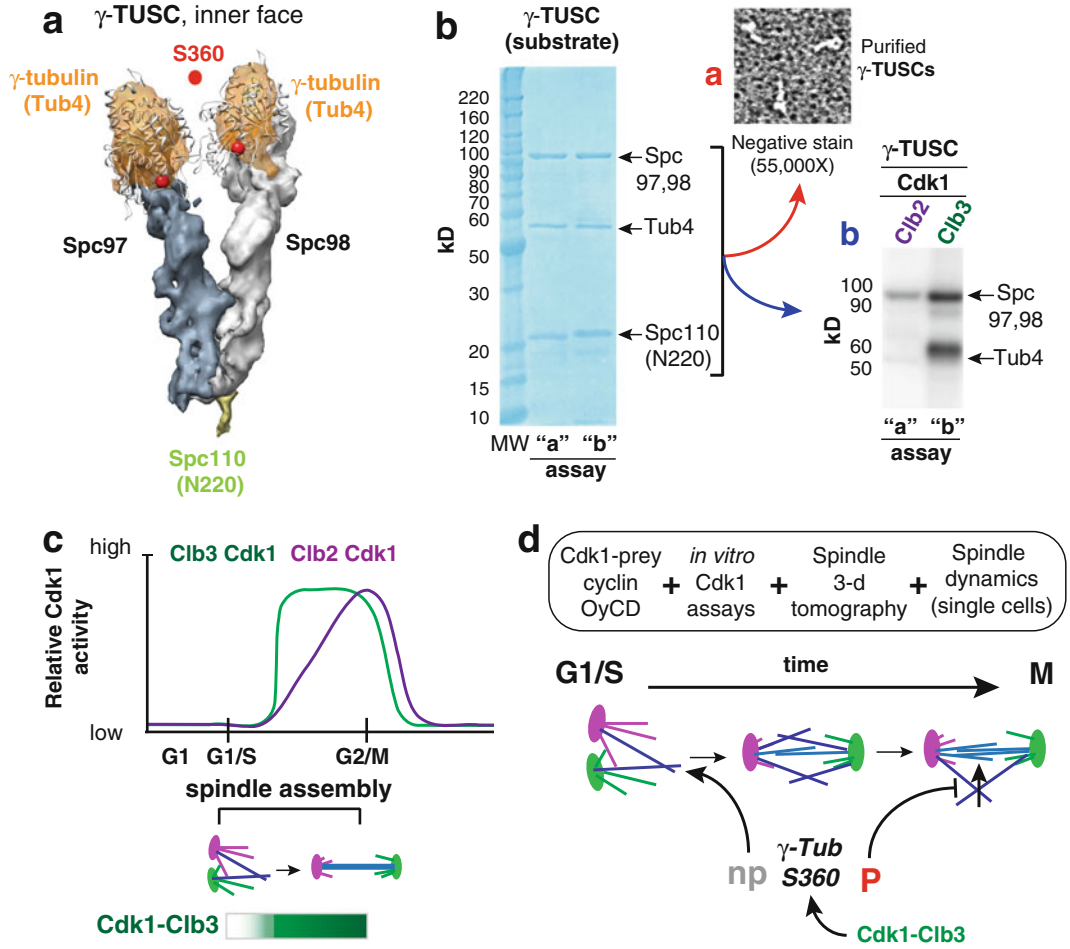

Fig. 3 Tub4 within the γ-TUSC is targeted by Cdk1-Clb3 in vitro. (**a**) The reconstituted γ-TUSC is composed of two molecules of Tub4, one molecule of Spc97 and of Spc98, and at least one molecule of an N-terminal fragment of Spc110 (Spc110-N220). (**b**) The purified complex is treated with KCl to form γ-TUSCs (shown in *inset a*) and used for in vitro kinase assays using purified Cdk1-Clb2 and Cdk1-Clb3 complexes (shown in *inset b*). (**c**) Clb3 levels rise as cells enter S phase, concomitant to the formation of ip-MTs, an early step in spindle assembly. (**d**) Results from multiple types of experiments suggest a mechanism by which Cdk1-Clb3 phosphorylation controls the number of ip-MTs by blocking their formation as cells approach metaphase

(ip-MTs) that are formed during the earliest steps in spindle assembly [15]. Conversely, a S360A (alanine) phospho-inhibiting mutation increased the number of intermediates in ip-MT formation [15]. The identification of Cdk1-Clb3 interaction with Tub4 in the OyCD PCA screen suggested that the phosphorylation of S360 occurs early in spindle assembly during the formation of ip-MTs (*see* Fig. 3c). The OyCD and kinases assays, in combination with electron tomography of nm-scale microtubule organization within spindles, and microscopic measurements of spindle dynamical behaviors supports a novel role of Cdk1-Clb3 in controlling the number of ip-MTs formed during spindle formation. We have

shown that ip-MTs form when Clb3 levels are low, and S360 phosphorylation inhibiting the formation of new ip-MTs as cells progress through S phase and complete spindle assembly (*see* Fig. 3d).

Below we provide detailed protocols to perform the cell-based OyCD PCA to identify Cdk1-cyclin complexes that recognize specific substrates and in vitro biochemical methods to validate the in vivo-determined Cdk1-cyclin-substrate interactions using Tub4 and the yeast γ-tubulin small complex (γ-TUSC) as examples [15].

Finally, we note that all of the OyCD PCA expression plasmids are Gateway destination vectors (pAG413GAL1-ccdB-OyCD-F[1] and pAG415GAL1-ccdB-OyCD-F[2]). It is thus straightforward to create C-terminal fusion constructs with the OyCD reporter fragments and test many pair-wise protein-protein interactions in parallel for Cdk1-substrate interactions or any interactions one may want to test.

2 Materials

2.1 Strains, Reagents, and Media Used for OyCD Assays

2.1.1 Enzymes

AccuPrime Pfx DNA polymerase, BP Gateway clonase, and LR Gateway clonase enzyme mixes are purchased from Invitrogen or other vendors.

2.1.2 Bacteria and Yeast Strains

1. DH5α bacterial competent cells.
2. Competent BY4741 *MAT***a** (*his*3Δ 1; *leu*2Δ 0; *met1*5Δ 0; *ura*3Δ 0) yeast strains with *fcy1*Δ single-gene deletion and with double-gene deletions to create cyclin deletion strains (deletion of *fcy1*Δ and one of the cyclins (*cln1*Δ, *cln2*Δ, *cln3*Δ, *clb1*Δ, *clb2*Δ, *clb3*Δ, *clb4*Δ, *clb5*Δ, or *clb6*Δ)) [16] prepared according to Knop et al. [17].

2.1.3 Bacteria Media

LB plates with 1.5 % (wt/vol) agar and 100 μg/mL of ampicillin or 50 μg/mL of kanamycin.

2.1.4 Yeast Media

1. SC-His-Leu: Synthetic complete solid medium lacking histidine and leucine with 2 % (wt/vol) glucose, and 2 % (wt/vol) agar petri plates.
2. SC-His-Leu+glucose+G418: Synthetic complete medium lacking histidine and leucine with 2 % (wt/vol) glucose and 200 μg/mL (wt/vol) of G418 with or without 3 % (wt/vol) agar.
3. SC-His-Leu+raffinose: Synthetic complete liquid medium lacking histidine and leucine with 2 % (wt/vol) raffinose.

4. OyCD selection plates: Synthetic complete solid medium lacking histidine and leucine with 2 % (wt/vol) raffinose, 2 % (wt/vol) galactose, 200 μg/mL of G418, and 3 % agar in NUNC omniplates with or without 1 mg/mL of 5-FC.
5. YPD liquid: 1 % (wt/vol) yeast extract, 2 % (wt/vol) peptone, 2 % (wt/vol) dextrose, 2 % (wt/vol) agar.
6. Deletion plates: YPD medium with 200 μg/mL G418, 100 μg/mL nourseothricin, 100 μg/mL 5-FC, and 2 % (wt/vol) agar plates (*see* **Note 1**).

2.1.5 Other Reagents

1. Dimethylsulfoxide (DMSO).
2. Galactose.
3. PLATE solution: 40 % PEG 3350, 100 mM lithium acetate, 10 mM Tris–HCl pH 7.5 and 0.4 mM EDTA.
4. Plasmid Miniprep kit.
5. Sorbitol buffer: 1 M sorbitol, 1 mM EDTA, 10 mM Tris–HCl pH 8.0, 100 mM lithium acetate.
6. Water (distilled and sterile).

2.1.6 Equipment

1. Omniplates (NUNC).
2. Pintool: Robotically manipulated (96 pintool (0.787 mm flat round-shaped pins, #FP3N, V&P Scientific Inc., San Diego, CA) and 384 pintool (0.457 mm flat round-shaped pins, custom #FP1N, V&P Scientific Inc., San Diego, CA)) or manually manipulated 96 pintool (1 μL slot pins, 1.58 mm, VP 408Sa, V&P Scientific Inc., San Diego, CA).
3. Plate imaging: At least a 4.0 Mega pixel camera (Powershot A520, Canon), a stationary arm (70 cm mini repro, Industria Fototecnica Firenze, Italy), and a plate-shooting platform.

2.2 Cells, Reagents and Media, and Equipment Used for γ-TUSC Purification

2.2.1 Cells (Sf9 and Bacterial)

1. Sf9 cells (a clonal isolate of *Spodoptera frugiperda* Sf21 cells).
2. pFastBac vectors (Invitrogen).
3. DH5α *E. coli* cells (pFastBac).
4. DH10BAC *E. coli* cells for bacmids (Invitrogen).

2.2.2 Reagents and Media for Bacterial Manipulation

1. Standard LB medium with 100 μg/mL ampicillin (DH5α cells).
2. LB medium supplemented with 50 μg/mL kanamycin, 7 μg/mL gentamicin, and 10 μg/mL tetracycline.
3. Standard SOC medium (pFastBac transformation).

4. DH10BAC plates: LB plates (or broth) supplemented with 50 μg/mL kanamycin, 7 μg/mL gentamicin, 10 μg/mL tetracycline, with or without 100 μg/mL X-gal and 40 μg/mL isopropyl β-d-1-thiogalactopyranoside (IPTG).

2.2.3 Reagents and Media for Sf9 Cell Culture, Protein Expression, and Protein Purification

1. Gibco SF900II media (Life Technologies) with 7 μg/mL gentamicin. Alternatively, Multicell I-Max serum-free media for insect cells (Wisent) can also be used as a less expensive option.
2. DMSO.
3. Escort IV transfection reagent (Sigma-Aldrich; Sf9 transfection).
4. Fetal calf serum (FCS) from Gibco (Life Technologies; BIIC stocks).
5. HB100 buffer: 40 mM HEPES, 1 mM EGTA, 1 mM $MgCl_2$, 100 mM KCl with 1 mM DTT, and 100 μM GTP added fresh, pH 7.5 (γ-TUSC purification).
6. KCl stock solution: 1 M in HB100 buffer.
7. Roche PhosSTOP phosphatase inhibitor cocktail and Roche cOmplete protease inhibitor cocktail [14].
8. TEV protease [18].
9. SF9 freezing solution: 90 % SF900II + 10 % DMSO.

2.2.4 Equipment

1. CASY cell counter (Roche Innovatis).
2. Heraeus multifuge 3S-R centrifuge (Thermo Scientific).
3. 45Ti Beckman Coulter centrifuge.
4. Micro Bio-Spin Chromatography columns (Bio-Rad).
5. Glutathione-Sepharose 4B resin (GE Healthcare).
6. Glass Dounce homogenizer.

2.3 Strains, Reagents and Media, and Equipment Used for In Vitro Kinase Assays

2.3.1 Strains

1. Yeast strains expressing Clb3-TAP and Clb2-TAP from the GAL1 promoter in a 2μ plasmid (URA3; described in Koivomagi et al. [19]).

2.3.2 Reagents and Media for Cdk1-Cyclin Purification

1. Synthetic complete medium without uracil (SC–ura) with 2 % galactose.
2. TAP affinity resins, binding, and elution buffers [20].

2.3.3 Reagents Used for In Vitro Kinase Assays

1. Kinase buffer (KB), 10× stock (Cell Signaling).
2. Cold ATP: 100 μM in 1× KB.

3. γ^{32}P-ATP 3000 Ci/mmol 10 mCi/ml, 100 μCi (Perkin-Elmer).
4. 4× SDS sample buffer: 0.25 Tris–HCl pH 6.8, 8 % SDS, 40 % glycerol, 0.008 % bromophenol blue. Add β-mercaptoethanol (β-ME) to 10 % before using.
5. Histone control substrate or γ-TUSC substrate: 0.4 μM.
6. Purified Clb2-Cdk1 (2 nM in 1× KB) and Clb3-Cdk1 (5 nm in 1× KB).

2.3.4 Equipment

1. Refrigerated centrifuges for pelleting cells from liquid culture, clarification of whole-cell lysates, and separation of lysates from resin.
2. Bead beater or Reutch P 100 cryo grinder (recommended) for yeast cell lysis.
3. SDS-PAGE and gel casting equipment for mini gels (Biorad).
4. Gel imaging station (MBI).
5. Phosphorimager: Typhoon Trio (GE).

3 Methods

3.1 Deletion of the FCY1 Gene in Wild-Type and in Cyclin Deletion Strains

Timeline for generating *FCY1* knockout yeast: 4–7 days.

A list of plasmids and oligonucleotides used for the OyCD interaction assay is provided in Table 1.

1. Use the following oligos to amplify the nourseothricin resistance gene from the pAG25 plasmid [12] using the AccuPrime *Pfx* DNA polymerase.
   Forward-FCY1-KO oligo:
   TGAGAGCCAGCTTAAAGAGTTAAAAATTTCATAGC TAATGGCGCCAGATCTGT
   TTAGCTT
   Reverse-FCY1-KO oligo:
   ATAAAATTAAATACGTAAATACAGCGTGCTGCGTG CTCTAGGTTAACCTGGCTTATCGAA
2. Transform each cyclin deletion strain (available from Open Biosystems) with the PCR product: Mix 50 μL of thawed competent cells with 5 μL (2 μg) of the PCR-amplified cassette DNA encoding the *NAT1* resistance marker. Mix and incubate for 30 min at room temperature. Add 500 μL of PLATE solution and 50 μL of DMSO followed by heat shock at 42 °C for 20 min. Centrifuge at 805 × *g* for 3 min, remove the supernatant, and resuspend cells in 1 mL YPD medium; incubate at 30 °C with shaking for 4 h. Centrifuge the cells, remove the supernatant, resuspend the cells in 200 μL of liquid YPD, and plate on the deletion plates (*see* **Note 1**).

Table 1
Plasmid and oligonucleotide list

Plasmids and oligos	Description	Reference or company
BG1805 plasmids with your genes of interest	Gateway yeast ORF collection expression clones	GE/Dharmacon/ Open Biosystems
pDONR221	Gateway donor vector	Invitrogen
pAG413GAL1-ccdB-Linker-OyCD-F[1] pAG415GAL1-ccdB-Linker-OyCD-F[2]	Gateway destination vector: to generate fusion genes with the OyCD reporter fragments, using the Gateway technology. OyCD-F[1]: amino acid residues 1–77 of yCD with A23L point mutation. OyCD-F[2]: amino acid residues 57–158 of yCD with the following point mutations: V108I, I140L, T95S, and K117E	Ear et al. [11]
pAG25 plasmid	Contains nourseothricin resistance gene which is used to knock out *FCY1* gene	Goldstein et al. [12]
p415GAL1-Cdk1-Linker-OyCD-F[2]	Used to study PPIs with Cdk1	Ear et al. [11]
p415GAL1-Linker-OyCD-F[2]	Serves as negative control when used alone	Ear et al. [10]
p413GAL1-GCN4 leucine zippers-Linker-OyCD-F[1] p415GAL1-GCN4 leucine zippers-Linker-OyCD-F[2]	Positive control plasmid pair	Ear et al. [10]
Forward-FCY1-KO oligo	TGAGAGCCAGCTTAAAGAGTTAAAAATTTCATAGCTAATGGCGCC AGATCTGTTTAGCTT	Ear et al. [11]
Reverse-FCY1-KO oligo	ATAAAATTAAATACGTAAATACAGCGTGCTGCGTGCTCTAGGTT AACCTGGCTTATCGAA	Ear et al. [11]

3. Incubate the plates at 30 °C for 3–5 days. Colonies can be further verified by colony PCR methods.

   Pause point: Prepare a glycerol stock of the correct strains and store at −80 °C (*see* **Note 2**).

3.2 OyCD PCA for Identification of Cdk1 Interacting Partners (Fig. 4)

Timeline for OyCD assays

BP reaction: 3 days.

LR reaction: 3 days.

Test for protein-protein interactions (PPIs) with Cdk1: 5 days.

Test PPIs with Cdk1 in the different cyclin deletion strains: 14 days.

1. Select genes from the Yeast ORF Collection (BG1805, expression clones) to transfer into a Gateway donor vector (pDONR221) to obtain ENTRY clones using the Gateway BP reaction. Perform a diagnostic PCR to determine the presence of your gene of interest or send the plasmids (ENTRY clones) for sequencing.

   Pause point: Store plasmids at −20 °C.

2. Perform the LR reaction with the ENTRY clones and the destination vector (pAG413GAL1-ccdB-OyCD-F[1]) to obtain the expression plasmid (pAG413GAL1-GeneX-OyCD-F[1]). Confirm by diagnostic PCR for the presence of your gene of interest or send the expression plasmids for sequencing.

   Pause point: Store plasmids at −20 °C (*see* **Note 3** and Table 1).

3. Transform each expression plasmid (pAG413GAL1-GeneX-OyCD-F[1]) into BY4741 *fcy1*Δ yeast containing either p415GAL1-Cdk1-OyCD-F[2] or p415GAL1-Linker-OyCD-F[2]. Mix 10 μL of cells with 200 ng of each yeast expression plasmid, 60 μL of PLATE solution, and 8 μL DMSO. Heat shock the yeast at 42 °C for 20 min. Centrifuge at 805 × *g* for 3 min. Remove the supernatant and resuspend cells in 50 μL sterile water; plate the cell suspension on SC-His-Leu. Incubate at 30 °C for 3 days (*see* **Notes 4** and **5**).

4. Inoculate colonies from each transformation in a 96-well plate containing 400 μL of SC-His-Leu+raffinose, and incubate in a 30 °C shaking incubator for 16 h.

   Pause point: Prepare a glycerol stock of yeast harboring the two plasmids and store at −80 °C.

5. Add galactose to each culture at a final concentration of 2 % (wt/vol) and incubate at 30 °C for more than 1 h to induce the expression of the OyCD fusion proteins.

6. Pin the samples onto OyCD selection plates using manual or robotic pintools according to what is available in your laboratory (*see* **Note 6**).

7. Incubate the plates at 30 °C for 2–3 days. Take pictures of the plates at days 2 and 3.

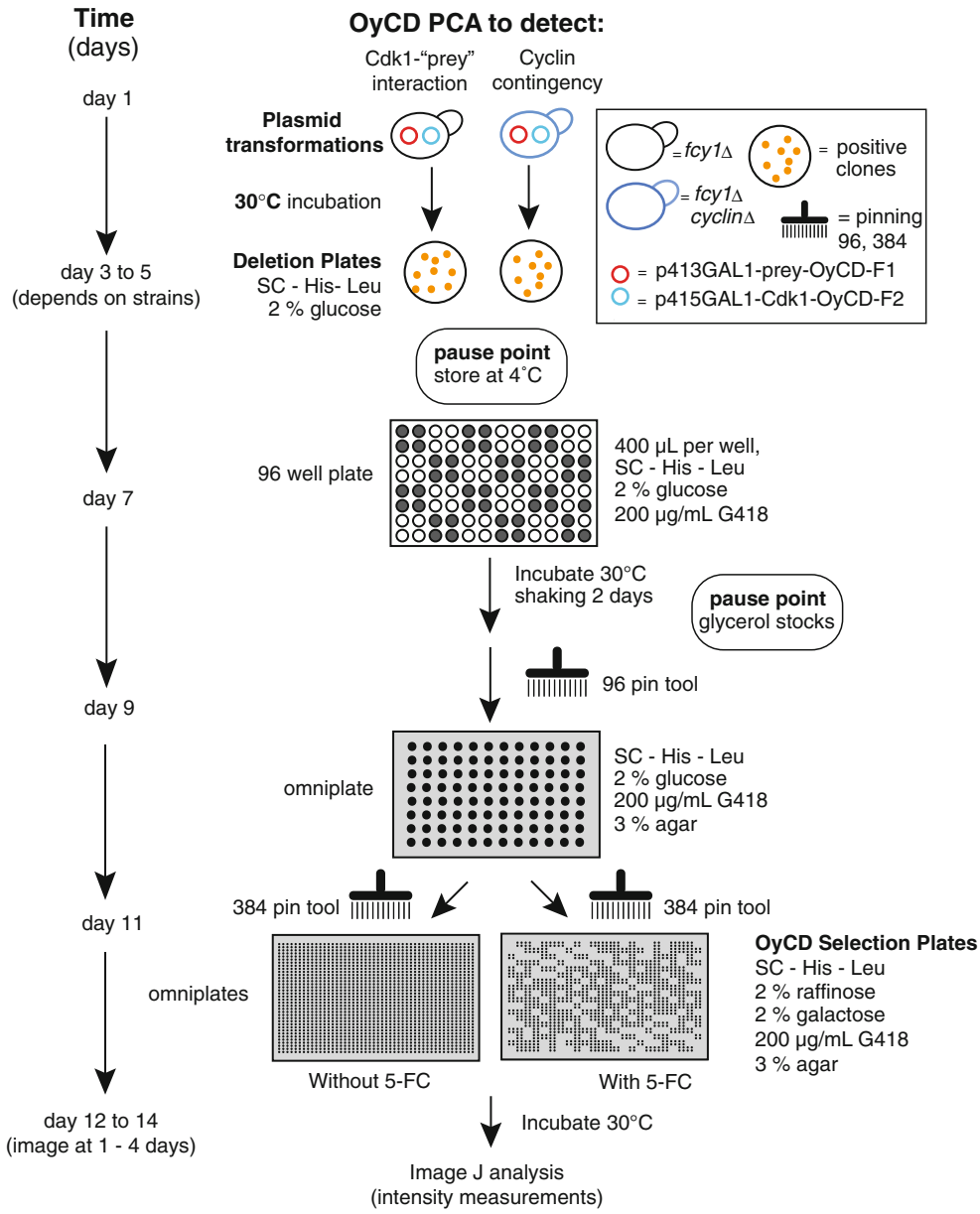

Fig. 4 Workflow chart for detecting protein-protein interaction between Cdk1 and its potential substrates in different yeast strains using the OyCD protein-protein interaction assay. Determine the activity of the OyCD PCA for Cdk1 and its potential substrates in a yeast strain harboring all nine cyclin genes or in different cyclin deletion strains. Transform yeast strains with expression plasmids carrying Cdk1 and its potential substrates fused to OyCD reporter fragments. Select for positive clones by plating onto deletion plates. Inoculate four positive clones per strain in a 96-well plate containing 400 µL per well of SC liquid medium-His-Leu with 2 % glucose and 200 µg/mL of G418. Grow with shaking to saturation and prepare glycerol stocks. Pin glycerol stocks onto an omniplate containing SC agar medium-His-Leu with 2 % glucose and 200 µg/mL G418 to reach, as much as possible, a uniform colony growth. Perform OyCD PCA by pinning onto OyCD selection plates. If a prey protein (potential substrate) does not interact with Cdk1, cells are resistant to 5-FC. If a prey protein interacts with Cdk1, cells are sensitive to 5-FC. For OyCD PCA activity in different cyclin deletion strains: If a cyclin is required for maintaining the interaction between Cdk1 and the prey protein, removal of the cyclin will affect 5-FC sensitivity. All growth steps are done at 30 °C

3.3 Detecting Protein-Protein Interactions in Wild-Type or Cyclin Deletion Strains (Fig. 4)

1. Screen the interaction between Cdk1 and its potential substrate in yeast strains expressing all nine cyclin genes or lacking one of the nine cyclin genes. The potential substrate genes fused to the OyCD-F[1] sequence in Gateway expression vectors are co-transformed with p415GAL1-Cdk1-OyCD-F[2] into the *FCY1* deletion (*fcy1*Δ) strain and the nine single-cyclin and *FCY1* double-deletion strains (*see* **Note 4**). *See* Subheading 3.2, **step 3**, for transformation protocol.
2. Inoculate four clones from each transformation and grow them to saturation in SC-His-Leu+glucose+G418.
   Pause point: Prepare glycerol stocks of these cultures and store at −80 °C.
3. Pin all samples from their glycerol stock onto plates containing the same medium with 3 % agar and grow for 4 days.
4. For evaluating the OyCD PCA activity, pin the colonies onto OyCD selection plates using a robotically manipulated 384 pintool.
5. Take pictures after 1, 2, 3, and 4 days of incubation at 30 °C.
6. Cell growth is quantified using ImageJ [21] by calculating the integrated intensity of each colony. The activity of the OyCD PCA is measured by taking the ratio of integrated intensity of each colony grown on 1 mg/mL of 5-FC over the integrated intensity of colonies grown in the absence of 5-FC (*see* **Note 7**).

3.4 Purification of Budding Yeast γ-TUSCs (See Fig. 5)

Timeline for γ-TUSC expression and purification

Bacmid transposition and glycerol stock production: 5 days.

Growing Sf9 cells from a frozen stock: 7–14 days.

Bacmid DNA preparation: 2 days.

Preparation of P1 virus stock: 5–7 days.

Preparation of BIIC stocks: 3–4 days (not including the time it takes to grow initial Sf9 cell culture).

Transfection with γ-TUSC BIIC stocks: 13–15 days (not including the time it takes to grow initial Sf9 cell culture).

γ-TUSC purification from frozen Sf9 cells: 1–2 days.

1. pFastBac vectors (Invitrogen) containing one of each of the four γ-TUSC components (Tub4, Spc97, Spc98, and an N-terminal fragment of Spc110; a gift from Trisha Davis [22]) are transformed into DH5α and subsequently miniprepped to generate plasmid stocks.
2. In order to transpose the γ-TUSC components into Sf9 compatible bacmids, the four pFastBac vectors are transformed into DH10BAC *E. coli* cells (Invitrogen) as per the manufacturer's instructions. Briefly: 0.2 μL of each pFastBac vector containing one of the γ-TUSC components is added to 100 μL of DH10BAC cells. The cell mixture is incubated on ice for

30 min, heat shocked at 42 °C for 45 s, and then incubated on ice for 2 min. Nine-hundred microliters of SOC medium is added to the cells, which are then incubated at 37 °C with shaking for at least 4 h. 10 and 90 % of the mixture are plated on two separate DH10BAC plates. Plates are incubated at 37 °C for at least 36 h. Ideally, one of the plate dilutions should result in 100 colonies per plate to optimize blue/white colony selection.

3. Pick large, white colonies (indicative of cells with recombinant bacmids) and resuspend in 10 μL of sterile water. The white colonies are screened for proper transposition using colony PCR.
4. Three microliters of a positive colony-water mixture is added to 2 mL of LB medium supplemented with 50 μg/mL kanamycin, 7 μg/mL gentamicin, and 10 μg/mL tetracycline. The culture is grown at 37 °C to stationary phase (up to 24 h).

   Pause point: A glycerol stock is made from the bacterial cultures and kept at −80 °C for future use.
5. One to two weeks before transfection of the bacmids into Sf9 cells, the Sf9 cells are passaged and grown in SF900II media with gentamicin until there are two volumes of 25 mL of cells at a density of 1×10^6 cells/mL. To start the culture, a 1 mL Sf9 frozen DMSO stock is rapidly thawed at 27 °C and then added to 10 mL of SF900II media with gentamicin. This culture is incubated at 27 °C with shaking until the cell density reaches about 4×10^6 cells/mL. Cell density is measured using a CASY cell counter. The cells are passaged once by diluting back to 2×10^6 cells/mL in 20 mL of SF900II media with gentamicin and then allowed to grow with shaking at 27 °C until the cell density reaches 4×10^6 cells/mL again. The culture is passaged as before in 20 mL media. On the third passage, the cells are diluted back to 1×10^6 cells/mL into two volumes of 25 mL of SF900II media with gentamicin (*see* **Note 8**).
6. Two to three days before transfection of the bacmids into Sf9 cells, the recombinant bacmids are isolated from the DH10BAC cells by growing up the positive γ-TUSC bacmid clones in LB medium supplemented with 50 μg/mL kanamycin, 7 μg/mL gentamicin, and 10 μg/mL tetracycline. The bacmids are isolated from 1.5 mL of stationary-phase culture using commercially available miniprep kits.

   Pause point: The purified bacmids can be stored at −20 °C for a few months, although repeated freeze/thawing and extended freezing can reduce transfection efficiency.
7. Each of the recombinant bacmids containing one of the γ-TUSC components is transfected separately into Sf9 cells (*see* below and day 11 of Fig. 5).

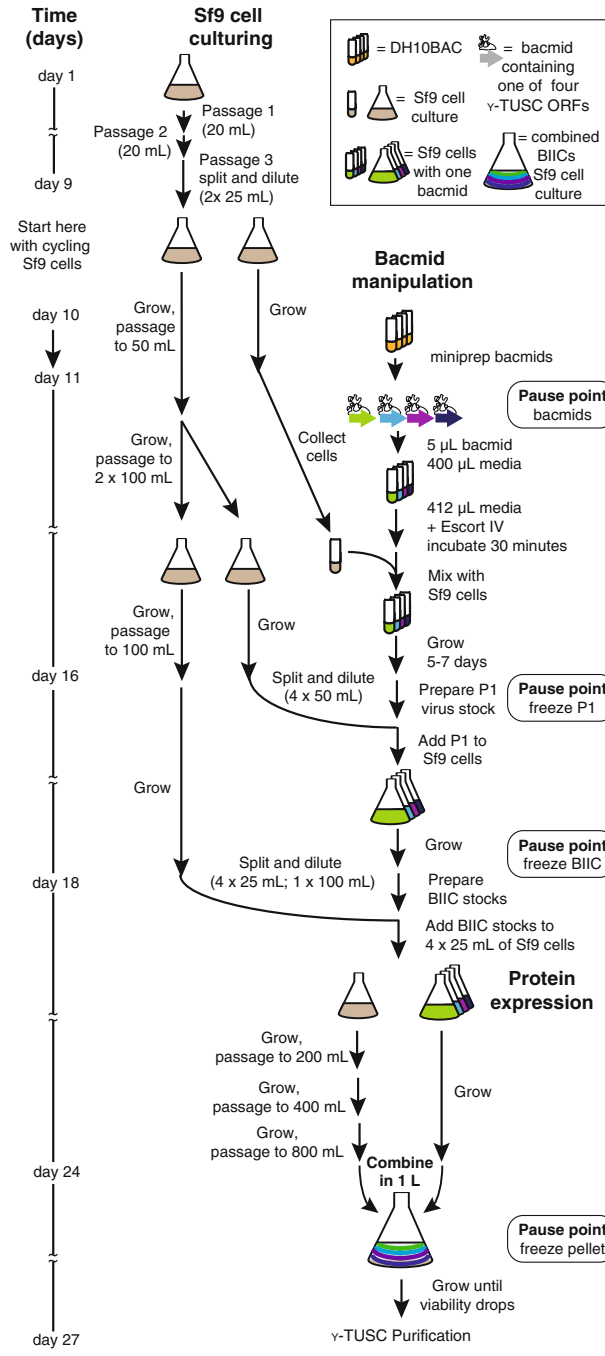

Fig. 5 Workflow chart for expression of the budding yeast γ-TUSC using Sf9 insect cells as a eukaryotic expression system. Sf9 cells must initially be cultured over an initial period of 9 days to obtain the desired cell concentration and volume for further manipulation. If cycling Sf9 cells already exist, then these steps may be skipped. Cultures of DH10BAC cells with bacmids containing each of the γ-TUSC components are set up 24 h prior to the day of transfection. Bacmid transfection into Sf9 cells occurs on day 11 after the bacmid miniprep. Transfection cell mixtures are grown for 5–7 days and are then used to prepare P1 virus stocks on day 16. The P1 virus stocks are added to fresh Sf9 cells in order to prepare the BIIC stocks on day 18. The BIIC stocks are then used to infect Sf9 cells. Once BIIC stocks have been made, Sf9 cells can be infected directly from the frozen stocks and all bacmid manipulation steps up until this point may be skipped (until BIIC stocks run out). BIIC-infected Sf9 cells are grown and then combined with uninfected cells to a 1 L final volume. This combined mixture is grown until cell viability drops to 85–89 %. Cells are then harvested and lysed for the γ-TUSC purification

8. A master mix of 400 μL of pre-warmed SF900II media with gentamicin and 12 μL of Escort IV reagent per transfection is mixed in a 15 mL conical tube.
9. A 400 μL aliquot of pre-warmed SF900II medium with gentamicin and 5 μL of each bacmid are added to four separate 15 mL snap-cap culture tubes.
10. A 412 μL aliquot of the SF900II media/Escort IV master mix is added to each snap-cap culture tube. The mixtures are incubated at room temperature for 30–45 min without shaking.
11. Measure the cell density of one of the two 25 mL volumes of Sf9 cells. A cell count of 2×10^6 cells/mL is ideal.
12. Calculate the volume required to obtain 1×10^7 cells (e.g., 5 mL of a 2×10^6 cells/mL culture yields a total cell count of 1×10^7 cells) and transfer the cells to a conical tube. The tube is centrifuged at $300 \times g$ in a Heraeus multifuge 3S-R centrifuge for 5 min at 27 °C.
13. The supernatant is decanted and the cells are washed once in 5 mL of pre-warmed SF900II medium, then centrifuged as before, and resuspended in 1 mL of pre-warmed SF900II medium with gentamicin.
14. A 200 μL aliquot of the concentrated cell mixture is added to each of the snap-cap tubes containing medium, Escort IV reagent, and a bacmid. This culture is then incubated at 27 °C for 5–7 days with shaking at 200 rpm. Check the culture daily for contamination and the presence of viral budding (indicating transfection).
15. Meanwhile, the second 25 mL culture of Sf9 cells is grown and passaged to 50 mL. Two days prior to the preparation of the P1 virus stocks (*see* **step 16**), cultures are diluted back to 1×10^6 cells/mL into two volumes of 100 mL of SF900II medium with gentamicin.
16. After the cultures have grown 5–7 days, P1 virus stocks are made (*see* Fig. 5, day 16). The cultures are transferred to conical tubes and centrifuged as before. The supernatants are filtered through 0.45 μm single-use sterile filters into 1.5 mL microfuge tubes, yielding ~500 μL per culture. This passage 1, or P1, virus stock can be stored at 4 °C for a few weeks.
17. The P1 virus stocks are then used to make baculovirus-infected insect cell stocks (BIIC stocks). One of the 100 mL volumes of Sf9 cells from **step 15** (at a final density of ~2×10^6) is used to prepare the BIIC stocks. The cell diameters are measured on a CASY cell counter and ideally are 18–19 μm.
18. FCS is added to the cell culture to a final concentration of 2 %, and then the cell culture is split and diluted into four 50 mL cultures at a concentration of 1×10^6 cells/mL. Each culture is

infected with 200 μL of one of the γ-TUSC P1 virus stocks (*see* Fig. 5, day 18).

19. The infected cells are placed at 27 °C for 36–48 h with shaking. The cells are monitored for diameter and cell density on a CASY cell counter.
20. Once the mean diameter of the cells reaches 22–23 μm, the culture is centrifuged as before and the supernatant is decanted.
21. The cell pellet is resuspended in 2 mL of Sf9 freezing solution (BIIC stock). Aliquots of 100 μL are prepared in cryotubes and are gradually frozen to −80 °C using a rack immersed in 100 % isopropanol.

    Pause point: The BIIC stocks can be kept at −80 °C but should be transferred to liquid nitrogen for long-term storage.
22. For purification of γ-TUSCs, the second 100 mL volume of Sf9 cells (from **step 15**) is grown until the cell density reaches 2×10^6 cells/mL. At this point, the culture is split and diluted into five flasks: four volumes of 25 mL and one volume of 100 mL, all at a cell density of 1×10^6 cells/mL (*see* Fig. 5, day 18).
23. A BIIC stock (100 μL) for each of the four γ-TUSC components is added to each of the four separate 25 mL volumes and the resulting cultures incubated with continuous shaking at 27 °C for about 1 week.
24. Meanwhile, the fifth volume of 100 mL of uninfected cells are grown and passaged as previously described (*see* **Note 8**), doubling the total volume of the cell culture at each passage until a final volume of 800 mL is reached.
25. Once the uninfected Sf9 cells reach a volume of 800 mL, the four flasks of 25 mL BIIC-infected cells are added to the 800 mL to make a final volume of 1 L of cells (*see* Fig. 5, day 24).
26. The cell density, cell diameter, and percent viability of the cells are measured using a CASY cell counter every 1–2 days. Once the culture reaches a percent viability of 85–89 % (the starting percent viability should be >95 %), the cells are harvested (*see* Fig. 5, day 27).
27. All subsequent steps are performed at 4 °C using HB100 buffer. A typical yield from 1 L of Sf9 cell culture is ~5 mL pellet. One liter of Sf9 cell culture is pelleted at $2000 \times g$ for 15 min.
28. The supernatant is poured off and 25–30 mL of HB100 buffer is added. The pellet is gently loosened off the side of the tube with a metal spatula and then transferred to a 50 mL conical tube.
29. The cell mixture is pelleted at $2000 \times g$ for 15 min. All the supernatant is removed.

    Pause point: The cell pellet may be flash frozen in liquid nitrogen in this point for future processing. Thaw the frozen pellet in a beaker of cold water before processing.

30. Whole-cell lysates are prepared by resuspending the cell pellet in 12.5 mL of HB100 buffer with 0.5 % Tween, and then using a 50 mL glass Dounce homogenizer pass 30 times for cell disruption.
31. Lysates are pre-cleared by centrifuging at 25,000 × *g* in a 45Ti Beckman Coulter rotor for 30 min.
32. During the centrifugation step, 500 μL glutathione-Sepharose 4B resin (GE Healthcare) per 1 L of final cell culture is transferred to a 50 mL conical tube, and then equilibrated by adding 9 mL of HB100 buffer, centrifuging at 500 × *g* for 5 min, removing the supernatant, and then repeating the wash.
33. After the second wash, enough supernatant is removed to leave the resin in 2 mL of buffer.
34. The clarified lysates are added to the equilibrated resin and incubated for 4 h on a nutator.
35. The resin with bound γ-TUSCs is centrifuged at 500 × *g* for 5 min and then washed once in 9 mL of HB100 buffer with 0.5 % Tween, and then twice in HB100 buffer.
36. The washed resin is transferred to a micro bio-spin chromatography column. Bound γ-TUSCs are cleaved from the resin by adding HB100 buffer with 5 μL of TEV protease (55 μM) and incubating on a nutator for 2 h.
37. The column is eluted and washed five to six times in HB100 buffer; each wash fraction is saved for further analysis. Typically, the first and second fractions contain the bulk of γ-TUSC, with a pooled concentration of 1.5 mg/mL as measured by Bradford assay. Sample homogeneity and the stoichiometry of the γ-tubulin complex components should be validated by SDS-PAGE (*see* Fig. 3b and **Note 9**).
38. Purified complexes, which can be in the form of rings filaments or γ-TUSCs [14], are diluted with HB100 buffer to 100 μg/mL. To produce predominantly γ-TUSCs (*see* inset b in Fig. 3b), KCl is added to 500 mM and the sample incubated on ice for 30 min.

3.5 Cdk1 Kinase Purification and Assays

Kinase purification: 1–2 days.

Kinase assay: 1–2 days.

Active Clb2-Cdk1 and Clb3-Cdk1 complexes are purified using the TAP method [20] as previously described [23] (*see* **Note 10**).

1. For each substrate, equivalent protein is used in the reactions for the two Cdk1-cyclin complexes. Reactions are run in parallel.
2. For each reaction, 100–200 ng of Cdk1-cyclin, 1–5 μg of substrate, 100 μM cold ATP, and 10 μCi γ^{32}P-ATP are

incubated for 30 min at 30 °C, and then the reaction is terminated by addition of 1/10th volume of β-ME and 1/4th volume of 4× SDS sample buffer.

3. Samples are run on an SDS-PAGE mini gel. Relative phosphorylation of Tub4, Spc97, and Spc98 by Cdk1-Clb2 and Cdk1-Clb3 are measured using a GE Typhoon Trio phosphorimager.

4 Notes

1. If no *fcyl*Δ and *cyclin*Δ double-mutant colonies are observed try optimizing the PCR reaction in order to get at least 100 ng of DNA/μL. Additionally use freshly made competent cells and increase the recovery time at 30 °C to 16 h instead of 4 h. To prepare 10 μg/mL stock solution of 5-FC, dissolve 100 μg of 5-FC in 10 mL of distilled water. Vortex the solution and incubate at 37 °C until it is dissolved. Filter the solution and use it right away or aliquot in sterile tubes and store at −20 °C.
2. The *fcy1*Δ yeast strain is the control strain in this screen and serves as a wild-type (wt) strain in the context of the OyCD Cdk1-prey assay since it expresses all nine cyclins.
3. If no colonies are observed some troubleshooting tips would be to try increasing the plasmid concentration, make sure that the enzymes have not lost their activity (get fresh enzyme if necessary), and ensure that your DH5α are high-efficiency competent cells.
4. Shorter or longer incubation times can result in decreased transformation efficiency. Use fresh competent cells in order to increase the transformation efficiency.
5. Before proceeding with a screen in the various cyclin deletion strains, verify that interactions between your proteins of interest can be detected by the OyCD PCA. Titrate the amount of 5-FC required for detecting your interactions. We normally try a range between 100 μg/mL and 1 mg/mL of 5-FC. For many cell cycle proteins and Cdk1 interactions, 1 mg/mL of 5-FC is required for detecting OyCD PCA activity. Use well-known interacting (Cdk1 and Swi6, or the homodimeric Gcn4 leucine zippers [Zip:Zip]) and non-interacting (Cdk1 and OyCD-F[2] alone) proteins as controls (Table 1).
6. Pintools exist in a variety of pin shapes and diameter sizes. 96 pintools generally come with thicker pins than 384 pintools. Hence, we advise using the latter to transfer liquid cultures (such as in Subheading 3.2, **step 6**). When transferring solid material (yeast colonies), first dip 96 or 384 pintools in autoclaved water or 75 % glycerol solution in order to homogenize

and dilute the colonies, and then perform the transfer. By doing so, technical variability between replicates can be reduced.

7. If there is no modulation of OyCD PCA activity in the deletion strain, it may be that the 5-FC concentration is too high. Try various 5-FC concentrations from 100 to 1000 μg/mL.
8. Once the Sf9 cells have been passaged a few times after reviving a frozen stock, it is best to continuously grow and passage 25–50 mL of cells so that they are available when needed. Grow the cells to 2×10^6 cells/mL and then passage them by diluting to 1×10^6 cells/mL.
9. The stoichiometry of the complex is 2 Tub4: 1 Spc97: 1 Spc98. Spc110-N220-GST is used as the bait for purification and will be the most abundant component. Typically Spc98 and Spc97 appear as a single band but may be resolved using an 8 % acrylamide gel.
10. Cdk1 kinase can be purified with cyclins bearing hydrophobic patch mutations to test the requirement for the RXL cyclin interaction domain on a given substrate [19], for example as an additional control for cyclin specificity for Cdk1 with Clb3-6.

References

1. Bloom J, Cross F (2007) Multiple levels of cyclin specificity in cell-cycle control. Nat Rev Mol Cell Biol 8:149–160
2. Mendenhall MD (1993) An inhibitor of p34CDC28 protein kinase activity from Saccharomyces cerevisiae. Science 259:216–219
3. Ghaemmaghami S, Huh WK, Bower K, Howson RW, Belle A, Dephoure N, O'Shea EK, Weissman JS (2003) Global analysis of protein expression in yeast. Nature 425: 737–741
4. Archambault V, Chang EJ, Drapkin BJ, Cross FR, Chait BT, Rout MP (2004) Targeted proteomic study of the cyclin-Cdk module. Mol Cell 14:699–711
5. Loog M, Morgan DO (2005) Cyclin specificity in the phosphorylation of cyclin-dependent kinase substrates. Nature 434:104–108
6. Agarwal R, Cohen-Fix O (2002) Phosphorylation of the mitotic regulator Pds1/securin by Cdc28 is required for efficient nuclear localization of Esp1/separase. Genes Dev 16: 1371–1382
7. Ubersax JA, Woodbury EL, Quang PN, Paraz M, Blethrow JD, Shah K, Shokat KM, Morgan DO (2003) Targets of the cyclin-dependent kinase Cdk1. Nature 425:859–864
8. Keck JM, Jones MH, Wong CC, Binkley J, Chen D, Jaspersen SL, Holinger EP, Xu T, Niepel M, Rout MP et al (2011) A cell cycle phosphoproteome of the yeast centrosome. Science 332:1557–1561
9. Kollman JM, Greenberg CH, Li S, Moritz M, Zelter A, Fong KK, Fernandez JJ, Sali A, Kilmartin J, Davis TN et al (2015) Ring closure activates yeast gammaTuRC for species-specific microtubule nucleation. Nat Struct Mol Biol 2:132–137
10. Ear PH, Michnick SW (2009) A general life-death selection strategy for dissecting protein functions. Nat Methods 6:813–816
11. Ear PH, Booth MJ, Abd-Rabbo D, Kowarzyk Moreno J, Hall C, Chen D, Vogel J, Michnick SW (2013) Dissection of Cdk1-cyclin complexes in vivo. Proc Natl Acad Sci U S A 110:15716–15721
12. Goldstein AL, McCusker JH (1999) Three new dominant drug resistance cassettes for gene disruption in Saccharomyces cerevisiae. Yeast 15:1541–1553
13. Liakopoulos D, Kusch J, Grava S, Vogel J, Barral Y (2003) Asymmetric loading of Kar9 onto spindle poles and microtubules ensures proper spindle alignment. Cell 112: 561–574
14. Kollman JM, Polka JK, Zelter A, Davis TN, Agard DA (2010) Microtubule nucleating gamma-TuSC assembles structures with 13-fold

microtubule-like symmetry. Nature 466: 879–882

15. Nazarova E, O'Toole E, Kaitna S, Francois P, Winey M, Vogel J (2013) Distinct roles for antiparallel microtubule pairing and overlap during early spindle assembly. Mol Biol Cell 24:3238–3250
16. Giaever G, Chu AM, Ni L, Connelly C, Riles L, Veronneau S, Dow S, Lucau-Danila A, Anderson K, Andre B et al (2002) Functional profiling of the Saccharomyces cerevisiae genome. Nature 418:387–391
17. Knop M, Siegers K, Pereira G, Zachariae W, Winsor B, Nasmyth K, Schiebel E (1999) Epitope tagging of yeast genes using a PCR-based strategy: more tags and improved practical routines. Yeast 15:963–972
18. Tropea JE, Cherry S, Waugh DS (2009) Expression and purification of soluble His(6)-tagged TEV protease. Methods Mol Biol 498: 297–307
19. Koivomagi M, Valk E, Venta R, Iofik A, Lepiku M, Morgan DO, Loog M (2011) Dynamics of Cdk1 substrate specificity during the cell cycle. Mol Cell 42:610–623
20. Rigaut G, Shevchenko A, Rutz B, Wilm M, Mann M, Seraphin B (1999) A generic protein purification method for protein complex characterization and proteome exploration. Nat Biotechnol 17:1030–1032
21. Abràmoff MD, Magalhaes PJ, Ram SJ (2004) Image processing with ImageJ. Biophotonics Int 11:36–42
22. Vinh DB, Kern JW, Hancock WO, Howard J, Davis TN (2002) Reconstitution and characterization of budding yeast gamma-tubulin complex. Mol Biol Cell 13:1144–1157
23. Koivomagi M, Valk E, Venta R, Iofik A, Lepiku M, Balog ER, Rubin SM, Morgan DO, Loog M (2011) Cascades of multisite phosphorylation control Sic1 destruction at the onset of S phase. Nature 480:128–131

Chapter 15

Cell Cycle Synchronization Using a Microfluidic Synchronizer for Fission Yeast Cells

Shujing Wang and Chunxiong Luo

Abstract

To produce synchronized cell colonies, many cell cycle synchronization technologies have been developed, among which the baby machine may be considered the most artifact-free. Baby machines incubate "mother cells" under normal conditions and collects their "babies," producing cell cultures that are similar not only in cell cycle phase but also in age. Several macroscale and microfluidic baby machines have been applied to synchronized cell research. However, for rod-shaped cells like fission yeast (*Schizosaccharomyces pombe*), it is still a challenge to immobilize only the mother cells in a microfluidic device. Here, we present a new baby machine suitable for fission yeast. The device fixes one end of the cell and releases the free-end daughter cell every time the cell finishes cytokinesis. A variety of structures for cell immobilization were attempted to find the optimal design. For the convenience of collection and to enable further assays, we integrated a cell screener into the baby machine, which exploits the deformation of polymer material to switch between open and closed states. The device, producing synchronous populations of fission yeast cells, provides a new on-chip tool for cell biology studies.

Key words Cell cycle, Synchronization, Microfluidic chip, Fission yeast, Baby machine, PDMS (polydimethylsiloxane)

1 Introduction

The synchronization of cells plays an essential role in experiments that focus on the molecular composition of the cell [1, 2]. There has been a rapid development of many cell cycle synchronization methods for more than half a century. These methods are generally divided into two sub-categories: selective or inductive [3–9]. The selective methods select a subgroup of cells from a normally dividing culture—usually with particular physical characteristics that correspond to a certain cell cycle phase. The inductive methods block a whole culture of cells at a certain cell cycle phase, usually by adding blocking agents or depriving nutrients to stop a necessary physiological event. But it is frequently argued that blocking agents (e.g. hydroxyurea, thymidine) or the starvation of cells may introduce pseudo-phenomena into experiments [10, 11].

Amanda S. Coutts and Louise Weston (eds.), *Cell Cycle Oscillators: Methods and Protocols*, Methods in Molecular Biology, vol. 1342, DOI 10.1007/978-1-4939-2957-3_15,

Of all the existing synchronization methods, "baby machine" synchronizers probably introduce the fewest artificial conditions and yield cells that are homogeneous both in terms of cell cycle stage and "age" [12]. A variety of baby machines have been developed for cells that have different shapes, sizes, cytokinesis patterns and that require different culture conditions. For example, anchorage-dependent cells tend to adhere to the container surface during interphase, and detach during mitotic phase. By shaking the container and collecting suspending cells, one can get a synchronous m-phase culture [4, 13]. In this case the container can be seen as a baby machine, although it requires many manual interventions. A more ingenious baby machine was realized by immobilizing cells on an adhesive-coated membrane, washing away newborn daughter cells with culture medium, and collecting effluent over a short period of time. Cells in this effluent are of similar age and cell cycle phase [7, 14, 15]. This baby machine is more automated and universal, being suitable for cells with no anchorage property, but it does require that the cell surface can bond to the membrane. Owing to the rapid development of microfluidic technology, many elaborate micro-devices have been invented and used for cell cycle synchronization in recent years. One device exploits pressure differences across thousands of holes in a silicon layer to hold a corresponding amount of leukemia cells, and elute "seed cells" with medium flow [5]. Every time a "seed cell" divides, the daughter cell plugging the hole stays in place, while the other one is emitted. However, with this kind of microfluidic synchronizer, it is challenging to generate synchronous cultures of some model organisms, such as fission yeast, because the rod shape and stiff cell wall make it difficult to obtain a sealed hole.

Using polymer materials with elasticity to constrain cells is a more convenient approach to realize baby machines [16]. Here, a new microfluidic synchronizer suitable for rod-shape bacterium and fungi cells is presented. With classic soft lithography technology, thousands of slits are fabricated along a 1 cm long zigzag PDMS (polydimethylsiloxane) channel. After pressurizing and centrifuging, rod-shaped cells can be loaded into slits and constrained firmly [17]. Introduction of a simple but robust pressure-controlled screener enables cell collection, and long-term culturing can be developed to cooperate with the slit array. Fission yeast cells have been used to test the performance of this novel synchronizer, and the degree of synchronization of shed baby cells was characterized [17].

2 Materials

2.1 Photolithography

1. Silicon wafers (100 mm in diameter, 525 μm thick, orientation <100>, Luoyang Hejing Electronic material CO., LTD, Henan, China). The wafers are used as the substrate for the chip pattern.

2. SU-8 3000 series and SU-8 developer (Clariant Corporation, The woodlands, TX, USA). SU-8 is a negative photoresist, which becomes insoluble in developer after exposure (*see* **Note 1**).
3. Spin coater (WS-650MZ-23NPP, Laurell Technologies Corporation, Pennsylvania, USA).
4. Exposure machine (BG-401A, No.45 Research Institute of China Electronics Technology Group Corporation, Beijing, China). Exposing under UV light changes the solubility of SU-8 in developer.
5. Hot plate (200 × 200 mm), capable of heating to 200 °C.
6. Petri dish (130 × 130 mm, thermo-stable at 80 °C). The petri dish serves as a container during the whole process.
7. Tweezers. These are used to protect the wafer surface when handling it.

2.2 Materials for Chip Fabrication

1. PDMS prepolymer (RTV615 (A, B)) (GE Toshiba Silicones Co. Ltd, Shizuoka, Japan).
2. Digital weighing scale.
3. Plasma cleaner (PDC-M-01, Harrick Plasma Inc., New York, USA). With plasma treatment, the PDMS binds to the microscope slide tightly and easily.
4. Vacuum pump linked with a desiccator. This is used to quickly remove air bubbles.
5. Puncher (Uni-Core-1.00, Ted Pella Inc., California, USA).
6. Microscope slide (24 × 60 × 0.15 mm). This serves as the substrate for the PDMS chip.
7. Two disposable syringes (1 mL).
8. Syringe pump (TS-1B/W0109-1B, Longer-Pump Company, Baoding, Hebei, China). This can be installed in a variety of syringes and reach a wide range of linear velocities (7.9 μm/min to 79.4 mm/min). The infusion rate is equal to the linear velocity multiplied by the cross-sectional area of the syringe.
9. Plastic gloves and masks. Due to the toxicity of SU-8, SU-8 developer and the non-curing PDMS, one should wear gloves and a mask (to protect nose and mouth from toxic gas) (*see* **Note 2**).
10. Scotch® magic tape. This is used to clean the PDMS without leaving any residue.
11. Tygon tubing, stainless blunt needles and steel wires that match the 1 mm puncher size (*see* **Note 3**).

2.3 Cell Preparation

1. The *Schizosaccharomyces pombe* strain AY160-14D (h90 ade6-216 leu1-32 lys1-131 ura4-D18 nuc1: nuc1-GFP-HA-Kanr), purchased from the Yeast Genetic Resource Center Japan

(YGRC/NBRP) is used [18]. The GFP in this strain acts as a nucleus marker, aiding determination of the exact time of anaphase.

2. YE5S culture medium: Add 5 g yeast extract, 30 g glucose, 225 mg adenine-HCl, 225 mg L-histidine, 225 mg L-leucine, 225 mg uracil and 225 mg L-lysine-HCl into a 1 L glass beaker or a bottle with scale. Make up to 1 L with water [19]. Filter with a 0.22 μm filter membrane. Sterilize at 120 °C for 30 min. Store at 4 °C.
3. The single colony is inoculated in YE5S culture medium, shaken at 30 °C, 200 rpm overnight, diluted to about 10^6 cells/mL with YE5S culture medium, and grown to produce a culture of about 10^7 cells/mL.

3 Methods

3.1 Mask Design

Our photomasks are designed with the software L-edit (Tanner Research, Inc.). Other commercially available software, such as Auto CAD (Autodesk, Inc.) or Ai (Adobe Systems, Inc.), can be used to draw microfluidic patterns. Figure 1 shows the layout of our device and details of the trap. The bottle-shaped traps, linked with

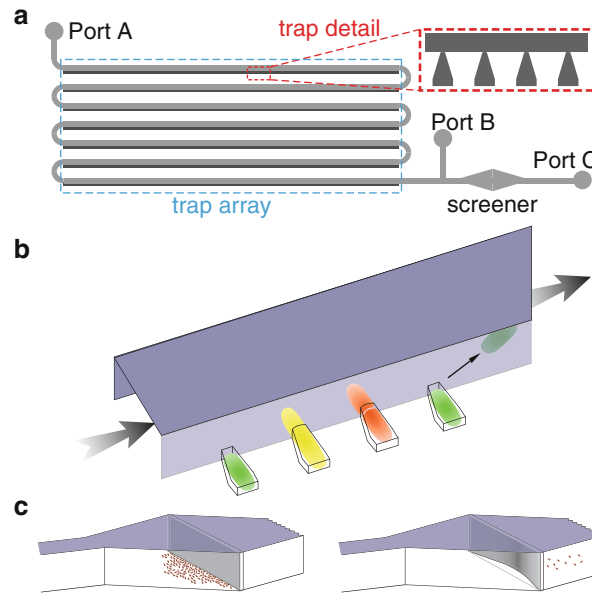

Fig. 1 The schematic drawing of the microfluidic baby machine. (**a**) Top view of the device; the flow channel is drawn in *grey*, the detail of the trap is shown in the *inset*. (**b**) The state evolution of cells in traps; *green* cells are newly divided, *yellow* cells are elongated, *red* cells are about to divide. (**c**) The shut/open state of the diamond cell screener

a 200 μm wide and 20 μm high zigzag flow channel, have 2.0 μm neck width, 75° neck corner (angle between trap side wall and main channel), and 14–15 μm trap length (with the same 8 μm in bottom width, and 4 μm in trap depth). Between ports B and C, the main channel expands to 1 mm wide and then shrinks to 200 μm wide, which is a diamond-shaped cell screener. The screener consists of a thin PDMS (60 μm thick) wall leaving a gap (narrower than 1 μm) at the bottom.

3.2 Photolithography

The procedure to fabricate the master mold should be carried out in an ultraclean chamber with yellow light. Before entering the chamber, one should wear protective clothing, shoe covers and gloves. The process is detailed below.

1. Print the mask patterns. The screener joint, the cell traps, and the main channel are the first, the second, and the third layers of photolithography fabrication, respectively (*see* **Note 4**).
2. Place a silicon wafer on a hot plate with tweezers (shiny side upwards). Heat at 190 °C for 5 min and then place it in a petri dish.
3. Program the spin coater according to the spin curve of SU-8. Usually a two-step procedure is set. The first step spinning at 500 rpm for 10 s, to make SU-8 spread over the wafer. The second step is to set an appropriate spinning speed, for 30 s, in order to obtain a SU-8 thickness of 1 μm (*see* **Note 1**).
4. Remove the wafer with tweezers and lay it in the spin coater. Centre the wafer on the spin coater holder (*see* **Note 5**).
5. Pour 2–3 mL SU-8 onto the shiny side of the wafer. Run the spin coater (*see* **Note 5**).
6. Carefully remove the wafer from the spin coater and place it onto the hot plate. Heat at 95 °C for 2 min (*see* **Note 1**).
7. Expose the first layer mask with the exposure machine. Adjust exposure time according to the energy of the UV light (*see* **Note 1**).
8. Place the exposed wafer onto the hot plate to cure the pattern. The bake condition (time and temperature) is the same as in **step 6** above.
9. Submerge the heated wafer into SU-8 developer to remove unexposed SU-8 until the shiny surface appears.
10. Rinse the wafer with fresh developer three or four times.
11. Blow-dry the surface with a nitrogen gun (*see* **Note 6**).
12. Repeat the photolithography from **steps 2** to **11** with the other two masks.

    The master mold is now obtained.

3.3 Chip Fabrication

1. Weigh 33 g PDMS prepolymer (the ratio of A:B is 10:1) and mix well so that uniform bubbles appear (*see* **Note 7**).
2. Cast the prepolymer into the master mold, which is fixed in a petri dish. Cover the dish with a lid.
3. Vacuum the dish from **step 2** in a desiccator for 3–4 min and place it on a table for about 30 min until all air bubbles disappear.
4. Put the dish into an oven at 75 °C for over 2 h (*see* **Note 8**).
5. Peel off the cured PDMS from the master mold.
6. Cut the PDMS from **step 5** to fit the microscope slide size.
7. Punch holes at port A, B, and C with a puncher.
8. Clean the PDMS surface with Scotch® magic tape.
9. Put the cleaned PDMS and the slide into the plasma cleaner and treat the surface with low level air plasma for 1 min.
10. Bond the oxidized PDMS to the slide (*see* **Note 9**).
11. Heat the bonded PDMS at 75 °C overnight.

3.4 Chip Operation

The whole process operates at room temperature unless otherwise specified. Figure 2 shows the key steps to load cells into the baby machine.

1. Cultivate the cell culture to 0.8 OD_{600} at 30 °C, 200 rpm.
2. Spin down the cell culture, remove a large proportion of supernatant and resuspend the cells, so that they are concentrated to a five times higher density.
3. Draw about 400 μL of cell suspension into a 1 mL disposable syringe (aseptic).
4. Use tygon tubing and stainless blunt needles to connect the syringe with the PDMS chip at port A.
5. Plug port C with a short piece of steel wire, and inject about 100 μL cell suspension into the microfluidic channel.
6. Plug port B with steel wire when the entire channel is filled with cells (except the air-filled branch leading to port C).
7. Place a rubber band over the syringe handle, stretch each end of the band and attach to the plunger ends as shown in Fig. 2a. Adjust the length of rubber band to generate a 5 N force, which corresponds to the application of a 2 bar pressure to the PDMS chip (*see* **Note 10**). A microscopic image in Fig. 2b shows the PDMS traps expanded by the syringe pressure.
8. Centrifuge at 200 × *g* for 2 min (*see* **Note 11**).
9. Remove the needle and wires from the chip, and connect two pumps to ports A and C to perfuse culture medium at high speed until all of the cell residue in the flow channel is washed away. Figure 2d shows a row of traps filled with fission yeast.

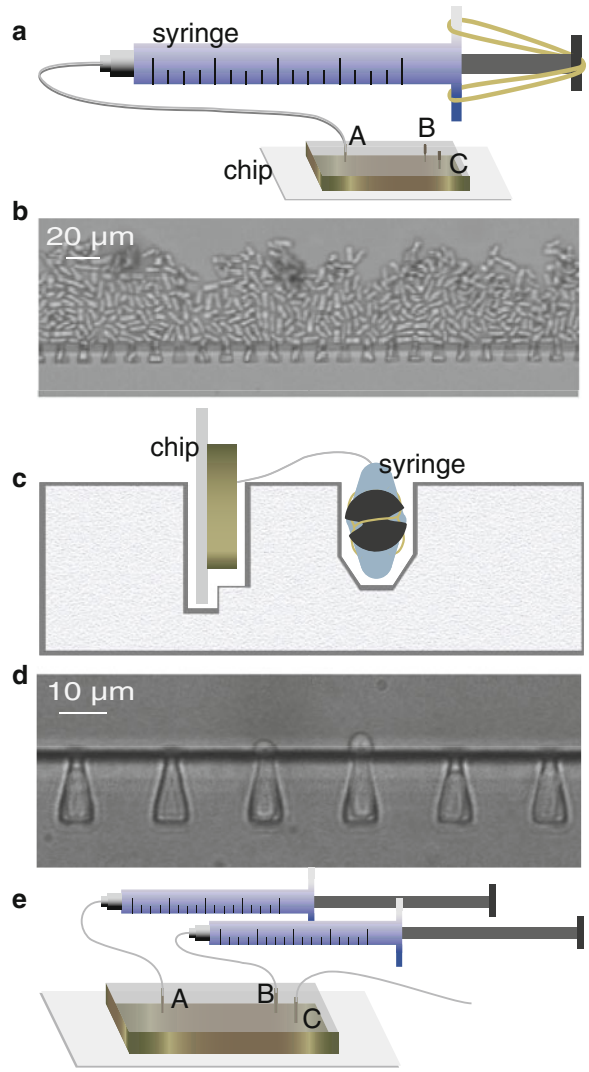

Fig. 2 The cell loading steps. (**a**) Apply high pressure into chip with a syringe bow. (**b**) The trap necks are broadened under pressure. (**c**) An adapter used for keeping the traps perpendicular to the centrifuge rotor. (**d**) A row of traps with cells loaded in them. (**e**) The tube connection when the device is in use (two syringes are connected to ports *A* and *B*)

10. Disconnect the pump from port C. Port C works as an exhaust.
11. Connect two pumps to ports A and B respectively to deliver medium (A at 200 μL/h, B at 10 μL/h) until a synchronous colony has been generated. Newborn cells shed from the trap array are carried to the cell screener by medium flow, where further culture, observation or assay can be performed.
12. At the beginning of every new round of cell collection, clear the cells previously accumulated at the cell screener by increasing

the inject speed of port B from 10 μL/h to an extremely high speed (about 10 mL/h) for a very short period (about 1 s) (*see* **Note 12**).

13. After cell collection, shut down port A, and maintain port B at the speed of 10 μL/h to keep the collected cells in situ and to prevent cells shed later from drifting downstream.

The complete device is shown in Fig. 2e, and the chip is now ready to be mounted onto a microscope for monitoring, or put into an incubator to produce a synchronized cell population (*see* **Note 13**).

4 Notes

1. The SU-8 data sheet, obtained from the company website, offers reference for the operation parameters for spin coating (Subheading 3.2, **step 3**) and curing (Subheading 3.2, **step 8**) (e.g. heating temperature, heating time, exposure energy). Download the data sheet: http://www.microchem.com/Prod-SU83000.htm
2. Latex hinders PDMS curing, so do not wear latex gloves when handling non-cured PDMS.
3. To prevent liquid leakage from the inlet and outlet, the diameter of the puncher should be a little smaller than that of the tubing.
4. In this protocol two kinds of photomask were used; a chrome plate mask printed by Institute of Microelectronics of Chinese Academy of Sciences and a high precision film mask purchased from Shenzhen MicroCAD Photo-mask LTD. In general, we use the chrome plate mask when the pattern size is between 2 and 20 μm. Otherwise, the high precision film mask is applied (larger than 20 μm).
5. Before placing the wafer in the spin coater, ensure the wafer surface is clean (without dust). Otherwise blow its surface with a nitrogen gun.
6. If there is not a nitrogen gun available, use a rubber pipette bulb. What is important is that the surface is dried under low-stress.
7. 33 g PDMS (A and B) is enough for a wafer that is 100 mm in diameter. The amount of PDMS can be adjusted according to the wafer's size. To achieve uniform coating, one should avoid visible air bubbles in the poured SU-8. A sucker can be introduced to remove bubbles.
8. Higher temperature accelerates curing of the PDMS mixture. Due to instability of the dish, we usually bake the PDMS mixture at 70–80 °C for at least 30 min.

9. For irreversible plasma bonding, make sure to align the PDMS and the slide before placing the PDMS onto the slide surface. Meanwhile, do not bend or twist the PDMS.
10. The force is determined by measuring the tension of the rubber band with a spring scale. To acquire the required force, the length of the rubber band can be adjusted.
11. The syringe pressurizer and the PDMS chip can be placed together into a chip holder, which can easily be constructed from foam, as shown in Fig. 2c. When centrifuging, the chip should be perpendicular to the centrifuge rotor while the trap neck points to the centre. In this way, cells can be forced into traps.
12. Continue the medium injection (Port A at the speed of 200 μL/h) for 10 min; about 300 cells could be collected, forming a synchronized population of similar age and cell cycle phase.
13. The temperature of the chip, microscope lens, and incubator is maintained at 30 °C in the yeast experiment.

Acknowledgement

Reproduced by permission of The Royal Society of Chemistry.
http://pubs.rsc.org/en/Content/ArticleLanding/2013/LC/c3lc50639h#!divAbstract

References

1. Whitfield ML, Zheng L-X, Baldwin A et al (2000) Stem-loop binding protein, the protein that binds the 3′ end of histone mRNA, is cell cycle regulated by both translational and post-translational mechanisms. Mol Cell Biol 20:4188–4198
2. Whitfield ML, Sherlock G, Saldanha AJ et al (2002) Identification of genes periodically expressed in the human cell cycle and their expression in tumors. Mol Biol Cell 13: 1977–2000
3. Maruyama Y, Yanagita T (1956) Physical methods for obtaining synchronous culture of Escherichia coli. J Bacteriol 71:542–546
4. Terasima T, Tolmach LJ (1963) Growth and nucleic acid synthesis in synchronously dividing populations of HeLa cells. Exp Cell Res 30:344–362
5. Shaw J, Payer K, Son S et al (2012) A microfluidic "baby machine" for cell synchronisation. Lab Chip 12:2656–2663
6. Lee WC, Bhagat AA, Huang S et al (2011) High- throughput cell cycle synchronisation using inertial forces in spiral microchannels. Lab Chip 11:1359–1367
7. Helmstetter CE, Cummings DJ (1963) The ultraviolet photochemistry of deoxyuridylyl (3′-5′) deoxyuridine. Proc Natl Acad Sci U S A 50:761–767
8. Creanor J, Mitchison JM (1979) Microbiol. Reduction of perturbations in leucine incorporation in synchronous cultures of Schizosaccharomyces pombe made by elutriation. J Gen Microbiol 112:385–388
9. Choi S, Song S, Choi C et al (2009) Microfluidic self-sorting of mammalian cells to achieve cell cycle synchrony by hydrophoresis. Anal Chem 81:1964–1968
10. Borel F, Lacroix FB, Margolis RL (2002) Prolonged arrest of mammalian cells at the G1/S boundary results in permanent S phase stasis. J Cell Sci 115:2829–2838

11. Samake S, Smith LC (1996) Effects of cell-cycle-arrest agents on cleavage and development of mouse embryos. J Exp Zool 274: 111–120
12. Cooper S (2002) Minimally disturbed, multicycle, and reproducible synchrony using a eukaryotic baby machine. Bioessays 24:499–501
13. Fox MH (2004) Methods for synchronizing mammalian cells. Methods Mol Biol 241:11–16
14. Helmstetter CE, Eenhuis C, Theisen P et al (1992) Improved bacterial baby machine: application to Escherichia coli K-12. J Bacteriol 174:3445–3449
15. Helmstetter CE, Thornton M, Romero A et al (2003) Synchrony in human, mouse and bacterial cell cultures—a comparison. Cell Cycle 2:42–45
16. Wang P, Robert L, Pelletier J et al (2010) Robust growth of *Escherichia coli*. Curr Biol 20:1099–1103
17. Tian Y, Luo CX, Ouyang Q (2013) A microfluidic synchronizer for fission yeast cells. Lab Chip 13:4071–4077
18. Hiraoka Y, Hayashi A, Da-Qiao D et al (2009) Localization of gene products using a chromosomally tagged GFP-fusion library in the fission yeast *Schizosaccharomyces pombe*. Genes Cells 14:217–225
19. Forsburg SL (2003) S. pombe strain maintenance and media. Curr Protoc Mol Biology, 13.15.1–13.15.5

Chapter 16

Detection of Protein–Protein Interactions in Tobacco BY-2 Cells Using Bimolecular Fluorescence Complementation

Gemma S. Puts and Natasha Spadafora

Abstract

Knowledge of protein–protein interactions in the plant cell is invaluable for furthering our understanding of the functions of these proteins. Many of the methods available for the study of these interactions, such as yeast two-hybrid and co-immunoprecipitation assays, rely on in vitro techniques. Here we describe the use of bimolecular fluorescence complementation for the study of protein–protein interactions in vivo, using simple techniques and accessible materials.

Key words BiFC, Protein–protein interaction, Tobacco, BY-2, Cell, Plant, Cell cycle

1 Introduction

Discovering the proteins with which core cell cycle components interact is useful for building networks in order to discover specific pathways, and also may point toward unknown functions of individual proteins. Several techniques are now available to researchers to build knowledge of protein–protein interaction networks (interactomes; [1, 2]). In this chapter we will focus on the use of bimolecular fluorescence complementation (BiFC) in plant cells, specifically in the tobacco BY-2 cell line. The BiFC procedure uses the linkage of two interacting proteins to bring together two fragments of yellow fluorescence protein (YFP) fused to these proteins by the use of complementary expression vectors both expressed in the same living cell (reviewed in [3]). This method allows visualization of the subcellular localization of specific protein interactions in the normal cellular environment (*see* Fig. 1). When the proteins interact and the portions of YFP are brought together, the resulting fluorescence can be viewed under a standard epifluorescence microscope. Two advantages of this technique for viewing protein–protein interactions in plant cells include the visualization of these interactions in vivo, and the discovery of the subcellular compartments in which they take place [4]. A disadvantage of the BiFC

Amanda S. Coutts and Louise Weston (eds.), *Cell Cycle Oscillators: Methods and Protocols*, Methods in Molecular Biology, vol. 1342, DOI 10.1007/978-1-4939-2957-3_16,

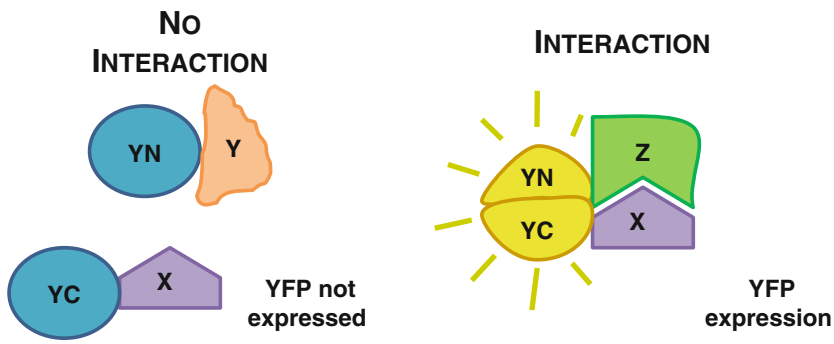

Fig. 1 Schematic representation of the principle of the BiFC assay. Two non-fluorescent fragments (YN and YC) of the yellow fluorescent protein (YFP) are fused to putative interaction partners (X, Y, or Z). The association of the interaction partners allows the two fragments of YFP to fuse and fluoresce

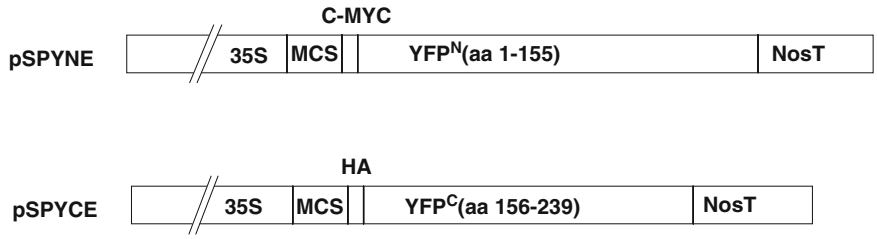

Fig. 2 Plasmid vectors designed for the use of BiFC in plant cells. Both vectors contain the cauliflower mosaic virus 35S promoter sequence, a multi-cloning site (MCS) containing target sites for the restriction enzymes Asc1 and Xma1 (among others) and the terminator for the Nos gene (NosT). The pSPYNE vector codes for the 155 amino acids from the N-terminus of the split-YFP, and contains a C-MYC affinity tag. The pSPYCE vector codes for the 83 amino acids from the C-terminus of the split YFP, and contains a hemagglutinin (HA) affinity tag (Diagram adapted from Walter et al. [6])

procedure is that the YFP fragments may associate non-specifically at high expression levels, which generates background fluorescence [5].

The BiFC vectors developed for use in plant cells are known as pSPYCE and pSPYNE (split YFP C-terminal/N-terminal fragment expression), enabling proteins of interest to be expressed and fused to either 86 amino acids of the C-terminus or 155 amino acids of the N-terminus of YFP, respectively ([6]; Fig. 2). Each plasmid contains an affinity tag—HA in pSPYCE and C-MYC in pSPYNE—which allows the fusion protein to be detected, for example by PCR or through the use of commercially available antibodies (Fig. 2). Transcription is driven by the 35S promoter of the cauliflower mosaic virus which ensures high levels of expression of the fusion proteins within plant cells (Fig. 2). The pSPYNE and pSPYCE vectors described here carry a gene conferring resistance to the antibiotic hygromycin, and to the herbicide glufosinate (BASTA) respectively [6].

Recently, new sets of vectors have been developed for multicolor BiFC (mc-BiFC), allowing the visualization of more than one protein–protein interaction simultaneously [7, 8]. BiFC and mc-BiFC have both been used successfully to show the interactions of proteins in BY-2 cells [9–12]. BiFC can in theory be used in all cell types of all organisms, and has been used to confirm protein–protein interactions in many plant processes, including the cell cycle [13–15], processes associated with protein degradation [16] and DNA damage [17]. We have successfully used this approach to confirm an interaction between a cell cycle regulatory gene, *Arath*;WEE1, and four proteins which may have a function in the cell cycle: *Arath*;GCN5, a histone-acetylating protein; *Arath*;TFCB, an α-tubulin folding cofactor; *Arath*;14-3-3ω, which may prevent dephosphorylation of *Arath*;WEE1; and *Arath*;GSTF9, a glutathione S-transferase involved in the cell's response to stress. This enzyme is involved in a redox pathway which may be linked to cell cycle control ([15, 16]; Fig. 3). As well as the previously published BiFC method using transient transformation of tobacco BY-2 cells, we have also developed a procedure for stable BiFC, enabling enrichment of pSPYCE and pSPYNE cells, with a subsequent improvement in efficiency.

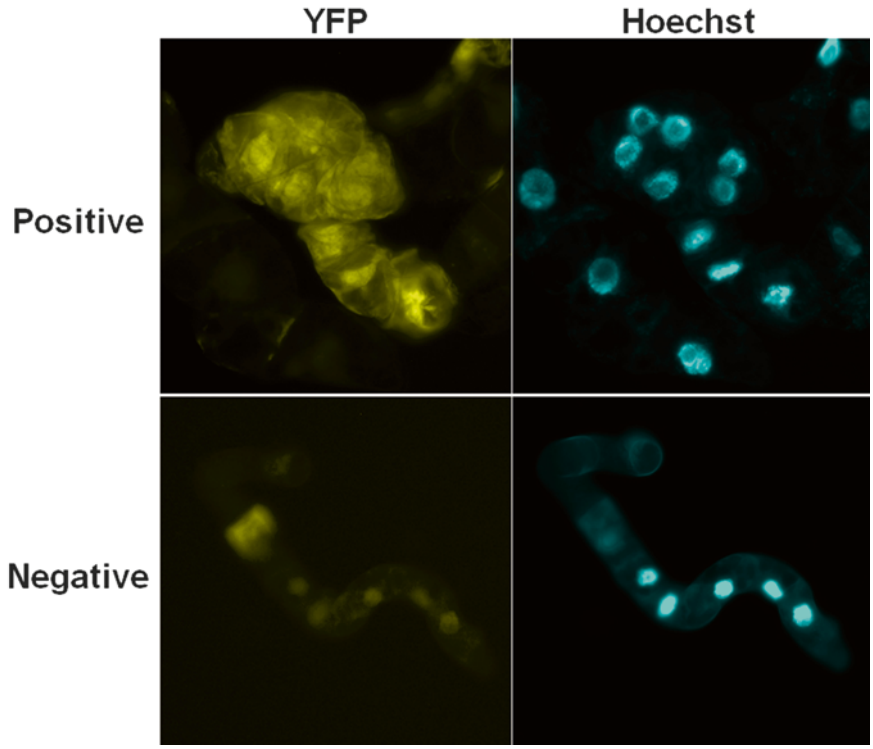

Fig. 3 Examples of positive and negative BiFC. Positive bright yellow fluorescence is observed when the two proteins of interest interact. In the negative control, background fluorescence can generally be observed, but is of a lower intensity compared to the positive

2 Materials

All standard chemicals can be sourced from Sigma-Aldrich, Poole, UK unless otherwise specified. Prepare and store reagents at room temperature unless otherwise specified.

2.1 Transformation and Maintenance of Agrobacterium

1. Plasmid DNA: must contain *in planta* antibiotic selection markers if to be used for stable transformation of tobacco BY-2 cells (*see* **Note 1**).
2. *Agrobacterium* LBA4404 competent cells.
3. Liquid nitrogen.
4. LB medium: Dissolve 10 g tryptone, 5 g yeast extract and 10 g sodium chloride in 800 mL water, adjust to pH 7 then make up to 1 L with water.
5. LB agar plate: To make agar plates add 0.8 % Difco agar, granulated (BD, Oxford, UK) to LB medium and autoclave. Allow to cool to approximately 60 °C before adding appropriate antibiotics. Pour 25 mL per 10 cm dish and allow to dry in a laminar flow cabinet.
6. Rifampicin: 50 mg/mL stock solution in dimethyl sulfoxide (DMSO; *see* **Note 2**).
7. Appropriate antibiotics, e.g., Kanamycin, hygromycin.
8. Glycerol (sterile).

2.2 BY-2 Cell Culture

1. Wild type BY-2 cells.
2. 1 N NaOH.
3. Prepare the following stock solutions in 100 mL sterile distilled water and store at −20 °C in 10 mL aliquots:
   (a) Myoinositol: 1 g.
   (b) Potassium dihydrogen phosphate: 2 g.
   (c) Thiamine hydrochloride: 100 mg.
4. 2,4-Dichlorophenoxyacetic acid: Dissolve 10 mg in 100 mL of 20 mM NaOH.
5. BY-2 medium: Dissolve 4.3 g Murashige and Skoog basal salts (Duchefa Biochemie, NL), 30 g sucrose, 0.1 g/L myoinositol (10 mL of stock solution), 0.2 g/L potassium hydrophosphate (10 mL of stock solution), 1 μg/L thiamine hydrochloride (1 mL of stock solution) and 0.2 mg/L 2,4-Dichlorophenoxyacetic acid (2 mL of stock solution) in 800 mL water and adjust to pH 5.7 using 1 N NaOH solution. Make up to 1 L with water, autoclave and store in a biosafety cabinet (*see* **Note 3**).
6. BY-2 agar plates: To make agar plates add 0.8 % Difco agar, granulated (BD, Oxford, UK) to BY-2 medium and autoclave. Allow to cool to approximately 60 °C before adding appropriate

antibiotics. Pour 25 mL per 10 cm dish and allow to dry in a biosafety cabinet.

7. 300 mL conical flasks.
8. Aluminum foil.

2.3 Bimolecular Fluorescence Complementation

1. Acetosyringone: Dissolve 19.6 mg of acetosyringone in 1 mL of 100 % ethanol (*see* **Note 2**).
2. Sterile cut-off pipette tips: Use scissors to cut off the points of pipette tips to make a wider opening, place in a tip box, and autoclave and dry before use.
3. Nesco film.
4. Hoechst stain: Add 1 % 10 mg/mL Hoechst stain (Bisbenzimide Ca) and 2 % Triton X-100 to water and mix.
5. Microscope slides and coverslips.
6. Fluorescence microscope.

2.4 Stable Transformation of BY-2 Cells

1. 0.5 M magnesium sulfate stock solution.
2. 250 mg/mL carbenicillin and/or timentin stock solutions (*see* **Note 2**).
3. Microporous tape (*see* **Note 4**).

3 Methods

3.1 Agrobacterium Transformation

1. Add DNA samples (0.2 μg/μL, *see* **Note 1**), in a volume of up to 10 μL, to separate aliquots of competent *Agrobacterium* LBA4404 cells that have been thawed on ice, and mix.
2. Freeze the cells in liquid nitrogen then thaw for 5 min at 37 °C.
3. Add 1 mL LB medium to the *Agrobacterium* and incubate for 4 h at 30 °C at 100 rpm.
4. Centrifuge the cells at 11,000 × *g* in a bench top microcentrifuge for 30 s, remove all supernatant, and resuspend in 100 μL LB medium.
5. Spread the cells onto LB agar plates in the presence of the antibiotic rifampicin (200 μg/mL).
6. Incubate the plates at 30 °C for 3 days and monitor for the appearance of *Agrobacterium* colonies.

3.2 Agrobacterium Glycerol Stocks

1. Set up liquid cultures by inoculating colonies of each bacterial transformant into growth tubes containing 3 mL LB and appropriate antibiotics. Incubate overnight at 30 °C at 100 rpm.

2. Make glycerol stocks of the cultures by pipetting 1.5 mL of each cell culture into 1.5 mL Eppendorf tubes and centrifuging at 4000 × *g* in a bench top microcentrifuge for 3 min.
3. Resuspend each of the resulting bacterial pellets in 4:1 LB medium: sterile glycerol (500 μL), mix thoroughly and store at −80 °C.

3.3 Wild Type BY-2 Culture

1. Culture the WT BY-2 cells under sterile conditions by adding 3 mL of 7-day-old culture to 95 mL BY-2 culture medium in a 300 mL conical flask, and seal using two layers of foil.
2. Grow at 27 °C in darkness at 130 rpm.
3. Subculture the cells using the above method every 7 days to maintain the cell line.

3.4 Transient Bimolecular Fluorescence Complementation (BiFC)

1. Plate *Agrobacterium* transformed with the appropriate constructs (*see* **Note 1**) from glycerol stocks onto LB agar plates in the presence of rifampicin (100 μg/mL) and appropriate antibiotics and grow at 30 °C for 3 days.
2. Subculture onto a fresh LB agar plate containing rifampicin and appropriate antibiotics and grow at 30 °C for 2 days (maintain these cell lines by subculturing onto fresh agar plates every 7 days).
3. Establish overnight cultures of the appropriate *Agrobacterium* cultures, inoculating from the 2-day-old colonies into 2 mL LB medium in 15 mL growth tubes, and grow shaking overnight at 30 °C.
4. To transiently transform BY-2 cells with plasmids, pipette 7 mL of 4-day-old BY-2 cells onto a BY-2 agar plate and swirl to fill the plate to the edges.
5. Add 12 μL acetosyringone and swirl to mix.
6. Add 100 μL of each appropriate *Agrobacterium* culture to the plate and swirl to mix.
7. Seal each plate in Nesco film, wrap in aluminum foil and incubate at 27 °C in the dark for 72 h.
8. Monitor YFP fluorescence as described below.

3.5 Stable BY-2 Transformation

Stable transformation of BY-2 cells is based on a method modified from An [18].

1. Establish overnight cultures of the appropriate *Agrobacterium* cultures, inoculating from the 2-day-old colonies (as described above) into 7 mL LB medium and 2 mM magnesium sulfate in 50 mL conical flasks and incubate overnight at 30 °C at 100 rpm.
2. Transfer 5 mL of each *Agrobacterium* culture to a 15 mL centrifuge tube and centrifuge at 1300 × *g* in a bench top centrifuge for 5 min.

3. Discard the supernatant, and resuspend the pellet in 5 mL BY-2 medium.
4. Dilute a 3-day-old BY-2 culture to 50 % using fresh BY-2 medium.
5. Add 100 μM acetosyringone to the 50 % BY-2 culture.
6. Co-cultivate 10 mL aliquots of this BY-2 culture mixture with 1 mL of the overnight *Agrobacterium* culture (transformed with the appropriate construct) in 50 mL conical flasks, seal using aluminum foil and incubate at 27 °C, 130 rpm in darkness for 48 h.
7. Wash BY-2 cells by transferring them into a 50 mL centrifuge tube and bring to 50 mL with BY-2 medium.
8. Centrifuge for 5 min at 1950 × *g* in a bench top centrifuge, and remove the supernatant.
9. Add fresh medium to the BY-2 pellet up to 50 mL, mix and centrifuge as above, and remove the supernatant.
10. Repeat **step 9**.
11. Resuspend the final pellet in 10 mL of BY-2 medium containing either 500 μg/mL carbenicillin (for vectors under kanamycin selection) or 250 μg/mL timentin (for vectors under hygromycin selection).
12. Plate aliquots of 2.5 mL onto plates of BY-2 medium containing either carbenicillin or timentin as above, and appropriate antibiotic selection.
13. Seal plates with microporous tape, wrap in foil and incubate at 27 °C in the dark (*see* **Note 4**). Antibiotic-resistant calli were isolated after 2–4 weeks.
14. Transformants appear as yellow calli on a background of dead white cells. Each individual callus is considered as an independent clone. Grow for a further 2 weeks on fresh plates until it reaches an area of approximately 2 cm^2.
15. To maintain a stable BY-2 cell line as either liquid or callus culture:
    (a) Liquid: Place a tiny piece of callus (approximately 0.05 cm^2) into 8 mL BY-2 medium containing appropriate selection in a sterile 25 mL conical flask and incubate at 27 °C in darkness, at 130 rpm until the culture reaches stationary phase (approximately 1.5–2 weeks). Subculture at 7- or 14-day intervals by transferring 250 μL of 7- or 14-day-old culture (depending on cell growth) to 8 mL BY-2 medium containing either carbenicillin or timentin as above, and appropriate antibiotic selection.
    (b) Callus: Transfer half of each callus to a fresh plate of BY-2 medium containing appropriate selection. Seal plates with microporous tape, wrap in foil, and incubate at 27 °C in the dark. Subculture onto a fresh plate once a month.

3.6 Monitoring YFP Fluorescence

1. To prepare slides, take 20 μL of culture using a sterile cut-off pipette tip, taking well-dispersed cells which look like normal subcultures and avoiding large masses.
2. Pipette onto a slide and spread out a little.
3. For counter-staining with Hoechst, add 1 μL dilute Hoechst stain to the cells on the microscope slide, mix with the pipette tip and apply a coverslip.
4. Observe and photograph the cells with a fluorescence microscope under a ×20 objective, using ultraviolet light (at a wavelength of 510 nm) to find cells positive for YFP fluorescence (*see* **Note 5** and Fig. 3).

4 Notes

1. The first step in using BiFC, not described here, is to clone your genes of interest into the pSPYCE and pSPYNE vectors. As a positive control, acquire the pSPYCE-BZIP63 and pSPYNE-BZIP63 constructs, which form a homodimer. As negative controls, pair your pSPYCE construct with the pSPYNE-BZIP63, and your pSPYNE construct with the pSPYCE-BZIP63 (unless, of course, you suspect that your protein of interest interacts with BZIP63).
2. Wear safety glasses and a dust respirator and work under a fume hood to prepare rifampicin, acetosyringone, carbenicillin, and timentin stock solutions.
3. For ease of BY-2 subculture, divide your 1 L of BY-2 medium between 10 × 300 mL conical flasks, 95 mL per flask, and seal with two layers of foil prior to autoclaving.
4. In our hands, sealing the plates with microporous tape gave the best chance of the development of calli, when compared with Nesco film.
5. Positive fluorescence events from BiFC are relatively rare, and background relatively high, which is why the positive and negative controls (*see* **Note 1**) are so important to help you know when you are looking at a real event. True positive BiFC will appear relatively bright compared to background (Fig. 3).

Acknowledgement

We especially thank Dr Dennis Francis for helpful suggestions and comments on the manuscript.

References

1. Zhang Y, Gao P, Yuan JS (2010) Plant protein-protein interaction network and interactome. Curr Genomics 11:40–46
2. Ngounou Wetie AG, Sokolowska I, Woods AG, Roy U, Deinhardt K, Darie CC (2014) Protein-protein interactions: switch from classical methods to proteomics and bioinformatics-based approaches. Cell Mol Life Sci 71:205–228
3. Kodama Y, Hu CD (2012) Bimolecular fluorescence complementation (BiFC): a 5-year update and future perspectives. Biotechniques 53:285–298
4. Bracha-Drori K, Shichrur K, Katz A, Oliva M, Angelovici R, Yalovsky S, Ohad N (2004) Detection of protein-protein interactions in plants using bimolecular fluorescence complementation. Plant J 40:419–427
5. Stephens DJ, Banting G (2000) The use of yeast two-hybrid screens in studies of protein:protein interactions involved in trafficking. Traffic 1:763–768
6. Walter M, Chaban C, Schutze K, Batistic O, Weckermann K, Nake C, Blazevic D, Grefen C, Schumacher K, Oecking C, Harter K, Kudla J (2004) Visualization of protein interactions in living plant cells using bimolecular fluorescence complementation. Plant J 40:428–438
7. Waadt R, Schmidt LK, Lohse M, Hashimoto K, Bock R, KUDLA J (2008) Multicolor bimolecular fluorescence complementation reveals simultaneous formation of alternative CBL/CIPK complexes in planta. Plant J 56:505–516
8. Kerppola TK (2013) Multicolor bimolecular fluorescence complementation (BiFC) analysis of protein interactions with alternative partners. Cold Spring Harb Protoc 9:798–803
9. Yano A, Kodama Y, Koike A, Shinya T, Kim HJ, Matsumoto M, Ogita S, Wada Y, Ohad N, Sano H (2006) Interaction between methyl CpG-binding protein and ran GTPase during cell division in tobacco cultured cells. Ann Bot 98:1179–1187
10. Lee LY, Fang MJ, Kuang LY, Gelvin SB (2008) Vectors for multi-color bimolecular fluorescence complementation to investigate protein-protein interactions in living plant cells. Plant Methods 4:24
11. Lentz Grønlund A, Dickinson JR, Kille P, Herbert RJ, Francis D, Rogers HJ (2009) Plant WEE1 kinase interacts with a 14-3-3 protein but a mutation of WEE1 at S485 alters their spatial interaction. Open Plant Sci J 3:40–48
12. Smaczniak C, Immink RGH, Muiño JM, Blanvillain R, Busscher M, Busscher-Lange J, Dinh QD, Liu S, Westphal AH, Boeren S et al (2012) Characterization of MADS-domain transcription factor complexes in Arabidopsis flower development. Proc Natl Acad Sci U S A 109:1560–1565
13. Boruc J, Inze D, Russinova E (2010) A high-throughput bimolecular fluorescence complementation protein-protein interaction screen identifies functional Arabidopsis CDKA/B--CYCD4/5 complexes. Plant Signal Behav 5:1276–1281
14. Van Damme D, Gadeyne A, Vanstraelen M, Inze D, Van Montagu MC, De Jaeger G, Russinova E, Geelen D (2011) Adaptin-like protein TPLATE and clathrin recruitment during plant somatic cytokinesis occurs via two distinct pathways. Proc Natl Acad Sci U S A 108:615–620
15. Cook GS, Lentz Grønlund A, Siciliano I, Spadafora N, Amini M, Herbert RJ, Bitonti MB, Graumann K, Francis D, Rogers HJ (2013) Plant WEE1 kinase is cell cycle regulated and removed at mitosis via the 26S proteasome machinery. J Exp Bot 64:2093–2106
16. Dowil RT, Lu X, Saracco S, Vierstra RD, Downes BP (2011) Arabidopsis membrane-anchored ubiquitin-fold (MUB) proteins localize a specific subset of ubiquitin-conjugating (E2) enzymes to the plasma membrane. J Biol Chem 286:14913–14921
17. Halimi Y, Dessau M, Pollak S, Ast T, Erez T, Livnat-Levanon N, Karniol B, Hirsch JA, Chamovitz DA (2011) COP9 signalosome subunit 7 from Arabidopsis interacts with and regulates the small subunit of ribonucleotide reductase (RNR2). Plant Mol Biol 77:77–89
18. An G (1985) High efficiency transformation of cultured tobacco cells. Plant Physiol 79: 568–570

Chapter 17

Tracking the Cyclin B1-GFP Sensor to Profile the Pattern of Mitosis Versus Mitotic Bypass

Victoria Griesdoorn, M. Rowan Brown, Marie Wiltshire, Paul J. Smith, and Rachel J. Errington

Abstract

This chapter provides a method for quantitative single cell analysis to track the transition of single cells from G_2, indicated by high cyclin B1 levels, to G_1 polyploidy phase (G_1(p)), indicated by low cyclin B1 levels, in a $4n$ population. The cell tracking methodology described provides a fluorescence fingerprint suitable for deriving G_2/M or G_2/G_1p transitions. Notably, during late G_2 the absolute cyclin B1-eGFP reporter levels obtained were high and the switch-off point identifiable, with destruction rates of a similar order across all cell cycle routing avenues. The three principle parameters extracted were defined as (1) G_2-to-G_1(p) transition duration ($tGFP^{off}$); (2) rate of sensor destruction ($kGFP^{off}$), and (3) peak sensor expression (GFP^{peak}).

Key words Cyclin B1-GFP, Time-lapse microscopy, Cell cycle transitions, Mitotic bypass

1 Introduction

The stable expression of the cyclin B1-GFP reporter in cells provides the ability to detect single cells progressing through the late cell cycle with high temporal resolution. This green fluorescent protein (GFP)-based sensor (Fig. 1) has expression, location, and destruction characteristics that shadow cyclin B1 dynamics in living cells [1] and its non-perturbing properties have been validated on high-content and high-throughput detection platforms achieving multi-well high-throughput screen (HTS) imaging, single cell kinetics tracking, and multi-parameter flow cytometry [1, 2]. Tracking cyclin B1 has been an approach previously used to track cells through mitosis and these first studies showed that cyclin B1 degradation began as soon as the spindle-assembly checkpoint was inactivated [3]. The focus of this chapter is to describe the typical methodology, including elements of quantitation. The method presented attempts to bring parameter readouts to characterize the

Amanda S. Coutts and Louise Weston (eds.), *Cell Cycle Oscillators: Methods and Protocols*, Methods in Molecular Biology, vol. 1342, DOI 10.1007/978-1-4939-2957-3_17,

Fig. 1 Structure of the cyclin B1-GFP sensor. Comprises three components that regulate the expression of the green fluorescent protein (*4*), without perturbing cell cycle transitions and checkpoint regulation: the cyclin B1 promoter (*1*); the destruction initiation (D-box) (*2*) and the Cytoplasmic Retention Sequence (CRS) (*3*)

cyclin B1 oscillator. The transitions to be measured include (1) G_2 phase through mitosis and (2) G_2 phase to G_1 polyploidy phase (G_1(p))—a novel cell cycle route called mitotic bypass that occurs due to perturbation of the G_2-decatenation checkpoint [4], using time-lapse fluorescence microscopy. The critical features of these transition phases include the measurement of initial cyclin B1 status at the point of switch-off, i.e. peak intensity; duration of the mitosis or bypass transition phase; and the initial destruction kinetics. Tracking cyclin B1 has been an approach previously used to track cells through mitosis and these first studies showed that cyclin B1 degradation began as soon as the spindle-assembly checkpoint was inactivated [3]. The first challenge for the creation of the single cell tracking described here is to ensure a non-invasive data collection approach so that the G_2-to-"next phase transition" is unperturbed, but which at the same time can provide sufficient signal-to-noise fluorescence intensity readouts suitable for measurement, and can establish a temporal sampling suitable for tracking cells through normal mitosis, i.e. a mitosis that is approximately 2 h in duration.

Overall, the priority here is to describe the instrument and accompanying acquisition methods that enable users to track an interphase morphology cell with sufficient temporal sampling. The designated wide-field time-lapse instrument, as described in this chapter's method, meets these requirements. The detailed methodology (with notes for improving the signal readout) provides the overall means for profiling and characterizing cyclin B1 dynamics, throughout the progression of a diploid cell, which either completes cell division to produce two progeny or bypasses mitosis to enter a single cell tetraploid state.

2 Materials

2.1 Cell Lines and Drug Treatments

1. U-2 OS osteosarcoma cells transfected with the cyclin B1-GFP sensor were obtained from GE Life Sciences [G2M Cell Cycle Phase Marker Vector from GE Healthcare Life Sciences].
2. Culture media in McCoy's 5A Modified Medium with 10 % fetal calf serum (FCS), 2 mM L-Glutamine (L-Glut) and penicillin/streptomycin antibiotics (pen/strep) with the addition of 0.4 M Geneticin (G418 sulfate) to maintain a stable GFP transfection.

3. ICRF-193 [bis(2,6-dioxopiperazine)] prepared in DMSO at 2 mg/ml and used at a peak concentration of 2 μg/ml (equivalent to 7.2 mM). This is an exemplar drug there are other agents that cause tumour cells to by pass mitosis.

2.2 Sample Preparation for Imaging

1. A 24-well SensoPlate™ [Greiner Bio-One, 662892]. Critically, the plate has to have a clear borosilicate coverslip bottom (175 ± 15 μm) enabling optimal imaging with standard infinity corrected objective lenses (*see* **Note 1**).

2.3 Fluorescence Time-lapse Microscopy Set-Up

1. The description here is of a wide-field instrument with well-calibrated temperature regulation and multi-well sampling, the decision was deliberately made not to employ confocal microscopy. The instrument comprises an inverted microscope [e.g. Zeiss Axiovert 100 (Zeiss, Welwyn Garden City, U.K.)].
2. A temperature-regulating incubator system and CO_2 supply. It is critical to ensure good temperature (36 ± 1 °C) and gas regulation (5 % CO_2) across the entire 24-well plate.
3. A motorized *x*, *y*, *z* microscope stage, with an extra recessed Microtiter plate holder suitable for a multi-well plate (*see* **Note 2**). An Orca I ER charge-coupled device camera capable of collecting 12-bit frames.
4. The camera, stage (*x*, *y*) and focus (*z*) were PC-controlled via the MetaMorph software package (Molecular Devices, Reading, U.K.).
5. Typically sequences can be collected with a 40×, 0.90 NA air objective lens, suitable for multi-well fluorescence time-lapse microscopy.
6. GFP fluorescence can be detected with 480/25 nm excitation and 525/30 nm emission, bandpass filters. This minimizes the interference of yellow-red autofluorescence.

3 Methods

3.1 Image Sequence Acquisition

1. Seed the 24-well plate with U-2 OS cyclin B1-GFP cells in densities ranging between 1300 and 5000 cells per well.
2. After 24 h treat the designated wells of the plate with different perturbations typically for control (media only), carrier (DMSO), or ICRF-193 (Drug) (*see* **Note 3**).
3. Immediately following the addition of the drug (or carrier) place the multi-well plate onto the plate holder on the microscope, ensure good placement into the holder, and that the plate is robustly gassing with 5 % CO_2.
4. Collect image sequences at intervals of 10–30 min over a course of 24 h, typically 98 frames per field of view; and at 3 fields per well (*see* **Notes 4–6**).

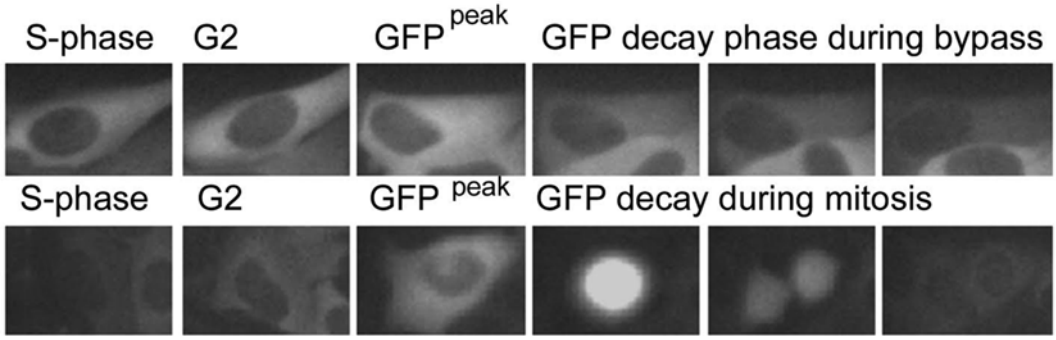

Fig. 2 Single cell GFP-cyclin B1 expression captured by fluorescence time-lapse microscopy. *Top*, typical sequence of GFP-cyclin B1 destruction in ICRF-193-treated cells (2 μg/ml) showing mitotic bypass. *Bottom*, typical sequence of GFP-cyclin B1 destruction in control cells showing commitment to mitosis

3.2 Manual Image Sequence Data Analysis

1. Pull up a relevant image sequence for analysis; place an ROI in the cytoplasm and another in the nucleus of the cell. Finally, place an ROI in the background. As the cell moves from frame to frame move the three ROIs to account for this movement. Typically, the levels of cyclin B1-GFP reporter fluorescence can be recorded from a 100×100 pixels square-shaped region of interest (ROI) (Fig. 2) (*see* **Note 7**).
2. Automated background subtraction can also be implemented to deal with non-uniform field illumination, or uneven patterns on the substrate of the cell substratum.
3. Readout the profiles into excel and compare the relevant tracks of cells between wells and between treatments. Subtract the background from each track and then normalize to peak of cyclin B1.
4. Extract parameters of interest, typically GFP^{peak} [the maximal fluorescence intensity measured for that track], the $kGFP^{off}$ [the cyclin B1 destruction rate measured as fluorescence intensity normalized over time], and $tGFP^{off}$ [the time in hours required for the fluorescence intensity to reach base level] (Figs. 3 and 4) (*see* **Notes 8** and **9**).

4 Notes

1. Other coverslip chambers are available and the user-choice depends on the microscope incubator system set-up and the integrated holder system, e.g. the Nunc™ Lab-Tek™ Chambered Coverglass, which provides optimum optical characteristics.
2. Also, use of a motorized focus option (PS3H122 Motorized Focus Drive) can provide step sizes as small as 0.002 μm and

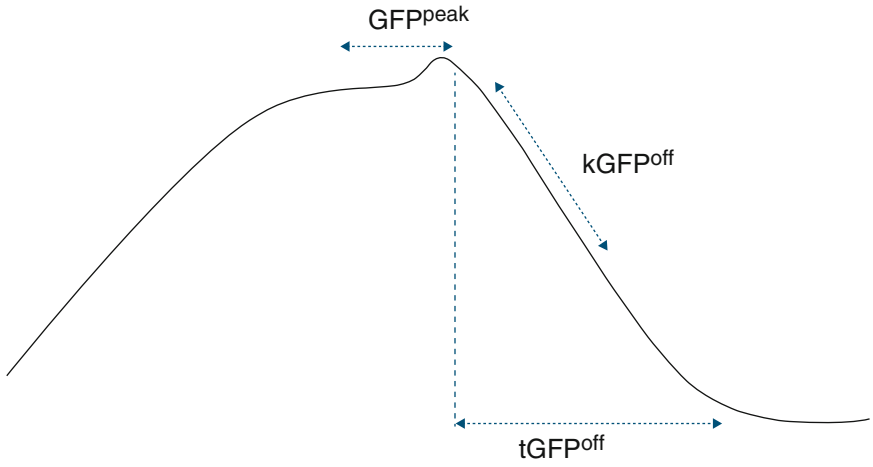

Fig. 3 Typical parameters measured from single cell fluorescence readouts. Schematic to show the location of the parameters including peak fluorescence intensity, GFP^{peak}; rate of decrease of fluorescence intensity normalized against time, $kGFP^{off}$; and the duration of the decline in hours, $tGFP^{off}$

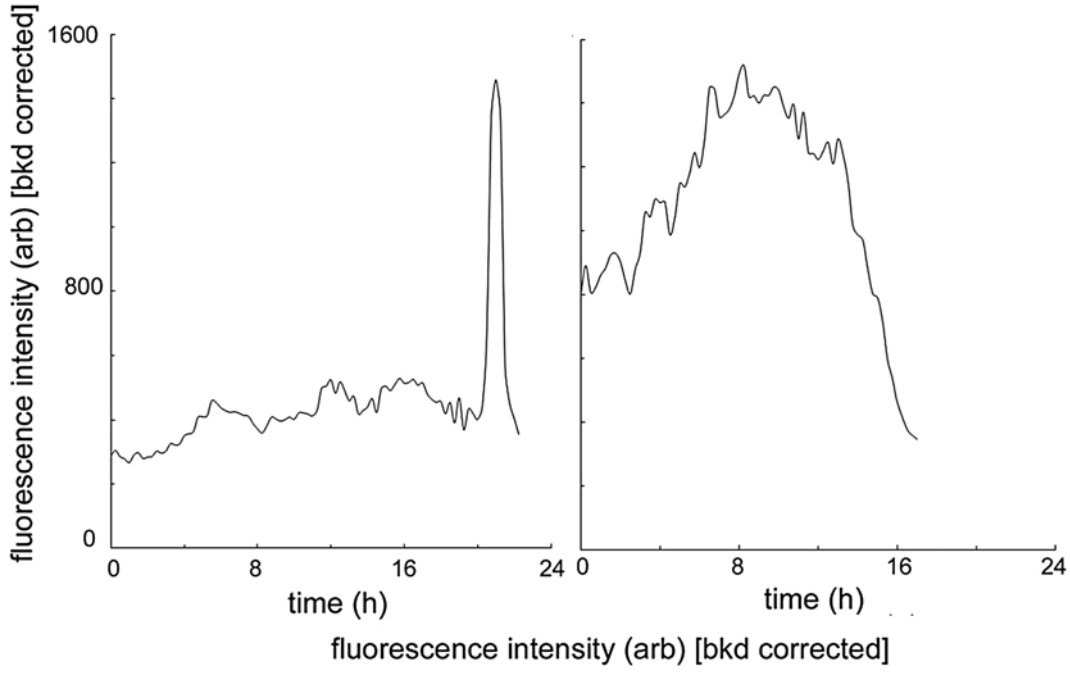

Fig. 4 Single cell cytoplasmic cyclin B1-GFP fluorescence profiles of human osteosarcoma. Plots show frame-by-frame mean fluorescence intensity over time with profiles of control cells undergoing normal mitosis (*panel left*) and mitotic bypass (*panel right*) after exposure to 2 μg/ml ICRF-193. Intensity profiles were background corrected

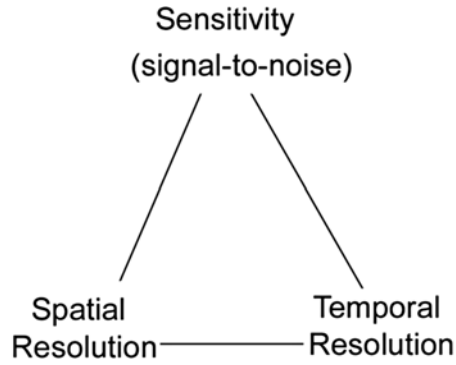

Fig. 5 Single cell imaging considerations and compromises. Experimental design and optimization in single cell fluorescence time-lapse is underpinned by the interrelated considerations or trade-offs between sensitivity, spatial resolution, and temporal resolution

provides excellent resolution for precise focus and repeatable positioning in the *Z*-axis.

3. Usually the treatment regimen is minimally repeated across 3 wells per treatment, this provides statistically enough data.
4. The experimental design described above and optimization is decided based on a triangle of interrelated considerations (Fig. 5) which represent the fundamental underpinnings of the implementation of time-lapse imaging, namely issues of sensitivity, spatial resolution, and temporal resolution [5].
5. Further acquisition optimization can be undertaken to improve the signal-to-noise, particularly so that cells in G_1 of the cell cycle with very little GFP expression could be detected. For instance, the camera frame binning can be increased to 4×4, i.e. each block of 4×4 pixels was averaged into 1 pixel 4× larger, decreasing the exposure time required but sacrificing spatial resolution. However, in doing so the cell cytoplasm and cell shape information was not compromised and the ability to detect nuclear translocation of the GFP signal, as an indicator of mitotic commitment, was maintained. Binned image files were smaller and as a result the camera could perform more efficiently. Binning has proven particularly useful for large data sets or live-cell imaging, and was used to ensure there was no phototoxicity effect on the cells.
6. In order to ensure that the temporal sampling does not perturb the biology, a time interval of 15 min was selected over a course of 24 h, yielding a 5× sampling of mitosis which was an acceptable sampling rate (mitotic duration is 2 h).
7. Placement of the region-of-interest (ROI) on to the images (*see* Fig. 2), in Fig. 3. Typically place an ROI onto the cell nucleus (the round 'empty hole); and place an ROI onto the

cytoplasm close to the nucleus to extract fluorescence intensities over time, placed in the cytoplasm bordering the nucleus.

8. The disadvantage of not having optical sectioning on a wide-field microscope means that rounding of the cells during mitosis—a drastic morphological change—results in a spike in fluorescence intensity that is due to cell rounding and not necessarily an enhanced GFP expression [4]. Thus the maximal nuclear intensity during mitosis is an artifact.
9. The disadvantage of not having optical sectioning on a wide-field microscope means that background (autofluorescence) from the media (probably due to tryptophans in the media) makes for a low signal-to-noise ratio during ramping-up or accumulation phase of the reporter and prevents the analysis of the S/G2 transition.

Acknowledgement

This work was supported by the EPSRC grant EP/F040954/1 and the BBSRC Sparking Impact Award for LineageP.

References

1. Thomas N, Goodyer I (2003) Stealth sensors: real-time monitoring of the cell cycle. Targets 2(1):26–33
2. Thomas N (2003) Lighting the circle of life: fluorescent sensors for covert surveillance of the cell cycle. Cell Cycle 2(6):545–549
3. Clute P, Pines J (1999) Temporal and spatial control of cyclin B1 destruction in metaphase. Nat Cell Biol 1(2):82–87
4. Smith PJ, Marquez N, Wiltshire M et al (2007) Mitotic bypass via an occult cell cycle phase following DNA topoisomerase II inhibition in p53 functional human tumor cells. Cell Cycle 6(16):2071–2081
5. White NS, Errington RJ (2005) Fluorescence techniques for drug delivery research: theory and practice. Adv Drug Deliv Rev 57(1): 17–42

Chapter 18

Measuring APC/C-Dependent Ubiquitylation In Vitro

Marc A. Jarvis, Nicholas G. Brown, Edmond R. Watson, Ryan VanderLinden, Brenda A. Schulman, and Jan-Michael Peters

Abstract

The anaphase-promoting complex/cyclosome (APC/C) is a 1.2 MDa ubiquitin ligase complex with important functions in both proliferating and post-mitotic differentiated cells. In proliferating cells, APC/C controls cell cycle progression by targeting inhibitors of chromosome segregation and mitotic exit for degradation by the 26S proteasome. To understand how APC/C recruits and ubiquitylates its substrate proteins and how these processes are controlled, it is essential to analyze APC/C activity in vitro. In the past, such experiments have been limited by the fact that large quantities of purified APC/C were difficult to obtain and that mutated versions of the APC/C could not be easily generated. In this chapter we review recent advances in generating and purifying recombinant forms of the human APC/C and its co-activators, using methods that are scalable and compatible with mutagenesis. We also describe a method that allows the quantitative analysis of APC/C activity using fluorescently labeled substrate proteins.

Key words Enzyme activity, Anaphase promoting complex/cyclosome, Ubiquitin, Mitosis

1 Introduction

The anaphase promoting complex/cyclosome (APC/C) is a ubiquitin ligase (E3 enzyme) which has essential functions in eukaryotes from yeast to man (reviewed in [1]; [2]). In metaphase of mitosis, APC/C ubiquitylates securin, an inhibitor of the cohesin protease separase, and B-type cyclins, the activating subunits of cyclin-dependent kinase 1 (CDK1). The APC/C recognizes specific "degron" sequences in these substrates, called the destruction box (D box) and the KEN box. The subsequent degradation of ubiquitylated securin and cyclin B by the 26S proteasome is essential for sister chromatid separation in anaphase and mitotic exit. APC/C also has functions in post-mitotic cells, for example during the terminal differentiation of cortical neurons [3, 4].

The APC/C is a 1.2 MDa protein complex composed of 14 protein subunits which are present in different stoichiometries (reviewed in [5]). To be able to recognize degron sequences in its

Amanda S. Coutts and Louise Weston (eds.), *Cell Cycle Oscillators: Methods and Protocols*, Methods in Molecular Biology, vol. 1342, DOI 10.1007/978-1-4939-2957-3_18,

substrate proteins, the APC/C has to associate with an additional co-activator protein, either with CDC20 in early mitosis or with CDH1 during mitotic exit, G1 phase, and in quiescent cells. CDC20 and CDH1 help to recruit substrates to the APC/C, presumably by directly binding their D and KEN boxes. Once associated with the APC/C, substrates are ubiquitylated by ubiquitin-conjugating (E2) enzymes. These small monomeric enzymes are first trans-esterified with an activated ubiquitin residue by the ubiquitin-activating (E1) enzyme, and subsequently this ubiquitin residue is transferred to epsilon-amino side chains of lysine residues in the APC/C substrate. The APC/C can interact with different E2s: UBCH5A, UBCH5B, UBCH5C (also known as UBE2D1, UBE2D2, UBE2D3, respectively), UBCH10, and UBE2S. UBCH10 is thought to be recruited to the APC/C via the RING finger domain of the APC/C subunit APC11. APC11 in turn is bound to the APC/C subunit APC2, which belongs to the cullin protein family [2]. Cullin and RING finger subunits are also found in a number of other ubiquitin ligase complexes, implying that these use related catalytic mechanisms for substrate ubiquitylation reactions [6].

The activity of the APC/C is tightly controlled to enable proper progression through the cell cycle (reviewed in [7]). For example, securin and cyclin B are only recognized by APC/C-CDC20 once all chromosomes have been properly attached to both poles of the mitotic spindle. Before this state (metaphase) has been reached, APC/C's ability to recruit securin and cyclin B is prevented by a four-subunit mitotic checkpoint complex (MCC). APC/C-CDH1 is also controlled by other mechanisms, for example the early mitotic inhibitor 1 (EMI1) [8].

Recent advances in single-particle electron microscopy have provided detailed insight into the structure of the APC/C [5, 9, 10]. However, the catalytic mechanism of APC/C-mediated substrate ubiquitylation reactions and their regulation remain incompletely understood. Studying these mechanisms requires the ability to measure the activity of the APC/C using purified components, and structure-function analyses of these components via mutagenesis. For many years, these assays have utilized APC/C purified from cultured cells (or sometimes from tissues), typically using immuno-affinity purification techniques (reviewed in [11, 12]). Although these approaches have been instrumental for analyzing APC/C, they were not easily scalable because the abundance of APC/C in cells is low and because the availability of APC/C antibodies needed for the affinity purification is often limited. These approaches were also not well suited for the analysis of APC/C loss-of-function mutants as these are difficult to generate in cells because APC/C is essential for cell viability.

To overcome these limitations, methods have been developed that enable the generation of recombinant forms of yeast and human

APC/C, expressed in baculovirus-infected insect cells [13–15]. These methods are more easily scalable and well suited for mutagenesis approaches. Here we describe one of these approaches for the generation of recombinant human APC/C. We also provide a brief description of how the other proteins can be purified that are required for the reconstitution of APC/C-mediated substrate ubiquitylation reactions and describe how these reactions can be measured using a fluorescently labeled substrate.

In brief, APC/C activity can be measured by incubating the respective purified proteins, i.e., APC/C, an APC/C co-activator, E1, one or several of the E2s that cooperate with the APC/C, ubiquitin, and a substrate protein in the presence of Mg^{2+}ATP. The reaction is stopped by the addition of SDS sample buffer and analyzed by sodium dodecyl sulfate-polyacrylamide gel electrophoresis (SDS-PAGE). Ubiquitin-substrate conjugates can be detected on a fluorescence scanner if either a fluorescently labeled substrate or a fluorescently labeled ubiquitin is used.

APC/C can ubiquitylate substrates at multiple lysine residues [16, 17] and, once the first ubiquitin residues have been linked to the substrate, also on lysine residues on the attached ubiquitin molecules (in the latter case APC/C typically modifies lysine residues 11, 48, and 63 on ubiquitin) [18–20]. APC/C-mediated ubiquitylation reactions, therefore, result in the formation of complex mixtures of different substrate-ubiquitin conjugates. These are resolved by SDS-PAGE into a characteristic "ladder" of bands, each containing a different number of ubiquitin residues coupled to the substrate molecule (*see* Fig. 1a). SDS-PAGE analysis can therefore be used to estimate how many ubiquitin residues are coupled to a substrate by the APC/C, but the identity of the modified lysines or whether linear or branched ubiquitin chains are formed can only be determined by mass spectrometric approaches [19]. Alternatively, APC/C-mediated ubiquitylation reactions can be performed in the presence of ubiquitin in which lysine residues have been chemically modified by methylation, so that ubiquitin itself cannot be ubiquitylated. Comparing reactions in the absence and presence of methyl-ubiquitin can, therefore, be used to determine if a substrate is modified by poly-ubiquitin chains, or by single-ubiquitin residues which are attached to multiple lysine residues, or by a combination of both.

In most cases, APC/C activity is measured by using fluorescently labeled substrate, but the activity can also be analyzed by using fluorescent-labeled ubiquitin (*see* Fig. 1b). This permits the visualization of not only substrate-ubiquitin conjugates, but also a covalent E1-ubiquitin adenylate, and—if SDS-PAGE is performed in the absence of reducing agents—of E2-ubiquitin thioesters (which are unstable in the presence of reducing agents such as β-mercaptoethanol or dithiothreitol). A limitation of using fluorescently labeled ubiquitin is, however, that it cannot be determined

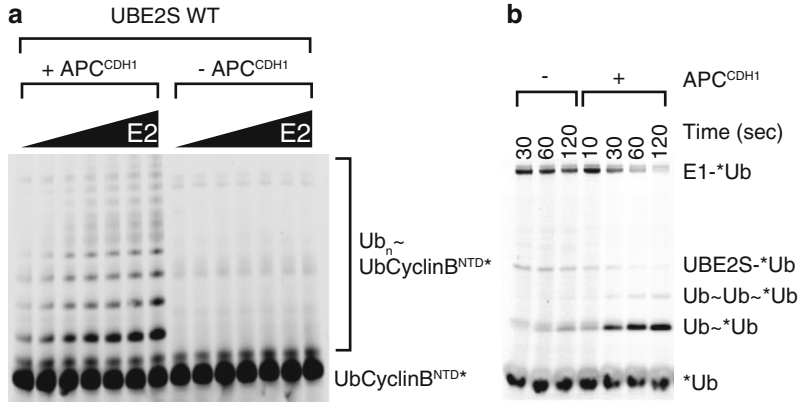

Fig. 1 (**a**) APC/C drives poly-ubiquitin chain formation. SDS-PAGE gel illustrating that APC/C-CDH1 drives poly-ubiquitin chain formation. Visualized using a fluorescently labeled substrate [22]. (**b**) APC/C-CDH1-dependent formation of free Ub chains by UBE2S visualized using a fluorescently labeled donor ubiquitin, similar to previously described [22]. For this experiment, the E1~*Ub conjugate is formed by incubating 50 mM $MgCl_2$ATP with Tube 2 containing E1 (10 μM) and fluorescent Ub (40 μM) for 10 min at room temperature. This reaction can be either left unquenched (shown) or, if desired, quenched by the addition of 50 mM ethylenediaminetetraacetic acid (EDTA) and/or desalting. The contents of Tube 2 are diluted tenfold into Tube 1 containing an unlabeled source of Ub (250 μM). Aliquots are then quenched by SDS sample buffer at the appropriate times and visualized by SDS-PAGE. In the experiment shown, the APC concentration used is 100 nM

to which protein the ubiquitin is conjugated (the substrate protein or to other proteins present in the reaction mixture).

When APC/C-mediated ubiquitylation reactions are to be analyzed in the presence of UBE2S it has to be kept in mind that this E2 preferentially ubiquitylates lysine residues (K11) in ubiquitin molecules, a property that enables it to elongate ubiquitin chains on substrate proteins [21]. UBE2S activity is, therefore, typically analyzed by using linear fluorescent ubiquitin-substrate fusion proteins, or by measuring the formation of fluorescent ubiquitin-ubiquitin conjugates (for an example, *see* [22]). Alternatively, UBE2S activity can also be analyzed in the presence of either UBCH5 or UBCH10, which both efficiently ubiquitylate lysine residues in substrate proteins, thereby generating conjugates which can then serve as substrate for ubiquitin chain elongation by UBE2S.

2 Materials

2.1 Bacterial Protein Expression

1. Bacterial cells: *E. coli* BL21 (DE3) CodonPlus-RIL (*see* **Note 1**).
2. Lysogeny broth—Miller (LB): 10 g tryptone, 5 g yeast extract, 10 g NaCl per liter.
3. 0.6 M Isopropyl β-d-1-thiogalactopyranoside (IPTG).

2.2 Baculovirus-Insect Cell Expression

1. Insect cells: Sf9/High Five (*see* **Note 2**).
2. Insect media: Hyclone SFX media (GE Lifesciences) (*see* **Note 2**).

2.3 Expression and Purification of Recombinant APC/C

1. Low- and high-speed centrifuges.
2. Phosphate-buffered saline (PBS).
3. APC/C lysis buffer: 50 mM Hepes pH 8, 250 mM NaCl, 5 % glycerol, 2 mM dithiothreitol (DTT), 2 mM benzamidine, 5 units/mL benzonase, 10 μg/mL aprotinin, 10 μg/μL leupeptin, 5 μg/μL avidin, and one Complete™ EDTA-free protease inhibitor tablet (per 50 mL buffer).
4. Sonicator.
5. Streptactin resin.
6. APC/C wash buffer: 50 mM Hepes pH 8, 250 mM NaCl, 5 % glycerol, 2 mM DTT.
7. Gravity flow column.
8. APC/C elution buffer: 50 mM Hepes pH 8, 250 mM NaCl, 5 % glycerol, 2.5 mM desthiobiotin, 2 mM DTT.
9. Bradford reagent.
10. SDS-PAGE gels and gel-running equipment.
11. APC/C buffer A: 50 mM Hepes pH 8, 5 % glycerol, 2 mM DTT.
12. APC/C buffer B: 50 mM Hepes pH 8, 1 M NaCl, 5 % glycerol, 2 mM DTT.
13. AKTA protein purification system.
14. POROS HQ 50 μm anion-exchange column.
15. Superose 6 size-exclusion column.
16. APC/C size-exclusion buffer: 20 mM Hepes pH 8, 200 mM NaCl, 1 mM DTT.

2.4 Expression and Purification of the Co-activators: CDC20 and CDH1

1. Low- and high-speed centrifuges.
2. PBS.
3. Co-activator lysis buffer: 20 mM Hepes pH 7, 100 mM $(NH_4)SO_4$, 20 mM imidazole, 5 % glycerol, 1 mM DTT, 1 Complete™ EDTA-free protease inhibitor tablet (per 50 mL buffer).
4. Dounce homogenizers.
5. Ni-NTA resin.
6. Co-activator wash buffer: 20 mM Hepes pH 7, 300 mM $(NH_4)SO_4$, 20 mM imidazole, 2.5 % glycerol, 1 mM DTT.
7. Gravity flow column.
8. Co-activator elution buffer: 20 mM Hepes pH 7, 300 mM $(NH_4)SO_4$, 250 mM imidazole, 2.5 % glycerol, 250 mM imidazole, 1 mM DTT.

9. Bradford reagent.
10. SDS-PAGE gels and gel-running equipment.
11. AKTA protein purification system.
12. Superdex 200 26/60 size-exclusion column.
13. Co-activator size-exclusion buffer: 20 mM Hepes pH 7, 300 mM NaCl, 2.5 % glycerol, 1 mM DTT.

2.5 Expression and Purification of Substrate: Cyclin B 1-95* and Ub-Cyclin B 1-95*

1. Low- and high-speed centrifuges.
2. PBS.
3. Substrate lysis buffer: 20 mM Tris pH 7.6, 150 mM NaCl, 1 mM DTT, 0.25 μg/mL lysozyme, 1 Complete™ EDTA-free protease inhibitor tablet (per 50 mL buffer).
4. Sonicator.
5. Glutathione sepharose.
6. Substrate wash buffer: 20 mM Tris pH 7.6, 150 mM NaCl, 1 mM DTT.
7. Tobacco etch virus (TEV) protease.
8. Gravity flow column.
9. SDS-PAGE gels and gel-running equipment.
10. Ni-NTA.
11. Substrate elution buffer: 20 mM Tris pH 7.6, 150 mM NaCl, 250 mM imidazole, 1 mM DTT.
12. Bradford reagent.
13. Amicon Ultra-15 centrifugal concentrator—3 kDa.
14. DTT.
15. PD-10 columns.
16. Substrate pre-label buffer: 50 mM Hepes pH 7, 150 mM NaCl (*do not include DTT*!).
17. Fluorescein-5-maleimide (F5M) in dimethyl sulfoxide (DMSO).
18. Substrate post-label buffer: 50 mM Hepes pH 7, 150 mM NaCl, 1 mM DTT.
19. AKTA protein purification system.
20. Superdex 75 16/60 column.
21. Substrate size-exclusion buffer: 20 mM Hepes pH 8, 200 mM NaCl, 1 mM DTT.

2.6 Expression and Purification of E1: UBA1

1. Low- and high-speed centrifuges.
2. PBS.
3. E1 lysis buffer: 20 mM Tris pH 7.6, 150 mM NaCl, 1 mM DTT, 0.25 μg/mL lysozyme, one Complete™ EDTA-free protease inhibitor tablet (per 50 mL buffer).

4. Sonicator.
5. Glutathione sepharose.
6. E1 wash buffer: 20 mM Tris pH 7.6, 150 mM NaCl, 1 mM DTT.
7. Gravity flow column.
8. E1 elution buffer: 20 mM Tris pH 7.6, 150 mM NaCl, 20 mM reduced glutathione, 1 mM DTT.
9. Bradford reagent.
10. SDS-PAGE gels and gel-running equipment.
11. AKTA protein purification system.
12. Resource Q anion-exchange column.
13. E1 buffer A: 20 mM Tris pH 7.6, 1 mM DTT.
14. E1 buffer B: 20 mM Tris pH 7.6, 1 M NaCl, 1 mM DTT.
15. Superdex 200 16/60 size-exclusion column.
16. E1 size-exclusion buffer: 20 mM Hepes pH 8, 200 mM NaCl, 1 mM DTT.

2.7 Expression and Purification of E2s: UBCH10 and UBE2S

1. Low- and high-speed centrifuges.
2. PBS.
3. E2 lysis buffer: 20 mM Tris pH 7.6, 150 mM NaCl, 1 mM DTT, 0.25 μg/mL lysozyme, one Complete™ EDTA-free protease inhibitor tablet (one tablet per 50 mL buffer).
4. Sonicator.
5. Ni-NTA resin.
6. E2 wash buffer: 20 mM Tris pH 7.6, 150 mM NaCl, 1 mM DTT.
7. Gravity flow column.
8. E2 elution buffer: 20 mM Tris pH 7.6, 150 mM NaCl, 250 mM imidazole, 1 mM DTT.
9. Bradford reagent.
10. SDS-PAGE gels and gel-running equipment.
11. AKTA protein purification system.
12. Superdex 200 16/60 size-exclusion column.
13. E2 size-exclusion buffer: 20 mM Hepes pH 8, 200 mM NaCl, 1 mM DTT.
14. Resource S cation-exchange columns.
15. E2 buffer A: 20 mM Tris pH 7.6, 1 mM DTT.
16. E2 buffer B: 20 mM Tris pH 7.6, 1 M NaCl, 1 mM DTT.
17. TEV protease.
18. Amicon Ultra-15 centrifugal concentrator—10 kDa.

2.8 Expression and Purification of Ubiquitin

1. Low- and high-speed centrifuges.
2. PBS.
3. Ub lysis buffer 20 mM Tris pH 7.6, 150 mM NaCl, 1 mM DTT, 0.25 μg/mL lysozyme and one Complete™ EDTA-free protease inhibitor tablet (per 50 mL buffer).
4. Glacial acetic acid.
5. SDS-PAGE gels and gel-running equipment.
6. Dialysis tubing—3 kDa cutoff.
7. Ub buffer A: 25 mM $NaC_2H_3O_2$, pH 4.5.
8. AKTA protein purification system.
9. Resource S cation-exchange column.
10. Ub buffer B: 25 mM $NaC_2H_3O_2$, pH 4.5, 1 M NaCl.
11. Amicon Ultra-15 centrifugal concentrator—3 kDa.
12. Superdex 75 16/60 size-exclusion column.
13. Ub size-exclusion buffer: 20 mM Hepes pH 8, 200 mM NaCl, 1 mM DTT.

2.9 APC/C Ubiquitylation Assay

1. 10 mg/mL BSA (Applichem) stock solution.
2. 50 mM $MgCl^{2+}$ATP pH 7 solution.
3. 4× SDS sample buffer: 250 mM Tris pH 6.8, 8 % SDS, 40 % glycerol, 400 mM DTT and 0.04 % bromophenol blue.
4. SDS-PAGE gels and gel-running equipment.
5. Fluorescence scanner.

3 Methods

3.1 Expression and Purification of Recombinant APC/C

Expression of recombinant APC/C is performed in insect cells. To date, published methods utilize co-expression techniques ranging from co-expressing each individual subunit from baculoviruses each containing the open reading frame of an individual APC/C subunit [14] to co-expression of the APC/C subunits using two baculoviruses containing a distribution of the individual subunits [15]. Here we briefly describe the expression and purification protocol we used to purify recombinant human APC/C which has been characterized in [8, 14, 22].

1. Co-infect Sf9 cells with the respective baculoviruses at a cell density of 1.0×10^6 and incubate at 27 °C at 100 rpm for 72 h to allow protein expression.
2. Harvest cells by centrifugation at 500 × *g* at 4 °C for 15 min, and wash once with PBS before resuspending in APC/C lysis buffer.

3. Sonicate cells for 15 s, and repeat three times, before centrifuging at 150,000 × *g* at 4 °C for 30 min.
4. Incubate the supernatant with equilibrated Streptactin resin on a rotor at 4 °C for 1 h (APC4 contains a C-terminal twin-Strep tag).
5. After binding, centrifuge the slurry at 1000 × *g* at 4 °C for 5 min, resuspend the Streptactin resin in APC/C wash buffer, transfer to a gravity flow column, and wash with 10 column volumes (CV) of APC/C wash buffer.
6. Elution of recombinant APC/C from the Streptactin resin is performed over 5 CV using APC/C elution buffer. Follow the elution by analyzing fractions using the Bradford assay.
7. Analyze the fractions by SDS-PAGE.
8. The relevant fractions should then be pooled, diluted with APC/C buffer A to a final concentration of 100 mM NaCl, and loaded onto a pre-equilibrated POROS HQ anion-exchange column. The bound recombinant APC/C is eluted using a gradient of APC/C buffer B.
9. Fractions should be analyzed by SDS-PAGE with the appropriate fractions pooled, concentrated, and loaded onto a Superose 6 size-exclusion column equilibrated in APC/C size-exclusion buffer (*see* **Note 3**).
10. The resulting fractions from size exclusion should then be analyzed by SDS-PAGE with respective fractions pooled and concentrated to 1 mg/mL, aliquoted, flash frozen, and stored at −80 °C.

3.2 Expression and Purification of the Co-activators: CDC20 and CDH1

Working with a recombinant form of the human APC/C allows great control over which co-factors in vitro experiments are performed with. As such the co-activators need to be purified separately. We briefly describe this below.

1. Infect Sf9 cells at a cell density of 1.0×10^6 with a baculovirus containing either the full-length reading frame of CDC20 or CDH1 with an N-terminal 3myc-his6 and incubate at 100 rpm at 27 °C for 72 h.
2. Following expression, harvest cells by centrifugation at 500 × *g* at 4 °C for 15 min, and wash once with PBS before resuspending in co-activator lysis buffer.
3. Dounce-homogenize cells 5×, and repeat three times, before centrifuging at 150,000 × *g* at 4 °C for 30 min.
4. Incubate the supernatant with equilibrated Ni-NTA resin on a rotor at 4 °C for 1 h.
5. After binding, centrifuge the slurry at 1000 × *g* for 5 min at 4 °C, resuspend in co-activator wash buffer, transfer to a gravity flow column, and wash with 10 CV of co-activator wash buffer.

6. Perform the elution over 5 CV using co-activator elution buffer. Follow the elution by analyzing fractions using the Bradford assay.
7. Analyze the fractions by SDS-PAGE.
8. Pool the appropriate fractions, concentrate, and load onto a Superdex 200 26/60 size-exclusion column equilibrated in co-activator size-exclusion buffer.
9. Fractions should be analyzed by SDS-PAGE with the respective fractions concentrated to ~1 mg/mL, aliquoted, flash frozen, and stored at −80 °C (*see* **Note 4**).

3.3 Expression and Purification of Substrate: Cyclin B 1-95* and Ub-Cyclin B 1-95*

This substrate construct is an iteration of previous versions of the N-terminus of cyclin B [17].

1. Substrate is bacterially produced and is expressed in the *E. coli* strain BL21 (DE3) CodonPlus-RIL. Bacteria are grown to an OD of 0.8, protein expression is induced by treatment with 0.6 M IPTG, and the culture is grown overnight at 16 °C.
2. Harvest cells by centrifugation at 4500 × *g* at 4 °C for 15 min, and wash once with PBS before resuspending in substrate lysis buffer.
3. Incubate cells rotating at 4 °C for 30 min before sonicating for 15 s, repeat four times, and then centrifuge at 25,000 × *g* at 4 °C for 30 min.
4. Incubate the supernatant with equilibrated glutathione sepharose resin on a rotor at 4 °C for 1 h.
5. After binding, centrifuge the slurry at 1000 × *g* at 4 °C for 5 min and wash with 5 CV substrate wash buffer.
6. Resuspend the resin in 1 CV substrate wash buffer supplemented with TEV protease and incubate on a rotor overnight at 4 °C.
7. The next morning transfer the slurry to a gravity flow column and collect the flow through. Add a further 1 CV pulse of substrate wash buffer and collect the flow through.
8. Analyze the flow through by SDS-PAGE.
9. Incubate the flow through with equilibrated Ni-NTA resin on a rotor at 4 °C for 1 h.
10. After binding, centrifuge the slurry at 1000 × *g* at 4 °C for 5 min, resuspend in substrate wash buffer, transfer to a gravity flow column, and wash with 10 CV of substrate wash buffer.
11. Elute the protein over 5 CV using substrate elution buffer. Follow the elution by analyzing fractions using the Bradford assay.
12. Analyze the flow through by SDS-PAGE.
13. Concentrate the flow through containing substrate to ~2.5 mL and continue to label the substrate of interest.

3.4 Fluorescent Labeling of the Substrate of Interest

1. Reduce the substrate by incubating with 20 mM DTT for 20 min.
2. Desalt the reduced substrate twice using PD-10 columns into substrate pre-label buffer.
3. Dissolve the F5M in dimethyl sulfoxide (DMSO).
4. The dissolved F5M is mixed with the substrate at a 10× higher concentration and incubated at room temperature for 3 h (*see* **Note 5**).
5. Quench the chemical reaction between the maleimide group and the cysteine in the substrate by the addition of a final concentration of 10 mM DTT.
6. Desalt the labeled substrate a further two times using PD-10 columns using substrate post-label buffer and further purify by size-exclusion chromatography using a Superdex 75 16/60 column equilibrated in substrate size-exclusion buffer.
7. Fractions should be analyzed by SDS-PAGE with the appropriate fractions concentrated to ~5 mg/mL, aliquoted, flash frozen, and stored at −80 °C [22].

3.5 Expression and Purification of E1: UBA1

The following method has been previously published [23].

1. GST-UBA1 (E1; a kind gift from Cynthia Wolberger) is bacterially produced and is expressed in the *E. coli* strain BL21 (DE3) CodonPlus-RIL. Bacteria are grown to an OD of 0.8, protein expression is induced by treatment with 0.6 M IPTG, and the culture is grown overnight at 16 °C.
2. Harvest cells by centrifugation at 4500 × *g* at 4 °C for 15 min, wash once with PBS, and resuspend in E1 lysis buffer.
3. Incubate cells by rotating for 30 min at 4 °C, before sonicating for 15 s, repeat four times, and centrifuge at 25,000 × *g* at 4 °C for 30 min.
4. Incubate the supernatant with equilibrated glutathione sepharose resin on a rotor at 4 °C for 1 h.
5. Following binding, centrifuge the resin at 1000 × *g* at 4 °C for 5 min, resuspend in E1 wash buffer, transfer to a gravity flow column, and wash with 10 CV of E1 wash buffer.
6. Elute the protein over 5 CV using E1 elution buffer. Follow the elution by analyzing fractions using the Bradford assay.
7. Analyze the fractions by SDS-PAGE.
8. The respective fractions should then be pooled, diluted with E1 buffer A to 50 mM NaCl, and loaded onto an equilibrated anion-exchange column. The bound UBA1 is eluted using a gradient of E1 buffer B.

9. Analyze fractions by SDS-PAGE, pool the appropriate fractions, concentrate, and load onto a Superdex 200 16/60 size-exclusion column equilibrated in E1 size-exclusion buffer.
10. Fractions should be analyzed by SDS-PAGE with the respective fractions concentrated to ~5 mg/mL, aliquoted, flash frozen, and stored at −80 °C.

3.6 Expression and Purification of E2s: UBCH10

1. UBCH10-His_6 is bacterially produced and is expressed in the *E. coli* strain BL21 (DE3) CodonPlus-RIL. Bacteria are grown to an OD of 0.8, protein expression is induced by treatment with 0.6 M IPTG, and the culture is grown overnight at 23 °C.
2. Post-expression, harvest cells by centrifugation at 4500 × *g* at 4 °C for 15 min, and wash once with PBS before being resuspended in E2 lysis buffer.
3. Incubate rotating for 30 min at 4 °C before sonicating for 15 s, repeat four times, and centrifuge at 25,000 × *g* at 4 °C for 30 min.
4. Incubate the supernatant with equilibrated Ni-NTA resin on a rotor at 4 °C for 1 h.
5. After binding, centrifuge the slurry at 1000 × *g* at 4 °C for 5 min, resuspend in E2 wash buffer, transfer to a gravity flow column, and wash with 10 CV of E2 wash buffer.
6. Conduct elution over 5 CV using E2 elution buffer. Follow the elution by analyzing fractions using the Bradford assay.
7. Analyze fractions by SDS-PAGE.
8. Pool the appropriate fractions, concentrate, and load onto a Superdex 200 16/60 size-exclusion column equilibrated in E2 size-exclusion buffer.
9. Fractions from size exclusion should be analyzed by SDS-PAGE with respective fractions pooled, concentrated to ~5 mg/mL, aliquoted, flash frozen, and stored at −80 °C.

3.7 Expression and Purification of E2s: UBE2S

1. His_6-TEV-Flag-PS-UBE2S is bacterially produced and is expressed in the *E. coli* strain BL21 (DE3) CodonPlus-RIL. Bacteria are grown to an OD of 0.8, protein expression is induced by treatment with 0.6 M IPTG, and the culture is grown overnight at 23 °C.
2. Harvest cells by centrifugation at 4500 × *g* at 4 °C for 15 min, and wash once with PBS before being resuspended in E2 lysis buffer.
3. Incubate cells rotating at 4 °C for 30 min before sonicating for 15 s, repeat four times, and centrifuge at 25,000 × *g* at 4 °C for 30 min.

4. Incubate the supernatant with equilibrated Ni-NTA resin rotating at 4 °C for 1 h.
5. After binding, centrifuge the slurry at 1000 × *g* at 4 °C for 5 min and wash with 5 CV E2 wash buffer.
6. Resuspend the resin in 1 CV E2 wash buffer supplemented with TEV protease and incubate on a rotor overnight at 4 °C.
7. The following morning transfer the slurry to a gravity flow column and collect the flow through. Pulse with a further 1 CV E2 wash buffer and collect the flow through.
8. Dilute the flow through with E2 buffer A to a final concentration of 50 mM NaCl, and load onto an equilibrated cation-exchange column. The bound UBE2S is eluted using a gradient of E2 buffer B.
9. Analyze fractions by SDS-PAGE, pool the appropriate fractions, concentrate, and load onto a Superdex 200 16/60 size-exclusion column equilibrated in E2 size-exclusion buffer.
10. Fractions from size exclusion should be analyzed by SDS-PAGE with respective fractions pooled, concentrated to ~5 mg/mL, aliquoted, flash frozen, and stored at −80 °C.

3.8 Expression and Purification of Ubiquitin

The following method has been previously published [25].

1. Ubiquitin is bacterially produced and is expressed in the *E. coli* strain BL21 (DE3) CodonPlus-RIL. Bacteria are grown to an OD of 0.8, protein expression is induced by treatment with 0.6 M IPTG, and the culture is grown overnight at 16 °C.
2. Harvest cells by centrifugation at 4500 × *g* at 4 °C for 15 min, and wash once with PBS before resuspending in Ub lysis buffer.
3. Incubate cells rotating at 4 °C for 30 min before sonicating for 15 s, repeat four times, and centrifuge at 25,000 × *g* at 4 °C for 30 min.
4. Acidify the supernatant with glacial acetic acid to approximately pH 4–4.5 (*see* **Note 6**).
5. Centrifuge the supernatant again at 25,000 × *g* at 4 °C for 30 min.
6. Analyze the supernatant by SDS-PAGE.
7. Dialyze the supernatant in 3 kDa dialysis tubing at 4 °C overnight in Ub buffer A.
8. Centrifuge the supernatant again at 25,000 × *g* at 4 °C for 30 min and load onto an equilibrated cation-exchange column. The bound ubiquitin is eluted using a gradient of Ub buffer B.

9. Analyze fractions by SDS-PAGE, pool the appropriate fractions, concentrate, and load onto a Superdex 7516/60 size-exclusion column equilibrated in Ub size-exclusion buffer.
10. Fractions from size exclusion should be analyzed by SDS-PAGE with respective fractions pooled, concentrated to ~10 mg/mL, aliquoted, flash frozen, and stored at −80 °C.

Figure 2 illustrates the purity to which the above-described individual proteins can be purified.

3.9 APC/C Ubiquitylation Assay

A typical APC/C ubiquitylation assay is conducted at room temperature in a volume of 20 μL. Below we describe the basic procedure of such an assay. Note that the components in the assay can be varied depending on the purpose of the experiment and the pipetted volumes may change depending on the stock concentrations of the purified components used (*see* **Note 7**).

1. The individual purified components (APC/C, co-activator, substrate, E2s) are mixed together, on ice, to reach the appropriate final concentrations. In a second tube, E1 and ubiquitin are mixed together.
2. The mixtures are then equilibrated to room temperature for 10 min.

Tube 1

Purified component	Concentration of stock	Volume (μL)	Final concentration in assay
BSA	10 mg/mL	0.5	0.25 mg/mL
$MgCl_2ATP$	50 mM	2	5 mM
Substrate	10 μM	1	500 nM
UBCH10	2.5 μM	2	250 nM
UBE2S	2.5 μM	2	250 nM
APC/C	150 nM	2	15 nM
Cdh1	20 μM	1	1 μM
Buffer	1×	5.5	–
Total volume: 16 μL			

Tube 2:

Purified component	Concentration of stock	Volume (μL)	Final concentration in assay
E1	1 μM	2	100 nM
Ubiquitin	1 mM	2	100 μM
Total volume: 4 μL			

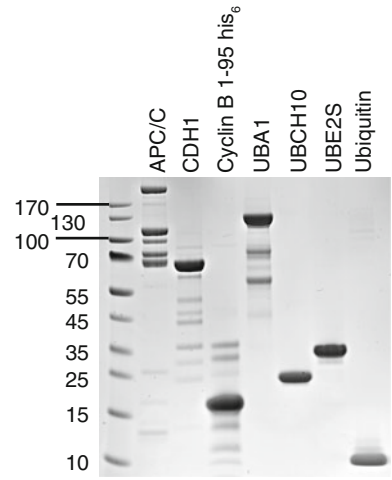

Fig. 2 SDS-PAGE gel of the individual purified protein components described in this chapter. From *left* to *right*: APC/C, CDH1, cyclin B 1-95, UBA1, UBCH10, UBE2S, ubiquitin

3. The ubiquitylation reaction is initiated by adding the volume in tube 1 to that of tube 2, with the assay allowed to proceed for 5–15 min at room temperature.
4. The reaction is stopped by the addition of 6 μL 4× SDS sample buffer to the reaction volume followed by a 5-min incubation at 95 °C.
5. The reaction products are then resolved in the dark by SDS-PAGE using a NuPAGE 4–12 % Bis-Tris, 8 cm × 8 cm, 1.0 mm thick, 15-well protein gel according to the manufacturer's recommendations. Alternatively, homemade polyacrylamide gels can also be used. The results are subsequently visualized by use of a fluorescence scanner set for detecting Alexa Fluor 488 (we use a Typhoon laser scanner in fluorescence scanning mode, with a voltage of 750 V) (*see* **Note 8**).

3.10 Quantification

This assay allows assaying of a wide range of parameters regarding APC/C activities with a range of different substrates, E2 combinations, and inhibitors, as have been published [8, 22]. We describe one typical scenario here for quantifying the apparent Km for the E2, UBE2S.

1. We determined assay conditions in the initial velocity range for 10-min reactions at room temperature to use 10 nM APC/C and 0.5 μM Ub-CyclinBNTD*.
2. Because UBE2S processively generates poly-ubiquitin chains, reaction products were quantified by determining the intensity

of all ubiquitinated species (individual bands) using Image Quant software, corrected for background by subtracting the sum of intensities in the corresponding lane for control reactions lacking APC/C.

3. The values for ½ Vmax and Km values can be calculated by fitting the initial velocity to a hyperbolic curve according to Michaelis-Menten kinetics using the equation $v = \mathrm{Vmax}[\mathrm{UBE2S}]/(\mathrm{Km} + [\mathrm{UBE2S}])$. Prism 6 software (GraphPad) is suitable for performing curve-fitting.

4 Notes

1. *E. coli* offers a fast and effective system for protein expression. There are many different strains of *E. coli* offering various advantages such as the co-expression of rare codon encoding t-RNAs (e.g., BL21 (DE3) CodonPlus-RIL), tight control of protein expression suitable for toxic proteins (e.g., BL21 (DE3) pLysS), and induction of proper protein folding (e.g., Origami (DE3)).
2. The baculovirus-insect cell expression system provides a mode of production that yields large quantities of recombinant proteins that require eukaryotic chaperones or the need to be posttranslationally modified by eukaryotic enzymes. There are various insect cell lines available such as Sf9 and High Five, as well as many different types of media including Grace's media (Sigma-Aldrich), Hyclone SFX (GE Lifesciences), Sf-900 III (Life Technologies), and ESF 921 (Expression Systems) offering many solutions in recombinant protein production.
3. Be conservative with respect to the fractions that you pool for size-exclusion chromatography. Focus on fractions that contain nice stoichiometric APC/C.
4. Do not concentrate the co-activators to higher concentrations than is necessary because these proteins tend to form aggregates and to precipitate.
5. Ensure that less than 5 % of the total volume contains DMSO as to limit the susceptibility of the substrate to DMSO.
6. Do not be concerned that a lot of protein is precipitating; these are bacterial host proteins!
7. We recommend making small working aliquots to avoid repeated freeze-thaw cycles of these enzymes. APC/C, the co-activators, and E1 are particularly sensitive to freeze-thaw cycles.
8. When setting up this assay it is worth testing different scan voltages to determine at which settings the best images are obtained.

References

1. Pines J (2011) Cubism and the cell cycle: the many faces of the APC/C. Nat Rev Mol Cell Biol 12:427–438
2. Primorac I, Musacchio A (2013) Panta rhei: the APC/C at steady state. J Cell Biol 201: 177–189
3. Delgado-Esteban M, García-Higuera I, Maestre C et al (2013) APC/C-Cdh1 coordinates neurogenesis and cortical size during development. Nat Commun 4:2879
4. Eguren M, Porlan E, Manchado E et al (2013) The APC/C cofactor Cdh1 prevents replicative stress and p53-dependent cell death in neural progenitors. Nat Commun 4:2880
5. Chang L, Barford D (2014) Insights into the anaphase-promoting complex: a molecular machine that regulates mitosis. Curr Opin Struct Biol 29:1–9
6. Duda DM, Scott DC, Calabrese MF et al (2011) Structural regulation of cullin-RING ubiquitin ligase complexes. Curr Opin Struct Biol 21:257–264
7. Craney A, Rape M (2013) Dynamic regulation of ubiquitin-dependent cell cycle control. Curr Opin Cell Biol 25:704–710
8. Frye JJ, Brown NG, Petzold G et al (2013) Electron microscopy structure of human APC/CCDH1–EMI1 reveals multimodal mechanism of E3 ligase shutdown. Nat Struct Mol Biol 20:827–835
9. Chang L, Zhang Z, Yang J et al (2014) Molecular architecture and mechanism of the anaphase-promoting complex. Nature 513: 388–393
10. Chang L, Zhang Z, Yang J et al (2015) Atomic structure of the APC/C and its mechanism of protein ubiquitination, Nature. advance online publication.
11. Herzog F, Peters J (2005) Large-scale purification of the vertebrate anaphase-promoting complex/cyclosome. Methods Enzymol 398: 175–195, Elsevier
12. Kraft C, Gmachl M, Peters JM (2006) Methods to measure ubiquitin-dependent proteolysis mediated by the anaphase-promoting complex. Methods 38:39–51
13. Schreiber A, Stengel F, Zhang Z et al (2011) Structural basis for the subunit assembly of the anaphase-promoting complex. Nature 470: 227–232
14. Uzunova K, Dye BT, Schutz H et al (2012) APC15 mediates CDC20 autoubiquitylation by APC/CMCC and disassembly of the mitotic checkpoint complex. Nat Struct Mol Biol 19: 1116–1123
15. Zhang Z, Yang J, Kong EH et al (2013) Recombinant expression, reconstitution and structure of human anaphase-promoting complex (APC/C). Biochem J 449:365–371
16. Dimova NV, Hathaway NA, Lee B-H et al (2012) APC/C-mediated multiple monoubiquitylation provides an alternative degradation signal for cyclin B1. Nat Cell Biol 14:168–176
17. King RW, Glotzer M, Kirschner MW (1996) Mutagenic analysis of the destruction signal of mitotic cyclins and structural characterization of ubiquitinated intermediates. Mol Biol Cell 7:1343–1357
18. Jin L, Williamson A, Banerjee S et al (2008) Mechanism of ubiquitin-chain formation by the human anaphase-promoting complex. Cell 133:653–665
19. Kirkpatrick DS, Hathaway NA, Hanna J et al (2006) Quantitative analysis of in vitro ubiquitinated cyclin B1 reveals complex chain topology. Nat Cell Biol 8:700–710
20. Meyer H-J, Rape M (2014) Enhanced protein degradation by branched ubiquitin chains. Cell 157:910–921
21. Wu T, Merbl Y, Huo Y et al (2010) UBE2S drives elongation of K11-linked ubiquitin chains by the Anaphase-Promoting Complex. Proc Natl Acad Sci 107:1355–1360
22. Brown NG, Watson ER, Weissmann F et al (2014) Mechanism of polyubiquitination by human anaphase-promoting complex: RING repurposing for ubiquitin chain assembly. Mol Cell 56:246–260
23. Eletr ZM, Huang DT, Duda DM et al (2005) E2 conjugating enzymes must disengage from their E1 enzymes before E3-dependent ubiquitin and ubiquitin-like transfer. Nat Struct Mol Biol 12:933–934
24. Pickart CM, Raasi S (2005) Controlled synthesis of polyubiquitin chains. Methods Enzymol 399:21–36

Chapter 19

Using the Fly-FUCCI System for the Live Analysis of Cell Cycle Dynamics in Cultured *Drosophila* Cells

N. Zielke, M. van Straaten, J. Bohlen, and B.A. Edgar

Abstract

Cultured *Drosophila* cells are an attractive system for live imaging experiments, as this cell type is not very demanding in terms of temperature and media composition. Moreover, cultured *Drosophila* cell lines are very responsive to RNAi without being prone to off-target effects, and thus have become important for use in high-content screening. We have developed a fly-specific *f*luorescent, *u*biquitination-based *c*ell *c*ycle *i*ndicator (FUCCI) system that enables faithful detection of G1, S, and G2 phases, and is thus a powerful tool for the analysis of cell cycle dynamics in living or fixed cells. Here, we describe a protocol for the generation of cell lines stably expressing the Fly-FUCCI sensors, followed by a description of how these cell lines can be employed in studies of cell cycle oscillation using live microscopy.

Key words *Drosophila*, FUCCI, S2 cells, Stable transfection, Live imaging, Cell cycle oscillation

1 Introduction

A major challenge of studying cell proliferation is to visualize cell cycle dynamics in living cells. In recent years, the *f*luorescent, *ubiquitination-based c*ell *c*ycle *i*ndicator (FUCCI) method, which assigns specific fluorescence labels to individual stages of the cell cycle, has become the standard approach for visualizing cell cycle oscillations by live microscopy [1]. We have generated a *Drosophila-specific* FUCCI system (Fly-FUCCI) that greatly simplifies the analysis of cell proliferation in developing flies, adults, and cultured cells [2]. The Fly-FUCCI system is based on the degradation signals (degrons) of *Drosophila* cyclin B and E2F1, which are targeted for proteolysis by the E3-ligase complexes APC/C and $CRL4^{Cdt2}$, respectively [3]. The APC/C is active from late mitosis throughout G1 phase and many of its substrates contain a destruction box (D-box) motif [4]. A functional D-box can be transferred to heterologous proteins, which prompted us to use a chimeric protein consisting of the N-terminal D-box containing region of *Drosophila* cyclin B (amino acid (a.a.) 1–266) coupled to red fluorescent

Amanda S. Coutts and Louise Weston (eds.), *Cell Cycle Oscillators: Methods and Protocols*, Methods in Molecular Biology, vol. 1342, DOI 10.1007/978-1-4939-2957-3_19,

protein (RFP) to label cells in S/G2/M phase. This signal is destroyed during mitosis and absent during G1. Similarly, we have fused green fluorescent protein (GFP) to the N-terminal region (a.a. 1–230) of the *Drosophila* transcription factor E2F1. This fragment contains a conserved PIP-box motif that confers S phase-specific degradation by $CRL4^{Cdt2}$ [5, 6]. Thus $GFP\text{-}E2F1_{1–230}$ marks cells residing in G1, G2, and M phases, but is absent from S-phase cells. Besides these degrons the Fly-FUCCI probes contain no other functional domains, and therefore cannot influence cell cycle progression. In contrast to the original FUCCI method, which only distinguishes between G1 and S/G2/M phase, the Fly-FUCCI system can be used to visualize all stages of interphase: G1 cells are marked by GFP, S-phase cells are marked by RFP, and cells in G2 phase express both markers and therefore appear yellow (Fig. 1b). The Fly-FUCCI probes were cloned into the pAc5-STABLE-2 vector (Fig. 1a), which allows efficient selection of stable cell lines [7]. This vector contains the *Drosophila actin5c* promoter, which is known to produce robust expression in commonly used *Drosophila* cell lines such as S2, S2-R+, and Kc [8, 9]. Key to this method is that both Fly-FUCCI probes and a neomycin resistance cassette are expressed as a single polypeptide (Fig. 1a). The components (cistrons) are separated by T2A sequences from the insect virus *Thosea asigna* [10, 11], which mediate self-cleavage of the multicistronic protein into individual peptides. 2A-like sequences do not have protease activity; the self-cleavage rather occurs co-translationally by a process termed "ribosome skipping" [12]. Essentially, the 2A-like sequence impinges on the peptidyltransferase center of the ribosome and thereby releases the nascent chain while the remainder of the polyprotein is translated. This design ensures that both Fly-FUCCI probes are always expressed at the same ratio and that only cells with robust expression will be selected. Using this strategy we generated a stable S2-R+ cell line that enables accurate tracking of cell cycle transitions by live microscopy (Fig. 2) [2], and thereby facilitates the detection of irregular cell cycle signatures.

The original FUCCI system has been successfully used as readout in high-content screening [13]. Although the FUCCI system has clear advantages over conventional proliferation markers, this strategy has not yet been broadly applied. A likely explanation is that high-throughput live imaging of cultured mammalian cells is technically demanding, and thus too expensive for many laboratories. *Drosophila* cell lines, by contrast, can be maintained at room temperature without the need of extensive environmental control. Furthermore, RNAi is more effective in *Drosophila* cell lines and less affected by off-target effects, which can obscure the results in mammalian cells. Hence, Fly-FUCCI-expressing *Drosophila* cells could provide a cost-effective answer for imaging-based screening

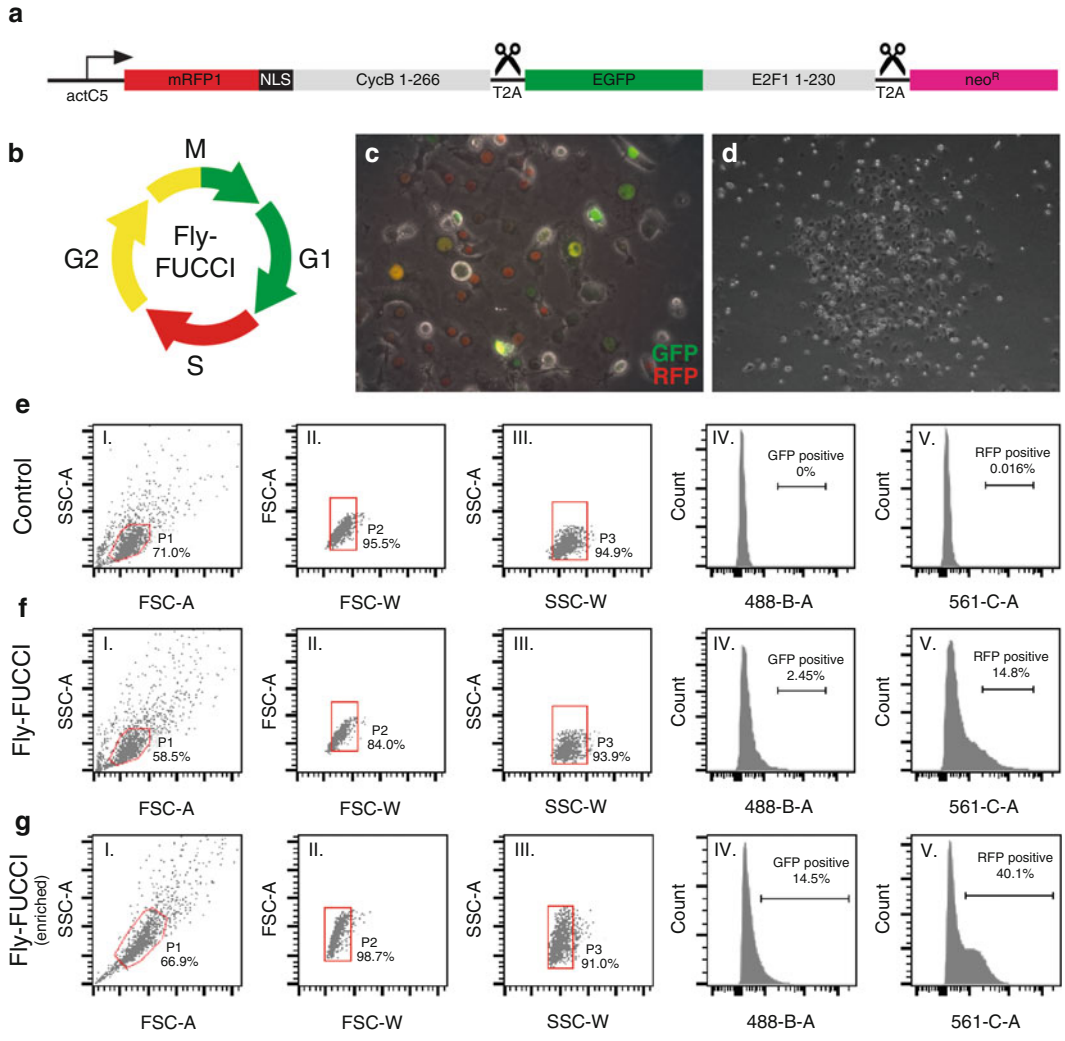

Fig. 1 Flow cytometric enrichment of Fly-FUCCI-expressing S2-R+ cells. (**a**) Schematic of the multicistronic Fly-FUCCI construct. mRFP1-CycB$_{1–266}$, GFP-E2F1$_{1–230}$, and the neomycin resistance gene are expressed as a single peptide under the control of the *act5C* promoter. T2A autocleavage sequences separate the coding regions of each cassette. (**b**) The Fly-FUCCI system labels cells in G1 phase with *green* fluorescence, cells in S phase are marked by *red* fluorescence, and cells in G2 phase are double positive and hence appear *yellow*. (**c**) Fly-FUCCI-expressing S2-R+ cells. GFP-E2F1$_{1–230}$ is shown in *green*, mRFP1-CycB$_{1–266}$ in *red*. (**d**) Phase-contrast image of a Geneticin-resistant cell colony. (**e**, **f**) Gating strategy for the flow cytometry-based enrichment of Fly-FUCCI-expressing S2-R+ cells. The brackets in panels *IV* and *V* indicate the gates that have been used for selecting GFP/RFP double-positive cells. (**g**) FACS profiles of Fly-FUCCI-expressing S2-R+ cells after enrichment. FSC-A: Forward scatter-area; FSC-W: forward scatter-width; SSC-A: side scatter-area; SSC-W: forward scatter-width; 488-B-A: area of the signal detected from 488 mm laser with 530/30 nm band-pass filter; 561-C-A: area of the signal detected from 561 mm laser with 582/15 nm band-pass filter

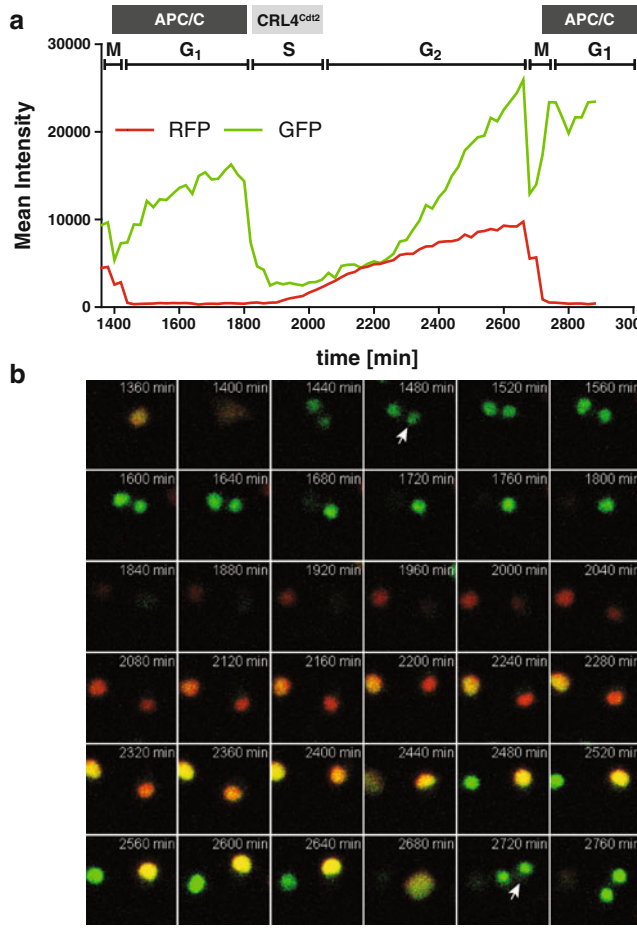

Fig. 2 Real-time imaging of cell cycle oscillations in Fly-FUCCI-expressing S2-R+ cells. (**a**) Time plot showing the sequential proteolysis of the Fly-FUCCI probes, mediated by the ubiquitin E3 ligases APC/C and $CRL4^{Cdt2}$. GFP-$E2F1_{1–230}$ accumulates during G1 phase, but is rapidly destroyed upon the onset of DNA synthesis. $CRL4^{Cdt2}$ is inactivated after completion of S phase, allowing the recovery of GFP-$E2F1_{1–230}$ levels during G2 phase. The proteasomal degradation mRFP1-$CycB_{1–266}$ is mediated by APC/C and lasts from mid-mitosis throughout G1 phase. During S phase the levels of mRFP1-$CycB_{1–266}$ start to increase and peak at the end of G2 phase. Hence, tracing color changes by live imaging allows precise determination of the duration of each cell cycle phase (G1 = 6.7 h, S = 4.7 h, and G2 = 8.7 h). (**b**) Image gallery illustrating the sequence of color changes of a cell executing a whole cell cycle. Images were taken every 20 min of overall time frame of 48 h. GFP is shown in *green* and RFP in *red*. The arrows indicate the daughter cells that were quantified in (**a**)

approaches [14–17]. Importantly, we have also generated a collection of transgenic *Drosophila* strains that express the Fly-FUCCI sensors under several different promoters [2]. These stocks are publically available at the Bloomington *Drosophila* Stock Center at Indiana University (http://flystocks.bio.indiana.edu/Browse/misc-browse/Fly-FUCCI.php), and will enable the researcher to do high-precision in vivo validation of results from cell-based experiments.

2 Materials

2.1 Drosophila Cell Culture

A general description of equipment and reagents required for insect cell culture can be found in [9, 15].

1. *Drosophila* cell line (*see* **Note 1**).
2. Multicistronic Fly-FUCCI vector [2], https://dgrc.cgb.indiana.edu/vectors/Catalog.
3. Incubator at 25 °C (no cooling needed if the ambient temperature is kept below 20 °C), sterile tissue culture hood, centrifuge.
4. Cell culture flasks 25 and 75 cm^2.
5. 15 and 50 ml polypropylene tubes, graduated, conical bottom, with screw cap sterile.
6. Schneider's medium (1×) with L-Glutamine (Gibco Cat#217020-024; *see* **Note 2**).
7. Fetal bovine serum (FBS) (PAN Cat# P30-1502, *see* **Notes 3** and **4**).
8. 500 ml vacuum filtration device, GP Millipore Express Plus Membrane, pore size 0.22 μm (Nalgene Cat#SCGPU05RE).
9. Penicillin-streptomycin, sterile filtered (10,000 U/ml–10 mg/ml).
10. Complete Schneider's medium: Schneider's medium supplemented with 10 % FBS, 100 U/ml penicillin, and 100 μg/ml streptomycin.
11. Phosphate-buffered saline (1× PBS), without Ca^{2+}, Mg^{2+}, sterile filtered.
12. Trypsin-EDTA (0.05–0.02 % in PBS), with phenol red, without Ca^{2+}, Mg^{2+}, sterile filtered.
13. Cell counter (e.g., Cellometer Auto T4, Nexcelom Bioscience) or hemocytometer.
14. 20 ml Syringe, sterile.
15. Syringe filter (33 mm), pore size 0.22 μm, sterile (Carl Roth AG Cat#KH54.1).

16. 2 ml cryo-vials.
17. Cryo freezing container (Nalgene Cat#5100-0001).
18. Dimethyl sulfoxide (DMSO) cell culture grade.
19. Freezing medium: 5 ml DMSO, 20 ml complete Schneider's medium, 25 ml FBS.

2.2 Selection of Stable Cell Lines

1. Calcium Phosphate Transfection Kit (Invitrogen Cat#44-0052).
2. Geneticin (50 mg/ml).
3. 1.5 ml polypropylene microcentrifuge tube.
4. 5 ml polystyrene round-bottom tube.
5. Glass Pasteur pipettes.
6. Cell culture microscope equipped with fluorescent light source (optional).

2.3 FACS Enrichment of FUCCI-Expressing Cells

1. Fluorescence-activated cell sorter fitted with 488 and 561 nm laser lines (e.g., FACS-ARIA III, BD-Biosciences).
2. 5 ml polystyrene round-bottom tube with Cellstrainer cap (BD-Falcon #352235).

2.4 Live Microscopy

1. Wide-field live imaging system (e.g., xcellence rt, Olympus).
2. 35 mm dish, high, ibiTreat (#81156).
3. µ-Slide 8-well, ibiTreat (#80826).

3 Methods

3.1 Drosophila Cell Culture

Since Schneider's medium does not rely on bicarbonate buffering and fly cells are quite tolerant to pH changes, *Drosophila* cells can be cultured without CO_2 control, which is a clear advantage over mammalian cell culture systems. We prefer S2-R+ cells [18] to the original S2 cell line [19], because these cells are adherent, and therefore better suited for live microscopy. However, different *Drosophila* cell lines respond differently to signaling cues such as Wingless or Ecdysone [18, 20], and thus certain experiments may require the use of other cell lines. Detailed information about the characteristics of the various currently available *Drosophila* cell lines can be found in [21] and on the webpage of the *Drosophila* Genomics Resource Center (https://dgrc.cgb.indiana.edu/cells/Catalog). Insect cells are usually cultivated in broth-like media, which are commercially available for the most commonly used cell lines. For the culture of S2-R+ cells we are relying on Schneider's medium supplemented with FBS, penicillin, and streptomycin and for the remainder of the text we will refer to this mixture as complete Schneider's medium ([22], *see* **Note 5**).

S2, S2-R+, and Kc cells are healthiest during their exponential growth phase, which occurs at concentrations between 5×10^5 and 1×10^7 cells/ml [9]. Under optimal growth conditions S2 cells divide approximately once per day [21], and thus the cells should be subcultured (split) twice a week.

Compared to mammalian cells, the karyotype of *Drosophila* cell lines is relatively stable [9]. Nevertheless, we recommend frequently inspecting the cells under the microscope and routinely freezing aliquots (*see* Subheading 3.1.2). Broth-type media are prone to contaminations by bacteria or fungi, and thus all operations should be conducted in a sterile laminar flow hood (*see* **Note 6**). Detailed guidelines for cultivating *Drosophila* cell lines can be found in [9, 15].

3.1.1 Subculturing

In contrast to other insect cell lines, which detach from the bottom of the flask by simple agitation, S2-R+ cells require trypsinization.

1. Carefully remove the medium without detaching the cells from the bottom of the flask.
2. Gently wash the cells with 1× PBS (e.g., 5 ml for a 25 cm^2 flask) to remove dead cells and residual medium, which otherwise will interfere with the trypsinization procedure.
3. Incubate the cells for 5 min with 1 volume trypsin-EDTA (e.g., 2 ml for a 25 cm^2 flask). Check under the microscope whether most of the cells have detached from the bottom of the flask. If the majority of the cells are still adhering, increase the incubation time accordingly.
4. Stop the trypsinization procedure by adding 2 volumes of complete medium (e.g., 4 ml for a 25 cm^2 flask). Use a pipette to flush the remaining cells from the bottom of the flask. Transfer suspended cells to a 15 ml polypropylene tube.
5. Centrifuge for 7 min at room temperature with 100 rcf (relative centrifugal force). Remove supernatant and add 10 ml of complete Schneider's medium.
6. Dilute cells 1:20 in complete Schneider's medium (e.g., 6 ml for 25 cm^2).

3.1.2 Freezing of Drosophila Cell Lines

To ensure high recovery rates, we disperse the cells of a well-grown 75 cm^2 flask (1×10^6 cells/ml) into two aliquots. Because DMSO is toxic to unfrozen cells, it is crucial that this procedure is carried out quickly.

1. Label the desired number of 2 ml cryo-vials (e.g., cell type, passage number, construct, and data). Utilize an alcohol and liquid nitrogen-resistant pen to prevent labels from washing off during the freezing/recovery procedure.
2. Place an isopropanol-filled cryo-freezing container in an icebox.
3. Prepare freezing medium and store it in the icebox until use.

4. Harvest cells by trypsinization as described in Subheading 3.1.1, **steps 1–4**.
5. Resuspend the pellet in 3.6 ml freezing medium and split the cell suspension equally between two cryo-vials. To ensure a smooth workflow we recommend unscrewing the lids beforehand.
6. Place the tubes in the cryo-freezing container and transfer it to a –80 °C freezer.
7. On the following day, transfer the aliquots to a liquid nitrogen tank for long-term storage (*see* **Note 7**).

3.1.3 Recovery of Drosophila Cell Lines from Liquid Nitrogen

Because of the toxicity of the DMSO in the freezing medium, it is essential that thawed cells will be rapidly transferred to fresh medium.

1. Prepare labeled 15 ml tubes with 10 ml complete Schneider's medium without antibiotics in the cell culture hood.
2. Retrieve aliquots from liquid nitrogen tank.
3. Thaw frozen aliquots quickly in a water bath set to 30 °C until the medium has almost completely thawed.
4. Before transferring the tubes to the cell culture hood, clean the outer surface of the tubes with 70 % ethanol from a spray bottle.
5. Transfer thawed cells with a 1 ml micropipette to the prepared 15 ml tube with complete Schneider's medium.
6. Centrifuge for 7 min at room temperature with 100 rcf, remove the supernatant, and add 6 ml complete Schneider's medium supplemented with appropriate antibiotics to maintain selection.
7. Plate cells in a 25 cm^2 flask and cultivate at 25 °C as described in Subheading 3.1.1.

3.1.4 Conditioned Medium

The term "conditioned medium" refers to media that has been harvested from exponentially growing cells. Conditioned medium is used to boost the growth rate of freshly established or poorly growing cultures, because it contains metabolites and growth factors that were secreted into the medium by the cultured cells. To prevent cross-contaminations it is important that conditioned medium is free of cells from the donor culture, which can be achieved by sterile filtration.

1. Collect medium of a growing culture (60–80 % confluency, *see* **Note 8**) in a 50 ml polypropylene tube.
2. Centrifuge for 7 min at room temperature with 100 rcf to separate debris and dead cells.
3. Fill a 20 ml syringe with conditioned medium, without detaching the pellet. Place a filter in front of the syringe and squeeze the medium into a fresh 50 ml polypropylene tube.
4. Store conditioned medium until use at 25 °C.

3.2 Calcium Phosphate Transfection and Selection of Stable Cell Lines

Although S2-R+ cells have been utilized in many different settings, they cannot be used universally. Certain situations may therefore require transfecting the Fly-FUCCI vector into alternative cell lines. The integration of exogenous DNA into the genome of S2 cells occurs by illegitimate recombination events, which lead to the formation of long head-to-tail arrays containing high numbers (>1000 copies) of the vector of interest [23]. Although liposome-based transfection has been successfully used in *Drosophila* cells, we prefer using the classic calcium phosphate transfection method, which leads to higher transfection efficiencies, thereby increasing the chance for stable integration. Calcium phosphate transfection relies on the formation of a calcium phosphate-DNA precipitate, which is believed to promote the binding of the DNA to the cell surface, from where it is internalized via endocytosis [24, 25]. To guarantee high reproducibility we rely on a commercially available transfection kit (calcium phosphate transfection kit, Invitrogen).

1. Seed 5 ml S2-R+ cells ($0.5–1 \times 10^6$ cells/ml in complete Schneider's medium) in a 25 cm^2 flask and incubate overnight at 25 °C.
2. Prepare the transfection mix (per 25 cm^2 flask) by mixing the following components in a microcentrifuge tube: 60 µl solution A (2 M $CaCl_2$) + 20 µg DNA. Add sterile water to a final volume of 500 µl.
3. Prepare 500 µl of solution B (2× HEPES-buffered saline = 50 mM HEPES, 1.5 mM Na_2HPO_4, 280 mM NaCl, pH 7.1) in a 5 ml polystyrene round-bottom tube.
4. Add solution A with a glass Pasteur pipette dropwise to solution B. To ensure proper production of precipitates, solution B has to be mixed continuously. The whole procedure should require 1–2 min.
5. Incubate the resulting solution for 30–40 min at room temperature. After approximately 30 min a precipitate should become visible.
6. Mix the solution and add dropwise to the cells.
7. Incubate for 14–18 h at 25 °C, then remove calcium phosphate solution, and wash the cells with complete Schneider's medium. Add fresh medium. At this step a cell culture microscope equipped with a fluorescent light source comes in handy for verifying the transfection efficiency.
8. After 2–3 days of recovery at 25 °C, add 240 µl Geneticin to the cells.
9. The selection has to be maintained for 4–6 weeks with frequent media changes to remove dead cells until discrete colonies of Fly-FUCCI cells appear.

10. Trypsinize the colonies (*see* Subheading 3.1.1) and replate the cells in a 75 cm^2 flask for propagation. Once stable cells have been established, the cell line can be maintained in complete Schneider's medium supplemented with 2 mg/ml Geneticin.
11. At this point we recommend freezing aliquots of the transformed cells (*see* Subheading 3.1.2).

3.3 FACS Enrichment of Fly-FUCCI-Expressing Cells

In a population of stably transformed cells most cells will be resistant to Geneticin and hence carry the Fly-FUCCI plasmid. However, the population will usually be highly heterogeneous in their expression levels due to variability of copy numbers with the arrays of inserted DNA. Because the variable expression of the Fly-FUCCI sensors complicates image acquisition and analysis, we utilize fluorescence-activated cell sorting (FACS) to obtain a homogenously expressing cell population. The gold standard for generating a homogenous cell population would be cloning of a single cell, but this procedure is laborious and technically challenging. Luckily, the Fly-FUCCI methods support tracking of single cells, and thus reliable results can be achieved by bulk sorting of well-expressing cells (*see* **Note 11**). An in-depth description of the use of flow cytometry on *Drosophila* cell lines can be found in [26].

1. Inoculate two 75 cm^2 flasks with Fly-FUCCI-expressing S2-R+ cells and one flask with untreated control cells. Incubate at 25 °C until the cultures have reached 60–80 % confluence.
2. Collect medium in 50 ml polypropylene tube and generate conditioned medium as described in Subheading 3.1.4.
3. Trypsinize cells as described in Subheading 3.1.1, **steps 1–4**, but resuspend pellets in 2 ml complete Schneider's medium.
4. Pool both cell suspensions in one tube and carefully transfer the liquid with a 1 ml micropipette to a 5 ml polypropylene tube fitted with a cell strainer cap. This step aims to remove any cell clumps that may clog the flow cytometer (*see* **Note 11**).
5. Use untreated S2-R+ cells to set the acquisition gates as described in Fig. 1e. The parameter forward scatter (FSC) represents the amount of light scattered in forward direction and reflects the size of the cell. Side scatter (SSC), by contrast, is the light scattered at large angles and indicates the internal complexity or granularity the cells. Height (*H*) is the maximum amplitude of the fluorescence signal. Width (*W*) stands for the duration of the signal and provides a measure for the amount of clumping. Area (*A*) is the integral of the emission peak.
6. Clumps of cells or cellular debris have different light-scattering properties; hence intact cells can be isolated by plotting SSC against FSC (Fig. 1eI).

7. Aggregates of cells may produce signals with the same amplitude as individual cells, and thus negative cells may be falsely recognized as positive. The signal amplitude of an individual cell is roughly proportional to the width of the peak, while cell aggregates produce signals of increased width. Hence, single cells can be distinguished by plotting parameters FSC-A vs. FSC-W (Fig. 1eII) and SSC-A vs. SSC-C (Fig. 1eIII) against each other.
8. Account for autofluorescence in the 488 nm and the 561 nm spectrum by placing the collection gates outside of the peaks of untreated S2-R+ cells (Fig. 1e).
9. Sort double-positive (GFP+ RFP+) cells into a labeled 15 ml polypropylene tube (Fig. 1e, *see* **Note 10**). We find that 1×10^6 cells are sufficient for successful recultivation.
10. Centrifuge for 7 min at 100 rcf. Remove as much of the supernatant as possible and resuspend the pellet in 6 ml conditioned medium (*see* Subheading 3.1.4).
11. Transfer cell suspension to 25 cm^2 flask and cultivate with regular media exchanges. After 2–3 weeks the culture can be expanded to 75 cm^2 flasks and aliquots may be frozen.

3.4 Live Imaging

Successful live imaging requires cell lines that flatten well on the cover slide. Therefore we prefer the S2-R+ line [18], which spreads much better than the more commonly used S2 or K2 cells. A major advantage of *Drosophila* cell lines is that they can be cultivated at room temperature, under atmospheric CO_2, and hence live imaging of Fly-FUCCI-expressing cells can be conducted with relatively simple hardware. In principle, any wide-field microscope that is fitted with a CCD camera (e.g., ORCA-R2, Hamamatsu) and capable of acquiring time series is sufficient for capturing movies of Fly-FUCCI-expressing cells. However, we find that more sophisticated setups that include motorized X, Y, and Z controls, hardware autofocus systems (*see* **Note 12**), and an EMCCD camera (e.g., ImagEM Enhanced, Hamamatsu) will substantially increase the success rate. Because S2-R+ cells require about 24 h to complete a cell cycle, images should be acquired for at least 48 h to ensure that each cell undergoes at least one cell cycle during the imaging period. Simultaneous imaging of multiple treatments in multi-well slides can help to compensate the relatively long acquisition times. Multiplex imaging involves extensive movements in X and Y direction that can cause problems with oil immersion objectives. For this reason we use high-quality dry objectives (e.g., 20× NA = 0.75 or 40× NA = 0.95) for imaging in multi-well plates.

1. Seed Fly-FUCCI-expressing S2-R+ cells in a 25 cm^2 flask and incubate at 25 °C until the culture reaches 60–80 % confluence.

2. Collect medium in 15 ml polypropylene tube and keep at 25 °C until **step 5**.
3. Trypsinize remaining cells as described in Subheading 3.1.1, **steps 1–4**, but resuspend the pellet in 5 ml complete Schneider's medium.
4. Determine cell density and dilute the culture with the conditioned medium collected in **step 2** to a final concentration between 5×10^4 and 1×10^5 cells/ml.
5. Seed 2 ml of this cell suspension in a 35 mm μ-dish or use 300 μl per well of a μ-Slide 8 well (*see* **Note 13**).
6. Incubate overnight at 25 °C (*see* **Note 14**).
7. Carefully mount the dish or the multi-well slide on an inverted microscope and capture a time series of z stacks. The exact imaging parameters should be tailored for each experimental layout, but a good starting point is to capture a z stack every 20 min for an overall time period of 48 h.
8. Figure 2b shows a typical image sequence of proliferating Fly-FUCCI cells. After quantification with ImageJ (http://imagej.nih.gov/ij/), the fluorescence intensities are ideally plotted against the time (Fig. 2a), which allows one to determine the duration of each cell cycle phase. G1 phase normally lasts for around 10 h; S phase requires approximately 4 h and G2 phase 6 h.

4 Notes

1. Over the last several decades more than 100 cell lines have been isolated from *Drosophila* embryos or larvae [21]. Many of these cell lines as well as the Fly-FUCCI-expressing S2-R+ cells described in [2] are publically available at the *Drosophila* Genomics Resource Center (https://dgrc.cgb.indiana.edu/cells/Catalog).
2. Schneider's medium can be purchased in liquid or powder form from many vendors. However, we find that not all brands of Schneider's medium support the growth of S2-R+ equally well. Therefore, we highly recommend comparing media from several manufacturers and not switching brands during an ongoing study. We obtained the most reproducible results with Schneider's medium from Gibco, but this does not mean that alternative products will not produce similar results.
3. We find that the growth rate of S2-R+ cells changes between different batches of serum and therefore we recommend testing the serum beforehand. Fortunately, many suppliers offer their customers small test samples if they obligate to purchase

a larger amount of serum. If a particular batch supports the growth of the cultures very well, a large quantity of this serum that will last the entire study should be acquired.

4. Before use, FBS should be heat-inactivated in a water bath for 30 min at 56 °C. Because many types of water baths are heated from the bottom, the serum should be mixed occasionally, to ensure that the serum is homogenously heated. To avoid contaminants from the serum, we routinely sterile filter the heat-inactivated serum in a 500 ml vacuum filtration device. The prepared serum can then be dispersed into 50 ml aliquots and stored at –20 °C.
5. All solutions and media required for the cultivation of *Drosophila* cell lines should be pre-warmed to room temperature. Therefore, we recommend installing a water bath that can be permanently kept at 25 °C. To prevent contamination from bacteria and fungus, the water bath should be frequently cleaned. Furthermore, addition of antimicrobial agents and subsequent spraying with ethanol helps to minimize the risk of contamination.
6. In many laboratories it is common practice to simultaneously work with flies and cell lines. Because fly cultures harbor all kinds of bacteria and fungi, and fly food is often supplemented with living yeast, extra care has to be taken not to contaminate the cultivated cell lines. Therefore, cell culture should be carried out in a designated room separated from the areas where the general fly work is executed. We highly recommend wearing designated lab coats while handling *Drosophila* cell lines. If possible we complete our cell culture work before we start working with living insects.
7. S2 cells can be securely stored at –80 °C for several months, but we recommend liquid nitrogen for long-term storage. Extra care should be taken when removing storage racks from liquid nitrogen tanks, and we highly recommend wearing a lab coat and safety goggles as protection. It is also important to accurately record the locations of the frozen vials in a journal or database.
8. The term confluency refers to the area in a cell culture vessel that is covered by adherent cells and is commonly used as an estimate of the density of adherent cells in a vessel. 100 % confluency indicates that the surface of the vessel is covered with cells, whereas 50 % confluency means that only half of the surface is covered with cells and that the culture is still growing.
9. Most antibiotics used in cell culture have a relatively short half-life in solution. Therefore, we recommend replacing the conditioned medium after 2–3 days with fresh complete Schneider's medium, ensuring that antibiotic selection is maintained.

Adding extra antibiotics to the conditioned medium could also work, but it is hard to estimate how much antibiotic is still left in the medium, and thus the fresh antibiotics may add up to inappropriately high concentrations.

10. Very high substrate concentrations may exceed the capacity of the E3 ligases APC/C and $CRL4^{Cdt2}$ and thereby impair the function of the Fly-FUCCI system. Therefore, we suggest setting the gates of the FACS in a way that cells with intermediate expression level will be enriched.
11. Modern flow cytometers such as the FACSARIA III (BD-Biosciences) work optimally with concentrated cell suspensions containing $1–10 \times 10^6$ cells. Higher cell numbers may be required if cells with suitable expression levels only occur at very low frequency; in this case we recommend splitting the cell suspension over multiple tubes.
12. Most of the currently available hardware autofocus systems were designed for imaging cells growing on glass substrates. Although the optical properties of thin-bottom plastic dishes are very similar to glass, we have observed that the autofocus systems from certain manufacturers have difficulty in maintaining accurate focus with plastic dishes. However, we have successfully used the VDC and VDC2 systems from Olympus, which allowed us to capture image sequences of up to 90 h without focus drift.
13. S2-R+ cells adhere poorly to the surfaces of glass-bottom dishes. Therefore, coatings such as poly-l-lysine or concanavalin A (ConA) are frequently used to enhance the flattening of the cells. However, we find that these coatings disturb proliferation of S2-R+ cells (e.g., cells on ConA fail to complete cytokinesis), making these unsuitable for long-time imaging. Instead, we recommend using thin-bottom plastic dishes or multi-well slides that have optical characteristics similar to glass.
14. We find that it is most practical to prepare the cells in the evening and start the live imaging experiment the next morning. This gives the cells sufficient time to recover from the trypsinization procedure and ensures that the cells are dividing when the image sequence starts.

Acknowledgements

We thank Monika Petersson and Jerome Korzelius for critical reading of the manuscript. The work on the Fly-FUCCI system was supported by the DKFZ, ERC Advanced grant 268515, and DFG SFB 873.

References

1. Sakaue-Sawano A, Kurokawa H, Morimura T, Hanyu A, Hama H, Osawa H, Kashiwagi S, Fukami K, Miyata T, Miyoshi H, Imamura T, Ogawa M, Masai H, Miyawaki A (2008) Visualizing spatiotemporal dynamics of multicellular cell-cycle progression. Cell 132(3):487–498. doi:10.1016/j.cell.2007.12.033
2. Zielke N, Korzelius J, van Straaten M, Bender K, Schuhknecht GF, Dutta D, Xiang J, Edgar BA (2014) Fly-FUCCI: a versatile tool for studying cell proliferation in complex tissues. Cell Rep 7(2):588–598. doi:10.1016/j.celrep.2014.03.020
3. Arias EE, Walter JC (2007) Strength in numbers: preventing rereplication via multiple mechanisms in eukaryotic cells. Genes Dev 21(5):497–518. doi:10.1101/gad.1508907
4. Glotzer M, Murray AW, Kirschner MW (1991) Cyclin is degraded by the ubiquitin pathway. Nature 349(6305):132–138. doi:10.1038/349132a0
5. Havens CG, Walter JC (2011) Mechanism of CRL4(Cdt2), a PCNA-dependent E3 ubiquitin ligase. Genes Dev 25(15):1568–1582. doi:10.1101/gad.2068611
6. Shibutani ST, de la Cruz AF, Tran V, Turbyfill WJ 3rd, Reis T, Edgar BA, Duronio RJ (2008) Intrinsic negative cell cycle regulation provided by PIP box- and Cul4Cdt2-mediated destruction of E2f1 during S phase. Dev Cell 15(6):890–900. doi:10.1016/j.devcel.2008.10.003
7. Gonzalez M, Martin-Ruiz I, Jimenez S, Pirone L, Barrio R, Sutherland JD (2011) Generation of stable Drosophila cell lines using multicistronic vectors. Sci Rep 1:75. doi:10.1038/srep00075
8. Krasnow MA, Saffman EE, Kornfeld K, Hogness DS (1989) Transcriptional activation and repression by Ultrabithorax proteins in cultured Drosophila cells. Cell 57(6):1031–1043
9. Cherbas L, Cherbas P (2007) Drosophila cell culture and transformation. Cold Spring Harb Protoc 2007:pdb.top6. doi:10.1101/pdb.top6
10. Szymczak AL, Workman CJ, Wang Y, Vignali KM, Dilioglou S, Vanin EF, Vignali DA (2004) Correction of multi-gene deficiency in vivo using a single 'self-cleaving' 2A peptide-based retroviral vector. Nat Biotechnol 22(5):589–594. doi:10.1038/nbt957
11. Osborn MJ, Panoskaltsis-Mortari A, McElmurry RT, Bell SK, Vignali DA, Ryan MD, Wilber AC, McIvor RS, Tolar J, Blazar BR (2005) A picornaviral 2A-like sequence-based tricistronic vector allowing for high-level therapeutic gene expression coupled to a dual-reporter system. Mol Ther 12(3):569–574. doi:10.1016/j.ymthe.2005.04.013
12. de Felipe P, Luke GA, Hughes LE, Gani D, Halpin C, Ryan MD (2006) E unum pluribus: multiple proteins from a self-processing polyprotein. Trends Biotechnol 24(2):68–75. doi:10.1016/j.tibtech.2005.12.006
13. Sakaue-Sawano A, Kobayashi T, Ohtawa K, Miyawaki A (2011) Drug-induced cell cycle modulation leading to cell-cycle arrest, nuclear mis-segregation, or endoreplication. BMC Cell Biol 12:2. doi:10.1186/1471-2121-12-2
14. Steinbrink S, Boutros M (2008) RNAi screening in cultured Drosophila cells. Methods Mol Biol 420:139–153. doi:10.1007/978-1-59745-583-1_8
15. Baum B, Cherbas L (2008) Drosophila cell lines as model systems and as an experimental tool. Methods Mol Biol 420:391–424. doi:10.1007/978-1-59745-583-1_25
16. Armknecht S, Boutros M, Kiger A, Nybakken K, Mathey-Prevot B, Perrimon N (2005) High-throughput RNA interference screens in Drosophila tissue culture cells. Methods Enzymol 392:55–73. doi:10.1016/S0076-6879(04)92004-6
17. Bettencourt-Dias M, Goshima G (2009) RNAi in Drosophila S2 cells as a tool for studying cell cycle progression. Methods Mol Biol 545:39–62. doi:10.1007/978-1-60327-993-2_3
18. Yanagawa S, Lee JS, Ishimoto A (1998) Identification and characterization of a novel line of Drosophila Schneider S2 cells that respond to wingless signaling. J Biol Chem 273(48):32353–32359
19. Schneider I (1972) Cell lines derived from late embryonic stages of Drosophila melanogaster. J Embryol Exp Morphol 27(2):353–365
20. Cherbas P, Cherbas L, Williams CM (1977) Induction of acetylcholinesterase activity by beta-ecdysone in a Drosophila cell line. Science 197(4300):275–277
21. Echalier G (1997) *Drosophila* cells in culture. Academic, New York, NY
22. Schneider I (1964) Differentiation of larval Drosophila eye-antennal discs in vitro. J Exp Zool 156:91–103
23. Kirkpatrick RB, Shatzman A (1999) Drosophila S2 system for heterologous gene expression.

In: Fernandez JM, Hoeffler JP (eds) Gene expression systems: using nature for the art of expression. Academic, San Diego, CA, pp 289–330

24. Wigler M, Silverstein S, Lee LS, Pellicer A, Cheng Y, Axel R (1977) Transfer of purified herpes virus thymidine kinase gene to cultured mouse cells. Cell 11(1):223–232
25. Graham FL, van der Eb AJ (1973) A new technique for the assay of infectivity of human adenovirus 5 DNA. Virology 52(2): 456–467
26. de la Cruz AF, Edgar BA (2008) Flow cytometric analysis of Drosophila cells. Methods Mol Biol 420:373–389. doi:10.1007/978-1-59745-583-1_24

Chapter 20

Imaging Cell Cycle Phases and Transitions of Living Cells from Yeast to Woman

Hadas Segev, Drora Zenvirth, Kobi J. Simpson-Lavy, Naomi Melamed-Book, and Michael Brandeis

Abstract

The eukaryotic cell cycle is comprised of different phases that take place sequentially once, and normally only once, every division cycle. Such a dynamic process is best viewed in real time in living dividing cells. The insights that can be gained from such methods are considerably larger than any alternative technique that only generates snapshots. A great number of studies can gain from live cell imaging; however this method often feels somewhat intimidating to the novice. The purpose of this chapter is to demonstrate that imaging cell cycle phases in living cells from yeast to human is relatively easy and can be performed with equipment that is available in most research institutes. We present the different approaches, review different types of reporters, and discuss in depth all the aspects to be considered to obtain optimal results. We also describe our latest cell cycle markers, which afford unprecedented "sub"-phase temporal resolution.

Key words Cell cycle, Live cell, Imaging, Cdc6, GFP, mCherry, APC/C

1 Introduction

Live cell imaging of cell cycle transitions has been pioneered more than 30 years ago using phase-contrast microscopy [1]. Mitosis, when cells round up and divide into two daughter cells, was the only event in the mammalian cycle that could be detected by this method. All other cell cycle transitions remained obscure.

The discovery in the early 1990s that fluorescent proteins can be expressed in mammalian cells [2] heralded a dramatic breakthrough in our capacity to visualize cell cycle transitions.

Using a title from yeast to man is not only chauvinistic but also wrong—all the human cells we used for this work—HeLa, HT1080 U2OS, and RPE1—are female cells.

Electronic supplementary material: The online version of this chapter (doi:10.1007/978-1-4939-2957-3_20) contains supplementary material, which is available to authorized users.

Amanda S. Coutts and Louise Weston (eds.), *Cell Cycle Oscillators: Methods and Protocols*, Methods in Molecular Biology, vol. 1342, DOI 10.1007/978-1-4939-2957-3_20,

Fluorescent proteins fused to proteins that are either degraded or redistributed in the cell, in specific phases of the cell cycle, could now be used to follow cell cycle transitions in real time. Jon Pines pioneered this approach by fusing green fluorescent protein (GFP) to cyclin B1 [3]. Cyclin B1 is degraded upon cell division and remains unstable throughout G1 until the onset of S phase [4]. The use of this fusion protein enables one to distinguish cells in G1 from cells during the rest of the cell cycle. We, and others, have since used multiple APC/C substrates like securin [5], Fzy [6], geminin [7], and Plk1 [8] fused to various fluorescent proteins to a similar effect.

Miyawaki and co-workers developed a marker based on a fragment of Cdt1, which is stable in G1 and degraded in S-G2-M, mirroring the stability of the markers based on APC/C-specific degradation like geminin or cyclin B1 [7]. Co-expression of these so-called FUCCI markers in cells generates red G1 cells and green S-G2-M cells, but it does not improve on the temporal resolution of either marker on its own.

Temporal resolution can be improved by using proliferating cell nuclear antigen (PCNA) fused to a fluorescent protein. PCNA is not degraded during the cycle, but its uniform nuclear distribution changes upon entry into S phase and forms typical nuclear foci [9]. DNA ligase I fused to a fluorescent protein can be used in a similar fashion [10]. Using these markers thus enables identification of all four cell cycle transitions and to some extent even distinguishes between different stages of S phase.

The most recent fluorescent marker we have started to use is the Cdc6-GFP fusion protein. Cdc6 is nuclear in late G1, cytoplasmic during S and G2, and degraded in mitosis and early G1 [11, 12]. By using Cdc6-GFP in conjunction with PCNA-mCherry we obtain unprecedented temporal resolution of multiple cell cycle transitions (*see* Fig. 1 and Supplemental Movie 1).

Live cell imaging in yeast has been greatly facilitated by the availability of a comprehensive collection of chromosomally GFP-tagged yeast strains [13], as well as by the relative ease with which yeast can be manipulated genetically. Yeast are smaller and their fluorescent signal is often weaker. On the other hand they have a much shorter cell cycle and, as cells start to bud upon entry into S phase and bud size corresponds to progress in the cycle, it is possible to follow their cell cycle by phase-contrast microscopy with excellent temporal resolution (*see* Fig. 2 and Supplemental Movie 2).

In this chapter we outline different approaches to live cell imaging to visualize the cell cycle and review a variety of reporters, which we believe can be easily used to give optimal results.

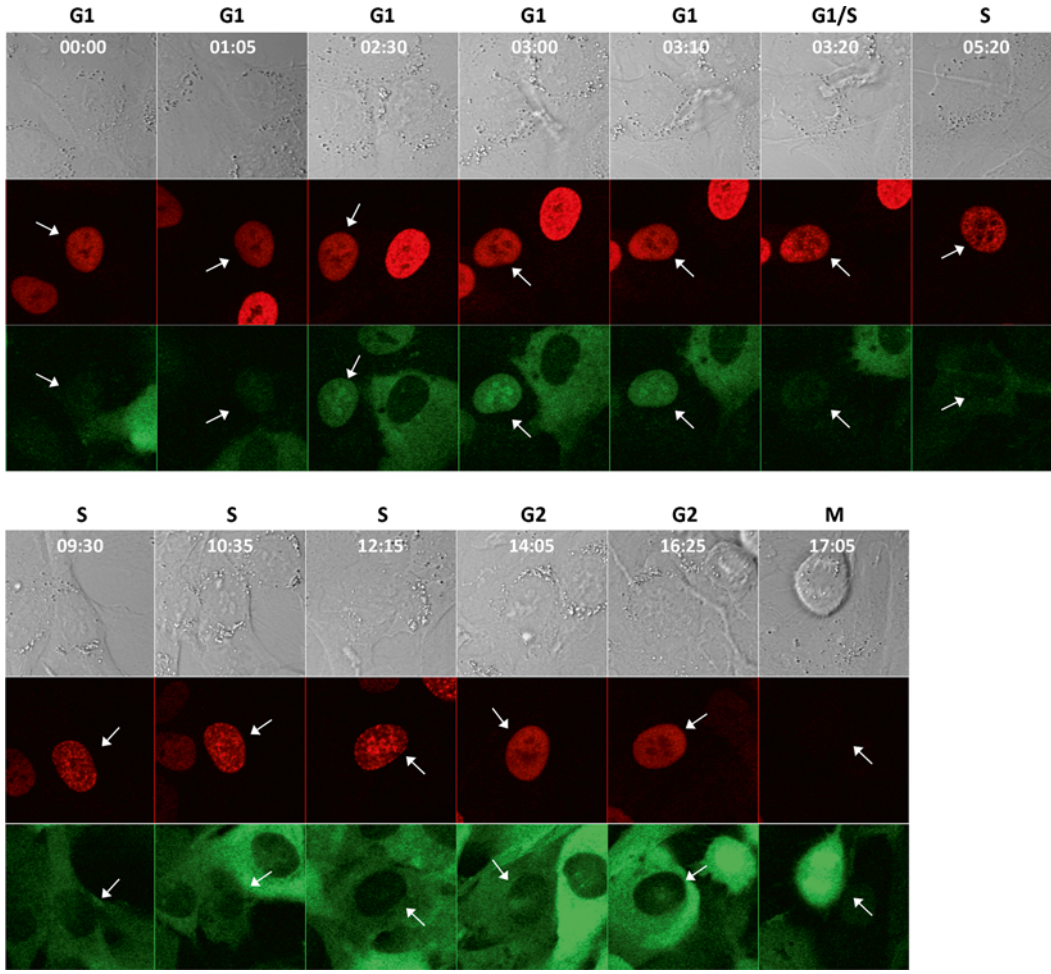

Fig. 1 RPE1 cells co-expressing Cdc6-GFP and PCNA-mCherry lentiviral vectors were imaged for 24 h on a laser scanning confocal microscope. See also Supplemental Movie 1

2 Materials

2.1 Cell Culture Materials

1. Cell lines: The choice of cell type depends on the experimental setup and biological question. In the past we used murine NIH3t3 and human U2OS and HT1080 cancer cell lines. We now prefer to use TERT immortalized human RPE1 (retina pigment epithelium) cells (*see* **Note 1**).
2. Budding yeast cells: Most yeast strains are suitable for live cell imaging (*see* **Note 2** for exceptions). The collection of yeast strains expressing full-length, chromosomally tagged GFP was generated in the S288C strain [13] and is most useful for microscopy. We further routinely use the W303 strain.

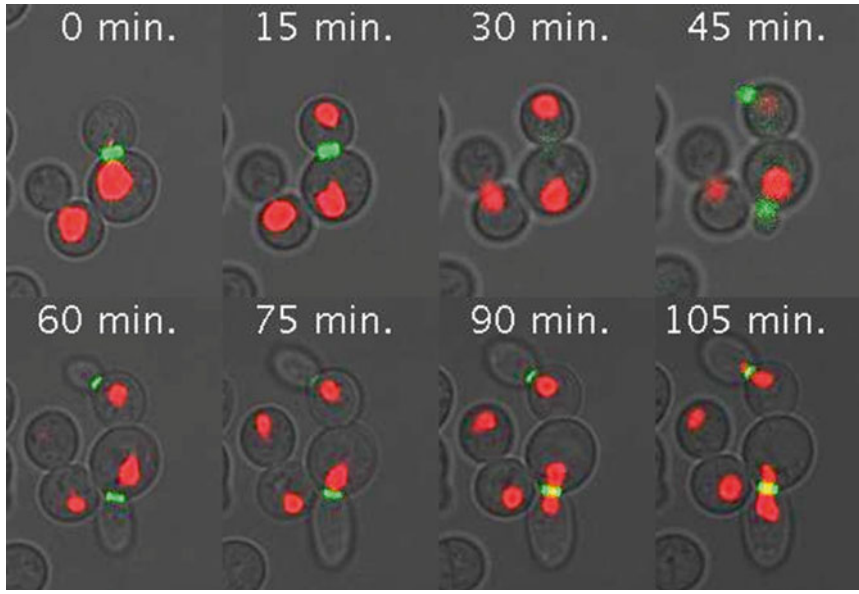

Fig. 2 Budding yeast co-expressing chromosomally tagged Hsl1-GFP and Pus1-RFP were imaged for 2 h on a laser scanning confocal microscope. See also Supplemental Movie 2

3. Fluorescent cell cycle markers: Multiple markers are available now and can be easily obtained from the Addgene™ repository (www.addgene.org) or from individual researchers, so that in most cases there is no need to design new ones (*see* **Notes 3–5**).
4. Cell culture media: Choose the appropriate media suitable for your cell type of choice. To improve the signal-to-noise ratio, especially in the green spectrum we generally use phenol red-free DMEM (*see* **Note 6**).
5. Yeast reagents: For imaging of yeast standard synthetic medium and growth reagents are required, as well as a 1 mg/ml concanavalin A (ConA, Sigma) solution for coating the culture dish.
6. Tissue culture dishes: For a single experiment 35 mm glass-bottom dishes are most convenient. For multiple simultaneous experiments 4- or 8-well "slide" dishes or a 35 mm dish divided into four are suitable. For a larger number of parallel experiments glass-bottom multi-well dishes should be used (*see* **Note 7** and Fig. 3). The dish sizes of different suppliers vary, so make sure in advance that the dish fits into your microscope stage holder.

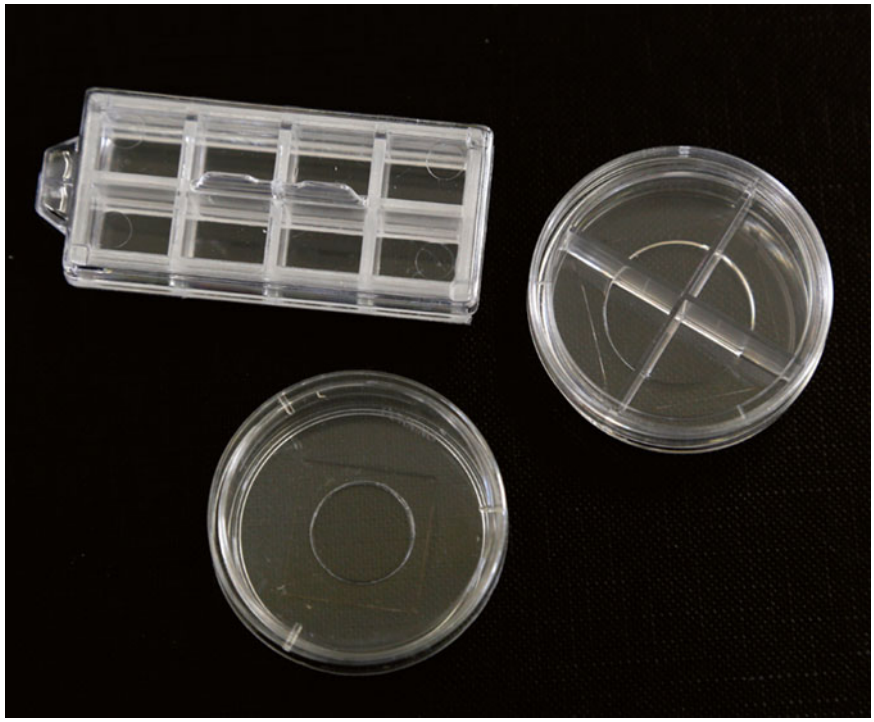

Fig. 3 A selection of glass-bottom tissue culture dishes for live cell imaging

2.2 Microscopy Materials

1. Epifluorescent wide-field microscope with a sensitive CCD camera, a laser scanning confocal microscope, or a spinning disc system are essential for live cell imaging (for various possible setups *see* **Note 8**).
2. An incubator that will keep the cells at constant temperature and if required in a controlled atmosphere (*see* **Note 9**).

2.3 Software and Image Analysis

Most systems come with their own proprietary software, for example our FV1000 and FV1200 Olympus laser scanning confocals run on Olympus Fluorview software. When integrating your own system it is possible to purchase expensive commercial software packages to run the shutter, CCD, microscope, stage, and filter wheel. It is however possible, and recommended, to use the free Micro-Manager package (https://www.micro-manager.org/) which interfaces with ImageJ (http://imagej.net). This system has drivers for most hardware configurations, is constantly updated, and boasts a large and helpful community.

3 Methods

3.1 Live Cell Imaging of Metazoan Cells

1. Choose the cell type.
2. Plate out the cells in an appropriate dish. Use a glass-bottom dish for higher quality images and when planning to use an immersion objective. We plate out about 2×10^5 RPE-1 cells per 35 mm dish. The density of cells in the dish is important. When there are too few cells they often do not grow well and you will have to collect many fields to obtain sufficient data. When there are too many cells they might become confluent and arrested and it is also difficult to follow cells that are too crowded.
3. Choose the appropriate fluorescent marker (*see* **Notes 3**–**5**) and express the fluorescent marker/s in the cells, preferably using stably expressing cells.
4. Grow the cells for at least 16 h until they have settled well and express the fluorescent marker. Live cell image analysis is done at the individual cell level. In theory, and in most cases in practice, live cell synchronization is thus not required. If your experiment requires synchronization this should be done now (*see* **Note 10**). If synchronization is done by mitotic shake-off with or without nocodazole/taxol treatment this has to be done before plating on the imaging dish.
5. Replace the culture medium if necessary to medium without phenol red. Take care to equilibrate the temperature of the fresh medium to avoid cold or heat shocking the cells.
6. Pre-equilibrate the temperature of the incubator of the microscope to the desired temperature. Pre-equilibration is important not only for the sake of the cells but also for preventing focal drift.
7. Mount your plate on the microscope. Make sure in advance that your imaging dish snugly fits into your stage adaptor. Start the CO_2 pump if using one.
8. Define the magnification and focus on the cell. Magnification is a trade-off between the number of cells you wish to image and resolution of each cell. For metazoan cells 20× to 40× objectives are most suitable. Further magnification can be achieved by zooming in when using a confocal microscope. The problem with higher magnification, in addition to the reduced number of cells in the field, is a reduced depth of field. This requires more precise maintenance of focus throughout the entire experiment.
9. Define the wavelength and exposure to image the fluorescent markers.

   Choosing the correct exposure is not always easy as the strength of signals can change dramatically during the cell cycle. It is best to use the minimal exposure that will yield a

good signal-to-noise ratio. Extended exposure will damage the cells and affect the cell cycle. Overexposure will lead to saturated signals that cannot be quantified. The higher the magnification, the shorter the exposure.

10. If your microscope has an XY motorized stage choose multiple fields. If it has an autofocus option consider activating it. We routinely acquire up to 40 fields in a single experiment obtaining a large amount of data at once. As cells tend to move, it is advisable to acquire fields of adjacent cells (2×2 or 3×3 grids are useful and can be easily stitched together afterwards). Multi-field acquisition enables one to include different experiments and controls in the same experiment under identical conditions. As it might be difficult to position the dish completely flat and parallel to the objective each field may have a slightly different focal plane. Most software-controlled motorized XY stages are also controlled at the *Z*-axis so that each field will have its specific focus. It is advisable not to choose fields that are too far apart to save travel time.
11. Set the temporal pattern of your experiments and its length. For most cell cycle experiments acquisition at about 5-min intervals is sufficient. A typical mammalian cell cycle lasts for 20 h so that if you desire to visualize cells completing a full round it is best to acquire for at least 24 h. Often an entire cycle for each cell is not required, as individual cells will complete different phases over a given time, such that 16 h is often sufficient.
12. Start your experiment.
13. Check on your experiment after about 1 h to ensure that the focus has not drifted and that everything runs properly.
14. Download your data and analyze it with ImageJ or with a commercial software package (*see* **Note 11**).

3.2 Live Cell Imaging of Budding Yeast

Following the budding yeast cell cycle by live cell imaging bears many similarities with those of metazoan cells but there are also important differences. One of the big advantages of budding yeast for live cell imaging is the fact that, unlike metazoan cells, the stage of the cycle can be deduced by phenotypic appearance at any given point. A second advantage is that yeast are easy to manipulate genetically and endogenous genes can be readily tagged with a fluorescent marker.

On the downside yeast are much smaller, they auto-fluoresce, and the fluorescent signal, in particular the ones achieved by tagging endogenous genes, is often too weak to follow. The extended exposure to UV radiation required for detecting weak signals is deleterious to the yeast and might affect the cell cycle by activating

the DNA damage response. In addition yeast are non-adherent and must be attached to the glass as we describe below.

1. Choose the appropriate strain (*see* **Note 2**).
2. Choose the appropriate fluorescent marker. Ensure that bleed-through between channels is minimized.
3. Express the fluorescent marker/s in the cells (*see* **Note 12**).
4. Culture the cells overnight in synthetic medium, dilute, and grow to a logarithmic phase (*see* **Note 13**).
5. Pre-equilibrate the temperature of the incubator of the microscope to the desired temperature. Pre-equilibration is important as otherwise any changes in temperature will cause focal drift.
6. Coat a glass-bottom tissue culture dish with ConA by covering it with 1 mg/ml solution of ConA for several minutes and subsequently aspirating it.
7. Wash the cells in synthetic medium. Dilute the yeast (*see* **Note 13**) and put in the dish. Let the cells settle and stick to the ConA for 10 min; remove the cells that have not attached to the glass and add fresh medium.
8. Mount your plate on the microscope.
9. Define the wavelength and exposure to image the fluorescent markers (*see* **Note 14**).
10. Define the magnification and focus on the cell. For yeast 40× or 60× high N.A. oil immersion objectives are most suitable. Further magnification can be achieved by zooming in when using a confocal microscope.
11. If your microscope has an XY motorized stage choose multiple fields. If it has an autofocus option consider activating it. Unlike in metazoan cells, multiple fields of the same experiment might not be required because each field has many yeast cells. Multiple experiments (treatments, strains, etc.) can however be done in parallel achieving the best controlled conditions.
12. Set the temporal pattern of your experiments and its length. For most cell cycle experiments acquisition at about 3 ± 1-min intervals is suitable. More frequent sampling adds little information and exposes the cells to unnecessary radiation. A typical yeast cell cycle lasts, under optimal growth conditions, for about 90 min. In various mutant strains, and under suboptimal conditions, the cycle can be considerably longer. Following cells for several hours will, in most cases, enable one to follow several cell cycles.
13. Start your experiment.

14. Check on your experiment after about 20 min to check that the focus has not drifted and that everything is running properly.
15. Download your data and analyze it with ImageJ or with a commercial software package.

4 Notes

1. Many cell types are hard to transfect and as long as cells had to be transfected with expression vectors they were difficult to use. The use of viral vectors, which can be used to express proteins in virtually any cell line, broadens the range of cells that can now be used. Imaging of non-adherent cells is slightly more challenging than imaging of adherent ones but is definitely possible [14].
2. Ade2 or ade1 mutant yeast strains are to be avoided as they accumulate the fluorescent red pigment P-ribosylaminoimidazole (AIR).
3. The most widely used method to visualize the cell cycle is using fluorescent fusion proteins of substrates that are degraded by the anaphase-promoting complex/cyclosome (APC/C). The APC/C is active throughout G1 and G0 and fusion FP proteins are therefore absent in G1 (and G0) and present in S-G2-M. The most widely used fusion proteins are cyclin B1 [3] and geminin [7]. Cdc6 is also degraded by the APC/C [15] but has a more complex [16] and thus more informative pattern of degradation and cellular localization (*see* Fig. 1 and Supplemental Movie 1). A fragment of Cdt1 fused to a fluorescent marker is degraded in S-G2-M and stains cells in G1 and G0. PCNA [9] and DNA ligase I [10] fused to a fluorescent marker change their distribution in the nucleus upon entry into and exit from S phase. These proteins can be fused to the various GFP variants as well as to Cherry. In most cases it is sufficient to fuse only the fragment of the protein harboring the specific degron, rather than the entire active protein, to the fluorescent marker. For example instead of expressing full-length cyclin B1, which binds and activates cdk1, we use only the amino (N)-terminal 100 residues. This approach eliminates, or at least strongly reduces, the risk that the marker will affect the cell cycle. Whether the fluorescent protein is fused to the N- or carboxy (C)-terminus of the protein that is degraded can have a crucial effect. For example, fusing a fluorescent protein to the N-terminus of cyclin B1 generates a stable protein that cannot serve as a marker. We generally fuse the fluorescent protein to

the C-terminus of the protein but this is in no way a failproof approach. The fluorescent protein used for the FUCCI marker Cdt1, for example, is fused to the N-terminus of a small part of the protein, as expressing full-length Cdt1 leads to cell cycle arrest [7].

4. The number of fluorescent proteins has dramatically expanded over recent years and their description is beyond the scope of this chapter. We routinely use red mCherry and "yellow" YFP (or Venus which is a YFP variant). YFP and mCherry do not overlap when used with the appropriate filter sets and have excellent signal-to-noise ratio. It is possible to further use CFP (cyan; or other more advanced "blue" variants) but the blue light required for its imaging is more damaging to cells and should be used carefully. With appropriate filters CFP and YFP can be almost completely separated so that together with mCherry (or other red proteins) three markers can be followed simultaneously. Far-red variants are also becoming available so that a fourth marker can be used in parallel (but we have never done it). In general, the different fluorescent proteins do not alter the expression pattern of the proteins used for cell cycle imaging. In particular the different GFP variants (CFP, GFP, and YFP), which differ by only a few point mutations, as well as mCherry do not seem to affect the pattern of expression. Other fluorescent proteins can have some effect and it is essential to carefully test every new combination. Even if the different fluorescent proteins do not affect the expression pattern they have different maturation times. While this will not affect their degradation timing, it could alter the time their accumulation can be detected.

   Several fluorescent proteins change their color over time and can be used as timers [17, 18]. Another consideration is the maturation time of the fluorescent tag. While most FPs mature quickly, most red-fluorescent proteins (except mCherry) have a maturation half time in the hours range (e.g., DsRed at 10 h). Slow-maturing FPs are clearly unsuitable for tagging proteins whose abundance is cell cycle regulated. However, they are advantageous for tagging organelles, and the discrepancy between the maturation rates can serve as a molecular timer for studying inheritance of proteins or organelles.

5. In order to express the fluorescent markers in cells, the expression vectors have to be introduced into cells. Cells can be transfected by a large variety of transfection agents (depending on cell type) or by electroporation. Alternatively expression can be accomplished by using viral vectors like lentivirus or retroviruses. Viral vectors are slightly more complex to prepare and require additional biosafety measures. They are, however, much more convenient for preparing stable lines expressing

the fluorescent markers. Fluorescent markers can be expressed either transiently or stably in cells. Preparing stable cell lines can take several weeks and is a laborious process; however we nevertheless *strongly discourage* using transiently transfected cells. Transient transfection leads to the introduction of huge amounts of DNA into cells leading to high expression of the marker, which is likely to affect the cell cycle of the transfected cells. The selection process ensures that cells that express excessive levels of the transgene will not survive and that we will get a population of cells in which transgene levels do not arrest the cell cycle. In order to obtain cells that stably express the desired marker, the plasmid should also contain a resistance marker like Puro, Neo, and Hyg. Alternatively the expression vector can be co-transfected with another plasmid that carries such a resistance marker. After transfection, cells have to be selected for at least a fortnight to obtain expressing colonies. Selection can be initiated about 48 h after transfection but it is recommended not to add the selection immediately after splitting the cells. If a fair proportion of the stable colonies express the fluorescent marker it is possible to pool all colonies instead of picking individual ones. This is not only quicker and easier but also creates a population of cells with mixed integration sites. The integration position of a marker can have some effect on its expression and using a mixed population is a good safeguard against such an effect. Using viral expression vectors to express cell cycle markers is considerably easier and faster than the use of plasmids. Virtually every cell type can be infected and stable expression of most cells is rapidly achieved. It is useful to grow the cells for a few generations just to make sure that the transgene does not interfere with cell division. As always it is important to be aware of potential effects of the markers on the cell cycle. As cells will be tracked individually by live cell imaging it is not essential to obtain a population with 100% expression, so it is of minor concern if not all cells express the transgene. We tend to sort cells by FACS to obtain a population of expressing cells but in most cases this is not essential.

The viral CMV promoter is the most widely used promoter in commercial plasmids. This promoter is exceedingly strong and is rumored to be prone to epigenetic silencing. We therefore routinely prefer the EF1 promoter, which yields robust levels of expression and is not prone to silencing. It is possible also to use cell cycle-specific promoters to combine the effect of transcription and degradation.

6. Most cell culture media like DMEM or RPMI contain the pH indicator phenol red, which has some background fluorescence. This background slightly interferes with visualizing fluorescent proteins, in particular those in the green spectrum, especially

when their level is low. Red proteins suffer much less from this background problem. It is possible to obtain standard media without phenol red, from commercial suppliers (like Biological Industries Beit Haemek, Israel). Apart from removing phenol red it is very important not to change the growth conditions of cells prior to imaging as this could affect cells in various ways.

For researchers that lack a CO_2 incubator mounted on their microscope it is necessary to use CO_2-independent HEPES-based medium, but be aware that certain cell types do not tolerate HEPES. Again it is crucial to be aware of the effect of changing the type of medium when moving cells to the microscope.

7. Imaging in plastic cell culture dishes is possible for low magnification and resolution imaging; however glass-bottom dishes will yield much better results. Glass-bottom or specialized plastic-bottom dishes are essential when using immersion objectives. Glass-bottom dishes can be homemade or obtained from different suppliers (MatTek, Ibidi, Lab-Tek, IVS, Greiner, etc.), which differ in price, quality, and size. We have had good experience with all of them. We generally use "35 mm" dishes. Annoyingly, the dishes of different suppliers have a slightly different diameter (thus the quotation marks), so it is essential to make sure that the dish fits snugly into the adapter of your microscope.

   In most cases we perform several simultaneous experiments and use glass-bottom multi-well cell culture dishes. Various types of these dishes are commercially available from the abovementioned suppliers. We either use glass-bottom 35 mm dishes that are divided into 4- or 8-well dishes with a glass cover slip bottom that is in the shape of a microscope slide (again sizes vary). Glass-bottom multi-well (96, 48, 24, etc.) dishes are also commercially available. Certain cell types will require coating of the glass. It is also possible to purchase pre-coated dishes or coat them yourself. In addition dishes are now available with a special thin plastic bottom that is supposed to have the optical qualities a glass cover slip (Ibidi). Figure 3 shows a selection of dishes we use.

8. Live cell imaging of fluorescent markers requires an inverted microscope (there are some solutions if only an upright is available) that can be used to observe the required wavelength or wavelengths. Such a system can either be a laser confocal, a spinning disc, or a "wide-field" epifluorescent microscope. Most confocal and spinning disc systems will already include all the required hardware.

   A wide-field microscope must be fitted with a sensitive CCD camera. The required sensitivity of the CCD depends on the signal-to-noise ratio of the signal to be imaged, as well as

on the noise (*see* medium considerations, **Note 6**, above). Monochrome CCDs are as a rule more sensitive than color ones. We use a Coolsnap (Roper) and Sensicam (PCO) but other options abound. The microscope does not have to be motorized but at least one shutter (for imaging only a single channel) and two shutters (for imaging both a fluorescent marker and phase/DIC channels) are required. For multiple fluorescent wavelengths a motorized filter cube holder or external filter wheels are needed. The latter can be retrofitted to any non-motorized microscope. We use filter wheels produced by Sutter. These enable near-simultaneous imaging of multiple wavelengths using a single multipass dichroic mirror (Chroma). An XY motorized stage will be required for taking multiple fields for each experiment, which enables acquiring a large amount of data in a single experiment, as well as for acquiring different wells (with control cells, cells treated in different manner, etc. in parallel).

9. Following cells through the cell cycle requires maintaining them at optimal growth conditions. The most basic requirement is growth at a controlled temperature, usually 37 °C for mammalian cells and 23 or 30 °C for yeast. A second requirement for mammalian cells is growth at 5 % CO_2 to keep the bicarbonate buffer of most growth media at an optimal pH. Many cells do however thrive also in HEPES-buffered medium (sold as CO_2-independent medium) and can be maintained and imaged at ambient atmospheric conditions. Temperature is in most cases regulated by encasing the microscope in a Perspex incubator. The atmosphere is either regulated by maintaining the entire incubator at the desired CO_2 level or by covering the cells in a smaller internal chamber, which is kept at the desired CO_2 level and humidity.

   The way temperature and CO_2 are maintained depends on a balance between budgetary constraints and skill. With sufficient available funds it is best to order a custom-made Perspex incubator, heater, and gas regulator. We are using the excellent systems built by LIS (Fig. 4), but there are other manufacturers on the market. We have however successfully used homemade systems. We used a heater built by the Stanford workshop from a hair dryer. The internal gas chamber was built by the same workshop and kept at 5 % CO_2 by connecting it to a commercially available 5 % CO_2 mixture, which saved buying a gas mixer. Much of our work was done at even more frugal conditions by keeping the cells at 37 °C on a heated stage built at the workshop of the life science institute of the Hebrew University (Fig. 5) and using CO_2-independent medium. The latter system has some disadvantages as humidity cannot be regulated and over extended periods the medium evaporates. We are mentioning this setup only to emphasize that lack of funds is

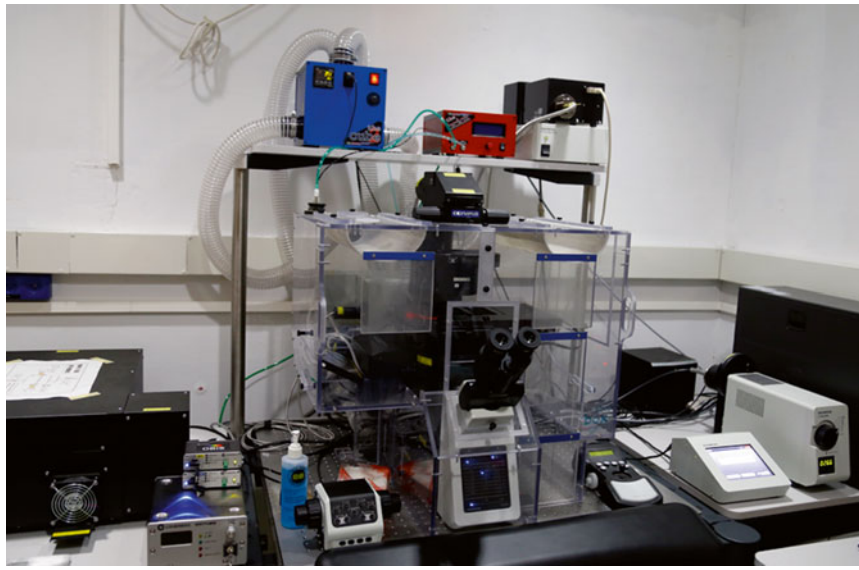

Fig. 4 Commercial microscope temperature-controlled incubator with internal CO_2 incubator (LIS)

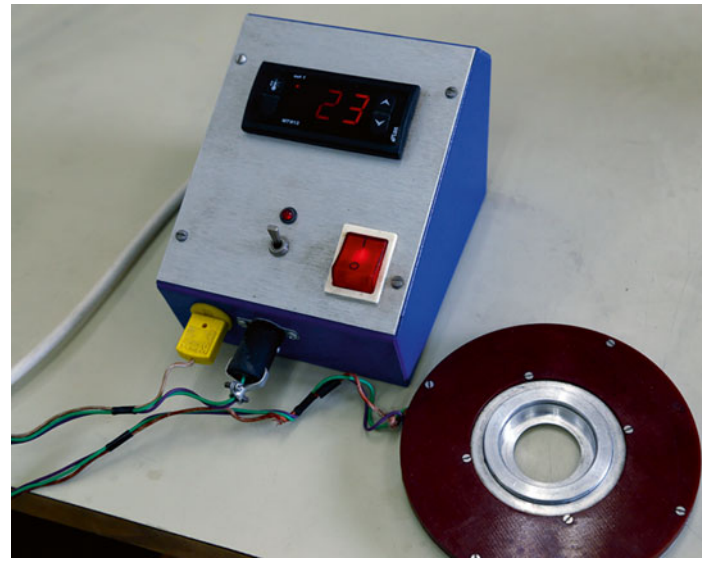

Fig. 5 A homemade heating device without CO_2 incubator

not an insurmountable obstacle to live cell studies (in fact this system gave rise to several high-impact publications). Such a simple setup is often sufficient for yeast imaging, which does not require CO_2 and is typically restricted in time to several hours.

10. Multiple methods have been developed to synchronize cells. All of these methods share the disadvantage that they perturb cellular pathways and the cell cycle. Some methods have a stronger effect and some a weaker one but as the basic instinct

of cells in culture is to proliferate, synchronization will inevitably have some effect. The big advantage of live cell imaging is that in general there is no need to pre-synchronize the cells. By following enough cells for sufficient time it is in most cases superfluous to enrich them in any specific phase of the cell cycle. Unlike any other assay, live cell imaging benefits in most cases from an unsynchronized and unperturbed cell population.

11. The analysis of cells from the experiment can sometimes be difficult due to cell motility and crowding. One way to facilitate analysis is to co-express a fluorescently tagged nuclear marker like PCNA or histone. Analysis of the cells can be done automatically, semiautomatically, or manually.
12. Expression of fluorescent markers can be done either by tagging an endogenous gene by homologous recombination or by expressing a plasmid with a tagged gene. It is further possible use a GFP-tagged strain from available libraries [14]. It is important to make sure that the desired gene has indeed been tagged. Tagging endogenous genes usually has a less deleterious effect on cells but will yield a weaker signal. The regulation of the endogenous tagged protein will be both at the transcriptional and protein stability level. It is best to choose a marker with a defined localization—the nucleus or the bud neck are both a good choice. Cytoplasmic markers are usually too dilute and not suitable due to the autofluorescence of the yeast cells.
13. Yeast cultured in rich medium prepared from yeast extract and peptone (YP) auto-fluoresce and the media is itself fluorescent. Synthetic defined (SD) medium should therefore be used for growing the cells. If the fluorescent reporter is expressed from a plasmid the medium should contain the appropriate selection.

    Finding the correct dilution can be a bit awkward, as adding too many cells to the dish will make it difficult to follow them along the cell cycle and subsequent cycles. It is better to start with a low concentration and add more cells if the desired number of cells has not been achieved within about 10 min.
14. Choosing the correct exposure is not always easy as the strength of signals can change dramatically during the cell cycle. It is best to use the minimal exposure that will yield a good signal-to-noise ratio. Extended exposure will damage the cells and affect the cell cycle. Moreover, overexposure will lead to saturated signals that cannot be quantified. The balance here is even more difficult to strike than in metazoan cells as most markers are relatively weak and yeast cells are more sensitive to radiation.

Acknowledgements

We would like to thank Aryeh Weiss, Amit Zur, Tamar Listovsky, Yuval Cinnamon, Julia Sajman, and the many other students and colleagues who helped to develop and practice live cell imaging in our laboratory over the last two decades. Special thanks to Tim Hunt who suggested that I should use live cell imaging in the first place. This research in our laboratory was funded over the years by grants from the ISF, BSF, GIF, AICR, ICRF, and HUJI.

References

1. Zetterberg A, Larsson O (1985) Kinetic analysis of regulatory events in G1 leading to proliferation or quiescence of Swiss 3T3 cells. Proc Natl Acad Sci U S A 82:5365–5369
2. Chalfie M, Tu Y, Euskirchen G, Ward W, Prasher D (1994) Green fluorescent protein as a marker for gene expression. Science 263: 802–805
3. Hagting A, Karlsson C, Clute P, Jackman M, Pines J (1998) MPF localization is controlled by nuclear export. EMBO J 17:4127–4138
4. Brandeis M, Hunt T (1996) The proteolysis of mitotic cyclins in mammalian cells persists from the end of mitosis until the onset of S phase. EMBO J 15:5280–5289
5. Zur A, Brandeis M (2001) Securin degradation is mediated by fzy and by fzr and is required for complete chromatid separation but not for cytokinesis. EMBO J 20:792–801
6. Listovsky T, Oren YS, Yudkovsky Y, Mahbubani HM, Weiss AM, Lebendiker M, Brandeis M (2004) Mammalian Cdh1/Fzr mediates its own degradation. EMBO J 23:1619–1926
7. Sakaue-Sawano A, Kurokawa H, Morimura T, Hanyu A, Hama H, Osawa H, Kashiwagi S, Fukami K, Miyata T, Miyoshi H, Imamura T, Ogawa M, Masai H, Miyawaki A (2008) Visualizing spatiotemporal dynamics of multicellular cell-cycle progression. Cell 132:487–498
8. Lindon C, Pines J (2004) Ordered proteolysis in anaphase inactivates Plk1 to contribute to proper mitotic exit in human cells. J Cell Biol 164:233–241
9. Leonhardt H, Rahn HP, Weinzierl P, Sporbert A, Cremer T, Zink D, Cardoso MC (2000) Dynamics of DNA replication factories in living cells. J Cell Biol 149:271–280
10. Easwaran HP, Leonhardt H, Cardoso MC (2005) Cell cycle markers for live cell analyses. Cell Cycle 4:453–455
11. Fujita M, Yamada C, Goto H, Yokoyama N, Kuzushima K, Inagaki M, Tsurumi T (1999) Cell cycle regulation of human CDC6 protein. Intracellular localization, interaction with the human mcm complex, and CDC2 kinase-mediated hyperphosphorylation. J Biol Chem 274:25927–25932
12. Clijsters L, Ogink J, Wolthuis R (2013) The spindle checkpoint, APC/C(Cdc20), and APC/C(Cdh1) play distinct roles in connecting mitosis to S phase. J Cell Biol 201:1013–1026
13. Huh WK, Falvo JV, Gerke LC, Carroll AS, Howson RW, Weissman JS, O'Shea EK (2003) Global analysis of protein localization in budding yeast. Nature 425:686–691
14. Cinnamon Y, Feine O, Hochegger H, Bershadsky A, Brandeis M (2009) Cellular contractility requires ubiquitin mediated proteolysis. PLoS One 4:e6155
15. Petersen BO, Wagener C, Marinoni F, Kramer ER, Melixetian M, Denchi EL, Gieffers C, Matteucci C, Peters JM, Helin K (2000) Cell cycle- and cell growth-regulated proteolysis of mammalian CDC6 is dependent on APC-CDH1. Genes Dev 14:2330–2343
16. Mailand N, Diffley JF (2005) CDKs promote DNA replication origin licensing in human cells by protecting Cdc6 from APC/C-dependent proteolysis. Cell 122:915–926
17. Terskikh A, Fradkov A, Ermakova G, Zaraisky A, Tan P, Kajava AV, Zhao X, Lukyanov S, Matz M, Kim S, Weissman I, Siebert P (2000) "Fluorescent timer": protein that changes color with time. Science 290:1585–1588
18. Subach FV, Subach OM, Gundorov IS, Morozova KS, Piatkevich KD, Cuervo AM, Verkhusha VV (2009) Monomeric fluorescent timers that change color from blue to red report on cellular trafficking. Nat Chem Biol 5:118–126

Chapter 21

Measurement of Cdk1/Cyclin B Kinase Activity by Specific Antibodies and Western Blotting

Cody W. Lewis, Ryan G. Taylor, and Roy M. Golsteyn

Abstract

Quantitative measurement of enzyme activity is a valuable approach to study how cells function. We present a method to measure the activity of the enzyme Cdk1/cyclin B. This enzyme is required by all eukaryotic cells to enter mitosis. Therefore, a biochemical assay to measure Cdk1/cyclin B activity can be used to identify cell populations that are in mitosis or to detect inhibitors of Cdk1/Cyclin B in vitro. A key distinction of the method presented here, compared to others, is that it uses a recombinant protein, a specific antibody, and a western blot apparatus, which makes the technique available to cell and molecular biology laboratories who do not wish to use radioisotopes, which are commonly required for other protein kinase assays.

Key words Cyclin-dependent protein kinase 1, Cyclin B, Phospho-antibodies, Protein kinase assay, Small-molecule inhibitors, Western blotting

1 Introduction

Mitosis is a key event in cell biology. During this phase of the cell cycle a cell distributes a copy of its genome to two daughter cells, which ensures the continuity of life [1]. Mitosis has a major impact upon disease, such as when a cell fails to segregate chromosomes correctly [2] or when the genome has been damaged and the cell escapes a checkpoint [3]. Given the importance of mitosis to biology, techniques are required to detect it in populations of cells or to identify chemicals that might act as antiproliferative drugs by inhibiting mitotic enzymes.

Cyclin-dependent kinase-1 (Cdk1/cyclin B) is a highly conserved protein kinase complex that is essential for entry into mitosis in eukaryotic cells [4]. It is a heterodimer composed of a 55 kDa regulatory subunit (cyclin B) and a 34 kDa catalytic subunit (Cdk1) [5]. During the cell cycle levels of the catalytic subunit remain constant while levels of cyclin B oscillate. In G_1 and S phases, cyclin B levels are low, but increase throughout G_2 phase until a

Amanda S. Coutts and Louise Weston (eds.), *Cell Cycle Oscillators: Methods and Protocols*, Methods in Molecular Biology, vol. 1342, DOI 10.1007/978-1-4939-2957-3_21,

maximal level is reached during the G_2/M-phase transition. During anaphase, cyclin B is selectively proteolyzed by the anaphase-promoting complex/cyclosome (APC/c) rapidly decreasing its levels, causing exit from mitosis [6]. Although cyclin B binding is essential for Cdk1 enzymatic activity, it is not sufficient to activate the complex. The Cdk1/cyclin B complex requires stepwise phosphorylation and dephosphorylation events that ensure accurate temporal and spatial activation in the cell cycle [7]. Because Cdk1/cyclin B protein levels and activity are highly regulated, a direct measure of its activity is the most reliable method to detect mitosis in cell populations [8].

Methods to measure Cdk1/cyclin B activity frequently use radiolabeled ATP as a substrate and measure the incorporation of phosphate onto the protein substrate histone H1 [9]. This assay is robust, quantitative, and well adapted to high-throughput screening approaches. There are, however, safety concerns and costs to handling radioisotopes in research laboratories. Those who investigate mitosis infrequently may not wish to invest in specialized laboratory equipment to handle or measure radioisotopes. These limitations have made it necessary to develop nonradioactive methods to measure Cdk1 activity. Fluorescence resonance energy transfer (FRET) is one method suitable for measuring Cdk1 activity in live cells [7]. We investigated another approach that uses western blotting and specific antibodies, because this technique will be more widely available to molecular and cellular biology laboratories and can be modified to provide quantitative measurements [10].

To design a western blot assay to measure Cdk1/cyclin B activity, we searched known Cdk1/cyclin B protein substrates for ones with a reliable antibody to the phosphorylated epitope. Protein phosphatase-1Cα (PP1Cα) is phosphorylated on threonine 320 by Cdk1/cyclin B [11] and can be detected by western blotting using phospho-Thr^{320}-specific antibodies. With this information, we synthesized an artificial substrate (GST-PP1C-S) that contained the Cdk1 canonical consensus sequence found within PP1Cα at threonine 320 in frame to the C-terminus of the GST protein. We then used the GST-PP1C-S substrate to develop a Cdk1 assay whereby GST-PP1C-S phosphorylation levels are quantified in cells or in vitro by western blotting. Specifically, we measure the fluorescence intensity of the secondary fluorescently coupled antibody that detects the respective phospho-antibody.

In this chapter, we describe how to measure Cdk1 activity by western blotting. The assay has been used to measure mitosis in cultured human cells undergoing checkpoint adaptation [3] and to detect Cdk1 chemical inhibitors [8]. This assay can be quantified without handling radioisotopes, such as those used in the histone H1 kinase assay.

2 Materials

All solution and reagents should be prepared in deionized and distilled H_2O.

2.1 Human Cell Extraction Preparation

1. 10× Phosphate-buffered saline (PBS): 685 mM NaCl, 13.5 mM KCl, 500 mM Na_2HPO_4, 88 mM KH_2PO_4. pH to 7.4 and sterilize by autoclaving.
2. Lysis buffer: 50 mM HEPES, 50 mM NaF, 10 mM EGTA, 50 mM β-glycerophosphate, 1 mM ATP, 1 mM dithiothreitol (DTT), 1 % Triton X-100, 10 μg/mL RNase A, 0.4 unit/mL DNase I, with Roche protease inhibitor tablet.
3. 26-G needle.
4. 1 mL syringe.
5. Trypsin–EDTA solution.
6. Nocodazole (200 mg/mL) in DMSO. Store at −20 °C.

2.2 Recombinant GST-PP1C-S and GST

1. BL21 bacteria previously transformed with pGEX-T1 plasmid.
2. BL21 bacteria previously transformed with pGEX-PP1Cα His plasmid (Fig. 1).
3. LB ampicillin agar plates.
4. 1 mM Isopropyl β-D-1-thiogalactopyranoside (IPTG).
5. 2× SDS sample buffer: 62.5 mM Tris, 35 mM DTT, 25 % glycerol, 694 mM sodium dodecyl sulfate, 150 μM bromophenol blue. Prepare aliquots and store at −20 °C.
6. Bacterial cell lysis buffer: 50 mM PBS, 1 mM EDTA, 100 mM NaCl, protease inhibitor (1/10 mL) at a ratio of 1 mL per g. Lysozyme solution (50 mg/mL Sigma L7651 in 10 mM PBS, 1 mM EDTA). Prepare aliquots and store at −80 °C.
7. Glutathione affinity chromatography purification system.
8. Elution buffer: 10 mM reduced glutathione, 50 mM Tris (pH 7.9).

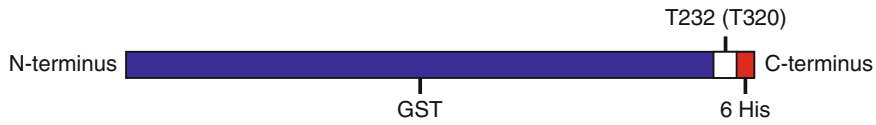

Fig. 1 The Cdk1/cyclin B recombinant protein substrate. A schematic diagram of the protein substrate is shown. The GST domain (*blue*) is located in the N-terminus, followed by the amino acids from PP1Ca that contain the T320 Phosphorylation site (*white*) with the phospho-residue at position 232. The six-histidine C-terminus is shown in *red*. The amino acid sequence of the phosphorylation site copied from human PP1-Ca with six histidines is GRPI**T**PPRNHHHHHH

9. Dialysis tubing.
10. 50 mM Tris (pH 7.9).
11. A protein chip (On-Chip-Electrophoresis; Agilent Technologies).
12. A Bioanalyzer 2100.

2.3 Kinase Assay

1. 2× Cdk1 phospho buffer: 100 mM β-glycerophosphate, 20 mM $MgCl_2$, 20 mM NaF, 2 mM DTT. Store aliquots at −20 °C.
2. 2× Sample buffer: 62.5 mM Tris, 35 mM DTT, 25 % glycerol, 694 mM sodium dodecyl sulfate, 150 μM bromophenol blue. Prepare aliquots and store at −20 °C.
3. Lysis buffer: 50 mM HEPES, 50 mM NaF, 10 mM EGTA, 50 mM β-glycerophosphate, 1 mM ATP, 1 mM DTT, 1 % Triton X-100, 10 μg/mL RNase A, 0.4 unit/mL DNase I, with Roche protease inhibitor cocktail.
4. 1 M ATP.
5. Cell extracts: 20,000 cells/μL in lysis buffer. *We recommend the use of nocodazole-treated and untreated cell extracts for mitotic and interphasic controls, respectively.*
6. Cdk1/cyclin B active enzyme (Millipore; 14-450). *For purified enzyme assay only.*

2.4 Polyacrylamide Gel Electrophoresis

1. Resolving gel buffer (1.5 M Tris base): 1.5 M Tris, pH to 8.8 and store at room temperature.
2. Stacking gel buffer (0.5 M Tris base): 0.5 M Tris, pH to 6.8 and store at room temperature.
3. 30 % acrylamide/bis solution. Store at 4 °C.
4. 10 % (w/v) Ammonium persulfate solution (APS). Prepare aliquots and store at −20 °C.
5. *N,N,N,N′*-tetramethyl-ethylenediamine (TEMED). Store at 4 °C.
6. 10 % (w/v) Sodium dodecyl sulfate solution. Store at room temperature.
7. SDS-PAGE running buffer: 24.8 mM Tris (hydroxymethyl) aminomethane, 190 mM glycine, 3.5 mM sodium dodecyl sulfate.
8. Coomassie blue stain: 0.1 % Coomassie blue R250, 25 % ethanol, 7.5 % acetic acid in distilled water.
9. Molecular weight marker (MWM).
10. Standard polyacrylamide gel electrophoresis equipment.

2.5 Western Blotting

1. Nitrocellulose membrane.
2. Thick Whatman blotting paper.

3. Towbin transfer buffer: 10 % Towbin buffer (2.4 M glycine, 313 mM Tris, 20 % methanol). Store at room temperature.
4. Ponceau-S stain: 1 % (w/v) of Ponceau-S in 5 % (v/v) acetic acid.
5. Tris buffer saline (TBS): 500 mM Tris and 1.5 M NaCl. Store at room temperature.
6. TBS with Tween®20 (TBST): 10 % TBS (500 mM Tris and 1.5 M NaCl), 0.1 % Tween®20. Store at room temperature.
7. 2 % BSA blocking buffer in TBS-T. Store at 4 °C.
8. 5 % milk powder blocking buffer in TBS-T. Store at 4 °C.
9. Alkaline phosphatase (AP) development buffer: To 10 mL of TBS, 66 μL of NBT (50 mg/mL nitroblue tetrazolium chloride in dimethylformamide) and 33 μL BCIP (50 mg/mL 5-bromo-4-chloro-3′-indolylphosphate p-toluidine in dimethylformamide) mixed immediately before use.
10. Standard western blotting apparatus.

2.6 Antibodies

1. Rabbit anti-glutathione S transferase antibody (Sigma; G7781-100UL).
2. Mouse anti-PPP1A (Phospho-T320) antibody (Abcam; ab62334).
3. Alkaline phosphatase-coupled anti-mouse antibody (Promega; S3721).
4. AlexaFluor 488-coupled anti-rabbit antibody (Invitrogen; A11008).
5. AlexaFluor 488-coupled anti-mouse antibody (Invitrogen; A11059).

2.7 Fluorescence Detection

1. Phospho-imager such as the Typhoon Trio™ Imager.
2. ImageQuant software.

3 Methods

3.1 Human Cultured Cell Extracts

1. In addition to the experimental extracts, prepare control extracts from cells either treated or not treated with 200 ng/mL nocodazole for 24 h (*see* **Note 1**). After treatment, mitotic (rounded) cells are separated from interphase (flattened) cells in both nocodazole and untreated populations by mechanical shake-off. Strike the flask of cells against a hard surface several times until the mitotic cells detach. After one or more strikes, observe the flask by light microscopy to detect cell release. Collect the suspension containing the mitotic cells from the nocodazole treatment by centrifugation. This sample serves as

a positive control that will contain Cdk1 activity. The remaining flattened adherent cells in the untreated population will be in interphase and will serve as a negative control that does not have Cdk1 activity. These cells can be collected by trypsinization. All cell samples should be processed without delay.

2. Use a cell counter to determine cell number.
3. Centrifuge cell suspensions at 350 × *g* for 5 min. After centrifugation, aspirate media without disturbing cell pellet.
4. Resuspend pellet in 1 mL of cold PBS and centrifuge (4 °C) by high-speed pulse centrifugation (20 s at 10,000 × *g*). Rotate tube 180° and repeat.
5. Resuspend cell pellet in precooled lysis buffer (4 °C) to a concentration of 20,000 cells/μL.
6. Pass cell suspension through a 26-G needle five times. Avoid creating a foam.
7. Store on ice for 30 min.
8. Centrifuge suspension for 10 min at 10,000 × *g* (4 °C).
9. Transfer the supernatant into a sterile precooled tube without disturbing the pellet. From this tube, note the volume, then transfer aliquots to sterile precooled tubes, and store them at −80 °C (*see* **Note 2**).

3.2 Preparation of Recombinant GST-PP1C-S and GST

1. Thaw BL21 bacteria (*E. coli*) that have been previously transformed with pGEX-PP1Cα His plasmid and thaw BL21 bacteria that have been previously transformed with the pGEX-T1 plasmid. Keep bacteria on ice (*see* **Note 3**).
2. Plate each bacteria preparation onto separate LB ampicillin (AMP) agar plates and incubate for 24 h at 37 °C.
3. Select one isolated colony from each plate and use it to inoculate separate flasks of LB + AMP liquid media.
4. Monitor the optical density of the culture, when it reaches an $OD_{600} = 0.6$, remove a 500 μL sample, and store on ice. Then induce the culture to express protein by adding IPTG to 1 mM.
5. Continue to culture the suspension for 3–4 h, then measure the OD_{600}, remove a 500 μL sample (induction sample), and store on ice (*see* **Note 4**). Combine induction samples with equal volumes of 2× SDS sample buffer and store at −20 °C.
6. Centrifuge the remaining culture at 10,000 × *g* for 20 min and then remove supernatant without disturbing the pellet. Store the pellet at −80 °C.
7. For purification, thaw the pellet on ice and resuspend in bacterial cell lysis buffer.
8. Add lysozyme solution at a ratio of 50 μL/10 mL of bacterial cell lysis buffer and incubate for 10 min.

9. Sonicate extract at 50 % duty cycle with a limit of eight cycles for 10 min. Remove a 100 μL sample (total extract sample).
10. Centrifuge the total extract for 10 min at 10,000 × *g*. Remove a 100 μL sample (total supernatant sample).
11. Remove supernatant without disturbing the pellet and store on ice in a precooled tube.
12. Gently wash the surface of the pellet with fresh lysis buffer and then resuspend the pellet to the original extract volume. Remove a 100 μL sample (total pellet sample) and discard the remaining sample.
13. Pass the supernatant (from **step 11**) through a column containing the glutathione-coated beads and then rinse three times with PBS (see the manufacturer's specifications). Collect a 100 μL sample from the flow through and each subsequent wash with PBS. Store the flow through and wash samples at –80 °C.
14. Add 50–100 μL of elution buffer per 1 mL of total supernatant used and then incubate at room temperature for 5–10 min with gentle agitation.
15. Centrifuge at 500 × *g* for 5 min, transfer the supernatant to a precooled tube or at –80 °C until dialysis, and repeat **steps 14** and **15** two more times.
16. Before proceeding to dialysis, confirm the presence of the GST-PP1C-S and/or the GST by SDS-PAGE. Load preinduction, post-induction, total extract, total supernatant, pellet suspension (total pellet), washes, and elution samples into a 12 % gel (*see* Subheading 3.4).
17. Once the gel has run, stain it with Coomassie blue. The GST-PP1C-S and/or the GST proteins should be visible at the 25 kDa marker position in the post-induction samples and not in the preinduction sample.
18. Prepare the dialysis tubing by tying one end closed.
19. If most of the substrate is in the first elution sample, pipette the contents into the dialysis tubing and seal, removing any bubbles. If a significant portion of the substrate is found in the other elution samples, they may be combined before adding to the dialysis tubing.
20. Place the filled dialysis tubing into a 1 L column filled with 50 mM Tris buffer (pH 7.9) for 6 h, gently inverting every 2 h.
21. Remove the dialysis tubing after 6 h. Open one end of the tubing and aliquot desired volumes into precooled tubes. Store at –80 °C.
22. Analyze the GST-PP1C-S and GST on a protein chip with a Bioanalyzer 2100. For best results, ensure that the purity is greater than 95 %.

3.3 Kinase Assay

1. Thaw cell extracts (Subheading 3.1, **step 9**) (or Cdk1 enzyme), GST-PP1C-S, and GST on ice (Subheading 3.2, **step 20**) and then centrifuge at 10,000 × *g* for 10 min at 4 °C.
2. Transfer the supernatant to new tubes without disturbing the pellet.
3. Prepare fresh 400 μM ATP solution in 2× Cdk1 phospho-buffer and store on ice. This amount is sufficient for 39 reactions.
4. Dilute GST-PP1C-S and GST substrates to a final volume of 80 ng/μL in 2× Cdk1 phospho-buffer. Store on ice.
5. Dilute cell extract to 100 cells/μL in lysis buffer or Cdk1 enzyme to 58 mg/L in 2× Cdk1 phospho-buffer. Store on ice.
6. Prepare each reaction by combining 5 μL of GST-PP1C-S or GST with 10 μL of 400 μM ATP in 2× Cdk1 phospho-buffer. Note that each cell extract should individually be reacted with both substrates (Table 1; Fig. 3).
7. Prepare one set of negative control reactions where 5 μL of substrate is combined with 15 μL of 400 μM ATP in 2× Cdk1 phospho-buffer with no cell extracts or Cdk1 enzyme.
8. Add 5 μL of the diluted cell extract or Cdk1 enzyme (positive control) to each tube and incubate at 30 °C for 15 min.
9. Stop the reactions by adding 2× sample buffer and store on ice or at −20 °C until analysis by western blotting.

3.4 SDS-PAGE

1. Prepare a 12 % resolving gel: Combine 6.7 mL of $^{dd}H_2O$, 5 mL of resolving buffer (1.5 M Tris, pH 8.8), 10 mL of acrylamide/bis (30 %), and SDS (10 % w/v) into a tube. Gently mix solution without introducing air bubbles. Add 100 μL of APS (10 % w/v) and 20 μL TEMED and gently mix. Pour gel immediately into a 1.5 mm cast. Leave approximately 2 cm for

Table 1
Final RXN conditions: 40 ng/μL substrate, 25 cell/μL cell extract, 1× Cdk1 reaction buffer (200 μM ATP)

Reaction	PP1Ca			GST		
Mitotic cell extract (μL)	5	X	X	5	X	X
Interphase cell extract (μL)	X	5	X	X	5	X
GST-PP1C-S: 80 ng/μL (μL)	5	5	5	X	X	X
GST protein: 20 ng/μL (μL)	X	X	X	5	5	5
2× Cdk1 reaction buffer + 400 μM ATP (μL)	10	10	15	10	10	15
Final volume (μL)	20	20	20	20	20	20

the stalking gel. Fill the remaining cast with 100 % ethanol. Allow the gel to polymerize for 30 min.

2. After the resolving gel has polymerized remove the ethanol and rinse three times with water.
3. Prepare a 4 % stacking gel: Combine 3.1 mL of $^{dd}H_2O$, 1.25 mL of 0.5 stacking buffer (0.5 M Tris, pH 6.8), 665 μL acrylamide/bis (30 %), 50 μL SDS (10 % w/v), 65 μL APS (10 % w/v), and 5 μL TEMED. Pour staking gel on top of the polymerized resolving gel. Insert the comb and allow gel to set for 30 min.
4. After the resolving gel has polymerized remove the comb, insert the cast containing the gel into the SDS-PAGE electrode box, and fill with SDS-PAGE running buffer.
5. Heat the kinase reaction samples to 95 °C for 5 min.
6. Vortex and load 10 μL of each sample into the gel lanes and load the molecular weight marker according to the manufacturer's recommendations. Samples should be run in duplicate to test for both GST and GST-PP1C-S.
7. Allow the SDS-PAGE system to run for 45 min at 200 V.

3.5 Western Blotting (Semidry)

1. Remove the protein gel from the cast and place the gel into Towbin transfer buffer for 10 min.
2. Separately pre-wet two pieces of Whatman blotting paper and nitrocellulose membrane (*see* **Note 5**) in Towbin transfer buffer (*see* **Note 6**).
3. Prepared a blotting "sandwich": Place one sheet of Whatman blotting paper directly on the positive plate of the transfer system. Next add the nitrocellulose membrane followed by the protein gel and another piece of Whatman paper.
4. Remove air bubbles by rolling a piece of tubing over the sandwich, close the negative plate over the sandwich, and load it into the transfer apparatus.
5. Run the transfer system for 45 min at 25 V.
6. After the transfer is complete carefully remove nitrocellulose membrane and add to TBS-T buffer.
7. Optional step: To confirm that protein transfer was successful, pour a few milliliters of Ponceau-S stain directly onto the membrane. After 1 min, rinse with distilled H_2O. Red bands (representing the GST/GST-PP1C-S) should be visible at the 25 kDa marker position.
8. Place membranes in either 2 % BSA blocking buffer for anti-PPP1A-phospho-T320 or 5 % milk blocking buffer for detection of anti-GST for 1 h.

9. Incubate membranes with either anti-PPP1A-phospho-T320 (1:30,0000) in 2 % BSA blocking buffer or anti-GST (1:10,000) in 5 % milk blocking buffer. Leave overnight at room temperature.
10. Wash with TBS-T for 15 min three times.
11. As an alternative step to the quantitative measure described below, Cdk1 activity can be detected using the alkaline phosphatase-coupled secondary antibodies (Fig. 2). The antibody handling and wash steps are similar to those for the fluorochrome-coupled antibodies. After the washes are completed, develop the nitrocellulose membrane by submerging the membrane in AP development buffer until bands are visible on a white background. Stop the development by rinsing the membrane with 1 mM EDTA. Dry the membrane and take an image by light scanner or camera.
12. For quantitative measurement, incubate the membranes at room temperature for 3 h with their respective AlexaFluor 488-couple antibodies (mouse or rabbit) at a dilution of 1:400.
13. Wash with TBS-T for 15 min three times.

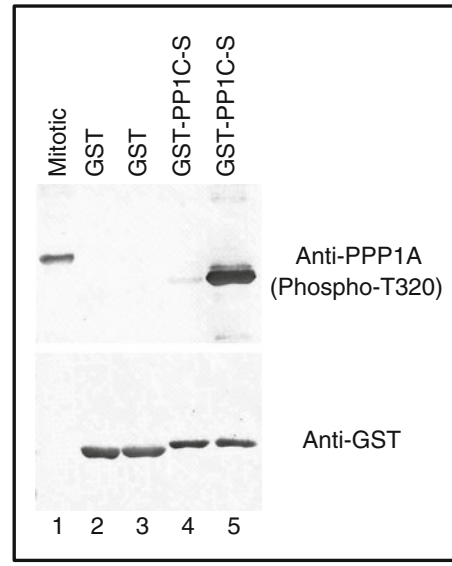

Fig. 2 The detection of phosphorylated PP1Ca in a mitotic extract (*lane 1*) and the phosphorylated form of GST-PP1C-S (*lane 5* positive control) is shown. In this assay, Cdk1/cyclin B enzyme was added to the reaction using the substrates GST (*lane 3*) and GST-PP1C-S (*lane 5*) but it was not added to samples shown in *lanes 2* and *4*. GST proteins and non-phosphorylated GST-PP1C-S were not detected by the anti-PPP1A antibody (*lanes 2, 3, 4*). The nitrocellulose membrane was developed with secondary antibodies coupled to alkaline phosphatase, which provides a qualitative estimate of signal strength. Reproduced from Lewis 2013 with permission from Elsevier [8]

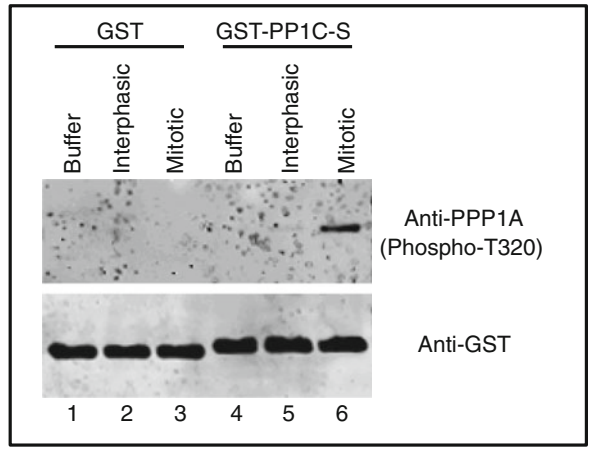

Fig. 3 Quantitative detection of phosphorylated GST-PP1C-S by western blotting with fluorochrome-labeled secondary antibodies. GST (*lanes 1–3*) or GST-PP1C-S (*lanes 4–6*) were incubated either with buffer, interphasic cell extract, or mitotic cell extract. The samples were processed by western blotting. The GST-PP1C-S substrate is detected by anti-PPP1A antibody when it is phosphorylated by a mitotic extract

14. Remove membranes from TBS-T and scan on a phospho-imager such as the Typhoon Trio™ Imager. Insure that the detection is set to scan fluorescent molecules. Use the 670BP30 emission filter with a 633 red laser for optimal scans. Set the voltage to between 450 and 500 V.
15. Analyze fluorescent signals using ImageQuant software (Fig. 3).
16. Normalize fluorescent signals collected from the membrane incubated with the anti-PPP1A phospho-T320 antibody by subtracting fluorescent signals obtained from the membrane incubated with the anti-GST antibody.

4 Notes

1. Prepare lysis buffer and store it on ice prior to harvesting cells with trypsin. In steps that handle cell extracts (including sonication), the extract must be kept cold or the Cdk1/cyclin complex will denature and become inactive.
2. Cell extract supernatants are first transferred to a new tube prior to preparing aliquots to ensure that the supernatant is homogenous prior to distribution.
3. GST-PP1C-S is composed of GST sequence (N-terminus) in frame with amino acids 316–324 of PP1Ca followed by 6-histidines at the C-terminus (Fig. 1). Although we did not use it in this protocol, the 6-histidine can be used to purify

GST-PP1C-S by the method of nickel chromatography. Furthermore, the 6-histidines present a convenient epitope with which to detect GST-PP1C-S by western blotting with an anti-histidine antibody [8].

4. The production of protein by IPTG induction should be carefully surveyed by examining the OD_{600} and removing samples at various time points. By knowing the time of relative maximum production, one can reduce the amount of undesired proteins present in the extract. Ideally, the OD_{600} will increase at lower rate after IPTG induction as compared to prior to induction. Analyze protein induction by SDS-PAGE. To load equal amounts of bacterial cells per gel lane, load an OD equivalent equal to 300 (i.e., volume bacterial suspension sample multiplied by its OD_{600}).
5. To minimize background levels on membrane, do not used powdered gloves or ink pens to mark the membrane when carrying out the steps in this protocol.
6. The Whatman blotting paper and nitrocellulose membrane should have slightly larger surface areas than the gel such that the edges of the gel do not hang over the membrane during the transfer.

References

1. Murray AW (2004) Recycling the cell cycle: cyclins revisited. Cell 116:221–234
2. Crasta K, Ganem NJ, Dagher R et al (2012) DNA breaks and chromosome pulverization from errors in mitosis. Nature 482:53–58. doi:10.1038/nature10802
3. Kubara PM, Kernéis S, Studeny A et al (2012) Human cells enter mitosis with damaged DNA after treatment with pharmacological concentrations of genotoxic agents. Biochem J 446: 373–381
4. Santamaria D, Barriere C, Cerqueira A et al (2007) Cdk1 is sufficient to drive the mammalian cell cycle. Nature 448:811–815
5. Pines J, Hunter T (1989) Isolation of a human cyclin cDNA: evidence for cyclin mRNA and protein regulation in the cell cycle and for interaction with p34. Cell 58:833–846
6. Dorée M, Hunt T (2002) From Cdc2 to Cdk1: when did the cell cycle kinase join its cyclin partner. J Cell Sci 115:2461–2464
7. Gavet O, Pines J (2010) Progressive activation of CyclinB1-Cdk1 coordinates entry to mitosis. Dev Cell 18:533–543
8. Lewis CW, Taylor RG, Kubara PM et al (2013) A western blot assay to measure cyclin dependent kinase activity in cells or in vitro without the use of radioisotopes. FEBS Lett 587: 3089–3095
9. Meijer L, Arion D, Golsteyn RM et al (1989) Cyclin is a component of the sea urchin egg M-phase specific histone H1 kinase. EMBO J 8:2275–2282
10. Fradelizi J, Friederich E, Beckerle MC et al (1999) Quantitative measurement of proteins by western blotting with Cy5-coupled secondary antibodies. Biotechniques 26: 484–490
11. Kwon YG, Lee SY, Choi Y et al (1997) Cell cycle-dependent phosphorylation of mammalian protein phosphatase 1 by cdc2 kinase. Proc Natl Acad Sci U S A 94:2168–2173

ERRATUM TO

Chapter 14
Combining the Optimized Yeast Cytosine Deaminase Protein Fragment Complementation Assay and an In Vitro Cdk1 Targeting Assay to Study the Regulation of the γ-Tubulin Complex

Po Hien Ear, Jacqueline Kowarzyk, Michael J. Booth, Diala Abd-Rabbo, Kristian Shulist, Conrad Hall, Jackie Vogel, and Stephen W. Michnick

Amanda S. Coutts and Louise Weston (eds.), *Cell Cycle Oscillators: Methods and Protocols*, Methods in Molecular Biology, vol. 1342, DOI 10.1007/978-1-4939-2957-3_14, © Springer Science+Business Media New York 2016

DOI 10.1007/978-1-4939-2957-3_22

The original version of this chapter unfortunately contained a mistake. In chapter 14 titled "Combining the Optimized Yeast Cytosine Deaminase Protein Fragment Complementation Assay and an In Vitro Cdk1 Targeting Assay to Study the Regulation of the γ-Tubulin Complex", the Materials section, on page 244, section 2.2.3 (Reagents and Media for Sf9 Cell Culture, Protein Expression, and Protein Purification), step 5 lists the components of the HB100 buffer. One of the components, GTP, is listed as 100 mM GTP. It should be 100 μM GTP.

The online version of the original chapter can be found at http://dx.doi.org/10.1007/978-1-4939-2957-3_14

Amanda S. Coutts and Louise Weston (eds.), *Cell Cycle Oscillators: Methods and Protocols*, Methods in Molecular Biology, vol. 1342, DOI 10.1007/978-1-4939-2957-3_22, © Springer Science+Business Media New York 2016

Index

Amanda S. Coutts and Louise Weston (eds.), *Cell Cycle Oscillators: Methods and Protocols*, Methods in Molecular Biology, vol. 1342, DOI 10.1007/978-1-4939-2957-3, © Springer Science+Business Media New York 2016

D

E

F

G

H

I

K

L

M

N

O

P

R

S

T

U

W

X

Y